

4

FILE COPY

TECHNICAL REPORT SL-88-22

SPALL DAMAGE OF CONCRETE STRUCTURES

by

Mark K. McVay

Structures Laboratory

DEPARTMENT OF THE ARMY
Waterways Experiment Station, Corps of Engineers
PO Box 631, Vicksburg, Mississippi 39180-0631

AD-A199 225



June 1988

Final Report

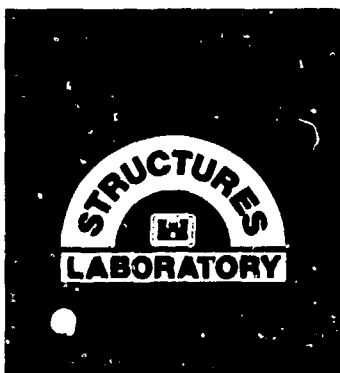
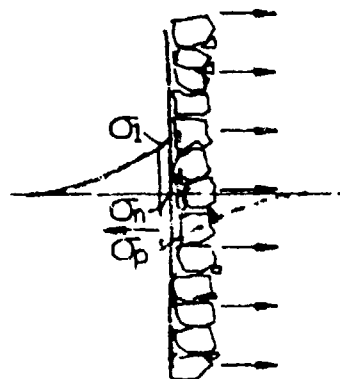
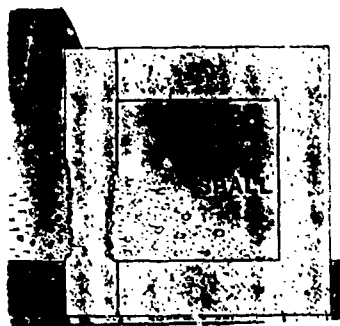
Approved For Public Release; Distribution Unlimited

DTIC
ELECTE
SEP 07 1988
S H

88 9 6 15 3

Prepared for DEPARTMENT OF THE ARMY
US Army Corps of Engineers
Washington, DC 20314-1000

Under Project No. 4A162719AT40
Task Area AO, Work Unit 023



Destroy this report when no longer needed. Do not
return it to the originator.

The findings in this report are not to be construed as an
official Department of the Army position unless so
designated by other authorized documents.

The contents of this report are not to be used for
advertising, publication, or promotional purposes.
Citation of trade names does not constitute an
official endorsement or approval of the use of such
commercial products.

Unclassified
SECURITY CLASSIFICATION OF THIS PAGE

AD-A199111

REPORT DOCUMENTATION PAGE				Form Approved OMB No 0704-0188 Exp Date Jun 30 1980	
1a REPORT SECURITY CLASSIFICATION Unclassified		1b RESTRICTIVE MARKINGS None			
2a SECURITY CLASSIFICATION AUTHORITY		3 DISTRIBUTION/AVAILABILITY OF REPORT			
2b DECLASSIFICATION/DOWNGRADING SCHEDULE		Approved for public release; distribution unlimited.			
4 PERFORMING ORGANIZATION REPORT NUMBER(S) Technical Report SL-88-22		5 MONITORING ORGANIZATION REPORT NUMBER(S)			
6a. NAME OF PERFORMING ORGANIZATION USAEWES Structures Laboratory	6b. OFFICE SYMBOL (If applicable) CEWES-SS	7a. NAME OF MONITORING ORGANIZATION			
6c. ADDRESS (City, State, and ZIP Code) PO Box 631 Vicksburg, MS 39180-0631		7b. ADDRESS (City, State, and ZIP Code)			
8a. NAME OF FUNDING/SPONSORING ORGANIZATION US Army Corps of Engineers	8b. OFFICE SYMBOL (If applicable)	9 PROCUREMENT INSTRUMENT IDENTIFICATION NUMBER			
8c. ADDRESS (City, State, and ZIP Code) Washington, DC 20314-1000		10 SOURCE OF FUNDING NUMBERS <i>See reverse.</i>			
		PROGRAM ELEMENT NO.	PROJECT NO.	TASK NO.	WORK UNIT ACCESSION NO.
11. TITLE (Include Security Classification) Spall Damage of Concrete Structures					
12. PERSONAL AUTHOR(S) McVay, Mark K.					
13a. TYPE OF REPORT Final report	13b. TIME COVERED FROM Jan 85 TO Oct 87	14 DATE OF REPORT (Year, Month, Day) June 1988		15 PAGE COUNT 430	
16 SUPPLEMENTARY NOTATION See reverse.					
17 COSATI CODES		18. SUBJECT TERMS (Continue on reverse if necessary and identify by block number)			
FIELD	GROUP	SUB-GROUP			
		See reverse.			
19. ABSTRACT (Continue on reverse if necessary and identify by block number)					
<p>Spall is defined as the ejection of fragments from the opposite side of a structural element from which it is impacted and/or impulsively loaded. This research was on the spall of reinforced concrete panels subjected to bomb fragment impacts and/or airblast loads from nearby bomb detonations. Theories of spall, tests involving spall, and current spall prediction methods were reviewed and evaluated. The current spall prediction methods did not satisfactorily predict all of the previous test results found in the literature. Forty tests were conducted on reinforced concrete walls to investigate parameters which affect spall, to evaluate prediction methods further, and to provide data with which theory and prediction methods could be improved.</p> <p>Theoretical calculations were conducted for airblast loads under the compressive elastic limit. The tests showed that spall is dependent upon the shape and duration of a</p> <p>(Continued)</p>					
20. DISTRIBUTION/AVAILABILITY OF ABSTRACT <input checked="" type="checkbox"/> UNCLASSIFIED/UNLIMITED <input type="checkbox"/> SAME AS RPT <input type="checkbox"/> DTIC USERS		21 ABSTRACT SECURITY CLASSIFICATION Unclassified			
22a. NAME OF RESPONSIBLE INDIVIDUAL		22b TELEPHONE (Include Area Code)		22c OFFICE SYMBOL	

DD FORM 1473, 84 MAR

83 APR edition may be used until exhausted
All other editions are obsolete

SECURITY CLASSIFICATION OF THIS PAGE

Unclassified

Unclassified

SECURITY CLASSIFICATION OF THIS PAGE

10. SOURCE OF FUNDING NUMBERS (Continued).

PROGRAM ELEMENT 62719A
PROJECT NO. 4A162719AT 7
TASK NO. AO
WORK UNIT ACCESSION NO. 023

16. SUPPLEMENTARY NOTATION (Continued).

Available from National Technical Information Service, 5285 Port Royal Road, Springfield, VA 22161. This report was also submitted to the Department of Civil Engineering, Mississippi State University, Starkville, MS, in partial fulfillment of the requirements for the degree of Master of Science.

18. SUBJECT TERMS (Continued).

Bare charges	Explosives	Spalling
Blast effects	Protective structures prediction	Structural response
Cased charges	Scabbing	Tests
Concrete walls--testing	Semi-hardened	Upgrading
Conventional weapons	Spall	Weapon effects
Dynamic loads		

19. ABSTRACT (Continued).

stress wave as well as peak pressure. Scale model structures subjected to model bomb threats incurred less damage than full-scale structures subjected to full-scale bomb threats due to strain-rate effects. Thus, empirical prediction curves based upon scaled standoff distance underpredicted the damage in the full-scale tests. Cased bombs caused worse damage than equal-size bare bombs at the same standoff distances from equal walls. Thick-cased bombs caused much worse damage than equal-size thin-cased bombs at the same standoff distances from equal walls. An increase in wall thickness slightly reduced the amount of spall. Walls with close-spaced reinforcing steel suffered less damage than walls with wider-spaced reinforcing steel. Walls made of high-strength concrete suffered worse spall damage than walls made of 4,000-psi concrete subjected to the same bomb threats. Walls made of 4,000-psi concrete with 191.7 lb/yd³ of acrylic latex additive suffered less spall damage than similar concrete walls without the latex additive subjected to the same bomb threats. Walls made of 4,000-psi concrete with 80 lb/yd³ of crimped steel fibers suffered less damage than similar concrete walls without steel fibers subjected to the same bomb threats.

Data on 334 tests were collected in addition to the data from the 40 tests in this study. Improved empirical prediction curves for bare and cased charges were made and are presented in this report.

(SDC)

Unclassified

SECURITY CLASSIFICATION OF THIS PAGE

PREFACE

The research reported herein was conducted by personnel of the Structural Mechanics Division (SMD), Structures Laboratory (SL), US Army Engineer Waterways Experiment Station (WES). This work was conducted for the Office, Chief of Engineers (OCE), as part of Project No. 4A162719AT40, Task Area AO, Work Unit No. 023, Deliberate Hardened Facilities. OCE Program Manager was Mr. R. L. Wight. This research is in partial fulfillment of the requirements for the degree of Master of Science in the Department of Civil Engineering at Mississippi State University for Mr. Mark McVay.

The work was accomplished during the period January 1985 through October 1987. The research was prepared under the general supervision of Messrs. Bryant Mather, Chief, SL; James T. Ballard, Assistant Chief, SL; and Dr. Jimmy P. Balsara, Chief, SMD, SL. Direct supervision was provided by Mr. David R. Coltharp, Project Manager, SMD, SL. Mr. Mark McVay, SMD, was the Project Engineer, Test Engineer, and author.

Dr. Sam A. Kiger was the resident advisor for Mississippi State University at the WES extension campus and provided constructive criticism throughout the study.

Dr. Keith H. Denson, Professor of Civil Engineering, Mississippi State University, chaired the thesis review committee and gave advice during the study.

COL Dwayne G. Lee, CE, was the Commander and Director of WES during the preparation of this report. Dr. Robert W. Whalin was the Technical Director.



Accession For	
NTIS GRA&I	<input checked="checked" type="checkbox"/>
DTIC TAB	<input type="checkbox"/>
Unannounced	<input type="checkbox"/>
Justification	
By _____	
Distribution/	
Availability Codes	
Dist	Avail and/or Special
A-1	

CONTENTS

	<u>Page</u>
PREFACE.....	iii
LIST OF ILLUSTRATIONS.....	iv
LIST OF TABLES.....	xi
CONVERSION FACTORS, NON-SI TO SI (METRIC) UNITS OF MEASUREMENT.....	xiii
PART I: INTRODUCTION.....	1
Background.....	1
Objectives.....	1
Approach.....	2
PART II: THEORY.....	4
Definition of Spall.....	4
Airblast Loads.....	5
Bomb Fragment Loads.....	8
Combined Loads.....	13
Induced Stress Waves.....	13
Changes in Stress Waves as They Propagate Through Concrete...	14
Reflection of Stress Waves at Various Angles of Incidence....	18
Dynamic Properties of Concrete.....	20
Types of Concrete.....	22
Effects on Spall of Stress Wave Shape and Magnitude.....	24
PART III: SPALL PREDICTION LITERATURE.....	57
General.....	57
Theoretical Spall Prediction Methods for Bare Charge Threats.....	58
Theoretical Spall Prediction Methods for Cased-Charge Threats.....	59
Empirical Spall Prediction Methods for Bare Charge Threats...	60
Empirical Spall Prediction Methods for Cased Charge Threats..	62
PART IV: EXPERIMENTS.....	70
Concrete Spall Tests.....	70
Test Structures.....	70
Concrete Properties.....	71
Reinforcing Steel Yield Stresses.....	73
Reaction Structure.....	73
Explosive Charge Parameters.....	74
Measurements.....	74
Test Procedure.....	77
PART V: TEST DATA.....	95
General.....	95
Pressure Data.....	95
Stress Data.....	97
Acceleration Data.....	98
Displacement Data.....	98
Strain Data.....	99
Measurements of Spall Damage, Velocity, and Cracks.....	99

	<u>Page</u>
Measurements of Scab Damage.....	100
PART VI: ANALYSIS.....	112
General.....	112
Analysis of Spall Caused by a Bare Bomb.....	112
Effect on Spall of Changing Scaled Standoff and Charge Weight at a Given Standoff Distance.....	114
Effect on Spall of a Bare Contact Charge.....	116
Effect on Spall of Changing the Bare Charge Weight and Standoff Distance at a Given Scaled Standoff Distance.....	118
Differences in Spall Damage in Cube-Root Scaled Tests of Bare Charges.....	118
Comparison of Damage Caused by Equal-Size Bare and Cased Charges.....	120
Effect on Spall of Casing Thickness.....	124
Differences in Spall Damage in "Cube-Root" Scaled Tests of Cased Charges.....	126
Effect on Spall of Wall Thickness.....	127
Effect on Spall of Rebar Spacing.....	128
Effect on Spall of Concrete Strength.....	130
Effect on Spall of Adding Acrylic Latex to Concrete.....	132
Effect on Spall of Adding Crimped Steel Fibers to Concrete...	133
PART VII: COMPARISON OF TEST RESULTS TO PREDICTIONS.....	138
General.....	138
Comparison of the Bare Charge Test Results to Predictions from References 39 or 40.....	138
Comparison of the Bare Charge Test Results to Predictions from Reference 33.....	139
Comparison of the Bare Charge Test Results to Predictions from Reference 45.....	139
Comparison of Cased Charge Test Results to Predictions from Reference 41.....	140
Comparison of the Cased Charge Test Results to Predictions from Reference 34.....	141
Comparison of the Cased Charge Test Results to Predictions From Reference 45.....	142
PART VIII: DISCUSSION OF SPALL PREDICTION.....	145
Discussion of Theoretical Prediction Methods.....	145
Discussion of Empirical Prediction Methods.....	145
Additional Data.....	146
Empirical Damage Curves for Bare Charges.....	146
Empirical Damage Curves for Cased Charges.....	147
PART IX: PREVENTION AND RETENTION OF SPALL.....	153
General.....	153
Methods of Spall Prevention/Reduction.....	153
Methods of Spall Retention.....	157
PART X: SUMMARY.....	165
Theory.....	165

	<u>Page</u>
Experiments on Spall.....	166
Evaluation of Existing Methods.....	169
Improved Prediction Methods.....	170
Spall Prevention and Retention.....	170
REFERENCES.....	171
APPENDIX A PLOTS OF THE ACTIVE MEASUREMENTS VERSUS TIME.....	A1
APPENDIX B PRESSURE DISTRIBUTIONS ON THE WALL PANELS.....	B1
APPENDIX C PRETEST AND POSTTEST PICTURES OF EACH TEST.....	C1
APPENDIX D DATA ON DAMAGE OF REINFORCED CONCRETE STRUCTURES CAUSED BY NEARBY BOMB DETONATIONS.....	D1

LIST OF ILLUSTRATIONS

<u>Figure</u>		<u>Page</u>
1.1	Spall caused by airblast and fragment loading.....	3
2.1	Stress wave propagating, reflecting, and causing spall.....	34
2.2	Typical free-field and reflected airblast histories.....	35
2.3	Airblast parameters versus scaled standoff distance for TNT spherical air burst (Reference 3).....	36
2.4	Airblast parameters versus scaled standoff distance for TNT hemispherical ground burst (Reference 3).....	37
2.5	Ratio of reflected pressure to incident pressure versus angle of incidence.....	38
2.6	Scabbing resulting from a concentrated zone of multiple bomb fragment impacts.....	39
2.7	Variation of primary fragment velocity with distance.....	40
2.8	Theoretical Hugoniot and experimental data of concrete in the stress range from 0 to 24 kbar.....	41
2.9	Schematic of stress waves changing due to different stresses above the HEL traveling at different velocities.....	42
2.10	Illustration of attenuation of a stress wave with stresses above the dynamic compressive strength of the material...	42
2.11	Illustration of cylindrical divergence of a stress wave induced by a cylindrically expanding airblast wave.....	43
2.12	Illustration of spherical divergence of a stress wave expanding from a bomb fragment.....	44
2.13	Dispersion of a stress wave hitting an air void.....	45
2.14	Reflection factors for the reflected primary and shear stresses from an incident primary stress wave.....	46
2.15	Reflection factors for reflected primary and shear stresses from stresses from an incident shear stress wave.....	47
2.16	Use of an imaginary mirror image of the incident stress wave to calculate the net stress at a given point and time.....	48
2.17	Comparison of static and impact stress-strain curves for a typical concrete.....	48

	<u>Page</u>
2.18 Ratio of dynamic to static compressive strengths of concrete versus strain-rate.....	49
2.19 Ratio of dynamic to static tensile strengths of concrete versus strain-rate.....	50
2.20 Effects on spall of rectangular stress waves.....	51
2.21 Effects on spall of triangular stress waves with no rise time.....	52
2.22a An exponentially decaying stress wave with no rise time....	53
2.22b An exponentially decaying stress wave and a triangular stress wave with the same total positive impulse.....	53
2.23 Ratio of spall depth predictions using a triangular approximation to spall depth predictions using an exponential approximation of stress waves.....	54
2.24 Effects on spall of a triangular wave with a short rise time.....	55
2.25 The effects on spall of a triangular stress wave with a long rise time.....	56
3.1 Variation of pressure wave form exponent (from Reference 39).....	64
3.2 Tensile stress at prescribed spall plane for scaled standoff distances and geometries (from Reference 41)....	65
3.3 Damage prediction curves from Reference 33.....	66
3.4 Empirical prediction curves from Reference 45 for damage to reinforced concrete panels subjected to nearby bare charge detonations.....	67
3.5 Required thickness of reinforced concrete slabs to resist explosions in air, Reference 34.....	68
3.6 Empirical prediction curves from Reference 45 for damage to reinforced concrete panels subjected to nearby charge detonations.....	69
4.1 A wall panel being mounted on the reaction structure.....	83
4.2 The box structure left over from another study, with walls tested in this study.....	83
4.3 Reinforcement layout for wall panels 1 through 7.....	84
4.4 Reinforcement layout for wall panels 8 and 9.....	85
4.5 Reinforcement layout for wall panel 10.....	86
4.6 A typical steel mat for wall panels 1 through 7.....	87
4.7 A typical reinforcing steel mat for wall panels 8 and 9....	88
4.8 The reinforcing steel mat and forms for wall panel 10.....	89
4.9 Reinforcement steel layout for the large reinforced concrete box.....	90
4.10 Existing reaction structure.....	91
4.11 A typical bare charge.....	92
4.12 A typical charge in a casing.....	92
4.13 Typical layout of the active instrumentation in a wall panel and inside the reaction structure.....	93
4.14 Airblast gage mounts and a stress gage installed in the reinforcing grid before the concrete was cast.....	94
6.1 Pressure-time histories at the PQ-0 gage location in tests 1A, 1D, and 2D for comparison.....	137
8.1 Log-log prediction curves for damage to concrete panels caused by bare charges.....	150

	<u>Page</u>
8.2 Prediction curves for damage to concrete panels caused by bare bombs.....	151
8.3 Log-log prediction curves for damage to concrete panels caused by cased charges.....	152
9.1a Test setup of a half-scale semi-hardened wall subjected to a cased bomb.....	158
9.1b Damage to the front of the wall caused by the bomb fragments.....	158
9.1c Spall damage to the back of the wall.....	158
9.2a A similar wall as in Figure 9.1 but with a soil berm in front of it.....	159
9.2b Posttest photograph showing very little damage to the front of the wall.....	159
9.2c Posttest photograph of the back of the wall with only a couple of hairline cracks.....	159
9.3a 8.5-inch-thick wall subjected to a cased 14-lb C-4 charge.....	160
9.3b Posttest photograph of the bomb fragment damage to the front of the wall.....	160
9.3c Posttest photograph of the spall damage to the back of the wall.....	160
9.4a 2-inch thick shield wall protecting an 8.5-inch-thick wall from a cased 14-pound C-4 charge.....	161
9.4b The shield wall and main wall after the test.....	161
9.4c The back of the main wall suffered only hairline cracks due to the test.....	161
9.5 Layered wall with the specific acoustic resistance of the first layer being 3 times that of the second layer. The incident stress wave splits into two waves with half the peak stress at the interface.....	162
9.6a Wall with 45° triangular corrugations on the back.....	163
9.6b Incident compression wave splits into a tensile and a shear wave upon reflection.....	163
9.6c Reflected tensile waves travel toward center of the triangular ridges.....	163
9.6d Spall will leave parallel to wall and impact neighboring spall.....	163
9.7a Wall similar to wall in Figure 9.1 except it has a spall plate.....	164
9.7b The front of the wall suffered severe bomb fragment damage.....	164
9.7c The spall plate over the back of the wall retained most of the spall.....	164
C.1 Test 1A with 3.626 pounds of C-4 in a cardboard tube 1.54 feet from an 8.5-inch-thick wall.....	C3
C.2 Test 1A did not damage the front of the wall.....	C3
C.3 Test 1A did not damage the back of the wall.....	C4
C.4 Test 1B setup with 3.626 pounds of C-4 in a 0.70-inch-thick casing at a standoff distance of 1.54 feet from an 8.5-inch-thick wall.....	C4
C.5 The fragment damage to the front of the wall caused by test 1B. The deepest penetration was 0.75 to 1.0 inch...	C5

	<u>Page</u>
C.6 The threshold spall caused by test 1B.....	C5
C.7 Cross-sectional view of the wall in test 1B.....	C6
C.8 Test 1C setup with a 1.074-pound C-4 bare charge in contact with an 8.5-inch wall.....	C7
C.9 The crater blown in the wall by test 1C.....	C7
C.10 Spall caused by test 1C.....	C8
C.11 Cross-sectional view of the wall in test 1C.....	C8
C.12 Test 1D setup with a 7.44-pound bare C-4 charge 1.54 feet from an 8.5-inch-thick wall.....	C9
C.13 Very light scabbing of the front of the wall caused by test 1D.....	C9
C.14 Spall caused by test 1D.....	C10
C.15 Cross-sectional view of wall in test 1C.....	C10
C.16 Test 2A with a 4.70-pound bare C-4 charge at 1.54 feet from an 8.5-inch-thick wall.....	C11
C.17 Test 2A did not damage the front of the wall.....	C11
C.18 Test 2A did not damage the back of the wall.....	C12
C.19 Test 2B with a 5.45-pound C-4 charge in a 0.088-inch- thick casing at 1.54 feet from an 8.5-inch-thick wall....	C12
C.20 Fragment damage caused by test 2B.....	C13
C.21 Cracks and a hollow area in the back of the wall caused by test 2B.....	C13
C.22 Test 2C with a 1.07 pound C-4 charge in 0.04-inch-thick casing 1.54 feet from an 8.5-inch-thick wall.....	C14
C.23 Crater 2.50 inches deep, blown in the front of the wall by the contact charge in test 2C.....	C14
C.24 Spall caused by test 2C.....	C15
C.25 Test 2D with a 5.45-pound C-4 bare charge 1.54 feet from an 8.5-inch-thick wall.....	C15
C.26 Test 2D did not damage the front of the wall.....	C16
C.27 Test 2D caused cracks and a hollow area in the back of the wall.....	C16
C.28 Test 3A with a 29.41-pound bare C-4 charge at 2.44 feet from an 8.5-inch-thick wall.....	C17
C.29 Outside view of the severe damage to the wall caused by test 3A.....	C17
C.30 Scattered spall damage and large flexural cracks in the back of the wall caused by test 3A.....	C18
C.31 Uncovered breach and 1.59-inch displacement of the bottom of the wall caused by test 3A.....	C18
C.32 Cross sectional view of the wall in test 3A.....	C19
C.33 Test 3B with 7.08 pounds of C-4 in 0.088-inch-thick casing at 1.54 feet from an 8.5-inch wall.....	C20
C.34 Bomb fragment damage to the front of the wall caused by test 3B.....	C20
C.35 1.38-inch-deep spall caused by test 3B.....	C21
C.36 Cross-sectional view of wall in test 3B.....	C21
C.37 Test 4A with a 14.39-pound C-4 charge in a 0.111-inch- thick casing at 5.0 feet from an 8.5-inch-thick wall.....	C22
C.38 Scab damage (2.25 inches deep) caused by the bomb fragments in test 4A.....	C22
C.39 Hairline cracks in the back of the wall in test 4A.....	C23

	<u>Page</u>
C.40	Hollow zone in the back of wall in test 4A..... C23
C.41	Cross-sectional view of the wall in test 4A..... C24
C.42	Test 4B with a 14.39-pound C-4 charge in a 0.111-inch-thick casing at 2.44 inches from an 8.5-inch-thick wall..... C25
C.43	2.25-inch deep scab in the front of the wall caused by bomb fragments in test 4B..... C25
C.44	1.81-inch-deep spall caused by test 4B..... C26
C.45	Cross-sectional view of the wall in test 4B..... C26
C.46	Test 5A with a 7.08-pound C-4 charge in a 0.088-inch-thick casing at 1.54 feet from an 8.5-inch-thick wall made of high-strength concrete..... C27
C.47	Scab damage (1.25 inches deep) in the front of the wall caused by bomb fragments from test 5A..... C27
C.48	Spall damage (3.75 inches deep) in the back of the wall is test 5A..... C28
C.49	Cross-sectional view of the wall in test 5B..... C28
C.50	Test 5B with a 3.63-pound C-4 charge in a 0.07-inch-thick casing 1.54 feet from an 8.5-inch-thick wall of high-strength concrete..... C29
C.51	Scab damage (0.94 inch deep) to the front of the wall caused by bomb fragments from test 5B..... C29
C.52	Spall damage (1.06 inches deep) to the back of the wall in test 5B..... C30
C.53	Cross-sectional view of the wall in test 5B..... C30
C.54	Test 5C with a 1.07-pound C-4 charge in a 0.047-inch-thick casing in contact with the 8.5-inch-thick wall of high-strength concrete..... C31
C.55	Scab damage (1.85 inches deep) to the front of the wall caused by test 5C..... C31
C.56	Close-up of the scab damage 1.85 inches deep..... C32
C.57	Spall damage (3.38 inches deep) to the back of the wall in test 5C..... C32
C.58	Cross sectional view of wall in test 5C..... C33
C.59	Test 6A with a 7.08-pound C-4 charge in a 0.088-inch-thick casing at 1.54 feet from an 8.5-inch wall of concrete with acrylic latex additive..... C34
C.60	Scab damage (1.08 inches deep) to the front of the wall in test 6A..... C34
C.61	Close-up of scab damage which was up to 1.08 inches deep... C35
C.62	Threshold spall in the back of the wall in test 6A..... C35
C.63	Cross-sectional view of the wall in test 6A..... C36
C.64	Test 6B with a 3.63-pound C-4 charge in a 0.070-inch-thick casing at 1.54 feet from an 8.5-inch-thick wall of concrete with acrylic latex additive..... C37
C.65	Scab damage (1.5 inches deep) to the front of the wall in test 6B..... C37
C.66	Threshold spall damage to the back of the wall in test 6B..... C38
C.67	Cross-sectional view of the wall in test 6B..... C38
C.68	Test 6C with a 1.07-pound C-4 charge in a 0.047-inch-thick casing in contact with an 8.5-inch-thick wall of concrete with acrylic latex additive..... C39

	<u>Page</u>
C.69 Scab damage (2.00 inches deep) to the front of the wall in test 6C.....	C39
C.70 Spall damage (3.75 inches deep) to back of the wall in test 6C.....	C40
C.71 Cross-sectional view of the wall in test 5C.....	C40
C.72 Test 7A with a 7.08 pound C-4 charge in a 0.088-inch-thick casing at 1.54 feet from an 8.5-inch-thick wall of steel fiber concrete.....	C41
C.73 Scab damage (2.00 inches deep) caused by bomb fragments from test 7A.....	C41
C.74 Threshold spall damage to the back of the wall in test 7A.....	C42
C.75 Cross-sectional view of the wall in test 7A. Main cracks were 2.0, 3.25, 5.0, and 6.5 inches deep.....	C42
C.76 Test 7B with a 14.39-pound charge in a 0.111-inch-thick casing at 2.44 feet from an 8.5-inch-thick wall of steel fiber concrete.....	C43
C.77 Scab damage (1.38 inches deep) caused by the bomb fragments in test 7B.....	C43
C.78 Threshold spall damage to the back of the wall in test 7B.....	C44
C.79 Cross-sectional view of the wall in test 7B.....	C44
C.80 Test 7C with a 1.07-pound C-4 charge in a 0.047-inch-thick casing in contact with an 8.5-inch-thick wall of steel fiber concrete.....	C45
C.81 Scab crater (2.25 inches deep) blown out of the front of the wall in test 7C.....	C45
C.82 Spall damage (1.75 inches deep) to back of the wall in test 7C.....	C46
C.83 Cross-sectional view of the wall in test 7C.....	C46
C.84 Test 8A with a 1.66-pound C-4 charge in a 0.054-inch-thick casing at 1.54 feet from a 5.38-inch-thick-wall....	C47
C.85 Bomb fragment damage up to 0.88 inches deep in the front of the wall in test 8A.....	C47
C.86 Faint hairline cracks on the back of the wall in test 8A...	C48
C.87 Cross-sectional view of the wall in test 8A.....	C48
C.88 Test 8B with a 3.63-pound C-4 charge in a 0.07-inch-thick casing at 1.54 feet from a 5.38-inch-thick wall....	C49
C.89 Bomb fragment damage up to 1.40 inches deep in the front side of the wall in test 8B.....	C49
C.90 Threshold spall in the back of the wall in test 8B.....	C50
C.91 Cross-sectional view of the wall in test 8B.....	C50
C.92 Test 8C with an 8.63-pound C-4 charge in a 0.22-inch-thick casing at 1.54 feet from a 5.38-inch-thick wall....	C51
C.93 Breach of the wall in test 8C.....	C51
C.94 Closeup of the wall with debris cleaned away.....	C52
C.95 Cross-sectional view of the wall breached by test 8C.....	C52
C.96 Test 9A with a 14.39-pound C-4 charge in a 0.111-inch-thick casing at 5.0 feet from a 5.38-inch-thick wall.....	C53
C.97 Scab damage up to 2.5-inch-deep caused by bomb fragments from test 9A.....	C53
C.98 Threshold spall in the back of the wall in test 9A.....	C54

	<u>Page</u>
C.99 Cross-sectional view of the wall in test 9A.....	C54
C.100 Test 9B with a 1.66-pound C-4 charge in a 0.54-inch-thick casing at 1.54 feet from a 5.38-inch-thick wall....	C55
C.101 Scab damage up to 0.62-inch-deep in the front of the wall in test 9B.....	C55
C.102 Threshold spall in the back of the wall in test 9B.....	C56
C.103 Cross-sectional view of the wall in test 9B.....	C56
C.104 Test 10A with a 14.39-pound C-4 charge in a 0.111-inch-thick casing at 2.44 feet from an 8.5-inch-thick wall with close spaced reinforcing (1.5 inch).....	C57
C.105 Scab damage up to 1.75-inch-deep caused by the bomb fragments from test 10A.....	C57
C.106 Close-up of scab damage up to 1.75 inches deep.....	C58
C.107 Spall of up to 1.25 inches from the back of the wall in test 10A.....	C58
C.108 Cross-sectional view of the wall in test 10A.....	C59
C.109 Test 10B with a 3.63-pound C-4 charge in a 0.07-inch-thick casing at 1.54 feet from an 8.5-inch-thick wall with close spaced reinforcing (1.5 inches).....	C60
C.110 Scab damage up to 1.00 inch deep in test 10B.....	C60
C.111 Hairline cracks in the back of the wall in test 10B.....	C61
C.112 Cross-sectional view of the wall in test 10B.....	C61
C.113 Test 10C with a 1.07-pound C-4 charge in a 0.047-inch-thick casing in contact with an 8.5-inch-thick wall with close spaced reinforcing (1.5 inches).....	C62
C.114 Scab damage up to 1.88 inches deep in the front of the wall in test 10C.....	C62
C.115 0.5-inch-deep spall damage to the back of the wall in test 10C.....	C63
C.116 Cross-sectional view of the wall in test 10C.....	C63
C.117 Test Box-1 with a bare 3.63-pound C-4 charge at 1.54 feet from an 11.25-inch-thick-wall.....	C64
C.118 Front of wall after charge was detonated in test Box-1.....	C64
C.119 Hairline cracks in the back of the wall in test Box-1.....	C65
C.120 Test Box-2 with a 3.63-pound C-4 charge in a 0.070-inch-thick casing at 1.54 feet from a 11.25-inch-thick wall...	C65
C.121 Damage to the front of the wall in test Box-2.....	C66
C.122 Close-up of the scab damage up to 1.0-inch deep in the front of the wall in test Box-2.....	C66
C.123 Spall damage (2.50 inches deep) to the back of the wall in test Box-2.....	C67
C.124 Test Box-3 with a 3.63-pound C-4 charge in a 0.22-inch-thick casing at 1.54 feet from a 11.25-inch-thick wall...	C67
C.125 Damage to the front of the wall in test Box-3.....	C68
C.126 Scab damage up to 2.50 inches deep in the front of the wall in test Box-3.....	C68
C.127 Spall damage up to 3.00 inches deep in the back of the wall in test Box-3.....	C69
C.128 Test Box-4 with a bare 7.44-pound C-4 charge at 1.54 feet from a 11.25-inch-thick wall.....	C69

C.129	Picture of the front of the wall in test Box-4 showing no damage to the wall.....	C70
C.130	Back of the wall in test Box-4 showing only a couple of small spall patches.....	C70
C.131	Test Box-5 with a 7.44-pound C-4 charge in a 0.088-inch-thick casing at 1.54 feet from a 11.25-inch-thick wall.....	C71
C.132	Damage to the front of the wall caused by bomb fragments in test Box-5.....	C71
C.133	Closeup of the crater and scab damage caused by test Box-5.....	C72
C.134	Spall damage up to 3.75 inches deep in the back of the wall in test Box-5.....	C72
C.135	Test Box-6 with a 7.44-pound C-4 charge in a 0.344-inch-thick casing at 1.54 feet from a 11.25-inch-thick wall...	C73
C.136	Scab damage up to 2.50 inches deep in the front of the wall in test Box-6.....	C73
C.137	Spall damage up to 3.75 inches deep in the back of the wall in test Box-6.....	C74
C.138	Test Box-7 with a 12.0-pound C-4 charge in a plastic pipe at 2.0 feet from a 11.25-inch-thick wall.....	C74
C.139	The front of the wall in test Box-7 slightly pitted.....	C75
C.140	Spall damage up to 3.00 inches deep in the back of the wall in test Box-7.....	C75
C.141	Test Box-8 with a 6.25-pound C-4 charge in a cardboard tube at 2.00 feet from a 11.25-inch-thick wall.....	C76
C.142	Picture of the front of the wall in test Box-8 showing no damage.....	C76
C.143	Picture of the back of the wall in test Box-8 showing no damage.....	C77
C.144	Test Box-9 with a 6.25-pound C-4 charge in a 0.156-inch-thick casing at 2.00 feet from a 11.25-inch-thick wall...	C77
C.145	Damage up to 1.5 inches deep to the front of the wall in test Box-9.....	C78
C.146	Spall damage up to 3.00 inches deep in the back of the wall in test Box-9.....	C78
C.147	Test Box-10 with a 9.00-pound C-4 charge in a plastic pipe at 2.00 feet from a 11.25-inch-thick wall.....	C79
C.148	Light damage to the front of the wall in test Box-10.....	C79
C.149	Threshold spall in the back of the wall in test Box-10.....	C80
C.150	Test Box-11 with a 3.86-pound C-4 charge in a 0.25-inch-thick casing at 2.00 feet from a 11.25-inch-thick wall...	C80
C.151	Scab damage up to 1.25 inches deep in the front of the wall in test Box-11.....	C81
C.152	Threshold to light spall damage (1.5 inches deep) in the back of the wall in test Box-11.....	C81

LIST OF TABLES

<u>Table</u>		<u>Page</u>
2.1	Averaged Free Air Equivalent Weights Based on Blast Pressure and Impulso.....	30
2.2	Explosive Constants.....	31
2.3	Spall Depths and Velocities Caused by Various Shapes of Stress Waves with no Rise Times in an Ideal Elastic-Brittle Material.....	32
2.4	Spall Depths and Velocities Caused by Various Shapes of Stress Waves with Rise Times in an Ideal Elastic-Brittle Material.....	33
3.1	Comparison of Calculations with Test Results of Reference 34.....	63
4.1	Wall Parameters.....	79
4.2	Average Concrete Properties.....	80
4.3	Reinforcing Steel Average Yield Stresses.....	81
4.4	Explosive Charge Parameters.....	82
5.1	Peak Pressures at Gage Locations for A, B, and D Tests.....	101
5.2	Rise Times, and Durations of Pressure-Histories on Portions of Walls Where Spall Damage was Expected.....	103
5.3	Unit Positive Impulse at Gage Locations for A, B, and D Tests.....	104
5.4	Peak Stresses, Rise Times, and Travel Times.....	106
5.5	Peak Acceleration, and Deflection Measurements at the Midheights of the Wall Panels.....	107
5.6	Displacement of the Wall Panels at the Floor.....	108
5.7	Permanent Strains in Wall Panels During A, B, and D Tests.....	109
5.8	Measurements of Damage and Spall Velocities.....	110
5.9	Scab Damage in the Fronts of Walls.....	111
6.1	Summary of Test Parameters and Resulting Damage.....	134
6.2	Damage Classifications.....	136
7.1	Comparison of Bare Charge Tests to Predictions.....	143
7.2	Comparison of Cased Charge Tests to Predictions.....	144
8.1	Ranges of Parameters for Bare Charge Data Used in Figures 8.1 and 8.2.....	148
8.2	Ranges of Parameters for Cased Charge Data Used in Figure 8.3.....	149

CONVERSION FACTORS, NON-SI TO SI (METRIC) UNITS OF MEASUREMENT

Non-SI units of measurement used in this report can be converted to SI (metric) units as follows:

<u>Multiply</u>	<u>By</u>	<u>To Obtain</u>
degrees	0.01745329	radians
feet	0.3048	meters
feet/pound ^(1/3)	0.3967012	meters/kilogram ^(1/3)
inches	2.54	centimeters
inches	25.4	millimeters
kilobars	100.00	megapascals
kip (force)	4.448222	(1,000) newtons
kip (force)/inch ²	6.894757	megapascals (or N/mm ²)
pounds (force)/inch ²	0.006894757	megapascals
pounds (mass)	0.4535924	kilograms
pounds (mass)/inch ²	27.6799	grams/centimeters ³

SPALL DAMAGE TO CONCRETE STRUCTURES

PART I: INTRODUCTION

Background

Spall is defined as the ejection of fragments of a structural element from the opposite side from which the structural element was impacted or impulsively loaded. In this study, the structural elements were made of reinforced concrete and the loads were applied by airblast and, for cased charges, bomb fragment impacts from nearby bomb detonations (Figure 1.1). Spall fragments can have large velocities if the loading is severe and of short duration. Spall with large velocities can severely damage equipment and personnel. Spall weakens the structural element, and is often one of the major steps during breach or perforation of a structural element.

Although spall is a very important design consideration for structures which could be subjected to nearby bomb detonation, there is very little design guidance for predicting or preventing spall. Recent tests of NATO structures (References 1 and 2) indicate that most of the spall prediction methods that do exist are not always accurate. The Department of the Army, Office, Chief of Engineers (OCE), funded a series of studies entitled Deliberate Hardened Facilities at the US Army Engineer Waterways Experiment Station (WES) to improve design procedures for semi-hardened and hardened facilities. Presented herein are the results of the spall study of the Deliberate Hardened Facilities program.

Objectives

The objectives of this study were to review the theory of spall of reinforced concrete caused by nearby detonations, to evaluate existing spall prediction methods, to investigate parameters which were suspected to affect spall, and to improve prediction methods, if possible.

Approach

The theory of spall of reinforced concrete caused by nearby detonations was reviewed in all the relevant literature which could be found. Existing spall prediction methods were also reviewed and evaluated.

Forty tests were conducted with various bare and cased bombs at various standoff distances from various types of reinforced-concrete walls. Twenty-nine of the tests were instrumented with active and passive gages and high-speed photography to obtain data on loading and response of the walls. Additional data from other tests with detonations of bombs near concrete structures were also collected in a literature search. The data were analyzed, the spall theory was improved, and spall prediction methods were improved.

AIRBLAST AND FRAGMENT LOADING

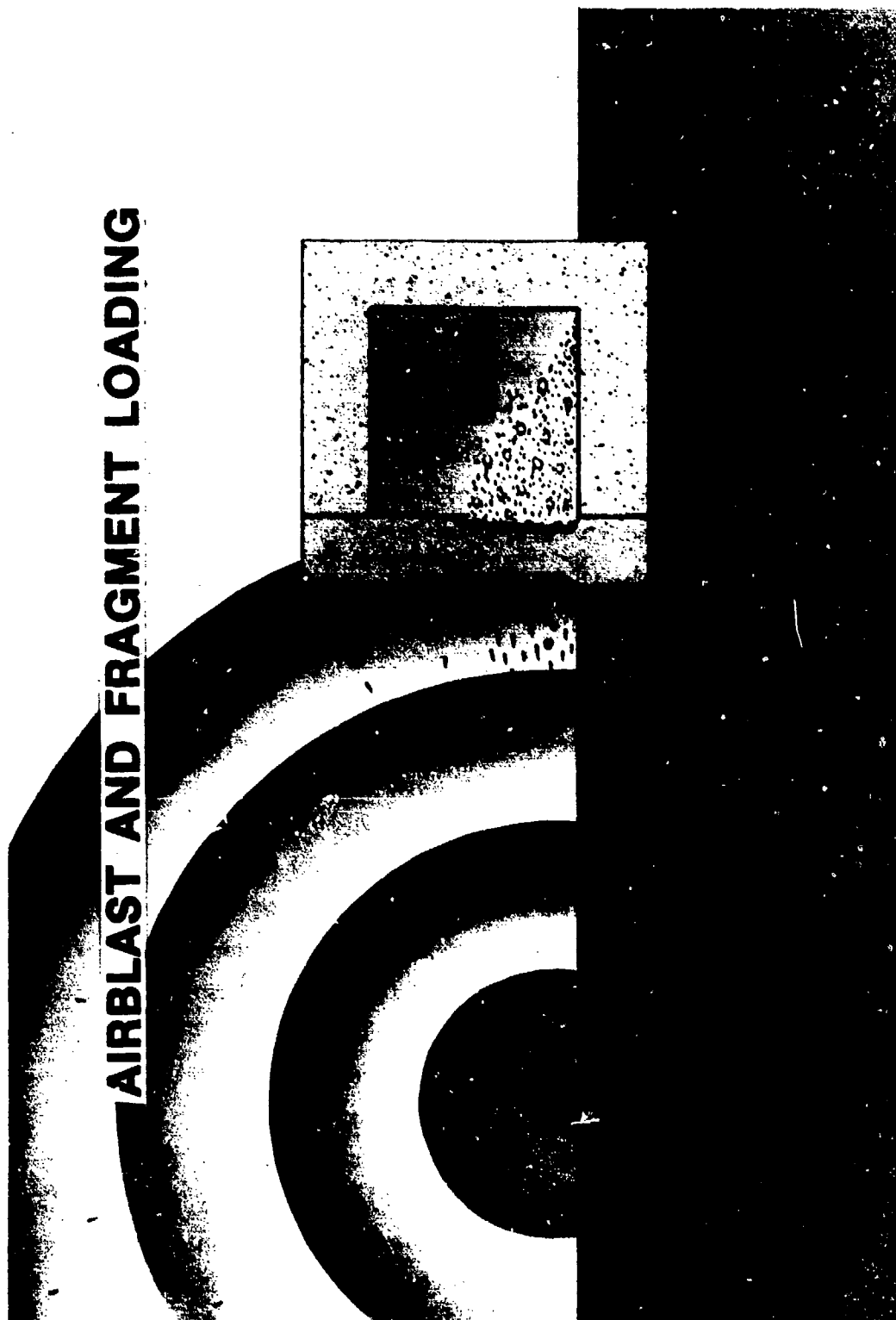


Figure 1.1 Spall caused by airblast and fragment loading.

PART II: THEORY

Definition of Spall

As stated in the Introduction, spall is defined as the ejection of fragments of a structural element from the opposite side from which the structural element was impacted and/or impulsively loaded. Basically, when a solid is impacted or impulsively loaded, stress waves are induced at the load-material interface and propagate through the material away from the load source (Figure 2.1a). When a stress wave reaches a free surface, it will reflect (Figure 2.1b). During reflection, the front reflected portion of the stress wave combines with the back incident portion to form a net stress wave. If the net stresses exceed the dynamic tensile strength of the material for a long enough time, the material will crack (Figure 2.1c). The impulse of the portion of the stress wave trapped between the crack and the back free surface equals the momentum imparted to the cracked off portion in the direction away from the structural element. However, forces such as bond, shear around the periphery of the cracked off portion, and mechanical interlocking resist against the cracked off portion separating from the structural element. If the trapped impulse is great enough to overcome these resistive forces, the cracked off part separates from the backside of the structural element at some velocity (Figure 2.1d). The actual momentum of the spall is equal to the trapped momentum less the impulses of the resistive forces. The remaining portion of the stress wave not trapped in the spall will reflect off the newly formed free surface (Figure 2.1d). If net stresses are again great enough to crack the material and overcome the resistive forces a second layer of spall will separate from the wall. This process will repeat itself until either the remaining stress wave cannot cause spall or the structural element is breached. Spall is a very complex phenomenon. The number of spall layers, spall depths, and spall velocities all depend upon the shape, magnitude, and angle of incidence of the stress waves; upon the dynamic tensile strength of the structural material and upon the resistive forces against spall.

This is a study of spall of reinforced concrete structural elements

caused by airblast loadings or combined airblast loadings and bomb fragment impacts from nearby bare or cased bomb detonations, respectively. In order to analyze this type of spall, one has to determine the airblast and bomb fragment impact loads; the angle of incidence; the changes in magnitudes and shapes of the stress waves as they propagate through the concrete; the net stresses during reflection; the dynamic tensile strength and ductility of the concrete element; and the dynamic bond, shear, and mechanical forces, which resist spall of cracked concrete.

Airblast Loads

There is a lot of information on airblast loads caused by common geometries of common explosives. Most people who are concerned about the design of structures for protection against nearby bomb detonations are familiar with airblast loads from bomb detonations. A brief overview of airblast loads is given below. For more details refer to References 3 and 4.

The magnitude and distribution of the airblast loads on a structure are a function of the type of explosive material, weight of explosive, shape of the bomb, thickness of casing, distance and location of the bomb relative to the structure, and the interaction of the shock front with the ground and the structure. Typical pressure-time histories for free-field and reflected airblast are shown in Figure 2.2. Most information on airblast loads is empirical. The most extensive data on airblast load parameters are for bare spherical TNT airbursts (Figure 2.3) and bare hemispherical TNT surface bursts (Figure 2.4). Airblast parameters can be scaled and plotted versus the scaled standoff distance, $(R/W^{1/3})$. The curves start at a scaled standoff distance of about $0.2 \text{ ft/lb}^{1/3}$. This is because the loadings of very close or contact charges are extremely severe and very difficult to measure. TNT is used as the standard or reference explosive for equating the airblast parameters of other explosives. The averaged free air equivalent weights of TNT required to produce the same peak pressures or impulses produced by unit weights of various types of explosives are given in Table 2.1 (Reference 5). There are not many data on other shapes of

bombs nor geometries, so most airblast parameters are approximated by the most similar of either spherical free airburst or hemispherical surface bursts. Airblast parameters are different for cased charges than for bare charges because of the energy required to break up the casing. The equivalent bare charge weight (W_{eq}) for a cased charge is given by the equation:

$$W_{eq} = \frac{W \left[1 + \frac{C(1-J)}{W} \right]}{1 + \frac{C}{W}} \quad (\text{eq 2.1})$$

where W is the actual charge weight, C is the case weight, and J is equal to the lesser of C/W and 1.0 (Reference 6). When an airblast wave impinges on a rigid surface at some angle, it is reflected and the pressures on the surface increase over those in the incident wave (Figure 2.2). The magnitude of the peak reflected pressure is a function of the peak incident pressure and the angle of incidence. Normal reflected peak pressures are given in Figures 2.3 and 2.4. The ratios of reflected pressures to incident pressures for various angles and pressures are given in Figure 2.5.

The pressure-time history of an applied airblast load can be approximated by equations. A loading front is usually so abrupt that it can be approximated by the linear equation:

$$P(t) = \frac{P_r(t - t_a)}{t_r} \quad \text{for } t_a \leq t \leq t_a + t_r \quad (\text{eq 2.2})$$

where

$P(t)$ = pressure as a function of time (t)

P_r = the peak reflected pressure

t_a = the time of arrival

t_r = the rise time.

No information on approximating rise times was found in the literature search. The equation $t_r = 0.24t_a$ roughly approximated the rise times of the airblast loads in this test series. The rise times for nearby detonations are usually very short in comparison with the positive pres-

sure duration (t_d) and are usually assumed to be zero. The three most common equations for approximating the unloading portion of an airblast load are the linear decay, exponential decay and modified Friedlander equations. The linear decay equation is:

$$P(t) = \frac{P_r(t_d + t_a - t)}{(t_d - t_r)} \quad \text{for } (t_a + t_r) \leq t \leq (t_a + t_d) \quad (\text{eq 2.3})$$

The exponential decay equation is:

$$P(t) = P_r \exp^{-b(t-t_a-t_r)} \quad \text{for } (t_a + t_r) \leq t \leq (t_a + t_d) \quad (\text{eq 2.4})$$

where b is solved for by either using a known pressure-time point in the equation or by iteration in the total reflected impulse (I_r) equation:

$$I_r = \frac{1}{2} P_r t_r + \left(\frac{P_r}{b}\right) \left[1 - \exp^{-b(t_d-t_r)}\right] \quad (\text{eq 2.5})$$

The modified Friedlander equation for unloading is:

$$P(t) = P_r \left[1 - \frac{(t - t_a - t_r)}{t_d - t_r}\right] \exp^{-b(t-t_a-t_r)/(t_d-t_r)} \quad \text{for } (t_a + t_r) \leq t \leq (t_a + t_d) \quad (\text{eq 2.6})$$

where b is solved for by iteration in the total reflected impulse equation:

$$I_r = \frac{1}{2} P_r t_r + P_r \left[(t_d - t_r)/b - (t_d - t_r)/b^2 + (t_d - t_r) (\exp^{-b})/b^2 \right] \quad (\text{eq 2.7})$$

An airblast loading can be determined for most common explosives and simple geometries. However, airblast loadings from contact or near contact charges, unusual explosives, bombs with shapes much different than spherical or hemispherical, or multiple reflections are very difficult to determine.

Bomb Fragment Loads

A casing or container of metal around an explosive will break into many relatively small, random size, high-velocity fragments upon detonation of the explosive. Detonation of a cased bomb near a structure will result in multiple fragment impact loads as well as airblast loads on the structure. The sum of all the fragment impact loads on a nearby structure is a large portion of the total load applied to the structure. The loads at the points of individual bomb fragment impacts are usually quite intense and cause localized damage. Most bomb fragments from nearby detonations penetrate concrete structural members upon impact and cause scabbing of the surface concrete around the penetration holes. Most of the fragments from cylindrical bombs usually radially disperse at very high velocities from the sides of the bomb and impact a nearby structure in a concentrated zone of multiple fragment impacts with a few random fragment impacts around this zone (Figures 1.1 and 2.6). Spalling often occurs on the opposite side of a concrete structural member from that which received multiple bomb fragment impacts.

Most of the bomb fragment characteristics which can be measured in the free field with high-speed photography and witness plates, have been extensively studied. However, no one has been able to measure the load-time histories applied by bomb fragments at the fragment-concrete interface. As a result, there are fairly reliable empirical equations for predicting free-field bomb fragment characteristics, but only unverified theoretical equations for applied loads by bomb fragments. The common empirical equations for free-field bomb fragment characteristics are briefly reviewed below and the theoretical equations for fragment applied loads are discussed afterwards.

The following empirical equations for free-field bomb fragment characteristics were obtained from References 7 and 8, and are presented

here for convenient reference. The equations are for bomb fragments from high-order detonations of evenly distributed explosives in cylindrical, mild steel, uniform thickness casings. The fragment mass distribution is given by:

$$\ln(N_f) = \ln(C'M_A) - \frac{M}{M_A} \quad (\text{eq 2.8})$$

where

N_f = the number of fragments with weights greater than a given fragment weight (W_f) in ounces

C' = fragment distribution constant = $\frac{C}{2M_A^3}$

C = total casing weight in ounces

$M = (W_f)^{0.5}$ in ounces^{0.5}

M_A = fragment distribution parameter = $B t_o^{5/6} d_1^{1/3} \left(1 + \frac{t_o}{d_1}\right)$ in ounces^{0.5}

t_o = average casing thickness in inches

d_1 = average inside diameter of the casing in inches

B = explosive constant from Table 2.2.

The average fragment weight (\bar{W}_f) is:

$$\bar{W}_f = 2M_A^2 \quad (\text{eq 2.9})$$

The initial fragment velocity (V_o) is given by:

$$V_o = G \left(\frac{W/C}{1 + 0.5W/C} \right)^{1/2} \quad (\text{eq 2.10})$$

where

G = the Gurney explosive energy constant in feet per second obtained from Table 2.2

W = the weight of the explosive in ounces

C = weight of the casing in ounces.

The fragment striking velocities (V_s) vary with distance as a function of:

$$V_s = V_o \exp^{-0.004R/W_f^{1/3}} \quad (\text{eq 2.11})$$

where

R = distance from the detonation in feet

W_f = fragment weight in ounces.

Figure 2.7 shows V_s/V_o versus W_f for various R . Reference 8 states "...within a short distance from the detonation, usually 20 feet, the striking velocity can be assumed to be equal to the initial velocity."

The load-time history applied by a bomb fragment as it penetrates a concrete element is difficult to measure. However, based upon the large momentums of most bomb fragments, the severe damage to concrete in areas around bomb fragment impacts and the stresses measured in the concrete at some distance from the impact areas - the applied load-time histories are believed to be extremely high (many kilobars) and of very short duration. An unverified theoretical method is the only method of approximating the load-time histories applied by bomb fragment impacts. Since bomb fragments usually penetrate concrete upon impact, a penetration-resistive force theory will be used. A summary of existing theoretical methods in penetration mechanics is given by Backman and Goldsmith in Reference 9. They observed that the penetration process is a complicated phenomena that depends upon many parameters, some of which are difficult to control. One of the popular theories is the Separable Force Law Theory postulated by Beth in Reference 10. The theory is that the resisting force against a penetrating body at a given instant is a function of its current velocity and current depth of penetration. Reference 8 developed the following equation for predicting bomb fragment penetration into concrete (X_f) based upon Beth's theory and empirical data:

$$X_f = 2 \sqrt{KND} d^{1.1} v_s^{0.9} \quad \text{for } 0 \leq x \leq 2d$$

or

(eq 2.12)

$$X_f = KND d^{1.2} v_s^{1.8} + d \quad \text{for } x > 2d$$

where

X_f = total penetration depth in inches

K = concrete penetrability constant = $\frac{6.53}{\sqrt{f'_c}} \frac{\text{inch}^{2.8} \text{ sec}^{1.8}}{\text{pounds kilofeet}^{1.8}}$

f'_c = concrete uniaxial compressive strength in ksi

N = nose shape factor = $0.72 + 0.25 \sqrt{n - 0.25}$

n = caliber radius of the tangent ogive of the fragment (0.5 for standard fragment shape)

D = Caliber density of the fragment = $\frac{W_f}{16d^3} \frac{\text{lb}}{\text{ounces}}$

W_f = fragment weight in ounces

d = diameter of the fragment in inches

V_s = striking velocity of fragment in kilofeet/sec

An equation for pressure (P_f) on the projected front of the fragment was derived from equation 2.12 and other relations and is:

$$P_f = \frac{47.79 \sqrt{f_c'} \sqrt{\text{ksi in.}} \frac{0.2 \text{ sec}^{0.2}}{d^{0.2} \text{ kft}^{0.2}} g(z)$$

$$\cdot \left[V_s^{1.8} - \frac{G(z) \sqrt{f_c'}}{5.51785 d^{0.2} D} \frac{(\text{lb}) (\text{kft})^{1.8}}{\text{in.}^{2.8} (\text{sec})^{1.8} \sqrt{\text{ksi}}} \right]^{0.1111} \quad (\text{eq 2.13})$$

where

$\frac{47.79 \sqrt{f_c'}}{d^{0.2}}$ = empirical factor based upon concrete penetrability and the assumed standard nose shape.

$g(z)$ = the depth dependent factor = $z/2.0$ for $0 \leq z \leq 2.0$ or
= 1.0 for $2.0 \leq z \leq$ total penetration depth

$z = x/d$ caliber penetration

x = depth at time t during penetration

$$\left[V_s^{1.8} - \frac{G(z) \sqrt{f_c'}}{5.51785 d^{0.2} D} \frac{\text{lb kft}^{1.8}}{\text{in.}^{2.8} \text{sec}^{1.8} \sqrt{\text{ksi}}} \right]^{0.1111}$$

= velocity dependent factor

$G(z) = z^2/4$ for $0 \leq z \leq 2.0$ or
= $z - 1$ for $2.0 \leq z \leq$ total penetration depth
and the other variables were described above.

The equations for time (t) at a given depth during penetration were derived by double integration and are:

$$t = \frac{1.89 x}{10,680 v_s^{3.6}} \frac{\text{kft}}{\text{in.}} \cdot \left(v_s^{1.8} - \frac{0.725 \sqrt{f'_c} d^{0.8} x^2}{W_f} \frac{\text{kft}^{1.8} \text{ ounces}}{\sqrt{\text{kip in.}}^{1.8} \text{ sec}^{1.8}} \right)^{1.445} \\ + \frac{x}{10,680 v_s^{1.8}} \frac{\text{kft}}{\text{in.}} \\ \cdot \left(v_s^{1.8} - \frac{0.725 \sqrt{f'_c} d^{0.8} x^2}{W_f} \frac{\text{kft}^{1.8} \text{ ounces}}{\sqrt{\text{kip in.}}^{1.8} \text{ sec}^{1.8}} \right)^{0.445}$$

for $0 \leq x \leq 2d$

(eq 2.14a)

or

$$t = \left(\frac{0.000064559 W_f \sqrt{\text{kip sec}}^{1.8} \text{ in.}^{0.8}}{\sqrt{f'_c} d^{1.8} \text{ kft}^{0.8} \text{ ounces}} \right) \\ \cdot \left[\left(\frac{10.1006 \sqrt{f'_c} d^{2.8}}{W_f} \cdot \frac{\text{ounces kft}^{1.8}}{\sqrt{\text{kip sec}}^{1.8} \text{ in.}^{1.8}} - v_s^{1.8} \right)^{0.445} \right. \\ \left. - \left(\frac{2.90063 \sqrt{f'_c} d^{1.8} x}{W_f} \cdot \frac{\text{ounces kft}^{1.8}}{\sqrt{\text{kip sec}}^{1.8} \text{ in.}^{1.8}} - v_s^{1.8} \right)^{0.445} \right] + t_{2d}$$

for $2d < x \leq X_f$

(eq 2.14b)

where

t = time at a given depth during penetration in seconds

t_{2d} = time at a penetration depth of $2d$ evaluated in equation 2.14a

Although the above equations are unverified approximations of the pressure-time histories applied by bomb fragments as they penetrate concrete, they are based upon equations which predict penetrations quite well. The peak pressures are usually extremely high compared with the dynamic compressive strength of the concrete. As a result, the induced stress waves in the concrete change rapidly as they propagate through the concrete failing it.

Combined Loads

Once the various airblast loads, multiple fragment loads, and the times at which they are applied have been determined, they must be combined to determine the total load-time history. An airblast wave decelerates with distance at a greater rate than bomb fragments as they travel through air. Therefore, the greater the standoff distance from the bomb, the greater the difference between the arrival times of the fragments and airblast. Combined loads from cased charges are quite complex and are usually very severe in the zone of multiple impacts.

Induced Stress Waves

When a solid material is impacted or impulsively loaded, two forms of stress waves are induced at the load-material interface and propagate through the material away from the load source. One of these stress waves is a primary or longitudinal wave and the other is a shear or transverse wave. The primary wave causes particle motions in the same direction which it propagates and can be either tensile or compressive in nature. The primary stress (σ) is related to the longitudinal particle velocity (V_L) at a given point by the equation:

$$\sigma = \rho c V_L \quad (\text{eq 2.15})$$

where

ρ = material mass density

c = the longitudinal propagation velocity

The propagation velocity c varies with material properties as given in

$$c = \left[\frac{3K(1 - \nu)}{\rho(1 + \nu)} \right]^{1/2} \quad (\text{eq 2.16})$$

where

K = bulk modulus

ν = Poisson's ratio

The shear wave causes particle motions perpendicular to the direction which it propagates and causes shear strains. The shear stress τ is

related to the shear particle velocity (V_t) at a given point by the equation $\tau = \rho c_t V_t$ where c_t is the shear propagation velocity. c_t varies with material properties as given by:

$$c_t = \left[\frac{3K(1 - 2\nu)}{2\rho(1 + \nu)} \right]^{1/2} \quad (\text{eq 2.17})$$

c is faster than c_t by a ratio of $\frac{c}{c_t} = \left(\frac{2 - 2\nu}{1 - 2\nu} \right)^{1/2}$ (eq 2.18)

Stress waves are usually described in terms of either stress versus time at given points or stress versus distance at a given time. The duration t_d of a primary stress wave is related to the wave length λ by the equation $t_d = \frac{\lambda}{c}$.

Bomb fragment impact and/or airblast loads induce primarily compressive primary waves and shear waves in structural members. The negative tail of an airblast wave is much smaller than the dynamic tensile strength of concrete and is ignored. The primary wave travels faster than the shear wave so it reflects off the back free surface before the shear wave. The portion of a structure with the lowest angle of loading incidence will receive the severest loading. At low angles of loading incidence, the induced compressive primary wave will reflect much higher tensile stresses than a shear wave. Thus the compressive primary wave is usually of main concern in spall analysis.

Changes in Stress Waves as They Propagate through Concrete

Stress waves change in magnitude and shape as they propagate through real materials. Once the stress waves induced in concrete by the applied loads are known, the changes in the stress waves as they propagate through the concrete, reflect and cause spall must be determined. The most common causes of change to stress waves in concrete are different stresses propagating at different velocities, attenuation, divergence of the wave energy over an expanding wave, and dispersion of stress waves upon striking air voids, reinforcing steel, or other imperfections.

Different stresses above the Hugoniot Elastic Limit propagate at different velocities. The longitudinal propagation velocity (c) of a

stress through a material varies with the bulk modulus, Poisson's ratio and density of the material by the relation given in equation 2.16. The bulk modulus is the slope of a Rankine-Hugoniot (or just Hugoniot curve). A Hugoniot curve is the locus of final stress - volume strain states that can be reached from an initial impulsive load. Figure 2.8 is a Hugoniot curve obtained from Reference 11, based upon tests on 4,000 to 6,000 psi concrete. The bulk modulus is constant for stresses below the Hugoniot Elastic Limit (HEL), but varies for stresses above the HEL. H. E. Read and C. J. Maiden assumed an HEL of about 1 kilobar (14,700 psi) for the curve shown here. The bulk moduli at stresses just above the HEL are abruptly much less than the elastic bulk modulus. The bulk moduli gradually increase with increased stresses above the HEL. At the hydrodynamic limit (σ_B) the bulk moduli start to exceed the elastic bulk modulus. This point is approximately 16 kbar on the given curve. Thus, if the peak stresses are below the HEL, and the changes in ρ and v are negligible, the propagation velocity will remain constant. If the peak stresses are between the HEL and the hydrostatic limit, the stress wave will separate into an elastic precursor, propagating at a constant elastic velocity, and a deformational shock wave with different stresses propagating at different velocities (Figure 2.9). If the peak stresses are above the hydrostatic limit, the deformational shock will travel at velocities greater than the elastic velocity and overtake the elastic wave so that a single shock wave is formed. Figure 2.9 illustrates an example of how a stress wave, with stress propagating at different velocities, changes shape as it travels.

Attenuation is the weakening of a stress wave as it does work on the material through which it propagates. The amount that a stress wave attenuates depends upon the amount of work it performs. W. Goldsmith states in Reference 12 that "... any material will behave as an elastic solid below a certain characteristic level, will exhibit attenuation above this level, but will regain its elastic behavior upon saturation of microscopic structural design." In other words, stress waves with stresses below the dynamic elastic limit of concrete will attenuate at very small rates, but stress waves with peak stresses above the dynamic elastic limit will attenuate rapidly by using energy to plastically deform and/or fracture the material. Unfortunately, there is very

little information on the rates of attenuation of plastic stress waves on concrete. J. S. Rinehart proved in Reference 13 that a simple square stress wave will shorten in height and lengthen in duration as it attenuates. A similar effect has also been observed in measurements of other various forms of stress waves. A drawing of how a stress wave changes magnitudes and shape as it attenuates is shown in Figure 2.10.

Divergence causes the magnitudes of the stresses to decrease as the stress wave expands. The total amount of energy in the stress wave is spread out over an increasing area as a stress wave expands. For example, figures in Reference 1 show that the early high pressure distributions on walls near detonations of cylindrical surface charges are also somewhat cylindrical. Assume that cylindrically expanding stress waves are induced into walls loaded by airblast from nearby cylindrical bombs. Also assume that radiant energy travels only in straight lines, the propagation velocity (c) remains constant, and the density remains constant. Looking at Figure 2.11, one sees that according to the conservation of energy law the radiant energy that passes through area A , must also pass through area B . In mathematical terms:

$$d(1/2 m_A V_A^2) = d(1/2 m_B V_B^2)$$

$$1/2 \rho A dr V_A^2 = 1/2 \rho B dr V_B^2$$

$$1/2 \rho A dr \left(\frac{\sigma_A}{\rho c}\right)^2 = 1/2 \rho B dr \left(\frac{\sigma_B}{\rho c}\right)^2$$

$$\sigma_A^2 A = \sigma_B^2 B$$

$$\text{but } \frac{A}{r_A} = \frac{B}{r_B} \quad \text{so } \frac{\sigma_A^2}{r_B} = \frac{\sigma_B^2}{r_A}$$

$$\text{or } \sigma_B = \sqrt{\frac{r_A}{r_B}} \sigma_A \quad (\text{eq 2.19})$$

where V_A and V_B are the velocities and σ_A and σ_B are the stresses at the distances r_A and r_B , respectively. If a

structure is far enough from the explosion so the structure front is fairly uniformly loaded, the induced stress wave can be assumed to be plane and no divergence will occur in the wall. The stresses induced in concrete by a bomb fragment impact may expand spherically away from the point of impact, see Figure 2.12. It can be proven that the stresses in a spherically expanding wave diverge according to:

$$\sigma_B = \frac{r_A}{r_B} \sigma_A \quad (\text{eq. 2.20})$$

When a stress wave hits an inclusion such as an air void or a reinforcing steel bar (rebar) in a concrete structure, it will at least partially scatter or disperse around it as illustrated in Figure 2.13. If the concrete has many air voids and/or if the rebars are very closely spaced, stress waves will be greatly dispersed. However, most protective structures are made of concrete with very few large air voids and conventional reinforcing steel spacings are large enough to allow large areas of stress waves to pass through undisturbed. A stress wave caused by a single bomb fragment impact is small enough that most of it would be dispersed by an air void or rebar. However, in zones where there are multiple fragment impacts very close to each other, many of the induced stress waves will pass through without being dispersed. So it is assumed that dispersion does not change the majority of the stress waves in normal concrete with conventional rebar spacing.

A later section will show how spall is very dependent upon the shape and magnitude of a stress wave. As discussed above, the shape and magnitudes of a stress wave can significantly change as it propagates through concrete. These changes depend upon the peak stresses, how the stress wave expands, and the size and number of inclusions in the concrete. A planar elastic stress wave in plain concrete will not change much in one transit, but a spherically expanding plastic stress wave in concrete with many inclusions will significantly change in one transit. Most airblast and bomb fragment impact loadings, which cause spall, induce stress waves in concrete which are above the HEL and are expanding, so changes in the shape and magnitudes of stress waves must be considered in the spall analysis.

Reflection of Stress Waves at Various Angles of Incidence

When a stress wave strikes a free surface of the material in which it is traveling, it will reflect. When a primary stress wave normally strikes a free surface it reflects as a primary wave of equal and opposite sense (i.e., a compressive wave reflects as a tensile wave or vice versa). When a shear wave normally strikes a free surface it reflects as an equal shear wave. However, when either a primary or a shear stress wave obliquely strikes a free surface, both a primary and a shear wave are reflected back. In all cases, the sum of the resultant stresses at and normal to the free surface must equal zero. The reflected tensile primary waves are of main concern in spall analysis.

Consider a primary stress wave striking a free surface at some given angle of incidence as illustrated in Figure 2.14a. Part of the wave is reflected as a primary wave at an angle equal to the angle of incidence α , and the other part is reflected as a shear wave at an angle of β . The relationship between the angle of incidence and the angle of reflected shear β is given by Snell's Law as:

$$\frac{\sin \alpha}{\sin \beta} = \frac{c}{c_t} = k = \left[\frac{2(1 - \nu)}{1 - 2\nu} \right]^{\frac{1}{2}} \quad (\text{eq 2.21})$$

where ν is Poisson's ratio for the material. β is always less than α . Since the sum of the resultant stresses normal to the free surface must equal zero, the stresses can be related by the equations:

$$\sigma' = r\sigma \quad (\text{eq 2.22})$$

$$\text{and} \quad \tau' = [(r+1) \cot(2\beta)]\sigma \quad (\text{eq 2.23})$$

where σ is the incident primary stress, σ' is the reflected primary stress part, τ' is the reflected shear stress part, and r is the coefficient of reflection:

$$r = \frac{[\sin(2\alpha) \sin(2\beta) - k^2 \cos^2(2\beta)]}{[\sin(2\alpha) \sin(2\beta) + k^2 \cos^2(2\beta)]} \quad (\text{eq 2.24})$$

Since β is related to α by k , and k is a function of v , the reflected stresses are dependent only on α and v . Figure 2.14b shows r as a function of α for various values of v . A positive r indicates that the reflected primary wave is the same sense as the incident primary wave and a negative r indicates that the reflected primary wave is the opposite sense of the incident primary wave. Most "average" strength concretes have v 's between 0.15 and 0.20. Notice that for a concrete with a v of 0.15, the r is negative for angles of incidence between 0 and 45 degrees, is zero for angles of incidence of 45 and 85 degrees, and r is positive for angles of incidence from 45 to 85 degrees. Therefore, a compressive primary wave at an angle of incidence between 45 and 85 degrees in concrete with $v = 0.15$ will reflect as a compressive primary wave and a shear wave, and no spall can occur.

A shear wave that strikes a free surface at an angle of incidence β , will partially reflect as a shear wave at an angle β and partially as a primary wave at an angle α , as shown in Figure 2.15a. An incident stress is related to the reflected stresses by the following equations:

$$\tau' = r\tau \quad (\text{eq 2.25})$$

and

$$\sigma' = [(r - 1) \tan^2(\beta)] \tau \quad (\text{eq 2.26})$$

where τ is the incident shear stress, τ' is the reflected shear stress part, σ' is the reflected primary stress part, r is the coefficient of reflection for $\sin \beta \leq \frac{1}{k}$, and k is as defined earlier. As in the previous equations, the reflected stresses are dependent only on the incident angle and v . Figure 2.15b shows r as a function of β and v . Recall that α is always greater than β , so these equations are limited to β equal to or below a critical angle of $\arcsin(1/k)$. For β greater than $\arcsin(1/k)$, the reflected primary stress part travels along the free surface with the wave front varying exponentially with distance from the surface (Reference 14). The shear wave is usually not considered in spall analysis because at low angles of incidence σ' is small and at medium to high angles of incidence,

the reflected primary wave is at large angles to the free surface.

As a primary stress wave reflects at a free surface, the front reflected stress wave overlaps the incident stresses of the back portion of the stress wave to form net stresses by superposition. It is convenient to imagine a normally reflected primary wave as a mirror image of the incident wave traveling into the concrete from the outside as shown in Figure 2.16 to help calculate the net stresses. For an incident plane primary stress wave at an oblique angle of incidence, the net primary stress ($\sigma_{net(i,t)}$) at a point i , distance δ from the free surface, at time t is given by:

$$\sigma_{net(i,t)} = \sigma_{i,t} + \sigma'_{i,t} = \sigma_{i,t} + r\sigma_{[i,t-(2\delta \cos\alpha)/c]} \quad (\text{eq 2.27})$$

where

$\sigma_{net(i,t)}$ = the net primary stress at point i at time t

$\sigma_{i,t}$ = the incident primary stress at point i at time t

$\sigma'_{i,t}$ = the reflected primary stress at point i at time t

$(2\delta \cos\alpha)/c$ = the time it took the stress wave to travel from point i , reflect at the free surface, and travel back to point i .

and all compressive stresses are positive and all tensile stresses are negative.

Spall will occur if the net primary stresses over an area exceed the dynamic tensile strength of concrete, and the trapped impulse overcomes resistive forces and pulls the cracked portion of concrete away at some spall velocity.

Dynamic Properties of Concrete

Most of the stress-strain properties of a concrete are dependent upon the rate at which the concrete is loaded. Figure 2.17 (obtained from Reference 15) shows the effect of loading rate on the stress-strain curves of compression and tension tests of a concrete. The ultimate compressive stress, ultimate tensile stress, and moduli of elasticity all increase with faster loading rates. The stress-strain curves become

straighter with faster loading rates, so many assume that concrete remains elastic up to its dynamic ultimate stress under very fast loading rates. The loading rates of bomb fragment impacts and/or airblast from nearby bomb detonations are extremely fast, as shown in earlier sections. Most laboratory tests measure strain rate in a specimen to indicate the rate of loading because it is an easier and more direct method to measure what a material actually receives.

Figure 2.18 shows the results of several experiments on compressive ultimate stress of concrete versus strain rate (Reference 15). Strain rates for most fragment impacts and/or airblast loads from nearby detonations on average concrete are well in excess of 10 sec^{-1} . Thus, the ratio of dynamic compressive strength to static compressive strength of "plain" concrete under bomb fragment and/or airblast loadings from nearby detonations is greater than 1.6.

Figure 2.19 (Reference 15) shows the results of several experiments on the tensile strength of concrete versus strain rate. Notice that the tensile strength increases faster than compressive strength as the strain rate increases. The ratios of dynamic tensile strength to static tensile strength for "plain" concrete are greater than 4.5 for strain rates greater than 10 sec^{-1} . D. L. Birkimer and R. Lindemann discuss in Reference 16 their experiments on a "plain concrete" at strain rates from approximately 2 sec^{-1} to 23 sec^{-1} . Contrary to the results of other studies at lower strain rates (Reference 17), they found the dynamic modulus of elasticity to be constant. They also assume that the critical fracture strain energy for a given concrete is constant. Their equation of critical dynamic tensile fracture strain (ϵ_{cr}) is:

$$\epsilon_{cr} = \left[\frac{(6U_{cr})}{EAc} \right]^{1/3} \left[\frac{1}{\dot{\epsilon}} \right]^{1/3} \quad (\text{eq 2.28})$$

where

U_{cr} = the critical fracture strain energy (which was 0.298 ft-lb for the 6,380-psi concrete they used)

E = dynamic modulus of elasticity

A = cross-sectional area

c = primary wave propagation velocity

$\dot{\epsilon}$ = strain rate

H. W. Rinehardt (Reference 18) determined that the bond stress between a given concrete and ribbed reinforcing bars, under a given displacement, increases with load rate according to:

$$\frac{u}{u_o} = \left(\frac{\dot{u}}{\dot{u}_o} \right)^n \quad (\text{eq 2.29})$$

where

u = bond stress for a given displacement δ at a load rate \dot{u}

\dot{u} = load rate

u_o = static bond stress for the same displacement

\dot{u}_o = static load rate

$$n = \frac{0.7(1 - 2.5\delta)}{f_o'^{0.8}}$$

f_o' = cubic uniaxial compression strength in megapascals

δ = displacement in mm

This also indicates that the bond stress increases with increasing load rate, less in high-strength concrete than in low-strength concrete.

The above curves and equations are based upon limited empirical data on just a few concrete strengths and mixes. One should not use the curves or equations for concretes much different than those from which the data were derived. Experiments on the dynamic properties of concretes need to be conducted at strain rates as fast as those caused by bomb fragment impacts and/or airblast loadings. Concretes with various static strengths should be tested at high strain rates to determine if different concretes increase differently in strength at different strain rates.

Types of Concrete

High-strength concrete, fiber-reinforced concrete, and polymer-portland cement concretes can all obtain higher tensile strengths than regular medium-strength concretes. They are, therefore, of interest for use in structures subjected to bomb fragment impacts and/or airblast to reduce the chances of spall. The characteristics of each type of concrete are discussed below.

High-strength concretes are defined by K. H. Gerstle in

Reference 19 as concretes with static uniaxial cylinder strengths above 9,000 psi. Stress-strain curves in Reference 19 show increasing stiffness, greater linearity and increasing brittle behavior with increasing static strength. Gerstle found a decrease in the ratio of static tensile strength to compressive strength for increasing compressive strengths. No information was found on the dynamic properties of high-strength concrete, but they are most likely also strain-rate sensitive.

Fiber-reinforced concrete has been extensively studied. Various types of fiber material, including nylon, glass, and steel, have been added to concrete to increase its ultimate tensile strength, ductility, and toughness. Most fibers are much stronger in tension than concrete. Steel fibers are the most popular. The properties of a steel fiber reinforced concrete depend upon the amount, length, strength, ductility, and shape of the steel fibers as well as the rest of the concrete mixture. Generally, fibers only slightly increase the elastic limit of the concrete, but greatly increase the ultimate strength and strain of the concrete. The fibers are randomly dispersed throughout the concrete matrix, strengthen local flaws and retard crack growth. Once a crack forms and crosses a fiber, the fiber has to be stretched or debonded for the crack to grow further. Details on the mechanics of fiber-reinforced concrete are given in References 20 and 21. References 16 and 22 discuss how the dynamic tensile strength of fiber-reinforced concrete increases with strain rate. There have already been many tests of fiber-reinforced concrete subjected to bomb fragment impact and/or airblast loads (see References 23 thru 27), and they all prove that sufficient amounts of fibers reduce spall.

Polymer-portland cement concrete is a type of polymer concrete which is produced by adding either a monomer or polymer to a fresh concrete mixture to allow polymerization within the concrete as it cures. A monomer is an organic molecule which is capable of chemically binding with other molecules to form a high-molecular weight material known as a polymer. A polymer consists of repeating monomer molecules and other molecules which form in long chemical chains. Latexes are the most common polymer added to concrete mixtures. Proper latex formulations greatly improve shear, bond, tensile, and flexural strengths of concretes. For more details on polymer-portland cement concretes and

other types of polymer concretes, see Reference 28. References 16, 29, and 30 illustrate that polymer concrete dynamic strengths increase with increasing strain rates. No information about spall tests on polymer concretes could be found.

Effects on Spall of Stress Wave Shape and Magnitude

The depth and velocity of spall depend greatly upon the shape and magnitude of the reflecting stress wave. To illustrate this, a few ideal plane stress waves with different shapes and magnitudes in an ideal linearly elastic-brittle material are compared. Assume for the moment that the stresses in the ideal plane stress waves all propagate at the same constant velocity, are normal to the back free surface, reflect perfectly, and do not attenuate, diverge, nor disperse. The ideal material is much stronger in compression than in tension, will immediately fracture when a tensile stress exceeds the dynamic tensile strength, and has no resistive forces to spall.

Consider first a rectangular ideal plane compressive wave with a wave length of λ and all stresses equal to σ_p as shown in Figure 2.20a. Once the wave starts to normally reflect off the back free surface (Figure 2.20b), the tensile reflected portion of the wave cancels the compressive incident portion and results in a zero net stress behind the leading edge of the reflected wave. The net stresses remain zero as the wave advances, until the reflected wave passes the end of the incident portion of the wave at $\frac{\lambda}{2}$ from the back free surface. At this instant, the net stress at the leading edge of the reflected wave equals σ_p (Figure 2.20c). If σ_p is greater than the dynamic tensile strength of the material (σ_{crit}) the material will crack and spall. The velocity of the spall (V) is found by equating the impulse of the stress wave to the momentum of the spall:

$$\rho \frac{\lambda}{2} V = \sigma_p \frac{\lambda}{c}$$

$$V = \frac{2\sigma_p}{\rho c} \quad (\text{eq 2.30})$$

where

V = spall velocity

ρ = density of the material

c = propagation velocity of primary waves

Notice that rectangular wave shapes have only one spall depth and it is independent of the magnitude of σ_p , as long as σ_p is greater than σ_{crit} . The spall depth is only dependent upon $\frac{\lambda}{2}$. As λ approaches zero, the spall depth approaches zero (Figure 2.20d). A special case is when λ is greater than or equal to two times the thickness of the material, then the leading edge of the reflected wave will strike the front free surface before or at the same time as the end of the incident portion of the wave arrives at the front surface (Figure 2.20e). The reflected wave reflects again at the front free surface as a compression wave. No spall is possible because the net stresses are never in tension.

Now consider a triangular ideal planar compressive wave with no rise length (90 degree front), a wave length of λ , and a peak stress of σ_p , which is greater than the dynamic tensile strength (σ_{crit}) of the material (Figure 2.21a). The net stress wave formed during reflection is a triangular tensile wave as shown in Figure 2.21b. The front of the net stress wave also has no rise length and travels even with the front of the reflected wave. The magnitudes of the peak net stress (σ_{net}) and wave length of the net stress wave increases as the reflected wave advances. At some point in time as the reflected wave advances, the peak net stress will equal the dynamic tensile strength, σ_{crit} , of the material and the ideal material will spall (Figure 2.21c). The spall depth (d) relates to the incident stress wave magnitudes by geometry as:

$$\frac{\sigma_p - \sigma_{crit}}{\lambda - 2d} = \frac{\sigma_p}{\lambda}$$
$$d = \frac{\lambda \sigma_{crit}}{2\sigma_p} \quad (\text{eq 2.31})$$

The velocity of the spall (V) is found by equating the impulse of the portion of the stress wave trapped in the spall, to the momentum of the spall:

$$\rho dV = \frac{\sigma_p + (\sigma_p - \sigma_{crit})}{2} \left(\frac{2d}{c} \right)$$

$$V = \frac{2\sigma_p - \sigma_{crit}}{\rho c} \quad (\text{eq 2.32})$$

The rest of the incident stress wave remaining in the structure will continue to propagate and will reflect off the newly formed free surface made by the spall (Figure 2.20d). The peak stress is now $\sigma_p - \sigma_{crit}$ and the wave length is now $\lambda - 2d$. A second spall will occur if σ_{net} again equals or exceeds σ_{crit} . The second spall traps a portion of the stress wave again, and follows the first spall at a lower velocity. The remainder of the original pulse in the structure will reflect off the newly formed free surface made by the second spall. The peak stress of the remainder is reduced to $(\sigma_p - 2\sigma_{crit})$ and the wave length is reduced to $\lambda - 4d$. This cycle of reflecting from a new surface and spalling another layer will continue until the peak stress of the remainder of the incident wave is less than σ_{crit} . So a triangular stress wave with no rise length can cause spall of multiple spall layers. The number of spall layers (k) is equal to the largest integer less than $\frac{\sigma_p}{\sigma_{crit}}$. The equation for the n^{th} spall layer depth (d_{tn}) is the same as for the first spall depth due to similar triangles:

$$d_{tn} = \frac{\lambda \sigma_{crit}}{2\sigma_p} \quad (\text{eq 2.33})$$

Notice that the spall depth equation for this shape has stress as well as wave length in it. Thus, the greater σ_p is compared with σ_{crit} the shallower the spall depth d_{tn} (Figure 2.21e); and the shorter λ the shallower the spall depth (Figure 2.21f). If λ is longer than 2 times the wall thickness and unloads gradually enough so σ_{net} never exceeds σ_{crit} , no spall will occur (Figure 2.21g). The equation for the velocity V_n of the n^{th} spall layer is a generalization of that for the first layer:

$$V_n = \frac{2\sigma_p - (2n - 1) \sigma_{crit}}{\rho c} \quad (\text{eq 2.34})$$

The spall velocity decreases with each successive layer.

Another shape is an exponentially decaying stress wave with no rise length (Figure 2.22a). The stress wave is described by the equation:

$$\sigma(x) = \sigma_p \exp^{-bx} \quad (\text{eq 2.35})$$

where $\sigma(x)$ is the stress a distance x behind the front of the wave, σ_p is the peak stress, c is the propagation velocity, and b is a constant determined from a known stress-distance point. Since this form also has a declining backside, multiple spall layers are possible. The equation for the n^{th} spall depth (d_{en}) is:

$$d_{en} = \frac{1}{2b} \ln \left[\frac{\sigma_p - (n-1) \sigma_{crit}}{\sigma_p - n \sigma_{crit}} \right] \quad (\text{eq 2.36})$$

The equation for the n^{th} spall velocity V_n is:

$$V_n = \left[\frac{\sigma_p - (n-1) \sigma_{crit}}{b d_n \rho c} \right] (1 - \exp^{-2bd_{en}}) \quad (\text{eq 2.37})$$

These equations work well except when σ_p is equal to or nearly equal to $n\sigma_{crit}$ at which time d_{en} approaches infinity and $V_n = 0$. This is because the duration of the function is infinite.

The difference between spall depths calculated for a triangular approximation of a stress wave compared with those calculated for an exponential approximation of the same stress wave can be significant. Consider a triangular stress wave and an exponential stress wave which both have no rise lengths, the same impulse, and the same peak stress (Figure 2.22b). The ratio of the n^{th} spall depth of the triangular stress wave (d_{tn}) to that of the exponential stress wave (d_{en}) is:

$$\frac{d_{tn}}{d_{en}} = \frac{2\sigma_{crit} \left(1 - \exp^{-b\lambda} \right)}{\sigma_p \ln \left[\frac{\sigma_p - (n-1) \sigma_{crit}}{(\sigma_p - n \sigma_{crit})} \right]} \quad (\text{eq 2.38})$$

where λ_e is the distance behind the exponential wave front to $\sigma_{(\lambda_e)}$ = $0.01 \sigma_p$, and b is calculated based upon the impulse and λ_e . Figure 2.23 is a plot of equation 2.38 for the first 3 layers of spall. It shows that the spall depth predictions can differ by large amounts depending upon the magnitudes and shape of the stress wave. For example, if σ_p is 10,000 psi, σ_{crit} is 3,500 psi, b is 16.5 msec^{-1} , c is 14.3 ft/msec and λ_e is 4.3 ft, then, for spall depth No. 1 $d_{t1}/d_{e1} = 1.61$ and for spall depth No. 2 $d_{t2}/d_{e2} = 0.90$. If σ_p is 5,000 psi, and all other values remain the same, then $d_{t1}/d_{e1} = 1.15$. Spall depth predictions using triangular approximations of stress waves with peaks the same or much higher than n times the dynamic strength of the concrete will differ greatly from spall predictions using exponential approximations of stress waves. Thus, it is recommended to fit stress waves from airblast loads with exponential or modified Friedlander equations.

Equations for spall depths and velocities for a few common shapes with no rise lengths are given in Table 2.3.

Now, consider shapes with rise lengths or loading fronts. Most real stress waves have some sort of rise length. Stress waves with rise lengths can theoretically only cause one main layer to spall. The spall depth and velocity equations are different for a stress wave with a loading portion smaller than the unloading portion of the stress wave, than they are for a stress wave with a loading portion larger than the unloading portion.

Consider first an ideal normal triangular stress wave with a rise length shorter than the fall length or unloading portion (see Figure 2.24a). The net stresses start out compressive as the loading portion of the stress wave reflects and then a portion of the net stresses become tensile after the peak stress is reflected (Figure 2.24b). The peak net tensile stress increases in magnitude as the wave advances. When the peak net tensile stress equals σ_{crit} , the material will crack and spall (Figure 2.24c). A middle portion of the stress wave is trapped in the spall and the loading portion and tail of the incident stress wave remains in the main structural element. The tail portion will now reflect off the new surface formed by the spall. Immediately after the material cracks, the loading and tail portions advance; the

peak net tensile stress again equals σ_{crit} ; and the material fails directly adjacent to the crack. As the loading and tail portions continue to advance, the peak net tensile stress continues to stay equal to σ_{crit} and causes a wide band of material to fail until the peak stress is reduced to some value less than σ_{crit} (Figure 2.24d). So a band of fine particles follows the initial spall layer.

Now consider an ideal normal triangular stress wave with a rise length longer than the fall or unloading portion and with σ_p greater than or equal to σ_{crit} (Figure 2.25a). The net stresses start out compressive as the stress wave reflects (Figure 2.25b) and the front net stress becomes tensile once the front of the reflected wave passes the back of the incident wave (Figure 2.25c). The peak net tensile stress increases as the wave advances. When the peak net tensile stress equals σ_{crit} the material will crack and spall (Figure 2.25d and e). In this case, most of the stress wave is trapped in the spall and only the portion of the loading front less than σ_{crit} remains in the structure. The spall depth (d) and velocity (v) are different in this case and can be calculated by:

$$d = \frac{\lambda}{2} - \left(\frac{\sigma_{crit}}{\sigma_p} \right) \left(\frac{a}{2} \right) \quad (\text{eq 2.39})$$

$$v = \frac{\lambda(\sigma_p - \sigma_{crit})}{(2d\rho c)} + \frac{\sigma_{crit}}{\rho c} \quad (\text{eq 2.40})$$

Equations for spall depths and velocities for other common shapes with rise lengths are given in Table 2.4.

Table 2.1
Averaged Free Air Equivalent Weights Based on Blast
Pressure and Impulse

<u>Explosive</u>	<u>Equivalent Weight Pressure</u>	<u>Equivalent Weight Impulse</u>	<u>Pressure Range</u>
AMATOL (60/40)	0.95		
AMATOL (50/50)	0.97		
ANFO (94/6 Am N1/ Fuel oil)	0.82		1-100
Composition A-3	1.09	1.07	5-50
Composition B	1.11	0.98	5-50
Composition C-4	1.37	1.19	10-100
Cyclotol (70/130) ^a	1.14	1.09	5-50
HBX-1	1.17	1.16	5-20
HBX-3	1.14	0.97	5-25
H-6	1.38	1.15	5-100
Minol II	1.20	1.11	3-20
Octol 70/30 ^b 75/25	1.06		
PETN	1.27		5-100
Pentolite	1.42	1.00	5-100
	1.38	1.14	5-600
Tetryl	1.07		3-20
75/25 ^c Tetrytol 70/30 65/35	1.06		
TNETB	1.36	1.10	5-100
TNT	1.00	1.00	Standard for pressure ranges shown
Tritonal	1.07	0.96	5-100

^aRDX/TNT

^bHMX/TNT

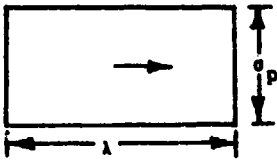
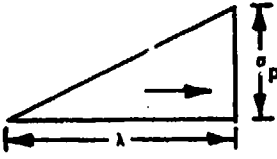
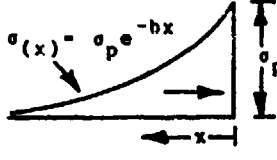
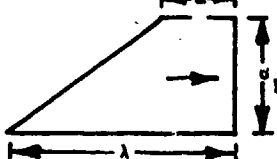
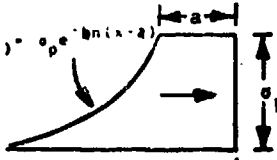
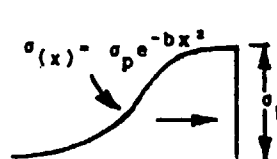
^cTETRYL/TNT

Table 2.2
Explosive Constants

Explosive	B(Equation 2.8) oz ^{1/2} /in. ^{7/6}	G(Equation 2.10) ft/sec
AMATOL	0.35	6,190
BARATOL	0.51	5,200
COMP. A-3	0.22	8,300
COMP. B (60/40)	0.22	8,800
COMP. C-3		8,800
COMP. C-4	0.22	8,300
CYCLONITE (RDX)		9,300
CYCLOTOL (75/25)	0.20	8,900
CYCLOTOL (20/80)		8,380
CYCLOTOL (60/40)	0.27	7,880
H-6	0.28	8,600
HBX-1	0.26	8,100
HBX-3	0.32	
HMX		10,200
HTA-3		8,500
OCTOL (75/25)		9,500
PENTOLITE (50/50)	0.25	8,100
PTX-2	0.23	
TETRYL	0.24	8,200
TNT	0.30	7,600
TORPEX		7,450
TRITON (80/20)		7,600

Table 2.3

**Spall Depths and Velocities Caused by Various Shapes of Stress Waves
with No Rise Times in an Ideal Elastic-Brittle Material**

*** Shape	n th Spall Depth	** n th Spall Velocity	* Max. n
	$d_1 = \frac{\lambda}{2}$	$V_1 = \frac{2\sigma_p}{\rho c}$	1
	$d_n = \frac{\lambda \sigma_{cr}}{2\sigma_p}$	$V_n = \frac{2\sigma_p - (2n-1)\sigma_{cr}}{\rho c}$	$\frac{\sigma_p}{\sigma_{cr}}$
	$d_n = \frac{1}{2b} \ln \left[\frac{\sigma_p - (n-1)\sigma_{cr}}{\sigma_p - n\sigma_{cr}} \right]$	$V_n = \frac{\sigma_p - (n-1)\sigma_{cr}}{b d_n \rho c} \left[1 - e^{-2b d_n} \right]$	$\frac{\sigma_p}{\sigma_{cr}}$
	$d_1 = \frac{\sigma_{cr}}{\sigma_p} \left(\frac{\lambda - b}{2} \right) - \frac{b}{2}$ $d_{n>1} = \frac{\sigma_{cr}}{\sigma_p} \left(\frac{\lambda - b}{2} \right)$	$V_1 = \frac{\sigma_p b}{\rho a d_1} + \frac{(2\sigma_p - \sigma_{cr})(\lambda - b)\sigma_{cr}}{\sigma_p 2 d_1 \rho \sigma}$ $V_{n>1} = \frac{2\sigma_p - (2n-1)\sigma_{cr}}{\rho \sigma}$	$\frac{\sigma_p}{\sigma_{cr}}$
	$d_1 = \frac{1}{2b} \ln \left[\frac{\sigma_p}{\sigma_p - \sigma_{cr}} \right] + \frac{\lambda}{2}$ $d_{n>1} = \frac{1}{2b} \ln \left[\frac{\sigma_p - (n-1)\sigma_{cr}}{\sigma_p - n\sigma_{cr}} \right]$	$V_1 = \frac{\sigma_p (ab) + \sigma_{cr}}{b d_1 \rho c}$ $V_{n>1} = \frac{\sigma_p - (n-1)\sigma_{cr}}{b d_n \rho c} \left[1 - e^{-2b d_n} \right]$	$\frac{\sigma_p}{\sigma_{cr}}$
	$d_n = \frac{1}{2} \sqrt{\frac{1}{b} \ln \left(\frac{\sigma_p}{\sigma_p - n\sigma_{cr}} \right)} - \frac{1}{2} d_{(1-1)}$	$V_n = \frac{[A_n - A_{n-1}] \sigma_p \sqrt{\pi}}{\rho a d_n \sqrt{b}}$ where: $A_n = \int_0^{t_n} \frac{1}{2\pi} e^{-t^2/2} dt$ and $t_n = \sqrt{2b} (2 d_n)^2$	$\frac{\sigma_p}{\sigma_{cr}}$

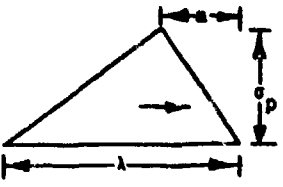
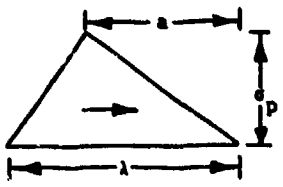
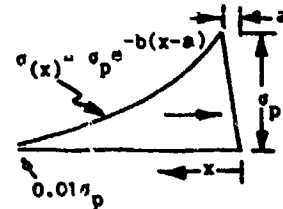
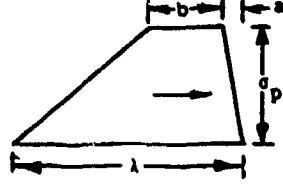
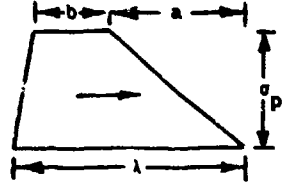
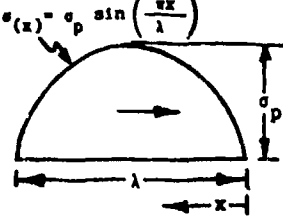
* Maximum number of spall layers is the ratio indicated truncated to an integer.

** The relation $x = ct$ was used to calculate the trapped impulses.

*** Shapes and magnitudes remain the same as they propagate through the material and σ_p is greater than the dynamic tensile strength σ_{cr} .

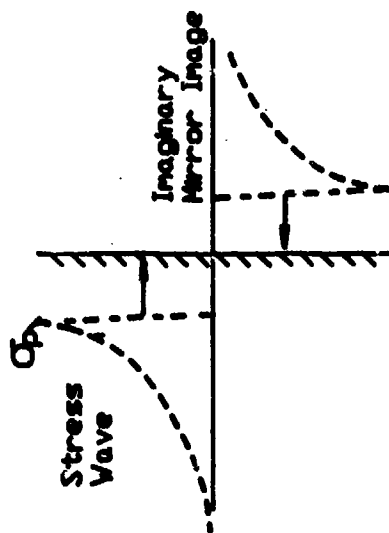
Table 2.4

Spall Depths and Velocities Caused by Various Shapes of Stress Waves with Rise Times in an Ideal Elastic-Brittle Material

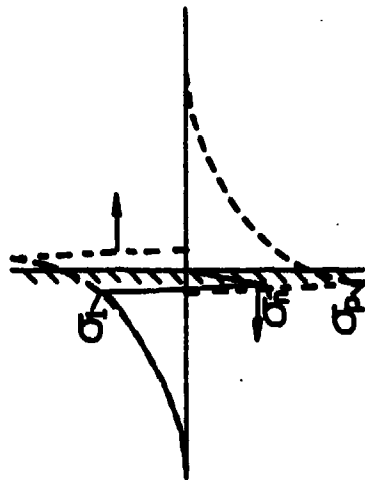
Shape	Spall Depth	n^{th} Spall Velocity	Max. n^{th}
	$d = \frac{\sigma_{cr}}{\sigma_p} \left(\frac{\lambda - a}{2} \right)$	$v_1 = \frac{2\sigma_p - \sigma_{cr}}{\rho_0 c}$	1
	$d = \frac{\lambda}{2} - \frac{\sigma_{cr}}{\sigma_p} \left(\frac{a}{2} \right)$	$v_1 = \frac{\lambda \left(\frac{\sigma_p - \sigma_{cr}}{2d\rho_0 c} \right) + \frac{\sigma_{cr}}{\rho_0 c}}{1}$	1
	$d = \frac{1}{2b} \ln \left(\frac{\sigma_p}{\sigma_p - \sigma_{cr}} \right) > a$	$v_1 = \frac{1}{\rho_0 c} \left(\frac{d\sigma}{2} \right) + \sigma_p b (1 - e^{-b2d})$	1
	$d = \frac{\sigma_{cr}}{\sigma_p} \left(\frac{\lambda - a - b}{2} \right) + \frac{b}{2}$	$v_1 = \frac{\sigma_p b}{\rho_0 c} + \frac{2\sigma_p - \sigma_{cr} (\lambda - a - b) (\sigma_{cr})}{2\sigma_p \rho_0 c}$	1
	$d = \frac{\lambda}{2} - \frac{\sigma_{cr} a}{\sigma_p 2}$	$v_1 = \frac{\sigma_{cr}^2 (\lambda + b) - \sigma_{cr}^2 a}{2\sigma_p \rho_0 c}$	1
	$d = \frac{\lambda}{2} - \frac{\lambda}{2} \sin^{-1} \left(\frac{\sigma_{cr}}{\sigma_p} \right)$	$v_1 = \frac{\sigma_p \lambda}{\pi \rho_0 c d} \left(1 - \cos \frac{\pi 2d}{\lambda} \right)$	1

* There can theoretically be only one spall band caused by stress waves with rise times. However, in real materials the strength is not uniform and multiple layers are possible.

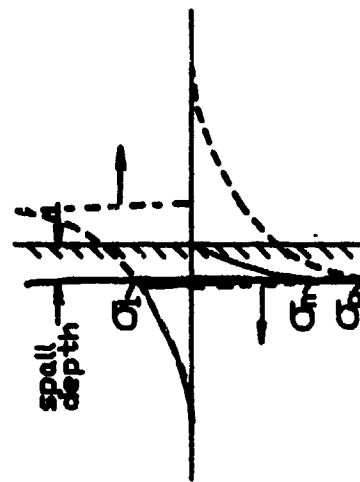
** The relation $x = ct$ was used to calculate the trapped impulses.



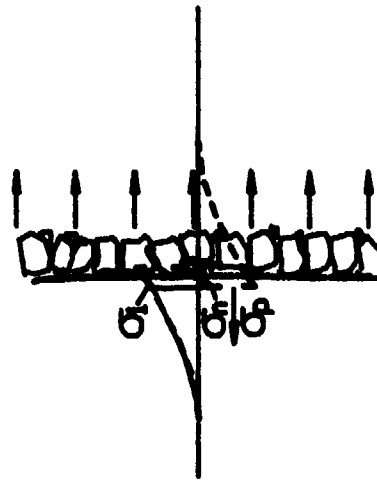
a. Stress wave induced by the loads.



b. Reflects as a tension wave on the backside of the wall.



c. A crack forms when $\sigma_h >$ dynamic concrete strength for a minimum time.



d. The trapped impulse forces the cracked concrete away at a spall velocity.

Figure 2.1. Stress wave propagating, reflecting, and causing spall.

TYPICAL REFLECTED PRESSURE-TIME HISTORY

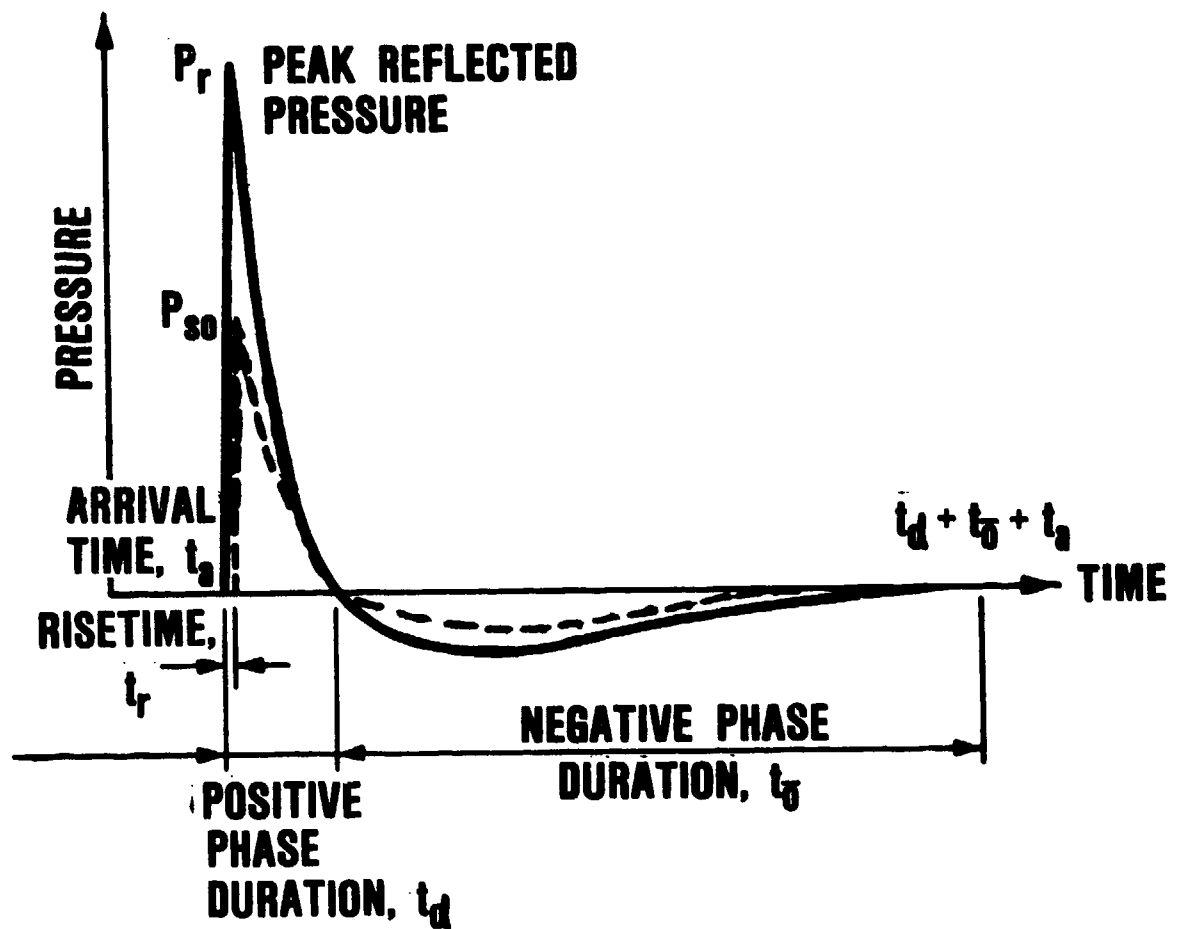
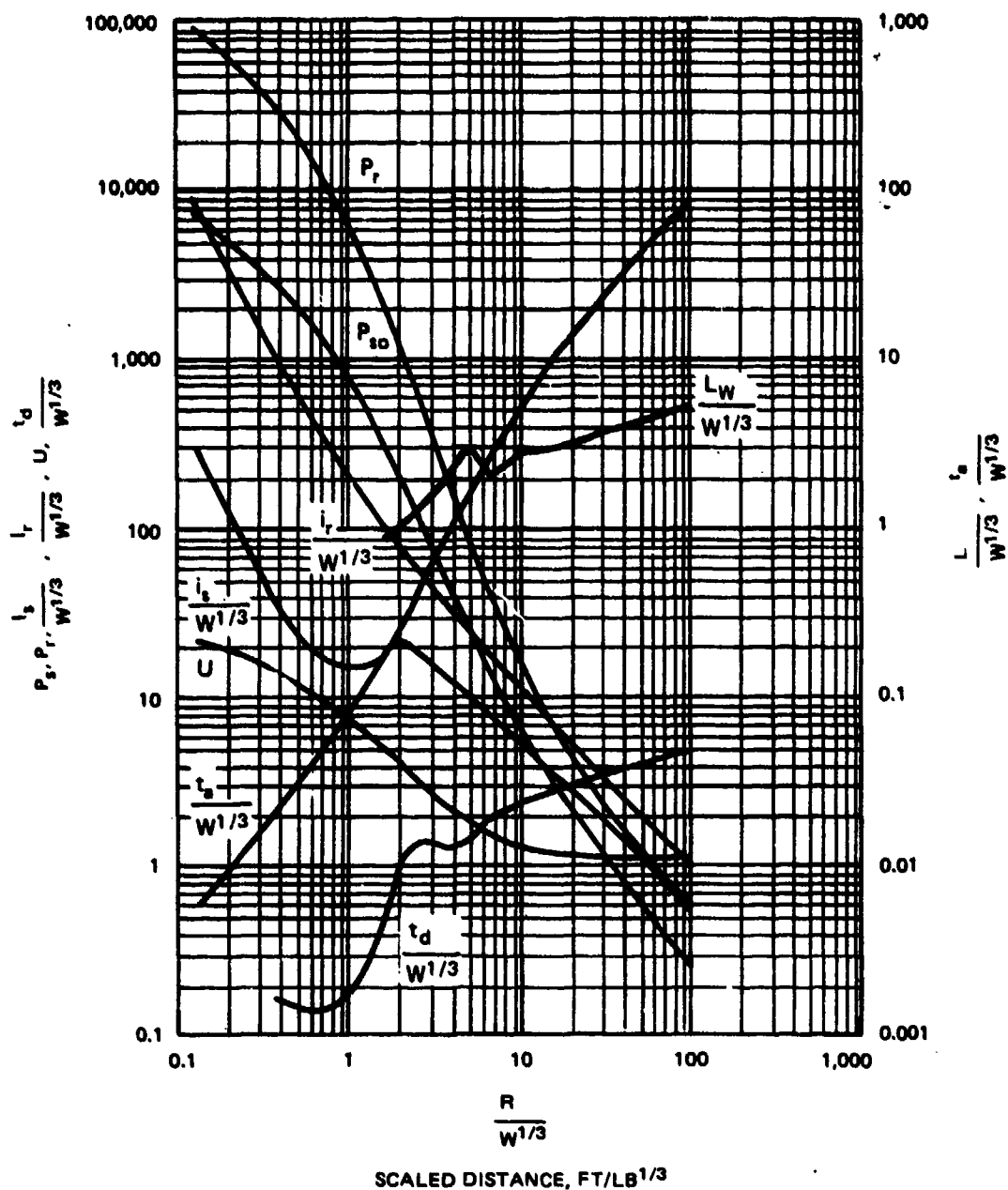


Figure 2.2. Typical free-field and reflected airblast histories.



R	= RADIAL STANDOFF DISTANCE, FT	$I_r/W^{1/3}$	= SCALED UNIT POSITIVE NORMALLY REFLECTED IMPULSE, PSI · MSEC/LB ^{1/3}
W	= CHARGE WEIGHT, LBS	U	= SHOCK FRONT VELOCITY, FT/MSEC
$R/W^{1/3}$	= SCALED STANDOFF DISTANCE, FT/LB ^{1/3}	$t_d/W^{1/3}$	= SCALED DURATION OF POSITIVE PHASE, MSEC/LB ^{1/3}
P_s	= PEAK POSITIVE INCIDENT PRESSURE, PSI	$t_a/W^{1/3}$	= SCALED TIME OF ARRIVAL, MSEC/LB ^{1/3}
P_r	= PEAK POSITIVE NORMALLY REFLECTED PRESSURE, PSI	$L/W^{1/3}$	= SCALED WAVE LENGTH OF POSITIVE PHASE, FT/LB ^{1/3}
$I_s/W^{1/3}$	= SCALED UNIT POSITIVE INCIDENT IMPULSE, PSI · MSEC/LB ^{1/3}		

Figure 2.3. Airblast parameters versus scaled standoff distance for TNT spherical air burst (Reference 3).

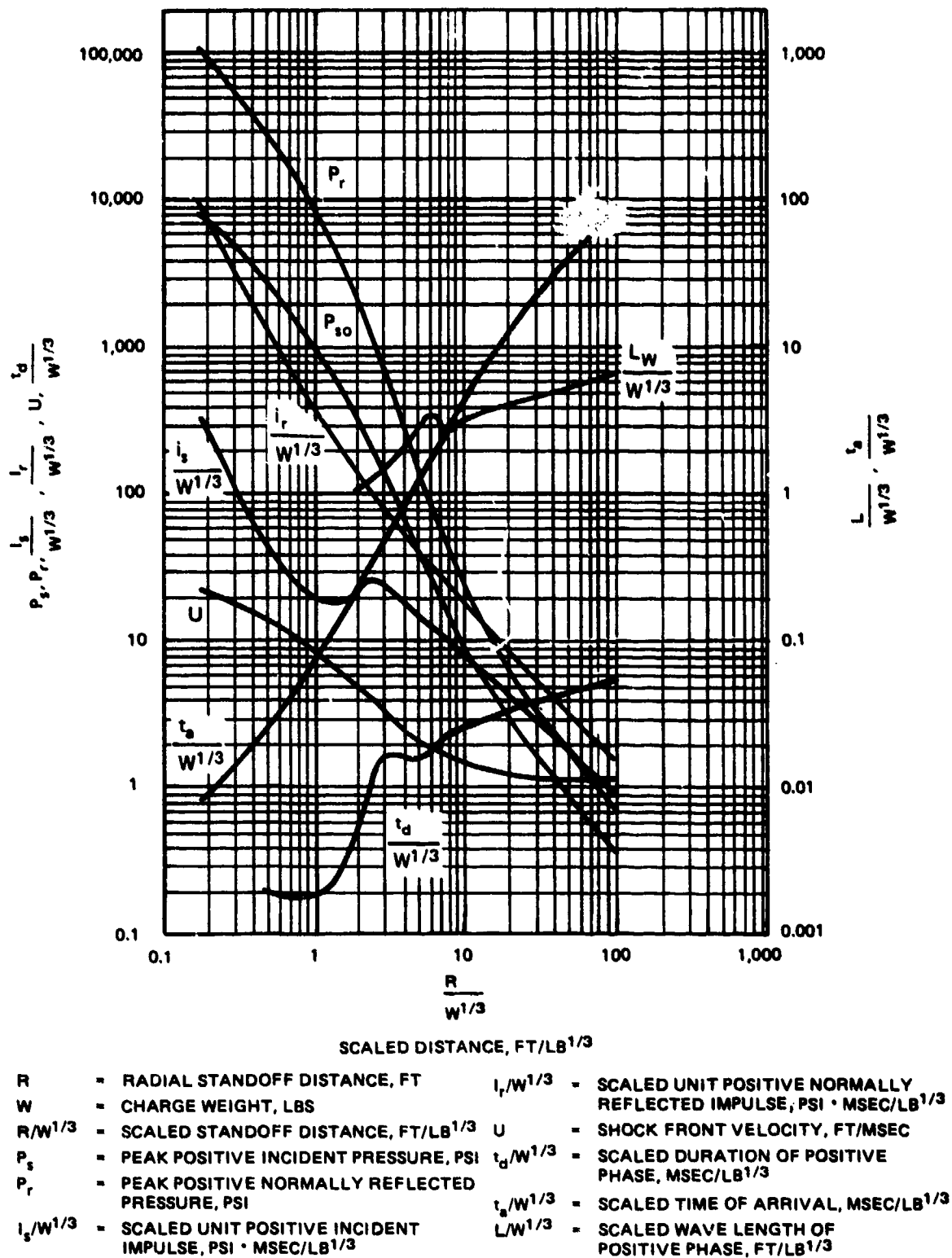
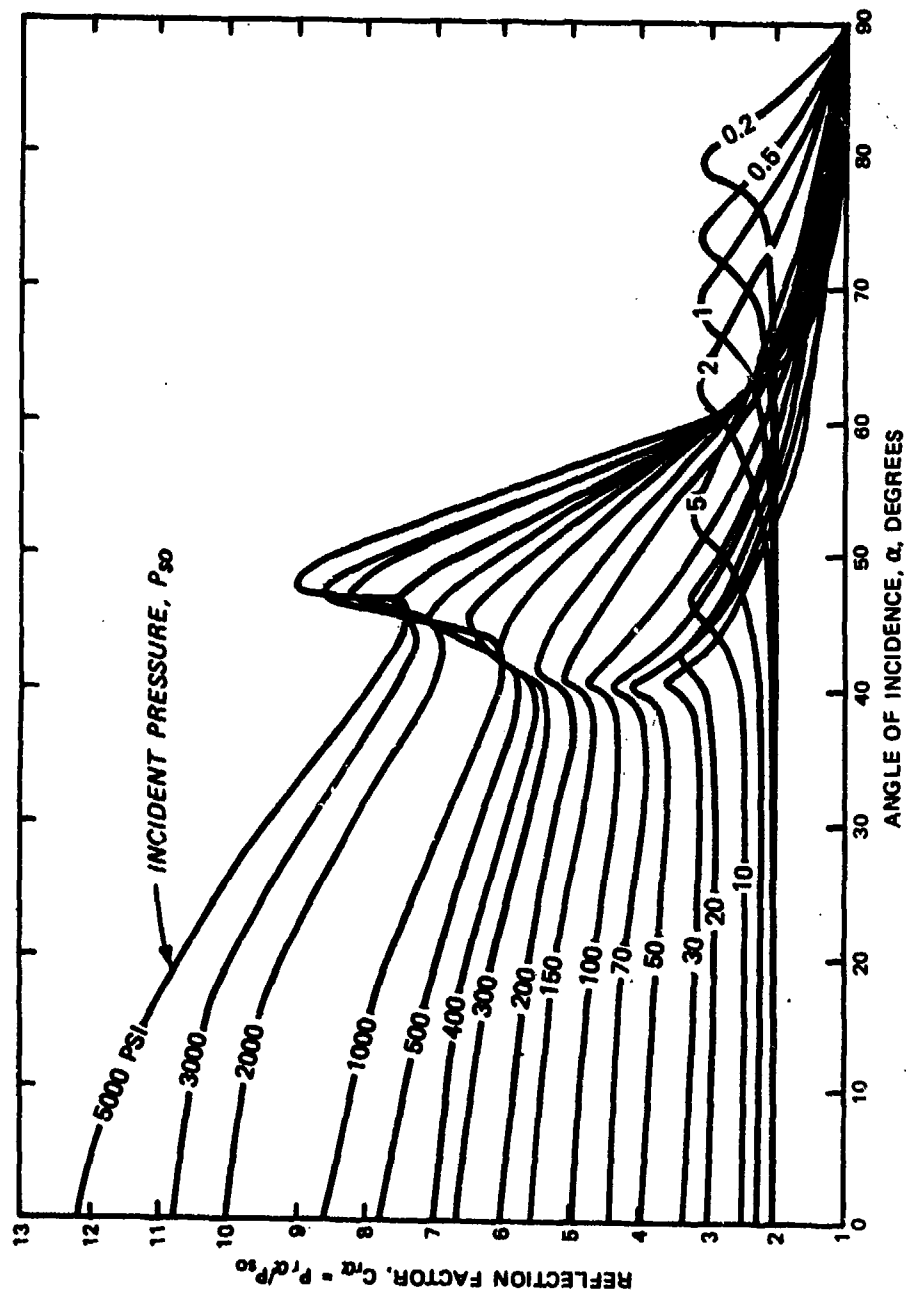


Figure 2.4. Airblast parameters versus scaled standoff distance for TNT hemispherical ground bursts (Reference 3).



SOURCE: AFWL TR 70-127

Figure 2.5. Ratio of reflected pressure to incident pressure versus angle of incidence.



Figure 2.6. Scabbing resulting from a concentrated zone of multiple bomb fragment impacts.

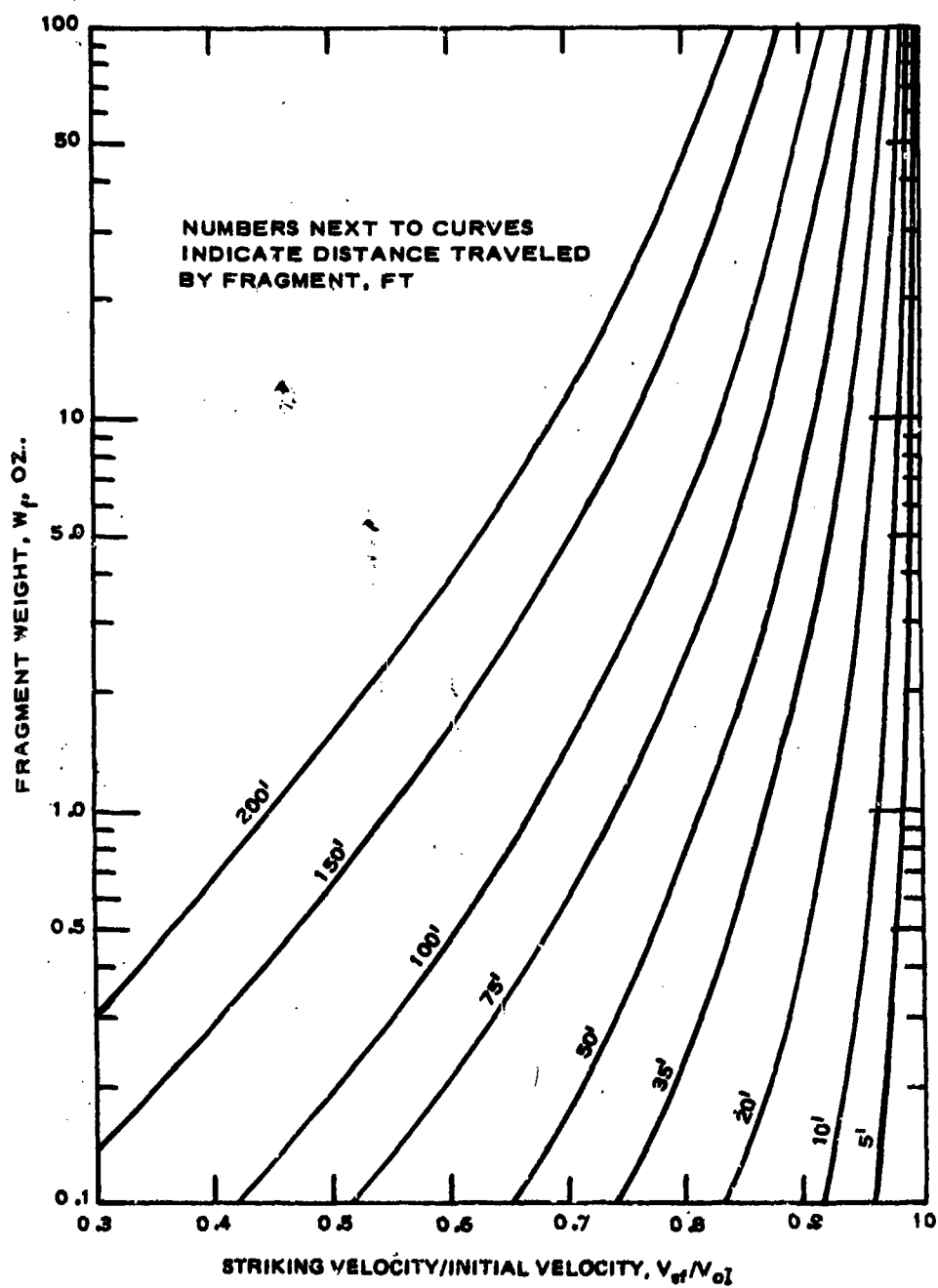


Figure 2.7 Variation of primary fragment velocity with distance.

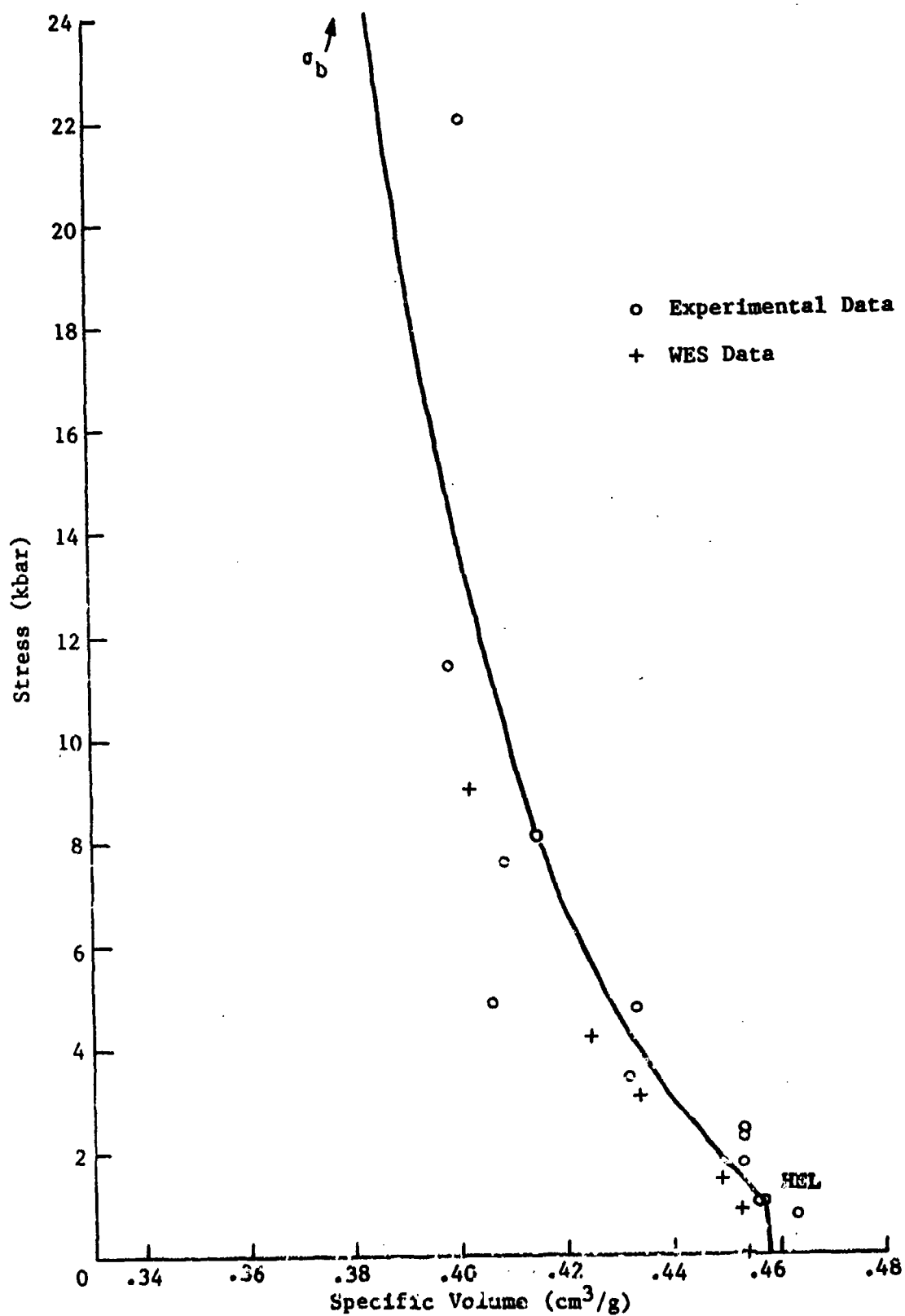


Figure 2.8 Theoretical Hugoniot and experimental data of concrete in the stress range from 0 to 24 kbar.

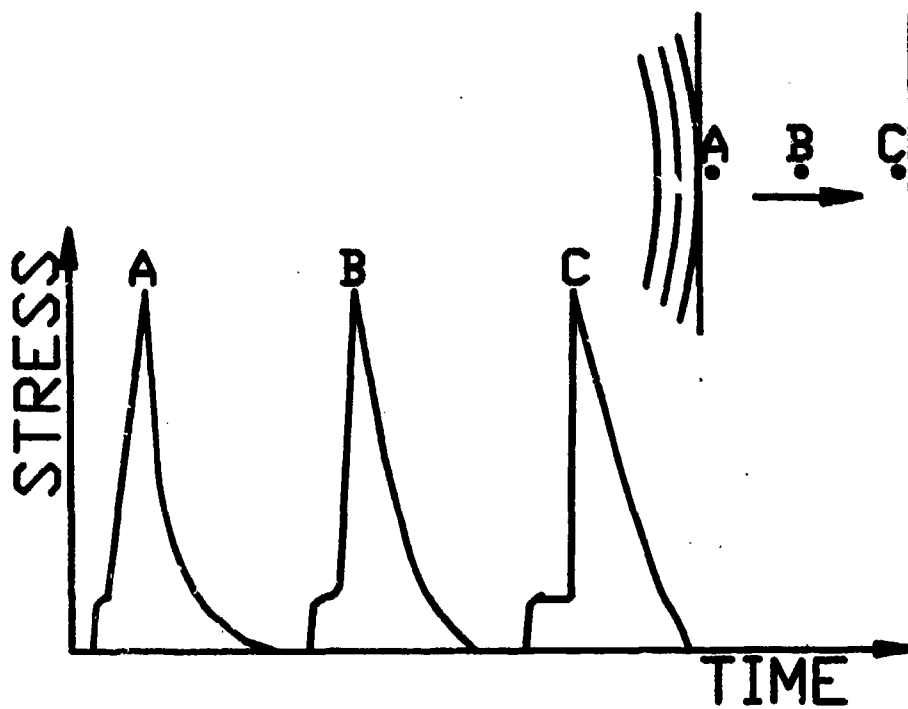


Figure 2.9. Schematic of stress waves changing due to different stresses above the HEL traveling at different velocities.

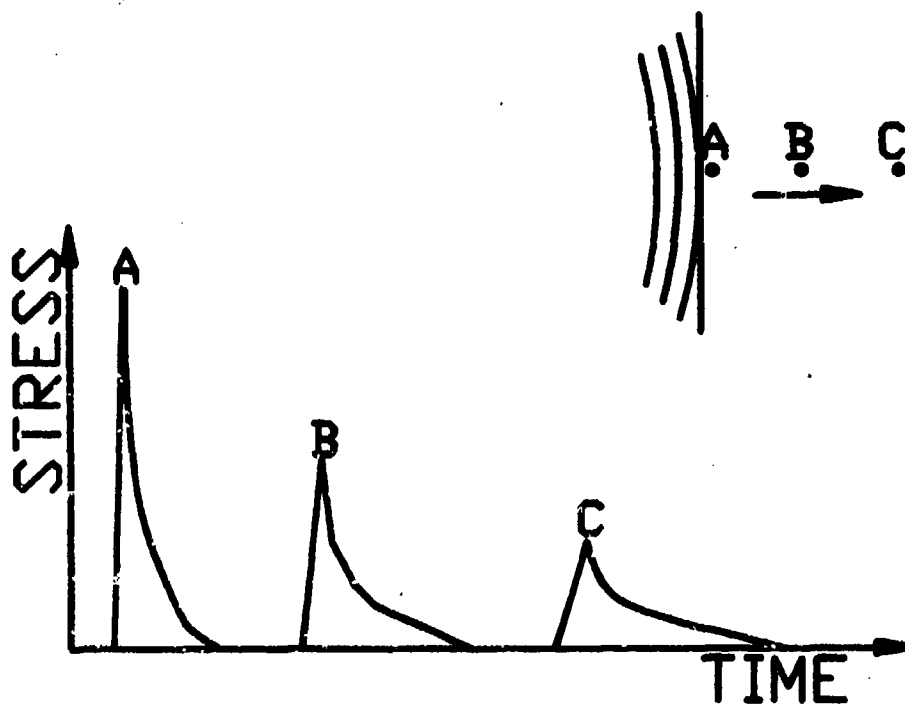


Figure 2.10. Illustration of attenuation of a stress wave with stresses above the dynamic compressive strength of the material.

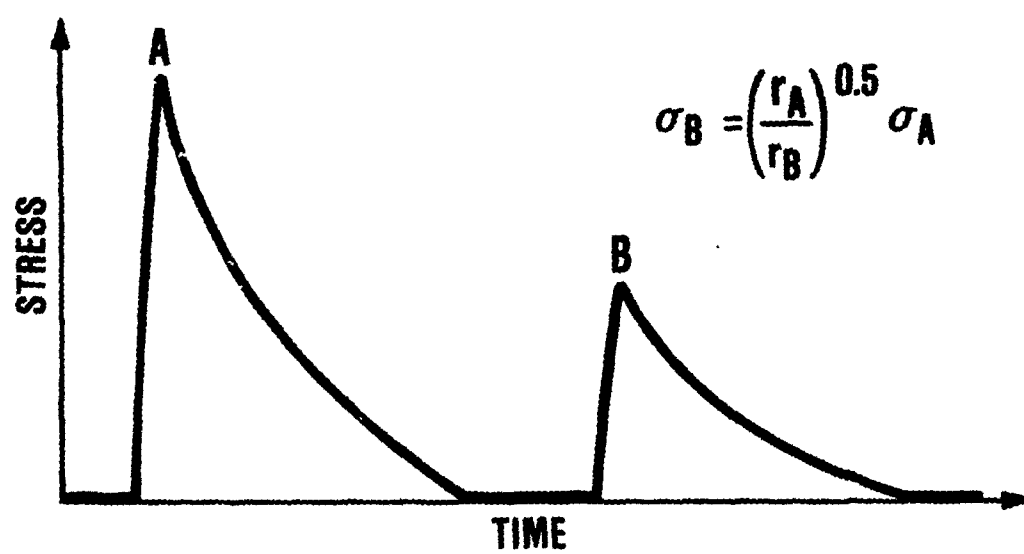
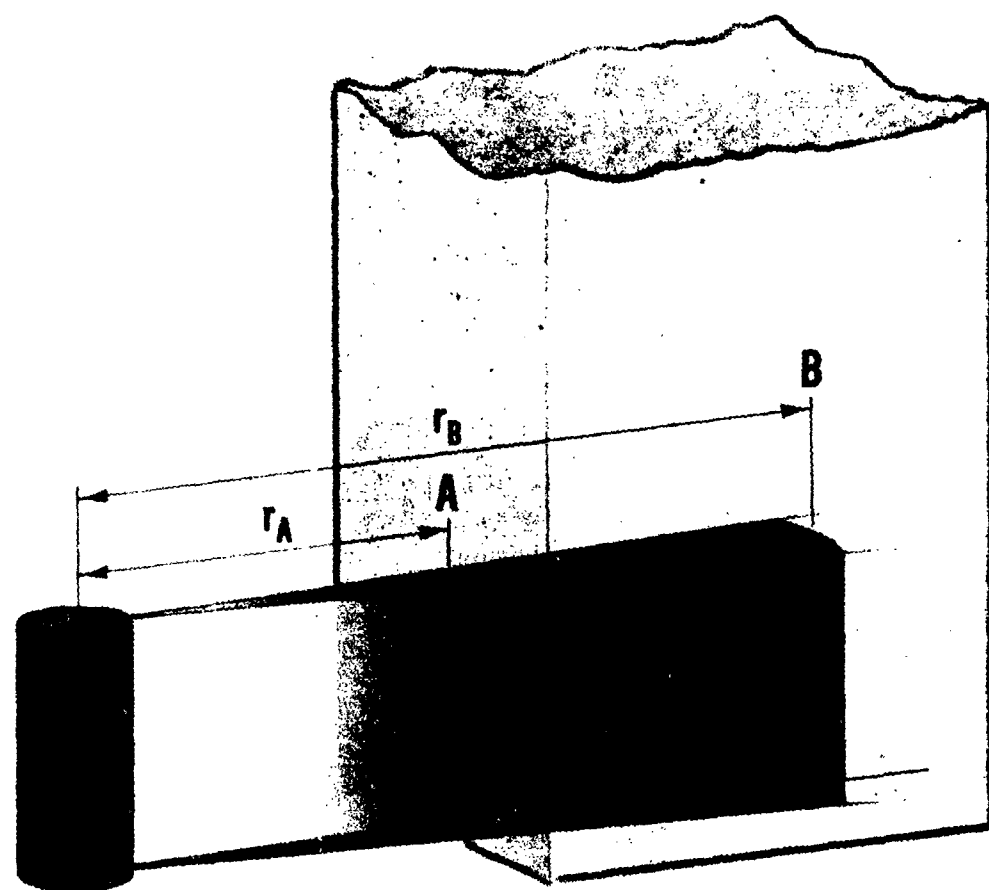


Figure 2.11. Illustration of cylindrical divergence of a stress wave induced by a cylindrically expanding airblast wave.

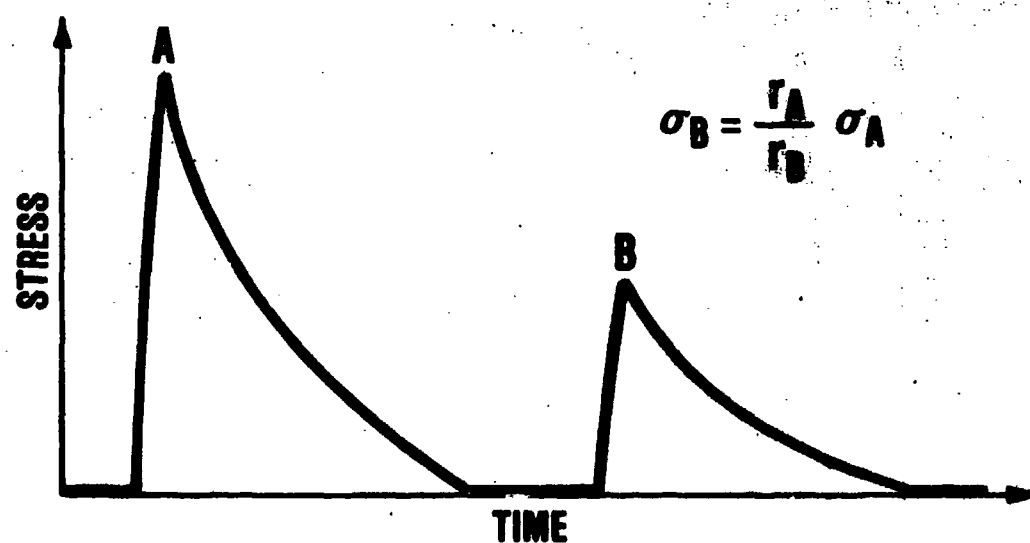
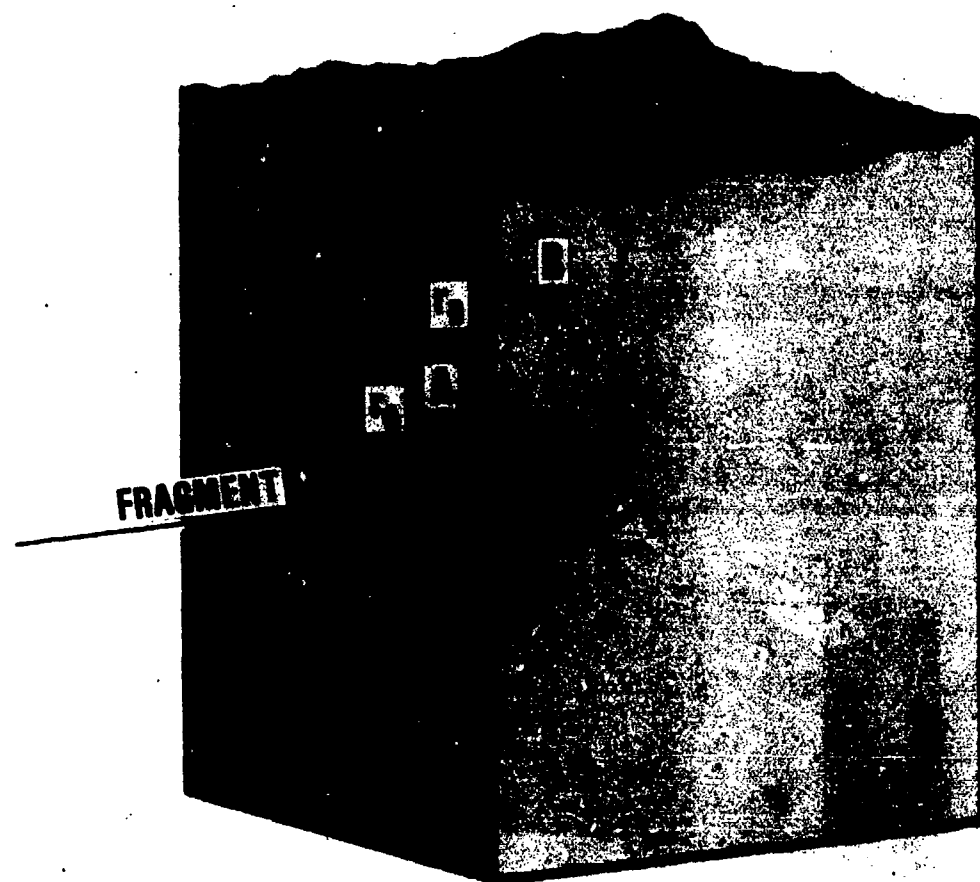


Figure 2.12. Illustration of spherical divergence of a stress wave expanding from a bomb fragment.

DISPERSION OF STRESS WAVE BY INCLUSIONS OR VOIDS

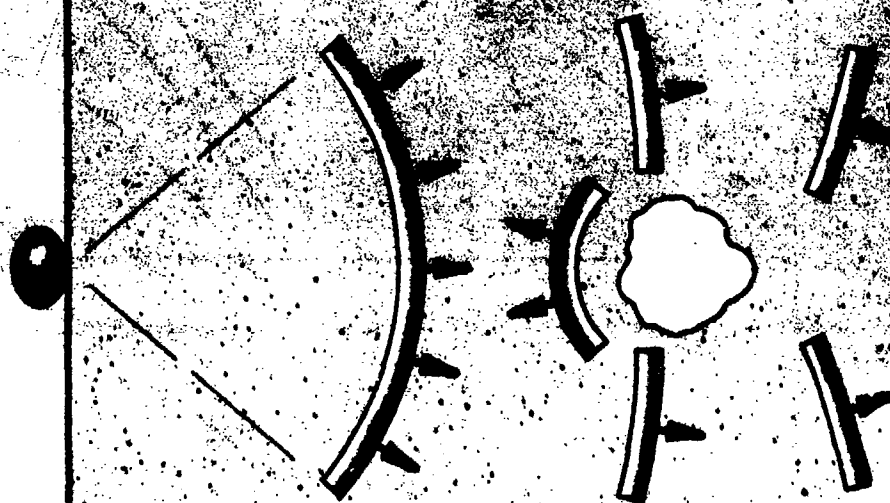


Figure 2.13. Dispersion of a stress wave hitting an air void.

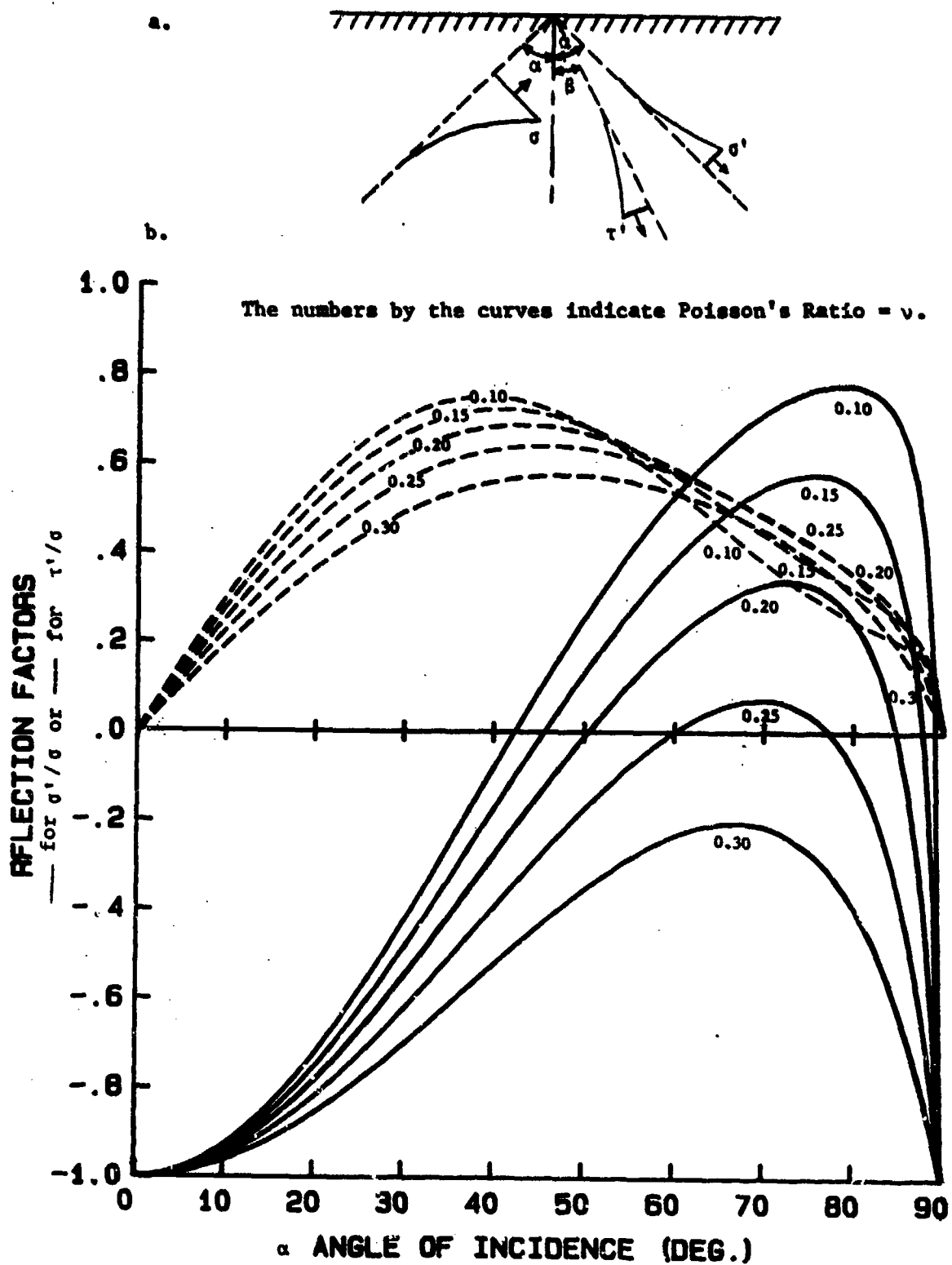


Figure 2.14 Reflection factors for the reflected primary and shear stresses from an incident primary stress wave.

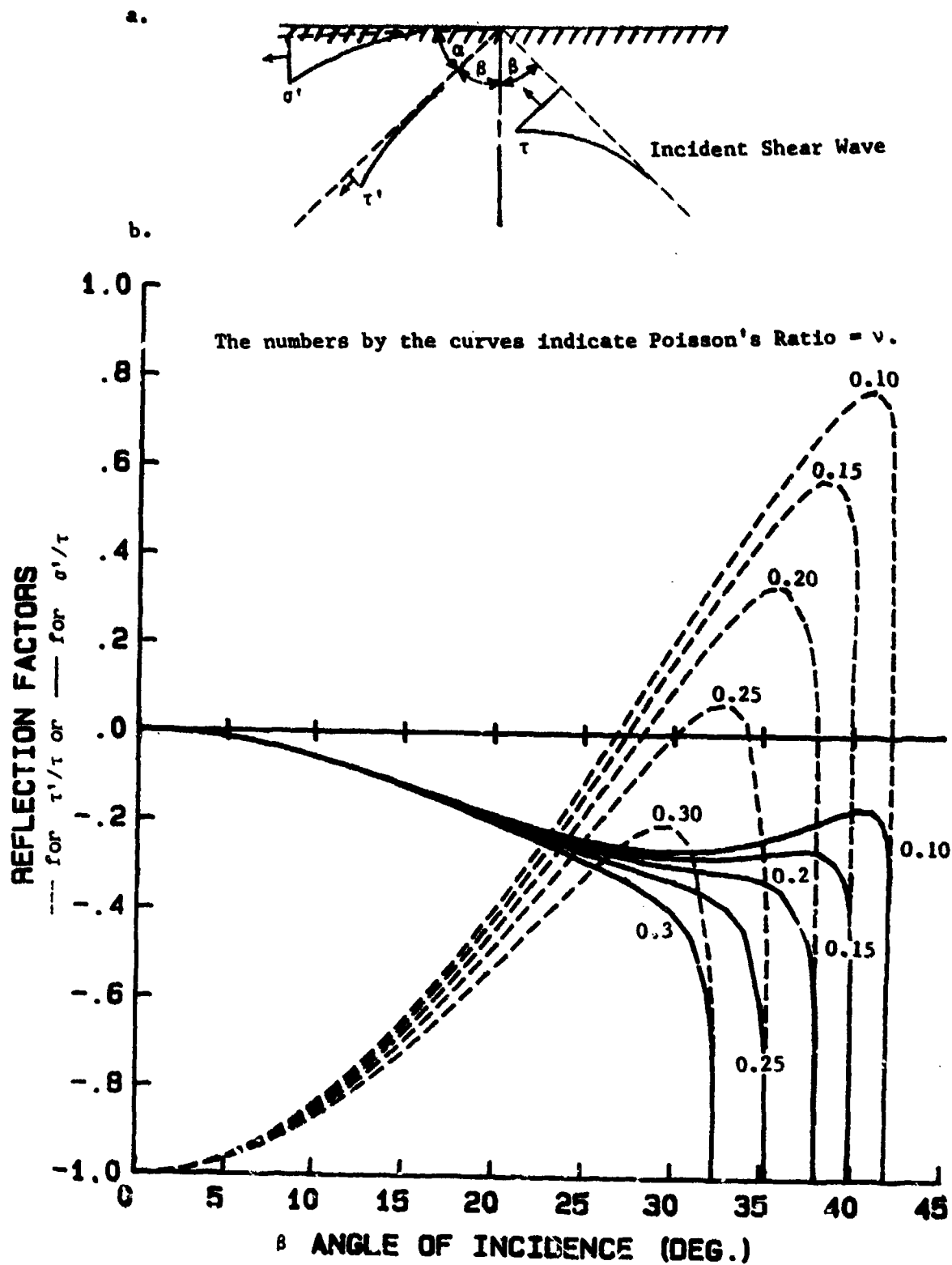


Figure 2.15 Reflection factors for reflected primary and shear stresses from stresses from an incident shear stress wave.

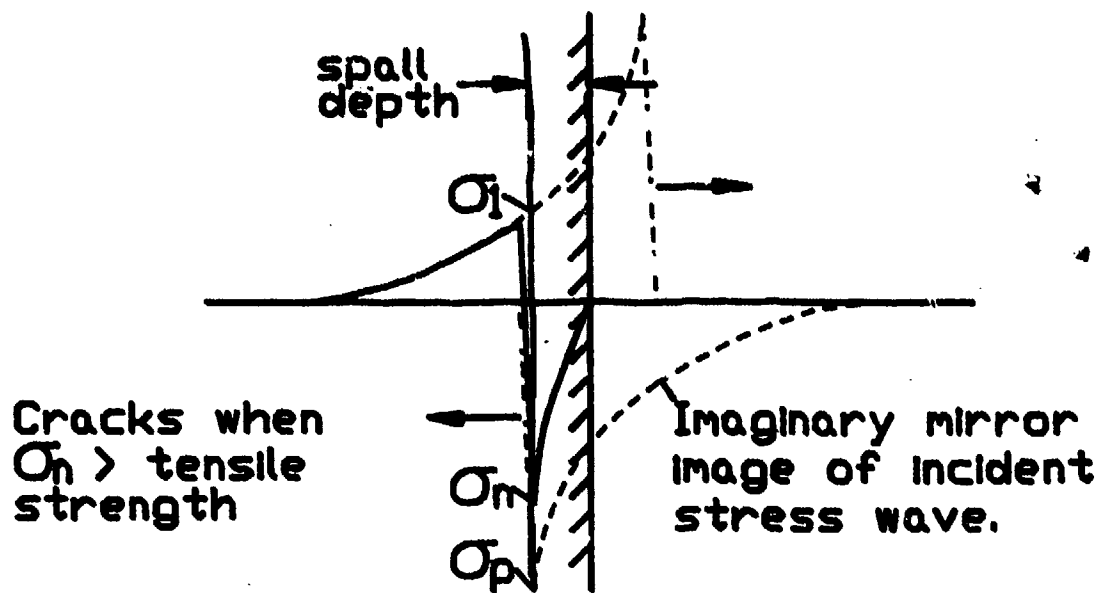


Figure 2.16. Use of an imaginary mirror image of the incident stress wave to calculate the net stress at a given point and time.

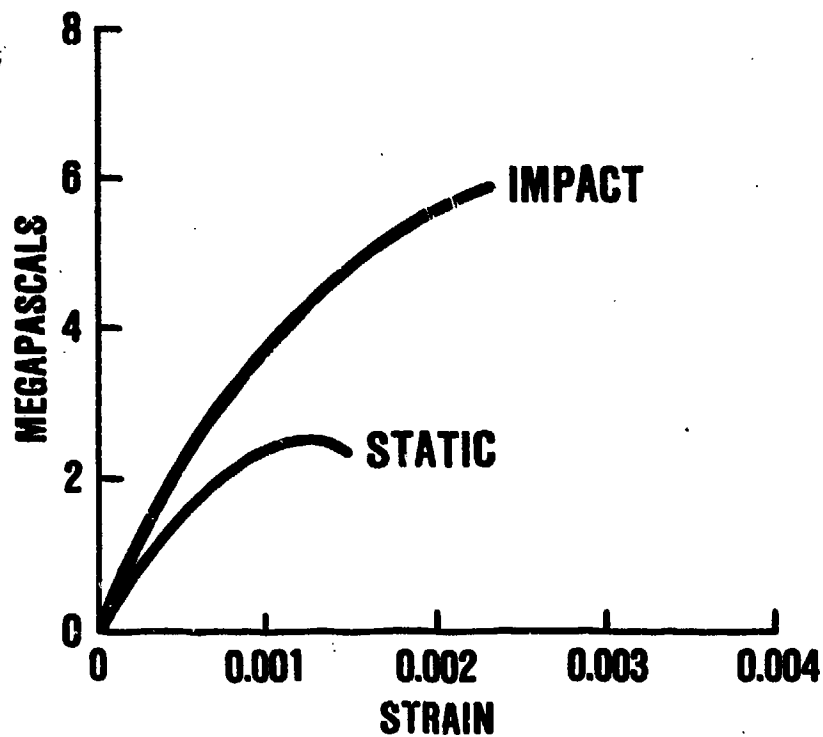


Figure 2.17. Comparison of static and impact stress-strain curves for a typical concrete (Reference 15).

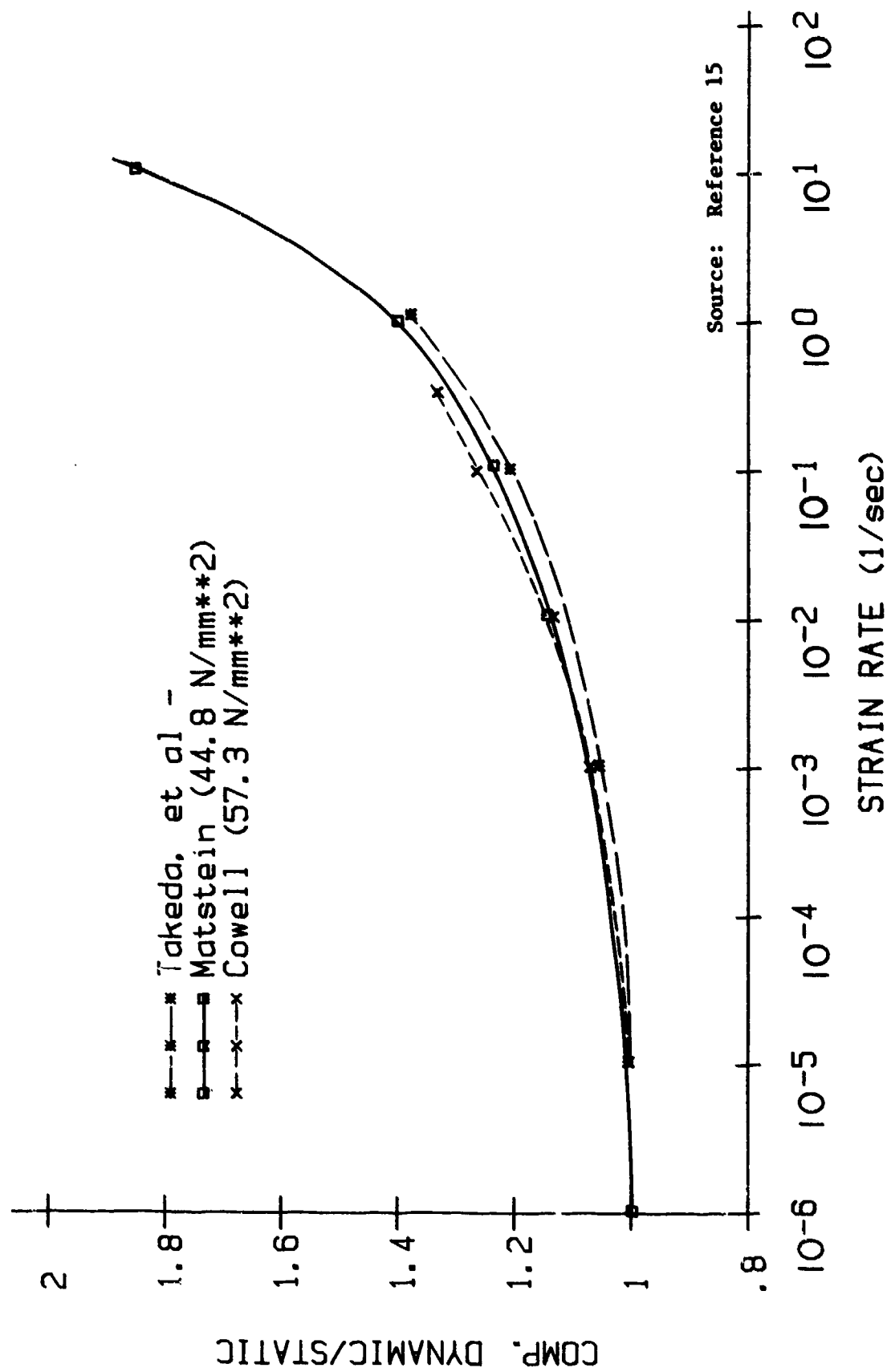


Figure 2.18. Ratio of dynamic to static compressive strengths of concrete versus strain-rate.

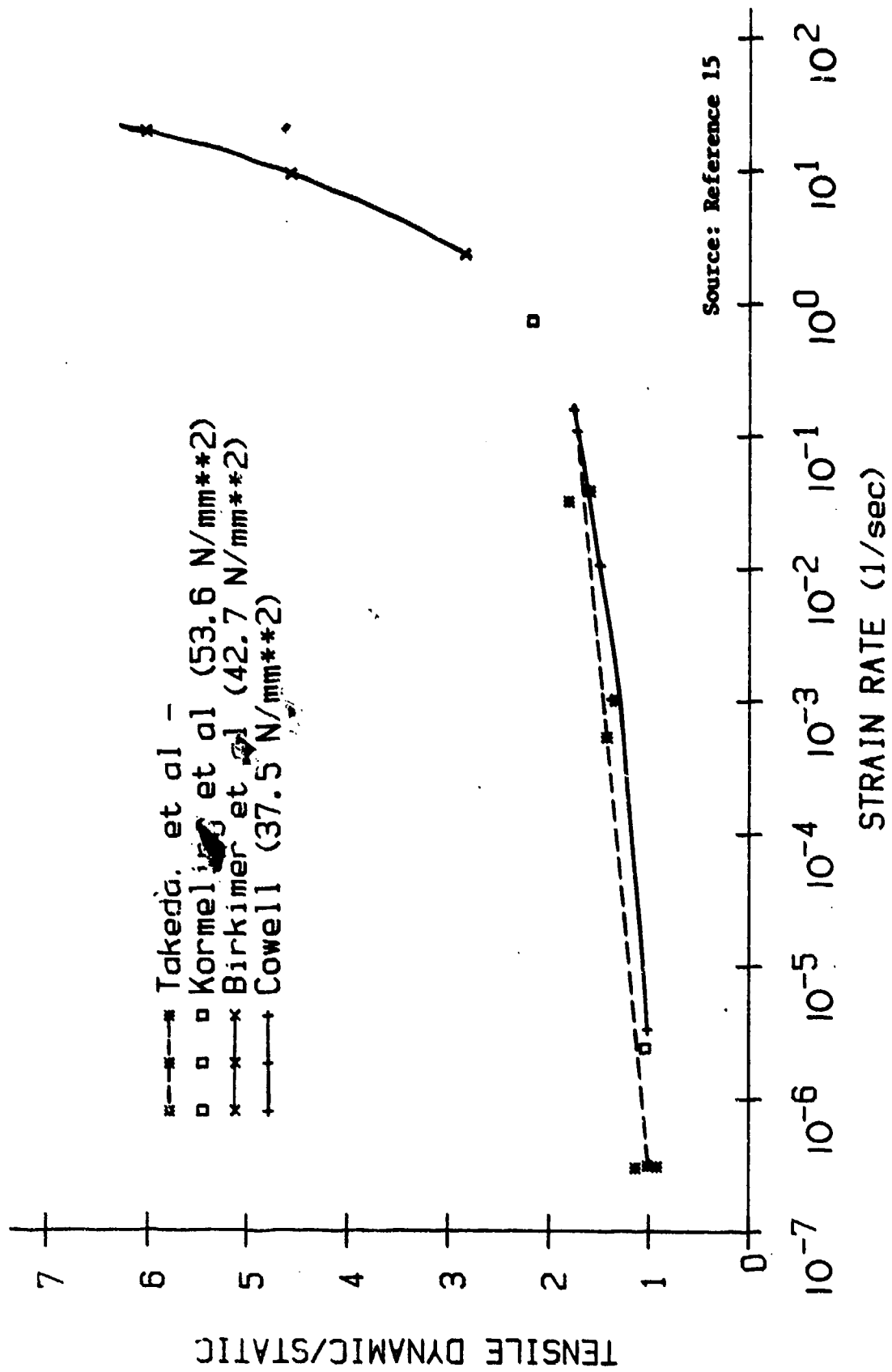


Figure 2.19. Ratio of dynamic to static tensile strengths of concrete versus strain-rate.

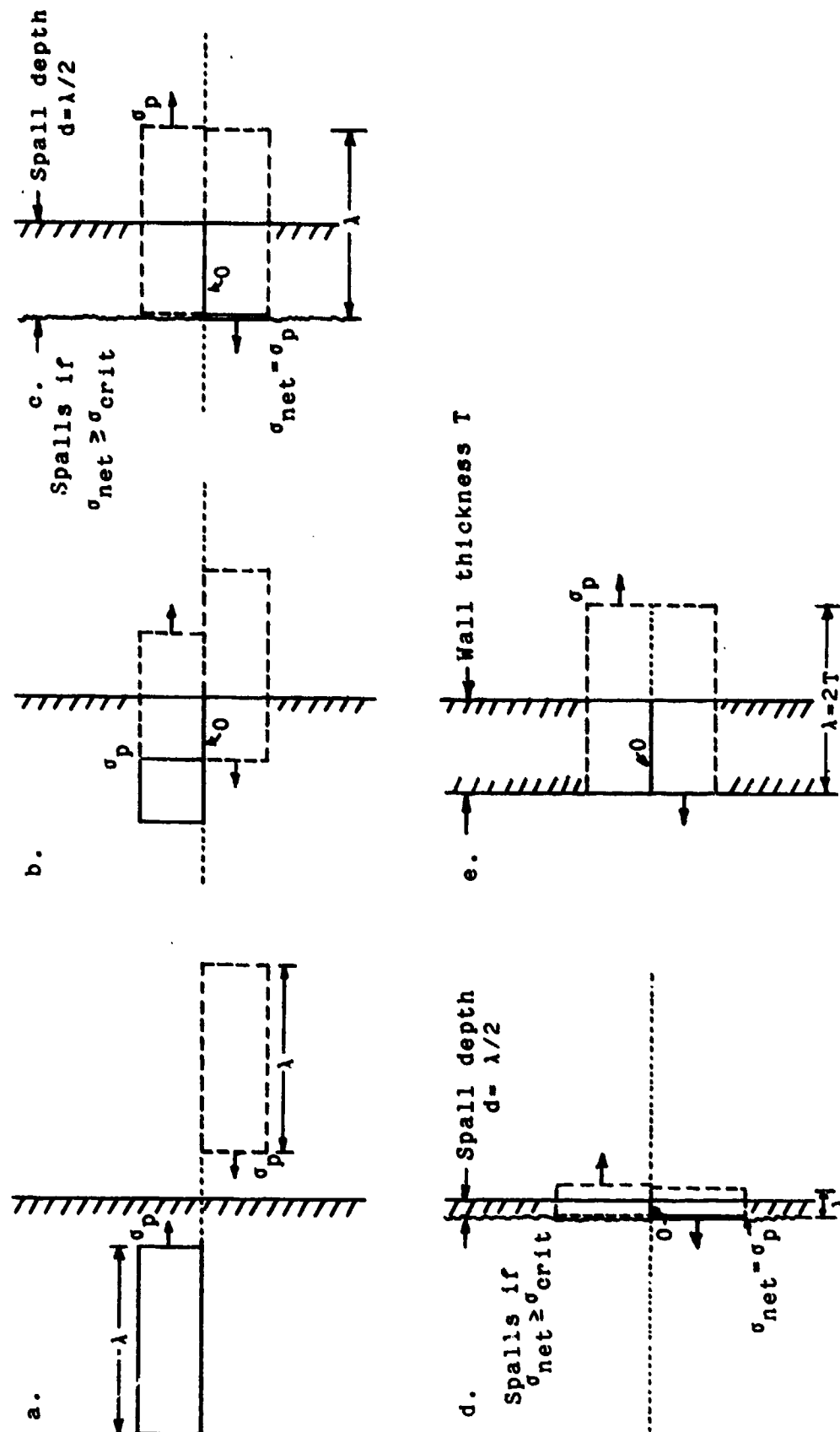


Figure 2.20. Effects on spall of rectangular stress waves.

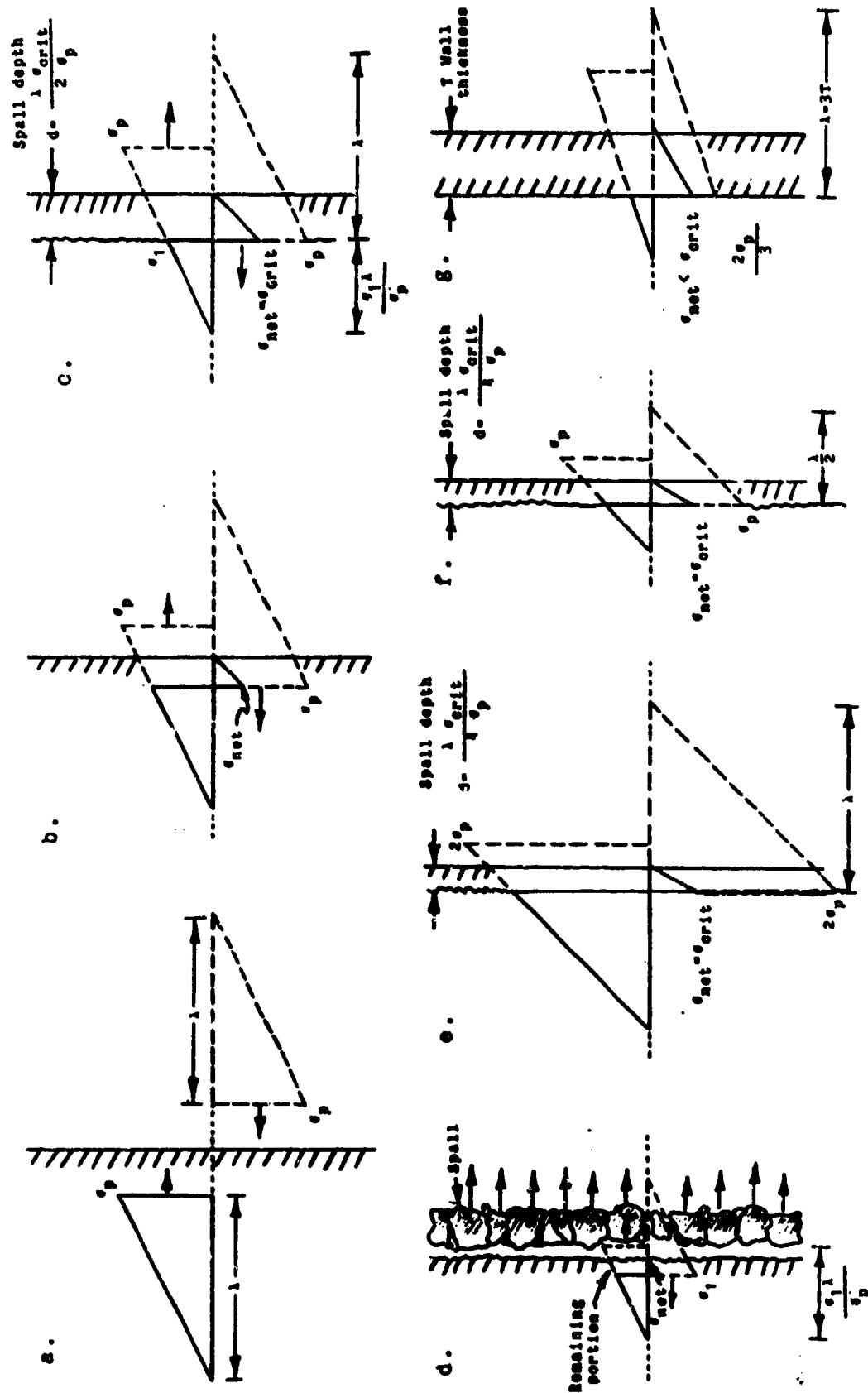
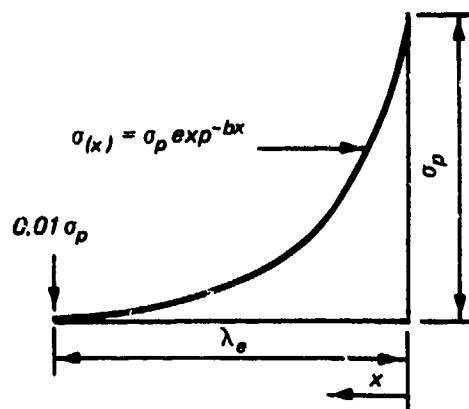
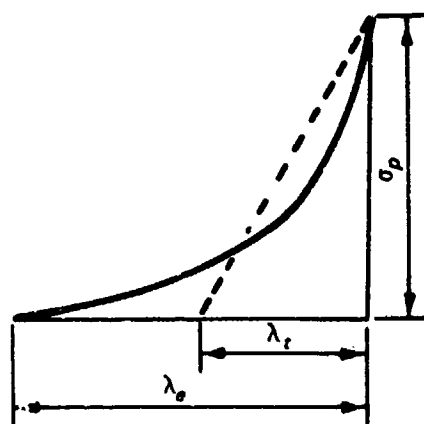


Figure 2.21. Effects on spall of triangular stress waves with no rise time.



NOTE $x = ct$
 AND $I_{\lambda_e} = \frac{\sigma_p}{cb} (1 - \exp^{-bct \lambda_e})$

Figure 2.22a. An exponentially decaying stress wave with no rise time.



$$I_{\lambda_t} = \frac{1}{2} \sigma_p t_{\lambda_t}$$

$$I_{\lambda_t} = I_{\lambda_e}$$

$$\frac{\sigma_p t_{\lambda_t}}{2} = \frac{\sigma_p}{cb} (1 - \exp^{-bct \lambda_e})$$

$$t_{\lambda_t} = \frac{2}{cb} (1 - \exp^{-bct \lambda_e})$$

$$\lambda_t = \frac{2}{b} (1 - \exp^{-bct \lambda_e})$$

Figure 2.22b. An exponentially decaying stress wave and a triangular stress wave with the same total positive impulse.

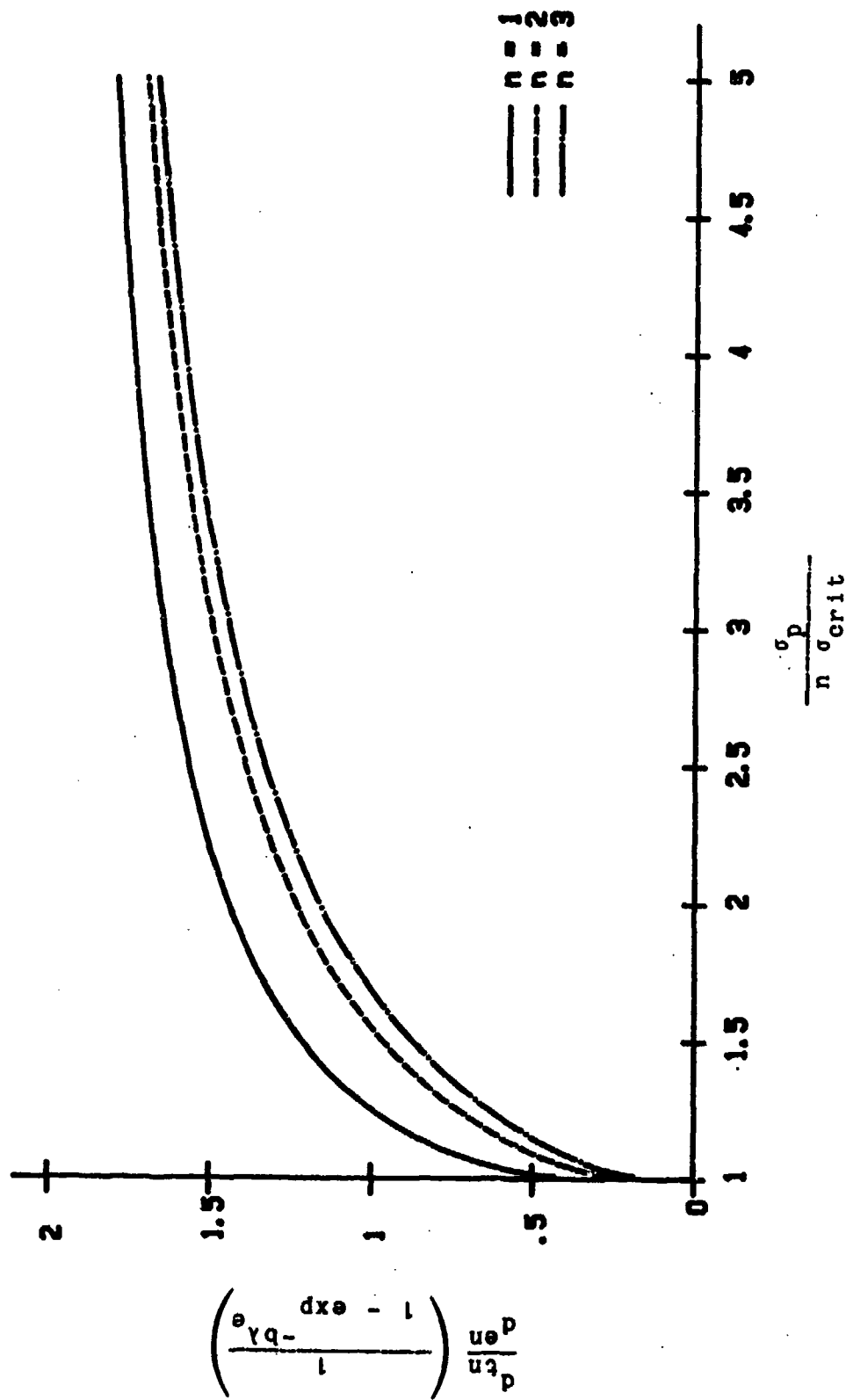


Figure 2.23 Ratio of spall depth predictions using a triangular approximation to spall depth predictions using an exponential approximation of stress waves.

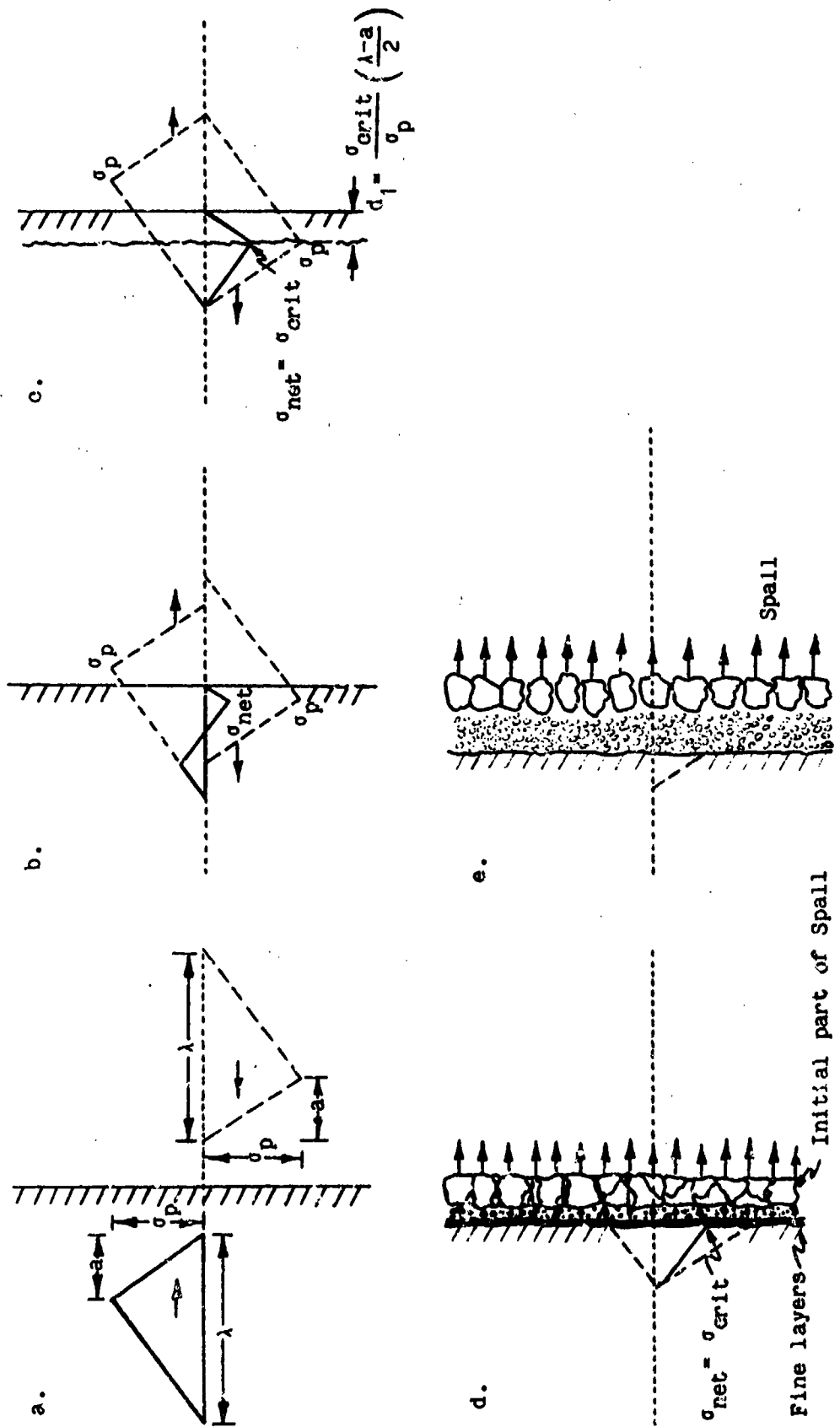


Figure 2.24. Effects on spall of a triangular wave with a short rise time.

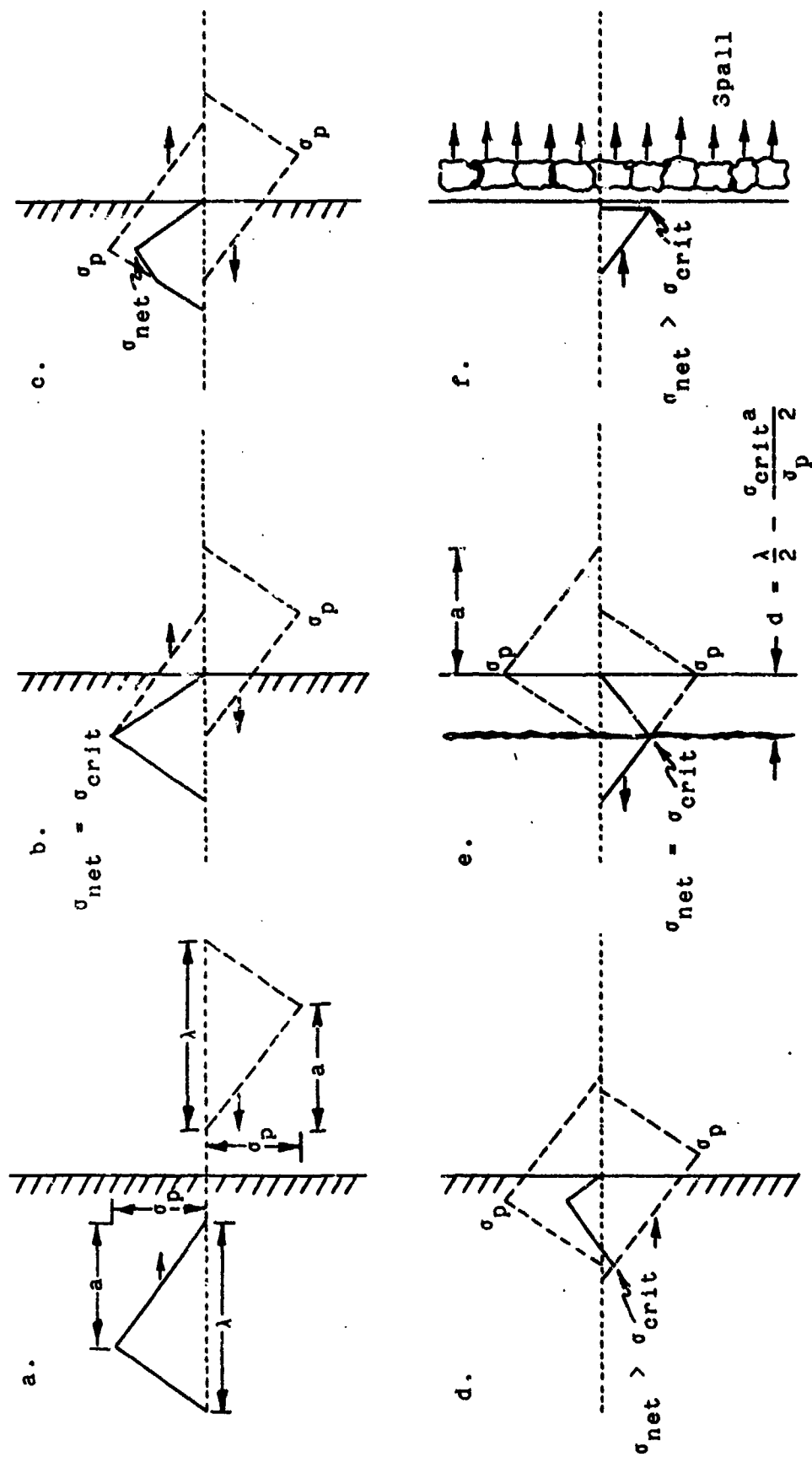


Figure 2.25. The effect on spall of a triangular stress wave with a long rise time.

General

The two main types of prediction methods are theoretical and empirical. A theoretical analysis of spall of concrete structures subjected to nearby bomb detonations is usually very complex and based on many unverified assumptions. The detonations of contact charges, very close charges, or nearby cased charges are so severe and destructive that fragment impact and/or airblast loads cannot be measured. Theoretical estimates of these loads cannot be verified. These loads in turn induce severe and rapidly changing stresses that cannot be measured. Theories on changes of stress waves cannot be verified. There is no information on the dynamic tensile strength of concrete at high strain rates caused by very close detonations or bomb fragment impacts. The few theoretical methods which the author found are limited to light to moderate bomb threats and are based upon several simplifying assumptions to make a solution possible. Since theoretical methods are so complicated and limited, empirical methods have been more popular. Empirical methods are faster and easier to use. However, there are some problems with empirical methods. Strain-rates are higher in small scale models than in a full scale structures while peak pressures are equal. Bomb fragment weight distributions do not scale the same as airblast so it is difficult to interpret scaled tests of concrete structures subjected to nearby cased bomb detonations. Field tests of concrete structures subjected to nearby detonations are expensive to conduct. Empirical prediction methods should be limited to scales and conditions similar to those under which the empirical data was collected.

There is a moderate amount of literature on spall. Reference 13 is a good reference on the basic theory of spall. Two good studies on spall of metals are reported in References 31 and 32. Several references contain empirical prediction methods for spall caused by a single projectile impact against concrete (References 5, 8, and 33 through 38). However, there are only a few references about spall of concrete structures caused by multiple bomb fragment impact and/or airblast loads for nearby bomb detonations. The next few paragraphs summarize the

principal theoretical and empirical prediction methods for spall of concrete structures subjected to nearby bare and cased bomb detonations.

Theoretical Spall Prediction Methods for Bare Charge Threats

C. A. Kot gives a method to predict spall in concrete walls under airblast loads in Reference 39. Kot assumes that the shape of the bomb is spherical; the stresses are below the dynamic compressive strength of the concrete (i.e., elastic); the stress wave keeps the same shape and duration as the incident airblast wave; the stress wave only changes by spherical divergence; the concrete is linearly elastic, the propagation velocity is constant; and the concrete will instantaneously spall once the peak net stress exceeds the dynamic tensile strength of the concrete. Kot approximates the airblast wave with the simple power law:

$$p(t) = p_a \left[1 - \left(\frac{t}{t_{dur}} \right)^\gamma \right] \quad (\text{eq 3.1})$$

where $p(t)$ is the pressure at a given time (t), p_a is the peak pressure at the back face, t_{dur} is the positive phase duration and γ is an exponent obtained from Figure 3.1. The equation for the n^{th} spall depth (d_n) caused by a stress wave at an angle of incidence of α is:

$$d_n = \frac{ct_{dur}}{2 \cos \alpha} \left\{ \left[(1 - |r|^n)^{1/\gamma} - (1 - |r|^{(n-1)})^{1/\gamma} \right] \left[1 + \frac{1}{1 - |r|} \frac{\sigma_{crit}}{p_a} \right]^{1/\gamma} \right\} \quad (\text{eq 3.2})$$

where n is the spall number, c is the propagation velocity, r is the coefficient of reflection, and all stresses are positive. The equation for the n^{th} spall velocity is:

$$v_n = \frac{2p_a \cos^2 \alpha}{(\gamma + 1) c_p} \left\{ (\gamma + |r|^\gamma) - \frac{(1 - |r|^\gamma) \sigma_{crit}}{(1 - |r|^\gamma) p_a} - \frac{\left[1 - |r| + \frac{\sigma_{crit}}{p_a} |r|^{(n-1)} \right]}{\frac{(1 - |r|^\gamma)^{1/\gamma}}{(1 - |r|^{n-1})^{-1}}} \right\} \quad (\text{eq 3.3})$$

Kot limits application of this prediction procedure to scaled standoff distances greater than $0.20 \text{ ft/lb}^{0.33}$ to insure the charge is not in contact with the concrete. No guidance is given on the dynamic tensile strength of concrete, but it is assumed that a 4,000-psi concrete has a dynamic tensile strength of 800 psi in an example. The same prediction method is given in Reference 40.

The assumptions that the stress waves are linearly elastic and only change by spherical divergence can result in incorrect predictions. There are many probable bomb threats which yield airblast loads above the dynamic compressive strength of the concrete and/or which diverge other than spherically.

Theoretical Spall Prediction Methods for Cased-Charge Threats

References 41 and 42 are the principal theoretical spall prediction methods for cased-charge threats.

C. E. Canada wrote Reference 41 for the U.S. Air Force. The prediction method is a computer program. The preferred lateral dimensions and thicknesses of concrete spall fragments are assumed to be equal to the spacing and concrete cover of the back layer of reinforcing bars, respectively. In other words, if spall occurs, it will form only along the reinforcing steel plane. The program calculates an average triangular blast load based upon blast data from References 7 and 40. The program calculates the bomb fragment characteristics based upon standard equations from References 7 and 8. Fragment loads are assumed to act simultaneously and with the same duration as the blast load. The computer program combines the blast and fragment loads linearly to form

a single triangular stress wave. The program calculates attenuation of the stress waves if the stresses are above the concrete strengths, but does not address other changes in the stress wave. Canada did not give guidance on determining the dynamic tensile strength of concrete, but assumed 14 percent of the unconfined compressive strength in an example. Figure 3.2 is a copy of a curve calculated for predicting the maximum standoff distance which spall will occur at a reinforcing steel plane 1.5 inches from the back free surface for a given dynamic tensile strength of concrete.

Major M. O. Kropatscheck describes a theoretical spall analysis used to analyze some of the test results in Reference 42. Triangular approximations of actual airblast measurements were used for the analysis, but the use of Reference 7 was recommended to determine airblast parameters for other threats. The bomb fragment characteristics were calculated using the standard equations in References 7 and 8. It was assumed that the velocities of the bomb fragments varied linearly from their striking velocities at the surface to zero at their penetration depths, in order to calculate durations of fragment loads. An average fragment load-history was calculated over an area. The airblast arrived at the structure before the bomb fragments in the tests, so spall was calculated using each load separately. Major Kropatscheck assumed the induced stresses reflected normally from the free surface, the duration of the stress waves did not change, and the stresses attenuated by 10 percent due to material properties and geometrical configurations. It was also assumed that the static tensile strength of concrete is 10 percent of the static uniaxial compressive strength, and for the loading rate of 10^8 psi/sec, the dynamic tensile strength is 350 percent of the static tensile strength. After the stress waves and concrete tensile strengths were determined, the spall depths were calculated using basic spall theory similar to that presented in the previous chapter. The results of this analysis are compared to the test results in Table 3.1.

Empirical Spall Prediction Methods for Bare Charge Threats

The Weapon Data Sheet 6A6 in the "Effects of Impact and Explosion" (Reference 33) is one of the original empirical prediction methods

for damage to reinforced concrete wall panels by nearby bare charge detonations in air. A copy of it is shown in Figure 3.3. It is based upon approximately 50 tests conducted during World War II. The tests were both model and full scale. The tests were on rectangular concrete test panels with face dimensions from 3 to 25 times their thickness. Various kinds of bare explosives were used. The charge weights varied from 0.08 to 1,700 lb. Test panels were supported along all four edges and results showed no appreciable difference between freely supported and fixed edges. The concrete compressive strength varied from 2,200 to 4,000 psi. Various steel reinforcing percentages were used. The curves are based upon data adjusted to TNT equivalent charges and 0.25 percent steel reinforcement. The slight damage curve defines the boundary between no damage and light cracking and average deflections less than 0.83 percent of the free span. The moderate damage curve defines the boundary between threshold spall and medium spall and deflections less than 4.17 percent of the free span. The heavy damage curve defines the boundary between medium and severe spall and average deflections less than 10 percent of the free span. The breach curve defines the boundary between severe spall and breaching or perforation. See Reference 43 for a more detailed report about the curves. Identical curves are also in Reference 44.

The only other set of empirical spall prediction curves found for bare charges is in recently published References 45 and 46. A copy of this set of curves is given in Figure 3.4. The curves are based upon 96 tests with various bare charges from 0.03 lb to 500.0 lb. The standoff distances varied from contact to 3.94 feet. The concrete test panels varied in wall thickness from 3.5 to 43.3 inches, static concrete compressive strengths from 2,900 to 7,977 psi, and reinforcing steel percentages from 0.64 to 1.91 percent. The minor damage zone defines the area of no damage to threshold spall. The spalling zone defines the area of light to severe spall. The perforation zone defines the area of breach or perforation.

Both sets of curves predict similar spall damage except for very small and very large scaled standoff distances. The first set of curves divides the degree of spall into slight, moderate, and heavy, whereas the second set has one large zone of spall. Test data from Reference 2

agree well with the curves.

Empirical Spall Prediction Methods for Cased Charge Threats

The Technical Manual 5-855-1 (Reference 34) has a short paragraph and a set of curves for predicting damage to reinforced concrete panels caused by nearby explosions in air. Figure 3.5 is a copy of the set of curves. It does not specifically state whether the curves are based upon bare or cased bomb threats. However, the curves predict worse damage than the curves for the bare charge surface threats previously discussed, and are assumed to be for cased bomb threats. Differences in concrete strength and reinforcing steel can be accounted for by multiplying the scaled distance by correction factors given with the curves. The zones of damage are defined in the figure.

Another set of empirical spall prediction curves for cased charge threats are in References 45 and 46. This is the same reference as for the curves for surface detonations of bare charges. A copy of the curves is shown in Figure 3.6. The curves are similar to those for the bare charges, but are higher and over a wider scaled distance range. The cased charge threats varied in weight from 0.45 to 48.5 lb and in standoff distance from contact to 16.4 ft. Charge to total bomb weight ratios ranged from 13 to 60 percent. The concrete walls varied in thickness from 4 to 47.24 inches, in strength from 2,900 to 7,977 psi, and in reinforcing steel from 0.64 to 1.91 percent. The effect of casing thickness or charge to total weight ratio was not well defined in the curves.

These two curves did not agree well on the prediction of breach and the effects of cased bombs at scaled standoffs greater than $2 \text{ ft/lb}^{.33}$. In addition, test data from References 1 and 2 did not agree with either curve. Additional tests were done to check the curves.

Table 3.1

Comparison of Calculations with Test Results of Reference 42

Test No.	TNT Equiv- alent Weight lb	Scaled Distance ft/lb ^{0.33}	Casing	Calculated Spall Depths		Actual Spall Depths inches
				Blast inches	Fragments inches	
1	76.23	1.16	uncased	1.88	--	3.9 to 4.7
2	66.14	1.21	uncased	--	--	No spall
3	66.14	1.21	cased	7.39	--	Breach
4	76.23	1.16	cased	6.51	4.44	3.9
5	15.76	1.16	cased	4.88	3.07	5.9
6	445.33	1.28	cased	16.27	12.20	3.9

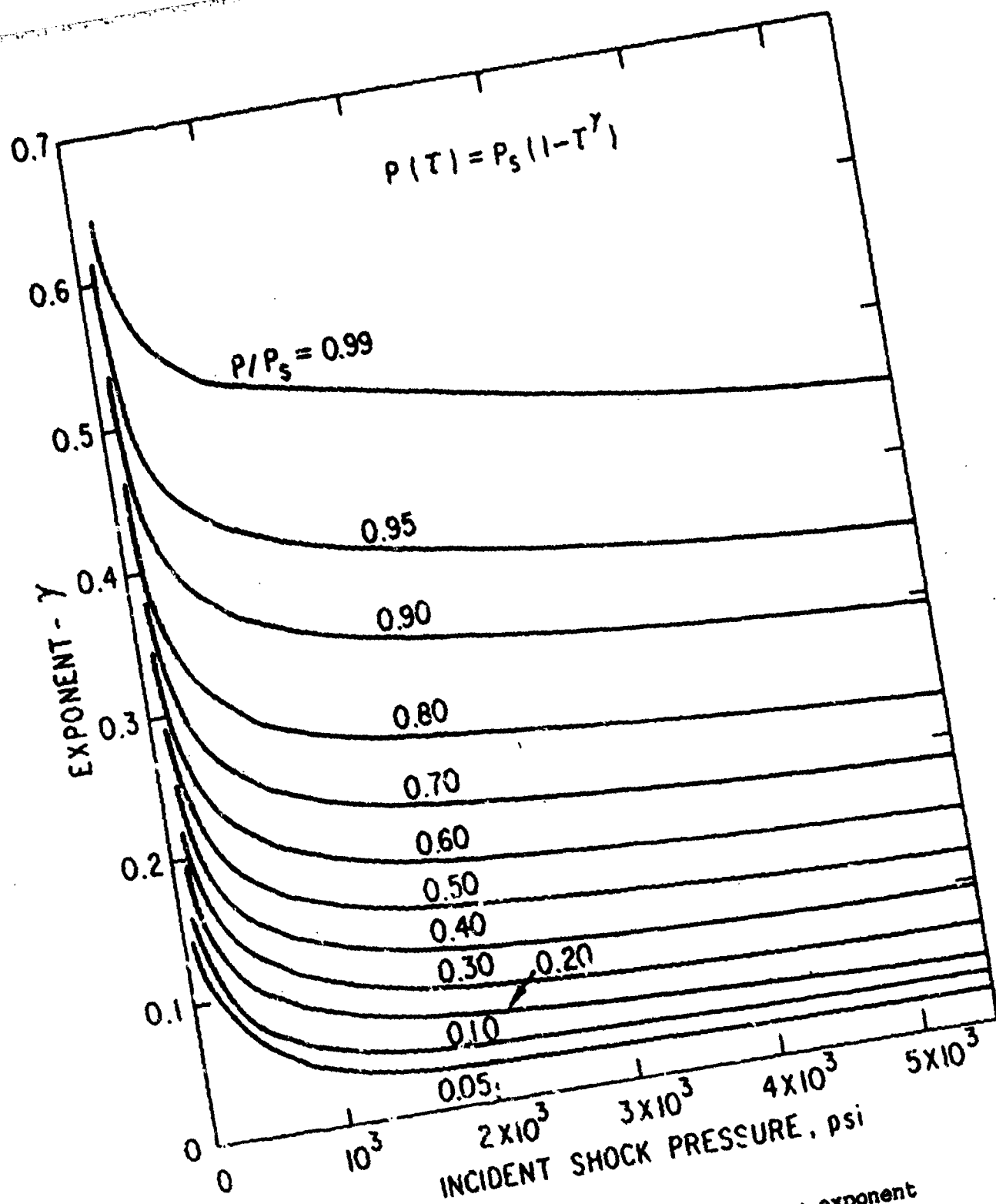


Figure 3.1. Variation of pressure wave form exponent (from Reference 39).

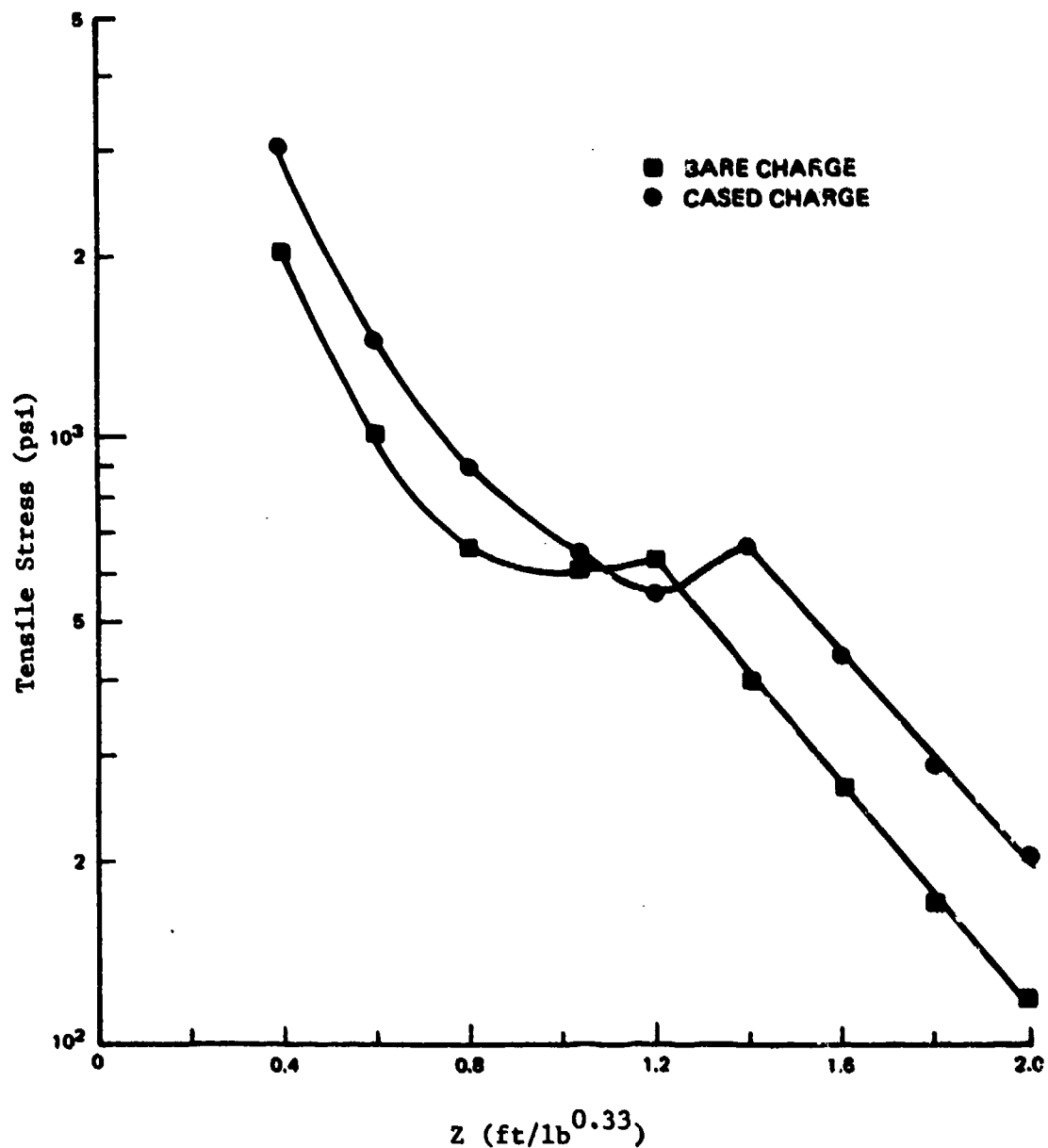
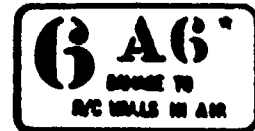


Figure 3.2. Tensile stress at prescribed spall plane for scaled standoff distances and geometries (from Reference 41).

DAMAGE TO REINFORCED CONCRETE WALL PANELS BY DETONATIONS IN AIR



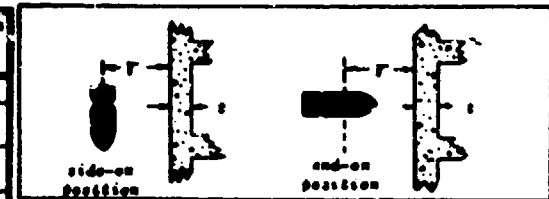
MINIMUM DISTANCE for indicated degree of damage, r in ft																		
WALL THICKNESS, t, ft	100-lb OF AN-FO			250-lb OF AN-FO			500-lb OF AN-FO			1000-lb OF AN-FO			2000-lb OF AN-FO			4000-lb OF TNT		
	MODERATE	HEAVY	BREACHING	MODERATE	HEAVY	BREACHING	MODERATE	HEAVY	BREACHING	MODERATE	HEAVY	BREACHING	MODERATE	HEAVY	BREACHING	MODERATE	HEAVY	BREACHING
1	2.1	2.2	1.2	2.4	2.5	1.3	2.7	2.8	1.4	3.0	3.1	1.5	3.3	3.4	1.6	3.6	3.7	1.7
2	1.5	1.6	0.9	1.7	1.8	0.7	1.9	2.0	1.0	2.1	2.2	1.1	2.3	2.4	1.2	2.5	2.6	1.3
3	1.1	1.2	0.7	1.3	1.4	0.5	1.5	1.6	0.8	1.7	1.8	0.9	1.9	2.0	1.0	2.1	2.2	1.1
4	0.9	1.0	0.6	1.1	1.2	0.4	1.3	1.4	0.7	1.5	1.6	0.8	1.7	1.8	0.9	1.9	2.0	1.0
5	0.8	0.9	0.5	1.0	1.1	0.3	1.2	1.3	0.6	1.4	1.5	0.7	1.6	1.7	0.8	1.8	1.9	0.9
6	0.7	0.8	0.4	0.9	1.0	0.3	1.1	1.2	0.5	1.3	1.4	0.6	1.5	1.6	0.7	1.7	1.8	0.8
8	0.6	0.7	0.3	0.8	0.9	0.2	1.0	1.1	0.4	1.2	1.3	0.5	1.4	1.5	0.6	1.6	1.7	0.7
10	0.5	0.6	0.2	0.7	0.8	0.2	0.9	1.0	0.3	1.1	1.2	0.4	1.3	1.4	0.5	1.5	1.6	0.6

The bombing efficacy is $\frac{W}{A}$ where W is the area in square feet within which any walls present will be damaged, and W is the weight of explosive charge in the bomb, in pounds. For area bombing of reinforced concrete walls the efficacy increases with the charge weight, so the various damage per pound of explosive will be attained by use of the bomb with the largest possible charge.

Similar reasoning shows that for area bombing of very long narrow targets having reinforced concrete walls, the bomb with the largest possible charge gives the greatest expectation of damage per pound of explosive.

DAMAGE CRITERIA ADOPTED:

DESCRIPTION OF DAMAGE	TYPE OF DAMAGE	Average Deflection, in.
SLIGHT	Slight Cracking and Bonding	0.1
MODERATE	Light Puncturing and Cracking with Possibly Some Spalling	0.5
HEAVY	Heavy Puncturing, Shattering, or Possible Perforation	1.2
BREACHING	Perforation with Extensive Scabbing. Bars May Be Bent or Bulged.	---



For contact and very near contact shots, end-on position of a bomb will cause less damage than side-on. Figures given correspond to side-on position; the bomb detonating not far from point opposite center of wall. Positions appreciably offside usually result in lessened damage.

The table gives min. distance at which an air-backed reinforced concrete wall or wall panel that will experience various degrees of damage due to explosion of TNT-filled bombs in air nearby or in side-on contact with the wall.

These data derive from tests, both model and full scale, on rectangular panels with face dimensions from 2 to 25 times the thickness. Charges used in tests ranged from about 1 lb. wt. to 1700 lb. Test panels were supported along all four edges, and results showed no appreciable difference between freely supported and fixed edges.

Tests involved various degrees of reinforcing and different explosives, but all data were reduced to a basis of 45 steel by volume and bombs filled TNT. Degree of damage and ratio of central deflection to span correlate fairly well for slight, moderate and heavy damage.

Tabulated data refer to about 45 reinforcing steel by volume. For 45 steel, multiply thickness values by 0.9 for breaching and by 0.7 for other degrees of damage.

Fragments from nearby bomb detonations usually cause surface scars and a few perforations; this type of damage is not included in the present analysis.

The graph gives damage curves in terms of scale variables $r/W^{1/3}$ and $t/W^{1/3}$, where t wall thickness (ft), r distance from wall to bomb (ft) and W weight of charge (lb).

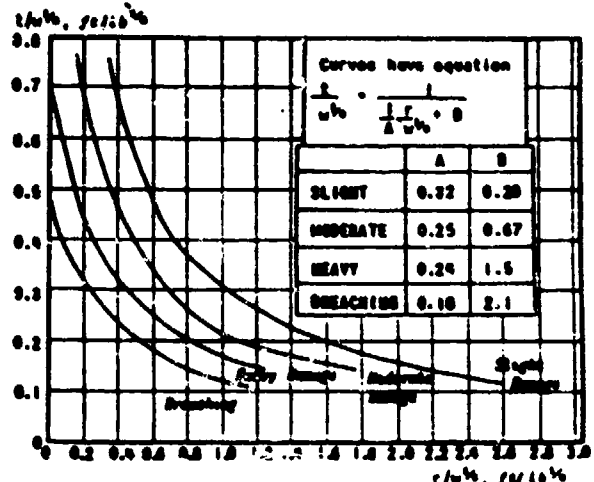


Figure 3.3. Damage prediction curves from Reference 33.

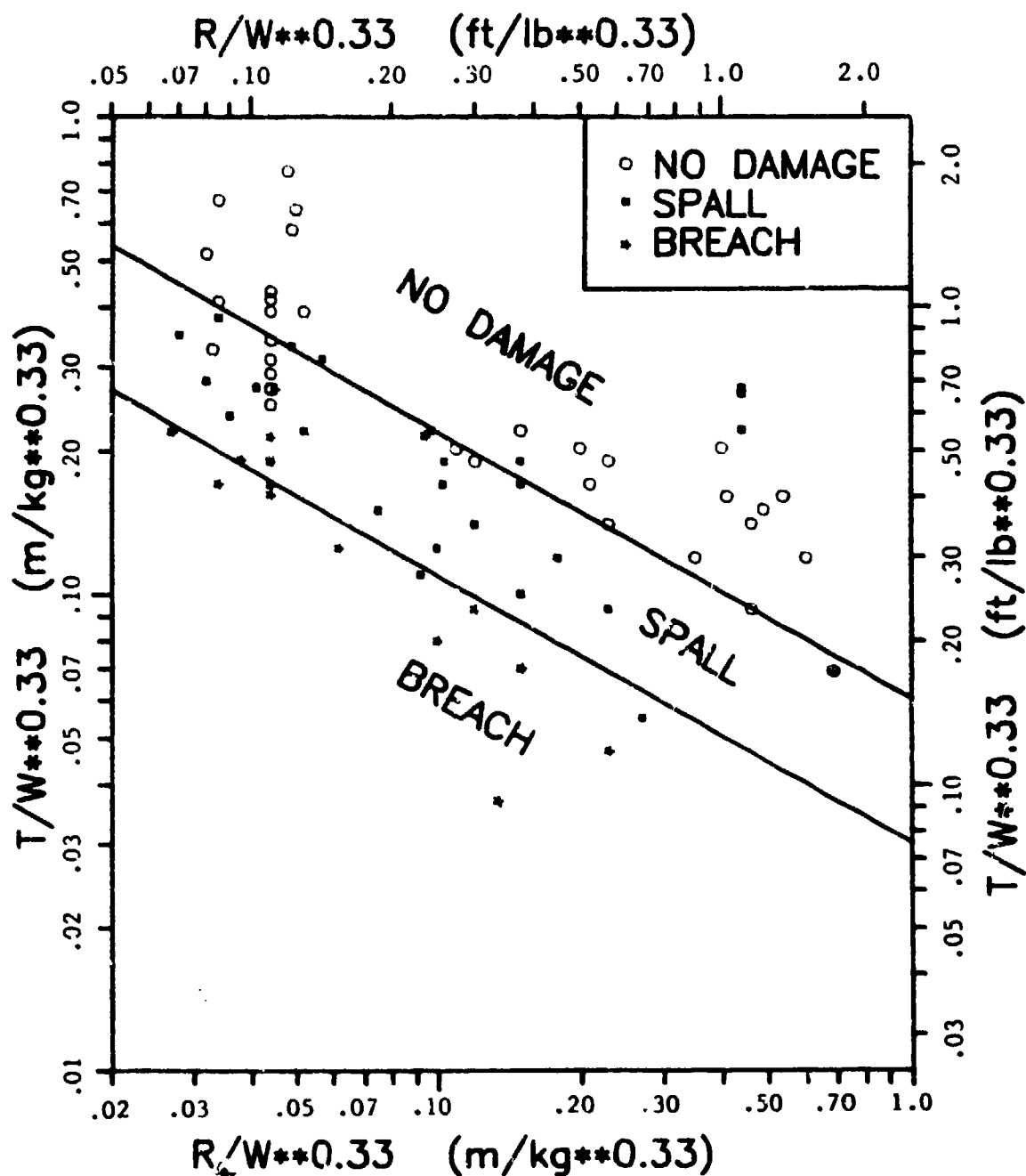
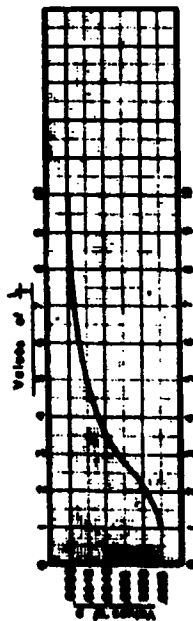
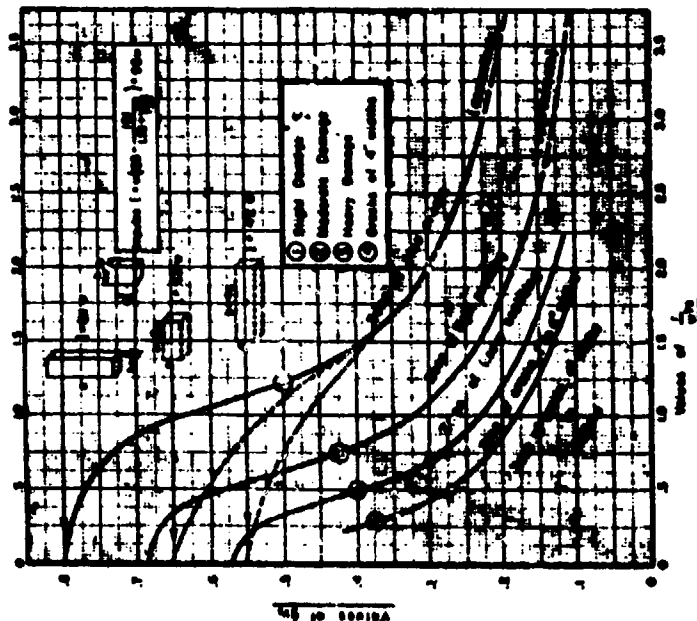


Figure 3.4. Empirical prediction curves from Reference 45 for damage to reinforced concrete panels subjected to nearby charge detonations.

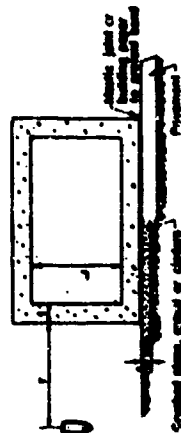
THE FOLLOWING EXAMPLES ILLUSTRATE THE USE OF THE CHARTS:



OPTIMUM RATIO OF EFFECTIVE TENSILE REINFORCEMENT



NOTE: The analysis for charts and illustrated examples are based on ζ (ultimate strength of concrete) = 4000 lbs. p.s.i. in cases where ζ is less than 4000 lbs. p.s.i., the value of ζ shall be multiplied by the correction factor $(\frac{\zeta}{4000})^{1/4}$.



Example No. 1: 0.2 for $\zeta_n < 3.0 \leq w < 8000$ lbs.

EXAMPLE NO. 1 - WALL DESIGN:

DESIGN:

1. 500 lb. G.P. Bars $w = 266$ lbs.
2. Distance $r = 15$ ft.
3. Clear span of wall $L = 6.9$ ft.

REQUIREMENTS (Per Seismic Damage):

1. Wall thickness
2. Optimum ratio of tensile reinforcing, p

SOLUTION:

1. Determine value of ζ_n
 $\zeta_n = \frac{r}{L} = \frac{15}{6.9} = 2.2$
2. Determine value of ζ_n and compute value of ζ : Enter value of $\zeta_n = 2.2$ and read value of $\zeta = 2.7$ from curve ①
 $\zeta_n = 2.7; 1.47 \times 0.40 = 0.59 \times 0.21$ inches
3. Determine value of ζ
Value of $\zeta = \frac{0.59}{0.21} = 2.83$
Enter value of $\zeta = 2.83$ and read value of $p = 0.0045$

EXAMPLE NO. 2 - WALL ANALYSIS:

DESIGN:

1. Wall thickness $t = 2.50$ ft.
2. Clear span $L = 6.5$ ft.
3. Ratio of tensile reinforcement, $p = 0.004$

REQUIREMENTS:

1. The optimum ζ_n for various degrees of damage from 1000 lb. G.P. Bars $w = 266$ lbs.

SOLUTION:

1. Determine the value of ζ_n
 $\zeta_n = \frac{r}{L} = \frac{6.5}{2.5} = 2.6$
2. Determine the value of ζ_n and compute the value of ζ : Enter value of $\zeta_n = 2.6$ and read value of ζ from curves 4, 3, 2, and 1.
For Grade of 4' walls: $\zeta_n = 4.0; r = 40 \times 0.07 = 3.2$
For Heavy Damage: $\zeta_n = 3.7; r = 37 \times 0.07 = 2.6$
For Moderate Damage: $\zeta_n = 3.0; r = 30 \times 0.07 = 2.1$
For Seismic Damage: $\zeta_n = 2.7; r = 27 \times 0.07 = 1.9$
3. Determine optimum ratio of tensile reinforcement p :
Enter value of $\zeta_n = 2.6$ and read value of $p = 0.0039$
Since the ratio of steel provided is greater than the optimum ratio of tensile reinforcement, the above distances are applicable.
It seems when the percentage of steel varies from the optimum p , the value of ζ_n should be multiplied by the correction factor:
$$\left(\frac{p}{p_{\text{optimum}}} \right)^{1/4}$$

Figure 3.5. Required thickness of reinforced concrete slabs to resist explosions in air, Ref. 34.

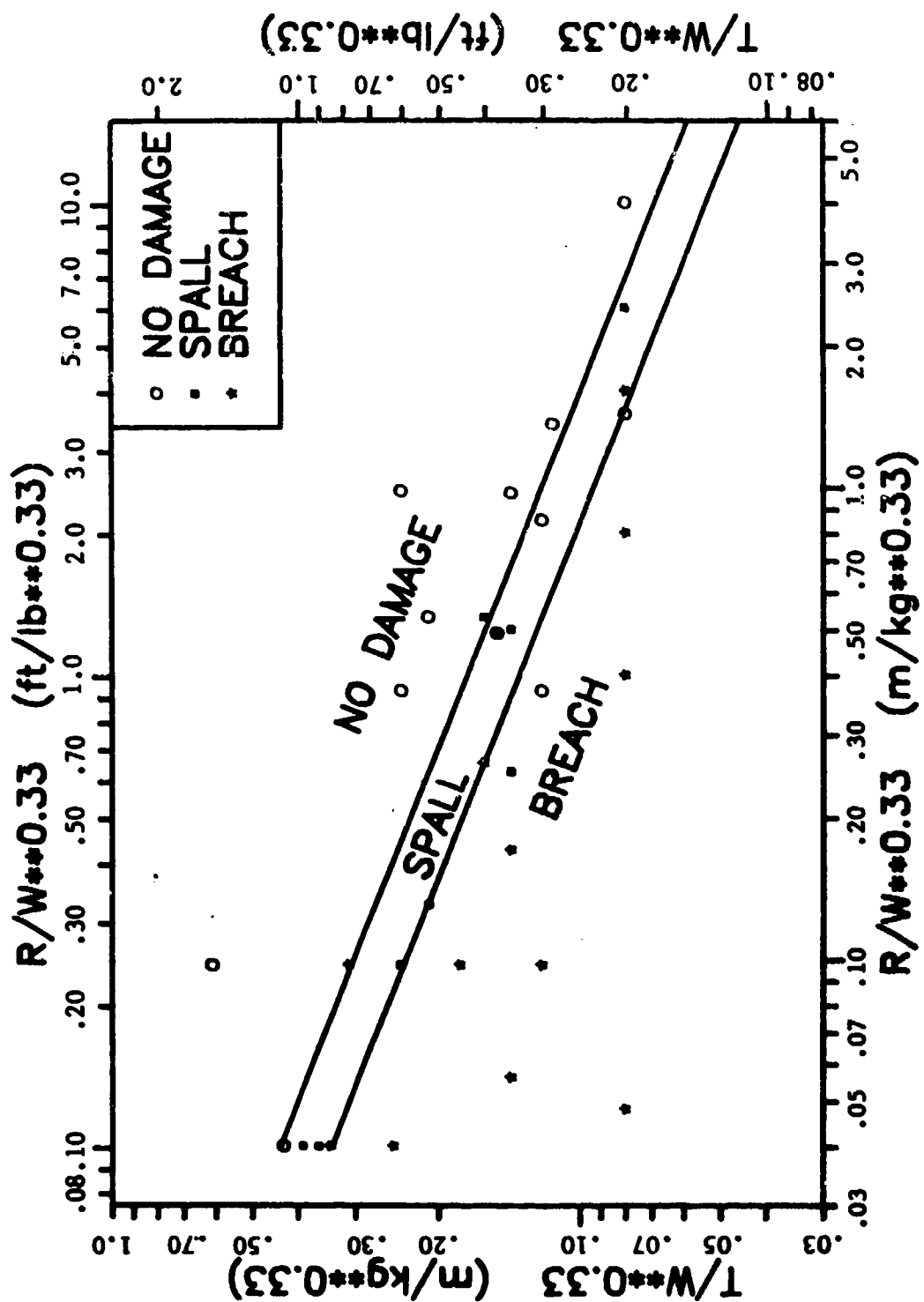


Figure 3.6. Empirical prediction curves from Reference 45 for damage to reinforced concrete panels subjected to nearby charge detonations.

PART IV: EXPERIMENTS

Concrete Spall Tests

Forty spall tests were conducted to investigate parameters which were suspected to affect spall, to check existing prediction methods, to take actual measurements of damage, and to provide additional data to refine prediction methods. The parameters which were investigated are:

- a. Scaled standoff distances (λ) which directly affect peak pressure. λ was varied from 0.076 ft/lb^{0.33} to 1.85 ft/lb^{0.33}.
- b. Charge weight, (W) and standoff distance, (R) for a given λ which affect the duration and shape of the load histories. The bomb sizes were varied from 1.47 to 40.30 lb equivalent TNT and the standoff distances were varied from contact to 60 inches.
- c. Casing thickness. The casing thicknesses were varied from no casings to thin casings (0.088 inches thick) to thick casings (0.344 inches) for the same size bombs.
- d. Concrete wall thickness (T). Similar tests were conducted on three different wall thicknesses: 5.375, 8.50, and 11.20 inches thick.
- e. Concrete strengths (f'_c). Similar tests were conducted on walls of normal 4,000-psi concrete and high-strength 13,815-psi concrete. The tensile strength of concrete increases with an increase in compressive strength.
- f. Concrete additives. Similar tests were conducted on normal 4,000-psi concrete, similar concrete with acrylic latex added to it, and similar concrete with crimped steel fibers. Both the acrylic latex and the steel fiber additives make concrete more ductile.
- g. Spacing of reinforcing steel bars (rebars). Similar tests were conducted on similar walls with rebar spacings of 5.50 inches and with rebar spacings of 1.50 inches center to center.

The experiments are described in detail below.

Test Structures

The 40 tests were conducted on 10 reinforced concrete wall panels and the walls of a large reinforced concrete box. The first 29 tests were conducted on the 10 reinforced concrete walls, each which were mounted on the side of a rectangular box reaction structure (Figure 4.1). The last 11 tests were conducted on the walls of a large

reinforced concrete structure left from another study. The roof of the box structure had been damaged during another study, but the walls were only damaged near the roof (Figure 4.2). The spall tests were conducted on the lower portions of the walls with surface detonations. Since spall is an early-time localized phenomenon, the author believes the roof damage from the previous study had no adverse effect on the spall tests. The walls are described in general in the next two of paragraphs and specific details for each wall are presented in Table 4.1.

The 10 reinforced concrete wall panels were all 15-ft long and 5.43-ft tall. Wall thickness, concrete properties, and spacing of the reinforcing steel were varied in some of the wall panels to determine their effects on spall (Table 4.1). All of the wall panels had 0.25 percent principal (vertical) reinforcing steel and 0.10 percent temperature (longitudinal) reinforcing steel per face. Plans of the reinforcement layouts for the various wall panels are shown in Figures 4.3 through 4.5. The shear stirrups hooked around the outsides of both reinforcing steel mats. The stirrups were staggered or offset by 1/2 spacings in each vertical row. Pictures of typical reinforcing steel mats are shown in Figures 4.6 through 4.8. Each wall panel had rows of bolt holes 4.875 inches from the top and the bottom edges in order to attach it to the reaction structure. The free span of each wall after it was mounted was 3.60 ft. The wall panels were cast at WES and transported to Fort Polk, LA, for testing.

The large reinforced concrete box was 33.87 ft long by 9.87 ft wide by 9.87 ft tall. The walls had an 8-foot clear span and were all 11.20 inches thick. The principal reinforcing steel was 1.0 percent in both faces. A layout of the reinforcing steel is shown in Figure 4.9.

Concrete Properties

The average properties of the concrete in each of the wall panels and in the box structure are given in Table 4.2. The average concrete properties for a particular wall were measured during the same days that field tests were conducted on that wall. The concretes in wall panels 1 through 4 and 8 through 10 were all made according to the same 4,000-psi mix design. The 4,000 psi mix design was 500 lb/yd³ of Type I portland

cement, 335 lb/yd³ of water, 1,582.2 lb/yd³ of 3/8-inch maximum crushed limestone aggregate (with 0.55 percent moisture) and 1634.9 lb/yd³ of manufactured limestone sand (with 0.66 percent moisture). The unconfined uniaxial compressive strengths were all above 4,000 psi, which is common because most mix designs are slightly over-designed to insure fluctuations in strength do not drop below the design strength. However, in spite of careful measuring, mixing, placement and curing, the strengths varied. The variations are attributed to testing at different ages and casting the concrete under different weather conditions.

The concrete in wall panel 5 was a high-strength concrete. It had a mix design of 850 lb/yd³ Type I portland cement, 150 lb/yd³ silica fume, 270 lb/yd³ of water, 995 lb/yd³ of 3/8-inch maximum crushed limestone aggregate (with 0.55 percent moisture), and 1,820 lb/yd³ of manufactured limestone sand (with a 0.66 percent moisture). The materials came from the same sources as those for the 4,000-psi concrete. Notice that the high-strength concrete had a uniaxial compressive strength almost 3 times and a split tensile strength almost 2 times those of the 4,000-psi concrete.

The concrete in wall panel 6 was similar to the 4,000-psi concrete, but was modified with an acrylic latex additive and adjusted to have a similar uniaxial compressive strength. The mix design of the acrylic concrete was 600 lb/yd³ of Type I portland cement, 126.6 lb/yd³ of water, 191.7 lb/yd³ of Rohm-Haas MC-76 acrylic latex (which is 47 percent solids so it contained 101.6 lb/yd³ of water), 1,993.7 lb/yd³ of 3/8-inch maximum crushed limestone aggregate (with 0.64 percent moisture), 1,581.1 lb/yd³ of manufactured limestone sand (with 0.89 percent moisture), and 1.9 lb/yd³ of anti-foam B. Addition of the acrylic latex to concrete slightly lowers the compressive strength. Therefore, the water to cement ratio was reduced to make a concrete with a compressive strength similar to the 4,000-psi concrete. The cement, aggregate and sand came from the same sources as for those in the other concretes in the wall panels.

The concrete in wall panel 7 was similar to the 4,000-psi concrete except it had crimped steel fibers added to it. The design mix for the fiber concrete was 470 lb/yd³ of Type I portland cement, 50 lb/yd³ of fly ash, 312 lb/yd³ of water, 1,697.3 lb/yd³ of 3/8-inch maximum crushed

limestone aggregate (with 0.29 percent moisture), 1444.8 lb/yd³ of manufactured limestone sand (with 0.38 percent moisture), 80 lb/yd³ of Dramix ZP 30/0.5 crimped steel fibers, and 31.2 ounces/yd³ of WRA plasticizer. The cement, aggregate and sand came from the same sources as for the other concrete in wall panels. The steel fibers were glued together in clips of up to 30 individual fibers. The glue broke down in the wet concrete mix allowing the individual fibers to disperse in the concrete matrix. Crimped steel fibers bond to the concrete better than plain fibers so fewer fibers were required. The fibers have a minimum tensile strength of 170,000 psi.

The concrete in the box structure was obtained from a local ready-mix concrete company near Fort Polk, Louisiana. The cement was Type I portland cement. The fine aggregate was a natural siliceous sand and the coarse aggregate was a natural gravel. No further details of the mix design were obtained.

Reinforcing Steel Yield Stresses

The reinforcing steel average yield stresses are given in Table 4.3. The reinforcing steel below size No. 3 were especially made for model structures. The model steel was deformed steel wire annealed to yield stresses similar to those of the normal size commercial Grade 60 reinforcing steel. The names of deformed wire start with a "D" and are followed by the cross-sectional area in hundredths of inches.

Reaction Structure

The 10 wall panels were mounted on a reaction structure (Figure 4.1). The reaction structure is a heavily reinforced rectangular concrete box with one open side to which the test slabs were attached (Figure 4.10). The open side of the reaction structure had a 5/8-inch-thick steel plate on its face for a hard smooth bearing surface for a wall panel. The wall panels were attached to the reaction structure with rows of 1-inch-diameter bolts along the open edges of the roof and floor. Both rows of bolts were 4.875 inches from the outside edges, and were 9-inches on center. A high-strength, quick-setting grout was

poured between each wall panel and the reaction structure before the bolts were securely tightened to insure good contact. The tests were conducted in a large pit in the ground to retain most of the bomb fragments at the test site. The back side of the reaction structure was placed against a side of the pit to minimize rigid-body translation and rotation. The bottoms of the reaction structure and wall panels were recessed 11 inches into the soil to make the inside floor of the reaction structure even with the ground level in the pit. This simulated common aboveground protective structures.

Explosive Charge Parameters

The explosive charge parameters are listed in Table 4.4. The standoff distances were the shortest distances from the centers of the bombs to the fronts of the walls. Standoff distances for contact charges were simply one-half of the outside diameter of the charge.

All of the explosive charges were made of Composition 4 (C-4) explosive. The equivalent TNT weights were calculated using the equivalent weight factor for peak pressure of 1.37 lb of TNT/1.00 lb of C-4 (see Table 2.1). The height to inside diameter ratios were all approximately 3 to 1. The bare charges were made by packing C-4 into cylindrical molds and then removing the molds. Figure 4.11 is a picture of one of the bare charges. The cased charges were made by packing C-4 into steel cylinder casings. Figure 4.12 is a picture of one of the cased charges. The steel casings were made from cold-drawn seamless mechanical tubings made of 1026 steel. The mechanical tubings were ordered close to the desired diameters and then machined to the proper dimensions. The thicknesses of the casings were varied to determine the effect of casing thickness on spall. The end caps on the cased bombs were all 1/4-inch mild steel. Notice that tests 1B and 4B and tests 1D and 3A have the same scaled standoffs ($R/W^{0.33}$) but different standoffs and explosive weights.

Measurements

Active measurements, passive measurements, and high-speed motion

pictures were taken during the first 29 tests, i.e., on the wall panels. There was no instrumentation or high-speed photography in the last 11 tests, i.e., the tests on the walls of the box structures. Posttest measurements of any damage to a wall were taken.

A typical layout of the active instrumentation for one of the wall panels is shown in Figure 4.13. (Note in Tests 3B, 4B, and 9B the "S" spacings were 9.5, 6, and 6 inches, respectively.) Two to four tests were conducted on each wall depending upon the area of damage caused by each test. The tests at the quarter points of the wall panels were with bombs at standoff distances and the tests at the centers of the wall panels were with either contact charges or thick-cased bombs. All of the tests at the quarter points had active measurements of the free-field pressure, pressure distribution on the wall, stresses in the wall, strains of the reinforcing steel, accelerations, displacements, and high-speed photography of the wall velocities. All of the tests at the centers of the wall panels only had active measurements of the stresses in the wall and high-speed motion pictures of the spall velocities.

All of the airblast pressure gages were Kulite Model HKS-375 in peak pressure sizes of 5,000 to 30,000 psi. The size of the gage used depended upon its position and the test. All of the pressure gages in the wall panels were mounted flush with the wall front and the free-field pressure gages were mounted flush with the ground surface. Figure 4.14 is a picture of the airblast pressure gage mounts installed in the reinforcing grid at the proper spacings. No protective baffles were used in front of the gages to insure that the high-pressure spikes were not filtered. The pressure gages in the wall panels were spaced in an array to one side of a quarter line. It was assumed that the wall panels were loaded symmetrically on either side of a quarter line. The spacings in a pressure gage array were related to the standoff distance from the bomb and geometry of the wall. According to Reference 7, an average pressure-time curve may be constructed using average values of the loading over a length $1.3 R$ but not greater than the width or 2 times the height of the wall. The pressure gages with a name ending in 0 are along a quarter line of the wall. The spacings of the columns of pressure gages with names ending in 1, 2, and 3, are $1.3 R/4$, $1.3 R/2$ and $1.3 R$ from the quarter points, respectively. The spacings of the

rows of pressure gages with names PB (bottom), PQ (quarter), PM (mid height), and PT (top) are 1 inch from the ground, 1.3 R/4 from the bottom row, the midheight of the wall, and 1 inch below the ceiling, respectively. No PB1 gages were installed for tests with cased charges and no PB gages were installed after test 3A because of the high destruction rate of gages in these positions. The free-field pressure gages were on the opposite side of a bomb from the wall and at the same standoff distance as the wall.

The stress gages were Dynasen Mini-Flat Packs (FP), Model C300-50-125CRS-WES. A stress gage was cast in the midplane inside the wall panel at each test location. The sensor portion of a stress gage was placed even with the height of the PQ0 pressure gage at each quarter point testing location, and 3 inches from the ground at each center test location. Figure 4.14 shows a stress gage installed in the reinforcing grid at the proper location for a quarter point test. Most of the stress gages were powered with 40 milliamps constant current excitation with a 400 ohm bridge. The stress gages of tests 1B and 10C were powered with a pulse power supply.

All the accelerometers were Endevco Model 2264A with ranges of 2,000 to 50,000 g's, depending upon the location of the gage and test. The accelerometers were placed at the midpoints of the ceiling (AR_), floor (AF_), and back of the wall panels at the quarter test locations (AWHM). The accelerometers which measured horizontal accelerations had an "H" in their name and those that measured vertical accelerations had a "V" in their name. The gages were mounted on small aluminum cubes attached to bolts cast in the concrete at the proper locations.

Micro-Measurements Model EA-06-250-BF-250-W, single axis, metal film strain gages were mounted on the inside (EI) and outside (EO) reinforcing steel bars at the quarter lines. The bottom pairs of strain gages (E_B) were mounted 1 inch above the ground level, the middle pairs (E_M) were mounted at midheight of the wall panels, and the top pairs (E_T) were mounted 1 inch below the ceiling.

An active and passive deflection gage were used to measure the deflection of the midheight of the wall panels at the quarter point test locations. The active gage was Celesco Model No. PT-101-10A-7556 "yo-yo" gage. The passive gage was a scratch type of gage.

The active instrumentation was connected to instrumentation equipment and recording devices in a trailer approximately 750 feet from the test pit. Up to 30 channels were recorded on a Sangamo Model III, 32-channel FM magnetic tape recorder. The data were recorded at tape speeds of 120 inches/second and later digitized at 200 KHz. A zero-time and time channel were recorded during each test to establish a common time reference for the test data. An aluminum wire screen (with holes cut out at the pressure gage locations) was taped to the front of the wall panels, starting with test 5A, to reduce the noise by acting as a Faraday Shield.

The response of the back of a wall panel to a test was photographed with a high-speed motion camera mounted inside the reaction structure. The responses of the wall panels in the first 9 tests were photographed by a Model 164 PHOTEC 16-mm high-speed motion picture camera manufactured by Photonics Systems, Inc. The frame rates for these tests were 1,000 frames per second. The responses of the wall panels in the 10th through the 29th tests were photographed with a Lowcam. The frame rates for these tests were 500 frames per second. Black lines were painted every 6 inches along the floor at the test centerline to provide a reference for measuring velocities and displacements.

Nine of the wall panels were cut along the vertical centerlines of each tested area in order to measure the depths of cracks, damaged concrete, and spall. Wall 2 was damaged by additional trial explosive tests and was not cut.

Test Procedure

Two to four tests were conducted on each wall panel and the last eleven tests were conducted at different locations along the sides of the box structure. The number of tests conducted on a wall panel depended upon the area of damage caused by the tests on that panel. The "A" tests were always conducted at the left quarter point, the "B" tests were always conducted at the right quarter points, and the "C" tests were always conducted at the center of each wall panel. The "D" tests were conducted at one of the quarter points if there was no damage caused by the previous test at that location. Each of the first

caused by the previous test at that location. Each of the first 29 tests were done according to the following procedures:

- a. A wall was bolted to the side of the reaction structure and high-strength grout was poured into any cracks between the wall and the reaction structure.
- b. Instrumentation was installed and calibrated.
- c. The high-speed camera was placed in a safe place inside the reaction structure and prepared for a test.
- d. A wire screen was taped to the front of the wall to act as a Faraday Shield (started after test 5A).
- e. The charge was placed and armed.
- f. The instrumentation was checked and then calibration steps were recorded.
- g. A countdown was initiated, the recording started, the camera started, and then the bomb was detonated.
- h. Still photographs and videos were taken of the damage.
- i. Measurements of the damage were taken.

A similar procedure was followed for the tests on the walls of the box structure, except there were no steps involving the installation of walls, instrumentation, and high-speed photography.

THIS
PAGE
IS
MISSING
IN
ORIGINAL
DOCUMENT

Table 4.2
Average Concrete Properties

Wall No.	Concrete Type	Uniaxial Compressive Strength "f _c ", psi	Uniaxial Modulus of Elasticity "E", psi	Poisson's Ratio "ν"	Split Tensile Strength "f _t ", psi	Propagation Velocity "C", ft/sec	Age when Tested days
1	4,000	5,010	4.8 × 10 ⁶	0.20	578	12,150	59
2	4,000	5,085	4.86 × 10 ⁶	0.17	595	12,120	64
3	4,000	4,980	4.95 × 10 ⁶	0.14	560	14,166	75
4	4,000	5,290	4.85 × 10 ⁶	0.18	440	14,285	105
5	High strength	13,815	6.00 × 10 ⁶	0.20	925	16,250	115
6	Acrylic latex	4,605	4.60 × 10 ⁶	0.17	485	15,260	102
7	Steel fiber	5,050	4.70 × 10 ⁶	0.36	470	12,200	126
8	4,000	4,140	4.60 × 10 ⁶	0.20	400	12,000	100
9	4,000	4,940	4.81 × 10 ⁶	0.18	520	12,150	111
10	4,000	4,320	4.50 × 10 ⁶	0.18	430	12,000	109
Box	4,000	5,100					~1 year

Table 4.1
Wall Parameters

Wall No.	Thickness "T" in.	Concrete Type	Principal Steel # - in.	Horizontal Steel # - in.	Stirrups Size - Vert. x Hor. Space # - in. x in.
1	8.50	4,000	#3 @ 5.50	#2 @ 5.50	D2.5 @ 5.50 x 5.50
2	8.50	4,000	#3 @ 5.50	#2 @ 5.50	D2.5 @ 5.50 x 5.50
3	8.50	4,000	#3 @ 5.50	#2 @ 5.50	D2.5 @ 5.50 x 5.50
4	8.50	4,000	#3 @ 5.50	#2 @ 5.50	D2.5 @ 5.50 x 5.50
5	8.50	High strength	#3 @ 5.50	#2 @ 5.50	D2.5 @ 5.50 x 5.50
6	8.50	Acrylic latex	#3 @ 5.50	#2 @ 5.50	D2.5 @ 5.50 x 5.50
7	8.50	Steel fiber	#3 @ 5.50	#2 @ 5.50	D2.5 @ 5.50 x 5.50
8	5.38	4,000	#2 @ 4.13	D2.5 @ 4.50	D2 @ 4.50 x 4.13
9	5.38	4,000	#2 @ 4.13	D2.5 @ 4.50	D2 @ 4.50 x 4.13
10	8.50	4,000	D3 @ 1.50	D1 @ 1.25	D1 @ 5.00 x 1.50
Box	11.20	4,000	#8 @ 8.00	#6 @ 8.00	2 x #6 @ 8.00 x 6.00

Table 4.3
Reinforcing Steel Average Yield Stresses

Wall No.	Principal Steel			Horizontal Steel			Stirrups		
	Size	Area in. ²	Yield psi	Size	Area in. ²	Yield psi	Size	Area in. ²	Yield psi
1	#3	0.11	68,725	#2	0.049	70,585	D2.5	0.025	60,730
2	#3	0.11	68,725	#2	0.049	70,585	D2.5	0.025	60,730
3	#3	0.11	68,725	#2	0.049	70,585	D2.5	0.025	60,730
4	#3	0.11	68,725	#2	0.049	70,585	D2.5	0.025	60,730
5	#3	0.11	68,725	#2	0.049	70,585	D2.5	0.025	60,730
6	#3	0.11	68,725	#2	0.049	70,585	D2.5	0.025	60,730
7	#3	0.11	68,725	#2	0.049	70,585	D2.5	0.025	60,730
8	#2	0.049	70,585	D2.5	0.025	60,730	D2	0.020	67,875
9	#2	0.049	70,585	D2.5	0.025	60,730	D2	0.020	67,125
10	D3	0.030	56,200	D1	0.010	57,830	D1	0.010	66,000
Box	#8	0.790	68,550	#6	0.440	63,340	#6	0.440	63,340

Table 4.4
Explosive Charge Parameters

Test Wall- Shot	Standoff R feet	C-4 Weight lb	Equivalent TNT Weight "W", lb	Bomb Size I.D. x Height in. x in.	Casing Thickness in.	R/W 0.33 ft/lb 0.33
1A	1.541	3.626	4.968	3.00 x 9.00	Bare	0.903
1B	1.541	3.626	4.968	3.00 x 9.00	0.070	0.903
1C	Contact	1.074	1.478	2.00 x 6.00	Bare	0.073
1D	1.541	7.442	10.195	3.81 x 11.44	Bare	0.711
2A	1.541	4.700	6.439	3.25 x 9.75	Bare	0.829
2B	1.541	5.455	7.473	3.75 x 8.69	0.088	0.788
2C	Contact	1.074	1.412	2.00 x 6.00	0.047	0.077
2D	1.541	5.455	7.473	3.44 x 10.31	Bare	0.788
3A	2.438	29.410	40.295	6.00 x 18.25	Bare	0.711
3B	1.541	7.082	9.702	3.75 x 11.25	0.088	0.723
4A	5.000	14.393	19.719	4.75 x 14.25	0.111	1.851
4B	2.438	14.393	19.719	4.75 x 14.25	0.111	0.902
5A	1.541	7.082	9.702	3.75 x 11.25	0.088	0.723
5B	1.541	3.626	4.968	3.00 x 9.00	0.070	0.903
5C	Contact	1.074	1.472	2.00 x 6.00	0.047	0.077
6A	1.541	7.082	9.702	3.75 x 11.25	0.088	0.723
6B	1.541	3.626	4.968	3.00 x 9.00	0.070	0.903
6C	Contact	1.074	1.472	2.00 x 6.00	0.047	0.077
7A	1.541	7.082	9.702	3.75 x 11.25	0.088	0.723
7B	2.438	14.393	19.719	4.75 x 14.25	0.111	0.903
7C	Contact	1.074	1.472	2.00 x 6.00	0.047	0.077
8A	1.541	1.661	2.275	2.31 x 6.94	0.054	1.172
8B	1.541	3.626	4.968	3.00 x 9.00	0.070	0.903
8C	1.541	3.626	4.968	3.03 x 9.00	0.219	0.903
9A	5.000	14.393	19.719	4.75 x 14.25	0.111	1.851
9B	0.948	1.661	2.275	2.31 x 6.94	0.054	0.721
10A	2.438	14.393	19.719	4.75 x 14.25	0.111	0.902
10B	1.541	3.626	4.968	3.00 x 9.00	0.070	0.903
10C	Contact	1.074	1.472	2.00 x 6.00	0.047	0.077
Box-1	1.541	3.625	4.966	3.00 x 9.00	Bare	0.904
Box-2	1.541	3.625	4.966	3.00 x 9.00	0.070	0.904
Box-3	1.541	3.625	4.966	3.00 x 9.00	0.219	0.904
Box-4	1.541	7.437	10.189	3.81 x 11.44	Bare	0.711
Box-5	1.541	7.437	10.189	3.75 x 11.25	0.088	0.711
Box-6	1.541	7.437	10.189	3.75 x 11.25	0.344	0.711
Box-7	2.000	12.000	16.440	3.94 x 17.50	Bare	0.787
Box-8	2.000	6.250	8.562	3.19 x 13.50	Bare	0.978
Box-9	2.000	6.250	8.562	3.06 x 14.31	0.156	0.997
Box-10	2.000	9.000	12.333	3.94 x 13.12	Bare	0.866
Box-11	2.000	3.860	4.979	3.06 x 9.38	0.250	1.171



Figure 4.1. A wall panel being mounted on the reaction structure.



Figure 4.2. The box structure left over from another study, with walls tested in this study.

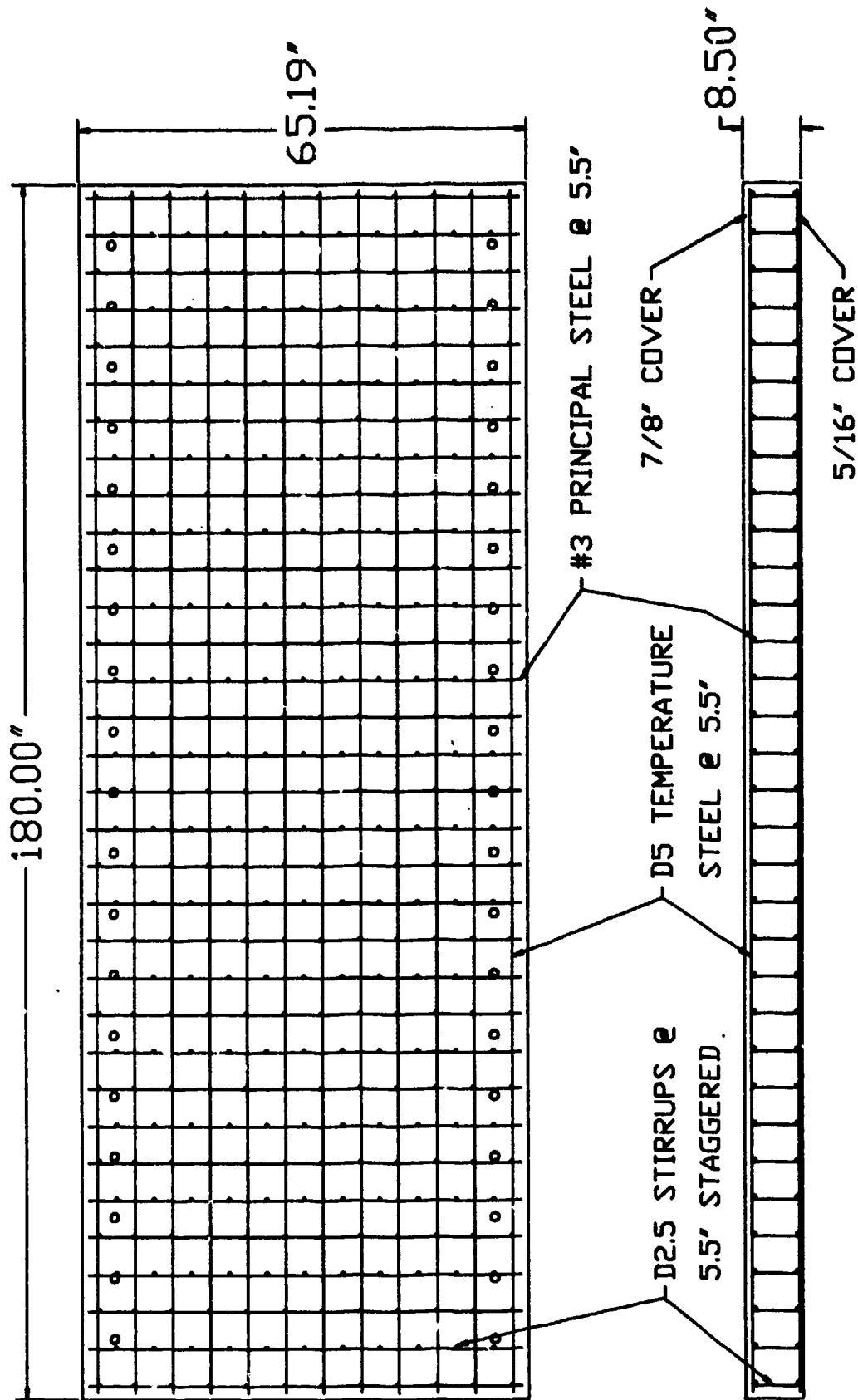


Figure 4.3. Reinforcement layout for wall panels 1 through 7.

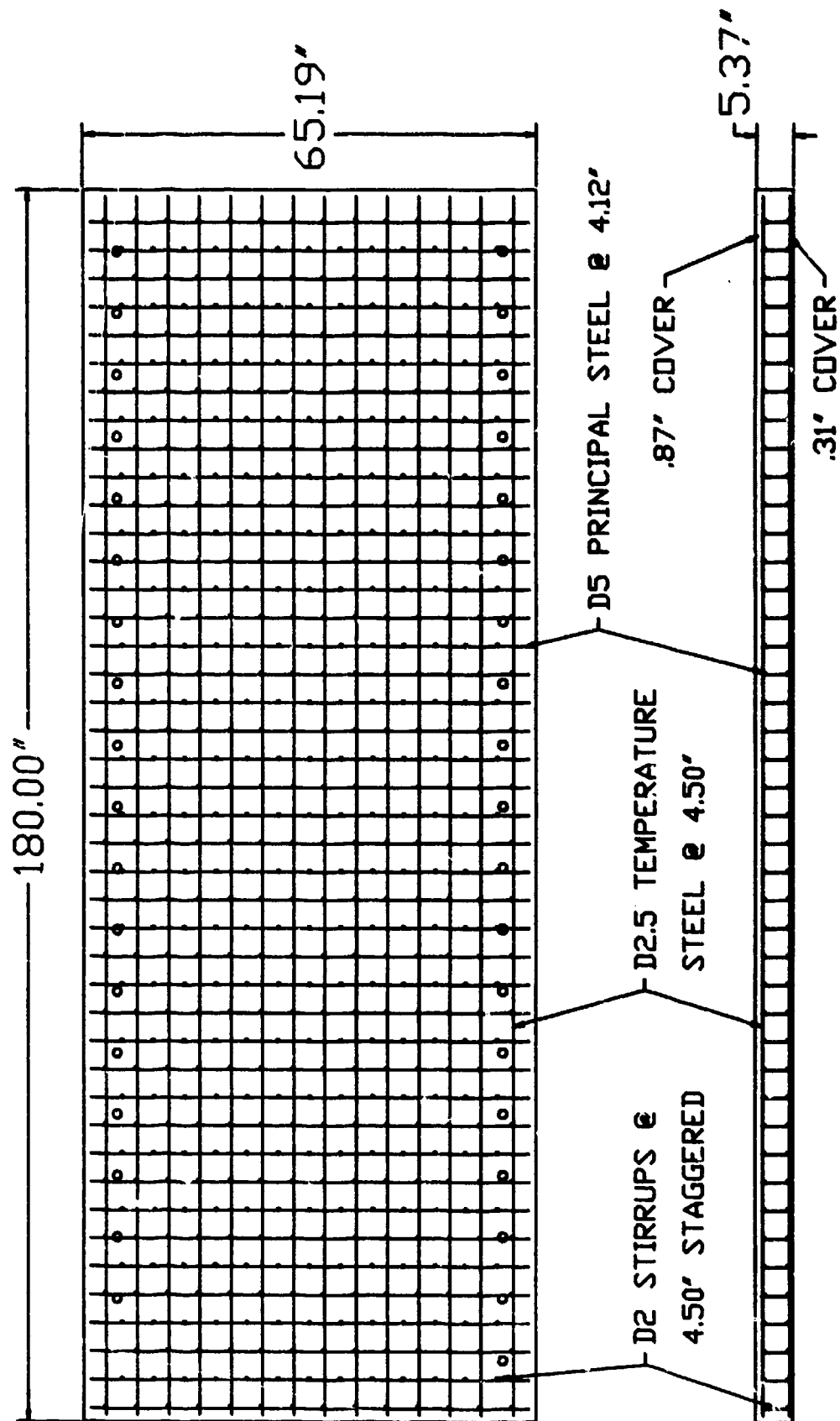


Figure 4.4. Reinforcement layout for wall panels 8 and 9.

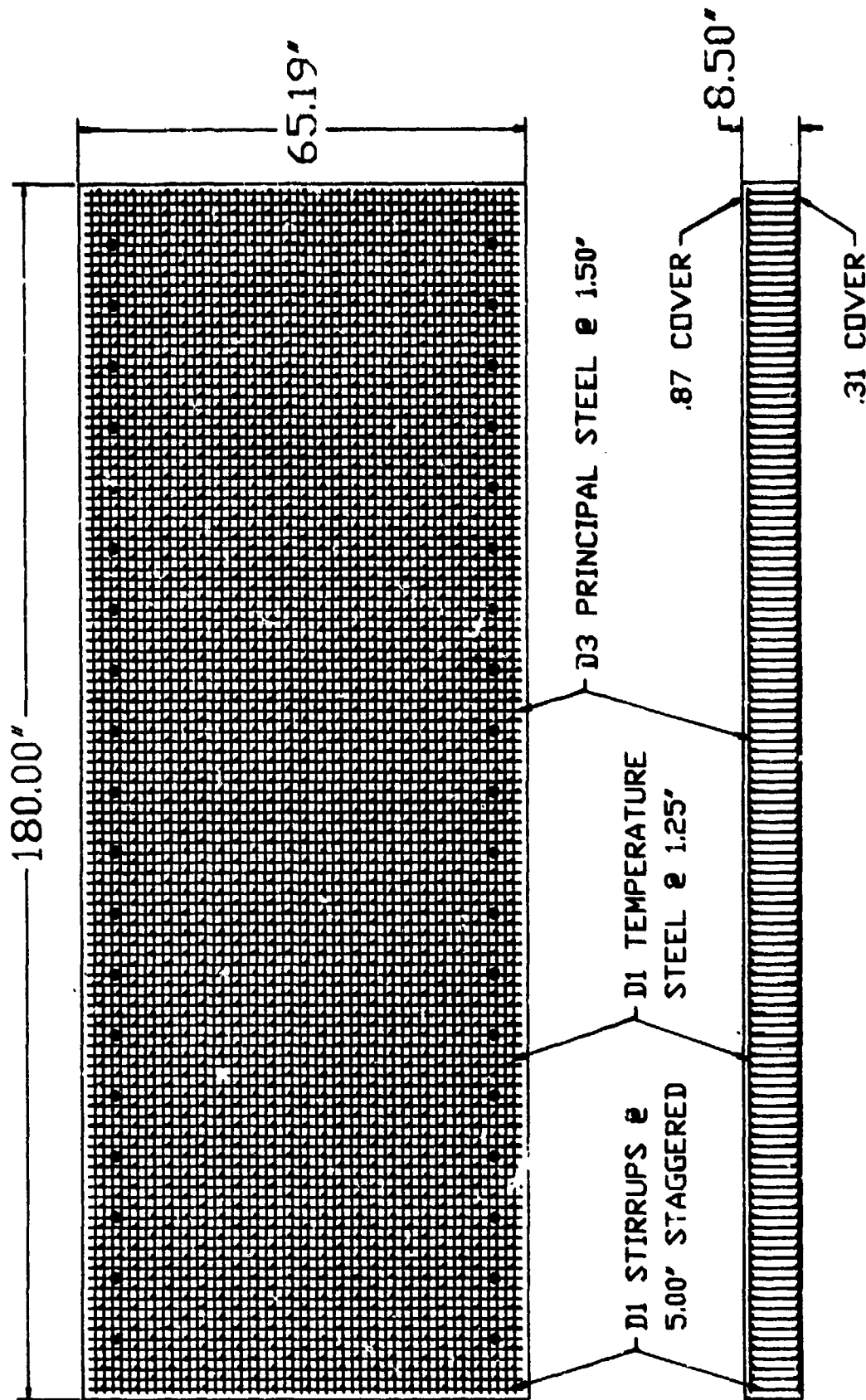


Figure 4.5. Reinforcement layout for wall panel 10.

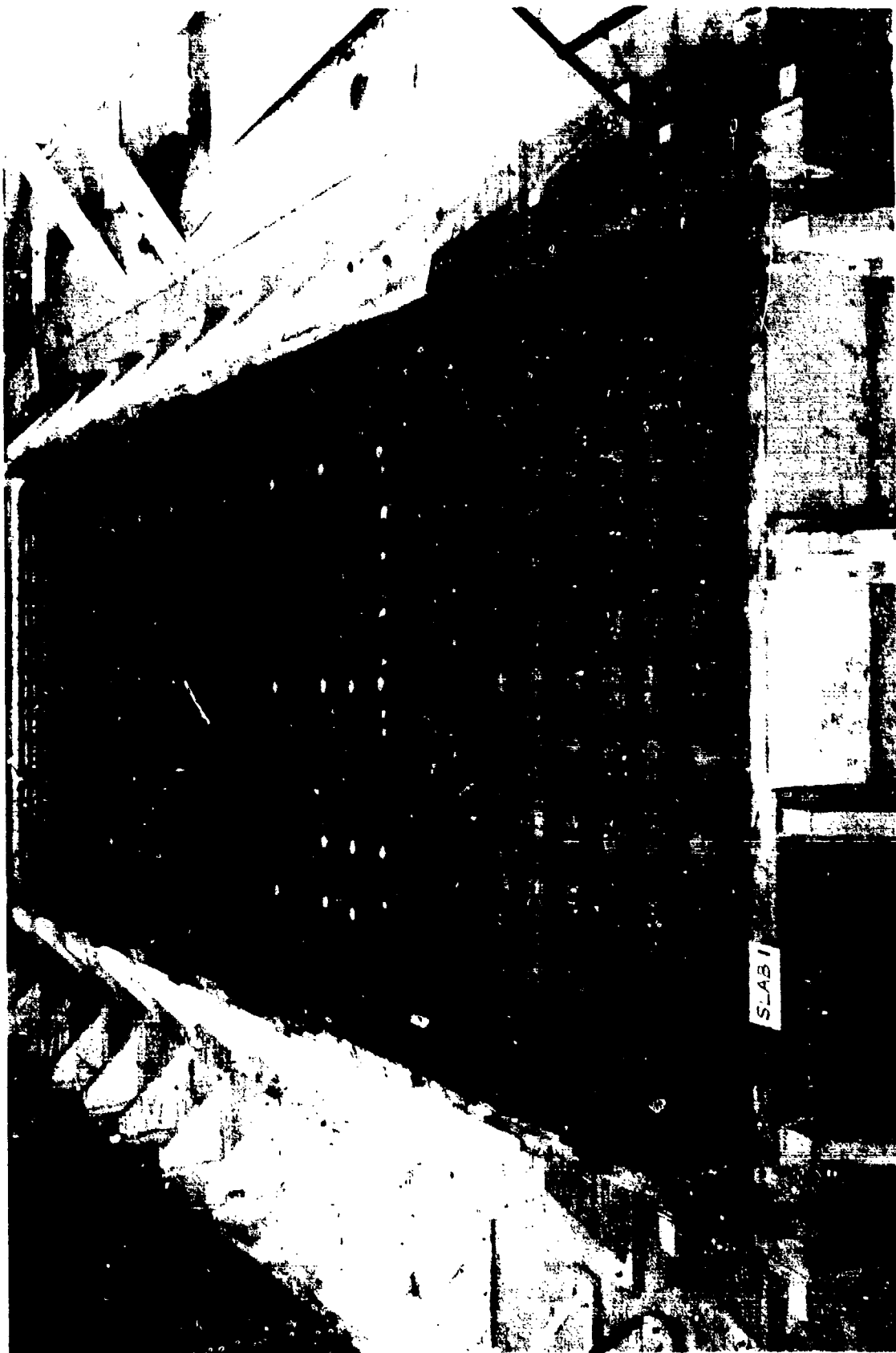


Figure 4.6. A typical steel mat for wall panels 1 through 7.



Figure 4.7. A typical reinforcing steel mat for wall panels 8 and 9.

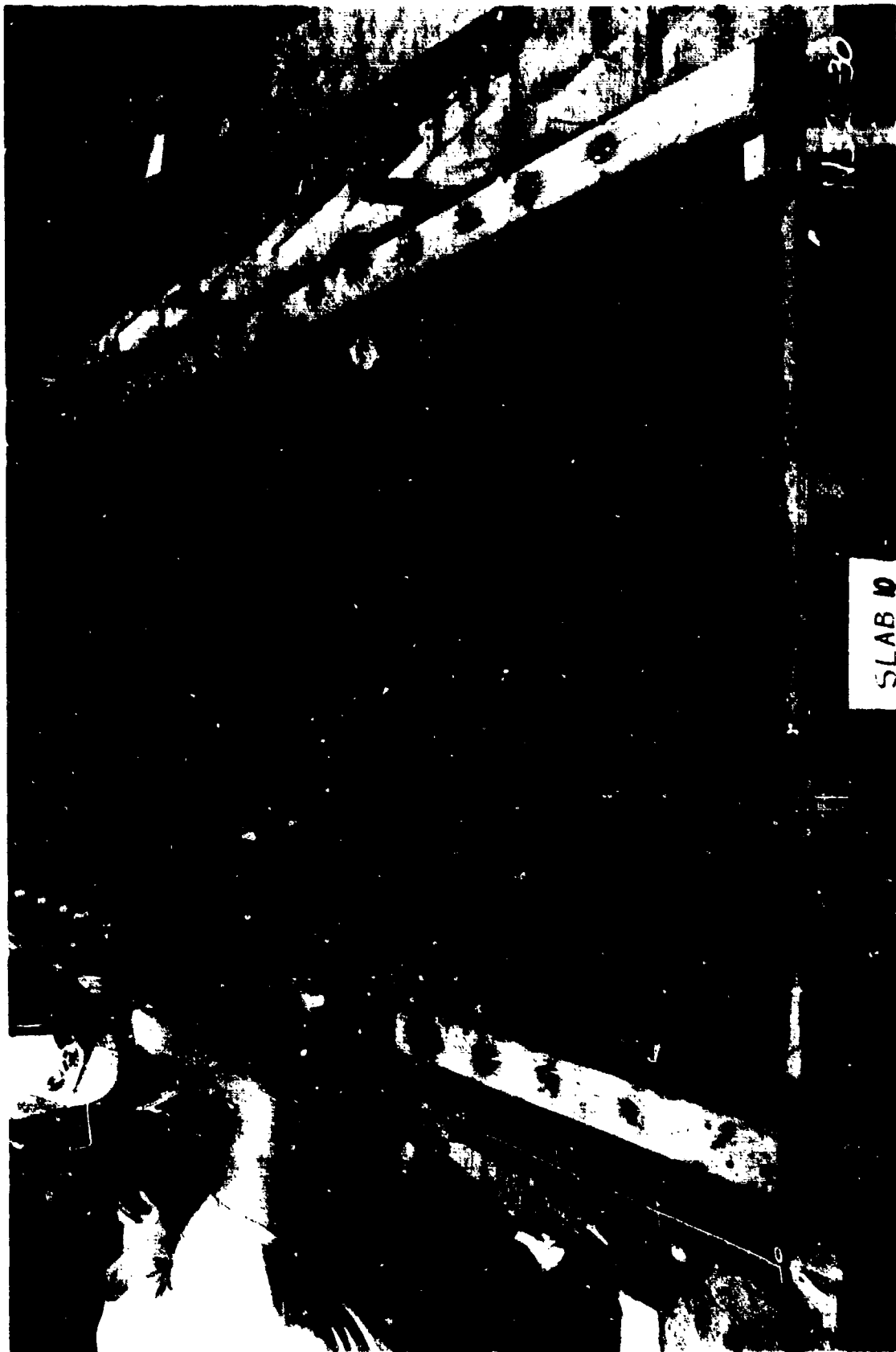


Figure 4.8. The reinforcing steel mat and forms for wall panel 10.

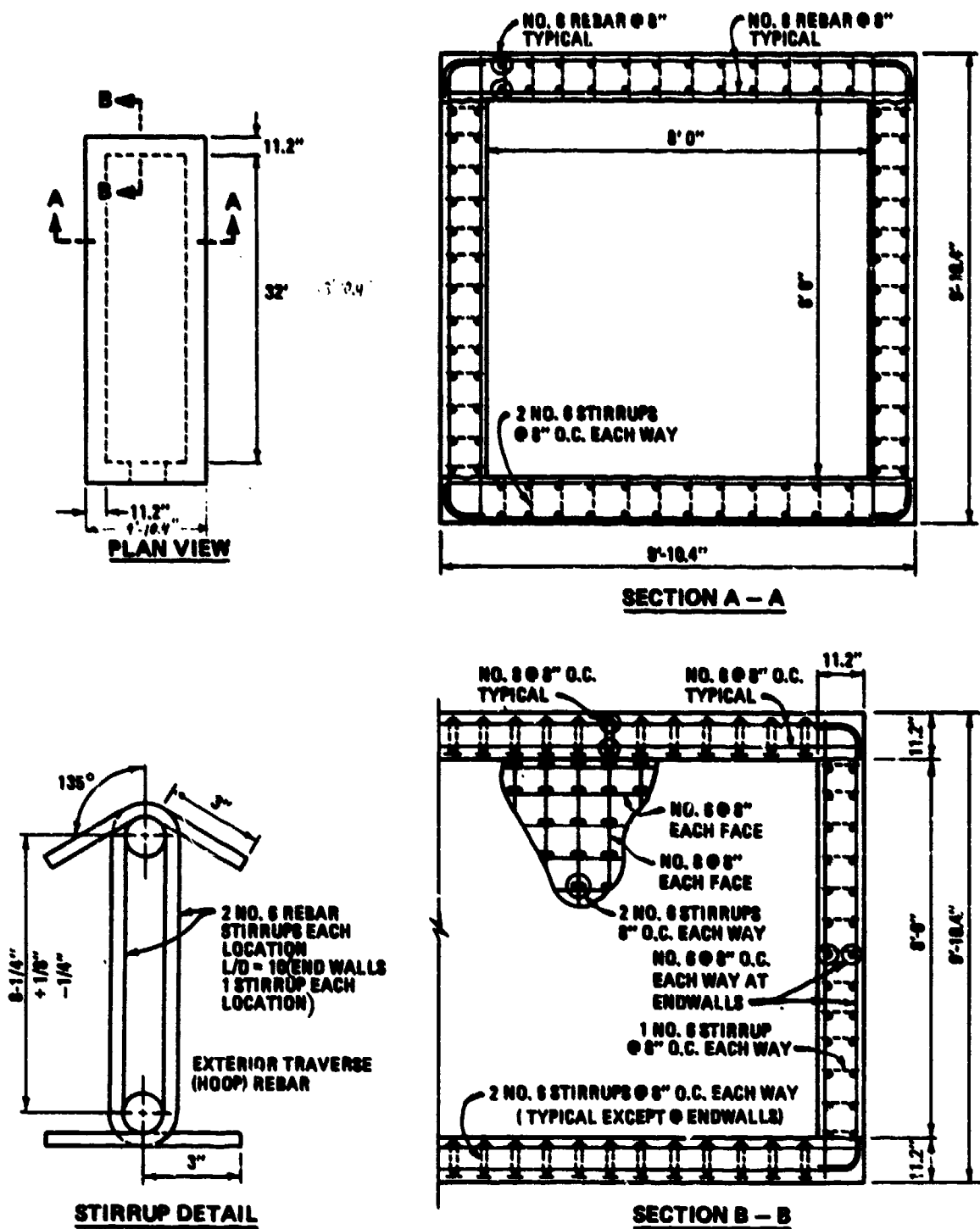


Figure 4.9. Reinforcement steel layout for the large reinforced concrete box.

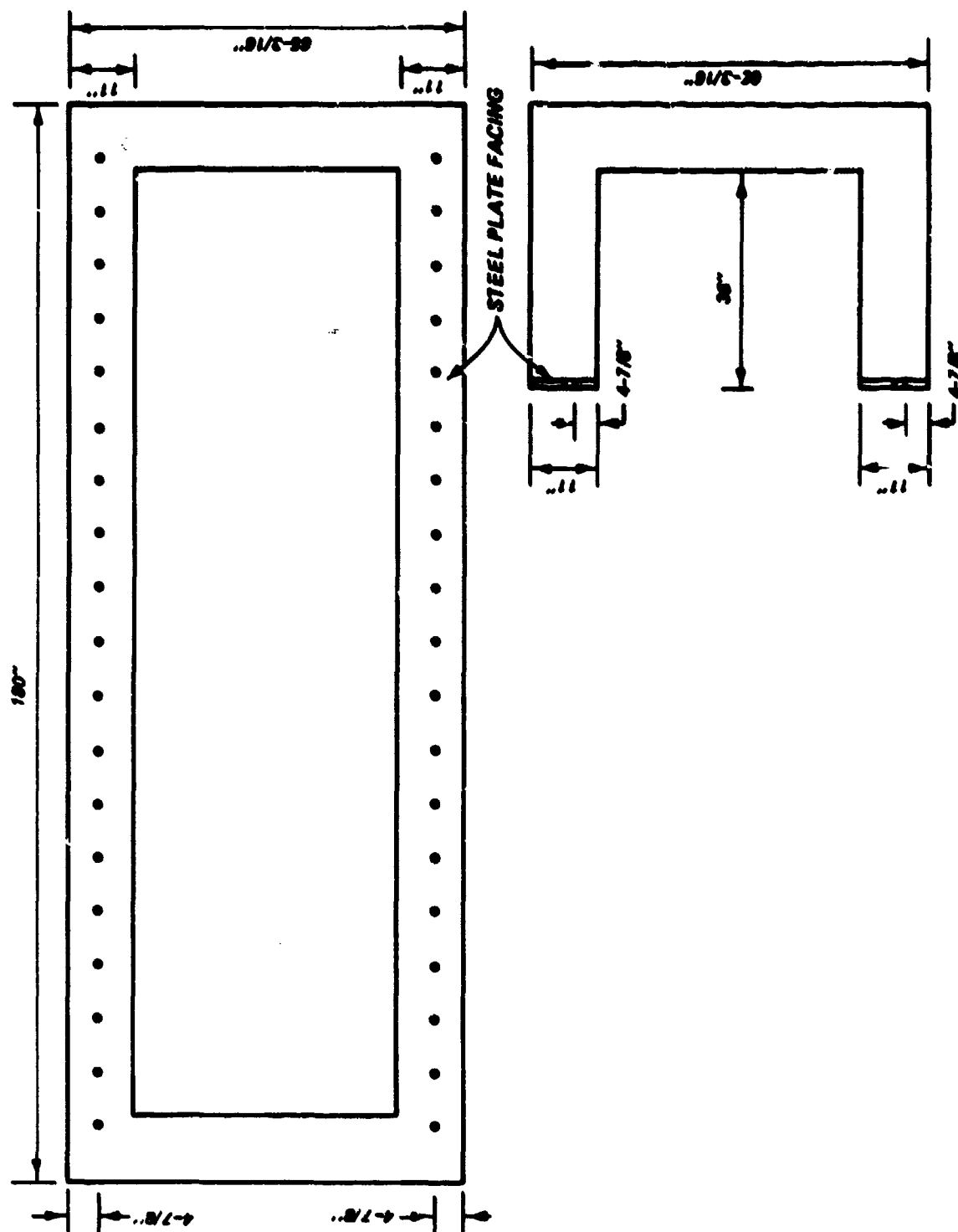


Figure 4.10. Existing reaction structure.



Figure 4.11. A typical bare charge.

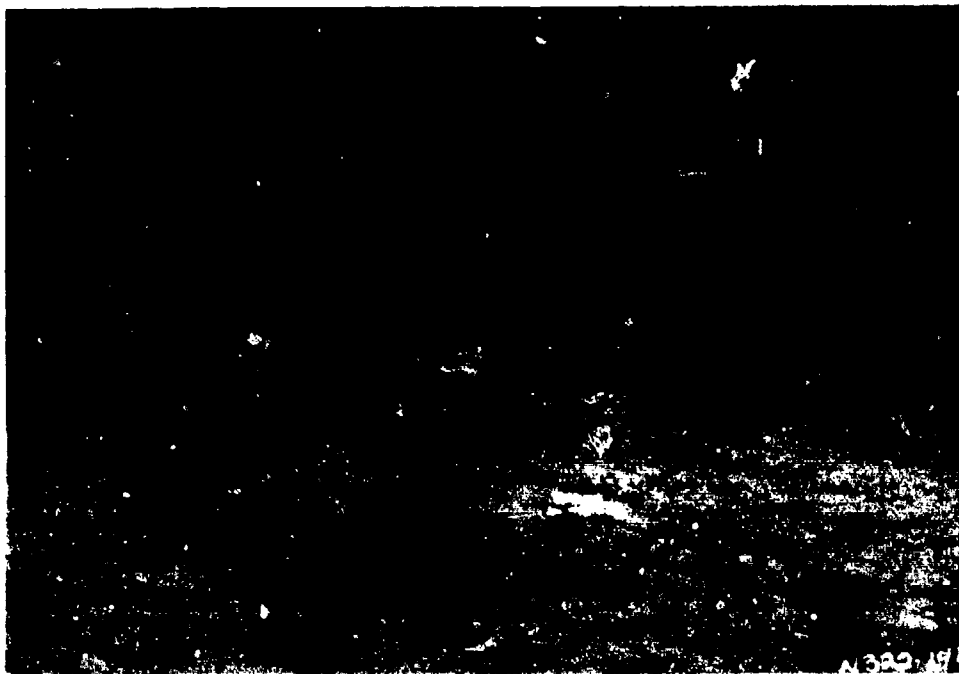


Figure 4.12. A typical charge in a casing.

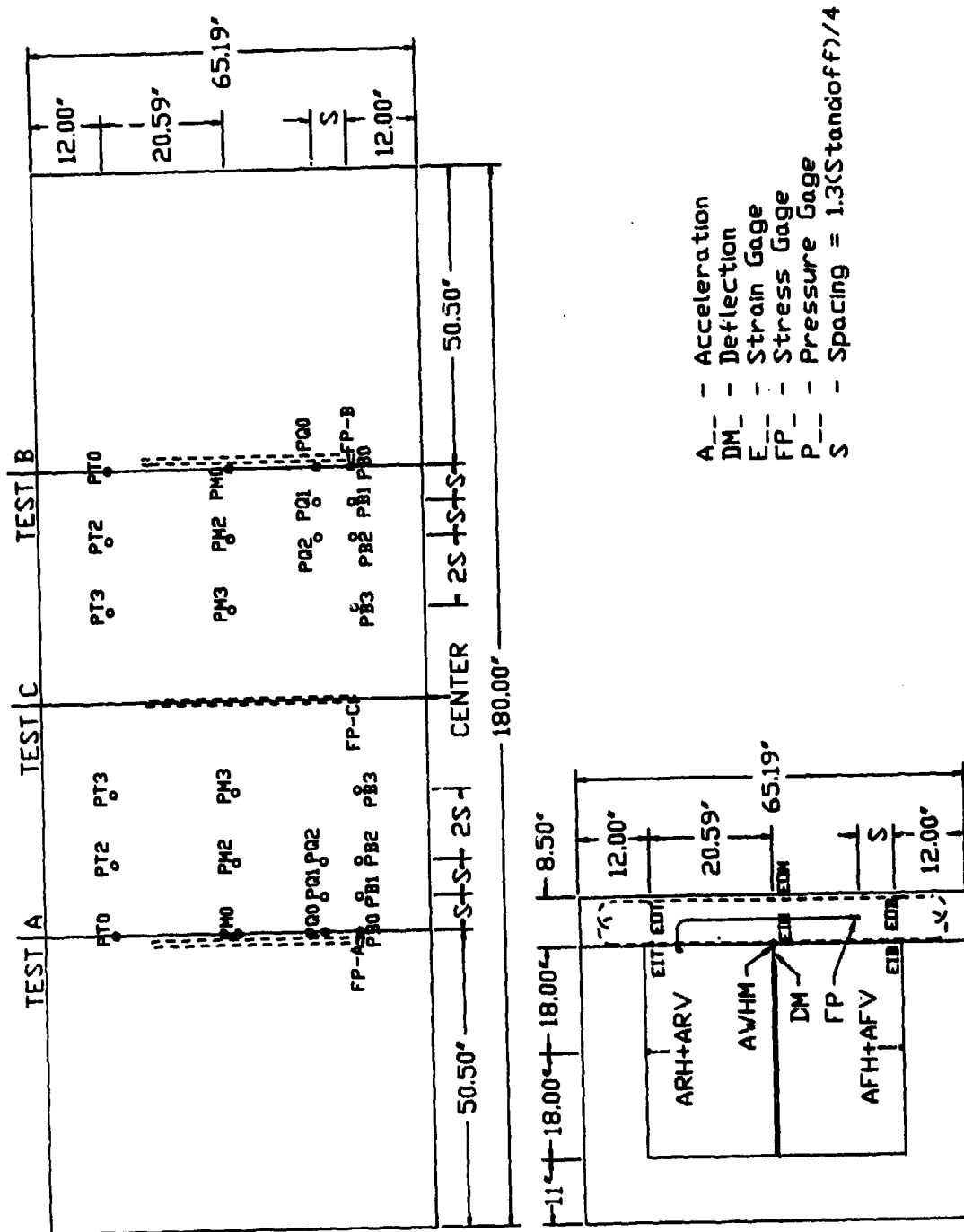


Figure 4.13. Typical layout of the active instrumentation in a wall panel and inside the reaction structure.

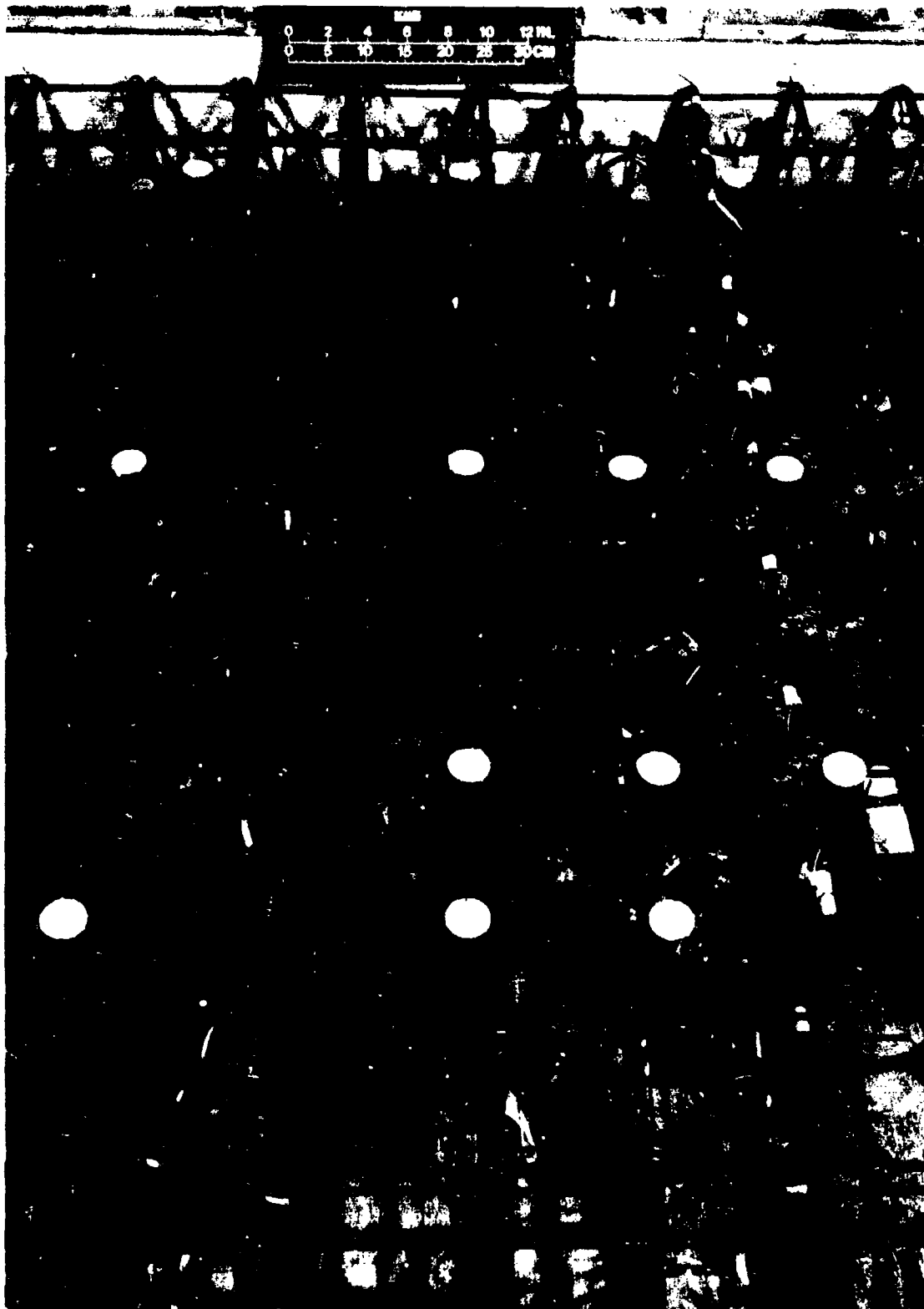


Figure 4.14. Airblast gage mounts and a stress gage installed in the reinforcing grid before the concrete was cast.

PART V: TEST DATA

General

Data for the tests consisted of over 700 measurements. Plots of all the active measurements versus time are given in Appendix A. The first few hundredths of milliseconds of each plot (before any data could occur) were made zero to eliminate any noise spikes from the detonation. Pressure distributions are given in Appendix B. Pretest and posttest pictures of each test are presented in Appendix C. The peaks of the active gages, the passive measurements, the spall velocities and the hand measurements of the damage are all summarized in various tables presented below. The measurements, trends, and major points of interest are discussed in the following sections.

Pressure Data

The peak pressure at the various pressure gage locations in all of the A, B, and D tests on wall panels are summarized in Table 5.1. The pressure measurements on the lower portion of the wall panels were of special interest because the lower back portions of the wall panels often spalled. Notice that many of the airblast gages in the bottom and quarter rows were destroyed or hit, so no realistic measurements were recorded for many of these gages. The airblast gages in these two lower rows were subjected to very sharp peaked pressure-time histories, intense heat from the fire ball of the bomb, ejecta from the bomb crater, and, if the bombs were cased, high-velocity bomb fragment impacts. The airblast gages in the bottom row were especially prone to destruction, almost all of the bottom airblast gages were destroyed during tests 1A through 4A. No more airblast gages were installed in the bottom row (PB row) after test 4A. Most of the airblast gages in the quarter row (PQ row) which survived, measured two main peaks. It is believed that the second peaks were from the airblast waves reflecting from the ground and arriving slightly after the main airblast wave. Most of the peak reflected pressure measurements did not match the predictions from curves in Figure 2.4 for equivalent weight hemispherical TNT charges

detonated at the surface. It is believed that the peak pressures which were extremely higher than the predictions were due to either multiple reflections, high temperatures, or excitation of the airblast gages natural frequencies. The peak pressures that were slightly lower or higher than the predictions were probably due to casing effects and geometry differences. References 1 and 47 also reported large discrepancies between measured and predicted peak reflected pressures during close-in cylindrical charge detonations. Agreement was better in the tests with the larger standoff distances.

The pressure distributions along the quarter lines at various times during each A, B, and D test are shown in Figures in Appendix B. In addition, the peak pressure distributions for the same tests are shown in Appendix B. Both types of pressure distributions indicate that the airblast waves expanded somewhat cylindrically.

The rise times and durations of the airblast-time histories can influence spall depth and velocities. The arrival times, rise times, and the durations of the airblast measurements at PQ-0 and PQ-1 (which are in front of the area where spall was expected) are given in Table 5.2. The arrival times of the bomb fragments are also given in Table 5.2 for comparison to the arrival times of the airblast. The airblast arrived before the bomb fragments in all of the tests, except for the tests with the largest standoff distances in which the bomb fragments arrived before the airblast arrived. The rise times of the airblast ranged from 0.016 to 0.220 msec with the majority of the rise times in the lower end of this range. The average ratio of rise time to arrival time for the good measurements was 0.24. For lack of better guidance on calculating rise times for theoretical analysis, this ratio can be used for similar bomb threats. The durations were all well below 1 msec. The corresponding wave lengths were, however, all many times greater than the thicknesses of the test panels. Thus, the airblast pressures had to unload rapidly to cause spall.

The unit positive impulses measured at the various airblast pressure gage locations during all A, B, and D tests are summarized in Table 5.3. The unit positive impulses were all under 1.02 psi × second.

Stress Data

The peak stresses, rise times, and durations measured by the Mini-Flat-Pack stress gages are given in Table 5.4. The Mini-Flat-Packs were experimental gages and did not always successfully measure stress. During the first 12 tests, 2 of the gages failed to respond well (including a gage with a pulse power supply), and the others measured strong electronic noise pulses from the bomb detonations. The intense electronic noise from the bomb detonations started immediately at time zero and quickly died down by 0.2 msec. The problem was the stress waves in all tests with standoff distances of 1.54 feet or less arrived at the stress gages before 0.2 msec and were mixed with high level noise. Only the stresses for tests with contact charges (which had very high peak stresses) or tests with standoff distances greater than 1.541 feet were measured successfully during the first 12 tests. Several of the first 12 tests were too noisy to distinguish any stress measurements.

Several attempts were made to reduce the electronic noise each successive test. A metal wire screen was taped to the front of the wall panel in test 5A to act as a Faraday Shield against the electronic noise. This reduced the intensity of the electronic noise tremendously and was used in the rest of the instrumented tests. However, 5 of the 16 tests with Faraday Shields did not have successful stress measurements. It appeared that the 5 gages did not respond. The stress measurements in those 5 tests had no strong stress waves, had multiple spikes with low peaks and appeared like medium-level noise.

In summary, a total of 7 stress gages were too noisy to read, 7 stress gages did not respond well, and 15 measured believable peak stresses. There were no large air voids seen, after cutting the panels, around the 7 stress gages which did not respond. Nothing was found wrong with the 7 gages that did not respond.

The minimum time it took the front of the stress wave to travel from the stress gage to the back of the wall and return to the gage is also given in Table 5.4 for comparison to the rise time and duration of the measured stress wave in each test. If the rise time was shorter than the travel time, then the front of the reflected portion of the wave arrived back at the stress gage after the peak incident stress had

passed the stress gage, which means that the peak stress measurement equaled the actual peak stress. However, if the rise time was equal to or greater than the travel time, then the front of the reflected portion of the wave could have arrived back at the stress gage before the peak incident stress arrived, and combined with the incident stresses to make a net stress lower than the actual peak stress. If the duration of the measured stress wave was longer than the travel time, then the front of the reflected portion of the stress wave arrived back at the gage before the end of the incident portion of the wave passed the gage and the unloading portion of the measured stress wave is different than that of the actual stress wave.

Acceleration Data

The peak accelerations, velocities, and displacements measured by the AWHM gages at the mid height of the wall panels are tabulated in Table 5.5. The accelerations of the floor and roof were measured for another study and will not be discussed further in this report. Notice that the AWHM acceleration measurements shown in Appendix A had early-time high frequency and very high peaked spikes in one direction. The AWHM measurements were all initially knocked off their base line shifts by large amounts. The baselines in the plots shown have been shifted to bring the initial and final accelerations back to zero. However, the peak displacements derived from the acceleration plots are many times greater than those measured by the displacement gages. Therefore, the high-frequency, high-peaked, initial acceleration measurements are believed to have been due to a portion of the stress wave traveling into the accelerometer and shocking it. The later accelerations may be due to the wall motions.

Displacement Data

The peak and permanent, active and passive displacement measurements at the mid height of the wall panels are tabulated in Table 5.5. There were no active displacement gages in tests 1A and 1B, because the first type of gages obtained interfered with the other gages. Another

type of displacement gage was obtained for the rest of the tests. The accuracy of the passive measurements were approximately ± 0.031 .

The permanent displacement of the bottom of the wall panels at the center of the test area are tabulated in Table 5.6. These measurements were taken from the back wall of the reaction structure to the wall panel at floor level. The measurements were sometimes just the displacement of threshold spall bulging from the wall and at other times were actual wall displacement. Some of the walls with severe loads, such as 3A, 8B, and 9A, sheared at the floor and displaced inward.

Strain Data

The strain gages also picked up the high-intensity noise from the bomb detonations for the first 0.1 msec. The actual strains did not occur until later, so, approximately the first 0.1 msec was made zero to eliminate the noise. The permanent strains were the most reliable and useful data from the strain measurements. The permanent strain measurements are tabulated in Table 5.7. Notice the permanent strain measurements at the bottom of the wall panels, which incurred spall damage, were many times larger than the permanent strains at the center and top of the wall panels. The large strains at the bottom were most likely caused by a combination of the "cracked-off" concrete pulling on the steel, a reduction in the effective depth of the steel due to spall and scabbing, loss of bond, and the much higher loads on the bottom portion of the wall.

Measurements of Spall Damage, Velocity, and Cracks

The depths of spall, areas of spall, depths of first cracks, depths of the deepest cracks, crack angles, and spall velocities are all tabulated in Table 5.8. The pictures of the cross-sections in Appendix C have scales in them, so additional measurements of damage can be obtained from the pictures, if desired. There are no measurements of crack depths or angles for the tests on wall panel 2 because this wall was subjected to additional tests for another study and was not cut. The spall depths were measured from a straight edge over the spall hole

to the deepest part of the spall hole. The spall depth measurements were only accurate to about ± 0.18 inches, because the spalled surface was very rough. The spall area length and height are the longest horizontal and vertical measurements across the spall holes. The spall holes were irregular in shape, but many of them were somewhat like a half circle. Most of the spall area heights were 1 to 2 times the bomb height. The spall holes in test 3A were very deep and scattered, and may have been partially due to large displacements. The crack depths were measured relative to the portions of the wall panels which had borne against the floor. The angles of the cracks were measured from the normal to the wall panels back face at the floor level. The walls with the severest loads had the sharpest crack angles. The cracks started at these angles and gradually curved to parallel the wall faces at the deepest point and to some oblique angle at the top ends of the cracks. The spall velocities are the velocities of the lead spall fragments. The various sized spall fragments behind the lead spall, traveled at various velocities and were difficult to follow in the film.

Measurements of Scab Damage

Scab is the ejection of concrete from the same side of the wall from which it was loaded. It is caused by extremely high compressive loads fracturing the concrete. Contact bombs or bomb fragments usually cause large areas of the front of a wall to scab. Some cased charges caused a continuous band to scab and others caused multiple scab areas in a zone across the lower portion of the wall panels. The scab zone depths, lengths, and widths for each test are given in Table 5.9. The scab depths were measurements from the bottom of a straight edge across the scab hole to the deepest part of the scab hole. The measurements were probably only accurate to within about ± 0.18 inches, because the scab hole was very rough and pitted. A few bomb fragments were found still sticking in the concrete in the scabbed area. The scab depths were probably close to the average penetration depth of the bomb fragments in the cased charge tests. Scab lengths and widths were the longest horizontal and vertical measurements of the zone severely scabbed or pitted. The scab heights in the cased charge tests were usually slightly less than the heights of the bombs.

Table 5.1
Peak Pressures at Gage Locations for A, B, and D Tests

Test No.	Peak Pressure, psi						
	PB-0	PB-1	PB-2	PB-3	PQ-0	PQ-1	PQ-2
<u>First Half of Gage Locations</u>							
1A	Hit	15,800	18,800	3,860	6,000	5,810	Hit
1B	No	Hit	Hit	Hit	10,850	Hit	Hit
1D	40,000	Hit	Hit	3,290	8,550	Hit	Hit
2A	Hit	Hit	Hit	4,750	8,170	10,500	7,550
2B	No	No	No	Hit	14,700	Hit	Hit
2D	Hit	Hit	Hit	4,020	Hit	Hit	8,060
3A	Hit	Hit	Hit	4,060	7,000	Hit	12,200
3B	No	No	No	No	6,950	Hit	4,580
4A	Hit	No	No	No	2,560	Hit	Hit
4B	No	No	No	No	Hit	Hit	5,990
5A	No	No	No	No	Hit	Hit	30,000
5B	No	No	No	No	7,600	10,600	4,180
6A	No	No	No	No	Hit	Hit	Hit
6B	No	No	No	No	Hit	16,000	Hit
7A	No	No	No	No	Hit	Hit	29,500
7B	No	No	No	No	Hit	Hit	18,600
8A	No	No	No	No	7,100	7,170	Hit
8B	No	No	No	No	Hit	Hit	5,300
9A	No	No	No	No	4,200	Hit	2,080
9B	No	No	No	No	10,000	Hit	2,380
10A	No	No	No	No	6,300	5,600	Hit
10B	No	No	No	No	Hit	>34,200	>26,500

(Continued)

Table 5.1 (Concluded)

Test No.	Peak Pressure, psi						BP
	PM-0	PM-2	PM-3	PT-0	PT-2	PT-3	
<u>Second Half of Gage Locations</u>							
1A	820	730	396	340	395	198	Hit
1B	297	526	487	170	182	152	Hit
1D	990	832	525	743	470	365	2,120
2A	600	495	515	431	420	222	1,695
2B	5,800	570	470	232	166	193	Hit
2D	1,840	632	450	585	244	371	1,980
3A	4,050	2,500	1,500	835	530	430	3,900
3B	Hit	9,300	440	222	252	170	Hit
4A	1,395	890	915	372	392	308	450
4B	660	1,610	1,250	436	438	337	9,900
5A	412	830	383	200	210	180	7,200
5B	427	1,000	382	370	265	180	
6A	940	825	680	306	270	265	Hit
6B	760	Hit	595	238	202	226	1,480
7A	800	810	314	188	202	176	1,480
7B	1,297	1,348	1,050	298	382	283	3,100
8A	242	204	168	97	96	80	1,500
8B	404	587	271	117	152	154	1,740
9A	1,700	1,530	950	600	424	460	900
9B	222	268	122	67	86	87	1,200
10A	1,438	1,100	1,500	Broken	302	320	1,500
10B	364	420	600	120	140	154	1,360

Table 5-2
Rise Times, and Durations of Pressure-Histories on Portions
of Walls Where Spall Damage Was Expected

Test No.	PQ-0			PQ-1			Fragments
	Arrival Time msec	Rise Time msec	Durations msec	Arrival Time msec	Rise Time msec	Durations msec	Arrival Times msec
<u>Gage Locations*</u>							
1A	0.110	0.035	0.53	0.105	0.020	0.50	--
1B	0.135	0.050	0.50	Hit	Hit	Hit	0.18
1D	0.119	0.047	0.53	Hit	Hit		--
2A	0.120	0.050	0.55	0.104	0.040	Hit	--
2B	0.185	0.029	Hit	Hit	Hit	Hit	0.18
2D	Hit	Hit	Hit	Hit	Hit	Hit	--
3A	0.185	0.025	Hit	Hit	Hit	Hit	--
3B	0.175	0.034	Hit	Hit	Hit	Hit	0.18
4A	0.610	0.220	0.63	No	No	No	0.59
4B	Hit	Hit	Hit	Hit	Hit	Hit	0.29
5A	Hit	Hit	Hit	Hit	Hit	Hit	0.18
5B	0.200	0.040	0.80	0.170	0.044	0.85	0.18
6A	Hit	Hit	Hit	Hit	Hit	Hit	0.18
6B	Hit	Hit	Hit	0.150	0.025	Hit	0.18
7A	Hit	Hit	Hit	Hit	Hit	Hit	0.18
7B	Hit	Hit	Hit	Hit	Hit	Hit	0.18
8A	0.185	0.020	0.53	0.176	0.016	0.30	0.18
8B	0.174	Hit	Hit	Hit	Hit	Hit	0.18
9A	0.606	0.138	Hit	Hit	Hit	Hit	0.59
9B	0.122	0.028	Hit	Hit	Hit	Hit	0.11
10A	0.228	0.070	Hit	0.255	0.035	Hit	0.29
10B	Hit	Hit	Hit	0.164	0.020	Hit	0.18

* Note the only PB-0 or PB-1 to survive was PB-1 in Test 1A. The arrival time, rise time, and duration of this measurement were 0.019 msec, 0.10 msec, and 0.53 msec respectively.

Table 5.3
Unit Positive Impulse at Gage Locations
for A, B, and D Tests

Test No.	Unit Positive Impulse, psi x sec						
	PB-0	PB-1	PB-2	PB-3	PQ-0	PQ-1	PQ-2
<u>First Half of Gage Locations</u>							
1A	Hit	1.000	0.950	0.480	0.505	0.514	Hit
1B	No	Hit	Hit	Hit	0.680	Hit	Hit
1D	Hit	Hit	Hit	0.435	1.000	Hit	Hit
2A	Hit	Hit	Hit	0.408	0.800	Hit	0.582
2B	No	No	No	Hit	Hit	Hit	Hit
2D	Hit	Hit	Hit	0.461	Hit	Hit	0.568
3A	Hit	Hit	Hit	0.720	Hit	Hit	Hit
3B	No	No	No	No	Hit	Hit	0.263
4A	Hit	No	No	No	0.463	No	No
4B	No	No	No	No	Hit	Hit	0.780
5A	No	No	No	No	Hit	Hit	1.000
5B	No	No	No	No	0.745	0.680	0.425
6A	No	No	No	No	Hit	Hit	Hit
6B	No	No	No	No	Hit	Hit	Hit
7A	No	No	No	No	Hit	Hit	1.665
7B	No	No	No	No	Hit	Hit	1.440
8A	No	No	No	No	0.512	0.322	Hit
8B	No	No	No	No	Hit	Hit	0.397
9A	No	No	No	No	>0.550	Hit	0.118
9B	No	No	No	No	Hit	Hit	0.215
10A	No	No	No	No	Hit	Hit	Hit
10B	No	No	No	No	Hit	Hit	Hit

(Continued)

Table 5.3 (Concluded)

Test No.	Unit Positive Impulse, psi x sec						BP
	PM-0	PM-2	PM-3	PT-0	PT-2	PT-3	
<u>Second Half of Cage Locations</u>							
1A	0.087	0.106	0.059	0.052	0.083	0.041	Hit
1B	0.035	0.060	0.059	0.035	0.033	0.034	Hit
1D	0.128	0.111	0.086	0.068	0.064	0.061	0.073
2A	0.092	0.085	0.075	0.061	0.056	0.046	0.076
2B	0.480	0.072	0.066	0.023	0.040	0.039	Hit
2D	0.355	0.082	0.065	0.650	0.052	0.052	0.073
3A	0.753	0.520	0.283	0.181	0.129	0.099	0.150
3B	Hit	1.020	0.072	0.045	0.046	0.053	Hit
4A	0.250	0.223	0.174	0.088	0.114	0.086	0.040
4B	0.123	0.218	0.189	0.085	0.075	0.066	0.81C
5A	0.048	0.103	0.070	0.040	0.035	0.046	Hit
5B	0.087	0.096	0.072	0.054	0.040	0.043	
6A	0.185	0.102	0.096	0.047	0.042	0.042	Hit
6B	0.045	Hit	0.087	0.039	0.042	0.034	0.035
7A	0.042	0.114	0.057	0.037	0.039	0.038	0.050
7B	0.250	0.256	0.174	0.081	0.088	0.081	0.325
8A	0.037	0.034	0.028	0.020	0.021	0.019	0.078
8B	0.068	0.069	0.049	0.027	0.029	0.032	Hit
9A	0.345	0.295	0.125	0.115	0.107	0.106	
9B	0.032	0.025	0.015	0.017	0.018	0.019	0.35
10A	0.236	0.218	0.258	Broken	0.083	0.090	0.072
10B	0.064	0.064	0.082	0.033	0.038	0.035	0.020

Table 5.4
Peak Stresses, Rise Times, and Travel Times

<u>Test No.</u>	<u>Peak* Stress psi</u>	<u>Rise- Time msec</u>	<u>Duration msec</u>	<u>Travel Time msec</u>
1A	2,000	0.020	0.035	0.058
1B	2 x Broken	--	--	0.058
1C	12,200?	0.012	0.150	0.058
1D	Noisy	--	--	0.058
2A	Noisy	--	--	0.058
2B	5,500?	0.019	0.083	0.058
2C	14,500?	0.020	0.140	0.058
2D	Noisy	--	--	0.058
3A	7,350?	0.050?	0.135	0.050
3B	7,350	0.039	0.055	0.050
4A	1,290?	Noisy	Noisy	0.050
4B	3,500?	0.020	0.107	0.050
5A	23,300	0.021	0.045	0.044
5B	5,350	0.018	0.046	0.044
5C	61,000	0.019	0.073	0.044
6A	18,500	0.045	0.093	0.046
6B	16,800	0.036	0.090	0.046
6C	Broken	--	--	0.046
7A	13,600	0.055	0.130	0.058
7B	8,150	0.030	0.116	0.058
7C	Broken	--	--	0.058
8A	Broken	--	--	0.047
8B	9,800	0.030	0.137	0.047
8C	No Gage	--	--	0.047
9A	2,450	0.02	0.395	0.037
9B	Broken	--	--	0.037
10A	14,800	0.040	0.135	0.077
10B	Broken	--	--	0.077
10C	32,920	0.029	0.152	0.077

* The "?" indicates the record was very noisy and the accuracy of the reading is questionable.

Table 5.5
Peak Acceleration, Velocity, and Deflection Measurements at
the Mid-Heights of the Wall Panels

Test No.	Gage AMHM			Gage DM		Scratch Gage	
	Peak Acceleration g's	Peak Velocity in./sec	Peak Deflection in.	Peak Deflection in.	Permanent Deflection in.	Peak Deflection in.	Permanent Deflection in.
1A	-8,000	-400	-2.33	--	--	0.094	0.090
1B	-7,000	-130	-0.80	--	--	0.156	0
1D	-10,100	-540	-4.40	0.225	0.135	0.467?	?
2A	-19,500	-835	-7.85	0.109	0.035	0.156	0.031
2B	9,500	-132	-0.93	0.184	0.055	0.125	0
2D	-24,300	-750	-2.50	0.142	0.032	0.188	0
3A	18,400	485	2.17	>1.59	>1.59	>1.75	0.125
3B	15,100	160	-0.21	0.007	0.003	0.188	?
4A	-26,400	-798	-9.10	0.190	0.083	0.094	0
4B	-11,800	-626	-4.85	0.380	0.225	0.500	0.3125
5A	-17,800	-505	-7.50	0.290	0.166	0.250	0.125
5B	-43,000	-1460	-11.45	0.148	0.110	0.062	0.062
6A	-51,000	-2550	-34.00	-0.490	0.080	0.188	0.125
6B	-40,150	-1215	-14.25	0.215	0.099	0.188	0.062
7A	-36,500	-1330	-18.20	-0.190	0.075	0.125	0.062
7B	-29,500	-4050	-51.80	0.440	0.240	0.375	0.188
8A	-12,300	-1860	-24.20	-0.114	0.040	0.062	0
8B	-20,400	-1050	-8.70	0.360	0.115	0.375	0.125
9A	-13,700	-1190	-12.25	0.750	0.480	0.500	0.438
9B	-29,200	-4400	-55.00	-0.140	0.330	0.125	0
10A	-19,800	-4400	-54.00	0.518	0.300	0.500	0.375
10B	-37,700	-2800	-36.25	0.098	0.044	0.062	0

Table 5.6
Displacement of the Wall Panels
at the Floor

<u>Test No.</u>	<u>Displacement in.</u>
1A	0
1B	0.30
1C	0
1D	0.25
2A	0
2B	0
2C	0.06
2D	0
3A	1.59
3B	0.22
4A	0
4B	0.25
5A	0
5B	0
5C	0
6A	0.50
6B	0.37
6C	0
7A	0
7B	0.50
7C	0.31
8A	0.12
8B	0.56
8C	1.31
9A	0.81
9B	0.38
10A	0.75
10B	0.19
10C	0.50

Table 5.7
Permanent Strains in Wall Panels During
A, B, and D Tests

Test No.	Gage Locations					
	EOB	E1B	EOM	E1M	EOT	E1T
<u>Strains, microin./in.</u>						
1A	-900	2,500	350	-300	500	0
1B	-30,000	10,000	0	500	360	20
1D	1,500	-3,000	-400	400	12,850	-100
2A	-750	8,600	Broken	200	165	20
2B	-400	11,500	130	-250	700	10
2D	-1,750	2,000	Broken	100	230	0
3A	4,500	47,100	2,500	13,000	-2100	-4200
3B	62,000	4,500	650	-800	800	120
4A	-400	Broken	1,250	-420	0	-420
4B	Broken	Broken	0	-2,600	-200	100
5A	>70,000	>61,000	820	Broken	1,140	850
5B	2,000	Broken	500	250	290	540
6A	0	0	Broken	3,250	200	Broken
6B	0	Broken	220	7,600	Broken	-50
7A	>72,200	>64,500	570	-50	525	-70
7B	>61,000	Broken	100	Broken	120	-80
8A	100	Broken	450	Broken	-200	0
8B	7,400	>62,800	1,000	-920	0	135
9A	0	>65,000	-100	30,700	-2,000	100
9B	3,000	Broken	840	-300	270	70
10A	Broken	Broken	250	Broken	10,000	400
10B	200	Broken	Broken	Broken	320	100

Table 5.8
Measurements of Damage and Spall Velocities

Test No.	Spall Depth in.	Spall Area Length/Height in. x in.	First Crack Depth in.	Deepest Crack in.	Crack Angle deg	Spall Velocity ft/sec
1A	No Damage	--	None	None	--	--
1B	Threshold	--	2.62	5.00	35	15
1C	2.50	23.5 x 14.8	3.19	4.25	25	53
1D	2.25	17.1 x 11.6	2.44	4.50	25	28
2A	No Damage	--	None	None	?	--
2B	Threshold	--	?	?	?	--
2C	2.25	28.0 x 13.5	?	?	?	57
2D	Threshold	27.0 x 3.0	?	?	?	--
3A	Breached	38.0 x 27.0	(4.87)	--	14	69
3B	1.38	23.4 x 15.0	2.31	4.50	50	39
4A	No Damage	--	7.06	Same	48	--
4B	1.81	11.0 x 22.0	3.75	4.75	16	44
5A	3.75	34.0 x 19.3	None	None	40	?
5B	1.06	13.5 x 11.0	1.50	3.56	50	17
5C	4.38	27.0 x 16.0	5.38	Same	56	89
6A	Threshold	--	2.75	7.50	19	--
6B	Threshold	--	2.44	5.75	15	--
6C	3.75	16.0 x 13.1	4.75	4.75	27	44
7A	Threshold	--	2.00	6.50	31	--
7B	Threshold	--	2.25	5.00	26	--
7C	2.00	8.0 x 10.0	3.00	7.25	39	35
8A	No Spall	--	4.75	Same	45	--
8B	Threshold	--	1.00	2.50	25	57
8C	Breached	?	--	--	?	65
9A	Flexure	--	0.87	3.25	28	69
9B	Threshold	--	0.94	2.44	35	--
10A	1.25	6.0 x 7.0	2.00	6.00	28	37
10B	Threshold	--	None	None	--	--
10C	0.62	15.0 x 11.5	1.37	4.75	16	70
Box-1	No Damage	--	--	--	?	--
Box-2	2.50	10.0 x 7.0	?	?	?	?
Box-3	3.00	20.0 x 16.0	?	?	?	?
Box-4	No Damage	--	--	--	--	--
Box-5	3.75	39.0 x 16.0	?	?	?	?
Box-6	3.25	50.0 x 20.0	?	?	?	?
Box-7	3.00	40.0 x 23.0	?	?	?	?
Box-8	No Damage	--	--	--	--	--
Box-9	3.00	40.0 x 20.0	?	?	?	?
Box-10	Threshold	--	1.12	?	?	--
Box-11	Threshold	--	1.50	?	?	--

Table 5.9
Scab Damage in the Fronts of Walls

Test No.	Scab Depth in.	Scab Area Length x Height in. x in.
1A	None	--
1B	0.75	? x 4.0
1C	2.44	17.0 x 12.8
1D	None	--
2A	None	--
2B	1.25	--
2C	2.50	15.0 x 13.0
2D	None	--
3A	Breached	--
3B	2.00	68.3 x 14.0
4A	2.25	110.0 x 5.0
4B	2.38	105.0 x 15.0
5A	1.25	54.0 x 14.0
5B	0.94	56.0 x 13.5
5C	1.85	12.0 x 12.0
6A	1.06	62.5 x 15.3
6B	1.50	?
6C	2.00	15.0 x 12.0
7A	2.00	?
7B	1.38	?
7C	2.25	?
8A	0.88	42.0 x 11.5
8B	1.40	53.0 x 11.6
8C	Breached	--
9A	2.50	83.5 x 17.2
9B	0.62	18.0 x 9.4
10A	1.75	83.0 x 14.0
10B	1.00	45.0 x 9.0
10C	1.88	13.8 x 12.0
Box-1	None	
Box-2	1.00	56.0 x 10.0
Box-3	2.50	60.0 x 13.0
Box-4	None	
Box-5	1.00	72.0 x 12.0
Box-6	2.50	75.0 x 17.0
Box-7	None	
Box-8	None	
Box-9	1.50	? x 18.0
Box-10	None	
Box-11	1.25	47.0 x 15.0

PART VI: ANALYSIS

General

A summary of the major test parameters and the resulting damage is compiled in Table 6.1. The damage classifications are based upon the criteria given in Table 6.2. The effect of various parameters on spall damage are discussed below.

Analysis of Spall Caused by a Bare Bomb

Test 1D is analyzed first to determine the conditions which caused spall. Test 1D was conducted on a "4,000 psi" concrete wall with a 7.44 lb bare charge at 1.54 feet from the wall. The spall appeared to be a single layer and the concrete was cracked two layers. The stress gage record is not good, so the stress wave will have to be calculated from the airblast record at PQ-0, which was in front of the area which spalled. Note the second peak in the airblast record is from a reflection of the airblast off the ground between the bomb and the wall. The initial rise time (0.000047 sec), peak stress (8,550 psi), and the static modulus of elasticity (4.8×10^6 psi) were used to approximate the strain rate of:

$$8,550 \text{ psi} / (4.8 \times 10^6 \text{ psi}) (0.000047 \text{ sec}) = 38 \text{ sec}^{-1}$$

According to Figure 2.18, the dynamic compressive strength of the concrete strained at 38 sec^{-1} is greater than 2 times the static strength. The static strength was 5,080 psi so the dynamic compressive strength was greater than 10,180 psi. The peak reflected airblast pressure of 8,550 psi was below the dynamic compressive strength, and is assumed to be below the Hugoniot elastic limit. Therefore, the propagation velocity was probably constant, attenuation was negligible, and the induced stress wave probably only significantly changed due to divergence. The pressure distribution on the wall indicates that the airblast wave expanded approximately cylindrically (see Appendix B). A cylindrically expanding airblast wave diverges according to equation 2.19. To calcu-

late the net stress at the spall plane (2.25 inches from the back of the wall), the peak reflected stress and the incident stress must be determined. The peak stress traveled 8.5 inches through the wall, reflected, and traveled back 2.25 inches for a total of 10.75 inches. It arrived at the spall plane at time 0.24 msec. It diverged to:

$$\sigma'(2.25, 0.24) = (8,550 \text{ psi}) \frac{\sqrt{18.5}}{\sqrt{18.5 + 10.75}} = 6,800 \text{ psi}$$

The incident stress at the spall plane is behind the peak stress by:

$$\frac{2d}{c} = \frac{2(2.25 \text{ in.})}{(12,150 \text{ ft/sec})(12 \text{ in./ft})} = 0.000031 \text{ seconds.}$$

The reflected airblast pressure 0.000031 sec after the peak reflected airblast pressure was 3,100 psi. This stress traveled from the front of the wall panel 6.25 inches to the spall plane. It diverged to:

$$\sigma(2.25, 0.24) = (-3,100 \text{ psi}) \frac{\sqrt{18.5}}{\sqrt{18.5 + 6.25}} = -2,680 \text{ psi}$$

The theoretical net stress at the spall plane was:

$$\sigma_{\text{net}}(2.25, 0.24) = 6,800 \text{ psi} - 2,680 \text{ psi} = 4,120 \text{ psi}$$

The ratio of this failure stress to the static split tensile strength was $4120/578 = 7.13$. This was close to the ratio extrapolated from the curve for dynamic tensile strength of concrete in Figure 2.19. The unit impulse trapped in the spall layer was theoretically 0.38 psi-sec. The lead spall velocity was measured at 28 ft/sec. The unit impulse required to cause the spall to travel at this velocity was:

$$i = mV = \frac{(150 \text{ lb/ft}^3)(2.25 \text{ in.})(28 \text{ ft/sec})}{(32.2 \text{ ft/sec}^2)(1,728 \text{ in}^3/\text{ft}^3)} = 0.17 \text{ psi} \times \text{sec}$$

The rest of the trapped impulse, 0.21 psi × second, was needed to overcome resistive forces such as bond, shear around the periphery of the spall zone, and mechanical interlocking. Thus, state of the art theory can be used to predict if and where a stress wave below the HEL will cause a tensile crack. However, theoretical methods for predicting any

changes in stress waves due to attenuation or stresses propagating at different velocities, and theoretical methods for predicting the forces which resist against the spall leaving the wall, are needed before spall can be theoretically predicted.

Effect on Spall of Changing Charge Weight at a Given Standoff Distance

Tests 1A, 1D, 2A, and 2D show how varying bare bomb sizes at a given standoff distance affects spall. The standoff distance for all 4 tests was 1.54 feet. The charges were bare and varied from 3.63 to 7.44 pounds of C-4 to cause various degrees of damage. Figure 6.1 compares the pressure-time histories at PQ-0 for tests 1A, 1D, and 2A (the PQ-0 gage in test 2D was hit). All of the peak pressures were less than the predictions from Figure 2-4. Notice that all three of the pressure plots have a second spike after the main peak. These second spikes were most likely from reflections of the airblast wave off the ground between the bombs and the wall panels. The second spikes actually helped to prevent spall because they arrived before the first peaks had unloaded very much and they unloaded at slower rates (were less sharp) than the first peaks. The bombs were ignited at their tops. Thus arrival times of the second spikes could be calculated by assuming the pressure comes from the point of ignition.

Test 1D, which caused medium spall was analyzed in the previous section.

Test 1A was conducted at the same standoff distance but with a smaller bomb (3.626 pounds) and scaled standoff distance than test 1D and caused no damage. The pressure-time history at PQ-0 had a smaller peak pressure and unit impulse in test 1A than in test 1D, as expected. The duration of the pressure-time history was the same in both tests. The strain rate was approximately $(6,000 \text{ psi}) / (4.8 \times 10^{-6} \text{ psi})$ $(0.000035 \text{ sec}) = 36 \text{ sec}^{-1}$. According to Figure 2.18, the dynamic compressive strength was greater than two times the static strength. Thus, compressive strength was greater than 10,180 psi again, and the peak pressure of 6,000 psi was below the HEL. The dynamic tensile strength in this test was roughly approximated at 4,000 psi, based upon the dynamic tensile strength in test 1D and upon Figure 2.19. The peak net

stress was calculated at several points in the wall panel and all of them were below 4,000 psi. The second spike, caused by the pressure wave which reflected from the ground, came early enough behind the first spike to keep to the peak net stresses below 4,000 psi. The second spike unloaded at a slower rate than the first spike and its peak reached the front surface of the wall before a peak net stress could exceed 4,000 psi. The largest peak net stress was when the peak reflected stress reached the front of the wall panel. At that point, the peak reflected stress had diverged to 4,331 psi and the incident stress was 1,580 psi, making a peak net stress of 2,751 psi. Therefore, no damage should have occurred.

Test 2A was at the same standoff distance, but with a bomb (4.70 pounds) between the sizes in test 1A and 1D. No damage was incurred. The strain rate was approximately 34 sec^{-1} , and the dynamic tensile strength was probably 3,900 psi, a little less than in test 1A. The largest peak net stress was 3,647 psi, when the peak reflected stress reached the front of the wall panel. This was below the dynamic tensile strength of approximately 3,900 psi. The second spike from the reflected airblast wave kept the incident portion of the stress wave high enough to keep net stresses below 3,900 psi before the peaks reflected again from the front of the wall.

Test 2D was at the same standoff distance as 1A, 1D, and 2A and had a bomb (5.45 pounds) between the sizes in test 2A where no damage occurred and test 1D where damage occurred. Test 2D caused a small threshold spall. Unfortunately, the airblast gages at PQ-0 and PQ-1 were damaged and no pressures were measured. The stress gage did not measure believable stresses and was noisy. No crack depth could be obtained because wall panel 2 was used in other tests and was not cut at the test locations. Thus, there are no data to analyze. It is believed that the airblast load was enough to cause the concrete to crack but the impulse trapped between the crack and the back surface was not enough to overcome the resistive forces.

These 4 tests illustrate how spall is dependent upon the magnitudes and the shape of the stress waves in the concrete. Spall can only occur when the peak reflected stress is greater than the dynamic tensile strength of the material, when either the wave length of the stress wave

is shorter than twice the wall thickness or the unloading portion of the stress wave unloads rapidly enough so that the sum of the peak reflected stress and the corresponding incident stress exceeds the dynamic tensile strength of the concrete, and when the impulse trapped between the crack and the back surface is enough to overcome forces resisting the portion behind the crack leaving the wall. The standoff distance and bomb have to be relatively small in order for an airblast wavelength to be smaller than twice most standard wall thicknesses. Refer to Figure 2.4 to see that peak reflected airblast pressure and scaled impulse ($i_p/W^{0.33}$) increase and scaled duration ($t_d/W^{0.33}$) decreases with increasing charge weight at a given standoff distance. The airblast loads unload or decay exponentially. The rate of unloading increases (i.e., the stress wave becomes sharper) with increasing unit impulse and decreasing duration. Since $t_d/W^{0.33}$ decreases as $W^{0.33}$ increases t_d does not change as rapidly as peak pressure or impulse. Thus increasing charge weight at a given standoff increases peak reflected pressure and impulse which make the unloading portion sharper and increases chances for spall.

Effect on Spall of a Bare Contact Charge

Test 1C was with a 1.074-pound bare charge in contact with the wall panel. The contact charge made a crater 2.44 inches deep by 17.0 inches wide by 12.8 inches high in the front of the wall panel. The formation of a crater implied that the stresses induced into the wall panel were above the dynamic compressive strength of the concrete. The stress wave probably changed magnitude and shape greatly as it propagated through the first few inches of concrete. The average velocity of the stress wave as it traveled from the front of the wall to the stress gage was 7,870 ft/sec. This is much less than the elastic propagation velocity of 12,150 ft/sec measured in a test cylinder. This discrepancy indicates the stress measurement was incorrect because at least an elastic precursor should have propagated at 12,150 ft/sec. The stress gage at the mid-plane in the wall measured a strong stress wave well above the noise. The first spike may have been an elastic precursor or noise. The peak stress measurement was 12,200 psi, the rise time was 0.012 msec and the duration was 0.150 msec. The approximate strain rate (using the

static modulus of elasticity) was 212 sec^{-1} . This is well above the limits of Figure 2.18, so the dynamic compressive strength of the concrete was probably much greater than just two times the static compressive strength of 5,080 psi. Assume for the moment that the dynamic compressive strength of the concrete was above the peak stress at the gage (2.4 times the static strength), then the stress wave would have only significantly changed by divergence and would have propagated at the elastic propagation velocity as it continued through the wall. If the elastic propagation velocity was 12,150 ft/sec, then the time it took the front of the stress wave to travel from the gage to the back of the wall, reflect as a tensile wave, and travel back to the gage was $(8.5 \text{ in.}) (1,000 \text{ msec/sec}) / (12,150 \text{ ft/sec}) = 0.058 \text{ msec}$. However, the elapsed time between the arrival time (0.045 msec) and the start of unload time (0.122 msec) at the gage was 0.077 msec, which was greater than 0.058 msec. One can not tell if the measured unloading portion was solely the tail of the incident wave or a combination of it and the reflected tensile portion of the wave. In either case, the propagation velocity had to have been less than 12,150 ft/sec in order for the stress measurement to be correct. A propagation velocity is needed to analyze the spall. The spall depth was 2.50 inches deep. One does not know if the spall was one or more layers. If it was one layer of spall, the peak stress of 12,200 psi at the gage would diverge to 7,583 psi by the time it reflected and arrived at the spall plane. If the concrete failed at the same dynamic tensile strength as in test 1D of 4,120 psi, then the corresponding incident stress at the spall plane was 3,463 psi. This stress would have diverged from a value of 4,115 at the gage location, and would have been 0.095 msec after the peak. The propagation velocity corresponding to these assumptions was:

$$\frac{(2)(2.50 \text{ in.})(1,000 \text{ msec/sec})}{(12 \text{ in./ft})/(0.095 \text{ msec})} = 4,385 \text{ ft/sec}$$

This was much lower than expected for this concrete. If there were more than one layer of spall, then the propagation velocity was even less. Thus, the stress measurement was inconsistent with other measurements which indicated the stress measurement was incorrect.

The test did demonstrate that contact bare charges can cause very high peak stresses, scabbing and spall.

Effect on Spall of Changing the Bare Charge Weight and Stand-off Distance at a Given Scaled Standoff Distance

Tests 1D and 3A demonstrated the effects on spall of two different size bombs at two different standoff distances, but the same scaled standoff distance. The peak normally reflected airblast pressure should theoretically be the same in both tests, but the peak pressure at location PQ-0 in test 1D was 8,550 psi and the peak pressure at PQ-0 in test 3A was 7,000 psi. The C-4 in the bomb in test 3A may have been slightly less dense than in the bomb in test 1D and this may have caused the normally reflected peak pressure to be less. For a given scaled standoff distance, the impulse and the duration increase with increasing bomb size and standoff distance. The increase in duration affects the shape of the pressure-time history the most. Freidlander's equation for describing the unload portion of an airblast wave (see equation 2.6) illustrates this well. The duration (t_d) is used twice in equation 2.6 and the constant (b) is a function of both the impulse and duration. The wall panels in both tests were identical. Since the size of the walls were not scaled with the standoff distance, the pressure distributions on the walls were very different (see the pressure distribution plots in Appendix B).

The total area of the wall which is severely loaded and the total impulse on the wall panel both increase with increasing bomb size and standoff distance for a given scaled standoff. The wall in test 1D had medium spall 2.25 inches deep and over an area 17 inches wide and 11 inches high; compared to the wall in test 3A which, breached, severed at the floor, had scattered deep spall areas (up to 4.9 inches deep), and severe flexural damage over an area approximately 90 inches wide and 43 inches high. This drastic difference in damage demonstrates the fallacy of saying that spall occurs at or below a certain scaled standoff distance (such as in Reference 7). Spall is dependent upon the shape of the stress wave as well as the peak reflected pressure.

Differences in Spall Damage in "Cube-Root" Scaled
Tests of Bare Charges

Tests 1A and 2D were scaled models of tests Box 10 and Box 7, respectively. The most important parameters of bomb sizes, standoff distances, wall thicknesses, and the concrete strengths were all properly scaled. The scale ratio of the wall thickness and standoff distance in the wall panel tests to those in the box tests was 1.0 to 1.3. The heights and widths of the box walls were larger than those of the wall panels, but were not scaled at the same ratio as the thicknesses. However, since the only damage which occurred was localized spall in the lower portions of the walls (no flexural damage), it did not matter if the heights and widths were not the exact scale. The steel ratios in the wall panels were 0.25 percent and the box walls were 1.00 percent. This difference should not have affected the spall depth, but may have affected the resistive forces against spall and the spall velocities. (If it had any effect it should have decreased the amount of spall in the box tests.)

Comparison of the spall damage in tests 1A and 2D with the spall damage in test Box 10 and Box 7, respectively, show that spall damage was worse in the larger scale box tests (see figures of tests in Appendix C). Test 1A had no damage, whereas, test Box 10 had threshold spall. Test 2D had threshold spall, whereas, Box 7 had medium spall. According to Hopkinson or cube-root scaling laws (Reference 5), the peak normal reflected pressure and velocities should have been the same in both tests, but length, time, and some other parameters scale. Time scales at the same scale ratio as length, thus, the rise times and durations in the wall panel tests should have scaled to those in the box tests by the same ratio of 1.0 to 1.3. Since the peak normally reflected pressures remain the same but the rise times scale, the strain rates should have scaled by 1.0 to $1/1.3$. The dynamic tensile strength of the concrete is dependent upon the strain rate of loading, so the dynamic tensile strengths in the wall panel tests were probably greater than in the larger box tests. Thus, the spall damage in the wall panel tests were less than in the larger scale box tests because the dynamic tensile strengths of the concrete were different for different strain

rates. This theory was confirmed by a series of tests on a full-scale box structure and a quarter-scale model of the same structure conducted later in another project (Reference 47). The quarter-scale model suffered no damage in scaled tests of tests which caused spall and breach of the full-scale box structure. Thus, caution should be exercised when using small scale models to predict the spall damage of full-scale structures, because they will under predict the damage. Empirical prediction curves such as in Figures 3.3 and 3.4 for bare charges should only be used to predict spall in similar scale tests to those upon which the curves were based.

Comparison of Damage Caused by Equal-Size Bare and Cased Charges

Several tests were conducted to determine the differences in damage caused by equal-size bare and cased charges at the same standoff distances from identical structures. See the pictures in Appendix C and the data in Table 6.1 to compare the spall damage in tests 1C with 2C, 1A with 1B, 2B with 2D, Box 1 with Box 2, Box 4 with Box 5, and Box 8 with Box 9. All of the tests with cased charges had worse damage than the tests with the same size bare charges at the same distance from identical walls, except the contact charge 2C. References 2, 46, and 47 also report worse damage in tests with cased charges than in similar tests with bare charges. The difference in damage caused by equal-size cased and bare charges was minimal for contact charges and increased with increasing standoff distance until the fragments became so scattered that they only had a small local effect on the structure. This is illustrated by comparing the damage prediction curves for bare and cased charges in Figures 3.4 and 3.6, which were obtained from Reference 46.

The difference in damage was due to the difference in loading caused by equal bare bombs and cased bombs at various standoff distances. The detonation of a bare charge results in primarily airblast load on a nearby structure, whereas the detonation of a cased charge results in primarily combined airblast and multiple fragment impacts loads on a nearby structure. Prediction methods for airblast and bomb fragment loadings were given in Chapter 2. The airblast from a cased

charge has a slightly lower peak pressure and unit impulse than the airblast from an equal-size bare charge at the same standoff distance. The stress waves induced by the multiple bomb fragment impacts are a function of the bomb fragment sizes, masses, velocities, hardness, and shape. Typical bomb fragments induce very sharp stress waves with very high stresses (usually several kilobars at the surface) and very short durations (much shorter than the airblast duration). The bomb fragments usually penetrate the concrete and cause a portion of the wall to scab (see posttest pictures of the walls in Appendix C). Spall damage will occur if the combined loads are severe enough. The difference in loadings in some of the bare and cased charge tests are analyzed below.

The contact charges in tests 1C and 2C made similar craters in the front of the wall panels and caused similar spall damage. The bare charge in test 1C even caused a slightly deeper spall (2.5 inches) than the spall caused by the cased charge in test 2C (2.0 inches). The craters in the walls indicate that both bombs generated extremely high airblast pressures (higher than the dynamic compressive strength of the concrete). The medium spall damage indicates that the airblast loads durations were short and they unloaded rapidly. According to theory, the airblast from the cased charge should have a slightly lower peak pressure and unit impulse than the airblast from the bare charge, because energy was used to break up the casing. There may have also been a slight difference in the airblast loading because the center of the cased charge was a casing thickness (0.047 inches) further from the wall than the bare charge was from the wall. A portion of the cased bomb was already against the wall before detonation, so the bomb fragments from this portion did not impact the wall at some high fragment velocity but were pushed into the wall by the pressure. Any stresses induced by bomb fragments from other parts of the casing which were not in contact with the wall, arrived at nearly the same time as the airblast and were overshadowed by the extremely high airblast load. Since the peak stresses induced at the surface of the wall were above the dynamic compressive strength of the concrete, the shape and magnitude of the stress waves changed due to attenuation and stresses traveling at different velocities, as well as due to divergence. Thus, the stresses measured by the stress gages in the middle of the wall were different than those induced

at the surface. Although the accuracy of the stress measurements are questionable, the stress wave measured in test 1C was less sharp and had a lower peak stress than the stress wave measured in test 2C. Test 1C was already analyzed in the previous section and the stress measurement was inconsistent with other measurements. The test 2C stress measurement had a rise time of 0.019 msec and a peak stress of 14,500 psi. The rise time, peak stress, and a static modulus of elasticity were used to approximate the strain rate of: $14,500 \text{ psi} / 0.000019 \text{ sec} / 4.86 \times 10^6 \text{ psi} = 157 \text{ sec}^{-1}$. This was well above the limits of Figures 2.18 and 2.19. It was assumed that peak stress of the stress wave was below the dynamic compressive strength of the concrete by the time it reached the gage location. Therefore, the propagation velocity of all the stresses beyond the gage was the elastic velocity of 12,120 ft/sec. The only major change to the stress wave as it propagated further was divergence. The peak pressure diverged to:

$$14,500 \text{ psi} \frac{\sqrt{4.25}}{\sqrt{10.5}} = 9,225 \text{ psi}$$

by the time it reached the spall plane. If there was only one spall layer, the time behind the peak stress at which spall would have occurred was: $(2)(2 \text{ in.}) / (12 \text{ in./ft}) / (12,120 \text{ ft/sec}) = 0.000027 \text{ sec}$. This corresponded to a stress of 6,550 psi at the gage location, and

$$6,550 \text{ psi} \frac{\sqrt{4.25}}{\sqrt{6.5}} = 5,256 \text{ psi}$$

at the spall plane. The dynamic tensile strength was $9,225 \text{ psi} - 5,256 \text{ psi} = 3,969 \text{ psi}$, which was slightly less than that calculated for test 1D. Thus, the stress measurement in test 2C was fairly consistent with other measurements.

The difference in spall damage caused by bare and cased charges varied more at larger standoff distances, because the airblast and bomb fragment loads varied differently with changes in standoff distance. The airblast load rapidly decreases in peak pressure, decreases in unit impulse, decreases in velocity, increases in duration, and unloads slower (becomes less sharp) with increasing standoff of a given bomb. The previous sections already discussed the effect of various bare

charges, i.e. airblast loads on spall damage. It was shown that several of the bare bombs in this test series produced airblast waves with wavelengths many times longer than the wall thickness and with unloading portions slow enough that the peak net stress would not exceed the dynamic tensile strength of the concrete. In comparison, the bomb fragments lost their momentum at a much slower rate than the airblast waves changed with distance. Reference 8 on bomb fragment effects states that "... within a short distance from the detonation, usually 20 feet, the striking velocity can be assumed to be equal to the initial velocity." In other words, there is negligible decrease in the velocity of most bomb fragments within the first 20 feet from cased bombs. The velocity of the fragments decreases with distance in accordance to equation 2.11, which is usually used for distances greater than 20 feet. Thus, the loads from most bomb fragment impacts do not significantly change within the first 20 feet from a given cased bomb. Of course, the number of bomb fragments which hit a wall per unit surface area, decreases with increasing standoff distance from a given bomb (This is a form of divergence). As stated earlier, typical bomb fragments induce very sharp stress waves at the surface, with very high stresses (usually several times the dynamic compressive strength) and very short durations (much shorter than the airblast duration). These stress waves change magnitudes and shapes as they propagate. Since the peak stress at the surface is usually higher than the dynamic compressive strength, the fragment penetrates the concrete, the stresses attenuate rapidly as the concrete is crushed and the stresses travel at different velocities. The stress wave expands as it travels away from the fragment causing divergence. Since the stress wave from a single bomb fragment impact is small, it could be dispersed easily. However, many of the multiple bomb fragment stress waves are still severe enough and sharp enough to cause spall by the time they reflect off the back of the wall. Thus, the bomb fragment stress waves become more dominant when compared with the airblast stress wave as the standoff distance for a given bomb is increased. Since the airblast velocity and bomb fragment velocities decelerate differently with distance, the difference in arrival times of each varies with distance. The airblast arrives after the bomb fragments at large distances from the bomb. If the arrival times of the

airblast and bomb fragments are close enough, their stress waves will combine or superimpose on each other. The stress measurements in tests 2C and 10C have no apparent spikes from stresses induced by bomb fragment impacts. The stress measurements in tests 3B, 6B, and 10A also have no extra spikes, but their peak stresses were higher than the peak reflected airblast pressures measured at the surface by nearby PQ-0 or PQ-1 airblast gages. This confirms that stress waves from the fragments combined with the stress wave from the airblast. Test 9A was conducted with a cased bomb at a relatively large standoff distance and the stress measurement in that test has two sharp, short duration, stress waves in front of a larger, longer duration stress wave. The two sharp stress waves are probably from bomb fragment impacts and the large stress wave is probably from the airblast load. This confirms the assumptions that bomb fragment stress waves have high peak stresses and short durations.

Effect on Spall of Casing Thickness

Other tests were conducted to examine the effect on spall damage of casing thickness. Cased bombs with different casing thicknesses, but the same charge weight and inside dimensions were detonated at the same standoff distance from identical concrete walls and the resulting damage was compared. Compare the damage, shown in the pictures in Appendix C, and the damage measurements, in Table 6.1, of tests 8B with 8C, Box 2 with Box 3, and Box 5 with Box 6. All of the comparisons support the theory that within certain limits of bomb sizes, standoff distances and casing thicknesses; thin-cased charges cause less spall than thick-cased charges.

This difference in damage is due to the difference in the stress waves induced by small and large bomb fragments. According to the equations given in Chapter 2, the average bomb fragments increase in mass, decrease in initial velocity, and decelerate slower; with increasing casing thickness. As stated before, the stress waves induced by multiple bomb fragment impacts are a function of the bomb fragment sizes, masses, velocities, hardness, and shapes. Equation 2.13 for pressure applied by a bomb fragment predicts that peak pressure decreases with a decrease in striking velocity and an increase in bomb fragment diameter

within certain limits. Equation 2.14 for time at a penetration depth of a bomb fragment, predicts that the duration of the stress wave increases with a decrease in velocity and an increase in fragment weight within certain limits. If the peak stresses are above the dynamic tensile strength, the stress waves unload rapidly, and if the wave length is less than 2 times the wall thickness; then, small increases in duration will result in deeper spall.

Tests 8B and 8C were analyzed for comparison. The bomb in test 8B had a casing thickness of 0.07 inches and it caused threshold spall. Whereas, the bomb in test 8C had the same charge weight, but a casing thickness of 0.22 inches and it caused breach. The calculated average fragment weights for test 8B and 8C were 0.00125 ounces and 0.0185 ounces, respectively (see equation 2.9). The initial bomb fragment velocities were calculated to have been 8,408 ft/sec in test 8B and 5,770 ft/sec in test 8C. The penetration depth of the average fragment in test 8B was calculated to have been 1.46 inches, which is close to the measured scab depth of 1.40 inches. The calculated penetration depth in 8C was 1.73 inches; no measurement of actual penetration was obtained because the wall was breached. The calculated peak stresses, using the equation 2.13, were 236,700 psi in 8B and 190,930 psi in 8C. The rise times and durations during penetration of the fragments were calculated, according to equation 2.14, to have been 0.00563 and 0.03348 msec, respectively in 8B, and 0.01507 and 0.0509 msec, respectively in 8C. Thus, the theoretical stress wave induced in the wall by an average bomb fragment in test 8C had a lower peak stress, longer rise times, and longer duration than the stress wave induced by an average bomb fragment in test 8B. Although the magnitudes and shapes of the stress waves changed as they propagated through the concrete, it was assumed that bomb fragment stress waves in test 8C still had lower peak stresses, longer rise times, and longer durations than the stress waves in test 8B at the same points in the concrete. The airblast arrived at PQ-0 at 0.17 msec in test 8B. The calculated arrival time of the bomb fragments was 0.18 msec in test 8B. Thus, the airblast wave arrived only 0.01 msec before the bomb fragments, and the peak stresses induced by the fragments and airblast probably superimposed. This is confirmed by the stress measurement in test 8B which only has one peak.

Unfortunately, no airblast gages were used in test 8C (none would have survived). According to equation 2.1, the equivalent bare weight of the cased charge in test 8C was 2.31 pounds, whereas it was 4.52 pounds in test 8B. Therefore, the peak pressure was lower and the arrival time was later in test 8C than in test 8B. Figure 2.4 shows an increase of arrival time of 1.2 times. Thus, the arrival time was estimated to be 1.2 by 0.17 = 0.20 msec. The calculated arrival time of the bomb fragments was 0.27 msec in test 8C. Thus, the peak of the airblast stress wave was induced about 0.07 msec before the peaks of the bomb fragment stress waves were induced and there were probably two major peaks in the combined stress wave. If the peak stresses were lower and the rise times longer for both peaks in test 8C than the single peak in test 8B, then the strain rates were slower in test 8C. If the strain rates were slower in test 8C, then the dynamic compressive and tensile strengths of the concrete in test 8C were lower than in test 8B. Thus, a lower net stress was needed to cause spall in test 8C than in test 8B. If the first peak in test 8C was longer and unloaded slower than the top of the combined stress wave in test 8B, then the spall depth should have been deeper in 8C than 8B. The second peak in test 8C may have helped push the "cracked off" concrete or spall, caused by the first peak, away at a high velocity and then may have caused additional layers to spall.

Prediction methods for damage caused by cased charges should consider casing thickness. One should use caution in using the prediction curves in Figures 3.6 for bombs with low or high charge to bomb weight ratios.

Differences in Spall Damage in "Cube-Root" Scaled Tests of Cased Charges

A couple of tests were modeled to study the effects of "cube-root" scaling on the damage caused by nearby cased bombs. Test 8B was a scale model of test 4B, and test 9B was a scale model of test 3B. The scale of both models was a ratio of 0.6 to 1.0. Test 8B had threshold spall, except one or two small spall fragments left the wall, whereas, test 4B had medium spall 1.81 inches deep. In addition, the bomb fragments in test 8B caused the outside of the wall to scab up to 1.38 inches deep and over a zone 53.0 inches wide by 11.6 inches high, whereas, the bomb

fragments in test 4B caused scabbing up to 2.38 inches deep and over a zone 105 inches wide by 15.0 inches high. Test 9B caused threshold spall, whereas, test 3B caused medium spall. Test 9B had scabbing up to 0.62 inches deep over a zone 18.0 inches wide by 9.4 inches high, whereas, test 3B had scabbing up to 2.0 inches deep over a zone 68.3 inches wide by 14.0 inches high. Both models had less spall and scab damage than the full-scale tests.

A previous section already discussed how strain rate scales by the inverse of the scale factor, so the dynamic tensile strength of the concrete is higher under the airblast load of the model than of the full-scale test, but the peak pressures are the same in both tests. A similar problem occurs with different size bomb fragments. The average size bomb fragments are larger in the full scale tests than in the model tests, but the initial velocities remain the same in both tests. Thus, the strain rate is slower in a full-scale test than in a scale-model test and a lower net stress is needed to cause spall. A third problem in scaling cased bombs with a large standoff distance is that the velocities of the scaled-bomb fragments decrease at a faster rate than the full-scale bomb fragments. A fourth problem in scaling cased bomb tests is the bomb fragment mass distribution does not scale. For example, the average bomb fragment in 8B was 0.0025 ounces and the average bomb fragment in 4B was 0.0073 ounces, which does not correspond to the volume scaled by $(0.6)^3$. Therefore, full-scale models of concrete walls subjected to nearby cased bomb detonations incur more spall and scab damage than scale models. Small scale model structures subjected to nearby cased bomb detonations should not be used to predict the spall and scab damage to full-scale structures because they would under predict the damage. Thus, the use of empirical prediction curves, such as Figures 3.5 and 3.6 should be limited to similar scale tests to those upon which the curves were based.

Effect on Spall of Wall Thickness

Several tests were conducted to study the effect on spall damage of wall thickness. The size of the bomb, casing thickness, standoff distance of the bomb, and concrete properties were all held constant while

the wall thickness was varied in several tests and the resulting damages were compared. Refer to Appendix C and Table 6.1 to compare the resulting damage in test 1A with test Box 1, test 1B with tests 8B and Box 2, test 1D with test Box 4, test 3B with test Box 5, and test 4A with test 9A. Note that the walls in the box structure had a different amount of reinforcing steel than the wall panels, but this was considered to have a minor effect on the spall damage. There was usually slightly less damage in the thicker walls than in the thinner walls. Other types of damage such as flexural bending, and shear were also affected by wall thickness. Reference 1 also examined the effect of wall thickness on spall and other types of damage and concluded that thicker walls do incur less damage than thinner walls.

An increase in the wall thickness is an increase in the distance the induced stress waves have to travel before they can cause spall. The further the stress waves have to travel, the more they can change their magnitudes and shapes, due to different stresses traveling at different velocities, attenuation, divergence, and dispersion. The tests in this study and in Reference 1 indicate that the wall thickness must be increased by large amounts to reduce medium spall to light spall or threshold spall to no damage. There are other less costly methods of reducing spall damage.

Effect on Spall of Rebar Spacing

The effect on spall damage of reinforcing steel spacing was studied in some of the tests. Similar wall panels with the same concrete mix design and the same percentage steel, but with different size reinforcing bars and spacing of the bars, were tested with the same size bombs at the same standoff distances. Tests 1B, 2C, and 4B were compared with tests 10B, 10C, and 10A, which had closer reinforcing steel spacings, respectively. Tests 1B, 2C, and 4B all had principal reinforcing steel of No. 3 bars spaced at 5.5 inches, longitudinal reinforcing steel of D5 bars spaced at 5.5 inches, and stirrups which hooked around the outside of the principal steel at 5.5-inch spacings (see Figure 4.3). Tests 10B, 10C, and 10A all had principal steel of D3 bars spaced at 1.5 inches, longitudinal steel spaced at 1.25 inches, and stirrups which

hooked around the outside of each principal steel bar at 5.0-inch spacings (see Figure 4.5). Refer to Appendix C and Table 6.1 to compare the damage of the tests. All of the tests on wall panel 10, with the smaller reinforcing steel spacing, had less spall damage than the tests on the wall panels with the larger reinforcing steel spacing. There were even less cracks and shallower cracks in all of the tests on wall panel 10 than in the similar tests on the other panels.

It is hypothesized that the spacing of the reinforcing steel in wall panel 10 was close enough to cause significant dispersion of the stress waves to reduce peak net stresses, and to partially confine spall. Evidently, the peak net stress was reduced below the dynamic tensile strength in test 10B, because there was no damage in test 10B, whereas, test 1B had threshold spall. If the peak net stress exceeds the dynamic tensile strength of the concrete behind the reinforcing steel grid, the closer reinforcing steel spacing provides a more uniformly distributed resistive force against the momentum trapped in the cracked off concrete. The cracked off layers of concrete must break into small pieces to pass through the small reinforcing grid. In test 10A, a few pieces of spall managed to break away from the wall, whereas, much more spall left the wall and at a higher velocity in test 4B. The closer spacing of the steel grid also caused the concrete around the steel plane to be weaker because there were more bars each with micro-cracks around them at closer intervals. The concrete cover in test 10C spalled (0.62 inches thick) and the cracked concrete was retained behind the reinforcing steel grid, whereas, the spall depth in test 2C was 2.0 inches and very little cracked concrete was retained behind the reinforcing steel grid. The spall in test 10C broke off at the weak steel plane as it tried to pull away. The velocity of the spalled concrete cover in test 10C was 70 ft/sec, whereas, the velocity of the spall in test 2C was 57 ft/sec.

Thus, a closely spaced reinforcement grid held securely with closely spaced stirrups does reduce the amount of spall and the spall depth, but weakens the concrete around the reinforcement plane to allow the concrete cover to spall more readily. It cost about twice as much to build wall panel 10 with very close reinforcement spacings than it cost to build one of the similar wall panels with wider reinforcement

spacings. Since the concrete cover over the reinforcing steel can in certain cases still spall at high velocities, the extra expense of making a very closely spaced reinforcing steel grid is not justified. A spall plate would be cheaper and would retain the concrete cover.

Effect on Spall of Concrete Strength

The effect on spall of concrete strength was studied. Since the tensile strength of the concrete increases with increasing compressive strength it was thought that spall would decrease with increasing compressive strength. The spall damages caused by detonation of bombs near wall panels made of 4,000 psi concrete were compared with spall damages caused by identical bombs at the same distances away from a similar wall panel made of high-strength concrete. The walls were all similar with the same reinforcing steel, the same spacing of the steel, and the same dimensions. Only the strength of the concrete was different. The tests on the walls made of 4,000-psi concrete were 3B, 1B, and 2C, and they were compared with the similar tests 5A, 5B, and 5C, respectively, which were on a wall panel made of high-strength concrete. Wall panels 1, 2, and 3 were all cast from the same batch of 4,000-psi concrete, which had an average unconfined compressive strength of 5,025 psi and an average split tensile strength of 578 psi. Wall panel 5 was made of high-strength concrete with an unconfined compressive strength of 13,815 psi and a split tensile strength of 925 psi. Compare the pictures of the spall damages in Appendix C and spall depths and velocities listed in Table 6.1. The spall depths and spall velocities in the tests on the wall panel made of high-strength concrete were much worse than in the similar tests on the 4,000-psi concrete.

It was hypothesized that since the high-strength concrete had a higher static compressive and tensile strength than the 4,000-psi concrete, it probably had higher dynamic compressive and tensile strengths. If the dynamic compressive strength of the high-strength concrete was higher than that of the 4,000-psi concrete, then the Hugoniot Elastic Limit (HEL) for the high-strength concrete was higher than the HEL for the 4,000-psi concrete. Thus, the stress waves with high peak stresses (such as those induced by a contact charge or bomb fragments) did not

change as much due to stresses traveling at different velocities and attenuation in the high-strength concrete as in the 4,000-psi concrete. This was confirmed by the fact that the stress waves measured in the tests on the high-strength concrete wall panels had much higher peak stresses, shorter rise times, and shorter durations than stress waves measured in the tests on the 4,000-psi concrete wall panels. Therefore, stress waves induced by similar loads started out in both concretes the same, but the stress waves in the high-strength concrete had higher peak stresses, shorter durations, and sharper shapes by the time they reached the back of the wall than in the 4,000-psi concrete. The high-strength concrete had a static compressive strength 2.75 times that of the 4,000-psi concrete, whereas, it had a static tensile strength only 1.60 times that of the 4,000-psi concrete. Although the strain rate was higher in the high-strength concrete, one cannot determine how much more the dynamic tensile strength of the high-strength concrete was over that of the 4,000-psi concrete. It was hypothesized that the higher peak stresses, shorter durations, and sharper shapes of the reflected stress waves overcame any benefits of a higher dynamic tensile strength in the high-strength concrete and caused multiple spall layers. The high-strength concrete also had a higher elastic propagation velocity (16,250 ft/sec) than the 4,000-psi concrete (12,200 ft/sec).

The impulse per mass of a cracked-off layer of concrete was higher because the dynamic tensile strength was higher in the high-strength concrete than in the 4,000-psi concrete. High-strength concrete is very brittle and fails more violently than the 4,000-psi concrete. Tests in Reference 18 show that the bond strength of concrete on deformed reinforcing steel increases with increasing strain rate at a lower amount for high-strength concrete than normal strength concrete. Therefore, the spall velocities of the high-strength concrete were greater than those of the 4,000-psi concrete, because the trapped impulse per mass of the cracked-off concrete was higher and the resistive forces were not much higher.

The strengths of the concretes used in protective structures have been increased over the years. Many have recommended using high-strength concrete in protective structures to make them harder or stronger. However, high-strength concrete can, under severe loads,

spall deeper and with higher velocities than normal strength concrete under the same loads, and should be used with caution in protective structures where spall is possible.

Effect on Spall of Adding Acrylic Latex to Concrete

The effects on spall of adding acrylic latex to the concrete mix were studied. It was believed that the acrylic latex additive would make the concrete more ductile and resistant to spall. Similar tests were conducted on wall panels with the same dimensions, same reinforcing steel at the same spacings, and similar 4,000-psi concrete mix designs, except acrylic latex was added to the concrete mixture in one of the walls. The 4,000-psi mix design was slightly modified to account for water in the acrylic latex and to have a uniaxial compressive strength similar to the regular 4,000-psi concrete. The tests on the walls made of 4,000-psi concrete were 3B, 1B, and 2C; they were compared with similar tests on the acrylic latex concrete, which were tests 6A, 6B, and 6C, respectively. Compare the pictures of the spall damage in Appendix C and spall depths and velocities listed in Table 6.1. The damage was greatly reduced in tests 6A and 6B as compared with tests 3B and 1B respectively. However, the contact charge caused deeper spall but with a lower velocity in test 6C than in test 2C.

The acrylic latex formed a matrix in the microstructure of the concrete, which helped bond the various concrete elements together. The acrylic latex bonds were very ductile and retarded rapid crack growth during the dynamic loading. The static compressive and tensile strengths of the acrylic latex concrete were less than those of the 4,000-psi concrete. However, the stress waves measured in the acrylic latex concrete had higher peak stresses and longer durations than those measured in the 4,000-psi concrete. The Hugoniot curve for the acrylic latex concrete may have had a higher HEL but lower tangent slopes above the HEL than that of the 4,000-psi concrete. It was hypothesized that the acrylic latex concrete had higher dynamic tensile strengths and higher resistive forces against spall than the 4,000-psi concrete.

Effect on Spall of Adding Crimped Steel Fibers to Concrete

The effects on spall of adding steel fibers to the concrete mix were studied. It was believed that the addition of crimped steel fibers would make the concrete more ductile and increase resistive forces against spall. Similar tests were conducted on wall panels with the same dimensions, same reinforcing steel at the same spacings, and similar 4,000-psi concrete mix designs except crimped steel fibers were added to the concrete mixture of one of the wall panels. The 4,000-psi mix design was slightly modified to allow the addition of 80 lb/yd³ of crimped steel fibers in the concrete of one wall. The static compressive strength, modulus of elasticity, and propagation velocity of the steel fiber concrete were about the same as those of the 4,000-psi concrete. The split tensile strength of the steel fiber concrete was less than that of the 4,000-psi concrete. The split tensile strength was only measured to the first crack of the cylinders, but the steel fibers increased the ductility of the concrete after the first crack. The tests on the walls made of 4,000-psi concrete were 3B, 4B, and 2C, and they were compared with similar tests on the crimped steel fiber concrete, which were 7A, 7B, and 7C, respectively. Compare pictures of the spall damage in Appendix C, and compare the spall depths and velocities listed in Table 6.1. The spall damage was much less in tests 7A and 7B (which had a few cracks) as compared with tests 3B and 4B (which had medium spall). The contact charge in test 7C did cause spall of the fiber concrete. The spall depth in test 7C was as deep as in test 2C, but the area of the spall and spall velocity in test 7C were smaller than in test 2C.

The crimped steel fibers were dispersed throughout the concrete mixture. The steel fibers increased the dynamic tensile strength of the concrete by retarding rapid crack growth during the dynamic loadings. Once a crack was formed, the fibers helped resist spalling by holding the concrete together until the bonds between the fibers and concrete were broken. Fewer crimped steel fibers were needed per cubic yard of concrete mix to reduce spall than straight steel fibers because the crimps enhanced the bond between the fiber and concrete.

Table 6.1
Summary of Test Parameters and Resulting Damage

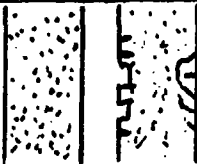
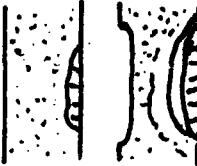



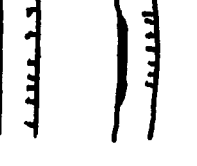
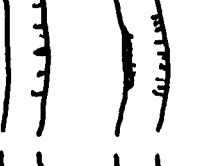
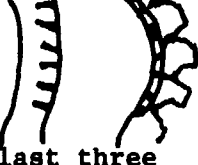
Test No.	C-4 Weight lb	Casing Thickness in.	$R/W^{0.33}$ ft/lb ^{0.33}	$T/W^{0.33}$ ft/lb ^{0.33}	Concrete f'_c + Additive psi	Rebars Bar-Spacings Size-in.	Damage
1A	3.626	Bare	0.903	0.415	5,010	#3 @ 5.5	No Damage
1B	3.626	0.70	0.903	0.415	5,010	#3 @ 5.5	Threshold
1C	1.074	Bare	0.073	0.623	5,010	#3 @ 5.5	Medium
1D	7.442	Bare	0.711	0.327	5,010	#3 @ 5.5	Medium
2A	4.700	Bare	0.829	0.381	5,085	#3 @ 5.5	No Damage
2B	5.455	0.088	0.788	0.362	5,085	#3 @ 5.5	Threshold
2C	1.074	0.047	0.077	0.623	5,085	#3 @ 5.5	Medium
2D	5.455	Bare	0.788	0.362	5,085	#3 @ 5.5	Threshold
3A	29.410	Bare	0.711	0.207	4,980	#3 @ 5.5	Breach
3B	7.082	0.088	0.723	0.332	4,980	#3 @ 5.5	Medium
4A	14.393	0.111	1.851	0.262	5,290	#3 @ 5.5	No Damage
4B	14.393	0.111	0.902	0.262	5,290	#3 @ 5.5	Medium
5A	7.082	0.088	0.723	0.332	13,815	#3 @ 5.5	Medium
5B	3.626	0.070	0.903	0.415	13,815	#3 @ 5.5	Medium
5C	1.074	0.047	0.077	0.623	13,815	#3 @ 5.5	Severe
6A	7.082	0.088	0.723	0.332	4,140 + Latex	#3 @ 5.5	Threshold
6B	3.626	0.070	0.903	0.415	4,140 + Latex	#3 @ 5.5	Threshold
6C	1.074	0.047	0.077	0.623	4,140 + Latex	#3 @ 5.5	Severe
7A	7.082	0.088	0.723	0.332	5,050 + Fiber	#3 @ 5.5	Threshold
7B	14.393	0.111	0.903	0.262	5,050 + Fiber	#3 @ 5.5	Threshold
7C	1.074	0.047	0.077	0.623	5,050 + Fiber	#3 @ 5.5	Medium

(Continued)

Table 6.1 (Concluded).

Test No.	C-4 Weight lb	Casing Thickness in.	$R/W^{0.33}$ ft/lb ^{0.33}	$T/W^{0.33}$ ft/lb ^{0.33}	Concrete f'_c + Additive psi	Rebars Bar-Spacings Size-in.	Damage
8A	1.661	0.054	1.172	0.341	4,140	D5 @ 4.12	No Damage
8B	3.626	0.070	0.903	0.262	4,140	D5 @ 4.12	Threshold
8C	3.626	0.219	0.903	0.262	4,140	D5 @ 4.12	Breach
9A	14.393	0.111	1.851	0.166	4,940	D5 @ 4.12	Flexure
9B	1.661	0.054	0.721	0.341	4,940	D5 @ 4.12	Threshold
10A	14.393	0.111	0.902	0.262	4,320	D3 @ 1.5	Medium
10B	3.626	0.070	0.903	0.415	4,320	D3 @ 1.5	No Damage
10C	1.074	0.470	0.077	0.623	4,320	D3 @ 1.5	Medium
Box-1	3.625	Bare	0.904	0.550	5,100	#8 @ 8.0	No Damage
Box-2	3.625	0.070	0.904	0.550	5,100	#8 @ 8.0	Light
Box-3	3.625	0.219	0.904	0.550	5,100	#8 @ 8.0	Medium
Box-4	7.437	Bare	0.711	0.432	5,100	#8 @ 8.0	No Damage
Box-5	7.437	0.088	0.711	0.432	5,100	#8 @ 8.0	Medium
Box-6	7.437	0.344	0.711	0.432	5,100	#8 @ 8.0	Medium
Box-7	12.000	Bare	0.787	0.369	5,100	#8 @ 8.0	Medium
Box-8	6.250	Bare	0.978	0.458	5,100	#8 @ 8.0	No Damage
Box-9	6.250	0.156	0.997	0.467	5,100	#8 @ 8.0	Medium
Box-10	9.000	Bare	0.866	0.406	5,100	#8 @ 8.0	Threshold
Box-11	3.860	0.250	1.171	0.549	5,100	#8 @ 8.0	Threshold

Table 6-2
Damage Classifications*

NO DAMAGE	From no change in the condition of the wall to a few barely visible cracks.	
THRESHOLD SPALL	From a few cracks and a hollow sound to a large bulge in the concrete with a few small pieces on the floor.	
MEDIUM SPALL	From a very shallow spall to a third of the wall thickness.	
SEVERE SPALL	From just over one third the wall thickness to almost breach.	
BREACH	From a small hole which barely lets light through to a large hole.	
LIGHT FLEXURE	From no permanent displacement but a few flexure cracks, to a ductility ratio of 3.	
MEDIUM FLEXURE	From a ductility ratio of 3 to 10.	
SEVERE FLEXURE	From a ductility ratio of 10 to almost breach.	

* The second through the fifth class are for spall and the last three are for flexure. Scabbing is shown in the second sketch for each class.

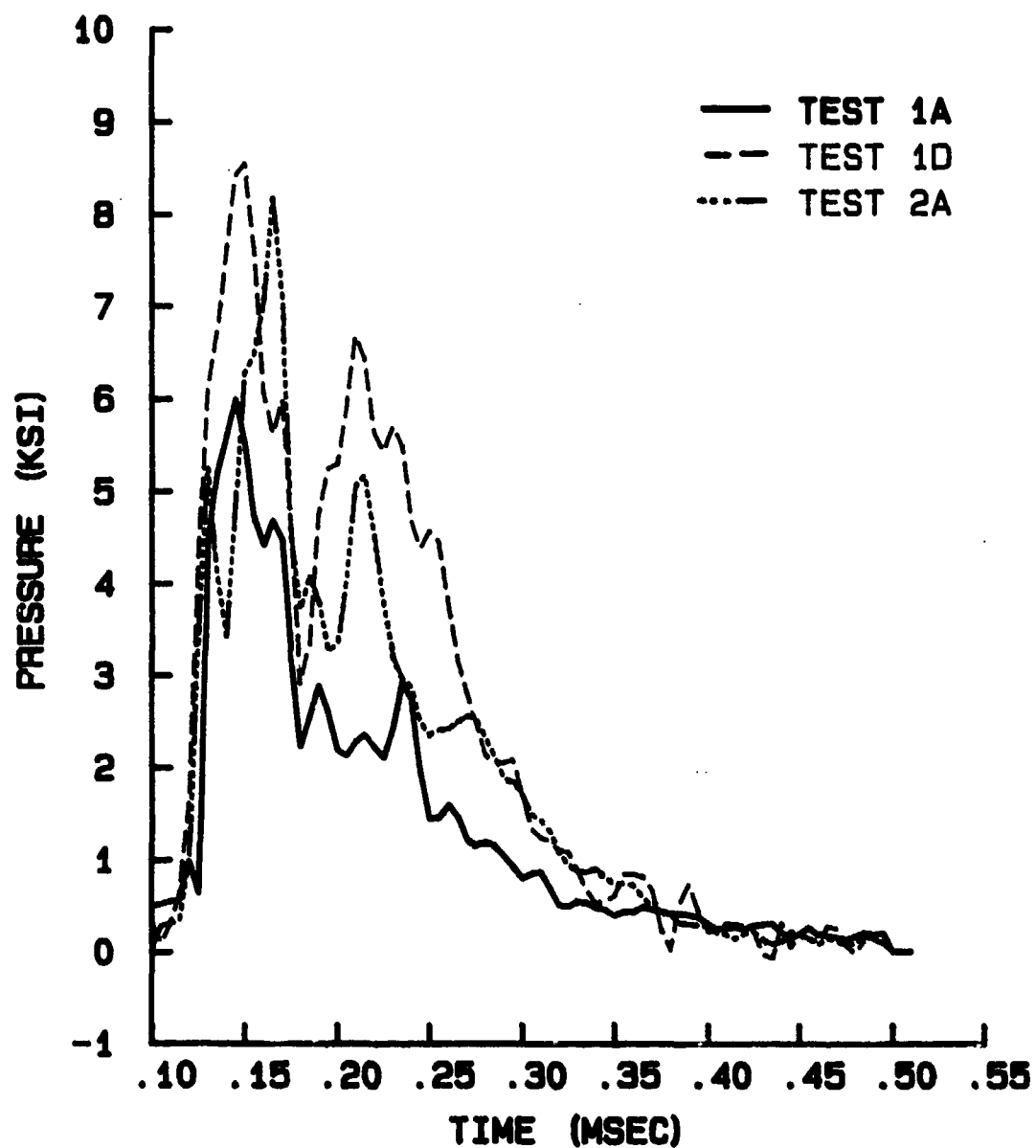


Figure 6.1 Pressure-time histories at the PQ-0 gage location in tests 1A, 1D and 2D for comparison.

PART VII: COMPARISON OF TEST RESULTS WITH PREDICTIONS

General

The test results of the bare charge tests are compared with the predictions of some of the more popular prediction methods in Table 7.1. The test results of the cased-charge tests are compared with the predictions of some of the more popular prediction methods for cased charges in Table 7.2. The comparisons, advantages, and disadvantages of each prediction method are discussed in the following sections.

Comparison of the Bare Charge Test Results with Predictions from References 39 and 40

The prediction method in References 39 and 40 is a theoretical prediction method. Although the authors of References 39 and 40 made several simplifications and assumptions just to illustrate trends in spall and propose a possible prediction method, many have used the reference for predicting spall damage. The prediction method was limited to bare charges at scaled standoff distances greater than $0.2 \text{ ft/lb}^{0.33}$ so the method was not used for predicting the damage in test 1C. The predictions from this method did not match well with the spall damage in any of the bare charge tests (see Table 7.1).

Several of the assumptions and simplifications used in this prediction method conflicted with other references and the test results. Some of these assumptions were that the concrete remained linearly elastic; the propagation velocity was constant; and the stress wave kept the same shape, rise time, and duration as it propagated through the wall. This means the stress wave cannot attenuate nor can different stresses travel at different velocities. However, the dynamic compressive strength of concrete varies with strain rate and can be exceeded by airblast loads from bare charges at scaled standoff distances greater than 0.2 ft/sec . If the dynamic compressive strength of the concrete is exceeded, the induced stresses will travel at different velocities and attenuate. For example, the stress measurement in test 3A, had a different shape and rise time than the airblast measurement. A further assumption was that a stress wave only changed by spherical divergence as it traveled from

the front of the wall to the back surface. However, the pressure distribution plots for the bare cylindrical charge tests indicated the airblast expanded somewhat cylindrically. Any form of divergence should continue even after the stress wave reflects off the back wall. The authors assumed a constant dynamic tensile strength of 800 psi for 4,000-psi concrete. The dynamic tensile strength of concrete varies with strain rate and can be above or below 800 psi depending upon the strain rate. Many of these assumptions were made due to a lack of information on dynamic compressive and tensile strengths of concrete, how stress waves attenuate and at what velocities various stresses propagate.

Comparison of the Bare Charge Test Results with Predictions from Reference 33

Although the prediction curves in Reference 33 (also shown in Figure 3.3) are for damage caused by nearby detonations in air instead of detonations at the surface, the predictions were compared with the test results (Table 7.1). The predictions agreed with the actual damage in 7 out of the 11 tests and slightly underpredicted the damage in the other 4 tests. Some of the differences may have been due to the differences in the definitions of damage.

Comparison of the Bare Charge Test Results with Predictions from Reference 45

All of the test parameters for the bare charge tests in this study were within the limits given for use of the damage prediction curve for bare charges in Reference 45. This curve was also shown in Figure 3.4. The predictions from this curve matched the actual damage very well in all of the bare charge tests, except test 3A and Box 7 (see Table 7.1). The discrepancy between the predictions and the damage in test 3A may be due to the difference in the definition of breach or perforation or due to problems with scaling. The previous chapter discussed possible problems with scaling spall damage due to strain rates changing, but peak pressures not changing with scales. The bomb and standoff distance used in Test 3A were larger than the majority of the bombs and standoffs used in the tests upon which the curve was based.

Comparison of Cased Charge Test Results with Predictions from Reference 41

The theoretical prediction method from Reference 41 only correctly predicted the spall damage of 6 out of 20 cased charge tests (see Table 7.2). There was either no damage or threshold damage in the 6 tests whose damages were correctly predicted. The prediction method overpredicted the spall damage of some of the tests with threshold damage and under predicted the damage in all the tests with medium and breach damage.

The discrepancies may have been due to some of the assumptions and simplifications made in the prediction method. Many of the assumptions and simplifications were made to make the calculations easier and because there was a lack of information on bomb fragment loads, stress wave changes, and dynamic concrete strengths. However, many of these assumptions conflict with recent studies and the measurements in this study. The author of the prediction method assumed that airblast loads can be approximated by average triangular airblast waves. The duration of the waves were calculated from the average impulse and peak pressure. Whereas, Figure 2.23 shows that the use of a triangular wave can be inaccurate. The prediction method also assumed that the bomb fragment impacts induced triangular stress waves with the same duration as the airblast. However, stress measurements showed that bomb fragments usually induced stress waves with much shorter durations than the airblast stress waves. The prediction method assumed that the airblast and bomb fragment stress waves could be directly combined if the airblast duration was less than the natural period of the wall. Whereas, spall is an early-time phenomenon and the natural period is a flexural response. The arrival times of the airblast and bomb fragments varied with distance. At large standoff distances, such as in test 9A, the bomb fragments arrived before the airblast. The prediction method assumed a $P-\alpha$ attenuation model to describe the attenuation, but did not address divergence nor other changes to stress waves. The pressure distributions indicated the airblast wave expanded somewhat cylindrically. The stress waves from the bomb fragments may have expanded spherically and also diverged. Although unsure what to assume for the

dynamic tensile strength of the concrete, the author of the prediction method assumed 14 percent of the static compressive strength. Whereas, References 15 through 19 and 22 show that the dynamic tensile strength of concrete varies with strain rate and is not a constant value. The worst assumption made by the prediction method is that the spall damage is only one layer and is always less than or equal to the plane of the reinforcing steel. Several tests in this series and in other studies on walls with normal reinforcing steel spacings had spall damage deeper than the reinforcing steel. The depth of spall is dependent upon the shape and magnitude of the stress waves, dynamic strengths of the concrete, and the resisting forces. If the peak net stress happens to exceed the dynamic tensile strength of the concrete near the reinforcing steel plane, there are probably enough microcracks around the steel to cause the cracks to occur in the steel plane. However, if the peak net stress exceeds the dynamic tensile strength of the concrete at some depth deeper than the reinforcing steel the cracks will form at that depth. The reinforcing steel grid helps prevent cracked-off concrete from spalling, but many times the impulse trapped in the cracked-off concrete is great enough and the steel spacing is large enough that the concrete can tear free and spall. This was illustrated in several of the tests with medium to breach damage in this study. The tests on wall 10 showed that if the spacings of the reinforcing steel and stirrups were extremely close, then the reinforcing steel grid would retain the loose concrete behind it. However, it is not common construction practice to space the reinforcing steel extremely close.

Comparison of the Cased Charge Test Results with Predictions from Reference 34

Although Reference 34 does not say whether the prediction curves (also shown in Figure 3.5) are for cased or bare charges, it was compared with the cased charge tests because the predictions were severe. The figure next to the curves shows a bomb in the air at midheight of the wall which indicates the curves were for airburst. However, the curves have been used for years by many to also predict damage caused by surface detonations. The prediction method only correctly predicted the damage of 4 out of 23 tests (see Table 7.2). The prediction method

overpredicted the damage in most tests. This may have been due to a difference in geometry, casing thicknesses or scales. There was not enough information about the curves to determine why there were so many discrepancies between the predictions and the actual damage.

Comparison of the Cased Charge Test Results
with Predictions from Reference 45

All of the test parameters for the cased charge tests on regular concrete were within the ranges given for use of the damage prediction curves for cased charges in Reference 45. Although, most of the charge to total bomb weight ratios were in the upper end of the given range. The prediction method only correctly predicted the damage in 4 out of 20 cased charge tests (see Table 7.2). The 4 tests for which the prediction method correctly predicted the damage were tests with bombs with relatively thick casings. Notice that the data points shown with the curves (Figure 3.6) that had worse damage class symbols than the curves predicted, were from either tests with bombs with very thick casings or from large-scale tests. The curves could be improved if casing thickness and scaling were taken into account.

Table 7.1
Comparison of Bare Charge Tests to Predictions

Test No.	R/W ^{0.33}		T/W ^{0.33}		Spall Damage Class/Depth		Spall Depth Prediction of Ref. 40		Spall Damage Prediction of Ref. 33		Spall Damage Prediction of Ref. 45	
	ft/lb	0.33	ft/lb	0.33	in.		in.		in.		in.	
1A	0.903		0.415		No Damage		0.166		No Damage		No-Minor	
1C	0.073		0.623		Medium/2.50		N/A		Moderate		Spalling	
1D	0.711		0.327		Medium/2.25		0.068		Slight		No-Minor	
2A	0.829		0.381		No Damage		0.116		No Damage		No-Minor	
2D	0.788		0.362		Threshold		0.095		Slight		No-Minor	
3A	0.711		0.206		Breach		0.086		Heavy		Spalling	
Box 1	0.904		0.550		No Damage		0.205		No Damage		No-Minor	
Box 4	0.711		0.432		No Damage		0.083		No Damage		No-Minor	
Box 7	0.787		0.369		Medium/3.00		0.104		Slight		No-Minor	
Box 8	0.978		0.458		No Damage		0.319		No Damage		No-Minor	
Box 10	0.866		0.406		Threshold		0.180		No Damage		No-Minor	

Table 7.2
Comparison of Cased Charge Tests to Predictions

Test No.	Case Thickness in.	R/W ^{0.33}		T/W ^{0.33}		Spall Damage Class/Depth in.		Spall Depth Prediction of Ref. #1 in.		Spall Damage Prediction of Ref. #34 in.		Spall Depth Prediction of Ref. #5 in.	
		ft/lb ^{0.33}		ft/lb ^{0.33}		in.		in.		in.		in.	
1B	0.070	0.903		0.415		Threshold		Threshold		Light		Spalling	
2B	0.088	0.788		0.362		Threshold		0.312		Heavy		Perforation	
2C	0.047	0.077		0.623		Medium/2.25		0.312		Heavy		Perforation	
3B	0.088	0.723		0.327		Medium/1.38		0.312		Heavy		Perforation	
4A	0.111	1.851		0.262		No Damage		No Damage		Light		Perforation	
4B	0.111	0.902		0.262		Medium/1.81		Threshold		4 in. wide crack		Perforation	
5A	0.088	0.723		0.332		Severe/3.75		---		Heavy		---	
5B	0.070	0.903		0.415		Medium/1.06		---		Heavy		---	
5C	0.047	0.077		0.623		Severe/4.38		---		Heavy		---	
8A	0.054	1.172		0.341		No Damage		No Damage		Moderate		Spalling	
8B	0.070	0.903		0.262		Threshold		Threshold		1 in. wide crack		Perforation	
8C	0.219	0.903		0.262		Breach		Threshold		1 in. wide crack		Perforation	
9A	0.111	1.851		0.166		Light Flexure		No Damage		2 in. wide crack		Perforation	
9B	0.054	0.721		0.341		Threshold		0.312		1 in. wide crack		Perforation	
10A	0.111	0.902		0.262		Medium/1.25		Threshold		2 in. wide crack		Perforation	
10B	0.070	0.903		0.415		No Damage		Threshold		Heavy		Spalling	
10C	0.047	0.077		0.623		Medium/0.62		0.312		Heavy		Perforation	
Box-2	0.070	0.904		0.550		Light/2.50		Threshold		Light		No to Minor	
Box-3	0.219	0.904		0.550		Medium/3.00		Threshold		Light		No to Minor	
Box-5	0.088	0.711		0.432		Medium/3.75		1.00		Light		Spalling	
Box-6	0.344	0.711		0.432		Medium/3.25		1.00		Light		Spalling	
Box-9	0.156	0.997		0.468		Medium/3.00		1.00		Light		No to Minor	
Box-11	0.250	1.171		0.549		Threshold		1.00		No Damage		No to Minor	

PART VIII: DISCUSSION OF SPALL PREDICTION

Discussion of Theoretical Prediction Methods

The previous chapter showed that two of the popular theoretical prediction methods did not correctly predict the damage in most of the tests of this study.

The theory of spall is difficult to apply to predictions, because many parameters are unknown such as, airblast loading from cylindrical bombs, stress waves induced by multiple bomb fragment impacts, attenuation rates of stress in concrete, change of stress waves due to different stresses propagating at different velocities, dispersion effects, how bomb fragment stress waves diverge, dynamic compressive and tensile strengths at strain rates greater than 10 sec^{-1} , resisting forces against spall, and other items. These parameters need to be researched. As a result of a lack of information on these parameters, many assumptions have to be made to predict spall damage with theoretical calculations. Even if assumptions are made the theoretical calculation can be cumbersome and difficult unless simplifications are made.

It is also difficult to predict combined spall, scab, shear, and flexure damage with a theoretical method. Most of the tests with severe damage or breach had combined damage mechanisms.

Discussion of Empirical Prediction Methods

Empirical prediction methods are expensive to develop and are limited to only situations similar to the data upon which the prediction methods were based. The previous chapter showed that the empirical damage prediction methods for bare charges from References 33 and 45 correctly predicted the spall damage of the majority of the bare charge tests in this study. However, the empirical damage prediction methods for cased charges from References 34 and 45 did not correctly predict the damage of most of the cased charge tests in this study. The empirical methods should be improved to account for scale and casing thickness effects.

Additional Data

The author collected data on 334 additional tests from References 1, 2, 25, and 47 thru 70 and from tests at WES not reported. The additional data was combined with the data in this study to make a large data base upon which empirical prediction methods could be made. All of the data are tabulated in Appendix D.

Empirical Damage Curves for Bare Charges

The data in Appendix D on bare charges were plotted in Figures 8.1 and 8.2 and prediction curves were drawn to fit the data. The prediction curves in Figure 8.1 are similar to, but slightly steeper than the curves in Reference 45. The prediction curves in Figure 8.2 are similar to, but lower and sharper than the curves in Reference 33.

Notice that the damage class of a few data points did not agree with the prediction curves and the surrounding data points. All of the discrepant points which had a damage class worse than the surrounding points, except one point, were from larger scale tests than the tests for the surrounding points. The one point that had a worse damage class but was not a large scale bomb, was a contact bomb on end. Vice versa, all the discrepant data points with damage less than the surrounding points were from smaller scale tests than the tests for the surrounding points. This again shows that spall damage and some other forms of damage are worse in large scale detonations than in small scale detonations. This indicates curves such as these would under predict the damage caused by nearby detonations of bare bombs as large or larger than the largest bare bombs in the data base. The curves should only be used to predict damage in similar scale detonations. The ranges of the test parameters for the data used in this plot are given in Table 8.1. The recommended range for use of these curves are also given in Table 8.1.

The author recommends making a prediction curve with the damage somehow scaled to the bomb size. For example, rate the damage on a scale from 0 to 100 for no damage to breach, respectively, and scale the damage rating. Unfortunately, there was no more time left in this study to try this idea or others.

Empirical Damage Curves for Cased Charges

The data in Appendix D on the cased charges were plotted in Figure 8.3 and prediction curves were drawn to fit the data. The data was plotted differently than in Reference 45. The scaled standoff distance ($R/W^{0.33}$) was multiplied times the ratio of the weight of the bomb to the weights of the bomb and the casing ($W/(W+C)$). The weight of the casing was only the weight of the metal around the sides of the explosive, and did not include the weight of any nose or tail portions of bombs. This charge to charge plus casing weight ratio helped account for the differences in damage caused by different casing thicknesses around the same size bombs and reduced the scatter of the data.

Notice that the damage class of a few data points did not agree with the prediction curves and the nearby surrounding data points, just as in the other curves. All of the discrepant points which had a damage class worse than the surrounding data points were from either much larger scale tests than the tests of the surrounding points or were from tests with close-in thick cased bombs. The discrepant points from the large scale tests again demonstrate that spall damage and some other forms of damage are worse from large scale detonations than from small scale detonations. The effect of casing thickness decreases with decreasing standoff distance. The results of tests 1A and 1B indicate that the damage caused by a contact cased charge may even be less than the damage caused by a contact bare charge. This was discussed in the analysis in Chapter 6. Thus, the use of the $W/(W+C)$ ratio may shift data points for close-in thick cased bombs too far to the left. Therefore, these curves should only be used to predict damage in similar scale detonations to the test data, and in tests with casing thicknesses similar to the casing thicknesses of the test data. The ranges of the test parameters for the data used in this plot and the recommended ranges for use of the curves are given in Table 8.2.

Table 8.1
Ranges of Parameters for Bare Charge Data Used
in Figures 8.1 and 8.2

<u>Parameter</u>	<u>Range</u>	<u>Recommended Use Range</u>
Standoff distance	Contact to 20.0 feet	Contact to 5.0 feet
Equivalent TNT charge weight	0.0276 to 299.3 pounds	0.0276 to 30.00 pounds
Scaled standoff	0.064 to 7.93 ft/lb ^{0.33}	0.064 to 2.00 ft/lb ^{0.33}
Wall thickness	2.50 to 43.31 inches	2.50 to 43.31 inches
Scaled wall thickness	0.167 to 1.95 ft/lb ^{0.33}	0.167 to 1.95 ft/lb ^{0.33}
Static compressive strength of concrete	1,535 to 8,888 psi	2,500 to 7,000 psi
Principle steel ratio	0.066 to 0.830 percent	0.066 to 0.830 percent

Table 8.2
Ranges of Parameters for Cased Charge Data
Used in Figure 8.3

<u>Parameter</u>	<u>Range</u>	<u>Recommended Use Range</u>
Standoff distance	Contact to 30.0 feet	Contact to 7.5 feet
Equivalent TNT charge weight	0.824 to 2,299 pounds	0.824 to 220 pounds
Charge weight to charge + casing weight	0.172 to 0.978	0.172 to 0.978
Scaled standoff	0.077 to 12.06 ft/lb ^{0.33}	0.077 to 5.00 ft/lb ^{0.33}
Wall thickness	3.94 to 84.0 inches	3.94 to 84.0 inches
Scaled wall thickness	0.155 to 1.08 ft/lb ^{0.33}	0.155 to 1.08 ft/lb ^{0.33}
Static compressive strength of concrete	2,500 to 7,110 psi	2,500 to 7,110 psi
Principle steel ratio	0.11 to 1.34 percent	0.11 to 1.34 percent

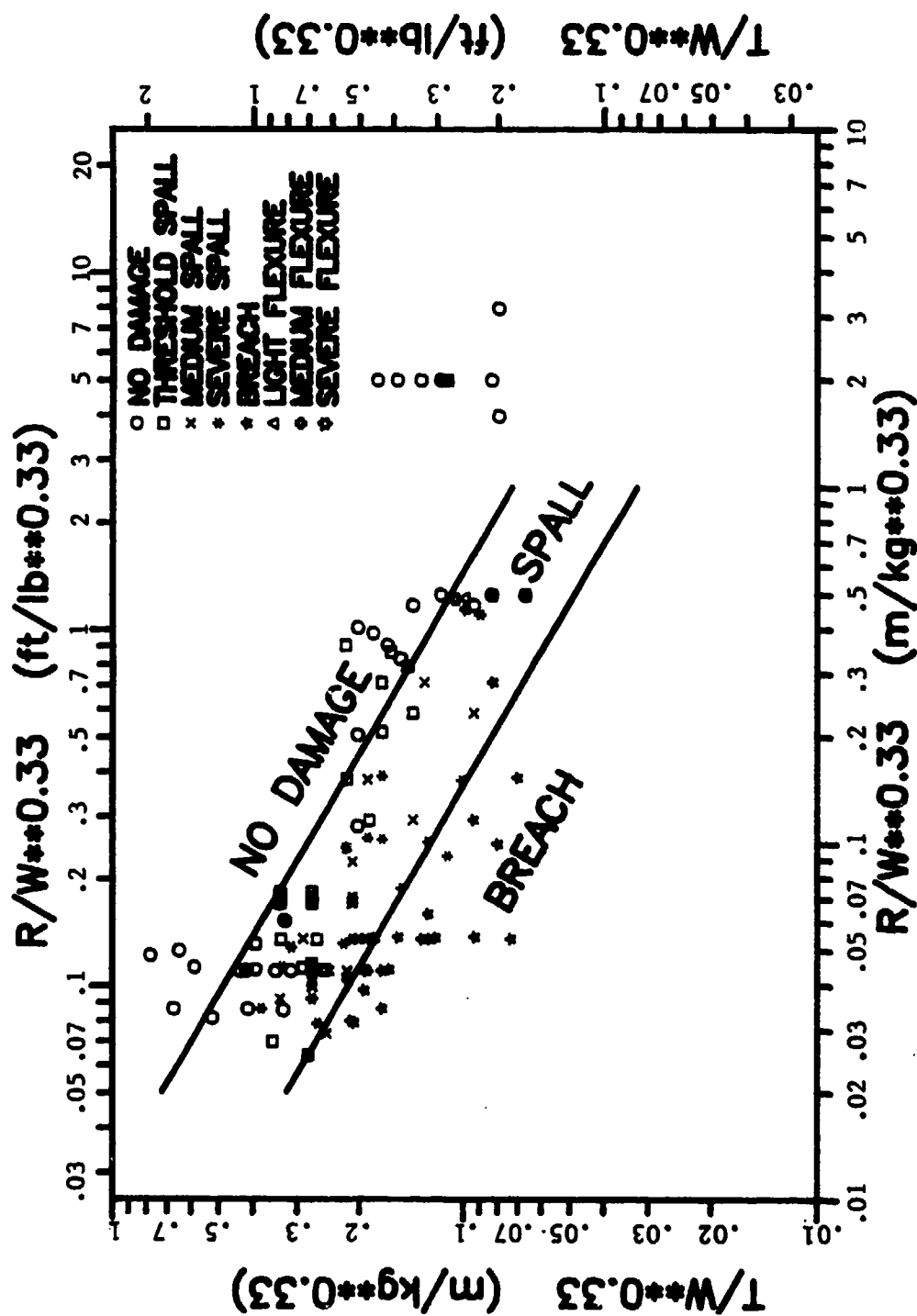


Figure 8.1. Log-Log prediction curves for damage to concrete panels caused by bare bombs.

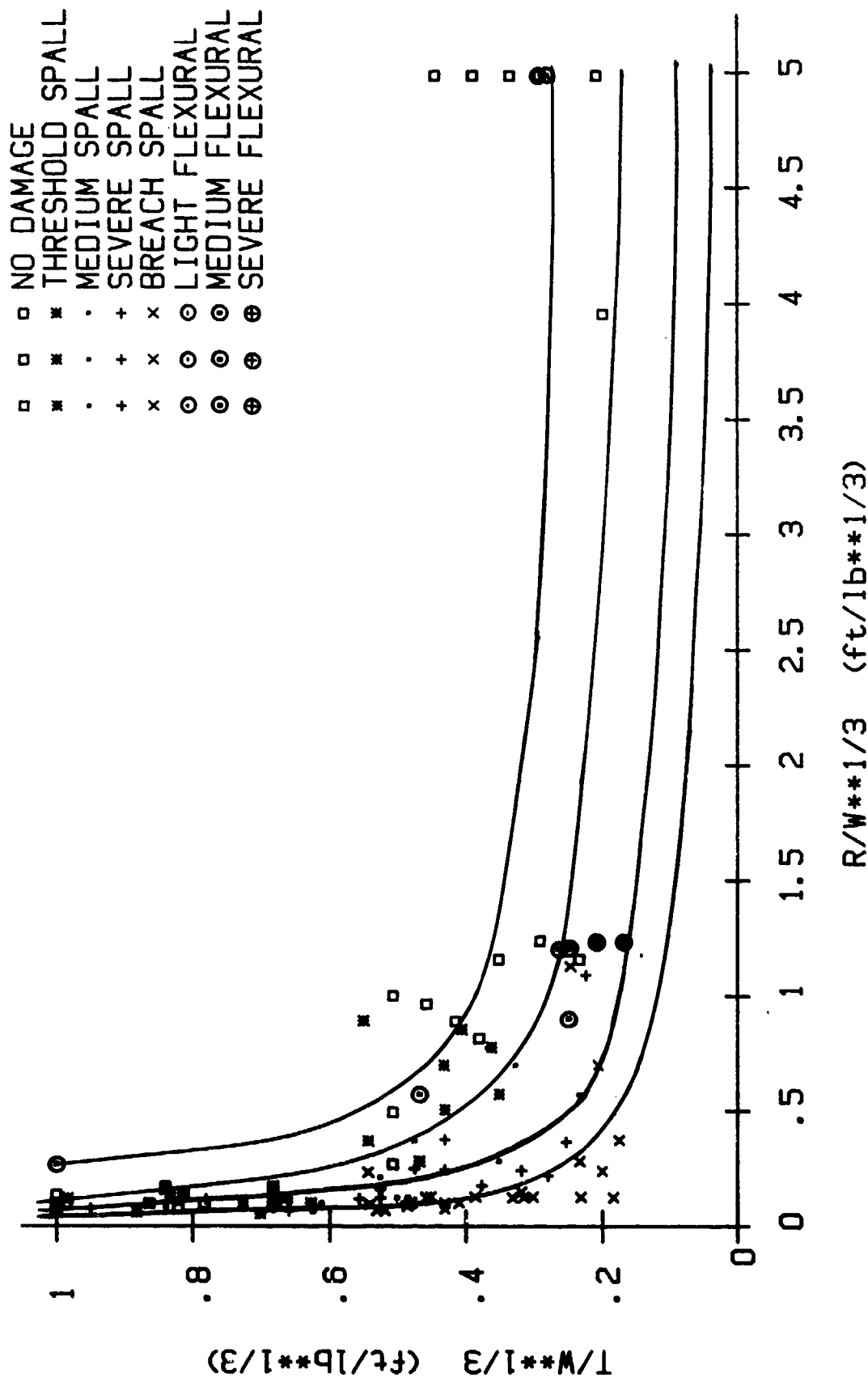


Figure 8.2. Prediction curves for damage to concrete panels caused by bare bombs.

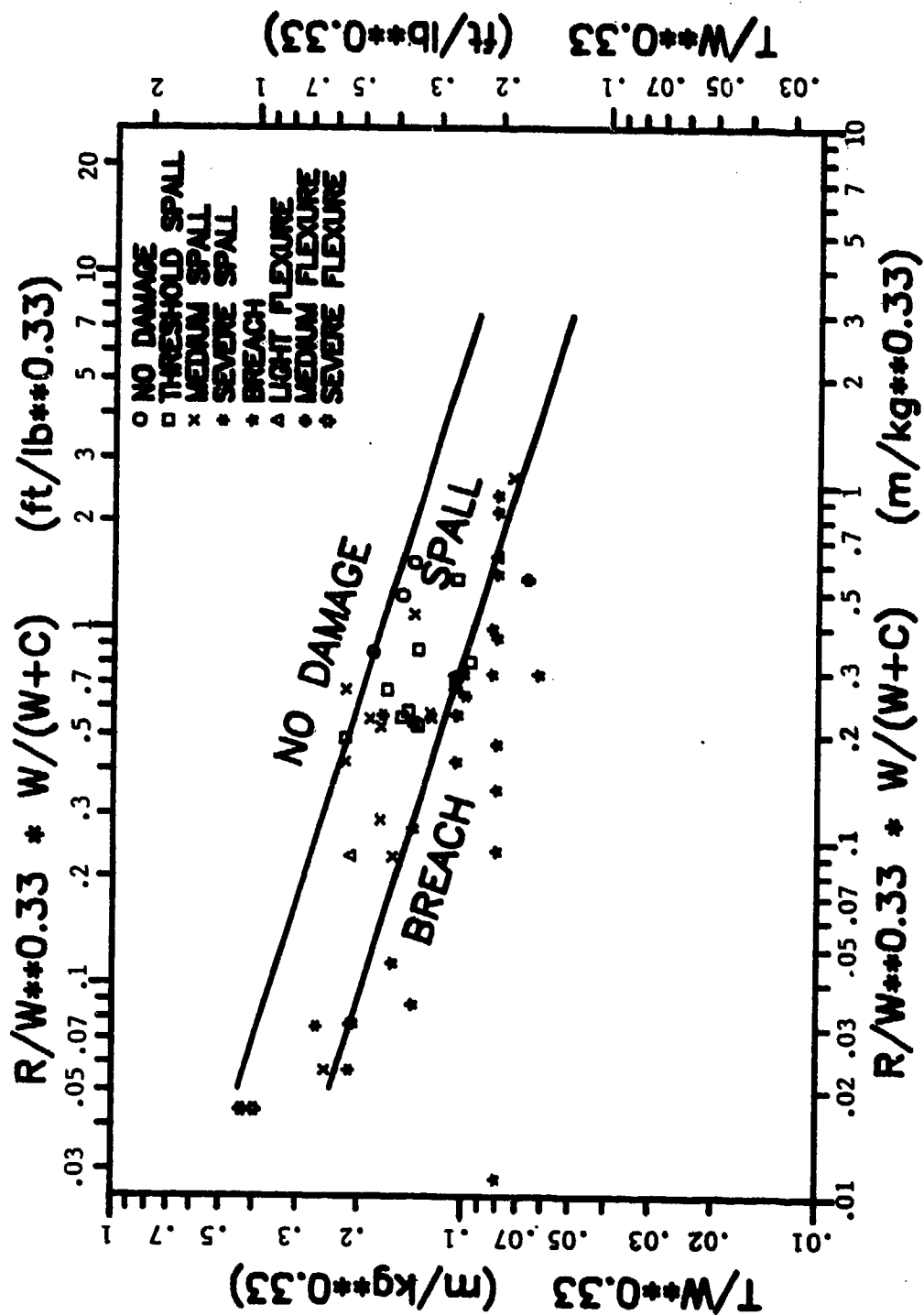


Figure 8.3. Log-Log prediction curves for damage to concrete panels caused by cased charges.

PART IX: PREVENTION AND RETENTION OF SPALL

General

There are several methods that have proven effective in either preventing or retaining spall. Both prevention and retention methods keep spall from leaving the backside of the wall. Spall prevention methods prevent or reduce the formation of any "cracked-off" concrete layers that could potentially spall, (i.e. prevents or reduces internal damage in the wall due to a reflected tensile wave). Spall retention methods keep spall from leaving the wall by either increasing the resistive forces holding the "cracked off" concrete to the wall or confining the cracked off concrete behind a plate. Some additives in concrete help both reduce damage and retain spall. Prevention methods are preferable because they prevent internal damage that could reduce the load-bearing and moment capacities of the walls. It is possible to severely damage a wall so it could not support the roof and still retain most of the spall.

Methods of Spall Prevention/Reduction

Most spall prevention methods either alter the loadings before they get to the wall, alter the stress waves induced in the wall before they reflect, or increase the ductility and dynamic tensile strength of the concrete. Some examples of spall prevention methods are discussed in the following paragraphs.

One of the best and most economical spall prevention methods is placement of a soil berm against the threatened walls. Tests have been conducted with identical bombs at the same standoff distances from similar walls with and without soil berms in front of them (see References 1, 2, 51, and 53). The walls without soil berms either breached or spalled severely (see Figure 9.1), whereas the walls with soil berms did not spall and suffered minor or no damage (see Figure 9.2). The soil berms not only prevented spall but also prevented scabbing by keeping most of the bomb fragments from reaching the wall. The walls with soil berms had peak soil stresses 0.051 to 0.089 times the peak

reflected airblast pressures on the walls without soil berms. The duration of the soil stresses were 5.90 to 11.66 times the durations of the airblast loads on the lower portion of the walls. However, there was not much difference in the impulse of the soil stresses and the airblast load on the lower portions of the walls. Thus, the wall without a soil berm received an airblast load with a high peak pressure, short duration and sharp shape; plus multiple bomb fragment impacts. The wall with the soil berm received only a soil stress load with a low peak, long duration and gradual unloading. This type loading does not cause spall. The loading was altered by the soil berm to a less severe form, but the total impulse remained about the same. Soil berms can prevent spall in multiple bomb detonations, as long as the bomb does not crater the soil berm.

Shield walls or blast absorbtive walls are another method of spall prevention (see Figure 9.3). References 2, 53, and 66 report tests conducted with identical bombs at the same standoff distances from similar walls with and without shield walls in front of them. The walls without shield walls in front of them suffered much worse scab and spall damage than the walls with shield walls in front of them. Figures 9.3 and 9.4 show the reduction in the damage to the main wall in tests from Reference 67. These tests indicated that the amount a shield wall reduces damage is proportional to its strength, stiffness, mass, and resistive forces to spall. The shield walls must be strong and stiff enough to resist the airblast loading long enough so the peak airblast pressures die down before the shield wall fails. The shield walls must also be strong and massive enough to either catch the bomb fragments or substantially reduce the velocities of the bomb fragments before they hit the main wall. The greater the resistive forces in the shield wall are against spall the smaller the impulse transmitted by any spall to the main wall. Even shield walls of several sheets of plywood have proven effective in reducing spall damage. Reference 33, states that "double slab construction with an air space between the slabs (i.e shield wall and main wall) may actually be more resistive to spall, perforation and contact explosions than the same amount of concrete poured as a single wall."

Layered walls with each layer decreasing in specific acoustic

resistance is another method of spall prevention (see Figure 9.5a). Specific acoustic resistance (ρc) is the product of the density (ρ) times the primary stress propagation velocity (c) in a layer. The equations governing the distribution of stresses at an interface are:

$$\sigma_t = \frac{2 \rho_2 c_2}{(\rho_2 c_2 + \rho_1 c_1)} \sigma_i \quad (\text{eq 9.1})$$

and

$$\sigma_r = \frac{\rho_2 c_2 - \rho_1 c_1}{(\rho_2 c_2 + \rho_1 c_1)} \sigma_i \quad (\text{eq 9.2})$$

where σ_t is the transmitted stress, σ_r is the reflected stress, σ_i is the incident stress, ρ_1 is the density of the first layer, c_1 is the propagation velocity of the first layer, ρ_2 is the density of the second layer and c_2 is the propagation velocity of the second layer. If $\rho_2 c_2$ is less than $\rho_1 c_1$, then σ_t is less than σ_i , and σ_r is negative and less than σ_i . A negative sign means the stress waves are reflected in opposite sense i.e. an incident compressive wave will reflect as a tension wave, and vice versa. Consider a wall with 2 layers where $\rho_1 c_1 = 3 \rho_2 c_2$ as an example. In this case $\sigma_t = \sigma_i/2$ and $\sigma_r = -\sigma_i/2$, see Figure 9.5b. The transmitted stress wave continues through the second layer and reflects as a tension wave off the back free surface (Figure 9.5d). Therefore, in this example, the incident stress was divided into 2 stress waves at the interface of the layers, each stress wave half of the incident stress wave. The reflected peak tensile stress in each layer is half of what the reflected peak stress would have been in a monolithic wall. If the dynamic tensile strengths of both layers exceed the reduced reflected stress waves no cracks will form. If the dynamic tensile strength of the first layer is exceeded, cracks will form but the second layer will retain any potential spall. Spall will only occur if the dynamic tensile strength of the second layer is exceeded by the reduced reflected stress. Several different layers could be used if desired. One popular type of layered or composite wall is a wall with 2 concrete panels separated by a sand filled cavity. The second concrete panel usually has a higher specific acoustic resistance than the sand, but is needed to retain the sand.

Addition of materials to enhance the ductility and dynamic tensile

strength of the concrete have also prevented or reduced spall. This study demonstrated that crimped steel fibers and acrylic latex additives prevented or reduced spall damage (see tests on wall panels 6 and 7). References 23 through 27 reported that proper amounts of steel, nylon, fiberglass, polypropylene, or polyethylene fibers can each prevent or reduce spall, depending upon the severity of the threat. Reference 65 reported that 3 percent entrained air in concrete helped prevent spall in some high explosive tests on concrete specimens.

Theoretically, the geometry of the back free surface can be made so the stress waves reflect at oblique angles from the surface (Figure 9.6). The portion of an incident compressive wave that reflects as a tensile wave decreases with increasing angle of incidence (see Figure 2.14). For example, the back free surface could be corrugated with 45° triangular ridges so a plane stress wave would reflect from the back free surface at 45° angles. If the Poisson's ratio of the concrete is 0.15 the reflected primary stress wave at 45° is nearly zero. Figure 9.6b shows a plane wave impacting the top of a triangular ridge. As the wave propagates further into the triangular ridge (Figure 9.6c) the left and right portions of the wave reflect from the sides and travel back toward each other. If the peak net stress exceeds the dynamic tensile strength of the concrete as the reflected waves are traveling the concrete will crack and any spall will pull away parallel to or at a low angle to the back wall and collide with neighboring spall or ridges. If the concrete does not crack before the reflected stress waves from each side of a triangular ridge meet in the middle, then the two reflected waves will add at the middle creating a peak net stress twice the peak of just one side, see Figure 9.6d. If the peak net stress in the middle exceeds the dynamic tensile strength of the concrete it will crack and any spall will, as described above, pull away parallel to or at a small angle to the back wall and collide with neighboring spall or ridges. Thus, 45° corrugations reduce the magnitude of the reflected tensile stress and cause any spall to leave at low angles to the wall. Other geometries could also theoretically reduce or prevent spall. However, no tests have been conducted on such walls.

Methods of Spall Retention

Spall retention methods usually do not reduce the damage to the wall, but retain the spall to keep the spall from damaging the contents in the structure. If a wall with a spall retention method is severely damaged by a nearby detonation it would not survive a second nearby detonation. Some examples of spall retention methods are discussed in the following paragraphs.

The most common method of spall retention is a steel spall plate attached to the backside of the target walls or roof. Figure 9.7 is a series of pictures of a test on a wall similar to the wall in Figure 9.1, but with a spall plate attached to the backside. Notice the front of the wall still suffers severe scabbing and the spall pushed the plate several inches inwards. Reference 7, gives recommended construction details for installation of spall plates. It is important to attach the spall plate to the wall with long anchors or studs which hook behind the reinforcing steel in the wall to insure the anchors do not break free. Spall plates are fairly expensive.

Close spacing of the back layer of reinforcing steel with close spacing of stirrups that hook around the back layer of steel will retain the majority of the deep or multiple spall behind the steel layer (see pictures of tests on wall 10 in Appendix C). However, the concrete cover over the back layer of steel can still spall. Construction of such walls is difficult and expensive.

Placing a synthetic or steel wire mesh in the concrete on the inner side of the back steel layer or securely attaching the mesh to the back steel layer will also retain some spall (see Figure 9.6). This is similar to the above two methods but may be less expensive.

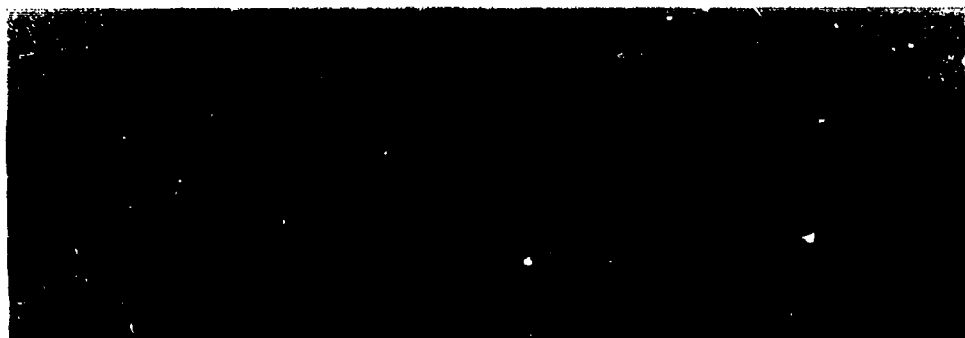


Figure 9.1a. Test set up of a half-scale semi-hardened wall subjected to a cased bomb.

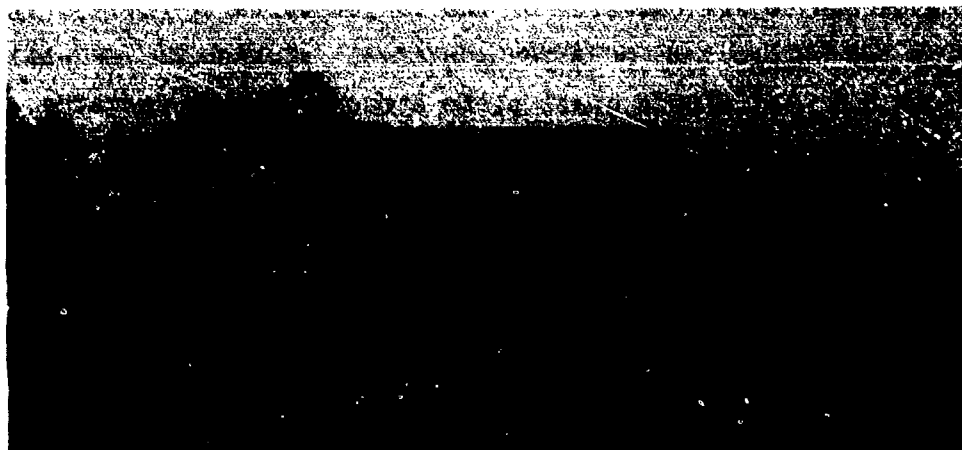


Figure 9.1b. Damage to the front of the wall caused by the bomb fragments.



Figure 9.1c. Spall damage to the back of the wall.

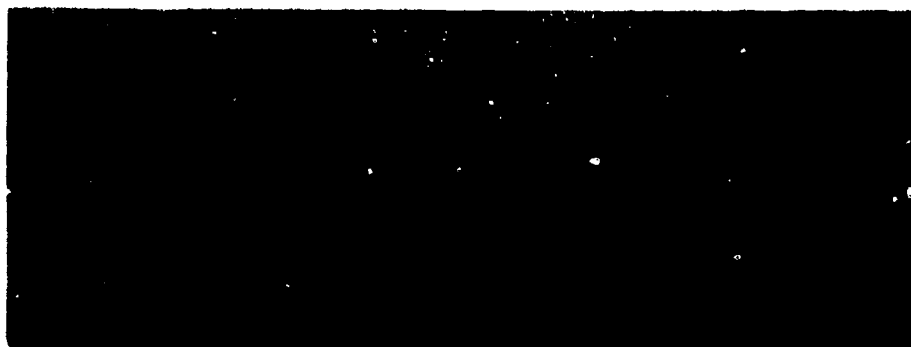


Figure 9.2a. A similar wall as in Figure 9.1 but with a soil berm in front of it.

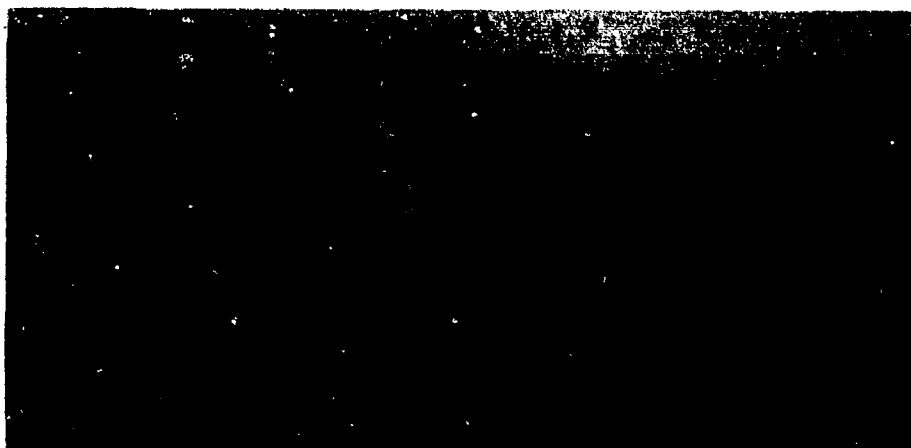


Figure 9.2b. The front of the wall suffered very little damage.



Figure 9.2c. The back of the wall suffered only two hairline cracks.



Figure 9.3a. 8.5-inch-thick wall subjected to a oased



Figure 9.3b. The bomb fragment damage to the front of the wall.



Figure 9.3c. The spall damage to the back of the wall.



Figure 9.4a. 2-inch thick shield wall protecting an 8.5-inch-thick wall from a cased 14-pound C-4 charge.



Figure 9.4b. The shield wall and main wall after the test.



Figure 9.4c. The back of the main wall suffered only hairline cracks due to the test.

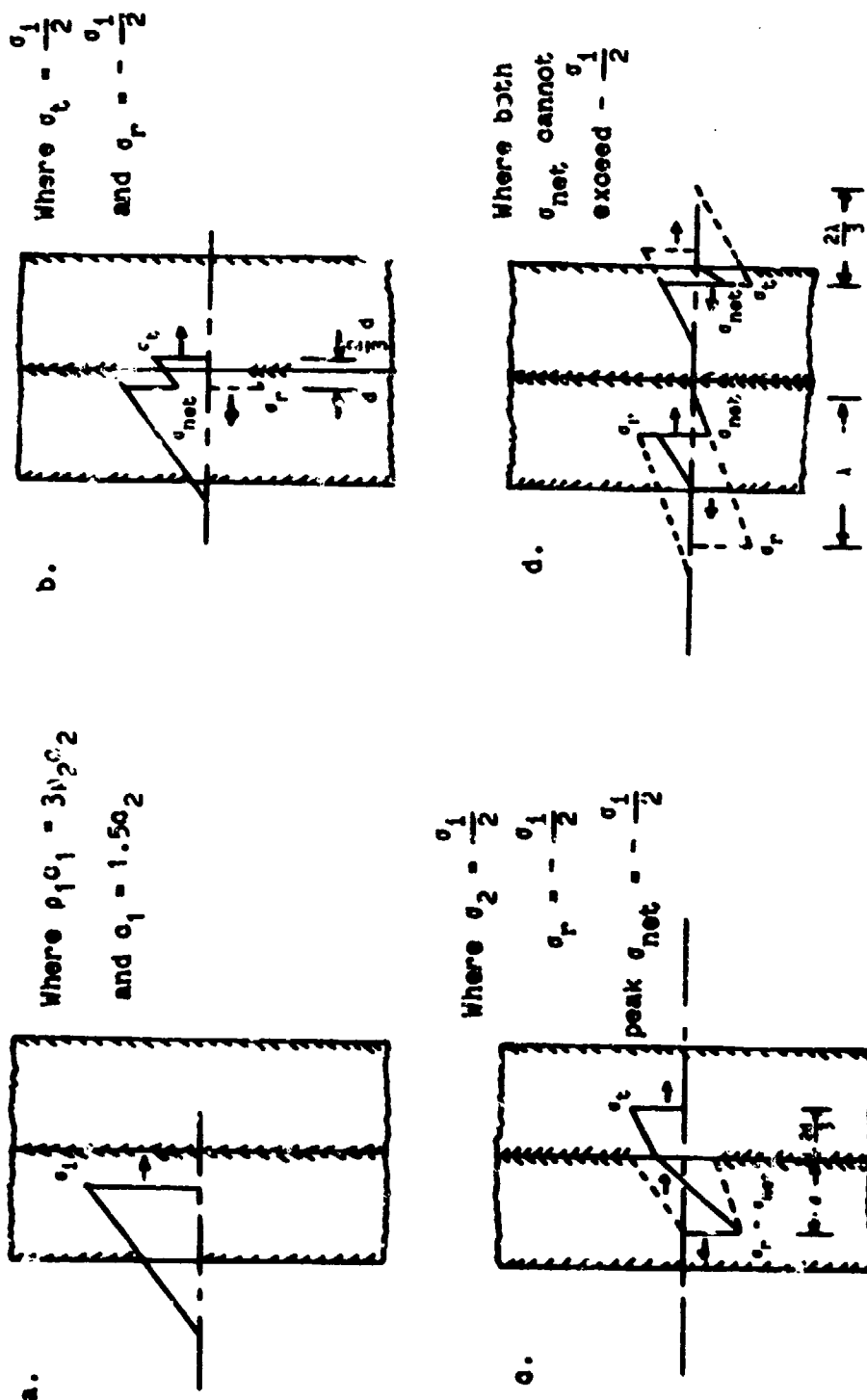


Figure 9.5. Layered wall with the specific acoustic resistance of the first layer being 3 times that of the second layer. The incident stress wave splits into two waves with half the peak stress at the interface.

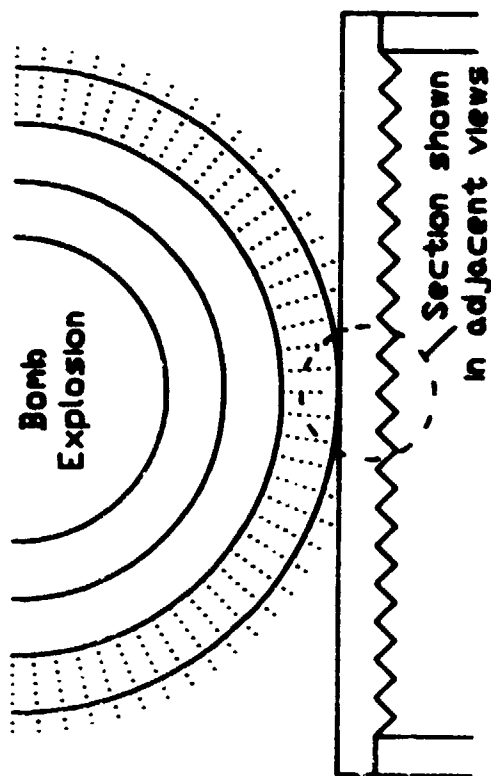


Figure 9.6a. Wall with 45° triangular corrugations on the back.

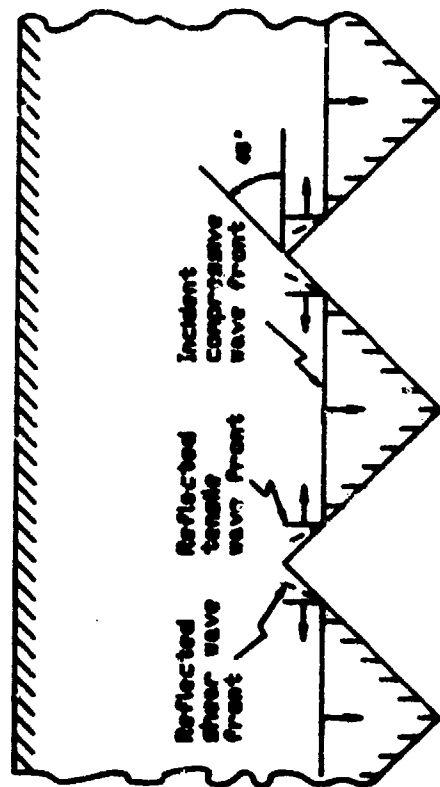


Figure 9.6b. Incident compression wave splits into a tensile and a shear wave upon reflection.

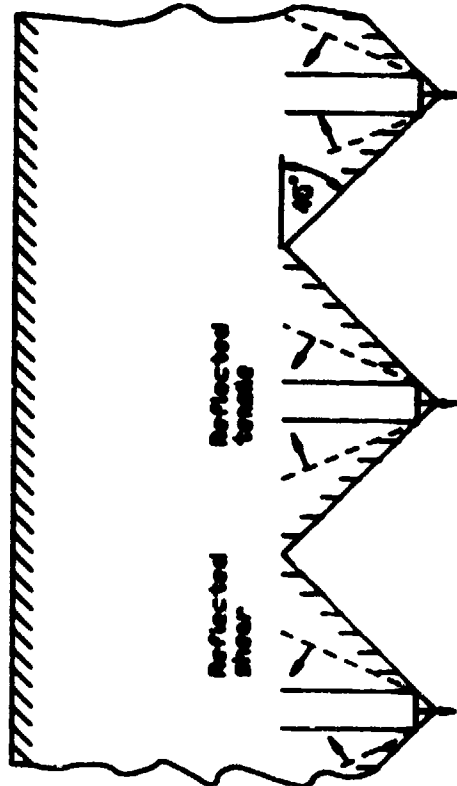


Figure 9.6c. Reflected tensile waves travel toward center of the triangular ridges.

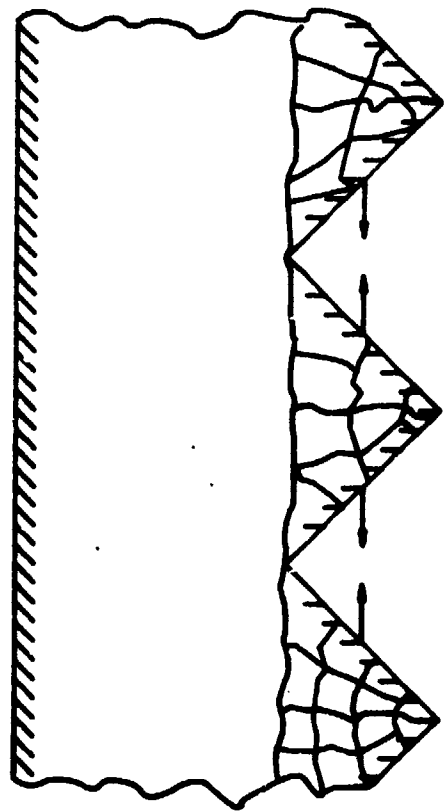


Figure 9.6d. Spall will leave parallel to the wall and impact neighboring spall.



Figure 9.7a. Wall similar to the wall in Figure 9.1 except for the addition of a spall plate.



Figure 9.7b. The front of the wall suffered severe bomb fragment damage.

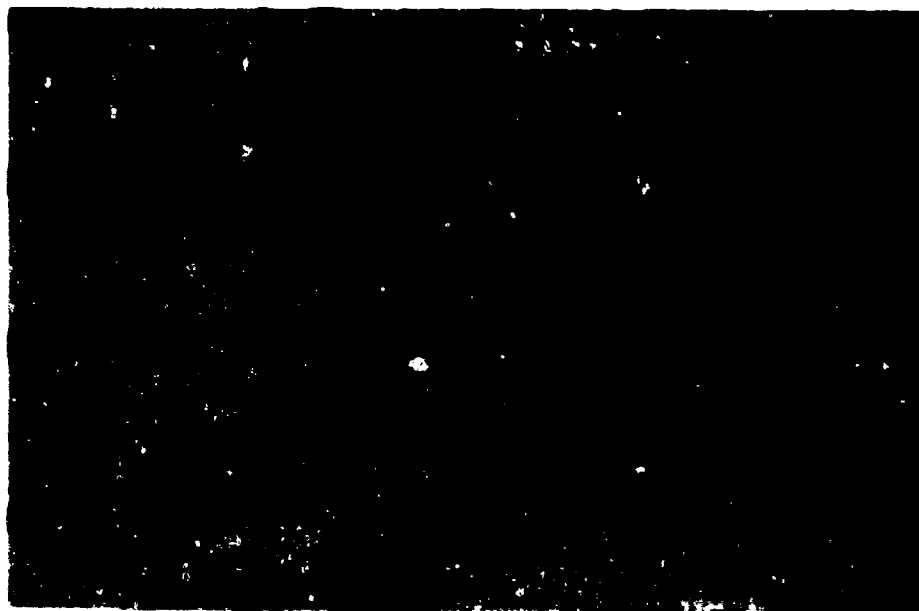


Figure 9.7c. The spall plate over the back of the wall retained most of the spall.

PART X: SUMMARY

Spall was defined herein as the ejection of fragments of a structural element from the opposite side from which it was impacted and/or impulsively loaded. This study was on spall of reinforced concrete structural elements caused by nearby bare and cased bomb detonations. Existing theories of spall were reviewed, additional improved spall theory was developed, existing spall prediction methods were reviewed, HE tests were conducted and analyzed, the existing spall prediction methods were evaluated with test results, improved prediction methods were developed, and methods of preventing spall were discussed.

Theory

Theoretical analysis of spall is quite complex. It was shown that spall is dependent upon the shapes, magnitudes, and angles of incidence of the applied airblast and bomb fragment impacts; upon changes in the stresses as they propagate through the structural member; upon the dynamic properties of the concrete; and upon forces such as dynamic bond, shear and mechanical retention which resist spall of cracked concrete. Each of these phenomena and their effects on spall were discussed in detail. Prediction of airblast loads were reviewed. It was shown that triangular approximations of airblast loads can yield incorrect spall predictions, therefore, exponential equations for airblast are recommended. Equations for bomb fragment loads were derived. Changes of stress waves due to different stresses above the Hugoniot Elastic Limit (HEL) traveling at different velocities were discussed, but there is not much information on these changes. Changes of stress waves due to attenuation were also discussed. Studies have shown that attenuation of stresses below the HEL are negligible and can be ignored, but stresses above the HEL plastically deform and fracture the material and thus attenuate substantially. There is little information on the rates of attenuation of various stress levels and shaped stress waves. Equations for changes of stress waves due to cylindrical and spherical divergence were given. The airblast loads from cylindrical bombs on the ground expanded somewhat cylindrically in close standoff distances

in the tests conducted. It was assumed that the stress waves induced by bomb fragment impacts diverged spherically from the bomb fragments imbedded in the concrete. Changes in stress waves in normal concrete due to dispersion seemed to be negligible but a few tests indicated that dispersion was significant in concretes with entrained air or closely spaced reinforcing steel. The peak stress and sense of a reflected stress wave is dependent upon the angle of incidence of the stress waves to the back free surface. It was shown that compressive stress waves with an angle of incidence between 45 and 85 degrees in concrete with a Poisson's ratio of 0.15 will reflect as compression waves. Thus, no spall would be possible for loads applied at these angles. Several studies showed that the dynamic properties of concrete are strain-rate dependent. There is information on the dynamic compressive and tensile strengths of "normal" concretes up to strain-rates of 23 sec^{-1} . However, the strain rates caused by most fragment impacts and severe air-blast loads on "normal" concrete are well in excess of 23 sec^{-1} .

A theoretical method for determining if and where a stress wave, induced into a normal concrete by airblast with peak reflected pressures below the HEL of the concrete, would cause the concrete to crack in tension was demonstrated in Part VI. In this case the changes in the stress wave caused by different stresses traveling at different velocities, attenuation, and dispersion were negligible. The only change in the stress wave which needed to be taken into account was divergence. However, even in this simplified case, spall could not be accurately predicted because the forces resisting the spall of the concrete behind the crack could not be predicted.

Thus states of the art in determining propagation velocities of stresses above the HEL, attenuation of stresses above the HEL, dispersion, dynamic tensile strength of concrete for strain rates greater than 23 sec^{-1} , dynamic bond, dynamic shear strength, mechanical retention of cracked concrete, and the effects of additives on the dynamic properties of concrete are not advanced enough to be able to theoretically predict spall of reinforced concrete.

Experiments on Spall

Forty tests were conducted on reinforced-concrete walls to

investigate parameters which affect spall.

Simple theoretical calculations of spall caused by airblast below the HEL of the concrete were verified. It was noted that surface bursts have a second main spike from the reflection of the airblast off the ground which helps reduce the chance of spall.

Several different size bare charges were detonated at the same standoff distance to demonstrate how spall is dependent upon the magnitudes and the shape of the stress waves in concrete. The larger a bomb at a given standoff distance the higher the peak pressure and the sharper the shape of the airblast wave. Thus the chances for spall increased with bomb size at a given standoff distance.

A small contact bare charge was tested and analyzed. It caused scabbing of the front of the wall and spall on the back of the wall. The stress gage at the midplane of the wall measured much smaller stresses than those estimated at the front surface, which indicates the stresses greatly attenuated.

It was demonstrated that different size bare bombs at different standoff distances but the same scaled standoff distance will cause much different damage to a given structure. Although the peak pressure scaled, the shapes and durations of the airblast waves were much different. In addition, the pressure distributions were very different since the structure was not scaled. The larger bomb at a greater distance caused worse damage over a much larger area. Thus scaled standoff should not be used as the only criterion for predicting spall (as done in some literature).

The scaling of spall damage due to bare charges was also studied. Tests confirmed that walls in small-scale tests incur less damage than similar larger scale walls in similar larger scale tests. This was again attributed to different strain-rates causing different dynamic strengths in the different scale tests.

The damage caused by equal-size bare and cased charges in tests on similar walls were compared. All of the tests with cased charges had worse damage than the tests with the same size bare charges, except for the tests with contact charges. The bare contact charge caused slightly worse damage than the cased charge. The difference in damage caused by equal-size bare and cased charges was minimal for contact charges and

increased with increasing standoff distance. The airblast load rapidly decreased in peak pressure, increased in duration and unloaded slower with increasing standoff distance. Whereas, the bomb fragments lost their momentum at a much slower rate than the airblast changed. At very close standoff distances the airblast was severe and long enough to overshadow the stresses induced by the bomb fragments. The stresses induced by multiple bomb fragments had very high peak stresses, very short durations and unloaded rapidly; so they could cause spall by themselves. The bomb fragment stress waves became more dominant as compared with the airblast stress wave as the standoff distance was increased.

The damage caused by equal-size cased bombs but with different casing thicknesses were compared in tests on similar walls. Within certain limits not yet defined, the thicker the casing, the worse the damage to a concrete wall. The average bomb fragments increase in mass, decrease in initial velocity and decelerate slower with increasing casing thickness. The peak induced stress decreases, the rise time increases and the duration increases with a decrease in striking velocity and increase in bomb fragment size within certain limits. Thus within certain limits thick cased bombs cause worse damage than equal size thin cased bombs because the rise times and durations of the bomb fragment stress waves are longer for thick cased bombs than for thin cased bombs.

Tests confirmed that walls in small-scale tests with cased bombs incur less damage than similar larger walls in larger scale tests. This is attributed to different strain-rates causing different dynamic concrete strengths in different scale tests, bomb fragment mass distribution does not scale, and velocities of scaled fragments decrease at a faster rate than full-scale bomb fragments.

Tests investigating the effect of wall thickness on spall indicated that large increases in wall thickness will decrease spall damage. The thicker the wall, the further the stress waves have to travel and the more they can change their magnitudes and shapes due to different stresses traveling at different velocities, attenuation, divergence and dispersion.

Various rebar spacing schemes can also affect spall. Tests indicate that a closely spaced reinforcement grid held securely with closely spaced stirrups does reduce the amount of spall. However, the concrete

cover over the reinforcing steel can still spall. In general, the extra expense of building walls with close-spaced reinforcement is not justified since the cover can still spall.

Spall depths and spall velocities in tests on "high-strength" concrete were much worse than in similar tests on "4,000 psi" concrete. The stress waves did not change magnitudes and shapes as much in the "high strength" concrete as in the "4,000 psi" concrete because it had a higher dynamic compressive strength, so the stress waves kept higher peak stresses, shorter rise times and shorter durations. The difference in the compressive strengths was much larger than the difference in the tensile strengths of the two concretes (i.e. the ratio of the dynamic tensile strength to compressive strength was higher for the 4,000 psi concrete). Although the tensile strength of the high strength concrete was higher than that of the "4,000 psi" concrete, the stress waves which reached the back of the wall were more severe in the high strength concrete than in the 4,000 psi concrete and caused worse spall damage. High strength concrete should be used with caution in protective structures where spall is possible.

Tests showed that walls of concrete with 191.7 lb/yd³ of acrylic latex additive suffered less spall damage than similar "normal" concrete walls subjected to identical bomb detonations. The acrylic latex formed a matrix in the microstructure which helped hold the various concrete elements together with a ductile bond and retarded rapid crack growth during dynamic loading.

Tests showed that walls of concrete with 80 lb/yd³ of crimped steel fibers suffered less damage than similar walls with similar normal concrete. The steel fibers were randomly dispersed throughout the concrete mixture and retarded rapid crack growth during the dynamic loadings.

Evaluation of Existing Methods

The principal theoretical and empirical prediction methods for spall of concrete structures subjected to nearby bare and cased bomb detonations were reviewed. The few theoretical methods which were found (References 39 and 40 by C. Kot and Reference 41 by C. Canada) were limited to light to moderate bomb threats and were based on several

simplifying assumptions to make them easier to solve. However, many of the simplifying assumptions compromised the accuracy of the calculations. As a result, none of the theoretical spall prediction methods compared very well with test data. The empirical prediction methods compared better with test data, although there were discrepancies. The data bases of the empirical prediction curves included a few large scale tests, but the majority of the data were from small scale tests. Most of the discrepancies were between empirical predictions and large-scale tests. An additional problem with scaling cased bomb tests is that bomb fragment weight distributions do not scale the same as airblast. The best spall prediction methods for bare charges reviewed were in Reference 33 by NDRC and References 45 and 46 by Firma E. Basler and Partner. The best spall prediction method for cased charges reviewed was in References 45 and 46 by Firma E. Basler and Partner.

Improved Prediction Methods

Data on 334 additional tests were collected and added to the data on the 40 tests in this study. Two forms of improved empirical damage prediction curves for bare charges were drawn to fit the data from bare charge tests and are shown in Figures 8.1 and 8.2. An improved empirical damage prediction curve for cased charges was also drawn to fit the data from cased charge tests and account for various casing thicknesses; it is shown in Figure 8.3. The limits on the parameters given for each prediction curve should be strictly adhered to in order to avoid under prediction due to problems of scaling spall damage.

Spall Prevention and Retention

Several methods for decreasing the chances of spall on retaining walls were discussed. Soil berms, shield walls, layered walls, additives in concrete, and corrugation of wall surfaces can reduce the chances of spall. Spall plates, wire mesh, and close spacing of reinforcing steel can be used to retain spall.

REFERENCES

1. Coltharp, D. R., Vitayaudom, K. P. and Kiger, S. A. 1985 (Sep). "Semihardened Facility Design Criteria Improvement," ESL-TR-85-32, Air Force Engineering and Services Center, Tyndall Air Force Base, Florida.
2. Loos, G., and Pahl, H. 1982 (Jan). "Quick-Look Report, Explosive Tests on Underreinforced Model Structures in Incirlik (Republic of Turkey) and Meppen (Federal Republic of Germany)," Infrastrukturstab Der Bundeswehr, TB-82-01.
3. Kingery, C. N., and Bulmash, G. 1984 (Apr). "Airblast Parameters from TNT Spherical Air Burst and Hemispherical Surface Burst," ARBRL-TR-02555, US Army Ballistic Research Laboratory, Aberdeen Proving Ground, Maryland.
4. Baker, W. E. 1983. "Explosions in Air," Wilfred Baker Engineering, San Antonio, Texas.
5. Structures Laboratory, Department of the Army. 1984 (Jul). "Fundamentals of Protective Design for Conventional Weapons," US Army Engineer Waterways Experiment Station, Vicksburg, Mississippi.
6. Fisher, E. M. "The Effect of the Steel Case on the Air Blast from High Explosives," NAVORD Report 2753, Explosives Research Department, US Naval Ordnance Laboratory, White Oak, Maryland.
7. Headquarters, Department of the Army. 1969 (Jun). "Structures to Resist the Effects of Accidental Explosions, "Technical Manual 5-1300.
8. Headley, J., Werner, H., Weissman, S., Dobbs, N., and Price, P. 1975 (Dec). "Primary Fragment Characteristics and Impact Effects on Protective Barriers," Technical Report 4903, Picatinny Arsenal, Dover, New Jersey 07801.
9. Backman, M. E., and Goldsmith, W. 1978. "The Mechanics of Penetration of Projectiles Into Targets," International Journal of Engineering Science, Vol 16, No. 1, pp 1-99.
10. Beth, R. A. 1946 (Mar). "Final Report on Concrete Penetration," Report No. A-388, National Defense Research Committee, Office of Scientific Research and Development.
11. Read, H. E., and Maiden, C. J. 1971 (Aug). "The Dynamic Behavior of Concrete," 3SR-707, Air Force Systems Command, Norton Air Force Base, California.
12. Goldsmith, W., Polivka, M., and Yang, T. 1966 (Feb). "Dynamic Behavior of Concrete," Experimental Mechanics, pp 65-79.
13. Rinehart, J. S. 1960 (Feb). "Practical Countermeasures for the Prevention of Spallation," AFSWC-TR-60-7, Air Force Special Weapons Center, Kirtland Air Force Base, New Mexico.
14. Graff, K. F. 1975. Wave Motion in Elastic Solids, Ohio State University Press.

15. Hatano, T. 1960. "Relations Between Strength of Failure, Strain Ability, Elastic Modulus, and Failure Time of Concrete," C-6001, Central Research Institute of Electric Power Industry, Tokyo.
16. Birkimer, D. L., and Lindermann, R. 1971 (Jan). "Dynamic Tensile Strength of Concrete Materials," American Concrete Institute Journal, pp 46-49.
17. Zielinski, A. J. 1982 (Nov). "Fracture of Concrete and Mortar and Uniaxial Impact Tensile Loading," Delft University Press.
18. Reinhardt H. W., 1982. "Concrete Under Impact Loading Tensile Strength and Bond," Heron, Vol 27, No. 3.
19. Gerstle, K. H. 1979 (Dec). "Material Behavior Under Various Types of Loading," Proceedings of the Workshop on High Strength Concrete, University of Illinois at Chicago Circle, Session II, pp 43-78.
20. "State-of-the-Art Report on Fiber Reinforced Concrete," ACI Manual of Concrete Practice 1985, ACI 544.1R-82.
21. Fanella, D., and Krojcinovic, D. 1985 (Aug). "Continuum Damage Mechanics of Fiber Reinforced Concrete," Paper No. 19925, Journal of Engineering Mechanics, Vol 111, No. 8.
22. Suaris, W. and Shah, S. P. 1983 (Jul). "Properties of Concrete Subjected to Impact," Paper No. 18111, Journal of Structural Engineering, Vol 109, No. 7.
23. Williamson, G. R. 1965 (May). "Fibrous Reinforcements for Portland Cement Concrete," Technical Report No. 2-40, US Army Engineer Division, Ohio River, Cincinnati, Ohio.
24. Williamson, G. R. 1966 (Jan). "Response of Fibrous-Reinforced Concrete to Explosive Loadings," Technical Report No. 2-48, US Army Engineer Division, Ohio River, Cincinnati, Ohio.
25. Mullins, R. K., and Baker R. K. 1979 (Sep). "Interim Report on Use of Steel Fibers in Concrete Slab Construction to Resist Spall Caused by High-Explosive Blast Effects," UCID 18251, Lawrence Livermore Laboratory.
26. Naus, D. J., and Williamson, G. R. 1976 (Apr). "Ballistics Tests of Fibrous Concrete Dome and Plate Specimens," US Army Construction Engineering Research Laboratory, Technical Report No. M-179.
27. Hulsewig, M., Stilp, A. J., and Pahl, H. 1982 (Mar). "Behaviour of Fiber Reinforced Concrete Slabs Under Impact Loading," Ernst-Mach-Institut, Freiburg i. Br., West Germany.
28. "Polymers in Concrete," ACI Manual of Concrete Practice 1985, ACI 548R-77.
29. Clifton, J. R., and Knab, L. I. 1983. "Impact Testing of Concrete," Cement and Concrete Research, Vol 14, pp 541-548.
30. Bhargava, J., and Rehnstrom A. 1982 (Jul). "Dynamic Behavior of Polymer-Cement Concrete," SP58-18, Polymers in Concrete, American Concrete Institute, Detroit, Michigan, Second Printing.

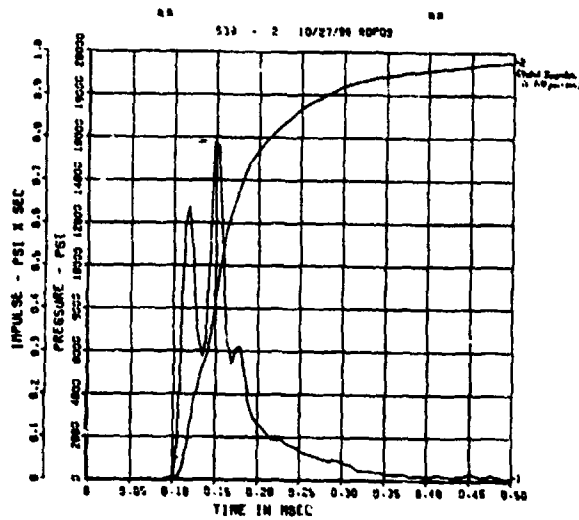
31. Kinslow, R. 1976 (May). "Spallation Resulting from High-Velocity Impacts," AD-A031907, Report 2179, US Army Mobility Equipment Research and Development Command, Fort Belvoir, Virginia.
32. Charest, J. A. 1972 (Aug). "Spall Data Compendium," EGG 1183-2274, EG&G Inc., Goleta, California.
33. National Defense Research Committee. 1946. "Effects of Impact and Explosion, Vol 1, Office of Scientific Research and Development, Washington, DC.
34. Headquarters, Department of the Army. 1965 (Jul). "Fundamentals of Protective Design (Nonnuclear), Technical Manual 5-855-1.
35. Kennedy, R. P. 1975 (Sep). "A Review of Procedures for the Analysis and Design of Concrete Structures to Resist Missile Impact Effects," Report NSS 5-940.1, Holmes and Narver Inc., Anaheim, California.
36. Kar, A. K. 1978 (May). "Local Effects of Tornado-Generated Missiles," Journal of the Structural Division, ASCE, Vol 104, No. ST5, pp 809-816.
37. Chang, W. S. 1981 (Feb). "Impact of Solid Missiles on Concrete Barriers," Journal of the Structural Division, ASCE, Vol 107, No. STZ, pp 257-271.
38. Hughes, G. 1984. "Hard Missile Impact on Reinforced Concrete," Nuclear Engineering and Design, Vol 77, pp 23-35.
39. Kot, C. A. 1977. "Spalling of Concrete Walls Under Blast Load," Transactions of the Fourth International Conference on Structural Mechanics in Reactor Technology, J 10/5, Vol J(b).
40. Kot, C. A., Valentin, R. A., McLennan, D. A., and Turula, P., 1978 (Oct). "Effects of Airblast on Power Plant Structures and Components," Report No. ANL-CT-78-41, Argonne National Laboratory, Argonne, Illinois.
41. Canada, C. E. 1984. "Combined Blast and Fragment Loading of Reinforced Concrete," Air Force Engineering and Services Center, Tyndall Air Force Base, Florida.
42. Kropatscheck, M. O. 1983 (10-13 May). "Tests and Evaluations of Close-In Detonations," Symposium Proceedings of The Interaction of Nonnuclear Munitions with Structures, US Air Force Academy, Colorado Springs, Colorado.
43. Freeman, I. M. 1946 (Jan). "Damage to Reinforced-Concrete Wall Panels by Detonation of Contact and Remote Charges," a paper in Study of the Physical Vulnerability of Military Targets to Various Types of Aerial Bombardment, NDRC Report No. A-385, Princeton University.
44. The JANNAF Hazards Working Group. 1971 (Oct). "Chemical Rocket/Propellant Hazards," CPIA Publication 194, Chemical Propulsion Information Agency, The John Hopkins University, Silver Spring, Maryland.

45. Firma E. Basler & Partner. 1982 (Sep). "Lokal Schadenwirkungen an Betonplatten Durch Sprengladungen," B3113.10-2, E. Basler & Partner, Zurich, Switzerland.
46. Hader, H. 1983 (10-13 May). "Effects of Bare and Cased Explosive Charges on Reinforced Concrete Walls," Paper presented in the Symposium on the Interaction of Nonnuclear Munitions With Structures, US Air Force Academy, Colorado Springs, Colorado.
47. Wright, R. S., Coltharp, D. R., Vretblad, B., and Balazs, P. 1987 (Mar). "Blast Response Tests of a Swedish-Norwegian Structure," Proceedings of: Internationales Symposium Interaktion Konventioneller Munition Mit Schutzbauten, Mannheim, West Germany.
48. Coltharp, D. R. 1986. "Explosive Tests on Reinforced Concrete Walls at Camp Shelby, Mississippi, Miscellaneous Paper SL-86-5, US Army Engineer Waterways Experiment Station, Vicksburg, Mississippi.
49. Ball, J. W. 1976 (Dec). "Essex-Diamond Ore Research Program," Technical Report N-76-10, US Army Engineer Waterways Experiment Station, Vicksburg, Mississippi.
50. Cummins, R. S., and Albritton, G. E. 1979 (Nov). "Federal Republic of Germany Structures Test Program, Dice Throw Event; Report 5: Small Scale High-Explosive Tests," Technical Report N-77-2, US Army Engineer Waterways Experiment Station, Vicksburg, Mississippi.
51. Hoot, B. B. 1974 (Aug). "Evaluation of Field Fortifications," Technical Report N-74-5, US Army Engineer Waterways Experiment Station, Vicksburg, Mississippi.
52. Coltharp, D. R. 1982. "Tests of the CEV Round Against Concrete Walls," Draft, US Army Engineer Waterways Experiment Station, Vicksburg, Mississippi.
53. Kropatscheck, M. 1982 (Aug/Sep). "Summary Report, Explosive Tests on Underreinforced Model Structures at Proving Ground 91 of the Federal Armed Forces of Germany at Meppen," WW-TB-82-12, Amt fur Studien und Uebungen der Bundeswehr Bericht Sonderaufgaben-Infrastruktur, Cologne, West Germany.
54. Bohnenblust, H. 1980 (Feb). "Sprengversuche an Betonwaenden," B922.10, Basler & Hofmann Ingenieure und Planer AG., Zurich, Switzerland.
55. Janser, P. 1981 (Mar). "Sprengversuche an Betonwaenden: Zusatzversuche Mai and Oktober 1980," B3113-1, Ernst Basler and Partner, Zurich, Switzerland.
56. Abteilung fur Passiven Luftschutz. 1941 (Jan). "Wirkungeiner 50 kg Bombe auf Permanente Splitterschutzobjekte," EMD, Bern, Switzerland.
57. Abteilung fur Passiven Luftschutz. 1941 (Jun). "Bericht uber Sprengversuche in Klotten am 12/13 Juni 1941," EMD, Bern, Switzerland.
58. Eidg. Militaerdepartement. 1942. "Bericht uber Sprengversuche an Massiven Betonplatten," Switzerland.

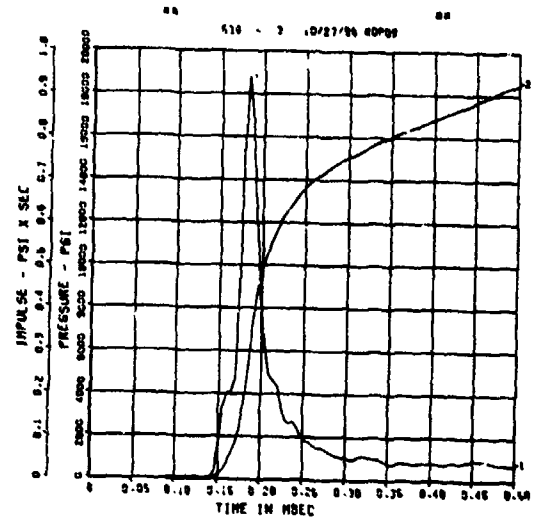
59. Schneider, T. 1979 (Dec). "Lokale Schadenwirkung auf Armierte Betonplatten bei der Explosion von Sprengladungen und Granaten," FMB 79-13 Forschungsinstitut fuer Militaerische Bautechnik, Zurich, Switzerland.
60. Heine, H. 1981. "Bugelbewehrung zur Vermeidung von Scabbing," E/K 47 E/80903/86090, Bundesamt fuer Wehrtechnik und Beschaffung, West Germany.
61. Kudicke, G. 1979. "Stahlfaserbeton Schutzban," T/K 47 E/81043/45160, Bundesamt fuer Wehrtechnik und Beschaffnug.
62. United States Office of Civil Defense. 1941. "Report of Bomb Tests on Materials and Structures."
63. Krefsinger, D. C. 1944 (Jun). "Interim Report No. 29 to the Chief of Engineers USA: Contact Explosions on Concrete," National Research Committee on Fortifications Design.
64. Clark, J. C., and Fleming, R. O. 1944 (May). "Pillbox Demolition by High Explosive Charges," Memorandum Report No. 29, Ballistic Research Laboratory, Aberdeen Proving Ground, Maryland.
65. Wasser, E. L. 1970 (Apr). "High Explosive Test Program for HRSD," Gulf General Atomic, Report GACD-10104(4-70).
66. Coltharp, D. R., Ball, J. W., and McVay, M. K. 1987 (Mar). "Effectiveness of Sacrificial Concrete Panels in Reducing Blast and Fragment Loadings," Proceedings of Internationales Symposium Interaktion Konventioneller Munition Mit Schutzbauten, Mannheim, West Germany.
67. McVay, M. K. 1988 (Mar). "Systems for Shielding Aboveground Structures from Severe Airblast, Bomb Fragments, and/or Projectiles," ESL-TR-88-Draft, Air Force Engineering and Services Center, Tyndall Air Force Base, Florida.

APPENDIX A
PLOTS OF THE ACTIVE MEASUREMENTS VERSUS TIME

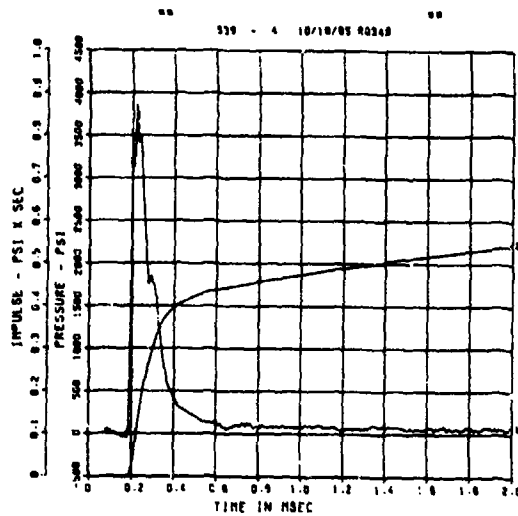
SPALL TEST 1A
PB-1
200000. HZ CAL= 15047.



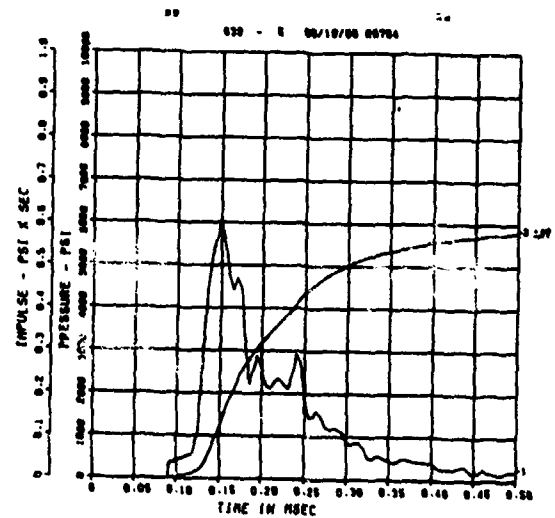
SPALL TEST 1A
PB-2
200000. HZ CAL= 10711.



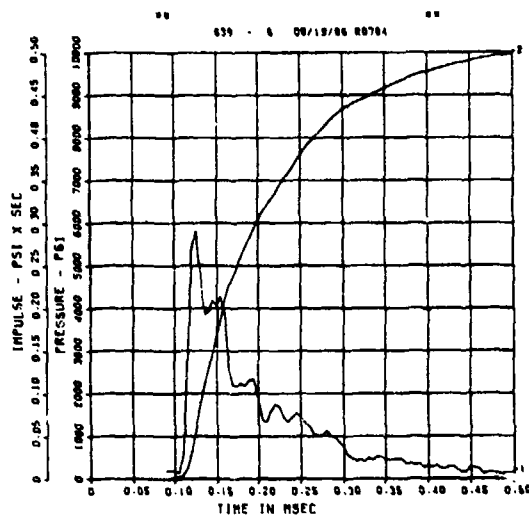
SPALL TEST 1A
PB-3
200000. HZ CAL= 4711.



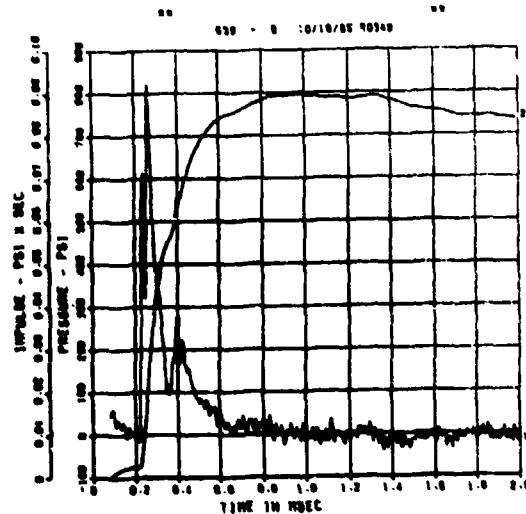
SPALL TEST 1A
PQ-0
200000. HZ CAL= 18352.



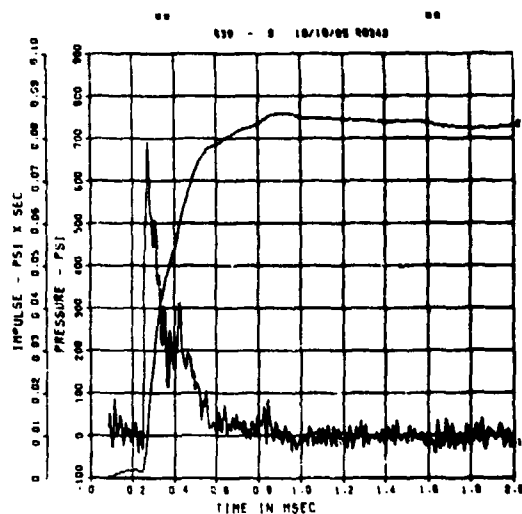
SPALL TEST 1A
PQ-1
200000. HZ CAL= 18204.



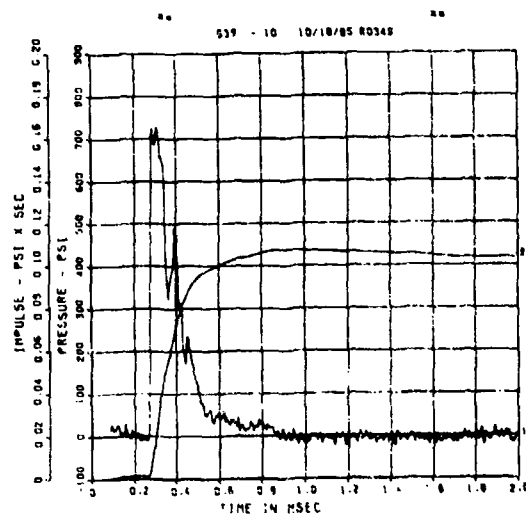
SPALL TEST 1A
PM-0
200000. HZ CAL= 4567.



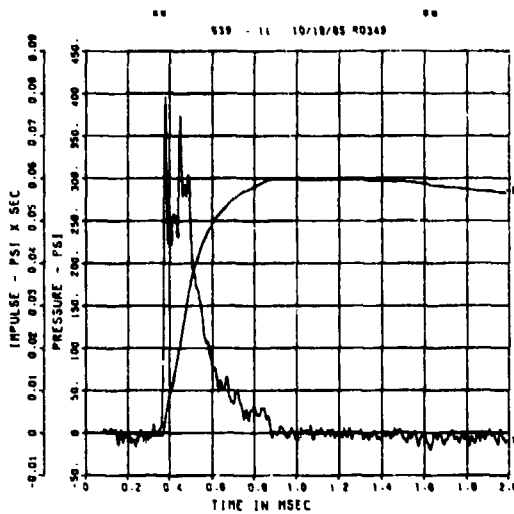
SPALL TEST 1A
PM-1
200000. HZ CAL= 4136.



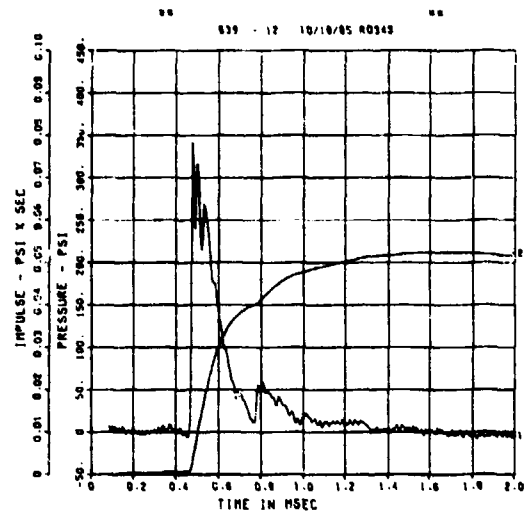
SPALL TEST 1A
PM-2
200000. HZ CAL= 2943.



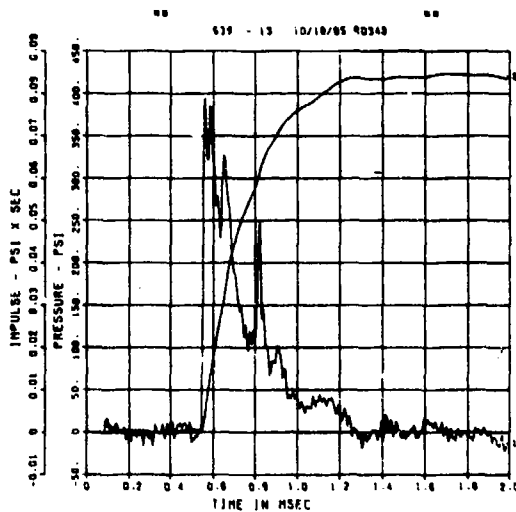
SPALL TEST 1A
PM-3
200000. HZ CAL= 1965.



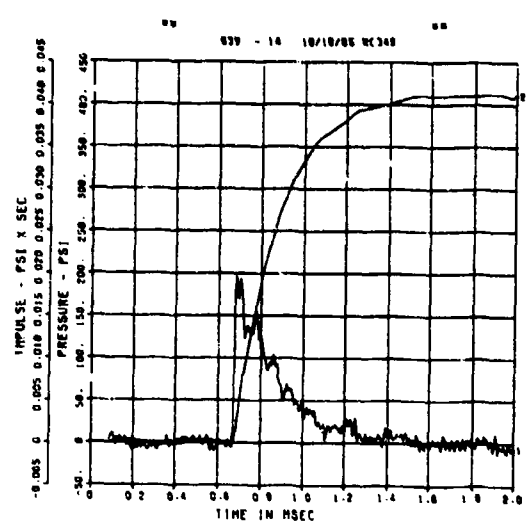
SPALL TEST 1A
PT-0
200000. HZ CAL= 952.3



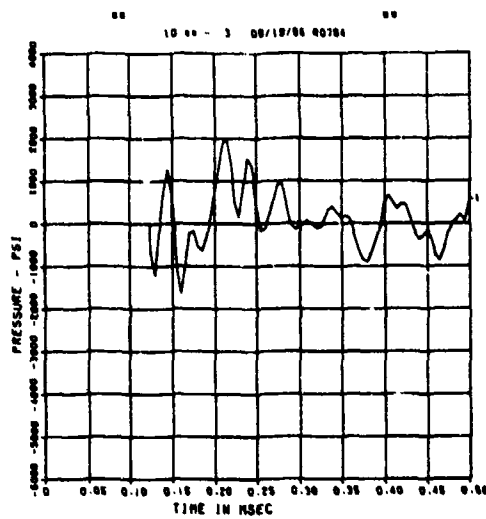
SPALL TEST 1A
PT-2
200000. HZ CAL= 1072.



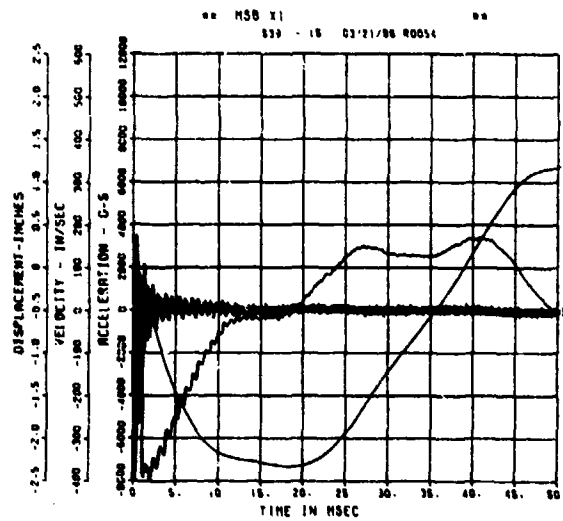
SPALL TEST 1A
PT-3
200000. HZ CAL= 1181.



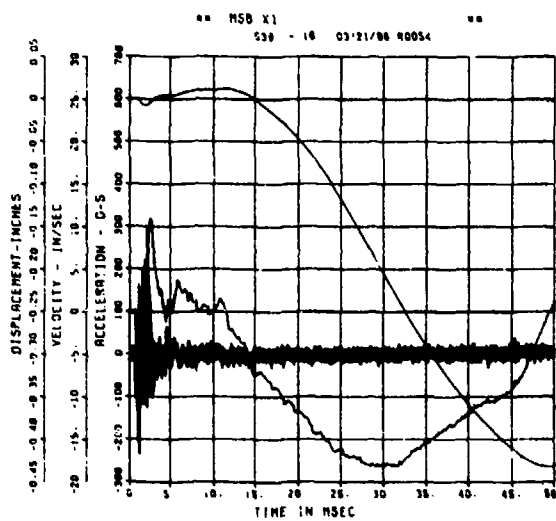
SPALL TEST 1A
 FP-A
 200000. HZ CAL= -0.060



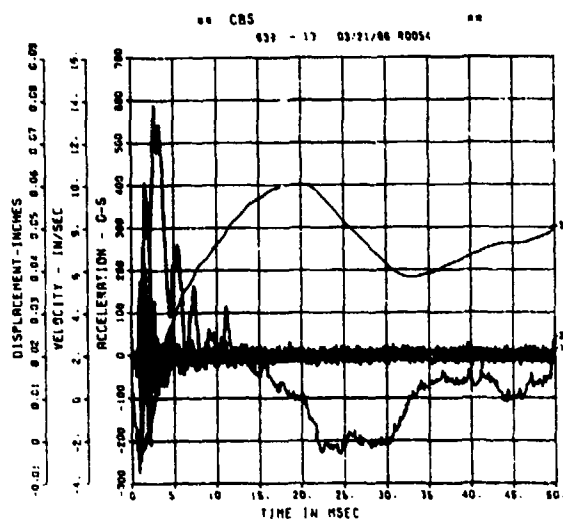
SPALL TEST 1A
 9WHM
 200000. HZ CAL= 26696.



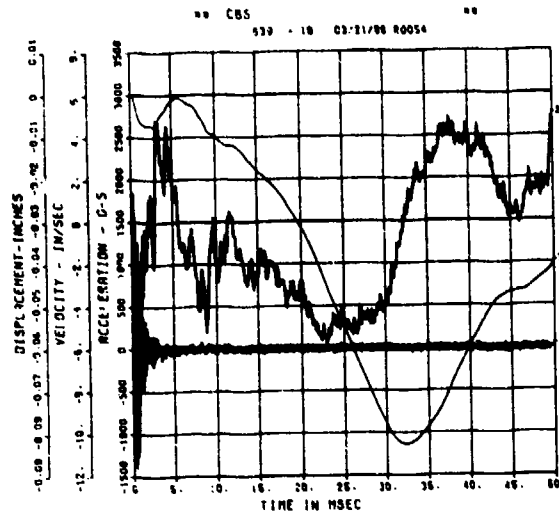
SPALL TEST 1A
 ARV
 200000. HZ CAL= 2532.



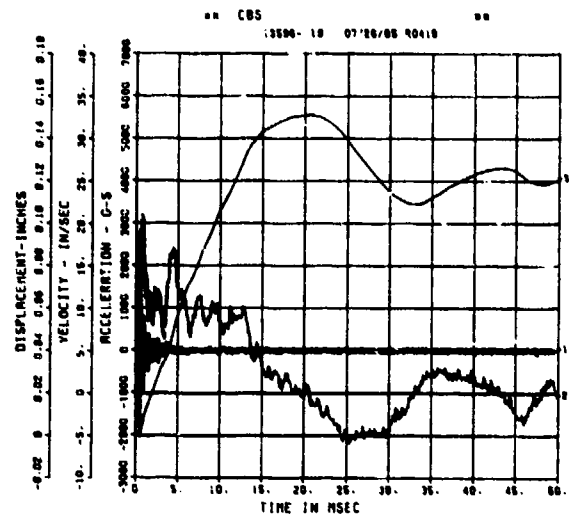
SPALL TEST 1A
 ARH
 200000. HZ CAL= 2336.



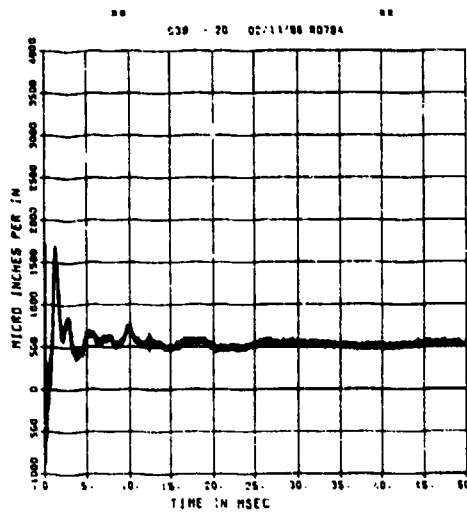
SPALL TEST 1A
AFV
200000. HZ CAL= 4983.



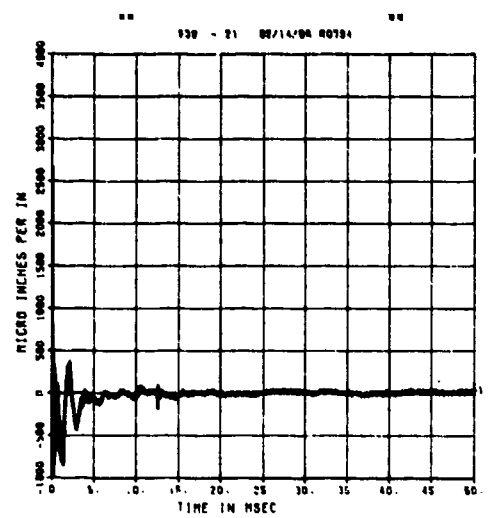
SPALL TEST 1A
AFM
200000. HZ CAL= 5966.



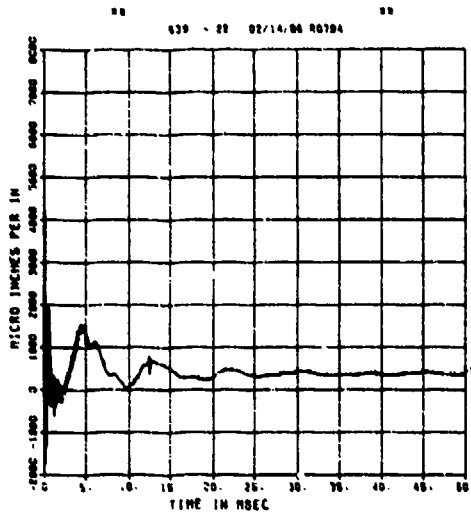
SPALL TEST 1A
EQT
200000. HZ CAL= 5004.



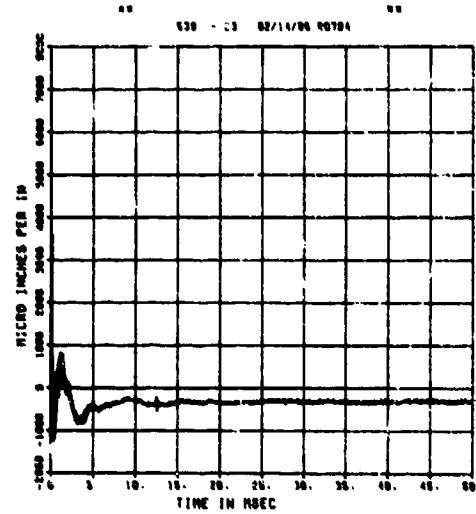
SPALL TEST 1A
EIT
200000. HZ CAL= 3026.



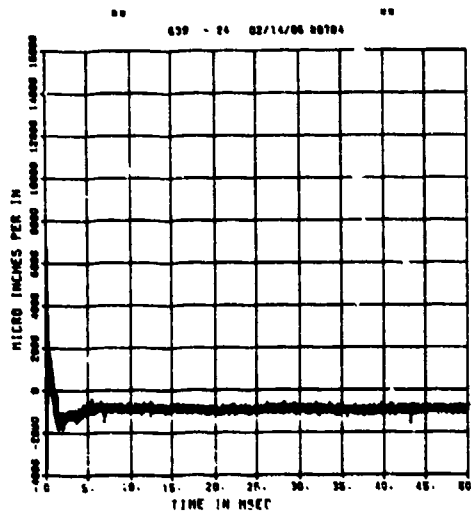
SPALL TEST 1A
EOM
200000. HZ CAL= 3026.



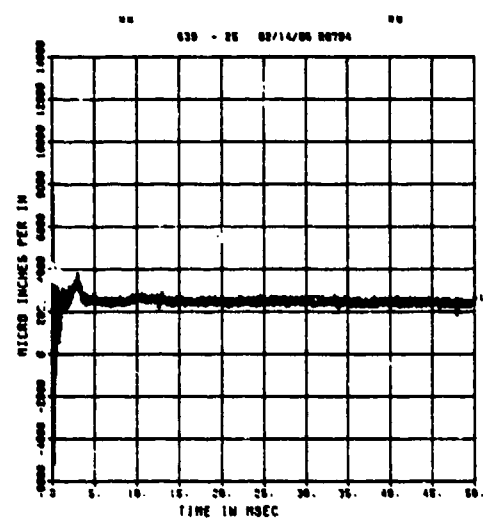
SPALL TEST 1A
EIM
200000. HZ CAL= 5004.



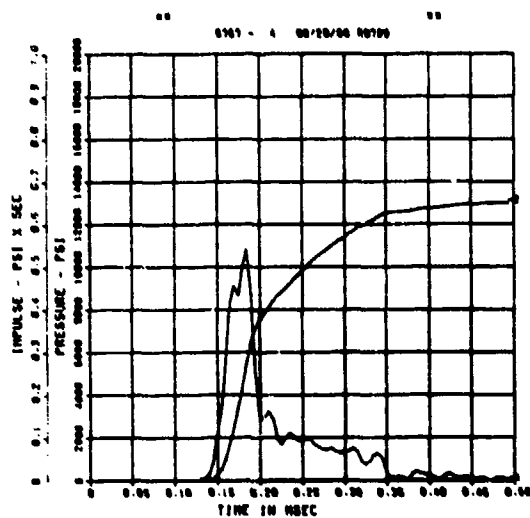
SPALL TEST 1A
E0B
200000. HZ CAL= 30324.



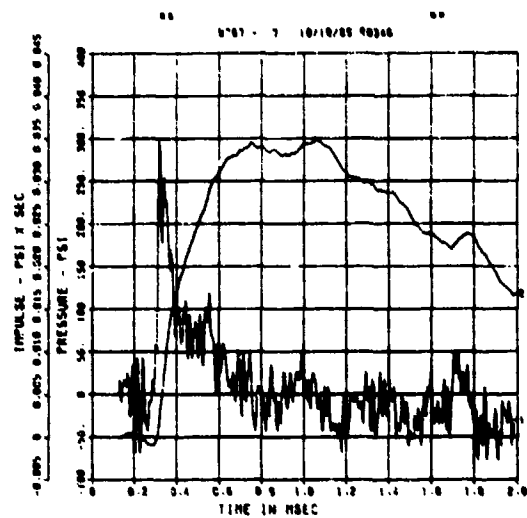
SPALL TEST 1A
E1B
200000. HZ CAL= 30324.



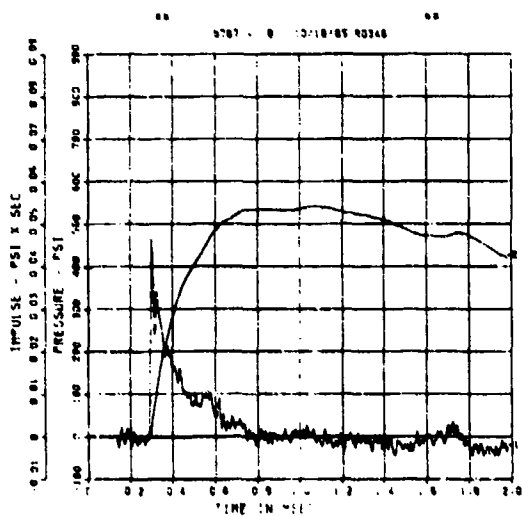
SPALL TEST 1B
PQ-0
200000. HZ CAL= 19659.



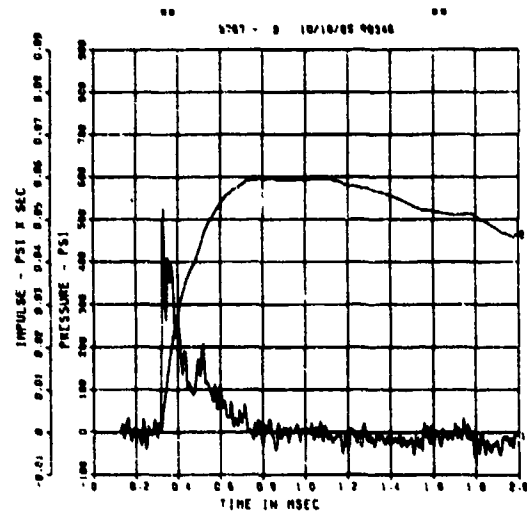
SPALL TEST 1B
PM-0
200000. HZ CAL= 8323.



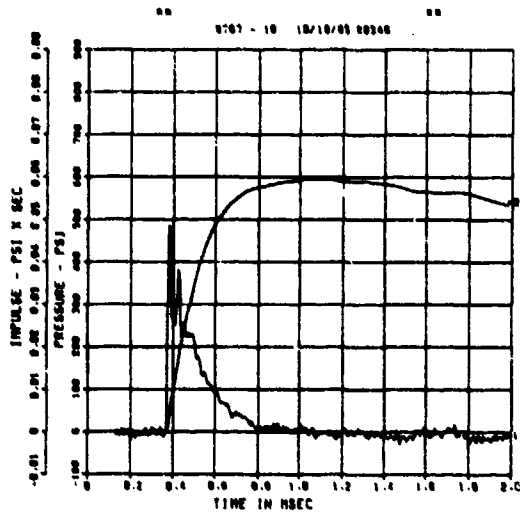
SPALL TEST 1B
PM-1
200000. HZ CAL= 4136.



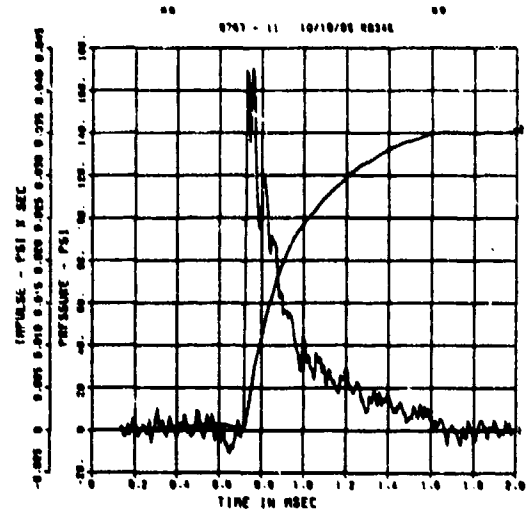
SPALL TEST 1B
PM-2
200000. HZ CAL= 2943.



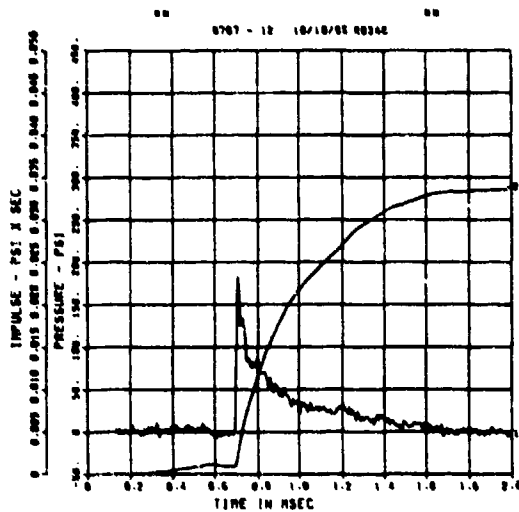
SPALL TEST 1B
PM-3
200000. HZ CAL= 1965.



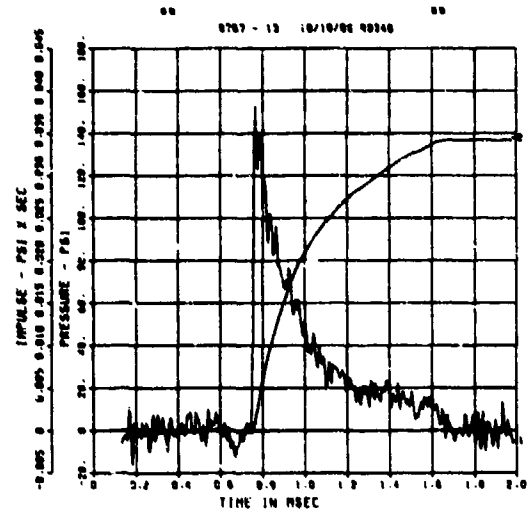
SPALL TEST 1B
PT-0
200000. HZ CAL= 952.3



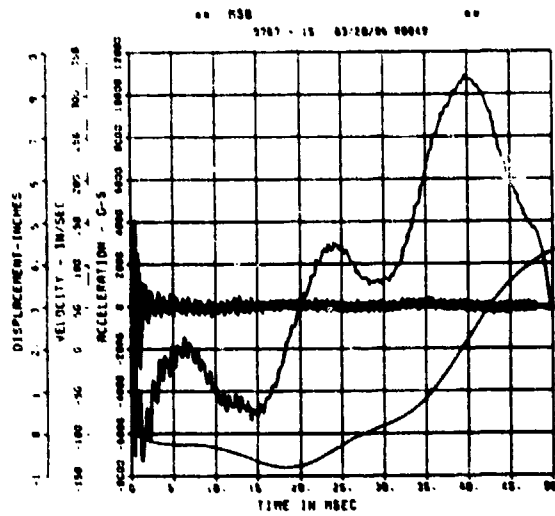
SPALL TEST 1B
PT-2
200000. HZ CAL= 1072.



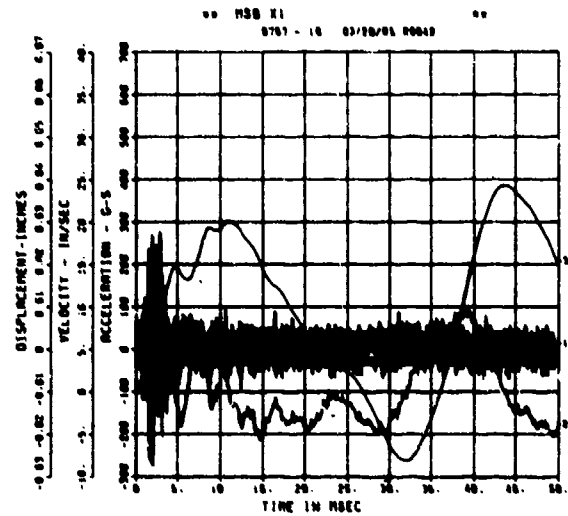
SPALL TEST 1B
PT-3
200000. HZ CAL= 1181.



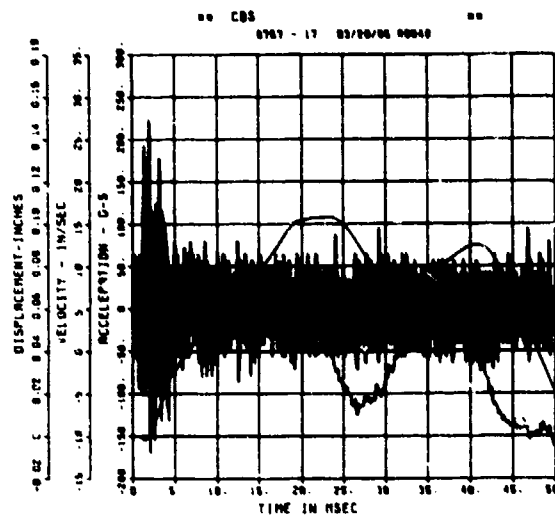
SPALL TEST 1B
 QWHM
 200000. HZ CAL= 30652.



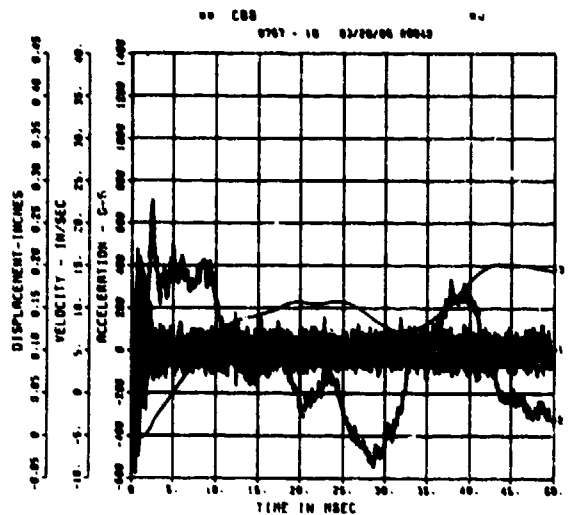
SPALL TEST 1B
 ARV
 200000. HZ CAL= 7452.



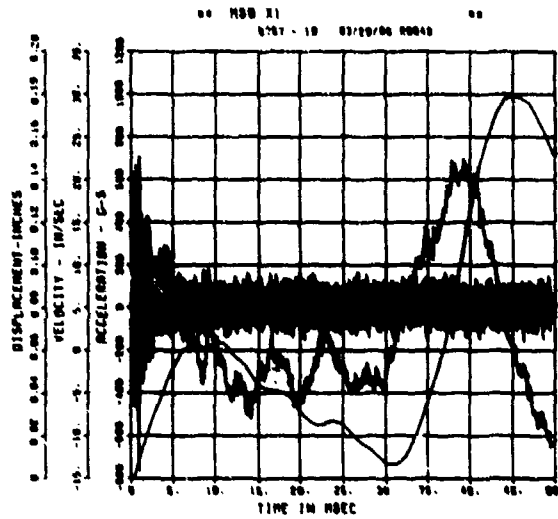
SPALL TEST 1B
 ARH
 200000. HZ CAL= 7556.



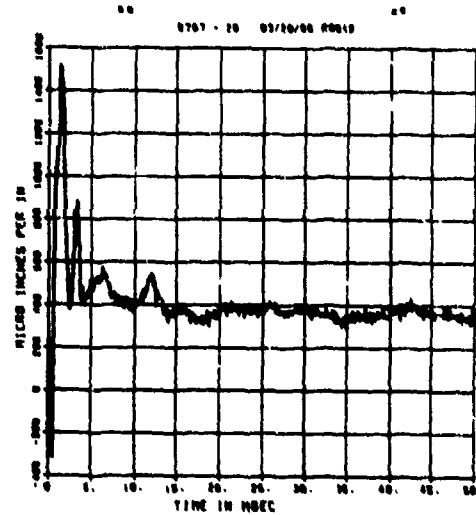
SPALL TEST 1B
 AFV
 200000. HZ CAL= 12297.



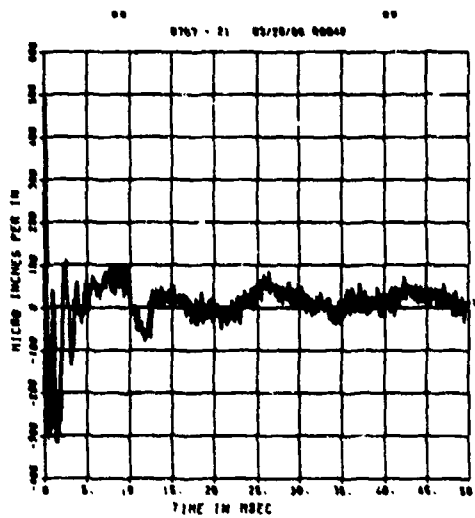
SPALL TEST 1B
 AFH
 200000. HZ CAL= 12019.



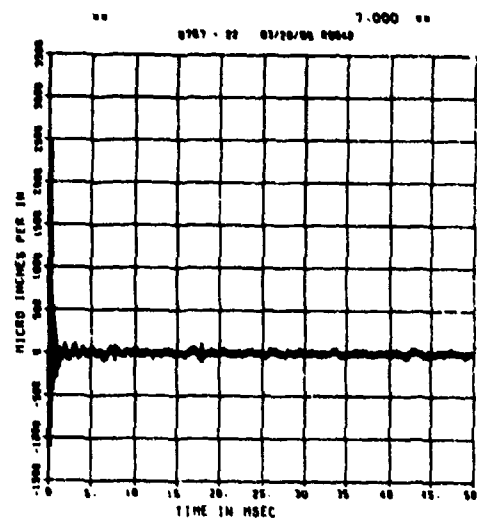
SPALL TEST 1B
 EDT
 200000. HZ CAL= 7469.
 LP4/0 70K CUTOFF= 9000. HZ



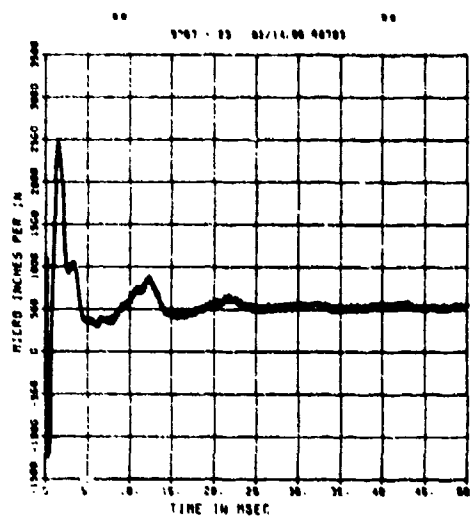
SPALL TEST 1B
 EIT
 200000. HZ CAL= 7469.
 LP4/0 70K CUTOFF= 9000. HZ



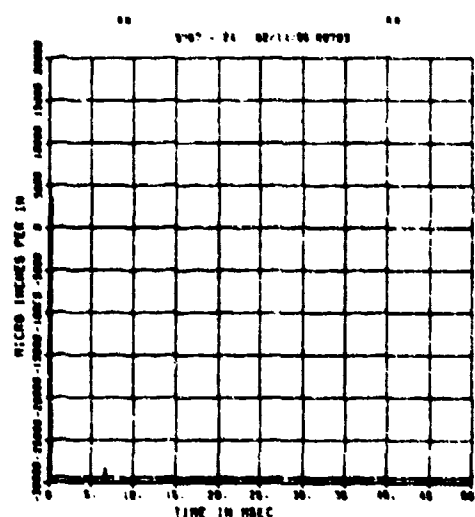
SPALL TEST 1B
 EDM
 200000. HZ CAL= 5004.



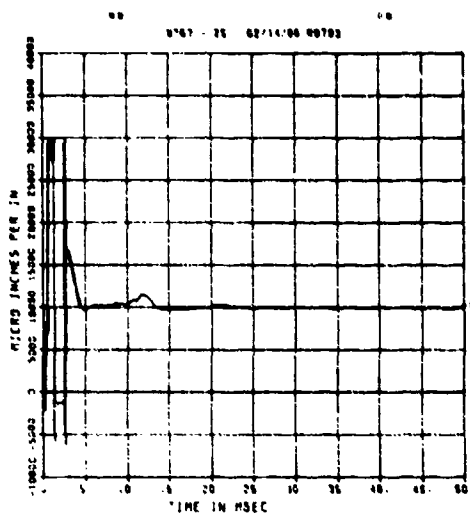
SPALL TEST 1B
E1M
200000. HZ CAL= 5004.



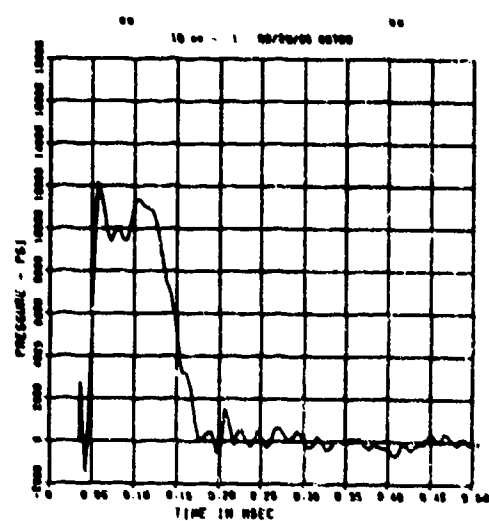
SPALL TEST 1B
E0B
200000. HZ CAL= 14816.



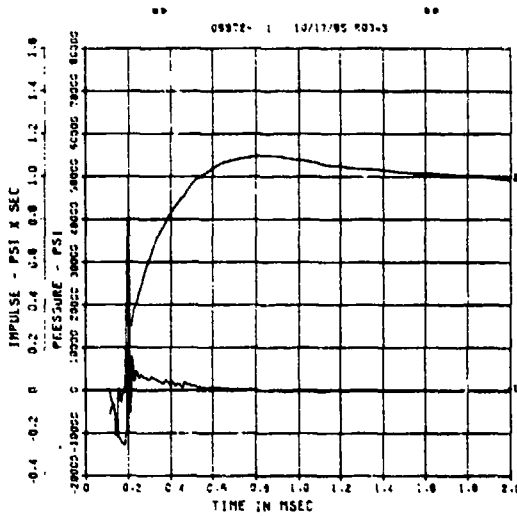
SPALL TEST 1B
E1B
200000. HZ CAL= 14816.



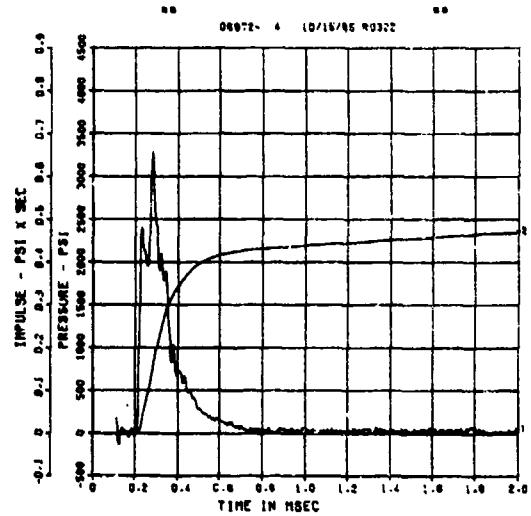
SPALL TEST 1C
FP-C
200000. HZ CAL= -0.210



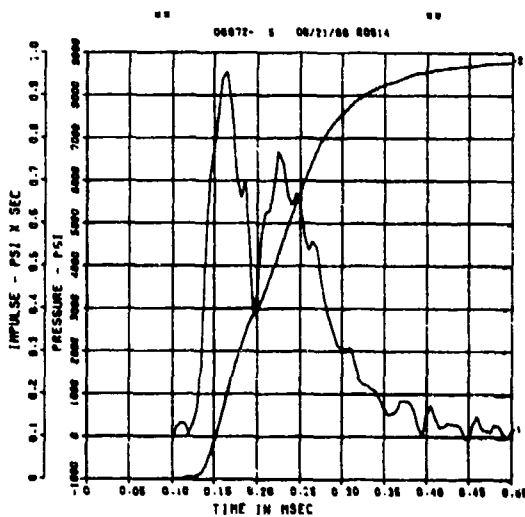
SPALL TEST 10
PB-0
200000. HZ CAL= 22037.



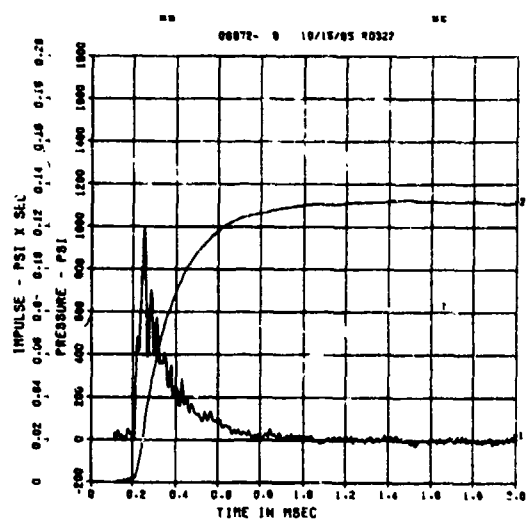
SPALL TEST 10
PB-3
200000. HZ CAL= 6246.



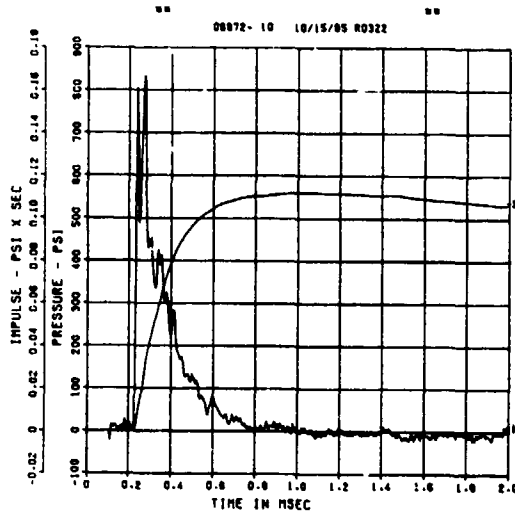
SPALL TEST 10
PG-0
200000. HZ CAL= 18352.



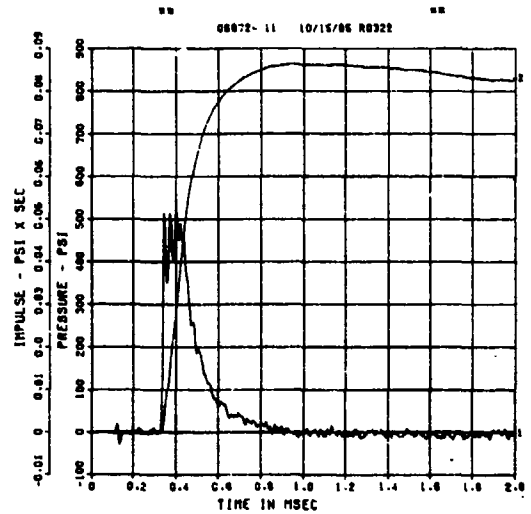
SPALL TEST 10
PM-0
200000. HZ CAL= 4567.



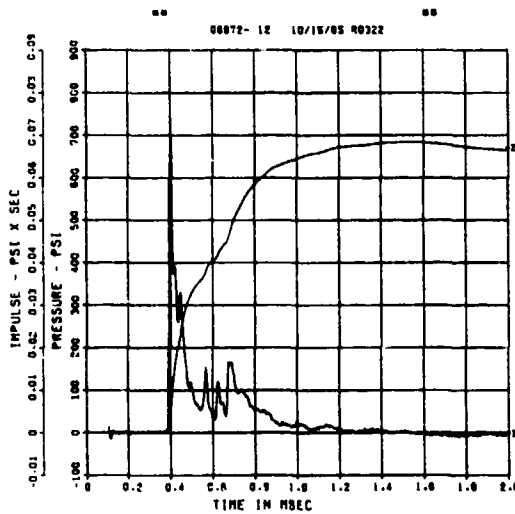
SPALL TEST 10
PM-2
200000. HZ CAL= 2943.



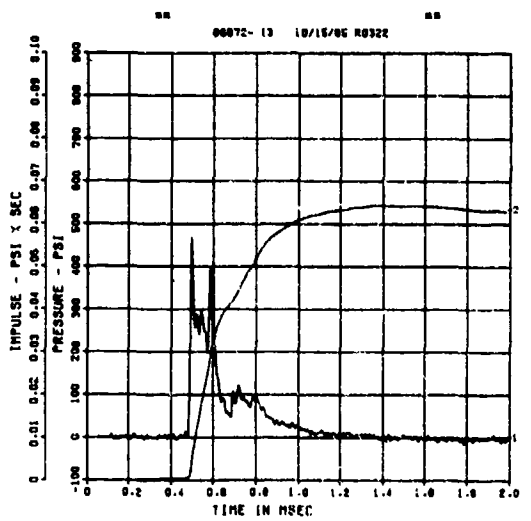
SPALL TEST 10
PM-3
200000. HZ CAL= 1965.



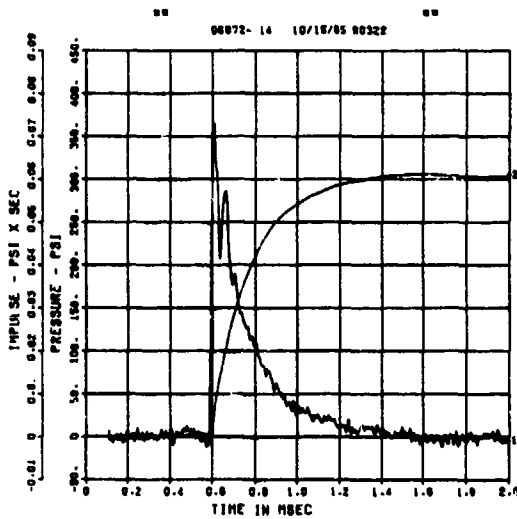
SPALL TEST 10
PT-0
200000. HZ CAL= 952.3



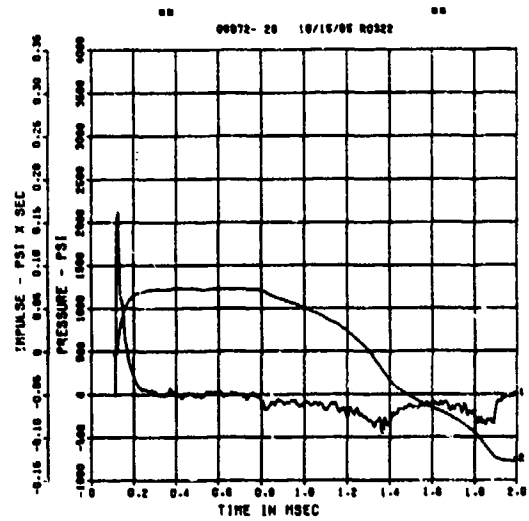
SPALL TEST 10
PT-2
200000. HZ CAL= 1072.



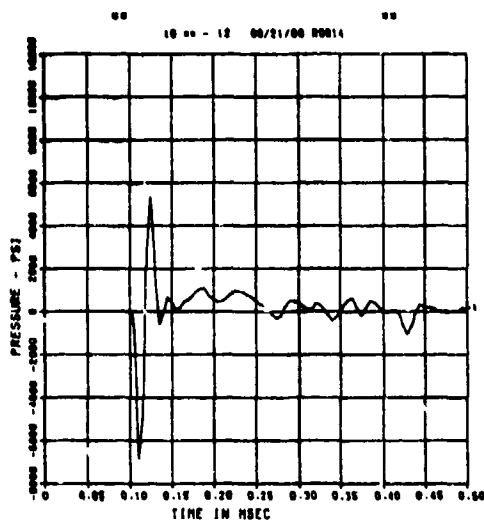
SPALL TEST 1D
PT-3
200000. HZ CAL= 1181.



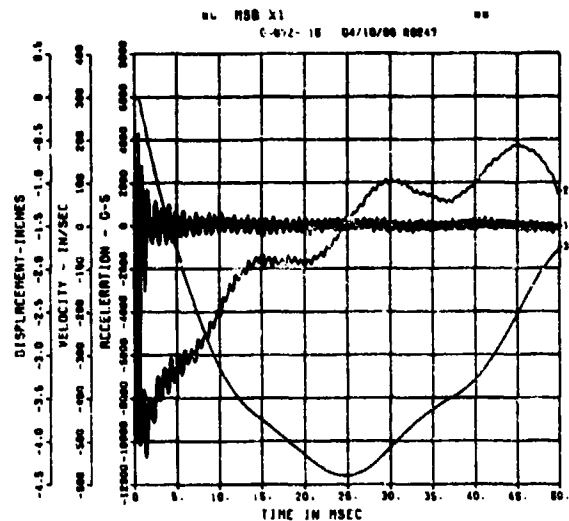
SPALL TEST 1D
BP-A
200000. HZ CAL= 4358.



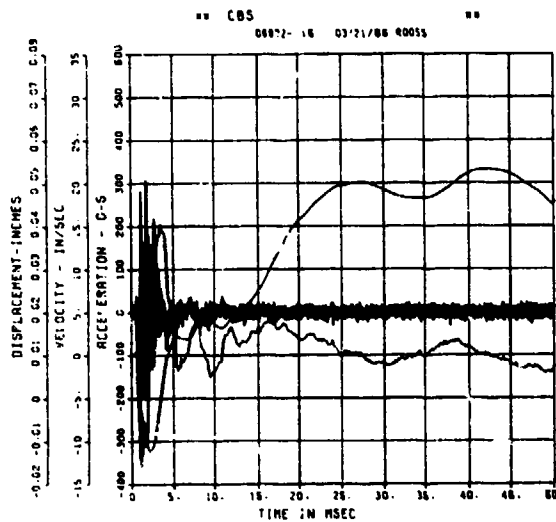
SPALL TEST 1D
FP-A
200000. HZ CAL= -0.080



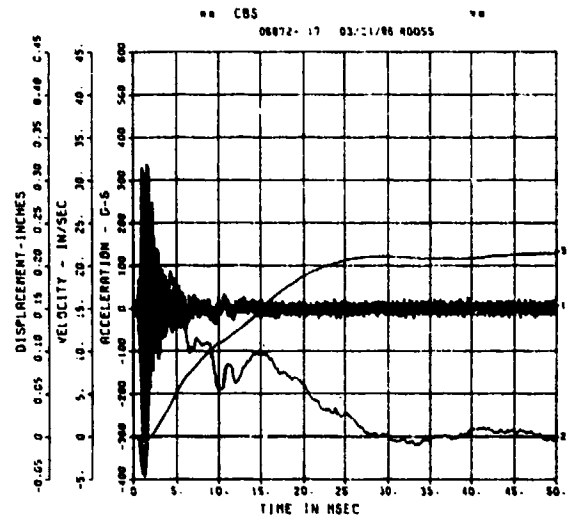
SPALL TEST 1D
AWHM
200000. HZ CAL= 26696.



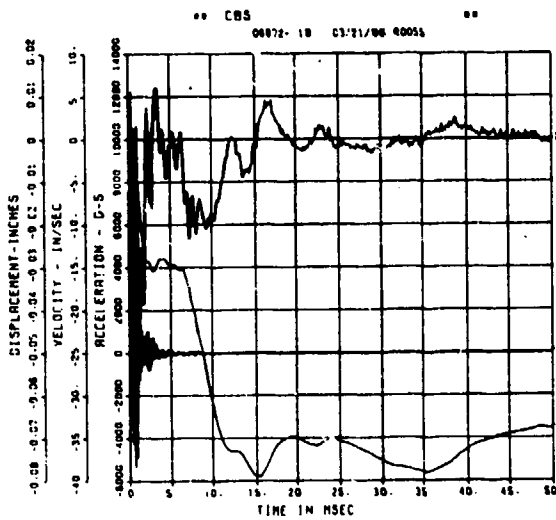
SPALL TEST 10
ARV
200000. HZ CAL= 2532.



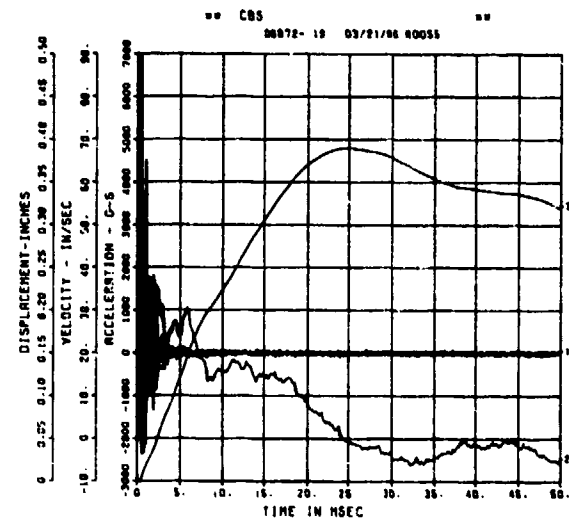
SPALL TEST 10
ARM
200000. HZ CAL= 2336.



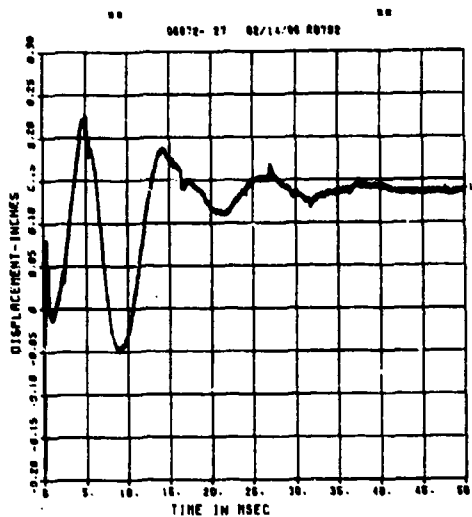
SPALL TEST 10
AFV
200000. HZ CAL= 4983.



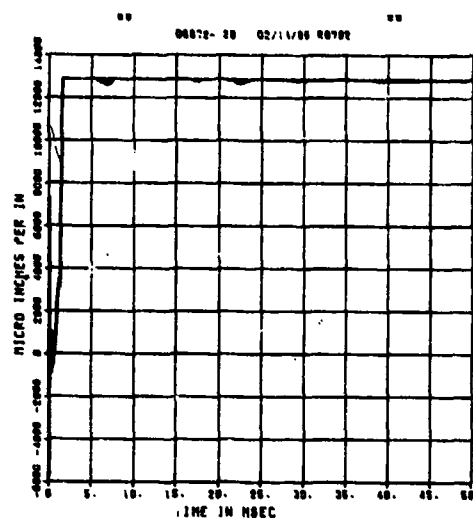
SPALL TEST 10
AFH
200000. HZ CAL= 5966.



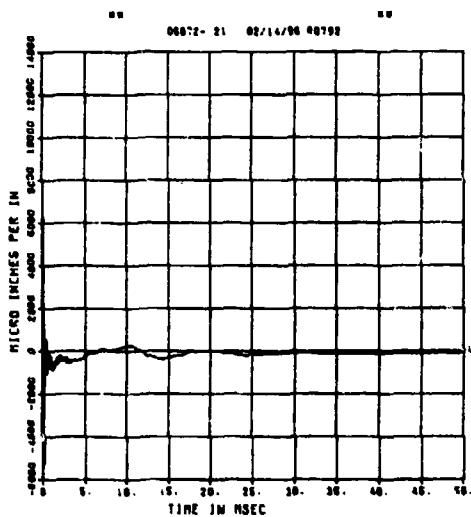
SPALL TEST 1D
 DM
 200000. HZ CAL= 0.434



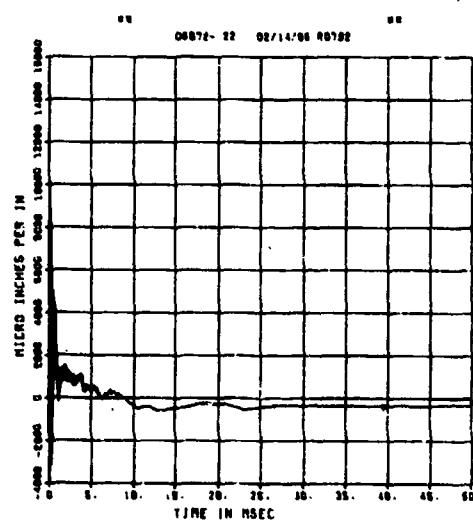
SPALL TEST 1D
 EOT
 200000. HZ CAL= 7469.



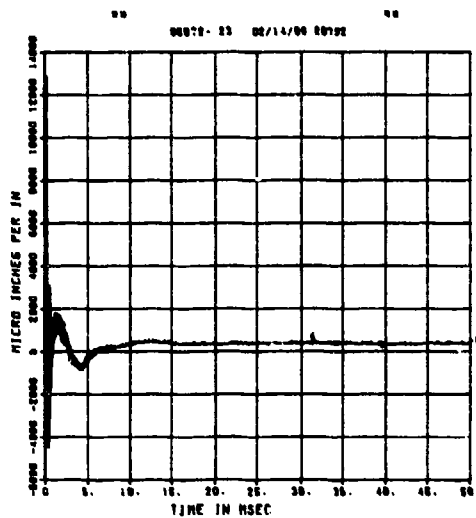
SPALL TEST 1D
 EIT
 200000. HZ CAL= 5004.



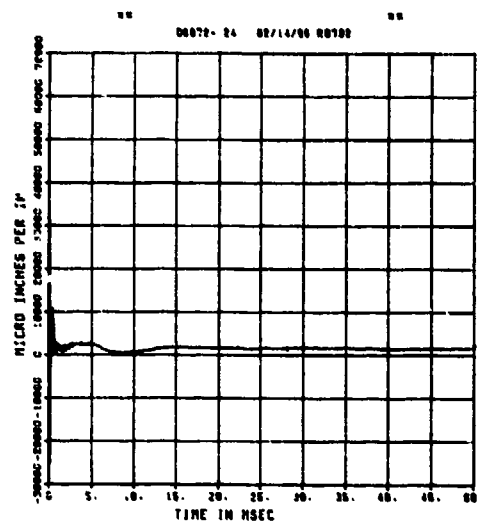
SPALL TEST 1D
 EOM
 200000. HZ CAL= 5004.



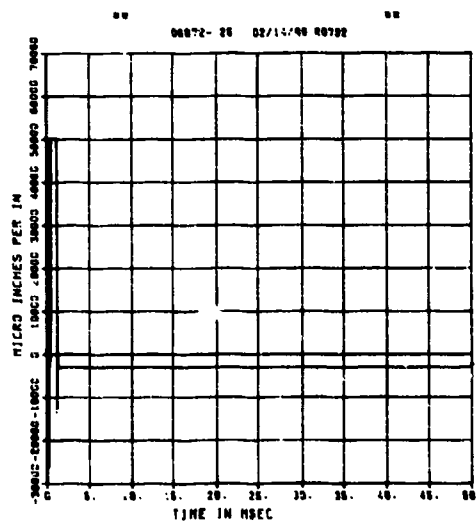
SPALL TEST 1D
EIM
200000. HZ CAL= 7469.



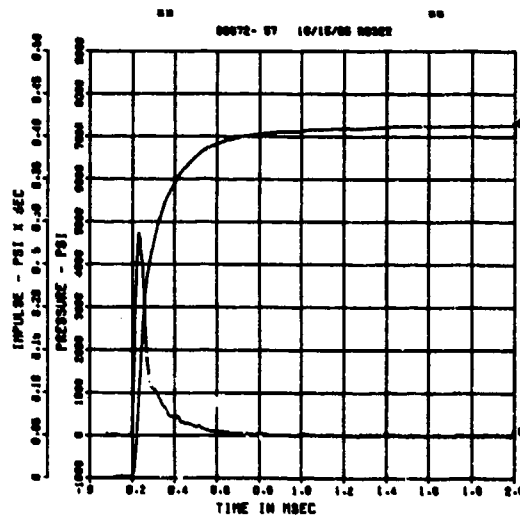
SPALL TEST 1D
EOB
200000. HZ CAL= 30324.



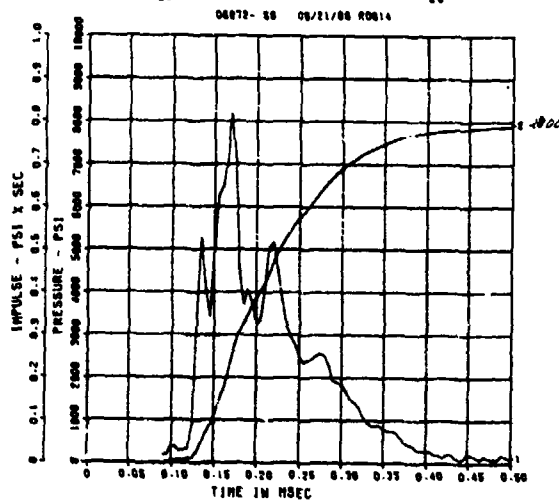
SPALL TEST 1D
EIB
200000. HZ CAL= 30324.



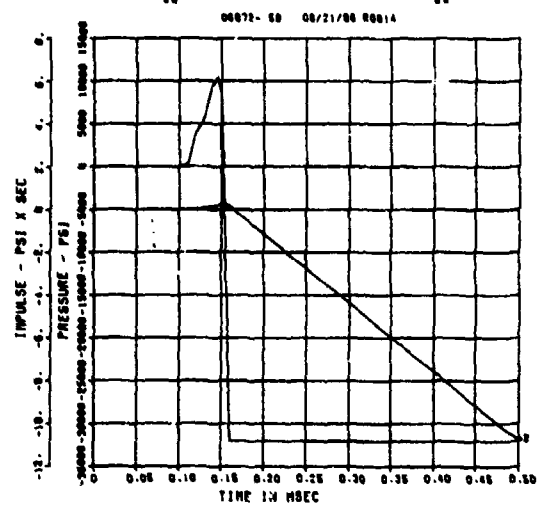
SPALL TEST 2A
PB-3
200000. HZ CAL= 4711.



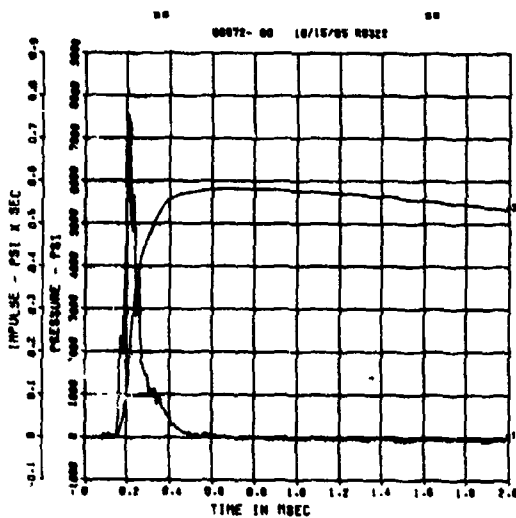
SPALL TEST 2A
PQ-0
200000. HZ CAL= 18352.



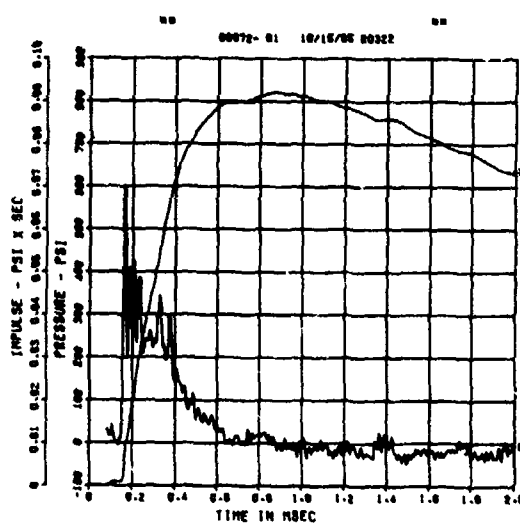
SPALL TEST 2A
PQ-1
200000. HZ CAL= 18652.



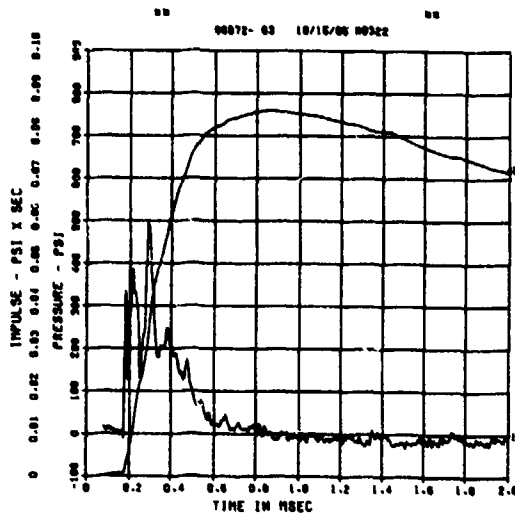
SPALL TEST 2A
PQ-2
200000. HZ CAL= 10131.



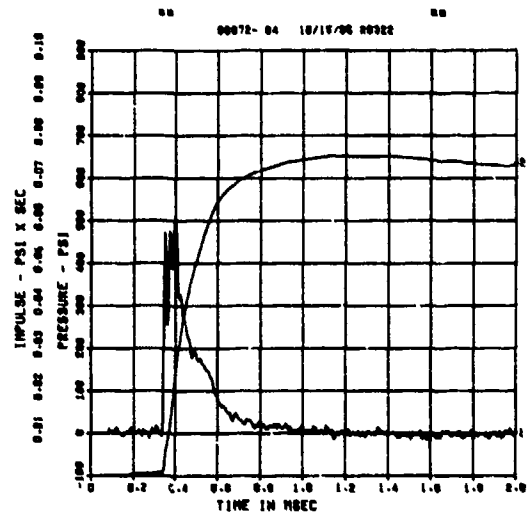
SPALL TEST 2A
PM-0
200000. HZ CAL= 4567.



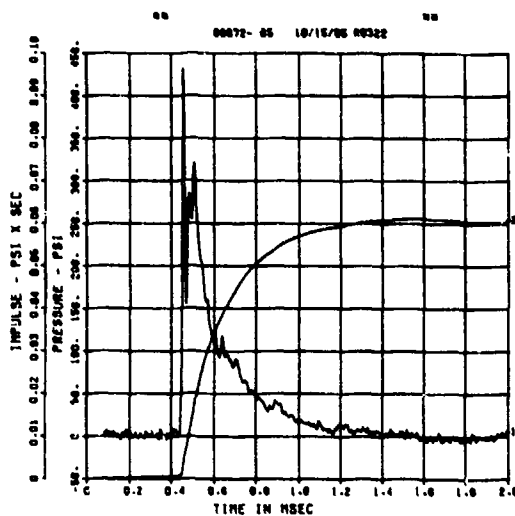
SPALL TEST 2A
PM-2
200000. HZ CAL= 2943.



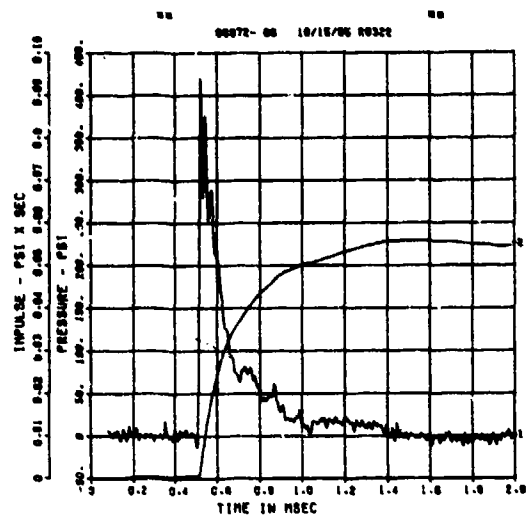
SPALL TEST 2A
PM-3
200000. HZ CAL= 1965.



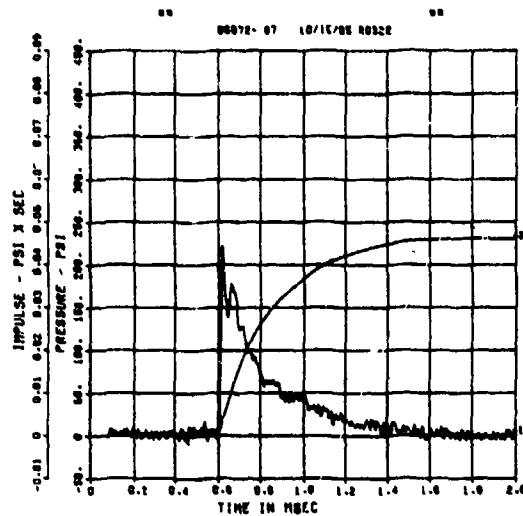
SPALL TEST 2A
PT-0
200000. HZ CAL= 952.3



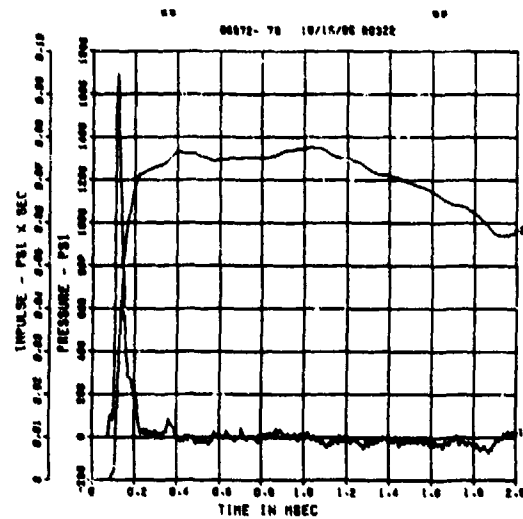
SPALL TEST 2A
PT-2
200000. HZ CAL= 1072.



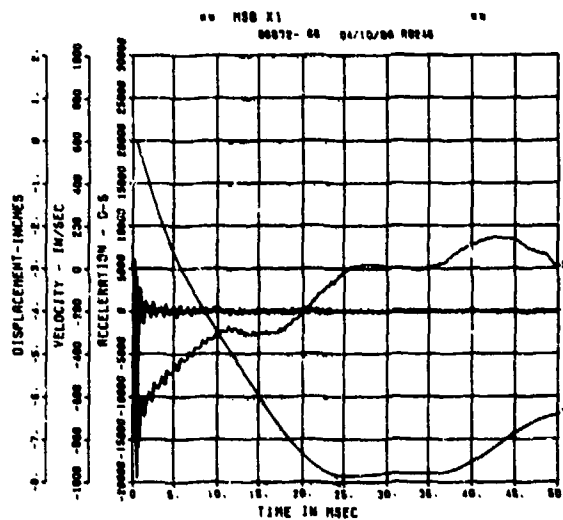
SPALL TEST 2A
PT-3
200000. HZ CAL= 1181.



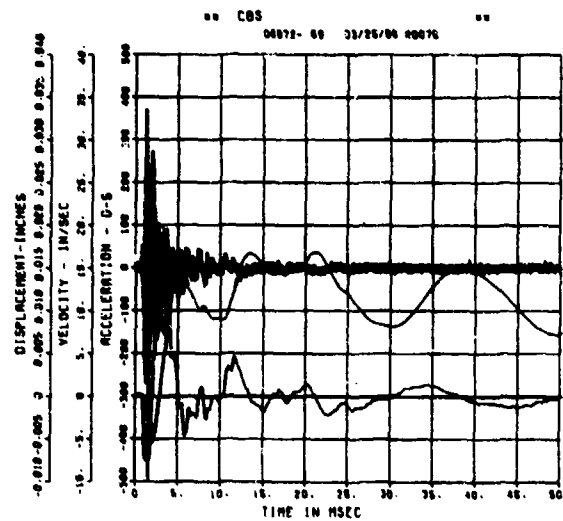
SPALL TEST 2A
BP-A
200000. HZ CAL= 4358.



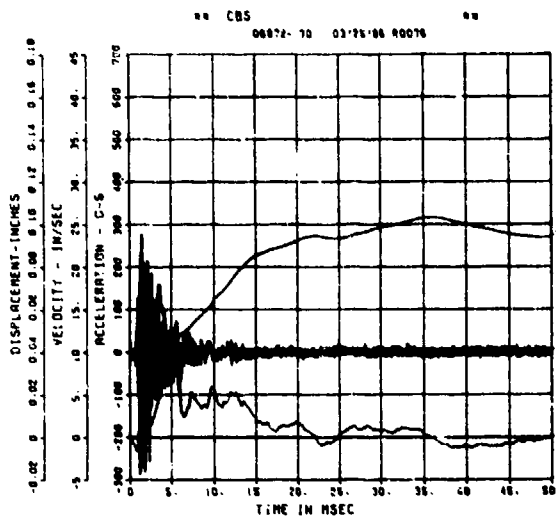
SPALL TEST 2A
AWHM
200000. HZ CAL= 26696.



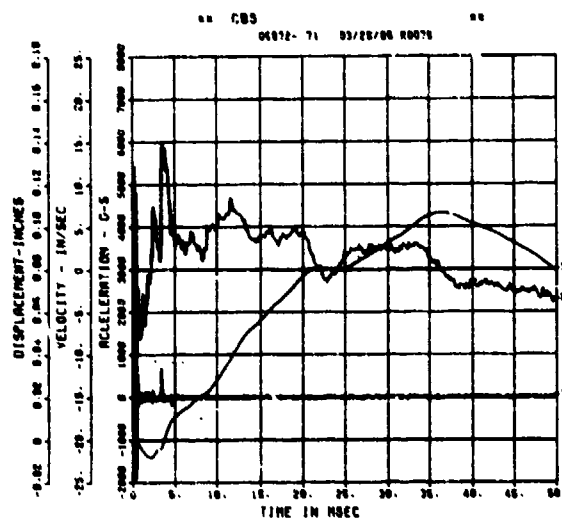
SPALL TEST 2A
ARV
200000. HZ CAL= 1513.



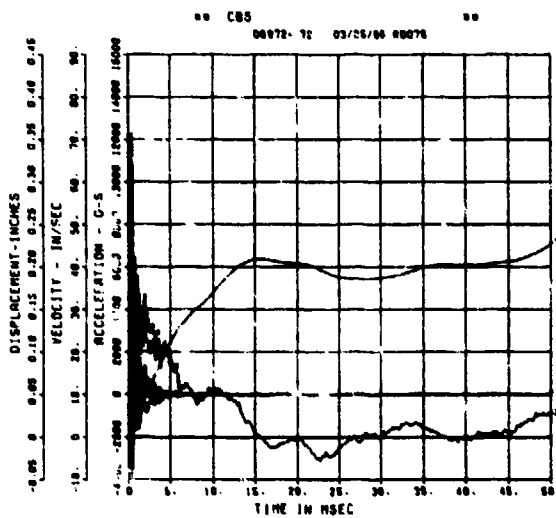
SPALL TEST 2A
 ARH
 200000. HZ CAL= 1672.



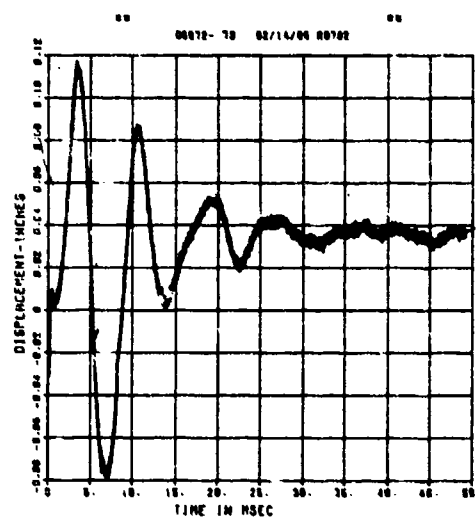
SPALL TEST 2A
 AFV
 200000. HZ CAL= 4983.



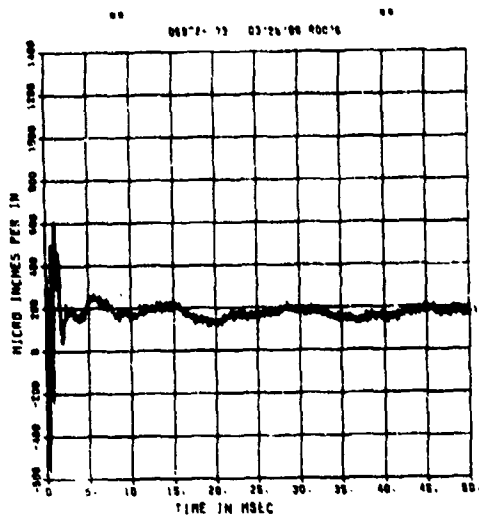
SPALL TEST 2A
 AFH
 200000. HZ CAL= 5966.



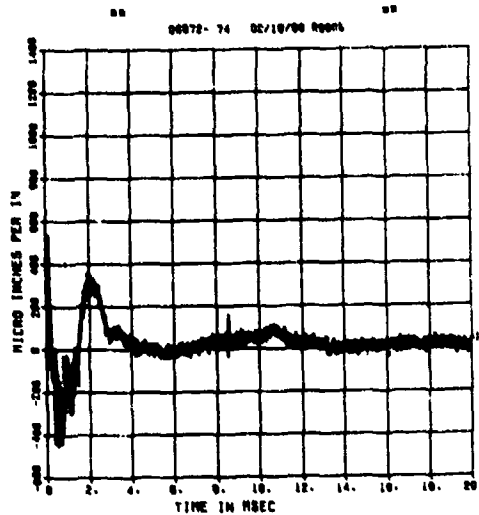
SPALL TEST 2A
 DM
 200000. HZ CAL= 0.434



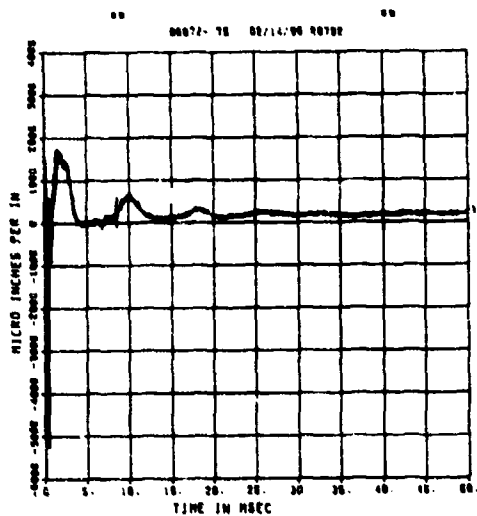
SPALL TEST 2A
EOT
200000. HZ CAL= 5004.
LP2 0.70% CUTOFF= 18000. HZ



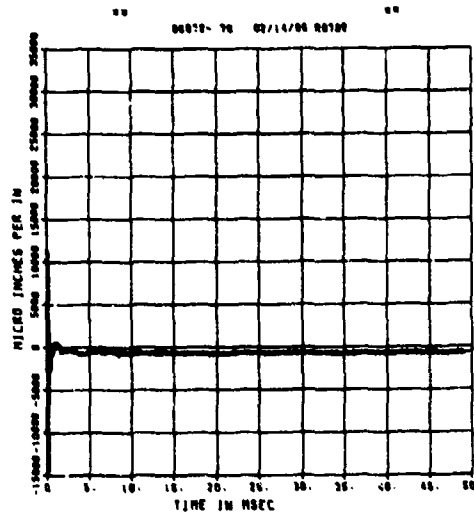
SPALL TEST 2A
EIT
200000. HZ CAL= 5004.



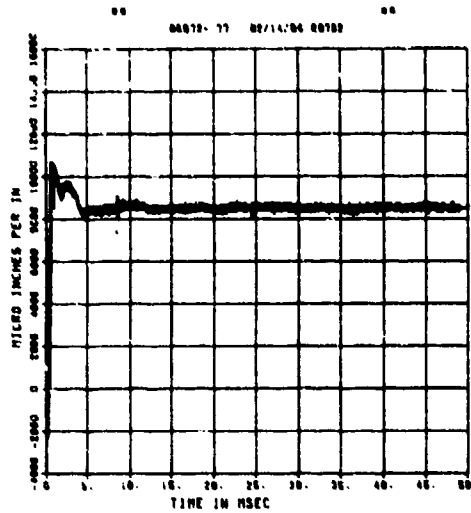
SPALL TEST 2A
EIM
200000. HZ CAL= 5004.



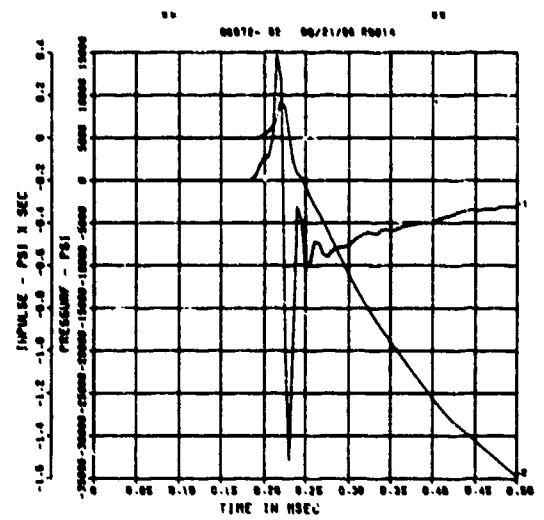
SPALL TEST 2A
EOB
200000. HZ CAL= 30324.



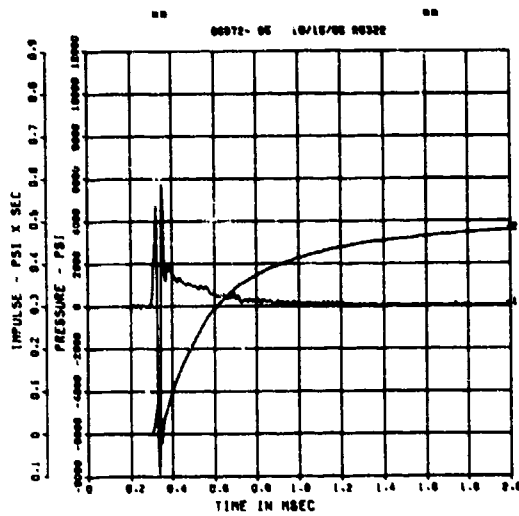
SPALL TEST 2A
E1B
200000. HZ CAL= 30324.



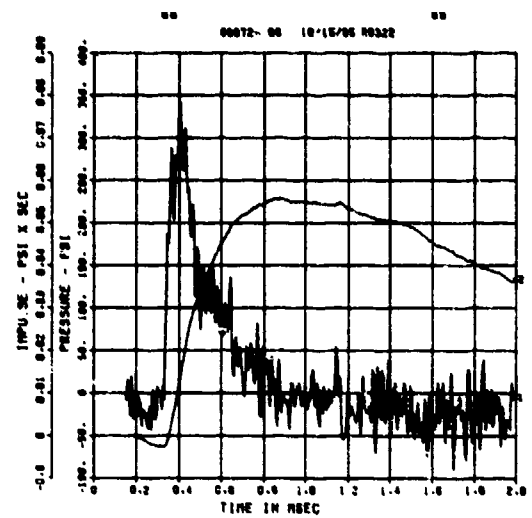
SPALL TEST 2B
PQ-0
200000. HZ CAL= 19019.



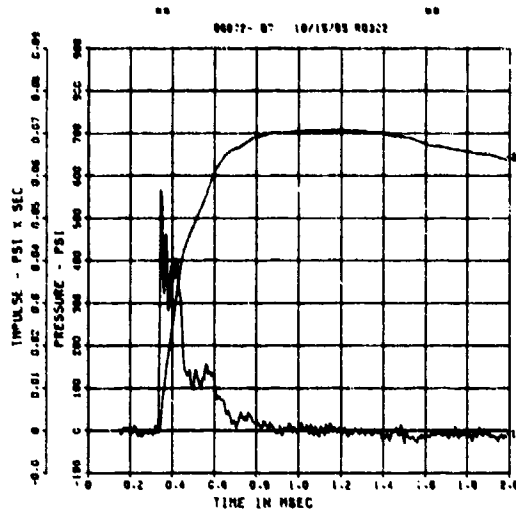
SPALL TEST 2B
PM-0
200000. HZ CAL= 4567.



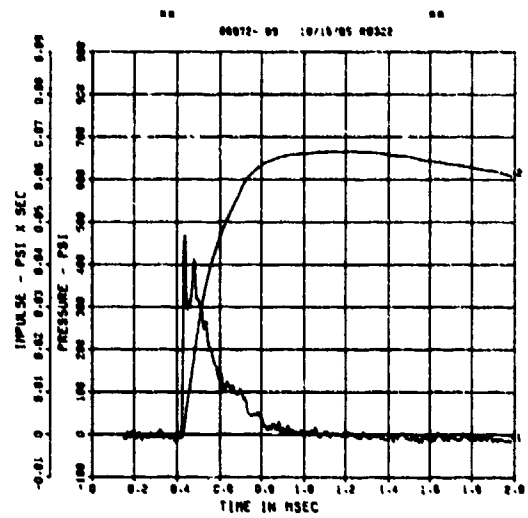
SPALL TEST 2B
PM-1
200000. HZ CAL= 4535.



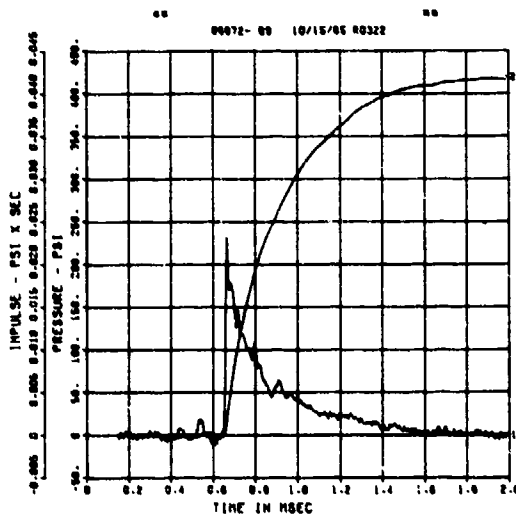
SPALL TEST 2B
PM-2
200000. HZ CAL= 2943.



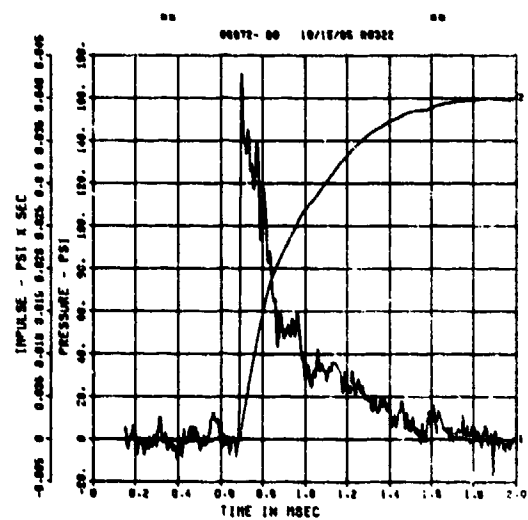
SPALL TEST 2B
PM-3
200000. HZ CAL= 1965.



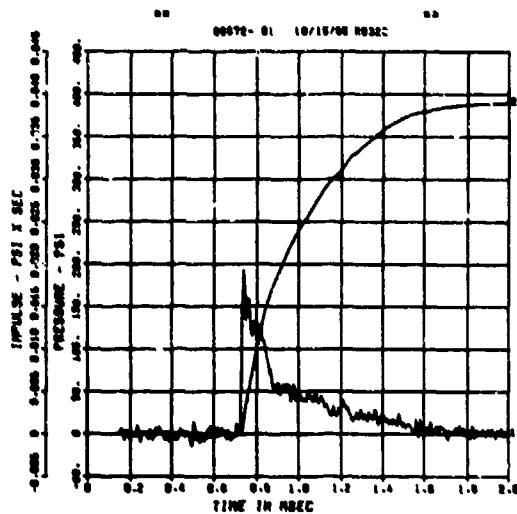
SPALL TEST 2B
PT-0
200000. HZ CAL= 952.3



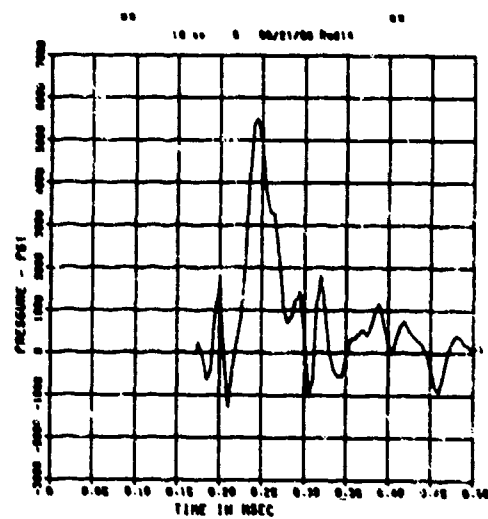
SPALL TEST 2B
PT-2
200000. HZ CAL= 1072.



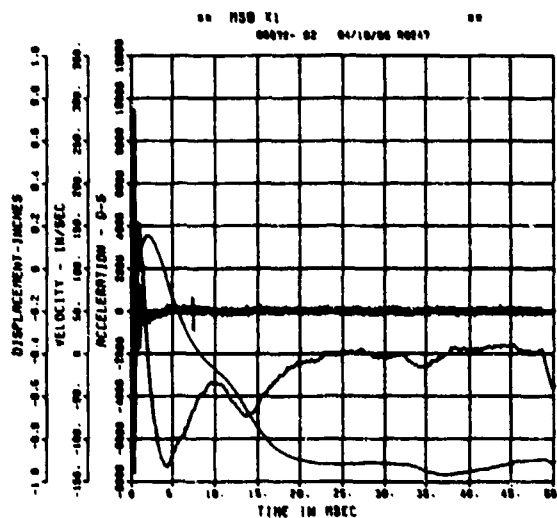
SPALL TEST 2B
PT-3
200000. HZ CAL= 1181.



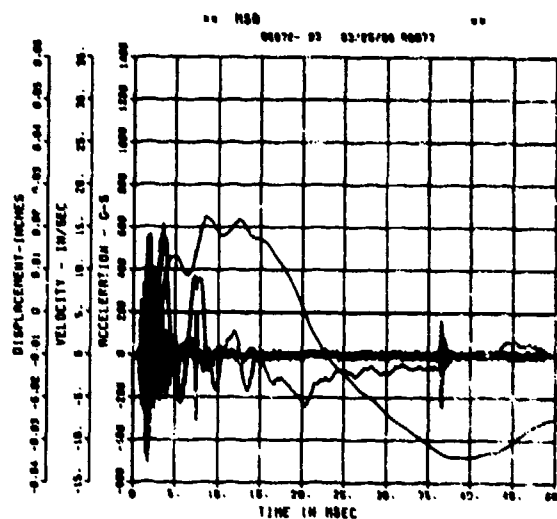
SPALL TEST 2B
FP-B
200000. HZ CAL= -0.083



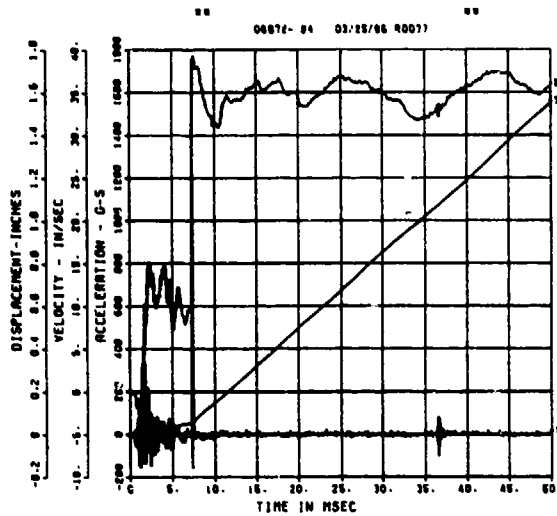
SPALL TEST 2B
AWHM
200000. HZ CAL= 24667.



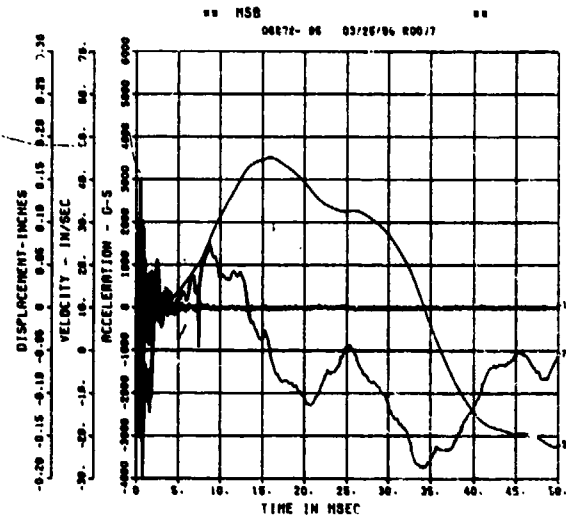
SPALL TEST 2B
ARV
200000. HZ CAL= 2701.



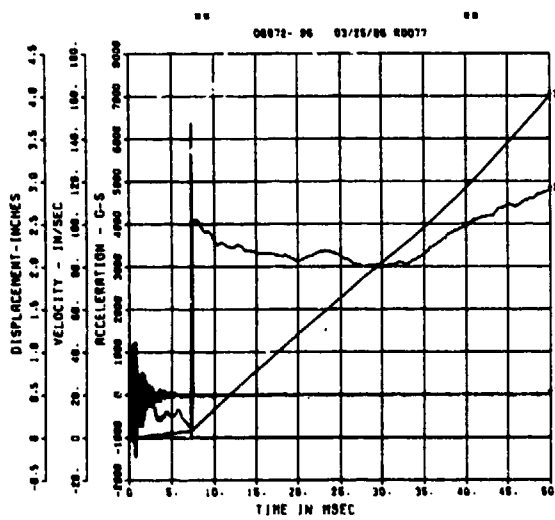
SPALL TEST 2B
ARM
200000. HZ CAL= 2738.
LP2/O 70% CUTOFF= 18000. HZ



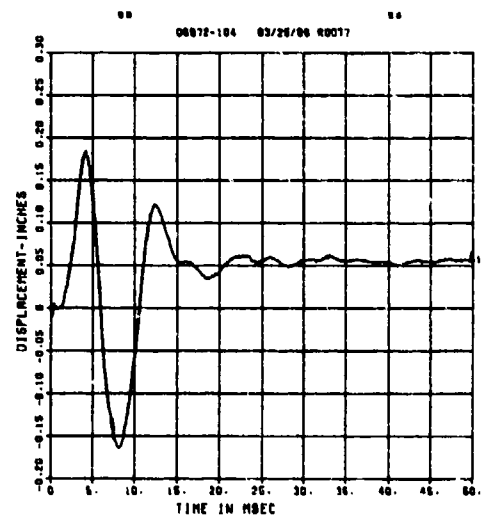
SPALL TEST 2B
AFV
200000. HZ CAL= 5366.



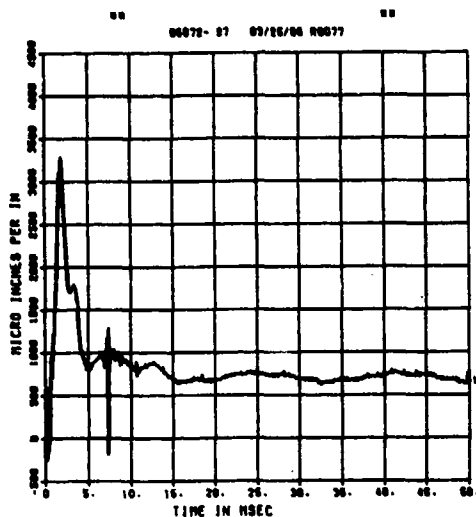
SPALL TEST 2B
AFH
200000. HZ CAL= 5686.
LP2/O 70% CUTOFF= 18000. HZ



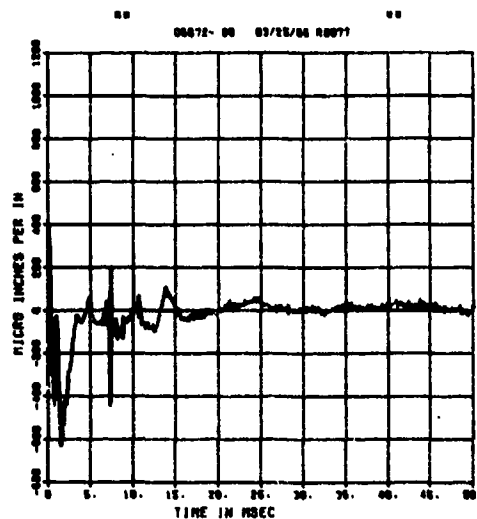
SPALL TEST 2B
DM
200000. HZ CAL= 0.434
LP4/O 70% CUTOFF= 9000. HZ



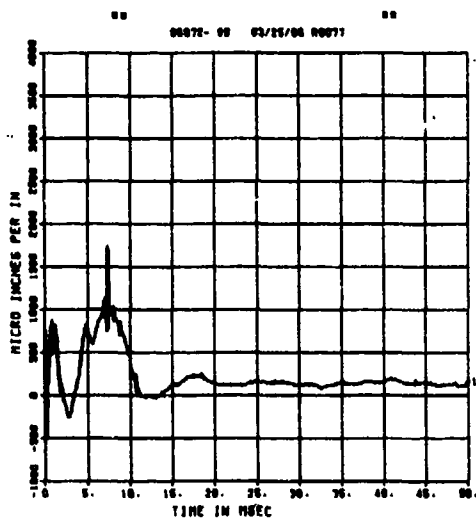
SPALL TEST 2B
EOT
200000. HZ CAL= 7469.
LP4/0 70% CUTOFF= 9000. HZ



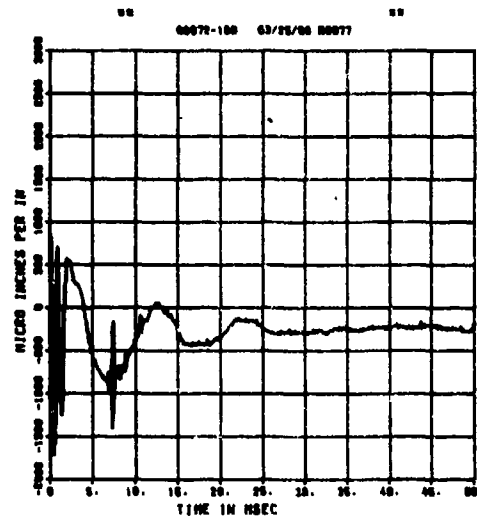
SPALL TEST 2B
EIT
200000. HZ CAL= 5004.
LP4/0 70% CUTOFF= 9000. HZ



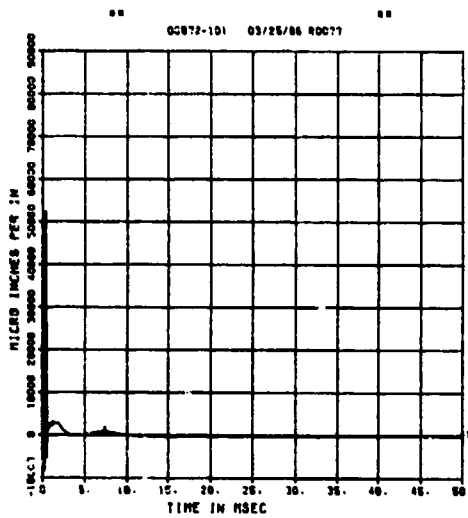
SPALL TEST 2B
EOM
200000. HZ CAL= 5004.
LP4/0 70% CUTOFF= 9000. HZ



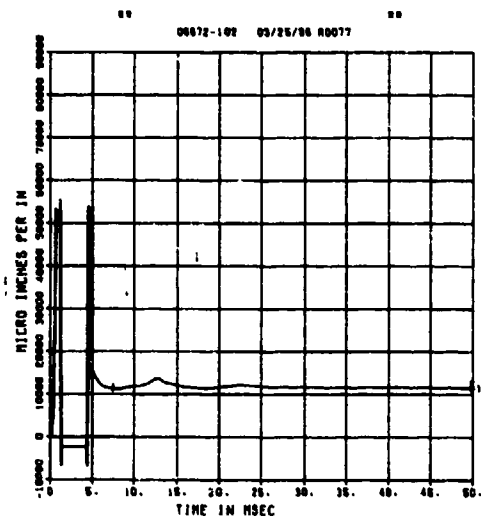
SPALL TEST 2B
EIM
200000. HZ CAL= 7469.
LP4/0 70% CUTOFF= 9000. HZ



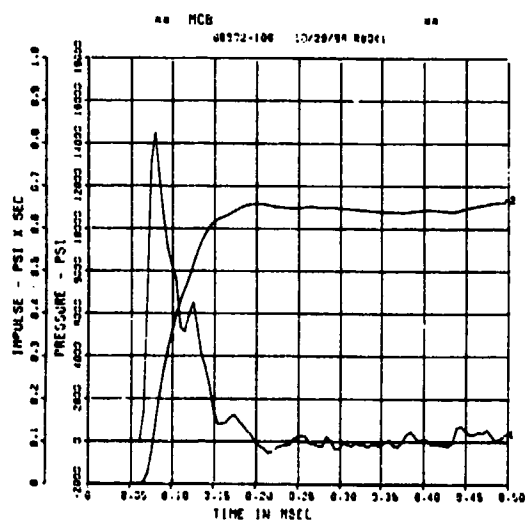
SPALL TEST 2B
E0B
200000. HZ CAL= 30324.
LP4/0 70% CUTOFF= 9000. HZ



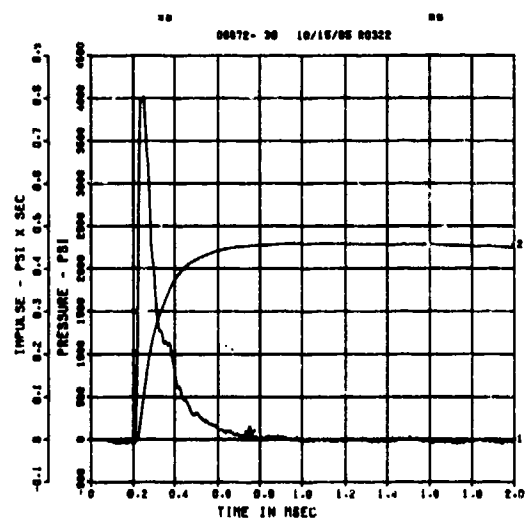
SPALL TEST 2B
E1B
200000. HZ CAL= 30324.
LP4/0 70% CUTOFF= 9000. HZ



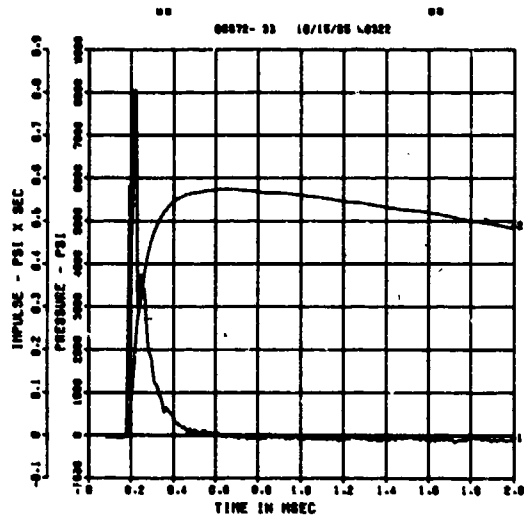
SPALL TEST 2C
FP-C
200000. HZ CAL= -0.210



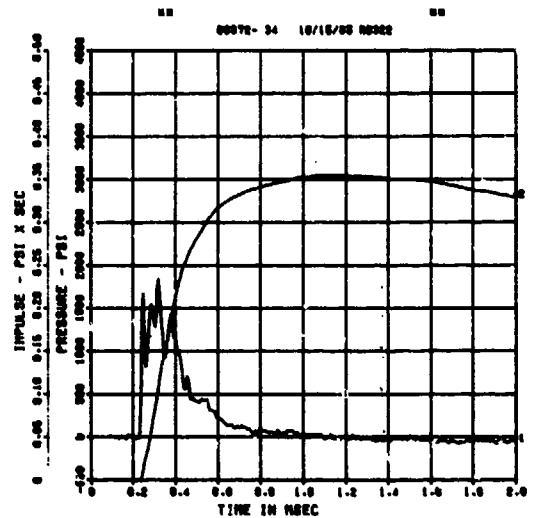
SPALL TEST 2D
PB-3
200000. HZ CAL= 4711.



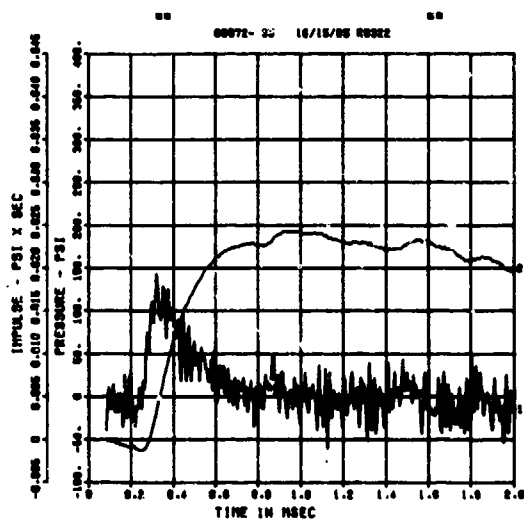
SPALL TEST 2D
PQ-2
200000. HZ CAL= 10131.



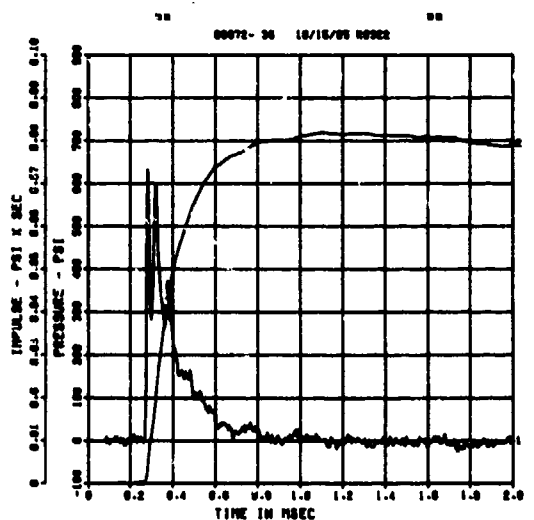
SPALL TEST 2D
PM-0
200000. HZ CAL= 4567.



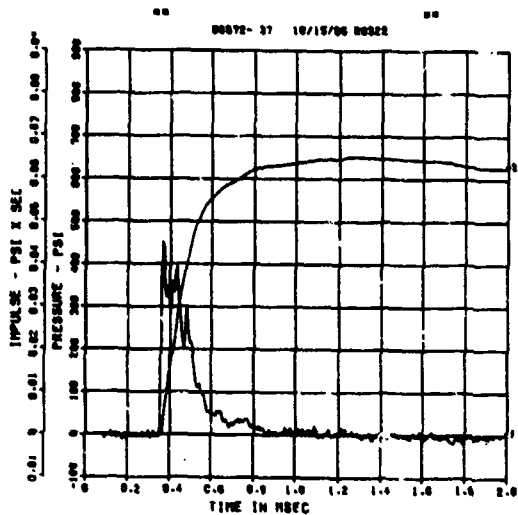
SPALL TEST 2D
PM-1
200000. HZ CAL= 4133.



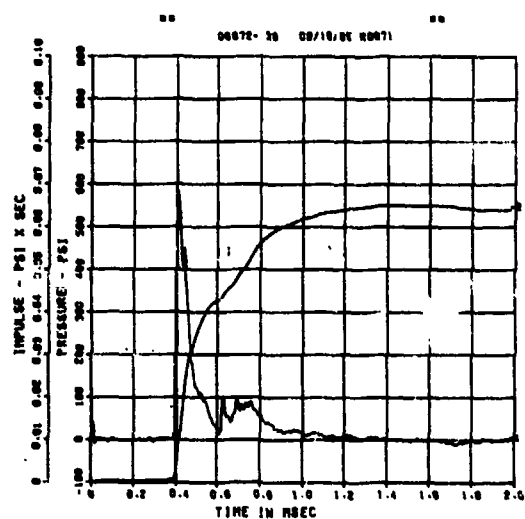
SPALL TEST 2D
PM-2
200000. HZ CAL= 2943.



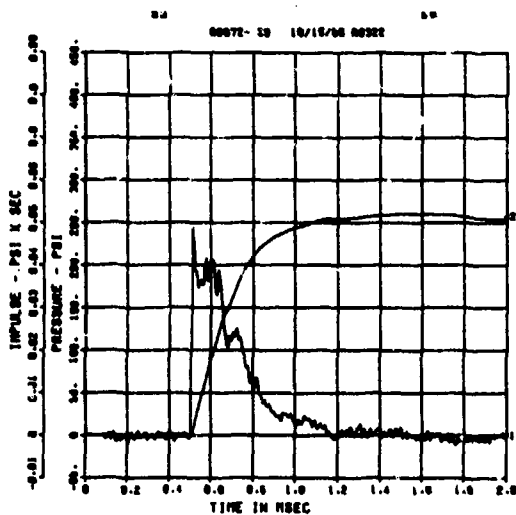
SPALL TEST 2D
PM-3
200000. HZ CAL= 1965.



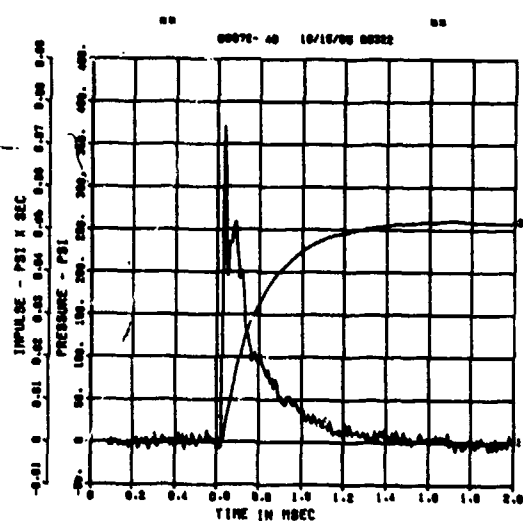
SPALL TEST 2D
PT-0
200000. HZ CAL= 952.3



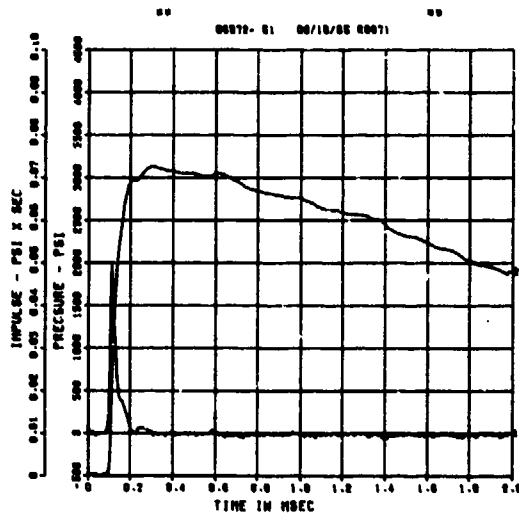
SPALL TEST 2D
PT-2
200000. HZ CAL= 1072.



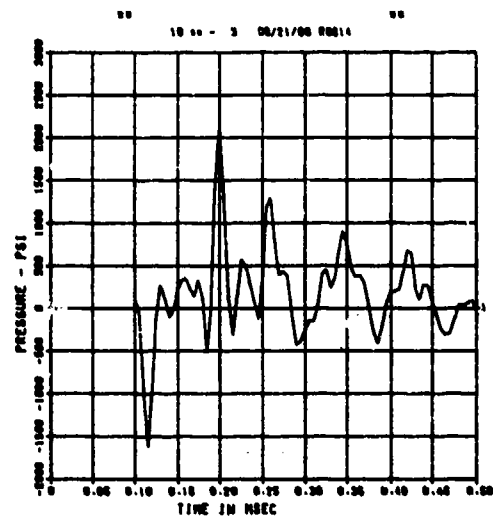
SPALL TEST 2D
PT-3
200000. HZ CAL= 1181.



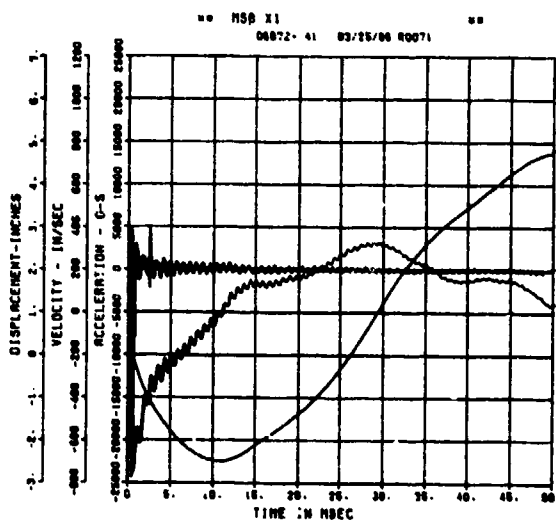
SPALL TEST 2D
BP-A
200000. HZ CAL= 4358.



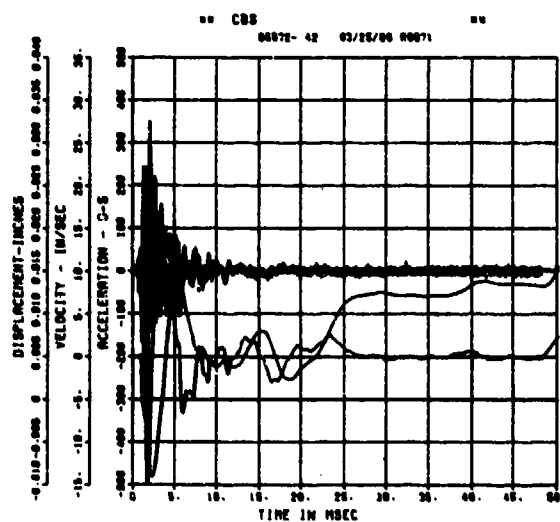
SPALL TEST 2D
FP-A
200000. HZ CAL= -0.080



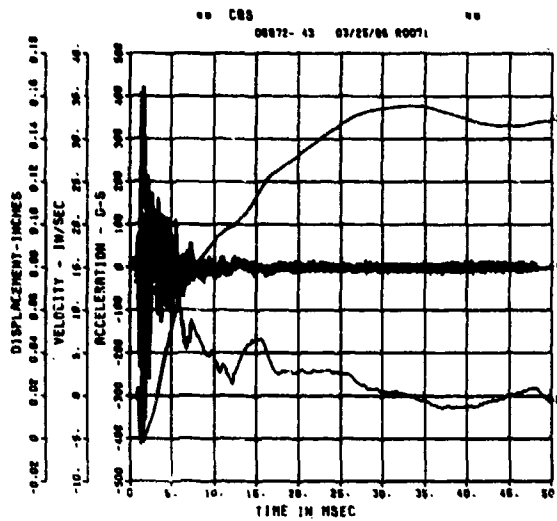
SPALL TEST 2D
AWHM
200000. HZ CAL= 26696.



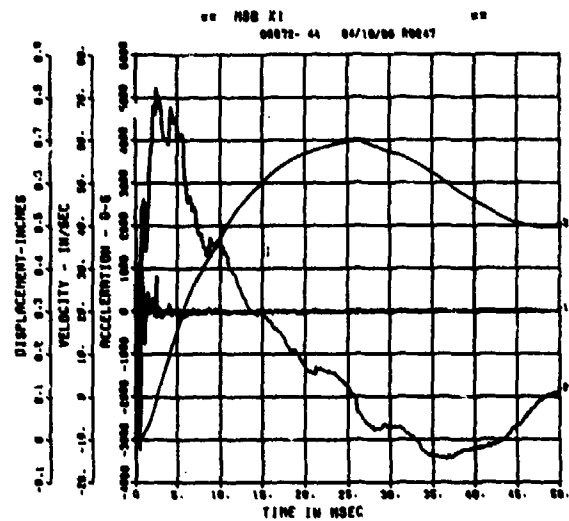
SPALL TEST 2D
ARV
200000. HZ CAL= 1513.



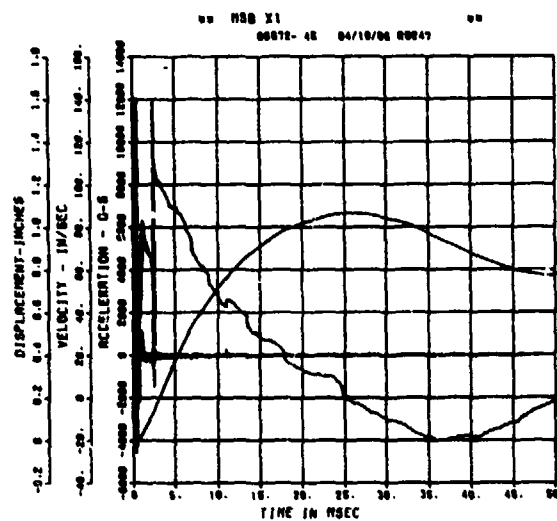
SPALL TEST 2D
ARH
200000. HZ CAL= 1672.



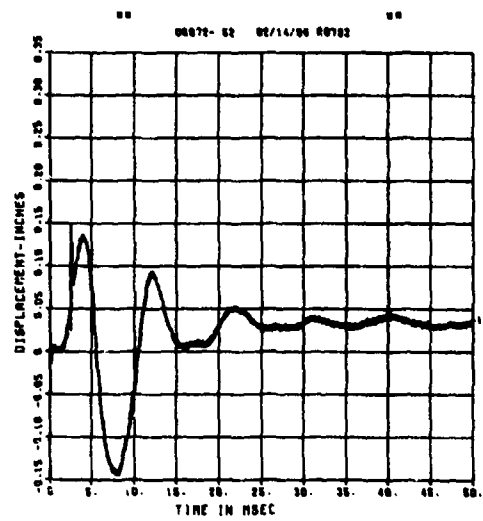
SPALL TEST 2D
AFV
200000. HZ CAL= 4983.



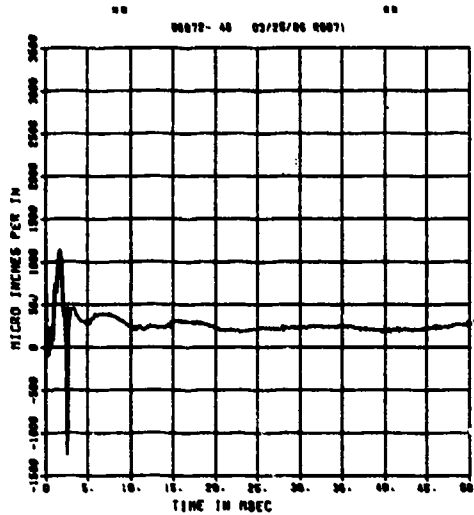
SPALL TEST 2D
AFH
200000. HZ CAL= 5966.



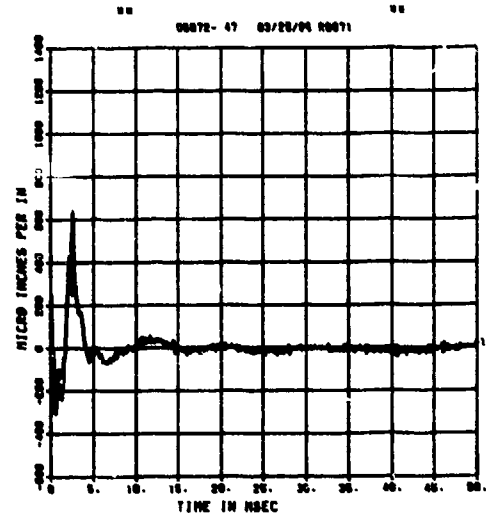
SPALL TEST 2D
DM
200000. HZ CAL= 0.434



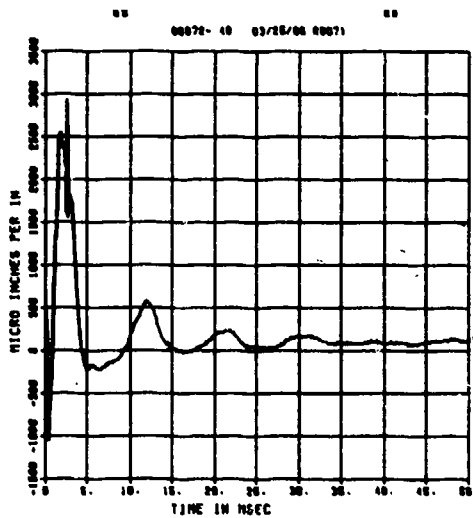
SPALL TEST 2D
EOT
200000. HZ CAL= 5004.
LP4/O 70X CUTOFF= 9000. HZ



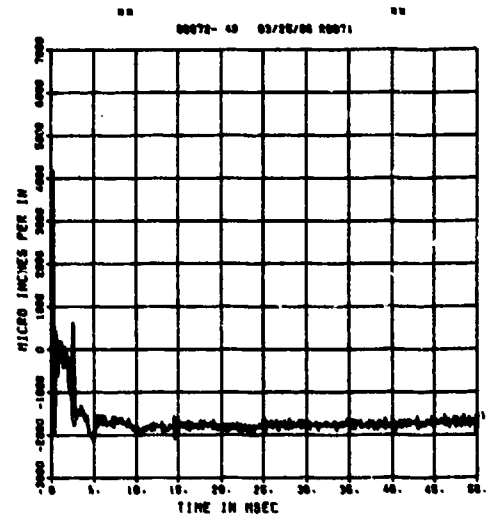
SPALL TEST 2D
EIT
200000. HZ CAL= 5004.
LP4/O 70X CUTOFF= 9000. HZ



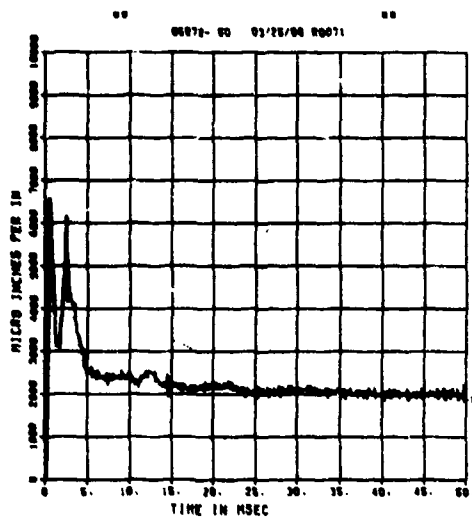
SPALL TEST 2D
EIM
200000. HZ CAL= 5004.
LP4/O 70X CUTOFF= 9000. HZ



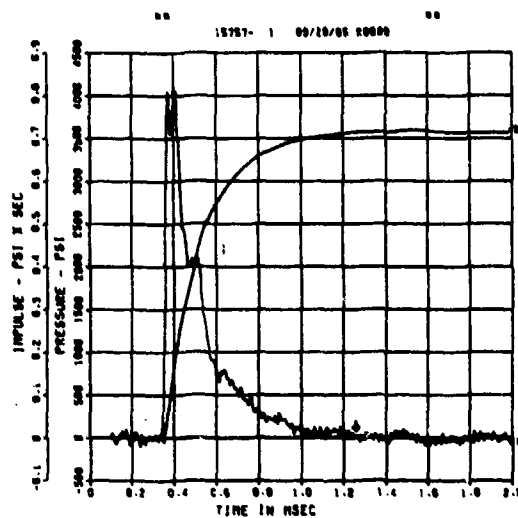
SPALL TEST 2D
EOB
200000. HZ CAL= 30324.
LP4/O 70X CUTOFF= 9000. HZ



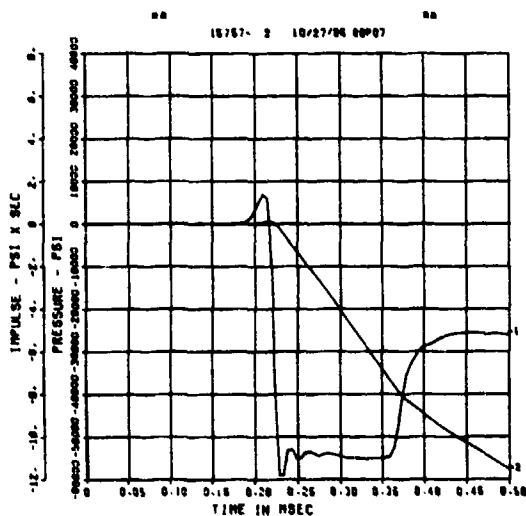
SPALL TEST 2D
E18
200000. HZ CAL= 30324.
LP4/0 70X CUTOFF= 8000. HZ



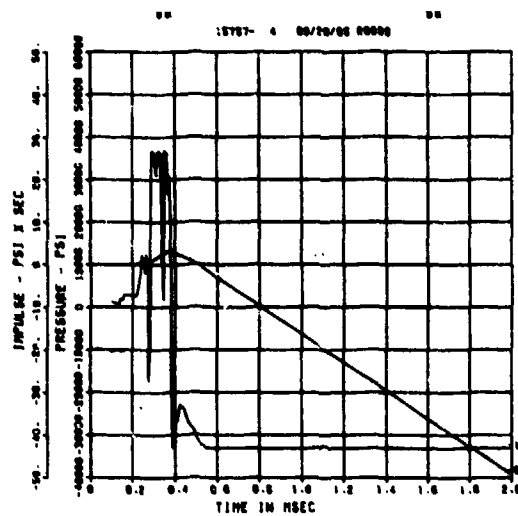
SPALL TEST 3A
PB-3
200000. HZ CAL= 12205.



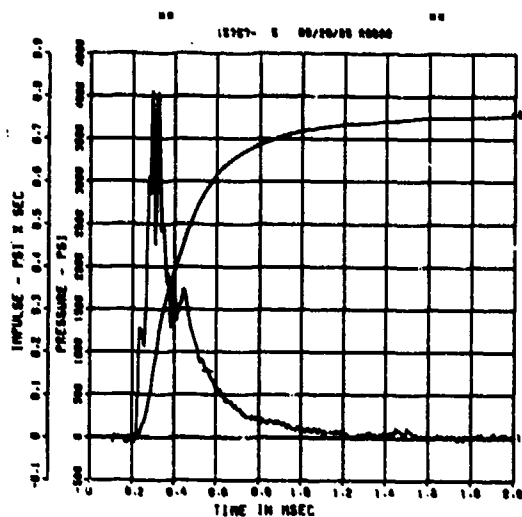
SPALL TEST 3A
PQ-0
200000. HZ CAL= 24003.



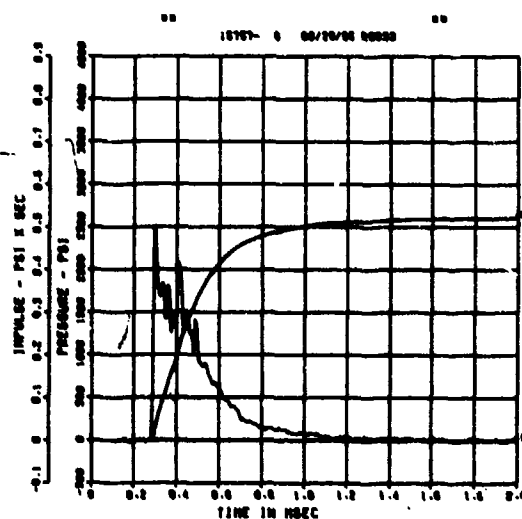
SPALL TEST 3A
PQ-2
200000. HZ CAL= 15787.



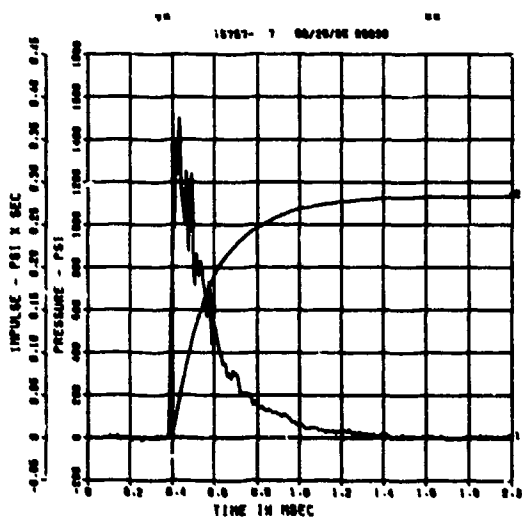
SPALL TEST 3A
PM-0
200000. HZ CAL= 8135.



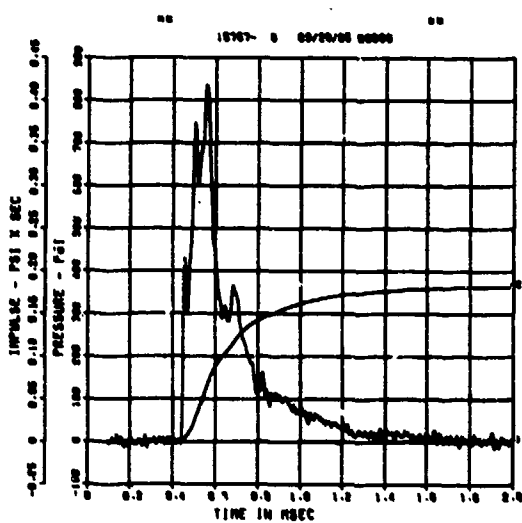
SPALL TEST 3A
PM-2
200000. HZ CAL= 4598.



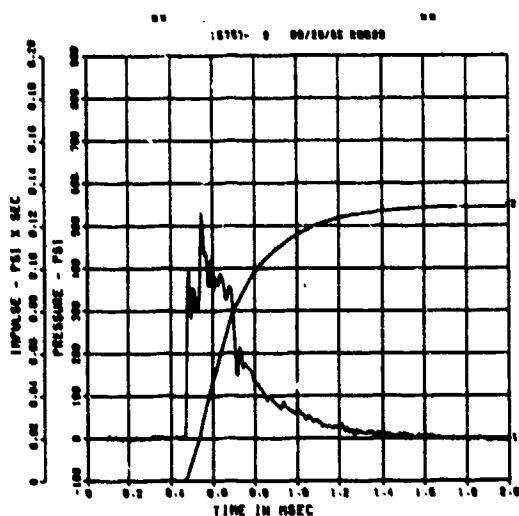
SPALL TEST 3A
PM-3
200000. HZ CAL= 1965.



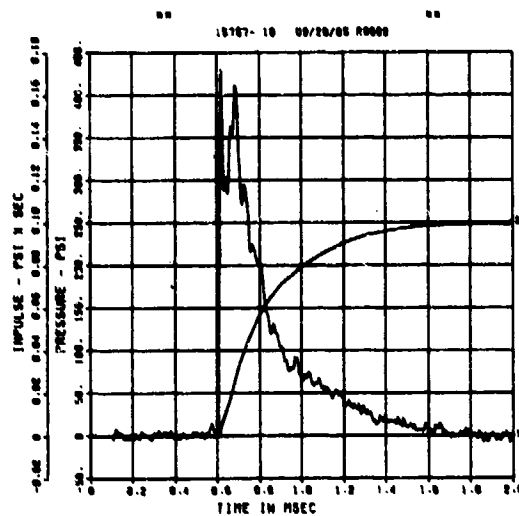
SPALL TEST 3A
PT-0
200000. HZ CAL= 1811.



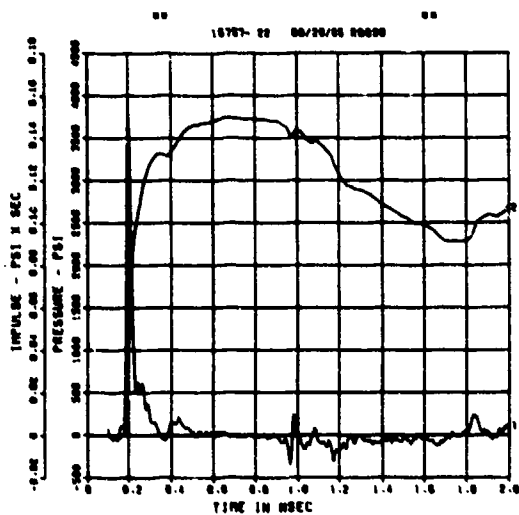
SPALL TEST 3A
PT-2
200000. HZ CAL= 1072.



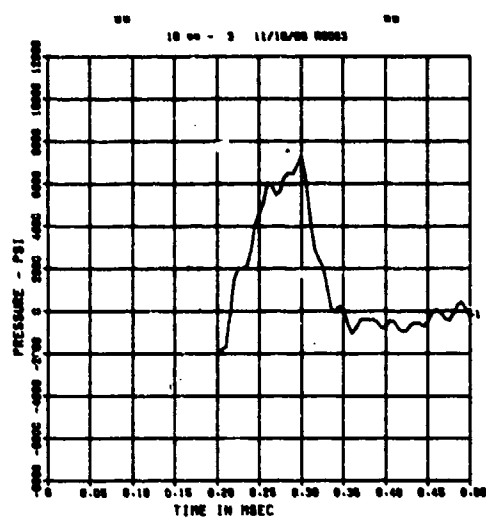
SPALL TEST 3A
PT-3
200000. HZ CAL= 1181.



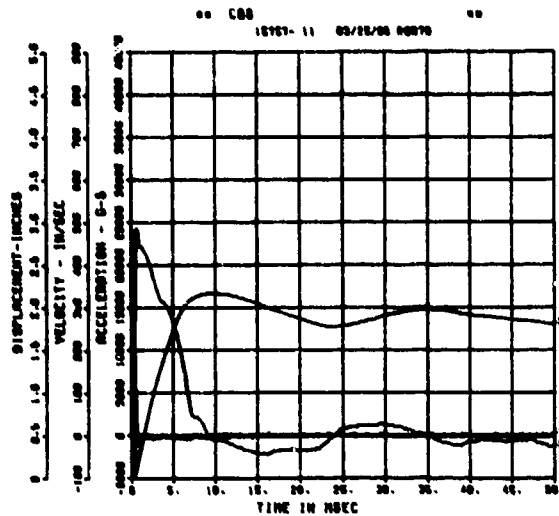
SPALL TEST 3A
BP-A
200000. HZ CAL= 4358.



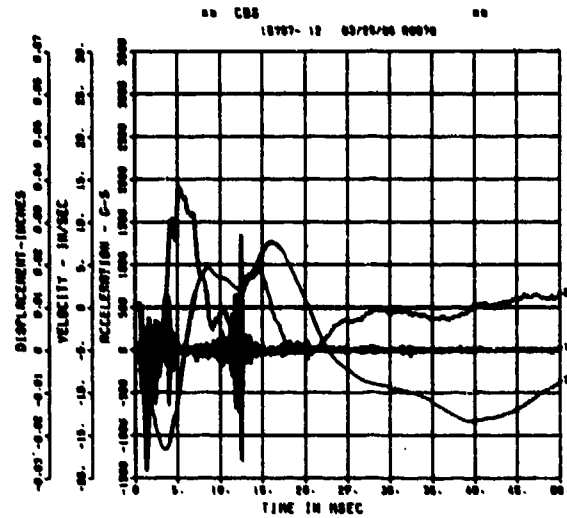
SPALL TEST 3A
FP-A
200000. HZ CAL= -0.080



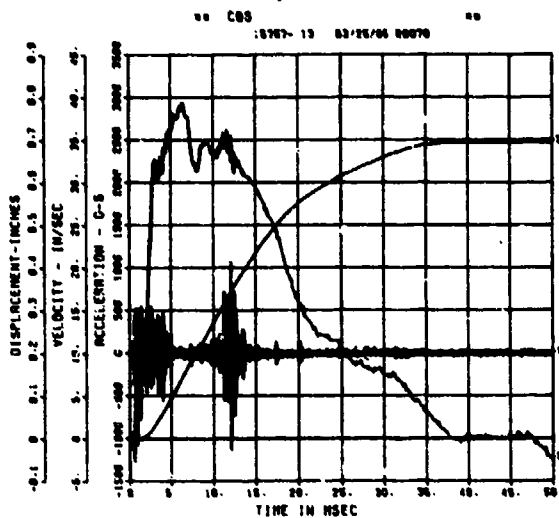
SPALL TEST 3A
AWHM
200000. HZ CAL= 29310.



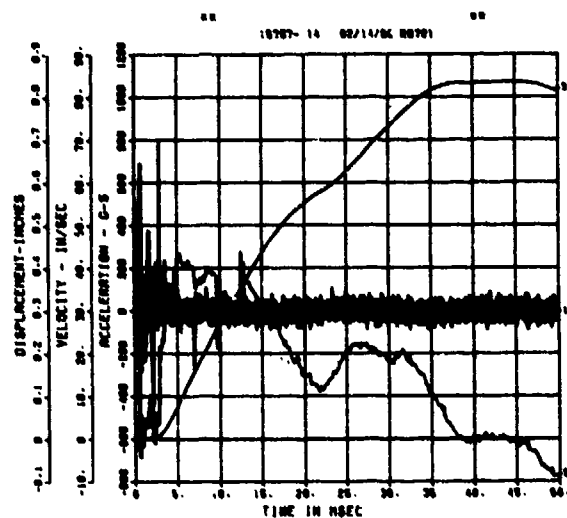
SPALL TEST 3A
ARV
200000. HZ CAL= 2532.



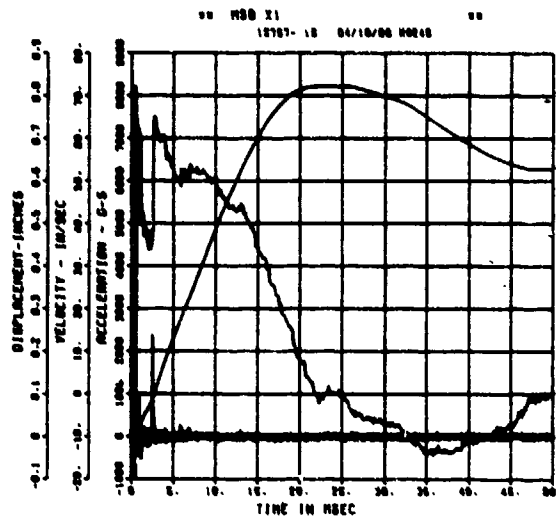
SPALL TEST 3A
ARH
200000. HZ CAL= 3691.



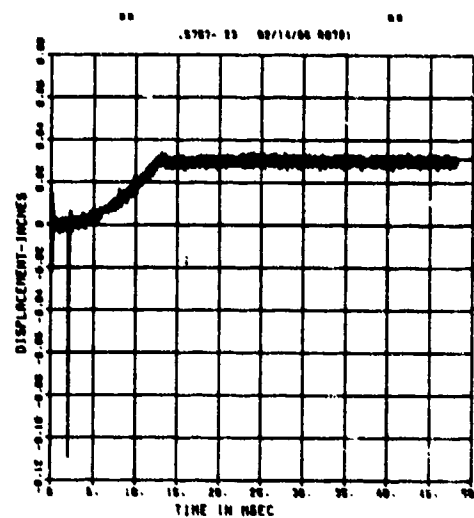
SPALL TEST 3A
AFV
200000. HZ CAL= 8902.



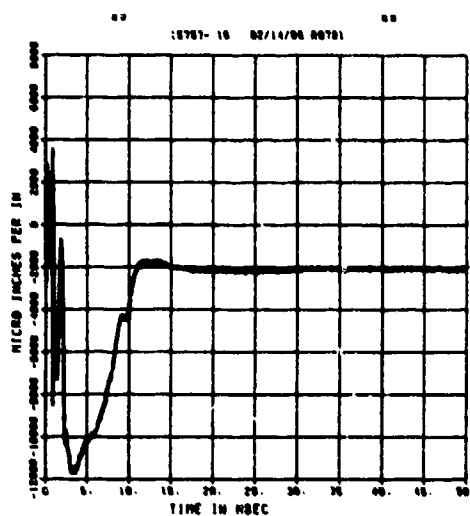
SPALL TEST 3A
AFM
200000. HZ CAL= 10167.



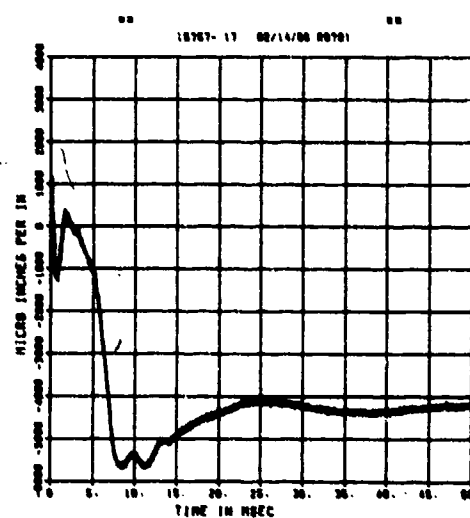
SPALL TEST 3A
DM
200000. HZ CAL= 0.449



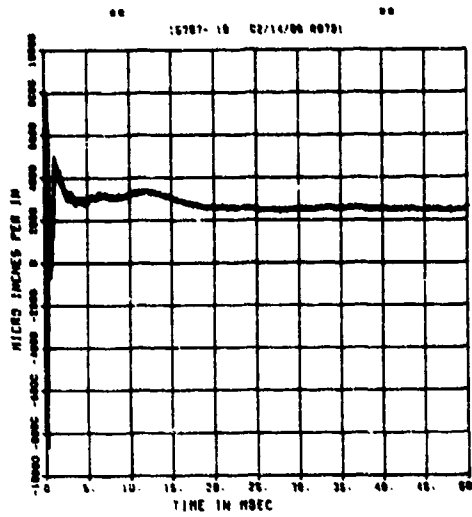
SPALL TEST 3A
EOT
200000. HZ CAL= 11176.



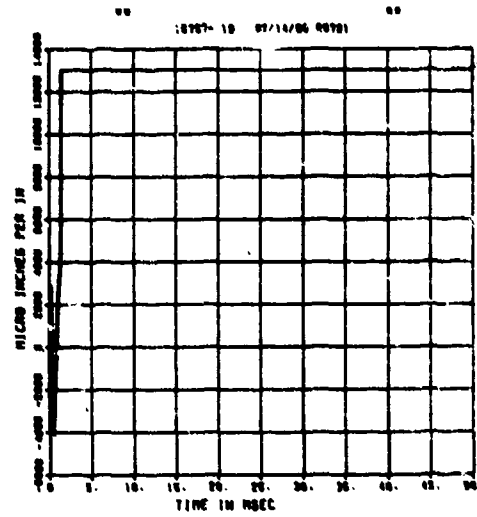
SPALL TEST 3A
EIT
200000. HZ CAL= 7469.



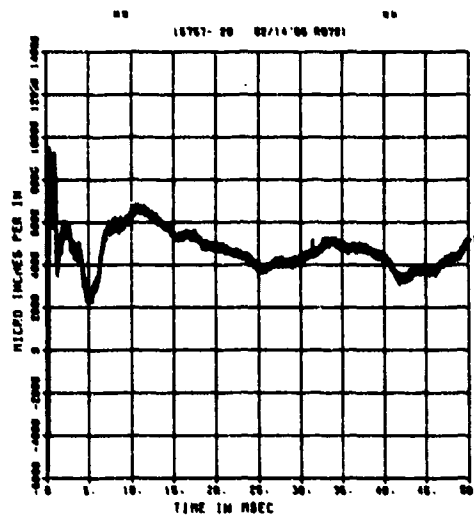
SPALL TEST 3A
EOM
200000. HZ CAL= 7469.



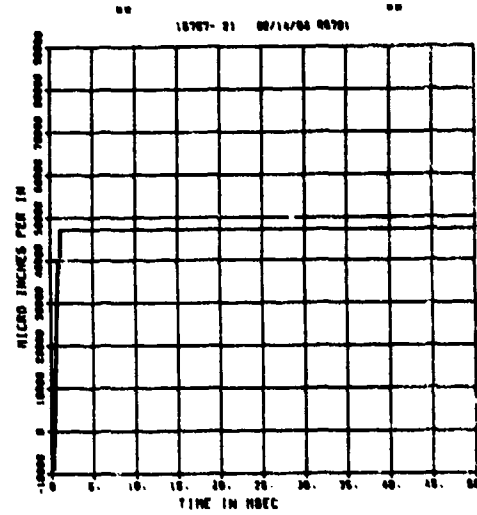
SPALL TEST 3A
EIM
200000. HZ CAL= 7469.



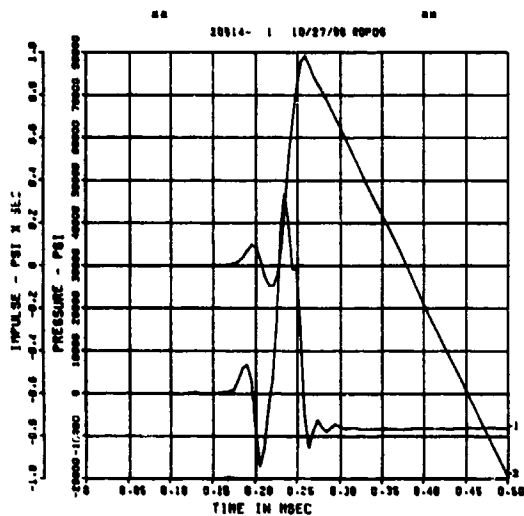
SPALL TEST 3A
EOB
200000. HZ CAL= 30324.



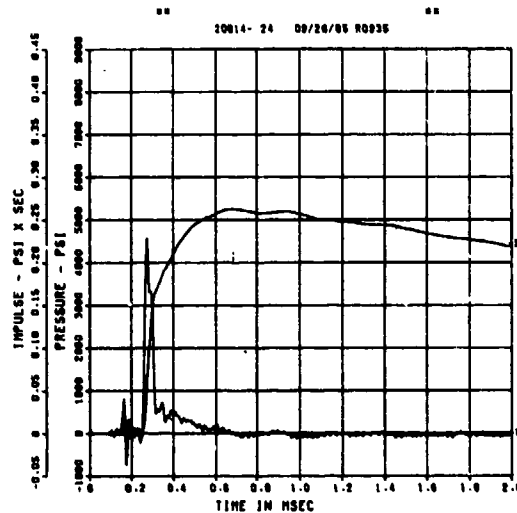
SPALL TEST 3A
EIB
200000. HZ CAL= 30324.



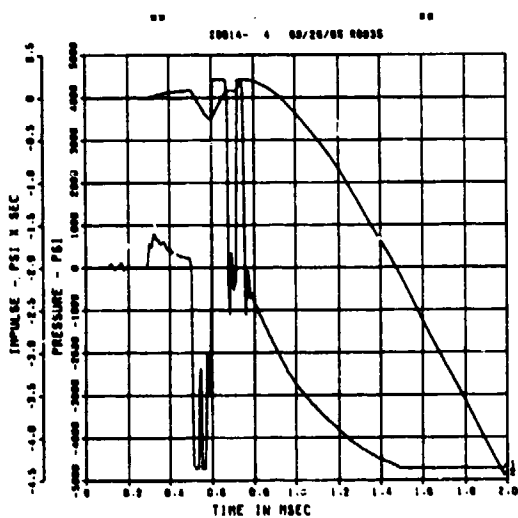
SPALL TEST 3B
PQ-0
200000. HZ CAL= 16987.



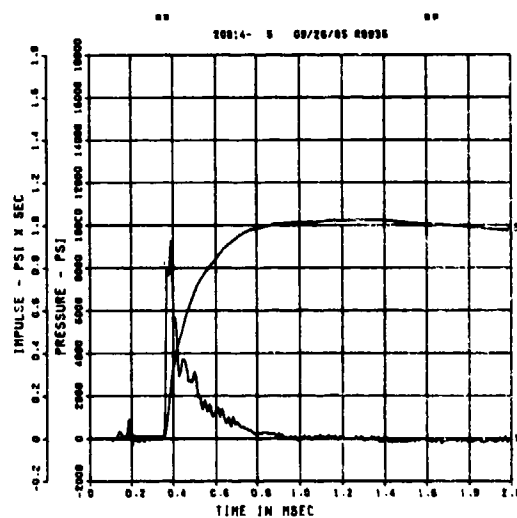
SPALL TEST 3B
PQ-2
200000. HZ CAL= 16181.



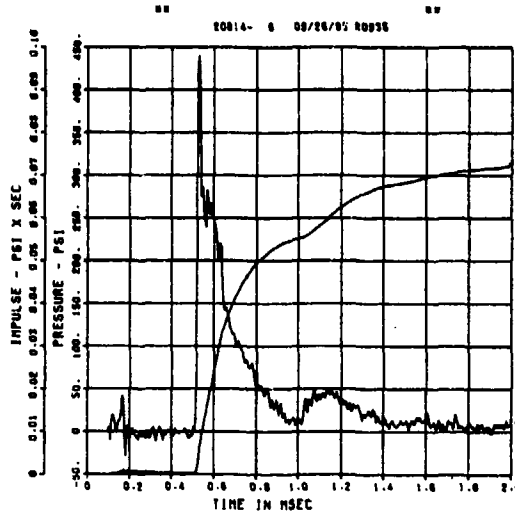
SPALL TEST 3B
PM-1
200000. HZ CAL= 3295.



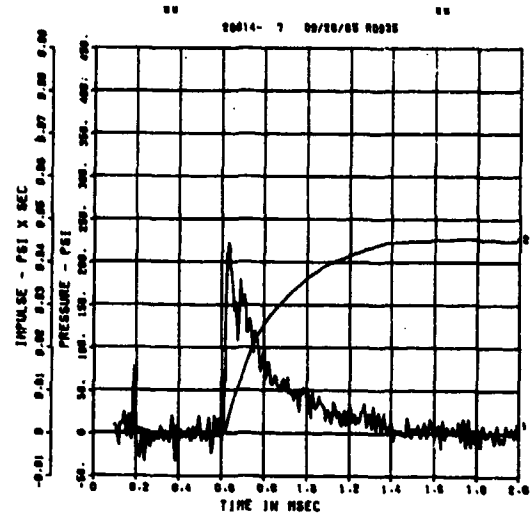
SPALL TEST 3B
PM-2
200000. HZ CAL= 19920.



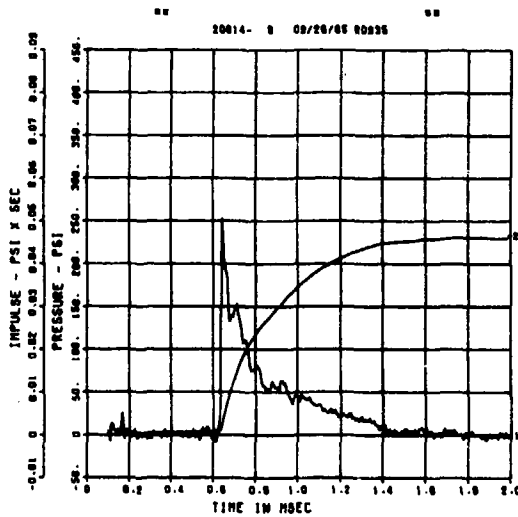
SPALL TEST 3B
PM-3
200000. HZ CAL= 1965.



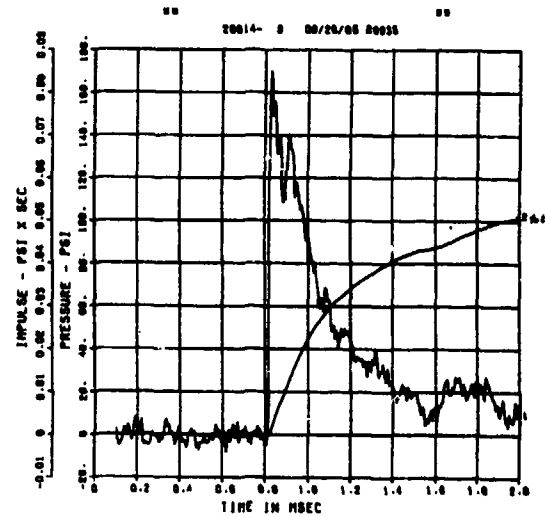
SPALL TEST 3B
PT-0
200000. HZ CAL= 1811.



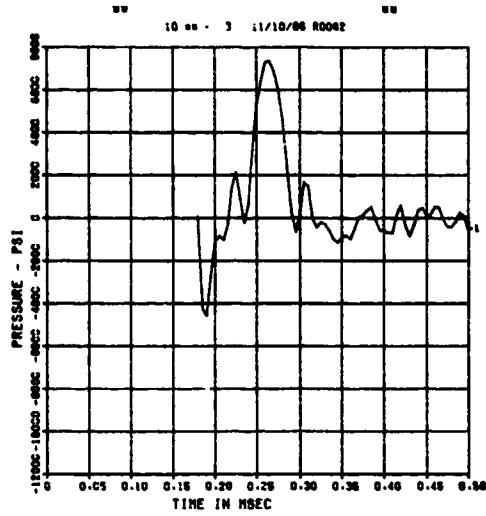
SPALL TEST 3B
PT-2
200000. HZ CAL= 1072.



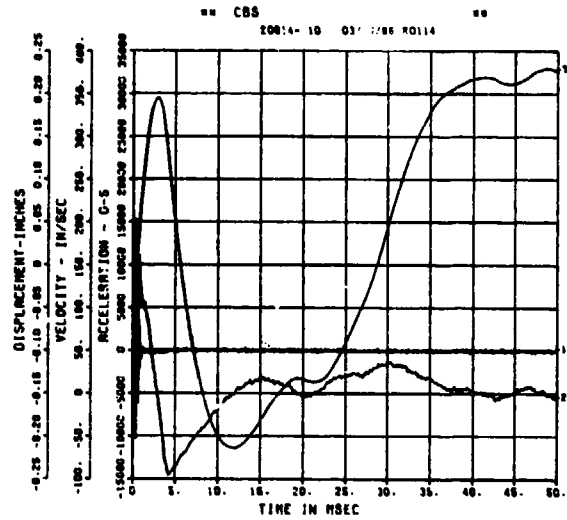
SPALL TEST 3B
PT-3
200000. HZ CAL= 1181.



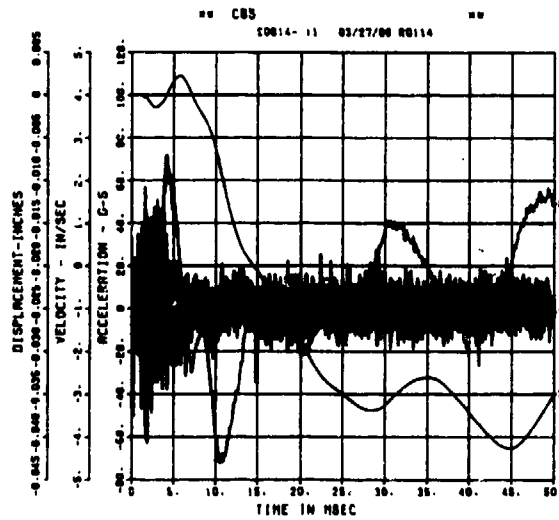
SPALL TEST 3B
 FP-B
 200000. HZ CAL= -0.080



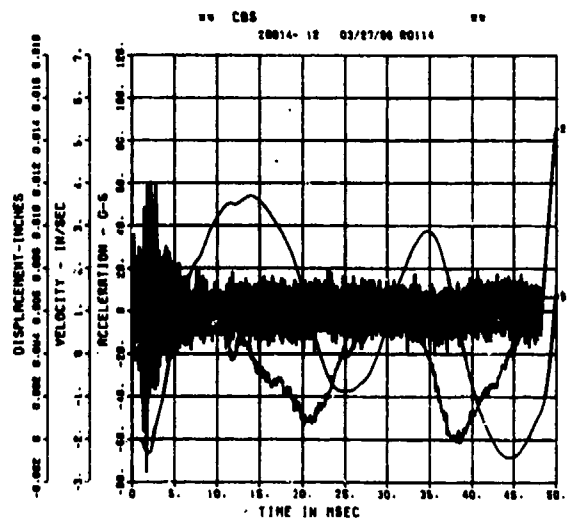
SPALL TEST 3B
 AWHM
 200000. HZ CAL= 29310.



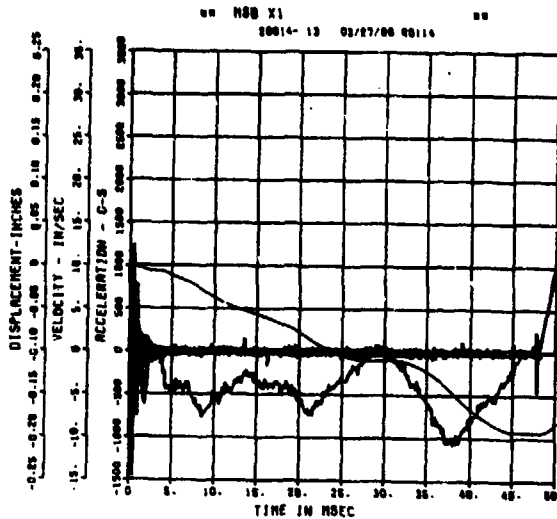
SPALL TEST 3B
 ARV
 200000. HZ CAL= 1513.



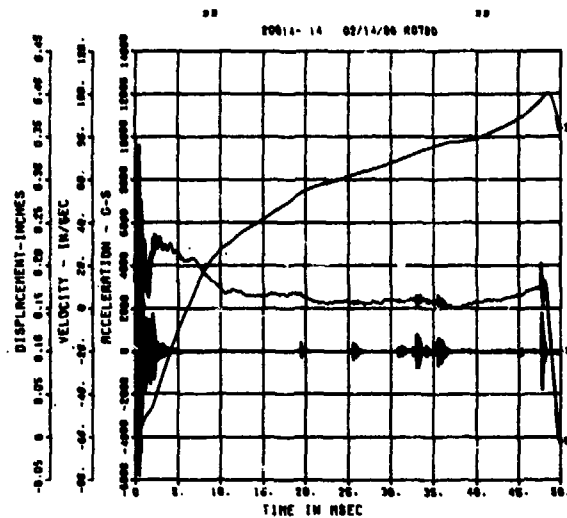
SPALL TEST 3B
 ARH
 200000. HZ CAL= 1672.



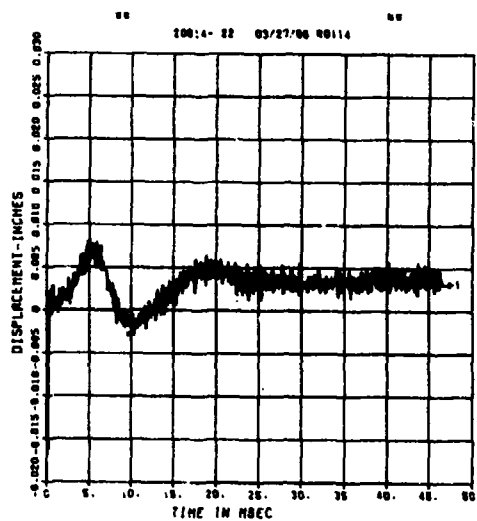
SPALL TEST 3B
AFV
200000. HZ CAL= 7063.



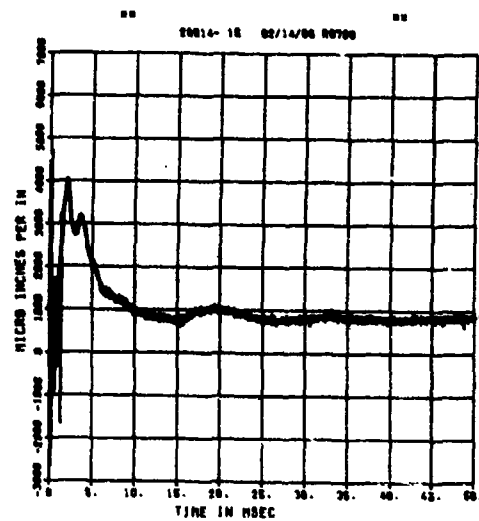
SPALL TEST 3B
AFH
200000. HZ CAL= 7036.



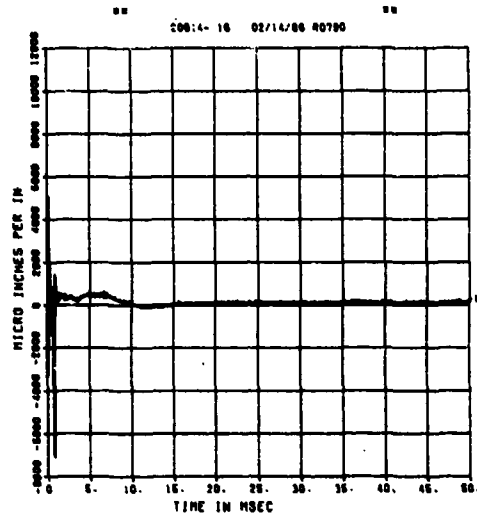
SPALL TEST 3B
DM
200000. HZ CAL= 0.449
LP4/0 70% CUTOFF= 9000. HZ



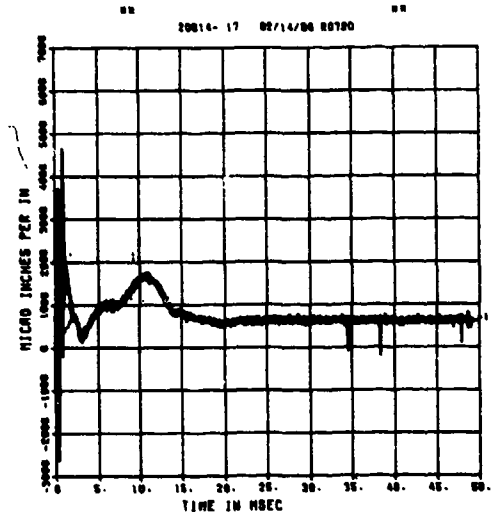
SPALL TEST 3B
EOT
200000. HZ CAL= 11176.



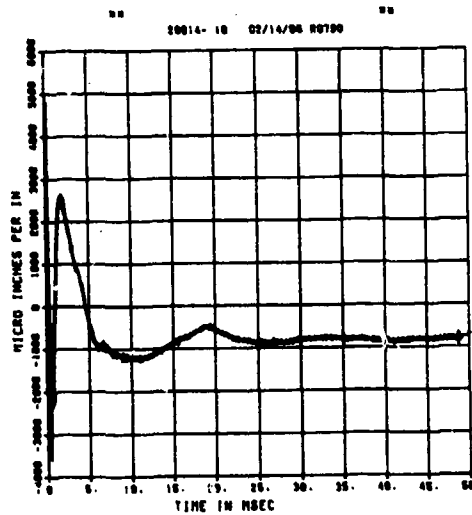
SPALL TEST 3B
EIT
200000. HZ CAL= 7469.



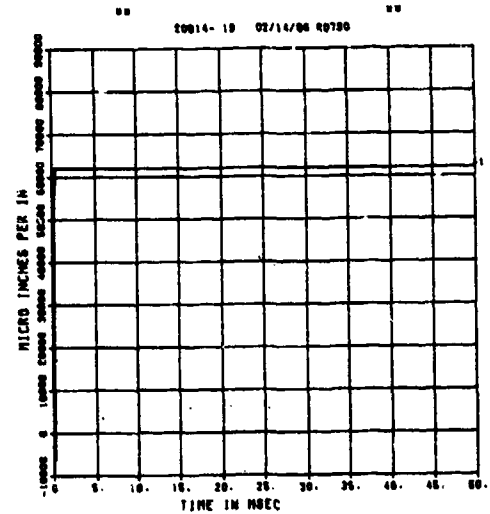
SPALL TEST 3B
EOM
200000. HZ CAL= 7469.



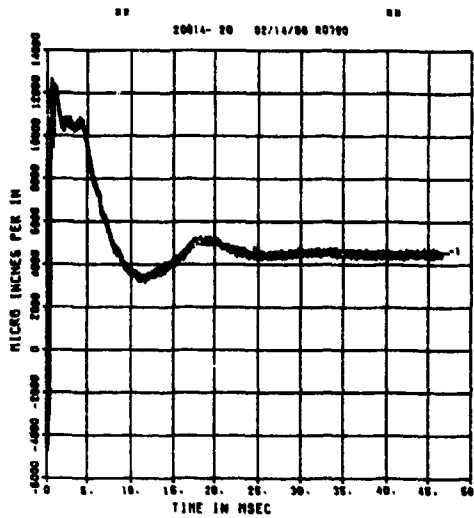
SPALL TEST 3B
EIM
200000. HZ CAL= 7469.



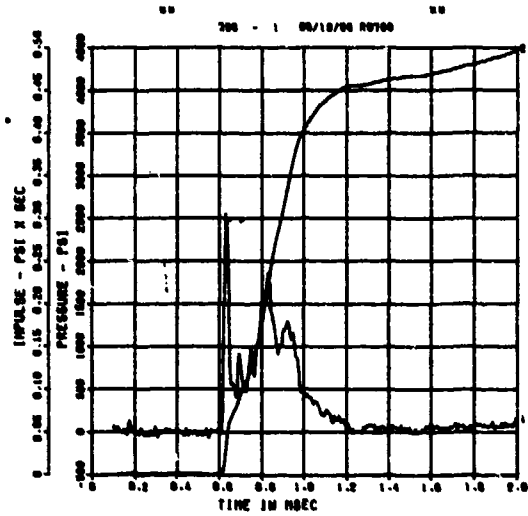
SPALL TEST 3B
E0B
200000. HZ CAL= 30324.



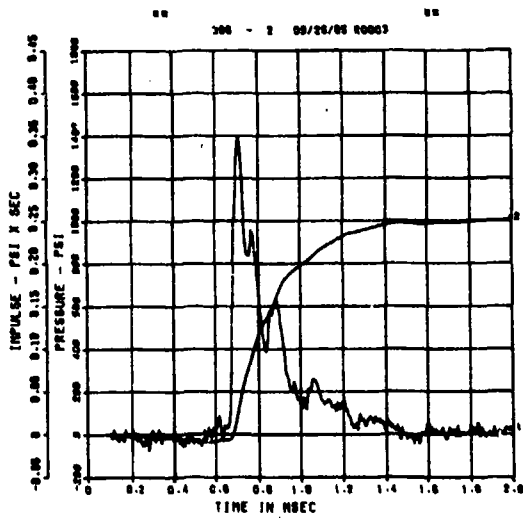
SPALL TEST 3B
E1B
200000. HZ CAL= 30324.



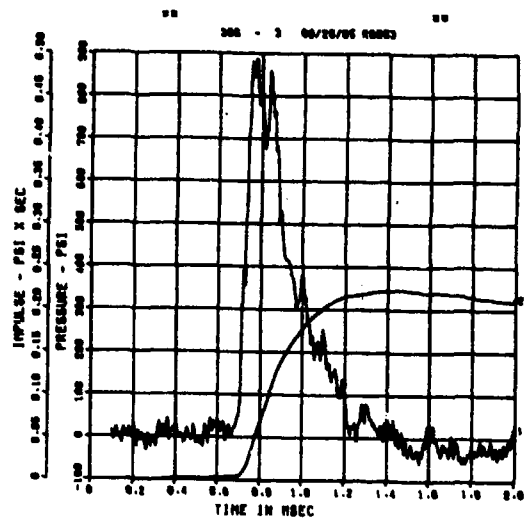
SPALL TEST 4A
PQ-0
200000. HZ CAL= 7040.



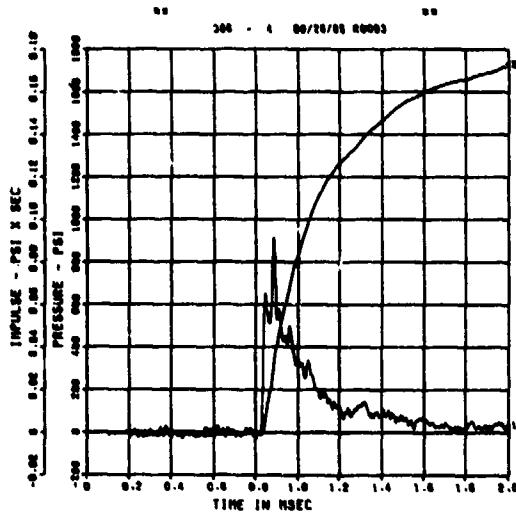
SPALL TEST 4A
PM-0
200000. HZ CAL= 7906.



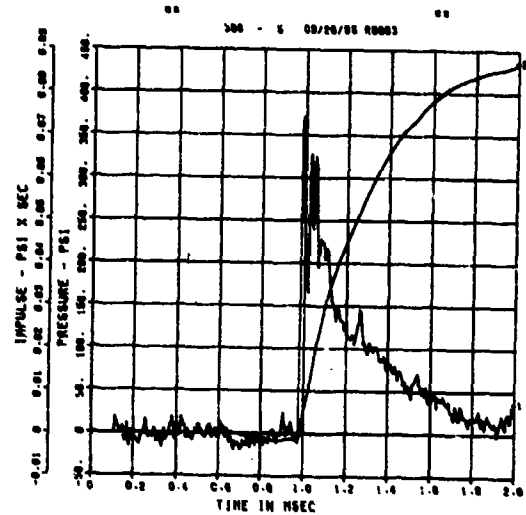
SPALL TEST 4A
PM-2
200000. HZ CAL= 7322.



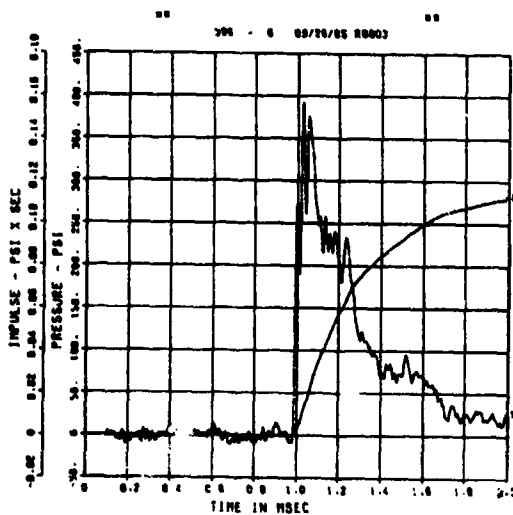
SPALL TEST 4A
PM-3
200000. HZ CAL= 5325.



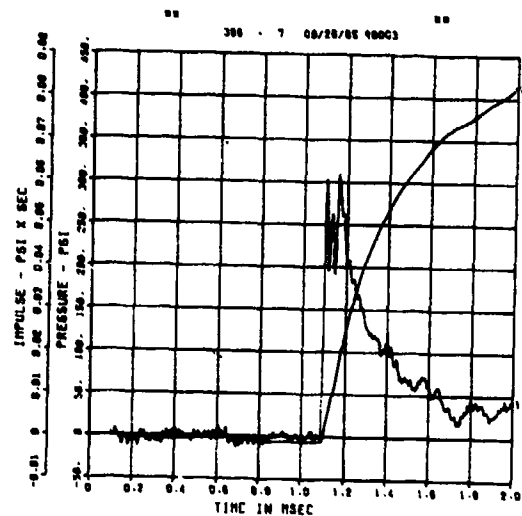
SPALL TEST 4A
PT-0
200000. HZ CAL= 2884.



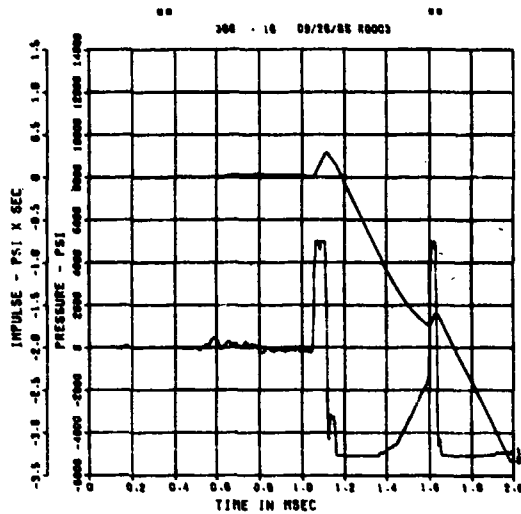
SPALL TEST 4A
PT-2
200000. HZ CAL= 1984.



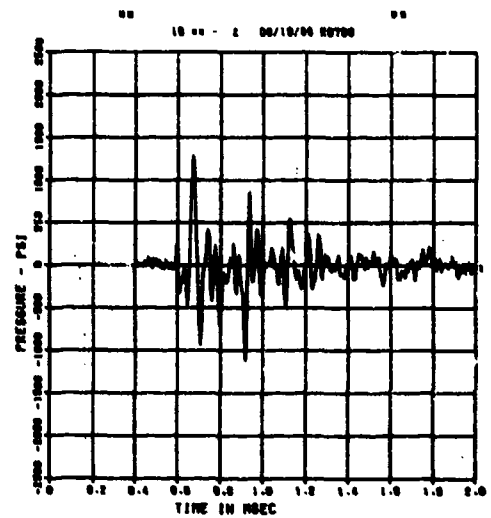
SPALL TEST 4A
PT-3
200000. HZ CAL= 1688.



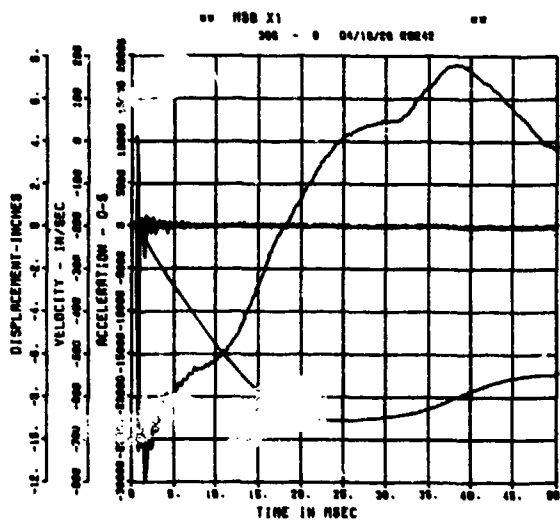
SPALL TEST 4A
BP-A
200000. HZ CAL= 2524.



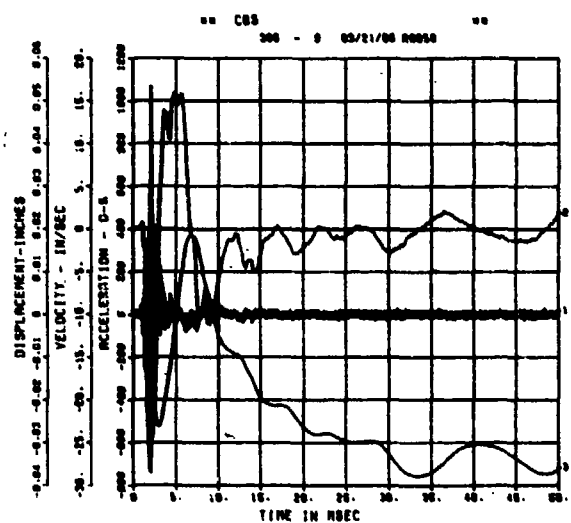
SPALL TEST 4A
FP-A
200000. HZ CAL= -0.030



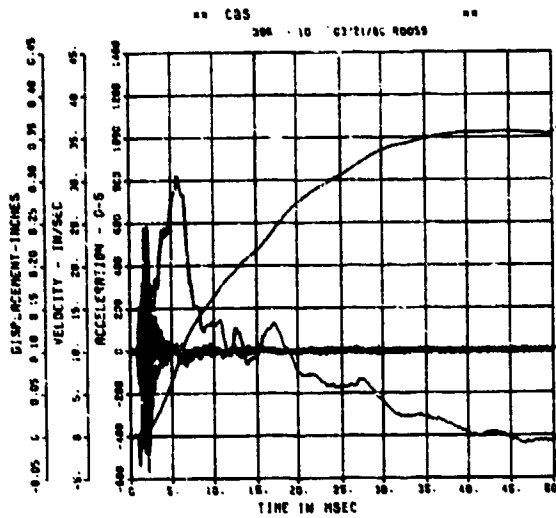
SPALL TEST 4A
AWHM
200000. HZ CAL= 27134.



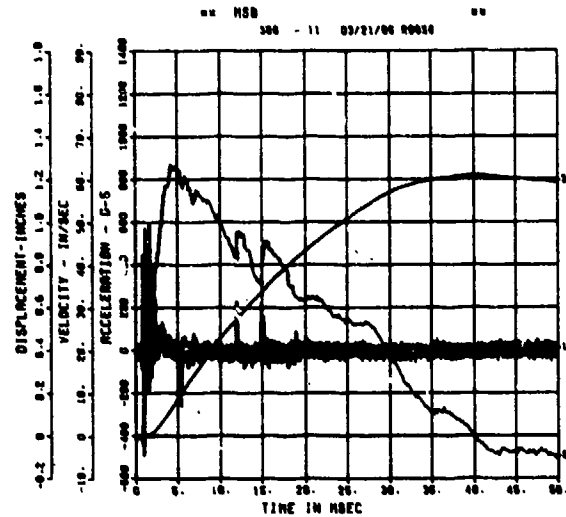
SPALL TEST 4A
ARV
200000. HZ CAL= 1542.



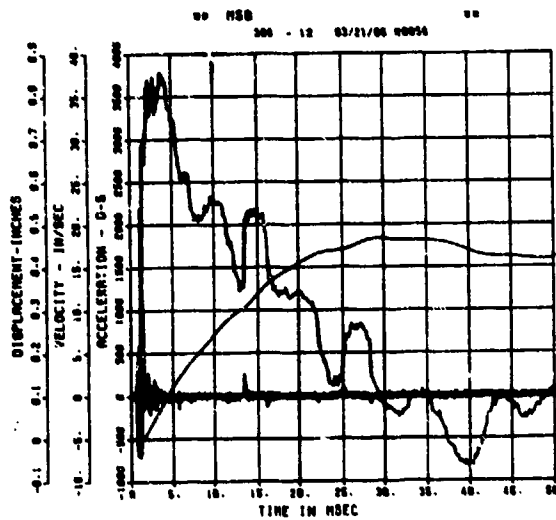
SPALL TEST 4A
ARH
200000. HZ CAL= 1672.



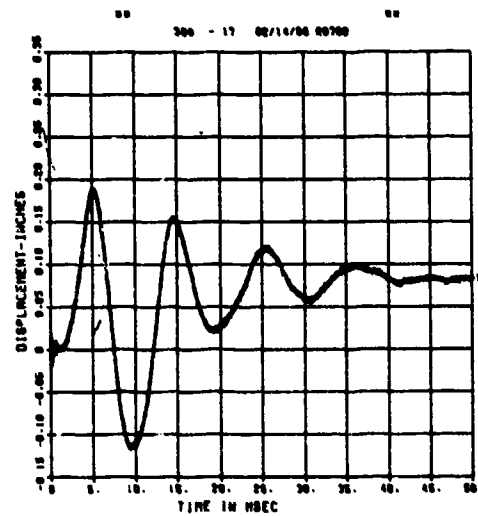
SPALL TEST 4A
AFV
200000. HZ CAL= 4983.



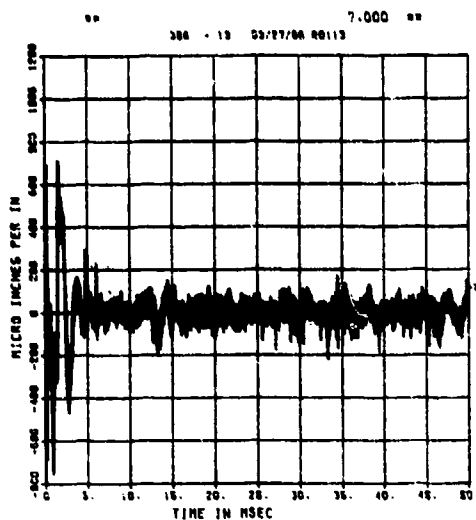
SPALL TEST 4A
AFH
200000. HZ CAL= 4944.



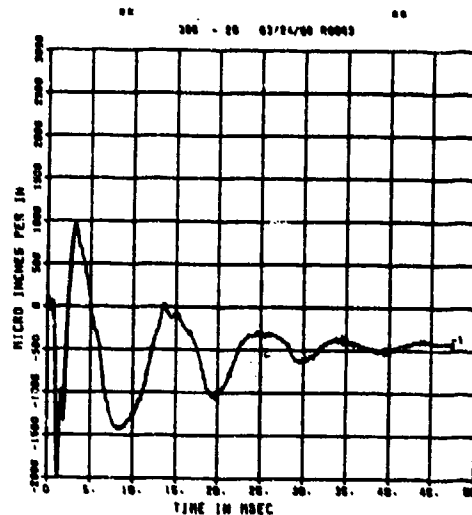
SPALL TEST 4A
DM
200000. HZ CAL= 0.449



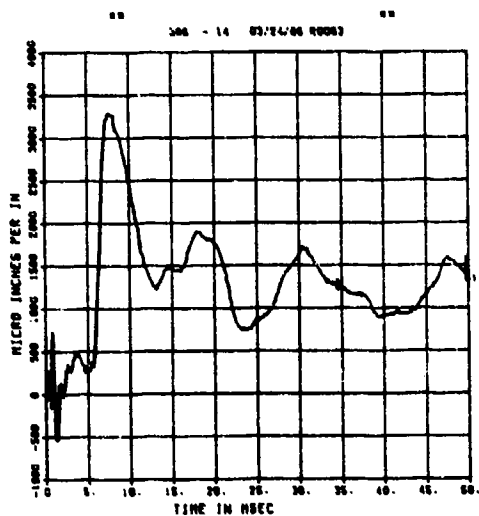
SPALL TEST 4A
EOT
200000. HZ CAL= 7469.



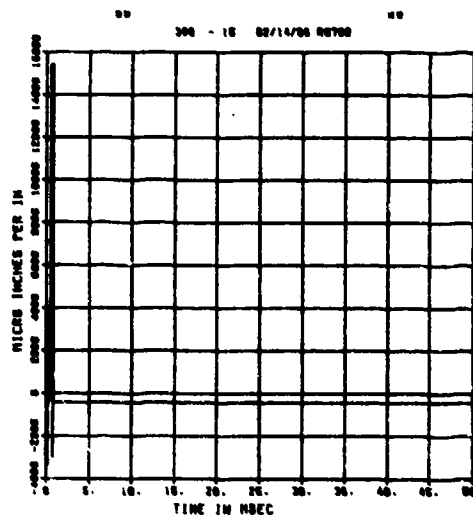
SPALL TEST 4A
~~EOT~~
200000. HZ CAL= 7469.
LP4/0 70% CUTOFF= 9000. HZ



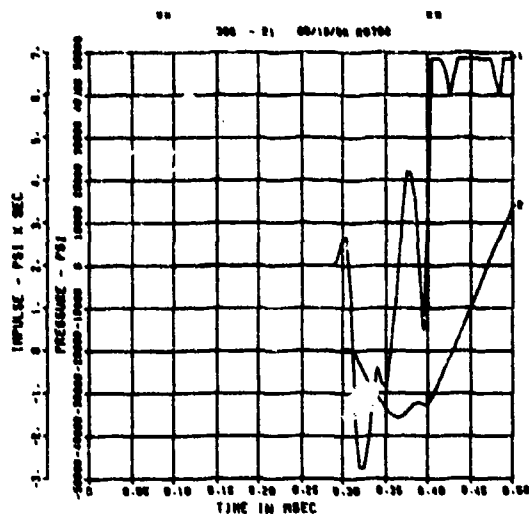
SPALL TEST 4A
EOM
200000. HZ CAL= 5004.
LP4/0 70% CUTOFF= 9000. HZ



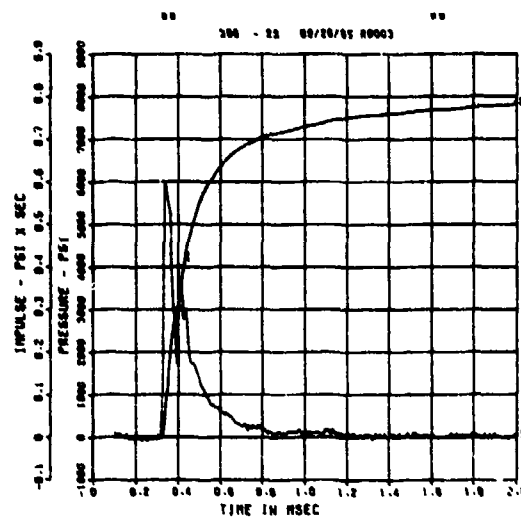
SPALL TEST 4A
~~EOM~~
200000. HZ CAL= 7469.



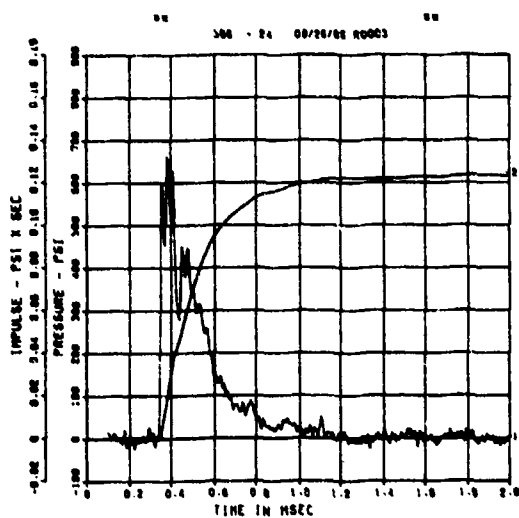
SPALL TEST 4B
 PQ-0
 200000. HZ CAL= 21261.



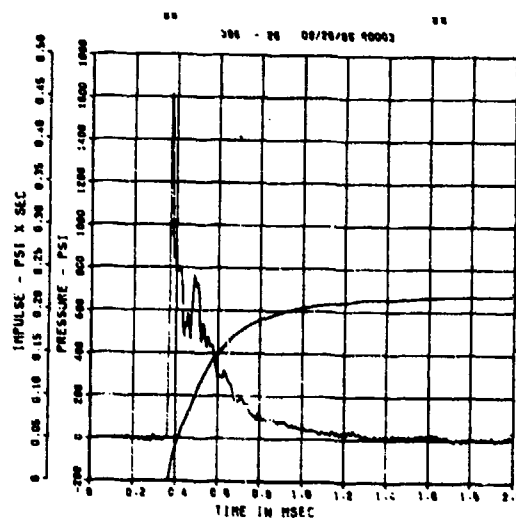
SPALL TEST 4B
 PQ-2
 200000. HZ CAL= 11435.



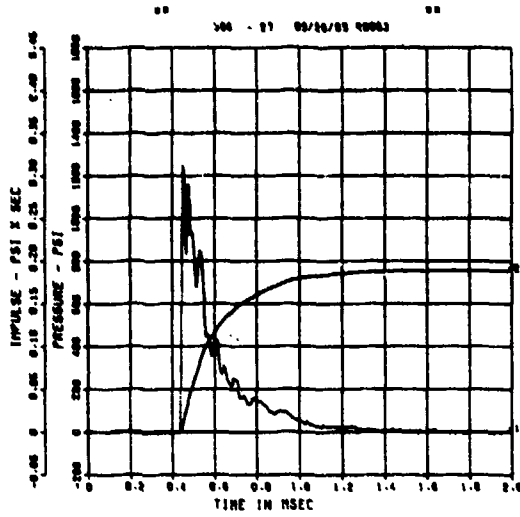
SPALL TEST 4B
 PM-0
 200000. HZ CAL= 3802.



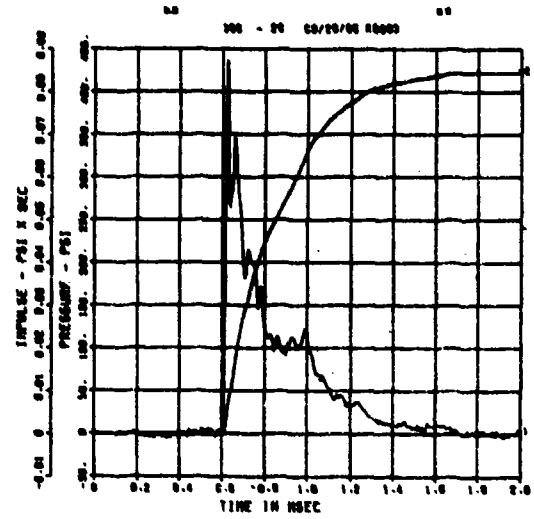
SPALL TEST 4B
 PM-2
 200000. HZ CAL= 2877.



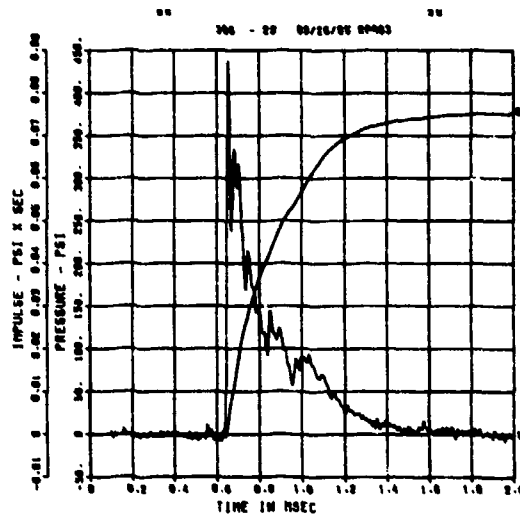
SPALL TEST 4B
PM-3
200000. HZ CAL= 1448.



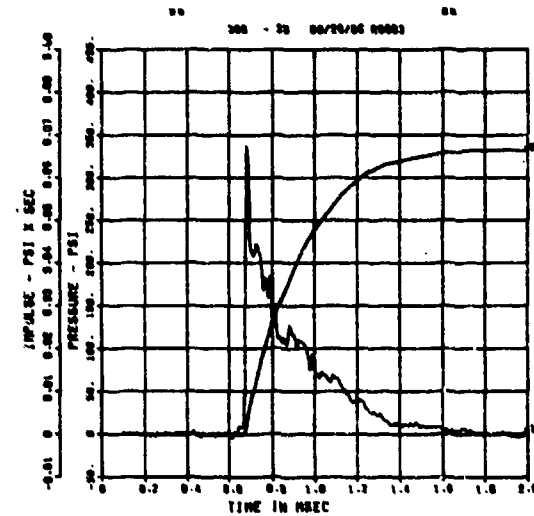
SPALL TEST 4B
PT-0
200000. HZ CAL= 631.3



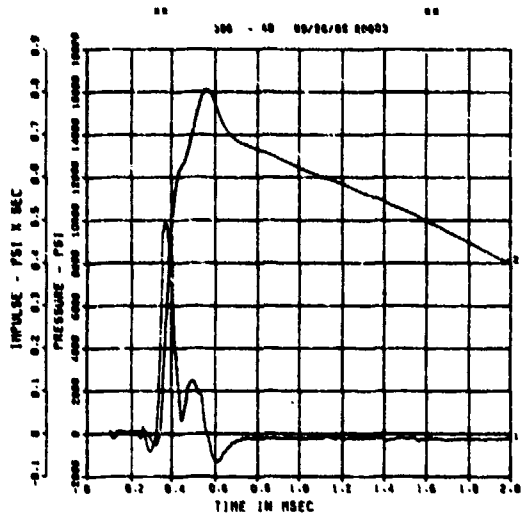
SPALL TEST 4B
PT-2
200000. HZ CAL= 621.8



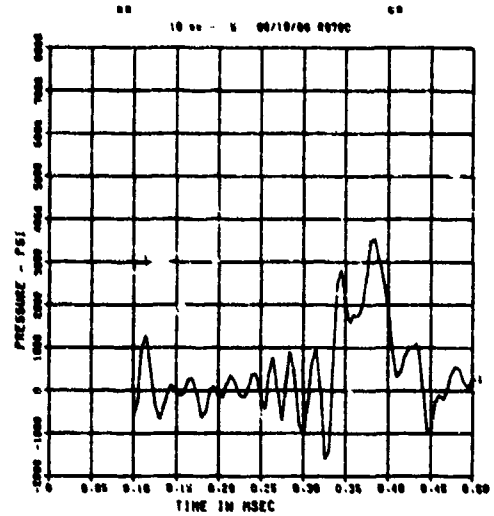
SPALL TEST 4B
PT-3
200000. HZ CAL= 529.0



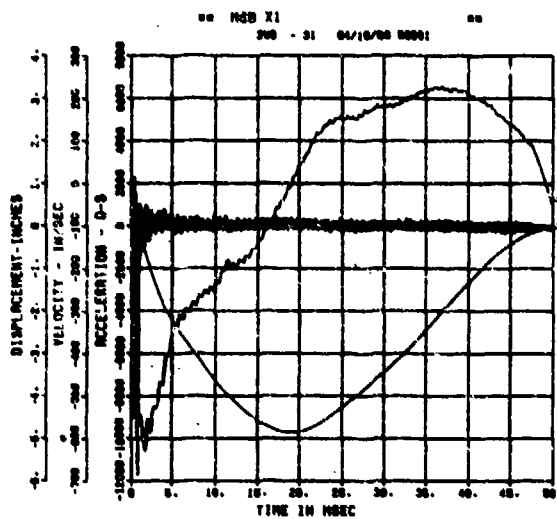
SPALL TEST 4B
BP-B
200000. HZ CAL= 4794.



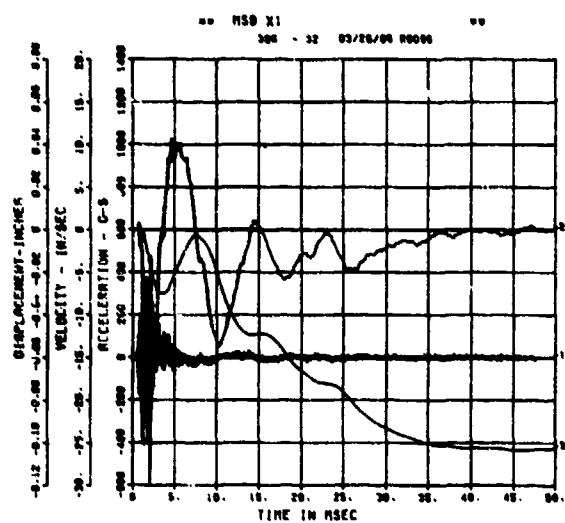
SPALL TEST 4B
FP-B
200000. HZ CAL= -0.065



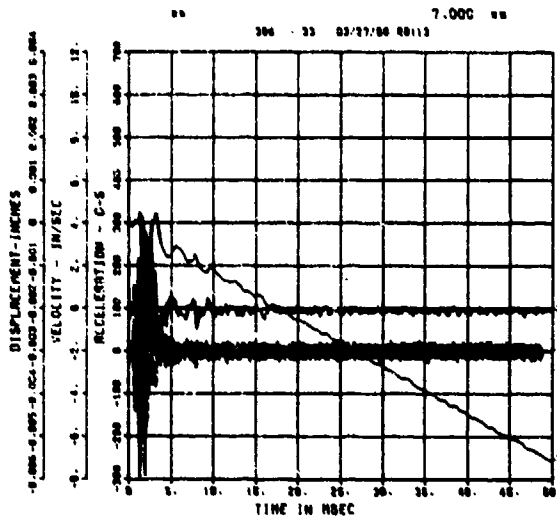
SPALL TEST 4B
AWHM
200000. HZ CAL= 30180.



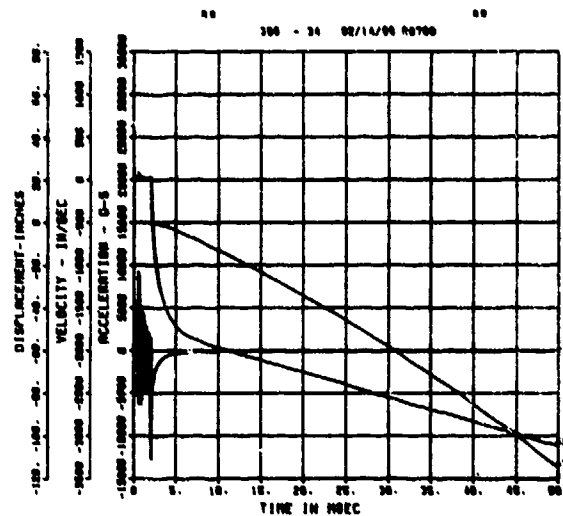
SPALL TEST 4B
ARV
200000. HZ CAL= 1552.



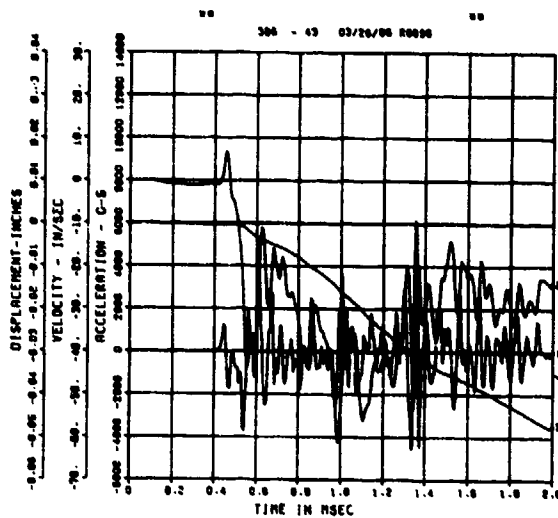
SPALL TEST 4B
AFH
200000. HZ CAL= 1832.



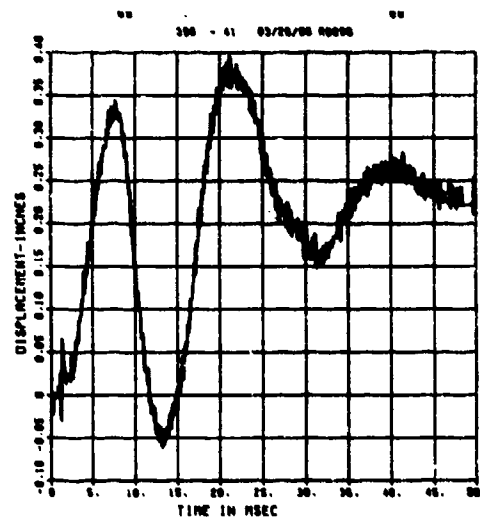
SPALL TEST 4B
AFH
200000. HZ CAL= 5624.



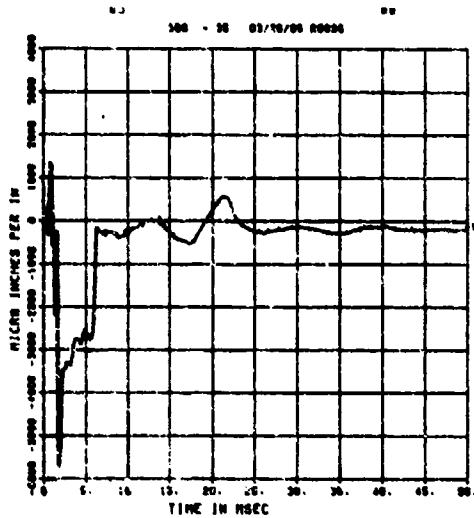
SPALL TEST 4B
AFV
200000. HZ CAL= 5366.



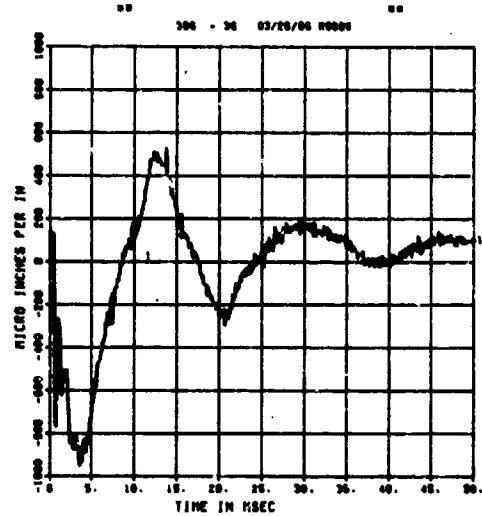
SPALL TEST 4B
DM
200000. HZ CAL= 4.497
LP4/O 70X CUTOFF= 9000. HZ



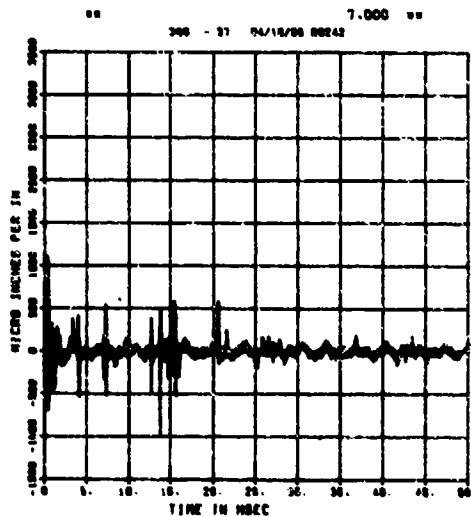
SPALL TEST 4B
EOT
200000. HZ CAL= 11176.
LP4/D 70X CUTOFF= 9000. HZ



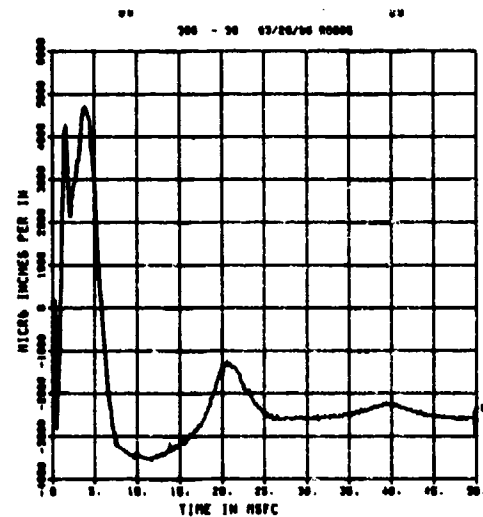
SPALL TEST 4B
EII
200000. HZ CAL= 7469.
LP4/D 70X CUTOFF= 9000. HZ



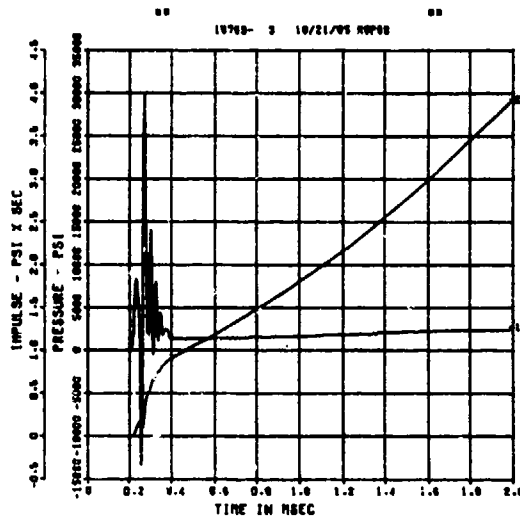
SPALL TEST 4B
EQM
200000. HZ CAL= 7469.



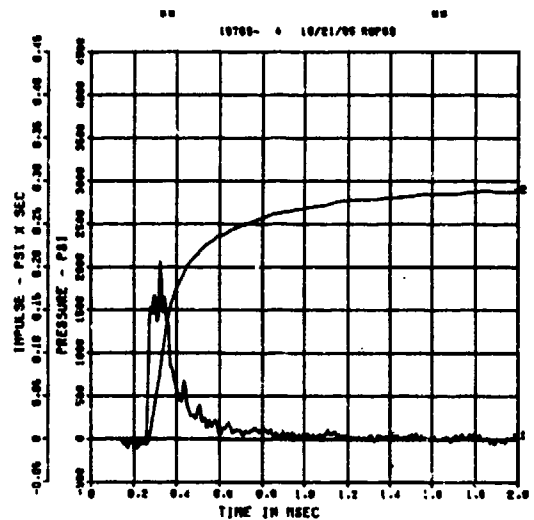
SPALL TEST 4B
EIM
200000. HZ CAL= 11176.
LP4/D 70X CUTOFF= 9000. HZ



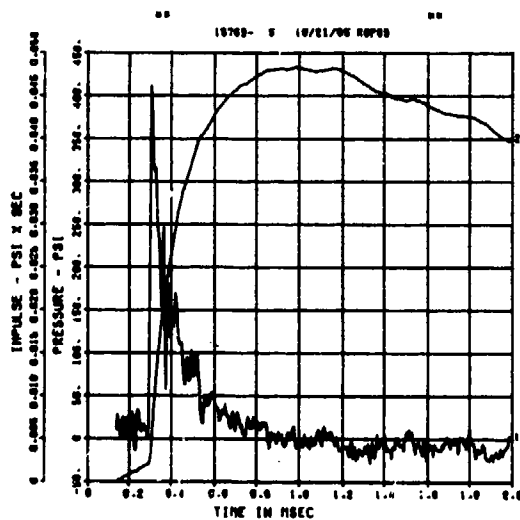
SPALL TEST 5A
PQ-2
200000. HZ CAL= 14343.



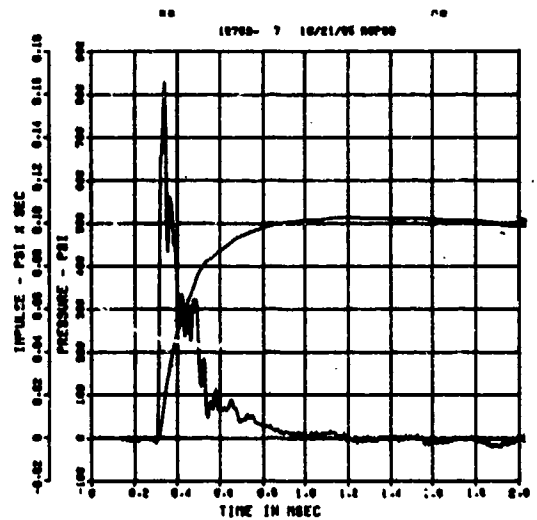
SPALL TEST 5A
PQ-3
200000. HZ CAL= 9618.



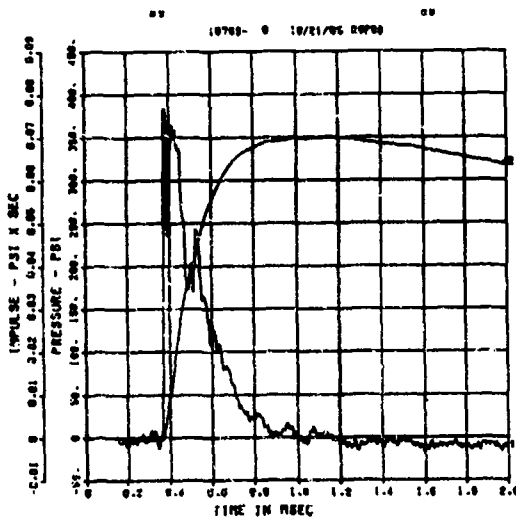
SPALL TEST 5A
PM-0
200000. HZ CAL= 2868.



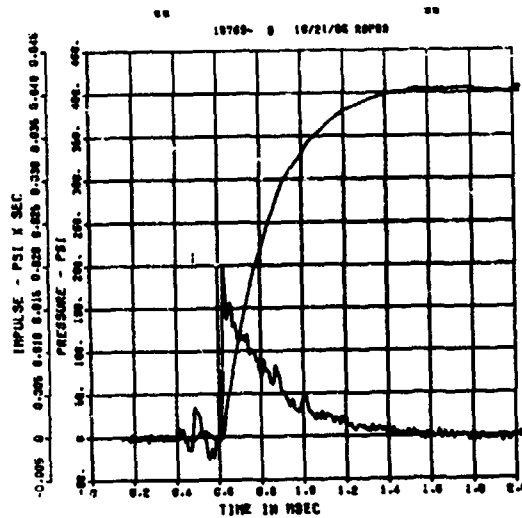
SPALL TEST 5A
PM-2
200000. HZ CAL= 1965.



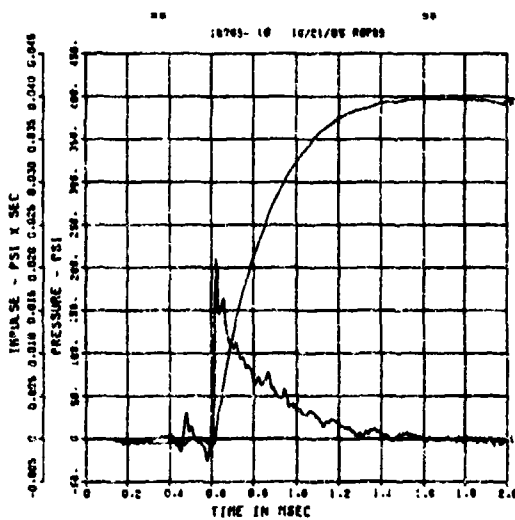
SPALL TEST 5A
PM-3
200000. HZ CAL= 1448.



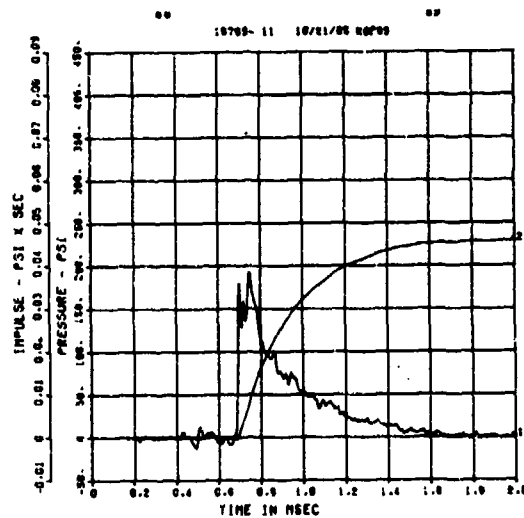
SPALL TEST 5A
PT-0
200000. HZ CAL= 631.3



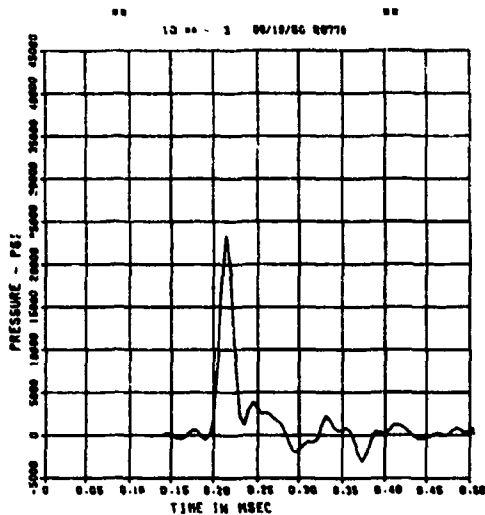
SPALL TEST 5A
PT-2
200000. HZ CAL= 621.8



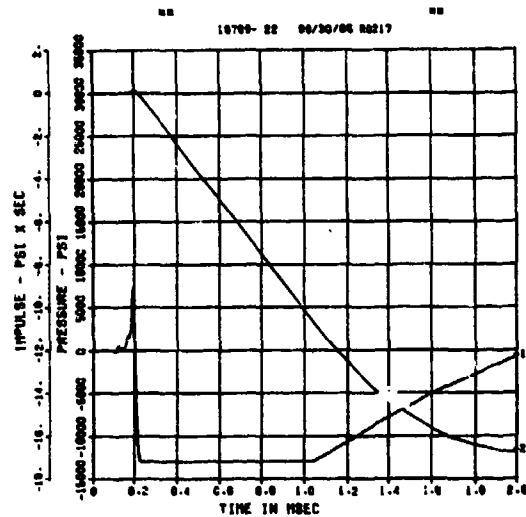
SPALL TEST 5A
PT-3
200000. HZ CAL= 529.0



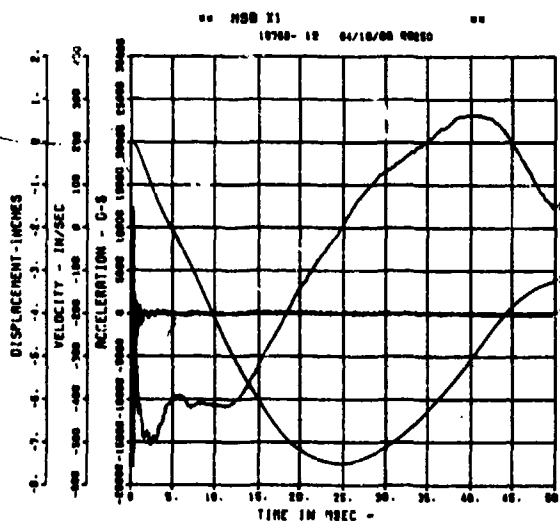
SPALL TEST 5A
 FP-A
 200000. HZ CAL= -0.055



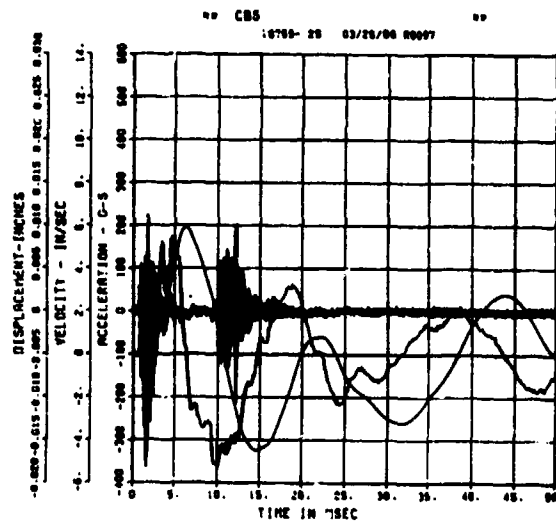
SPALL TEST 5A
 BP-A
 200000. HZ CAL= 6277.



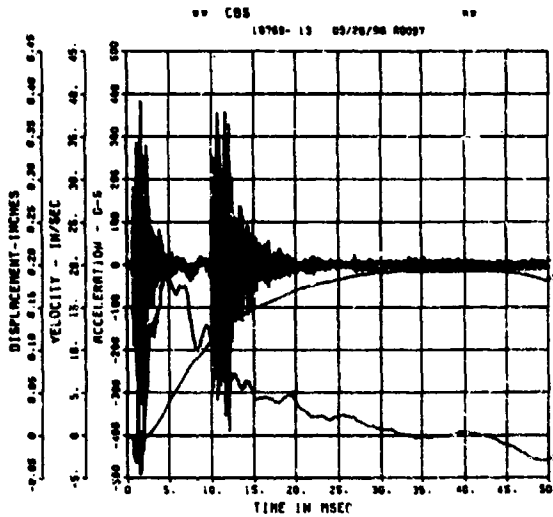
SPALL TEST 5A
 AWHM
 200000. HZ CAL= 25189.



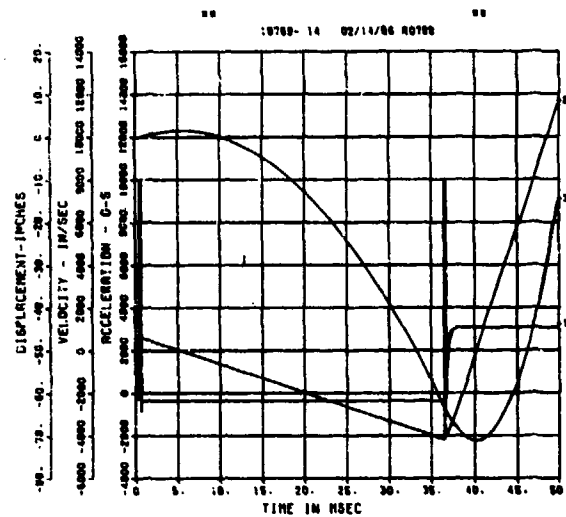
SPALL TEST 5A
 ARV
 200000. HZ CAL= 1105.



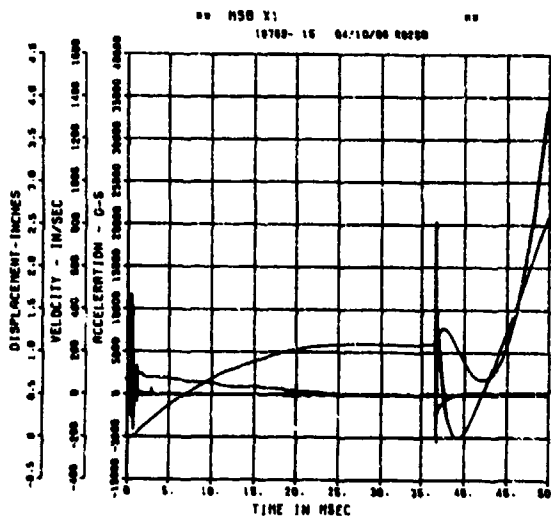
SPALL TEST 5A
ARH
200000. HZ CAL= 880.4



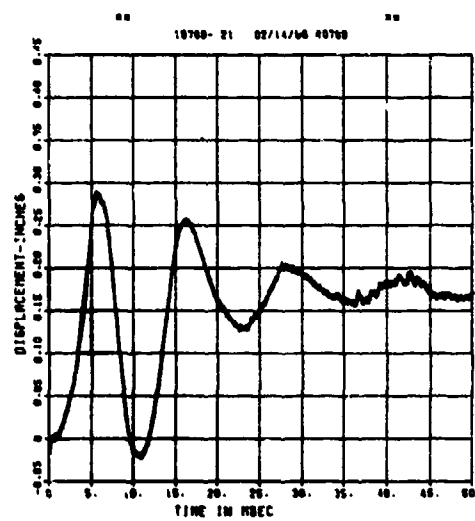
SPALL TEST 5A
AFV
200000. HZ CAL= 4983.



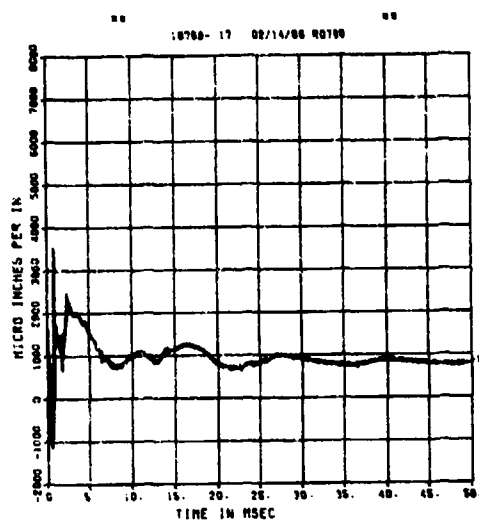
SPALL TEST 5A
AFH
200000. HZ CAL= 10167.



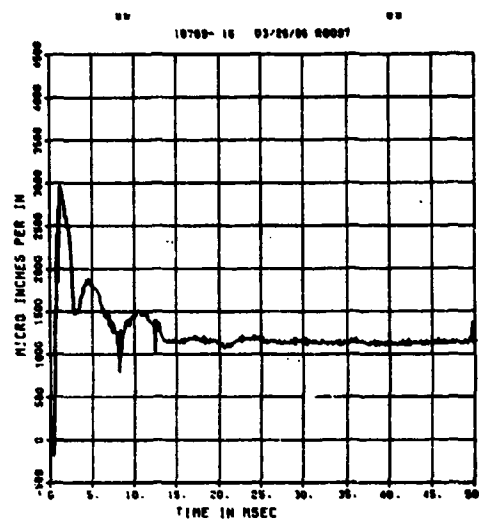
SPALL TEST 5A
DM
200000. HZ CAL= 0.431



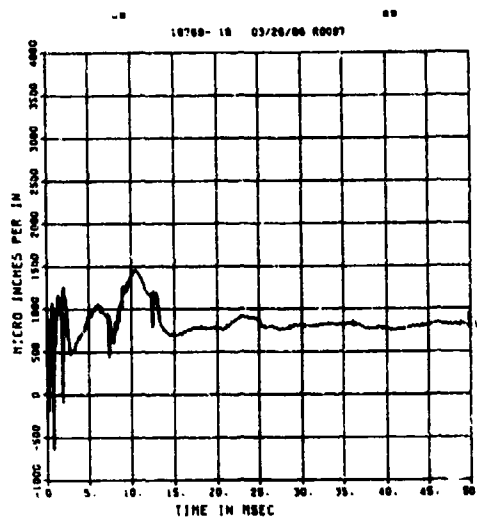
SPALL TEST 5A
EIT
200000. HZ CAL= 5004.



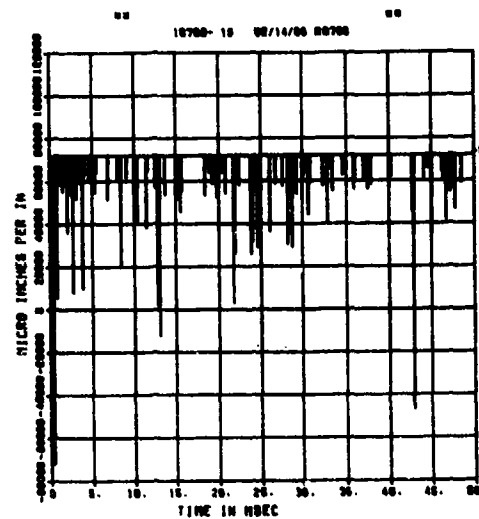
SPALL TEST 5A
EOT
200000. HZ CAL= 7469.
LP4/0 70% CUTOFF= 9000. HZ



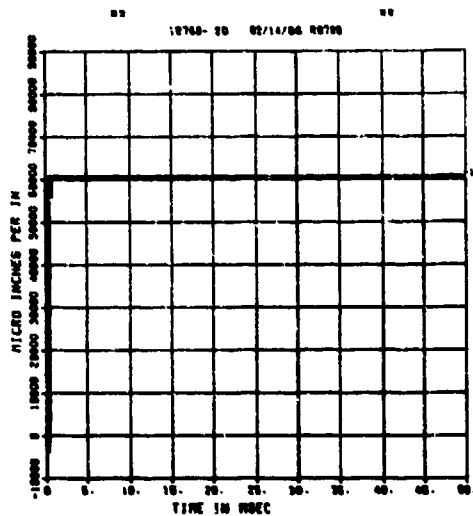
SPALL TEST 5A
EOM
200000. HZ CAL= 5004.
LP4/0 70% CUTOFF= 9000. HZ



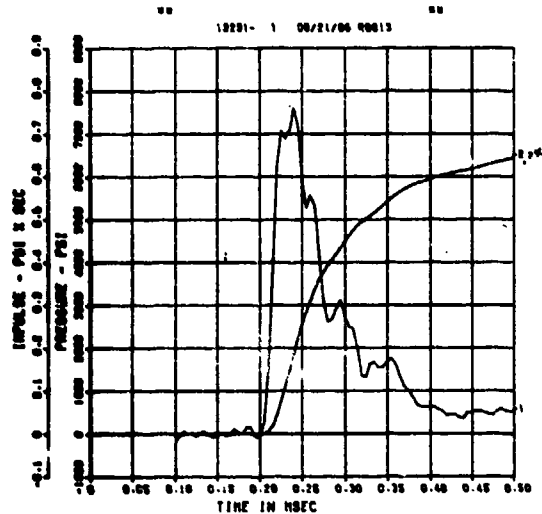
SPALL TEST 5A
EOB
200000. HZ CAL= 35703.



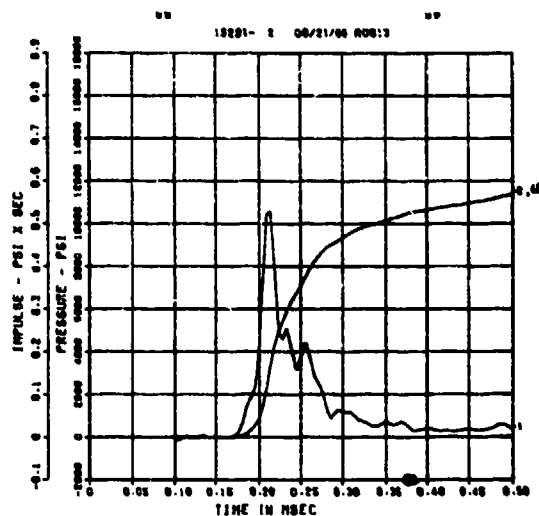
SPALL TEST 5A
E18
200000. HZ CAL= 30324.



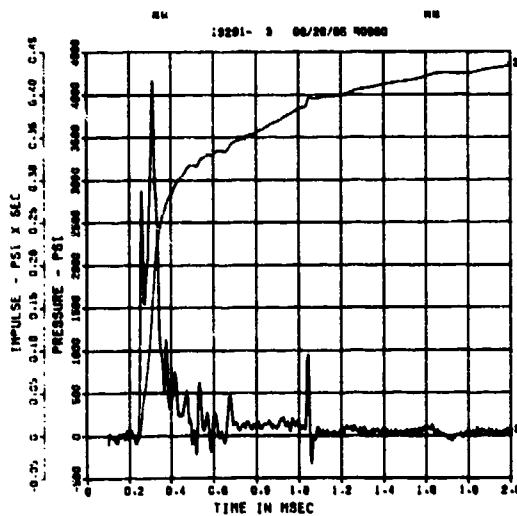
SPALL TEST 5B
PQ-0
200000. HZ CAL= 18408.



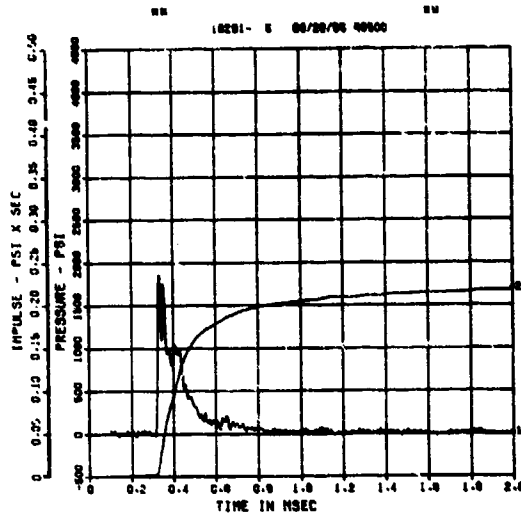
SPALL TEST 5B
PQ-1
200000. HZ CAL= 17253.



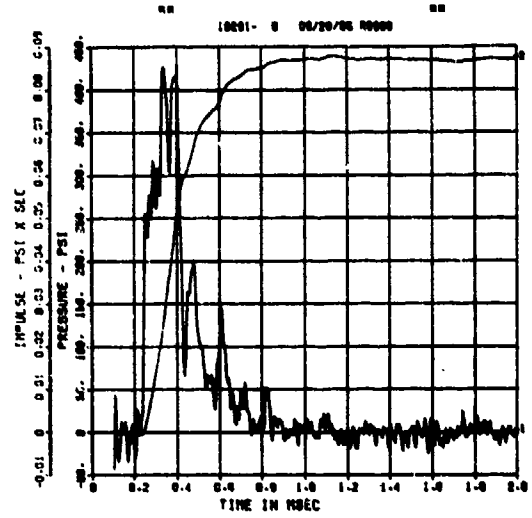
SPALL TEST 5B
PQ-2
200000. HZ CAL= 12240.



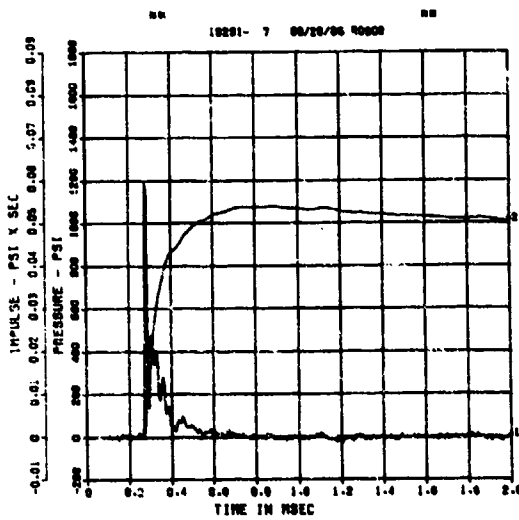
SPALL TEST 5B
PQ-3
200000. HZ CAL= 6485.



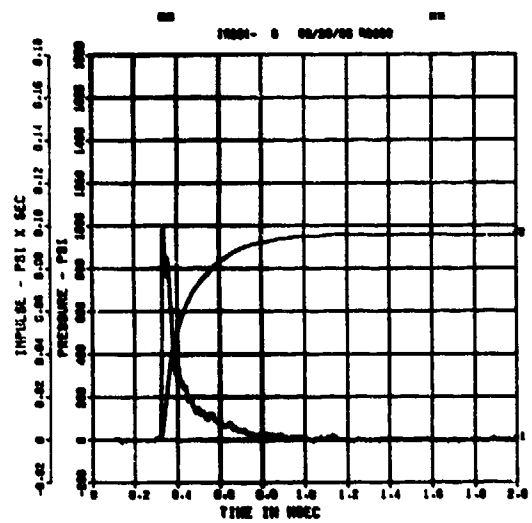
SPALL TEST 5B
PM-0
200000. HZ CAL= 3008.



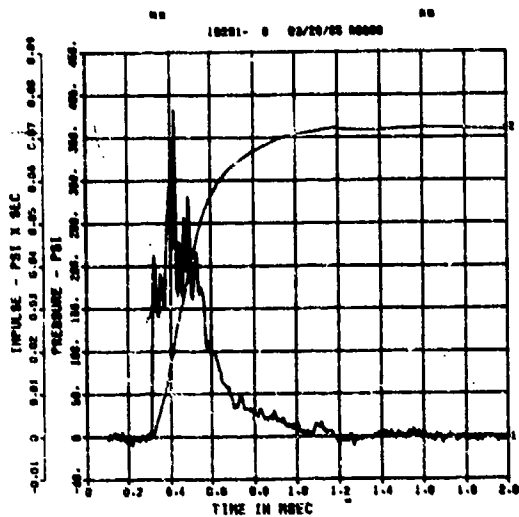
SPALL TEST 5B
PM-1
200000. HZ CAL= 2957.



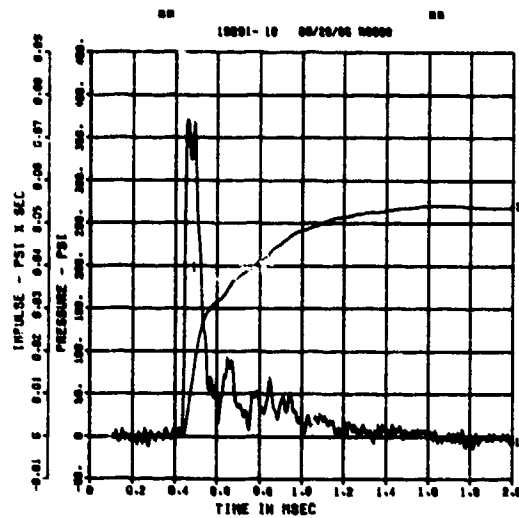
SPALL TEST 5B
PM-2
200000. HZ CAL= 1965.



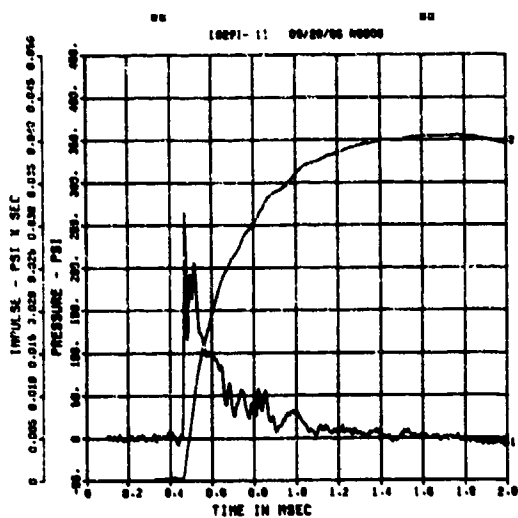
SPALL TEST 5B
PM-3
200000. HZ CAL= 1248.



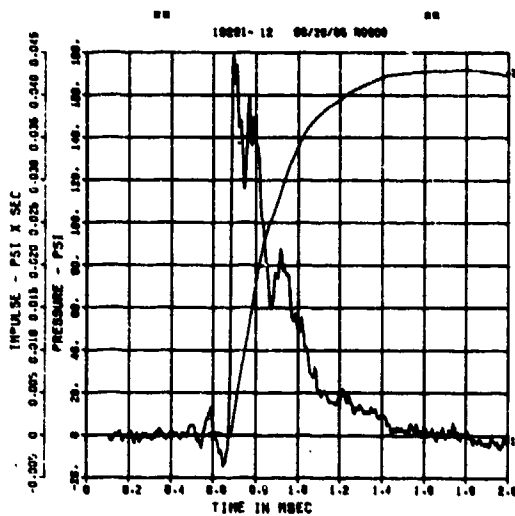
SPALL TEST 5B
PT-0
200000. HZ CAL= 936.0



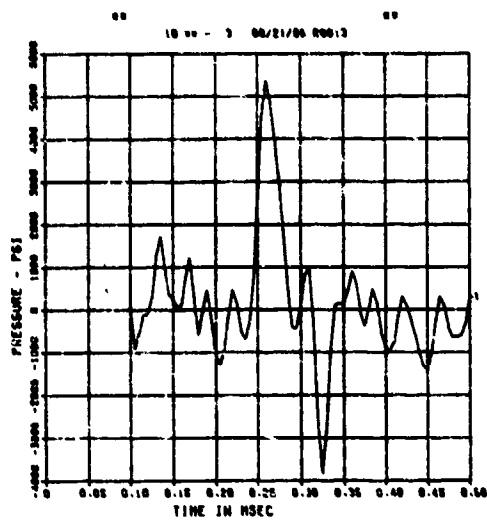
SPALL TEST 5B
PT-2
200000. HZ CAL= 732.0



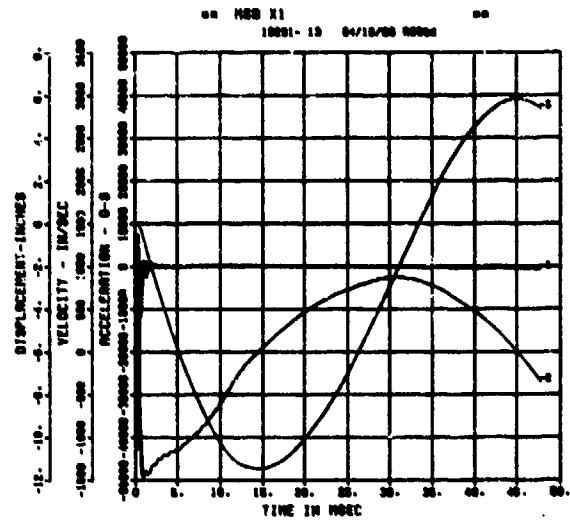
SPALL TEST 5B
PT-3
200000. HZ CAL= 529.0



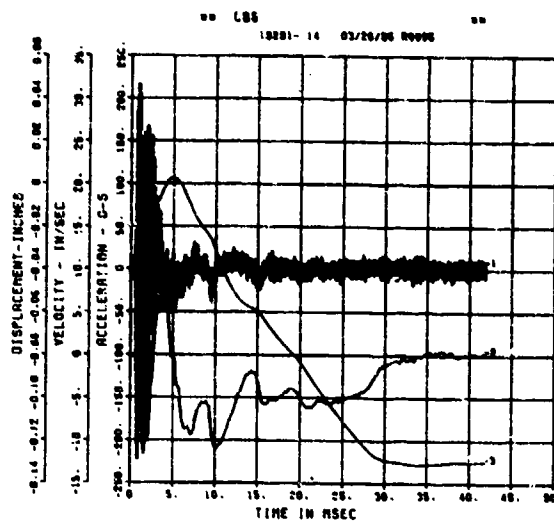
SPALL TEST 5B
FP-8
200000. HZ CAL= -0.045



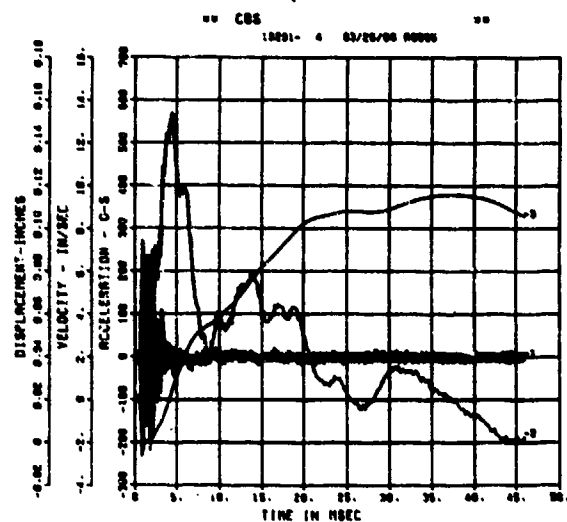
SPALL TEST 5B
AWHM
200000. HZ CAL= 23073.



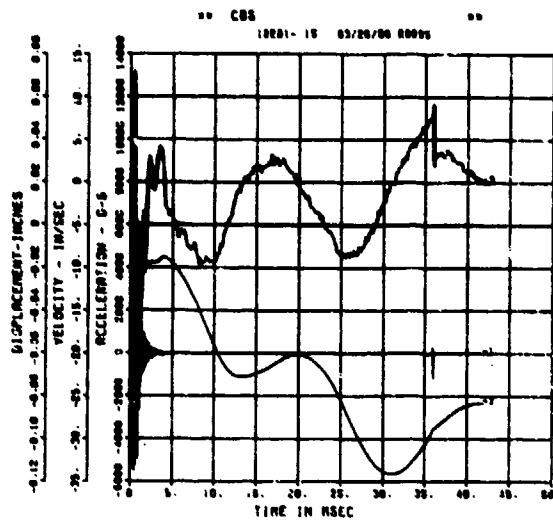
SPALL TEST 5B
ARV
200000. HZ CAL= 1211.



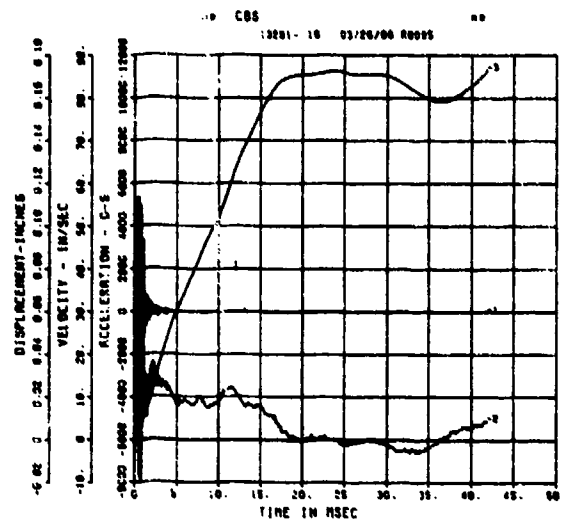
SPALL TEST 5B
ARH
200000. HZ CAL= 1228.



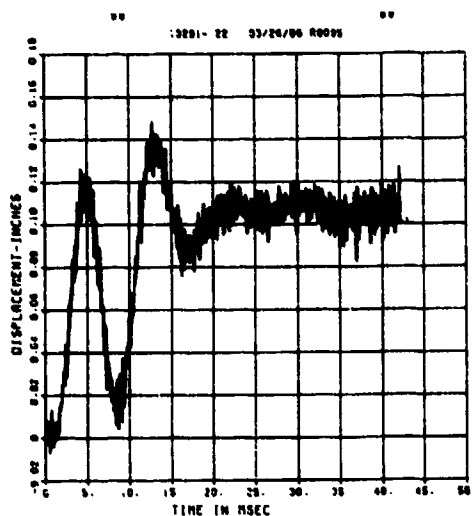
SPALL TEST 5B
AFV
200000. HZ CAL= 4963.



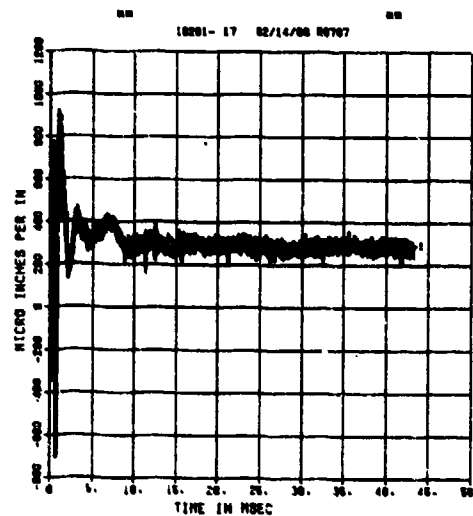
SPALL TEST 5B
AFH
200000. HZ CAL= 5624.



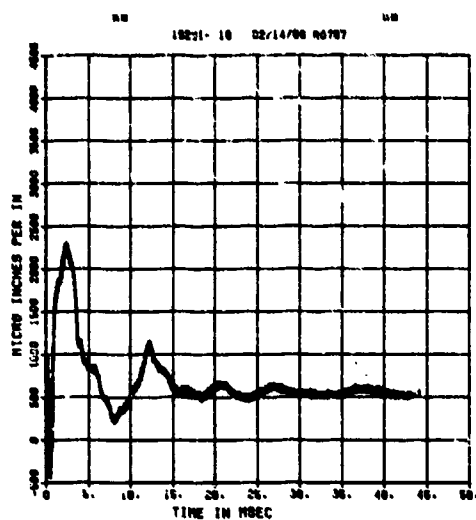
SPALL TEST 5B
DM
200000. HZ CAL= 3.106
LP4/0 70% CUTOFF= 9000. HZ



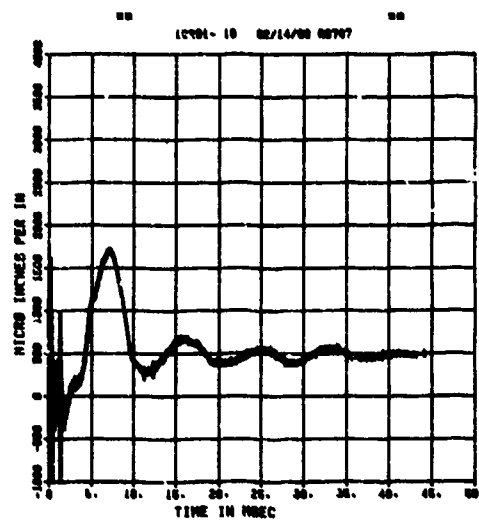
SPALL TEST 5B
EOT
200000. HZ CAL= 5004.



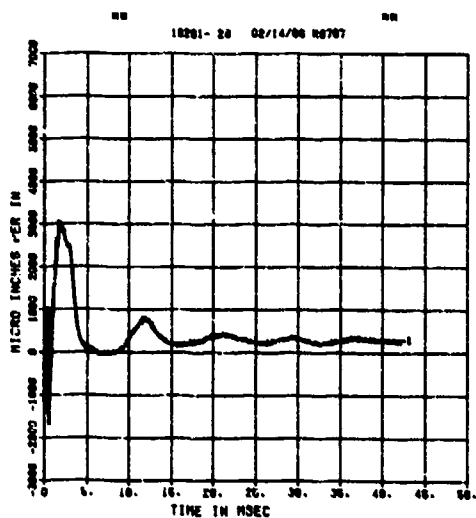
SPALL TEST 5B
EIT
200000. HZ CAL= 5004.



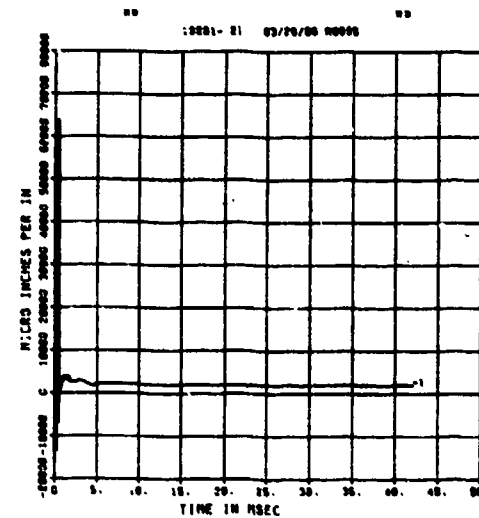
SPALL TEST 5B
EOM
200000. HZ CAL= 3022.



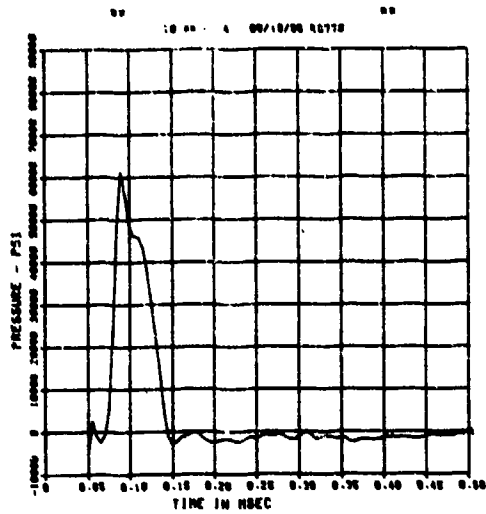
SPALL TEST 5B
EIM
200000. HZ CAL= 5004.



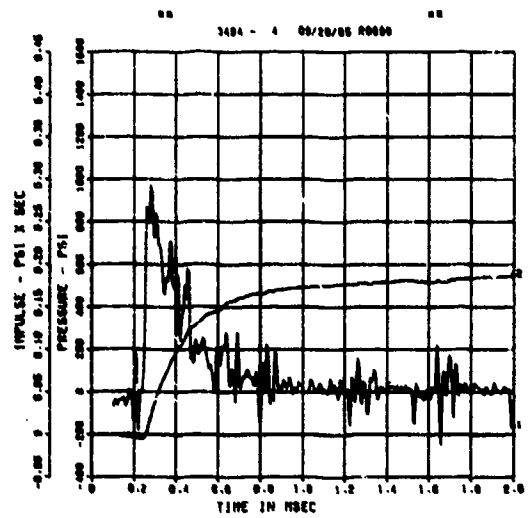
SPALL TEST 5B
EOM
200000. HZ CAL= 30324.



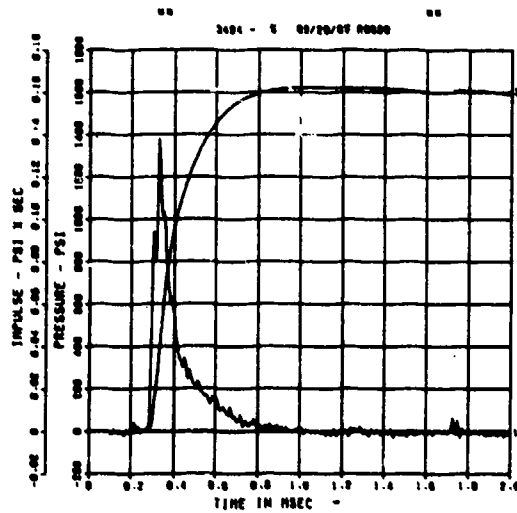
SPALL TEST 5C
 FP-C
 200000. HZ CAL= -0.210



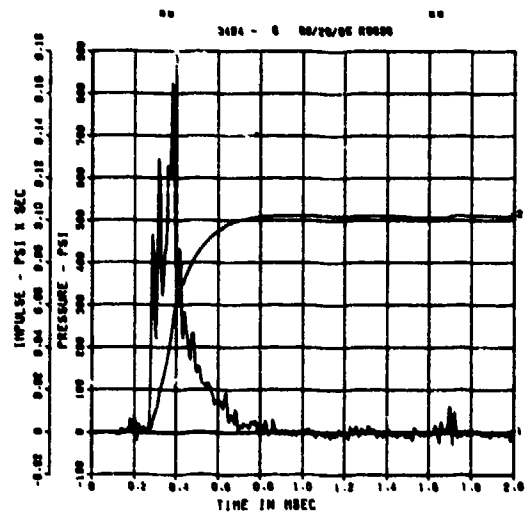
SPALL TEST 6A
 PM-0
 200000. HZ CAL= 3008.



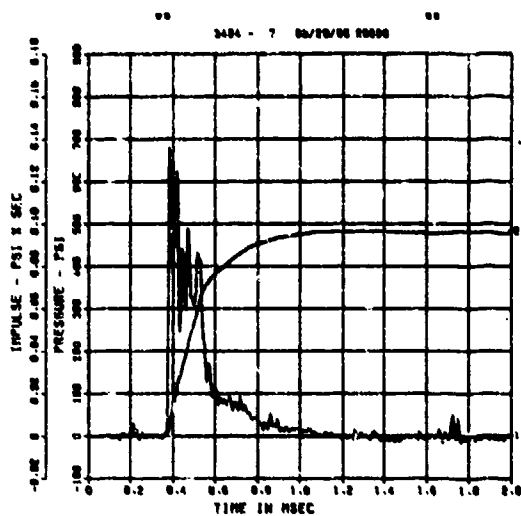
SPALL TEST 6A
 PM-1
 200000. HZ CAL= 2663.



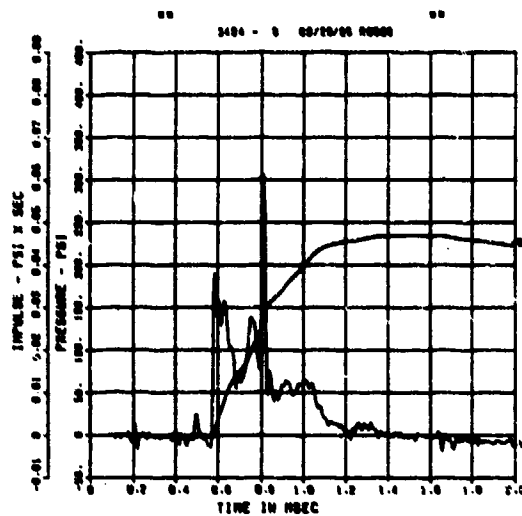
SPALL TEST 6A
 PM-2
 200000. HZ CAL= 1981.



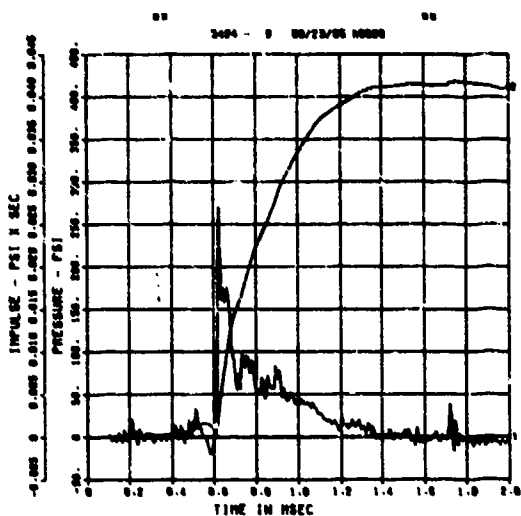
SPALL TEST 6A
PM-3
200000. HZ CAL= 1448.



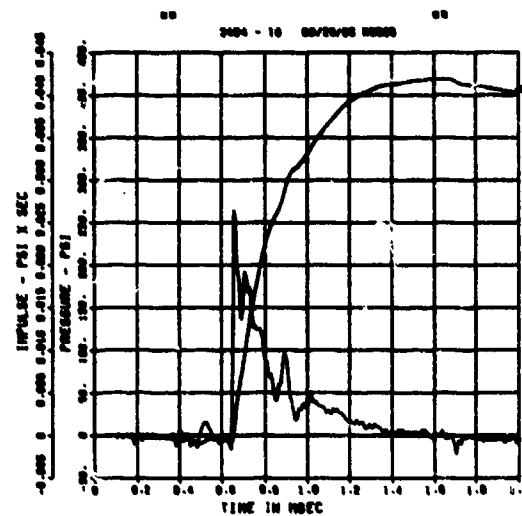
SPALL TEST 6A
PT-0
200000. HZ CAL= 631.3



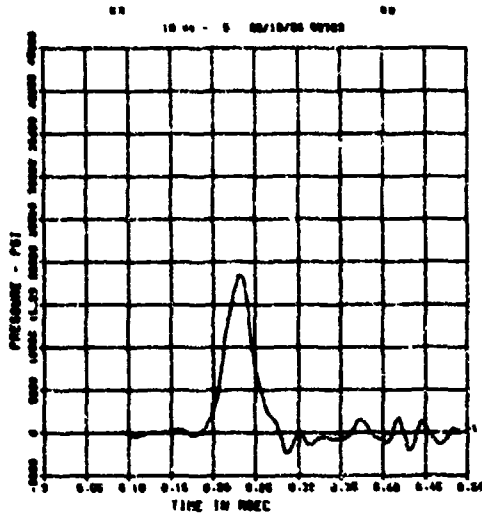
SPALL TEST 6A
PT-2
200000. HZ CAL= 638.5



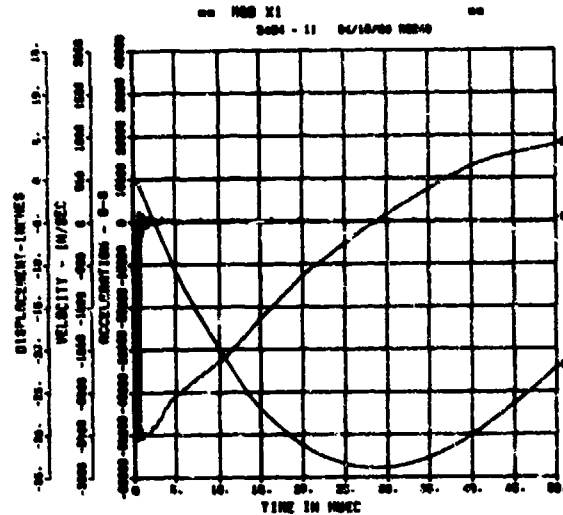
SPALL TEST 6A
PT-3
200000. HZ CAL= 533.4



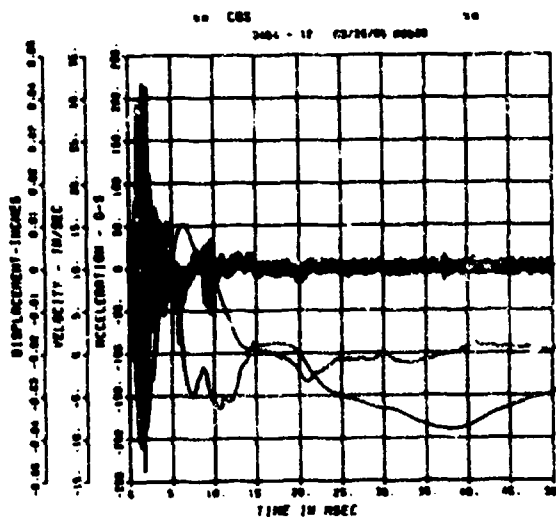
SPALL TEST 6A
FP-A
200000. HZ CAL= -0.055



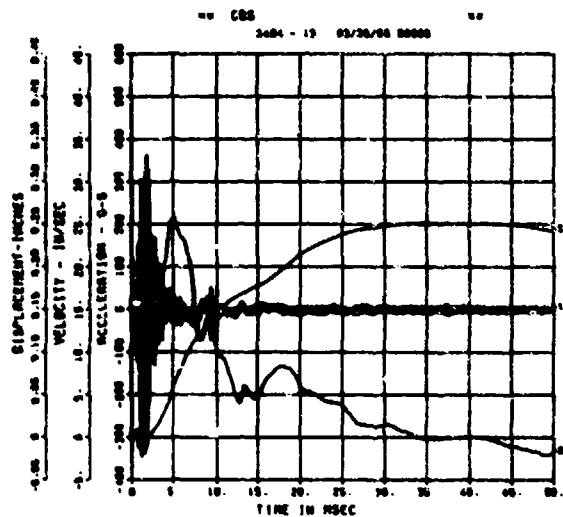
SPALL TEST 6A
AMHM
200000. HZ CAL= 25189.



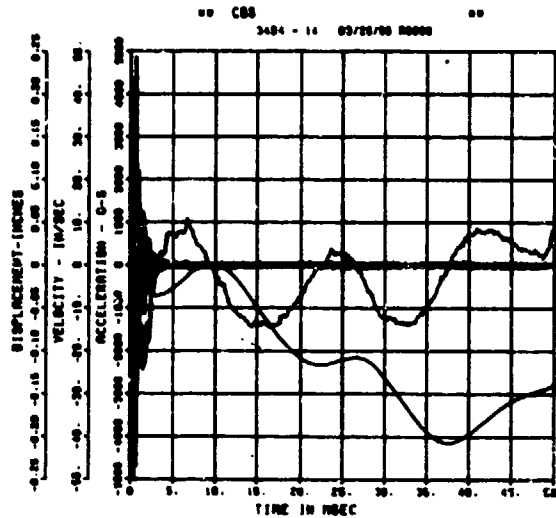
SPALL TEST 6A
ARV
200000. HZ CAL= 1105.



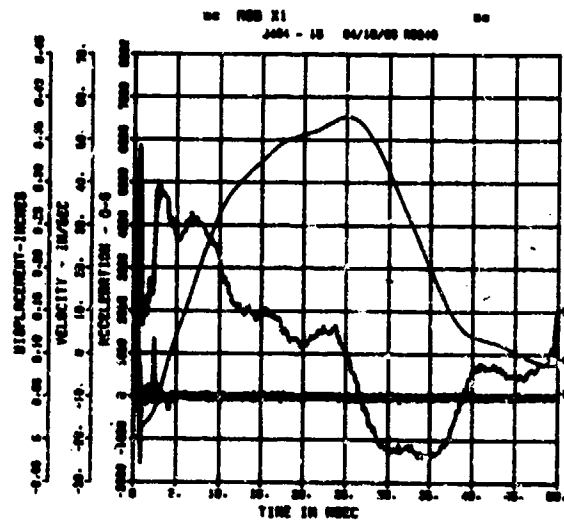
SPALL TEST 6A
ARH
200000. HZ CAL= 580.4



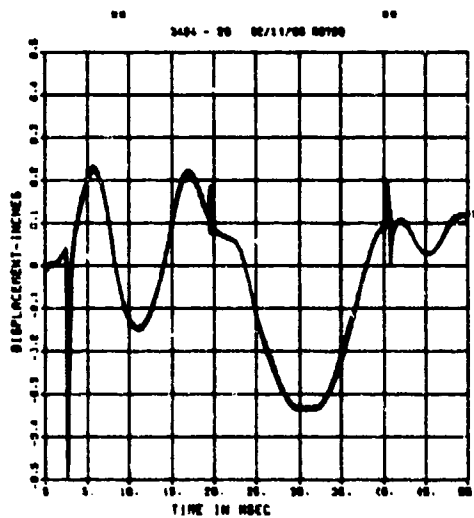
SPALL TEST 6A
AFV
200000. HZ CAL= 9259.



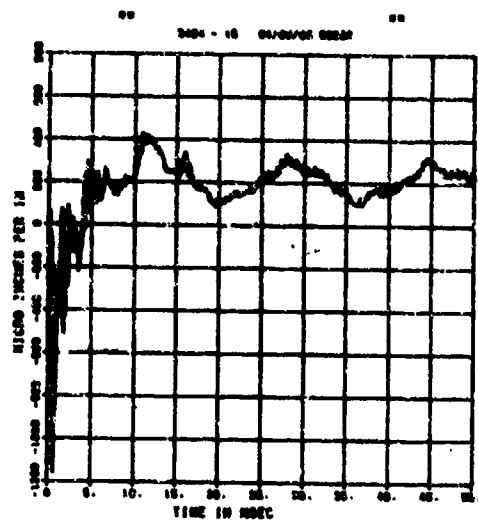
SPALL TEST 6A
AFH
200000. HZ CAL= 10167.



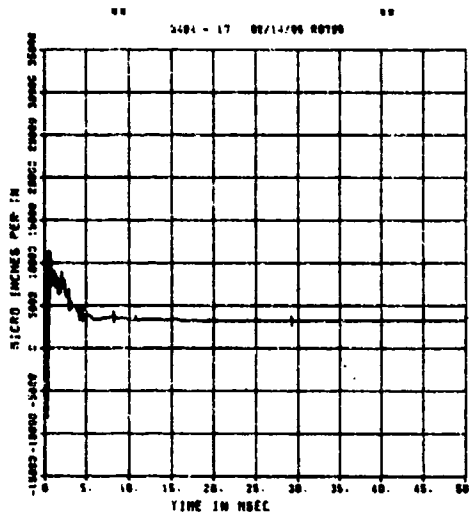
SPALL TEST 6A
DM
200000. HZ CAL= 0.431



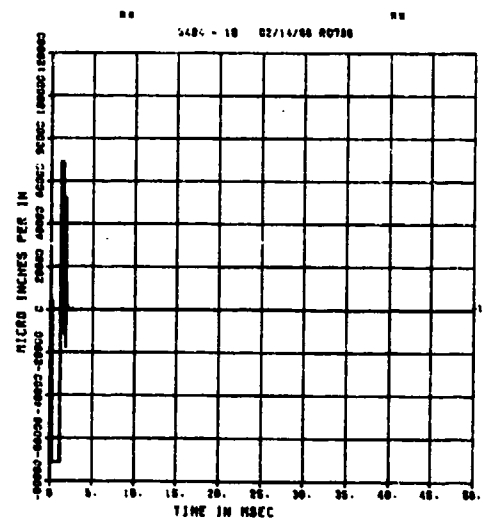
SPALL TEST 6A
EIT
200000. HZ CAL= 5004.
LPA/S 70X CUTOFF= 9000. HZ



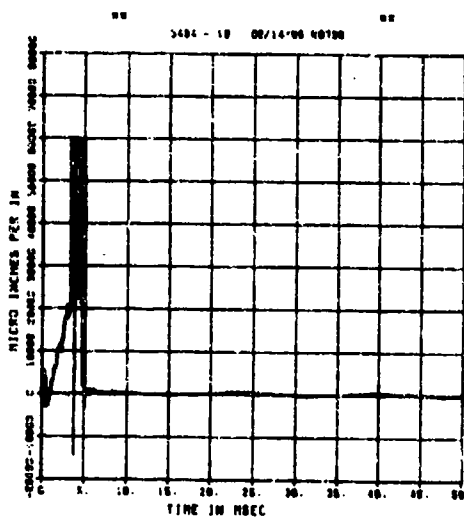
SPALL TEST 6A
EIM
200000. HZ CAL= 5636.



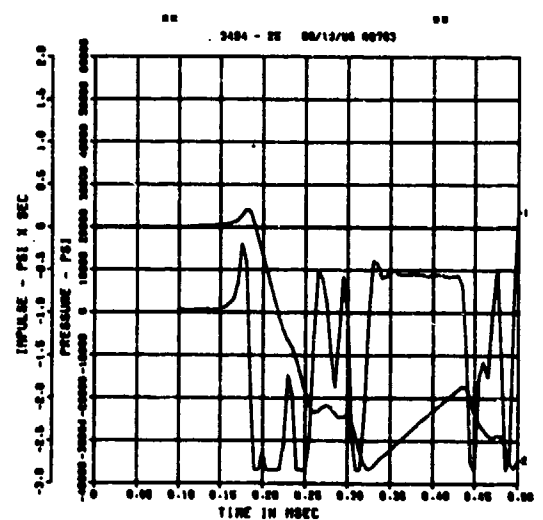
SPALL TEST 6A
EOB
200000. HZ CAL= 35703.



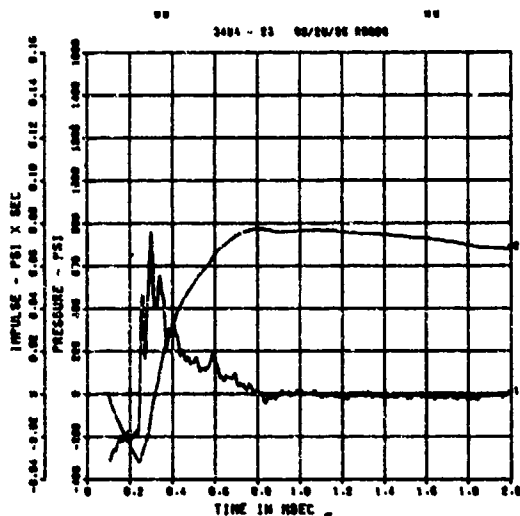
SPALL TEST 6A
EIB
200000. HZ CAL= 30324.



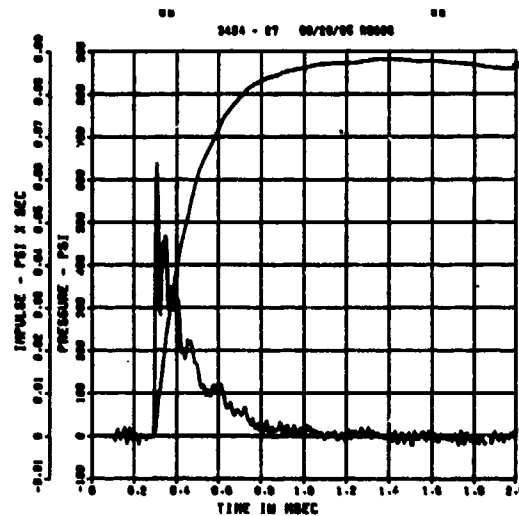
SPALL TEST 6B
PQ-1
200000. HZ CAL= 18232.



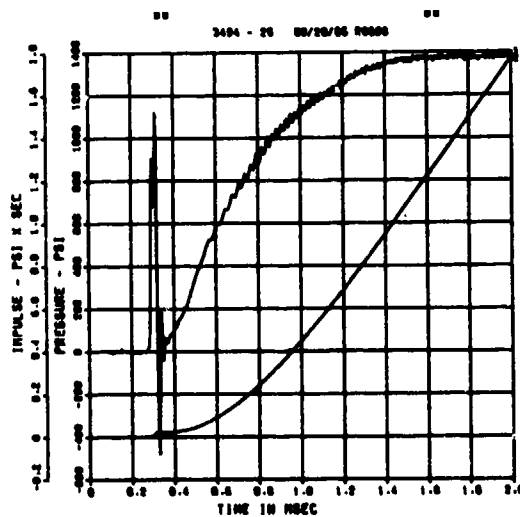
SPALL TEST 6B
PM-0
200000. HZ CAL= 3008.



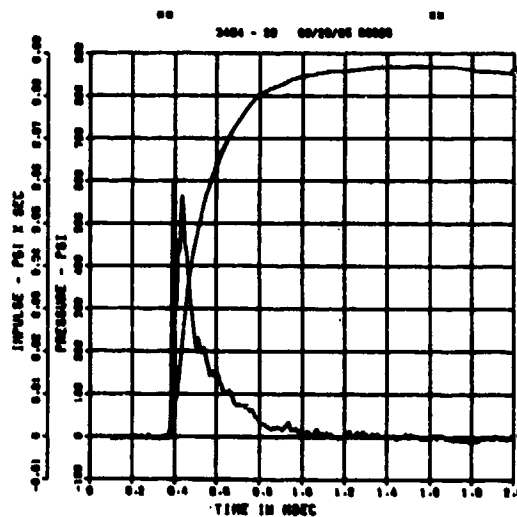
SPALL TEST 6B
PM-1
200000. HZ CAL= 2663.



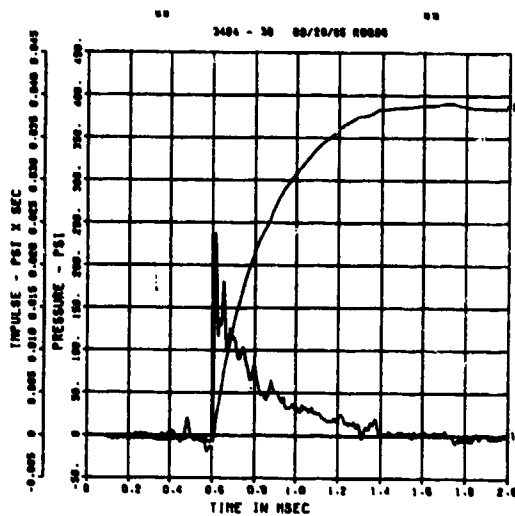
SPALL TEST 6B
PM-2
200000. HZ CAL= 1981.



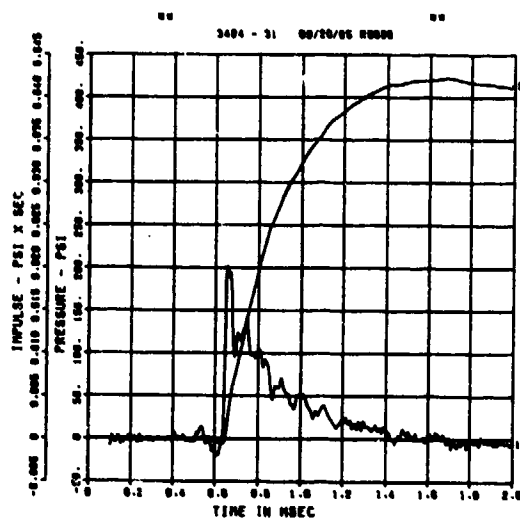
SPALL TEST 6B
PM-3
200000. HZ CAL= 1248.



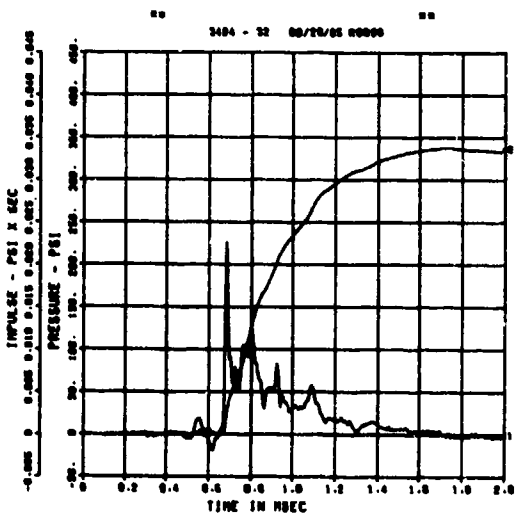
SPALL TEST 6B
PT-0
200000. HZ CAL= 936.0



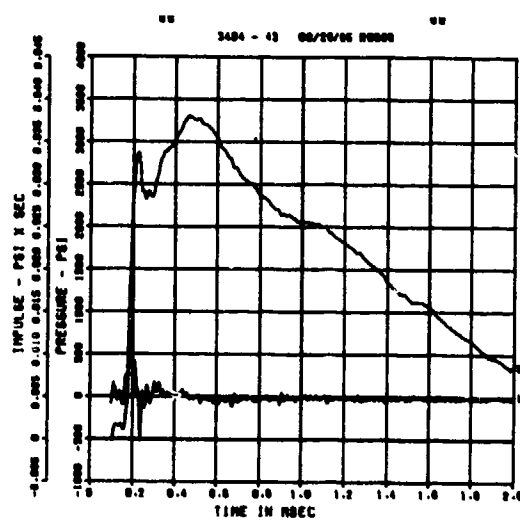
SPALL TEST 6B
PT-2
200000. HZ CAL= 713.7



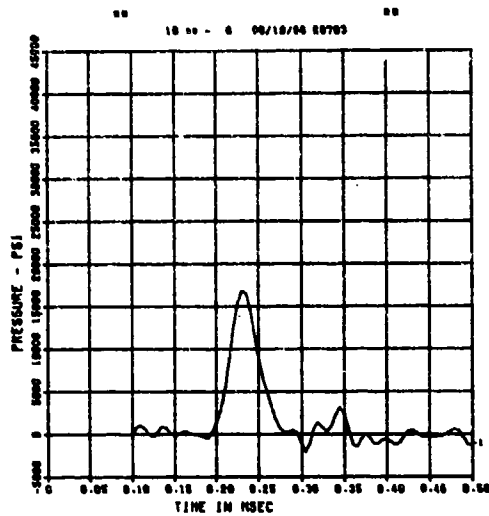
SPALL TEST 6B
PT-3
200000. HZ CAL= 505.3



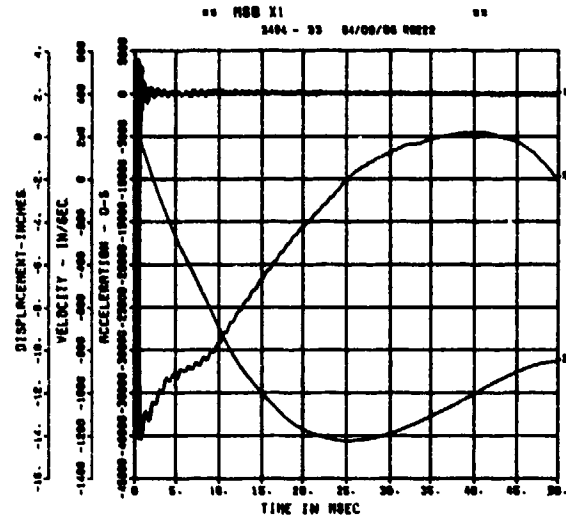
SPALL TEST 6B
BP-B
200000. HZ CAL= 4794.



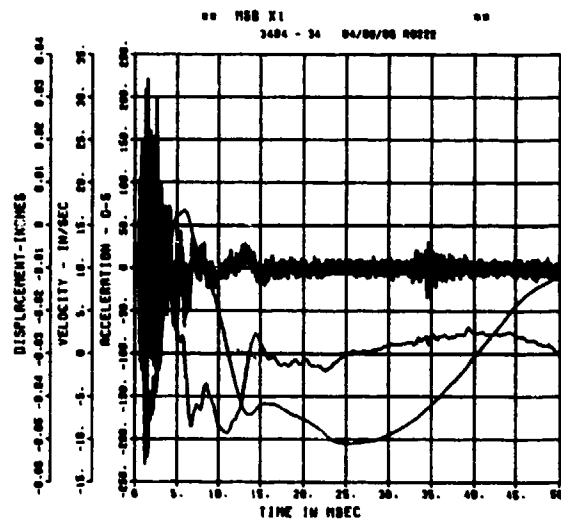
SPALL TEST 6B
 FP-B
 200000. HZ CAL= -0.045



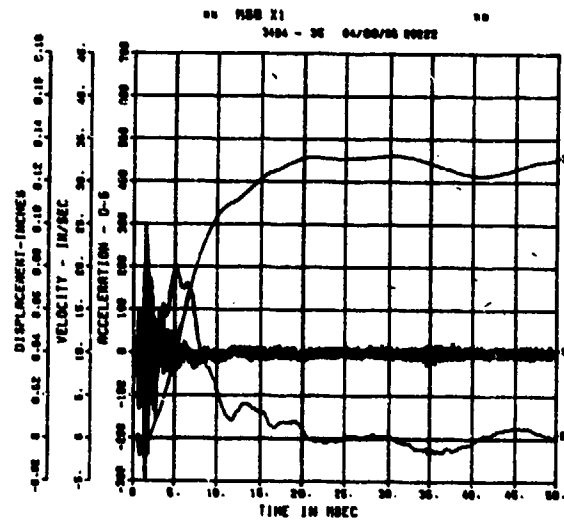
SPALL TEST 6B
 AWHM
 200000. HZ CAL= 23673.



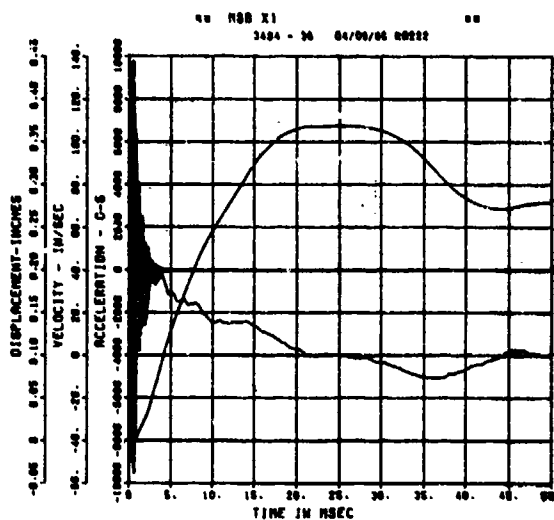
SPALL TEST 6B
 ARV
 200000. HZ CAL= 1211.



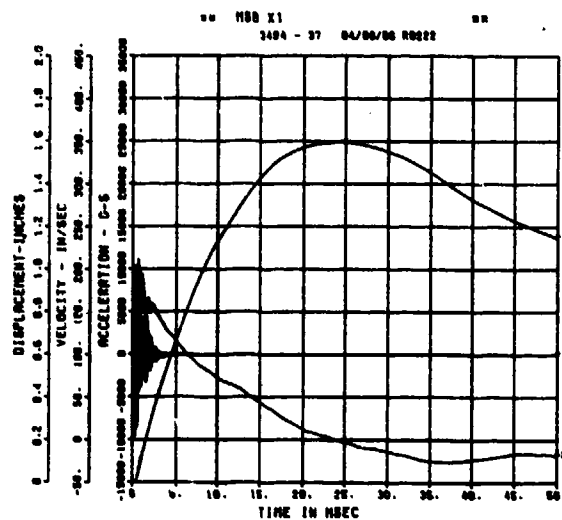
SPALL TEST 6B
 ARH
 200000. HZ CAL= 1228.



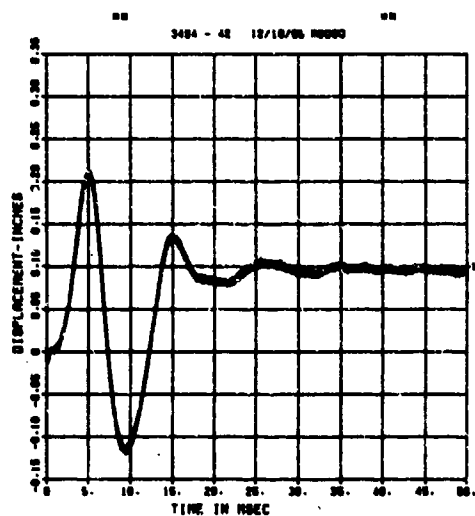
SPALL TEST 6B
AFV
200000. HZ CAL= 4963.



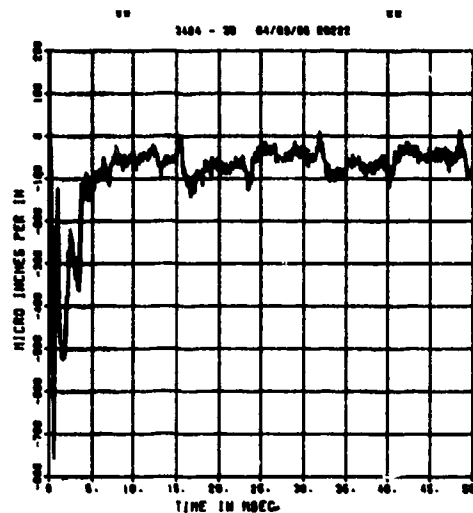
SPALL TEST 6B
AFH
200000. HZ CAL= 5624.



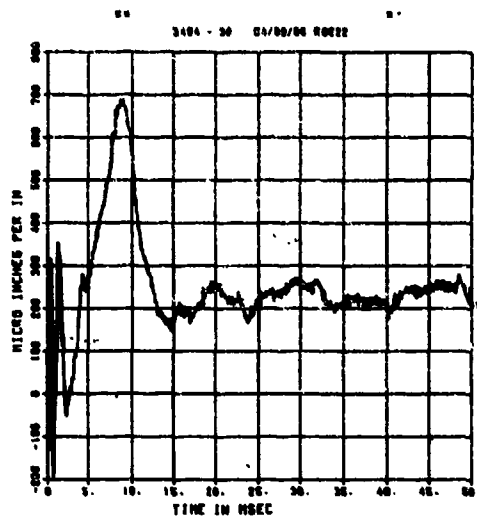
SPALL TEST 6B
DM
200000. HZ CAL= 0.435



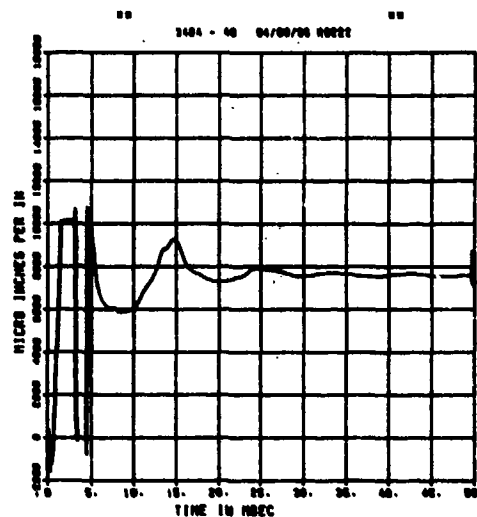
SPALL TEST 6B
EIT
200000. HZ CAL= 5004.
LP4/D 70X CUTOFF= 9000. HZ



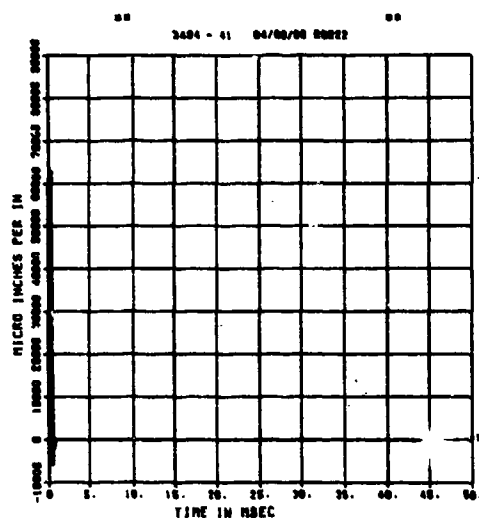
SPALL TEST 6B
EOM
200000. HZ CAL= 3022.
LP4/O 70% CUTOFF= 9000. HZ



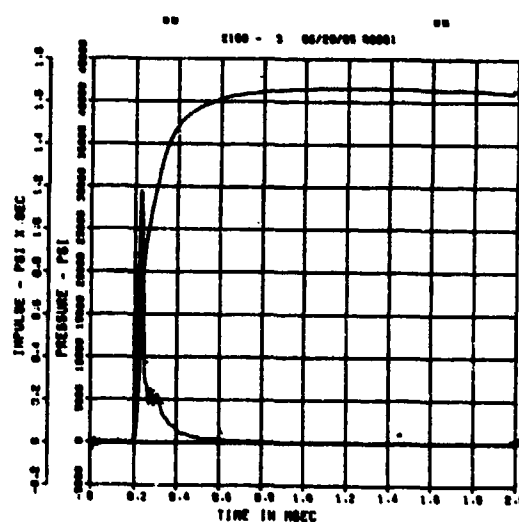
SPALL TEST 6B
EIM
200000. HZ CAL= 5004.
LP4/O 70% CUTOFF= 9000. HZ



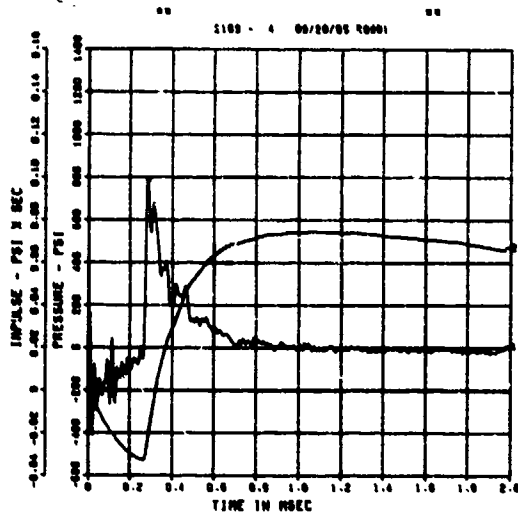
SPALL TEST 6B
EOB
200000. HZ CAL= 30324.
LP4/O 70% CUTOFF= 9000. HZ



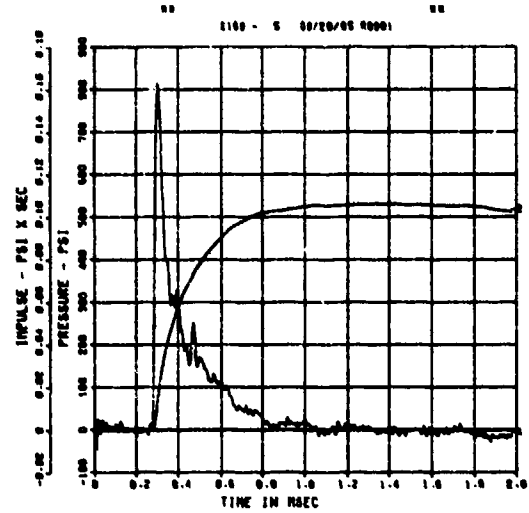
SPALL TEST 7A
PQ-2
200000. HZ CAL= 14595.



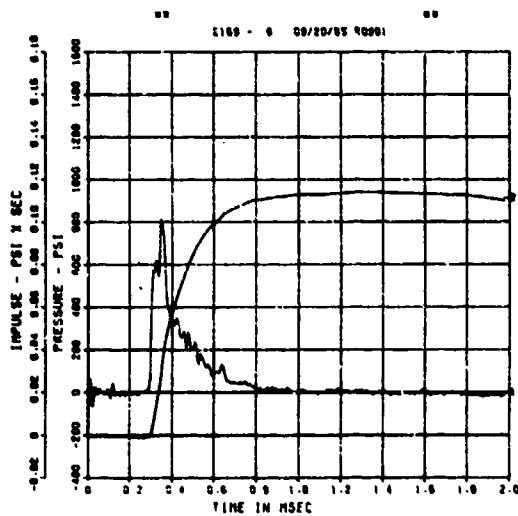
SPALL TEST 7A
PM-0
200000. HZ CAL= 3008.



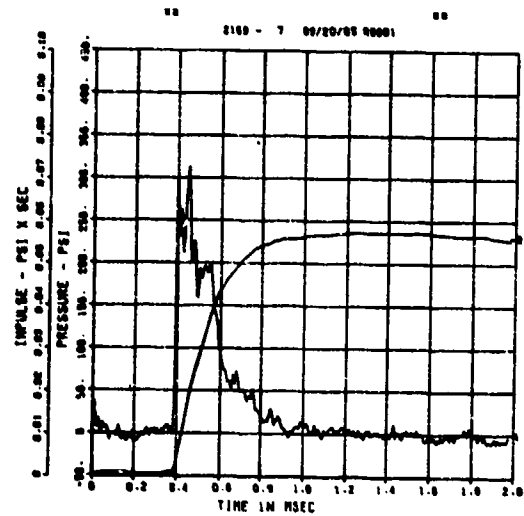
SPALL TEST 7A
PM-1
200000. HZ CAL= 2663.



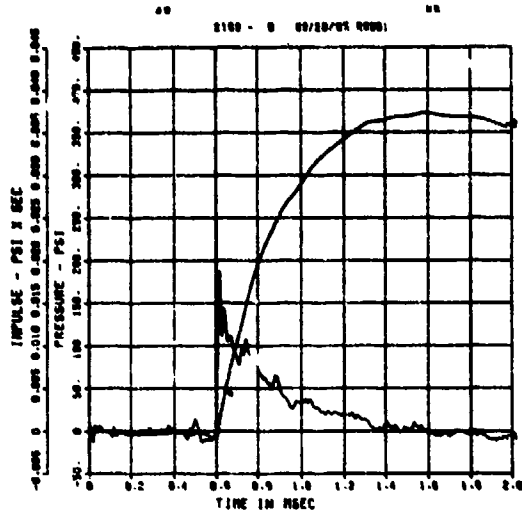
SPALL TEST 7A
PM-2
200000. HZ CAL= 1981.



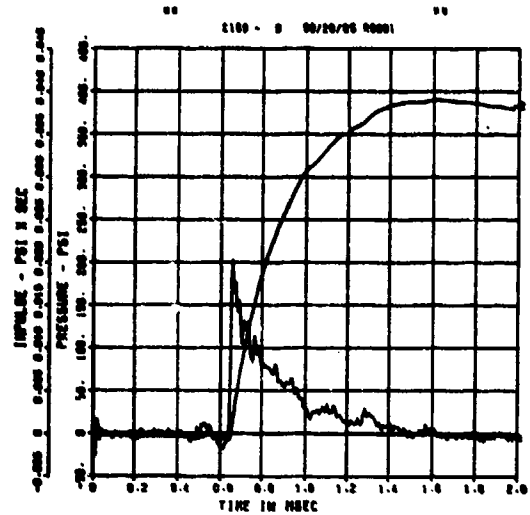
SPALL TEST 7A
PM-3
200000. HZ CAL= 1448.



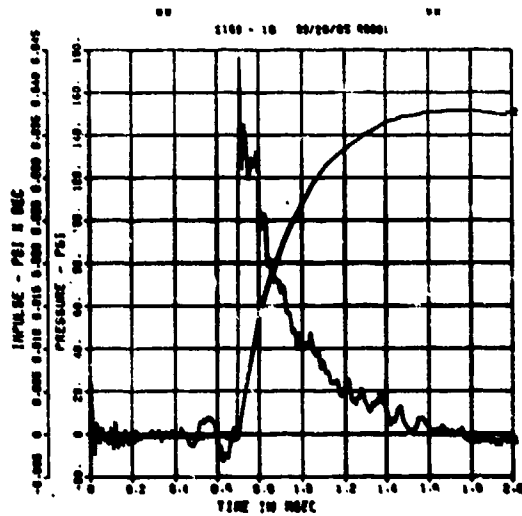
SPALL TEST 7A
PT-0
200000. HZ CAL= 831.3



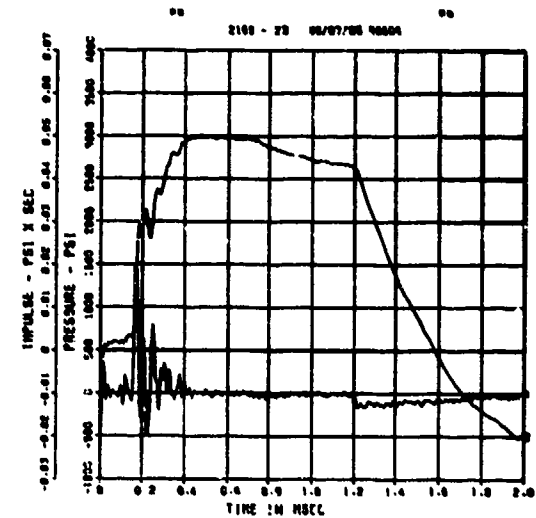
SPALL TEST 7A
PT-2
200000. HZ CAL= 838.6



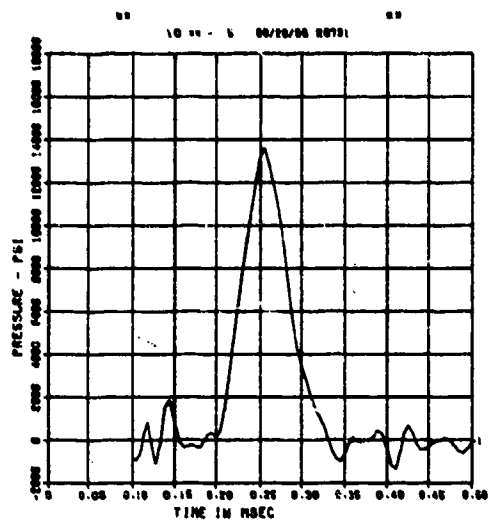
SPALL TEST 7A
PT-3
200000. HZ CAL= 533.4



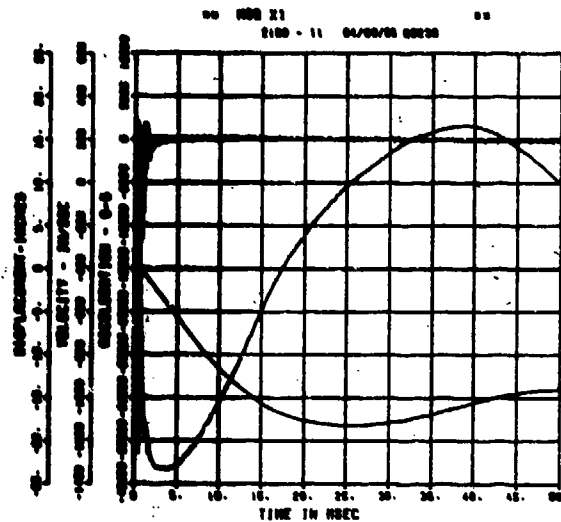
SPALL TEST 7A
BP-A
200000. HZ CAL= 6356.



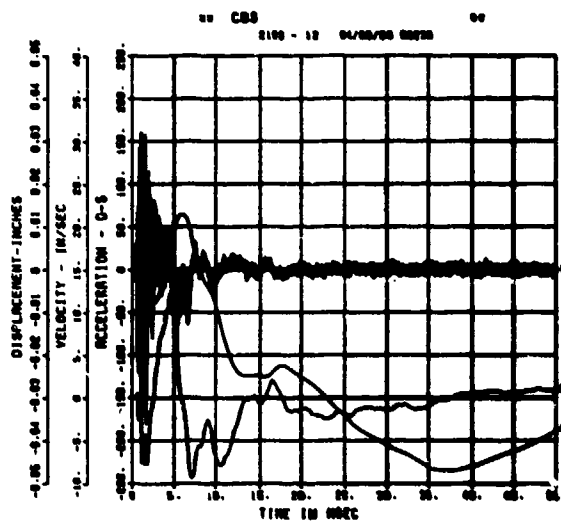
SPALL TEST 7A
 FP-A
 200000. HZ CAL= -0.055



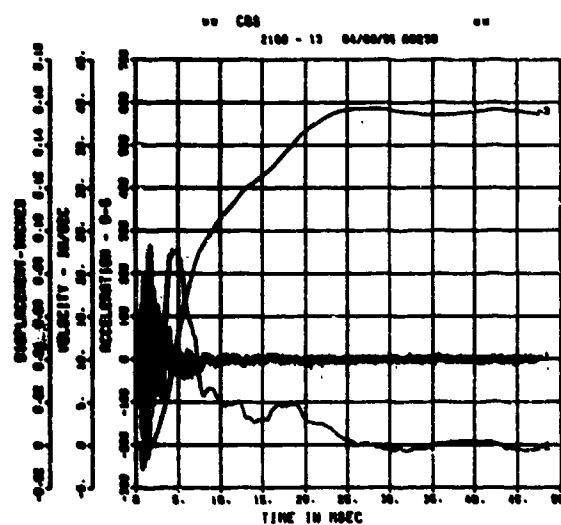
SPALL TEST 7A
 AWHM
 200000. HZ CAL= 25189.



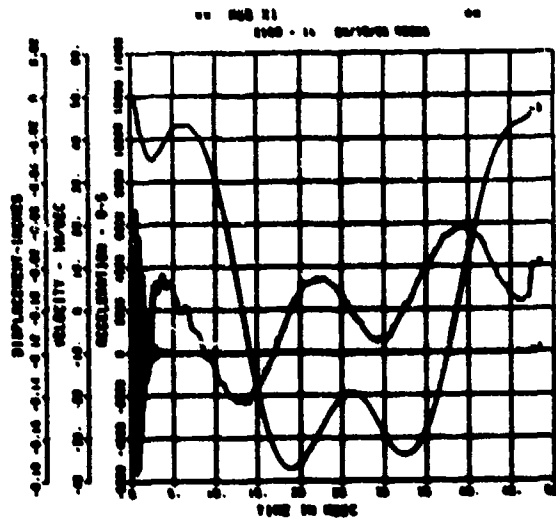
SPALL TEST 7A
 ARV
 200000. HZ CAL= 1105.



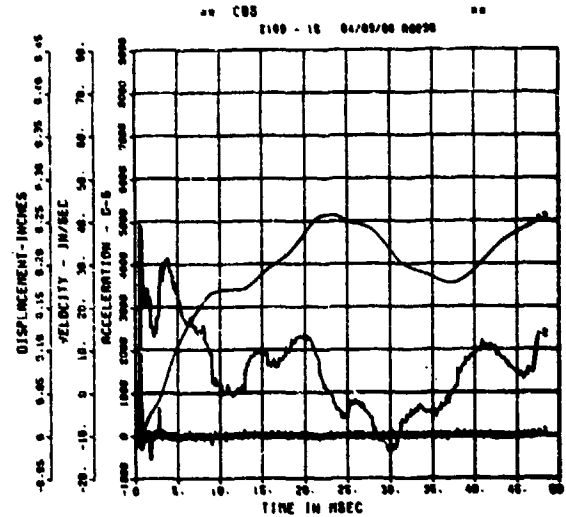
SPALL TEST 7A
 ARH
 200000. HZ CAL= 942.7



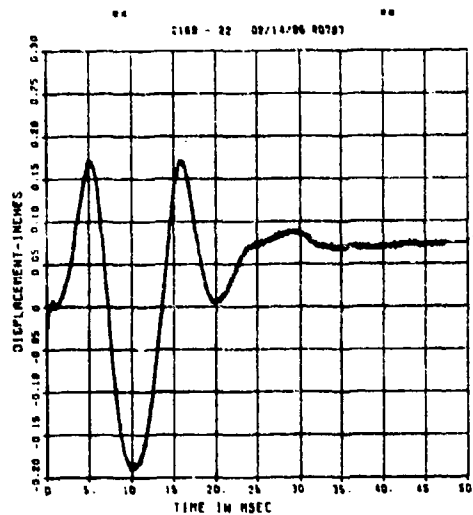
SPALL TEST 7A
AFV
200000. HZ CAL= 6259.



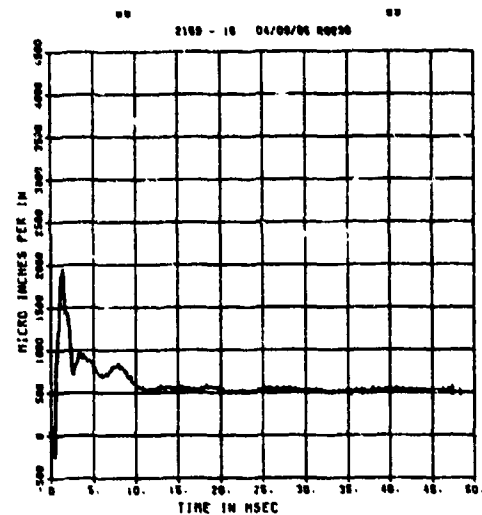
SPALL TEST 7A
AFH
200000. HZ CAL= 10167.



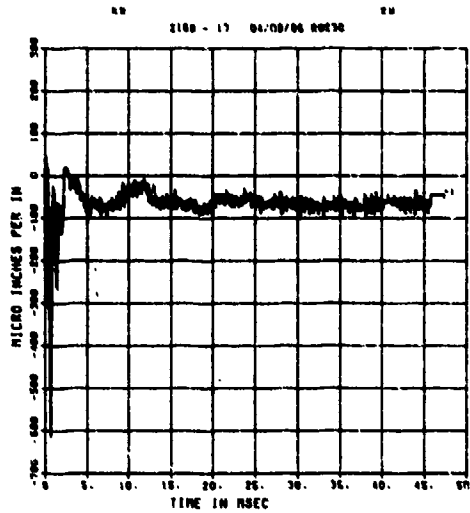
SPALL TEST 7A
DM
200000. HZ CAL= 0.431



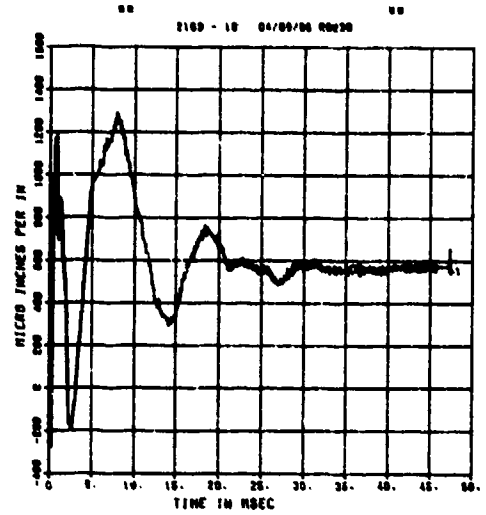
SPALL TEST 7A
EOT
200000. HZ CAL= 7469.
LP4/0 70% CUTOFF= 9000. HZ



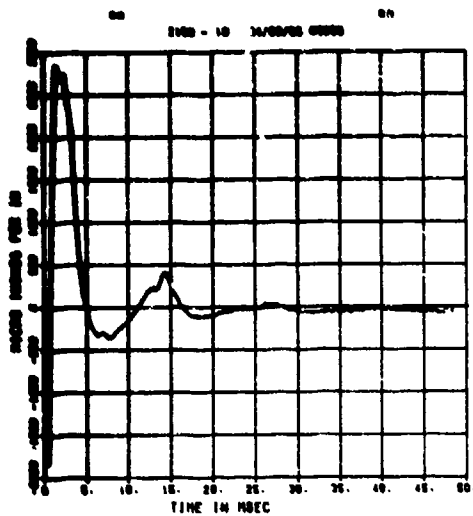
SPALL TEST 7A
EIT
200000. HZ CAL= 5004.
LP4/0 70% CUTOFF= 9000. HZ



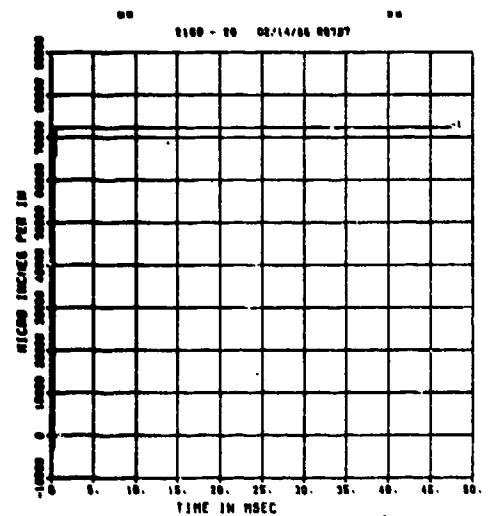
SPALL TEST 7A
EOM
200000. HZ CAL= 5004.
LP4/0 70% CUTOFF= 9000. HZ



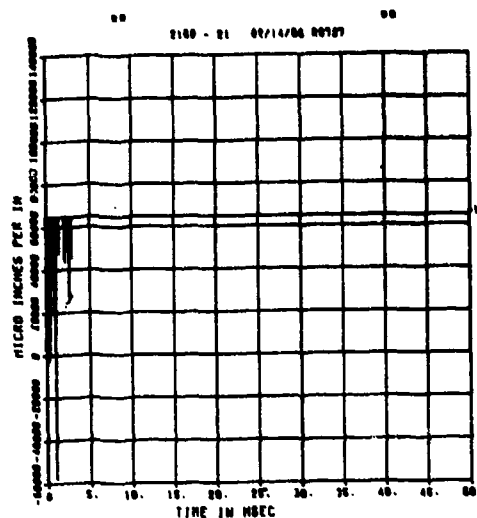
SPALL TEST 7A
EIM
200000. HZ CAL= 5636.
LP4/0 70% CUTOFF= 9000. HZ



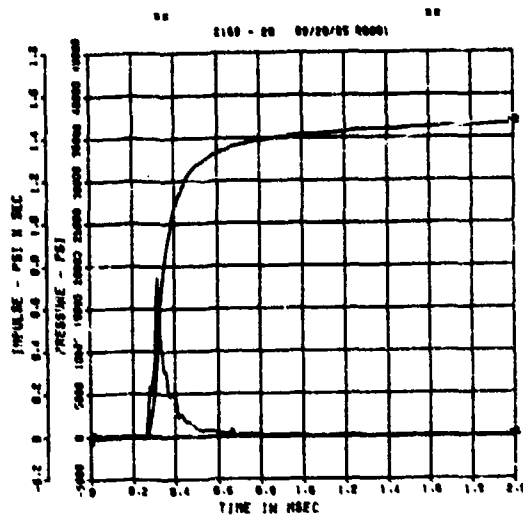
SPALL TEST 7A
EOM
200000. HZ CAL= 35703.



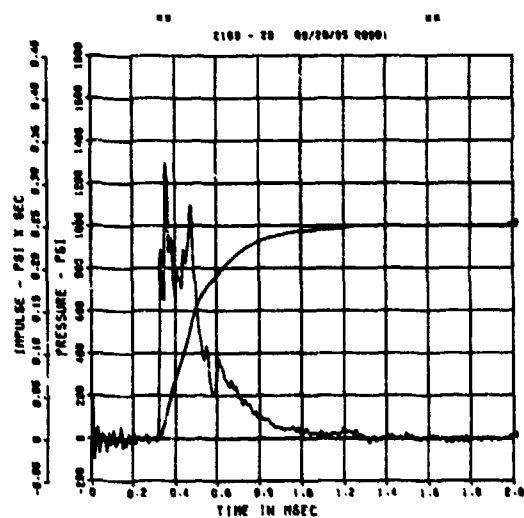
SPALL TEST 7A
E1B
200000. HZ CAL= 30324.



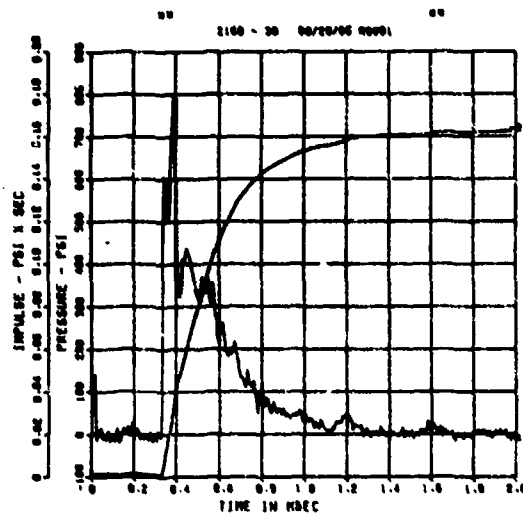
SPALL TEST 7B
PQ-2
200000. HZ CAL= 12586.



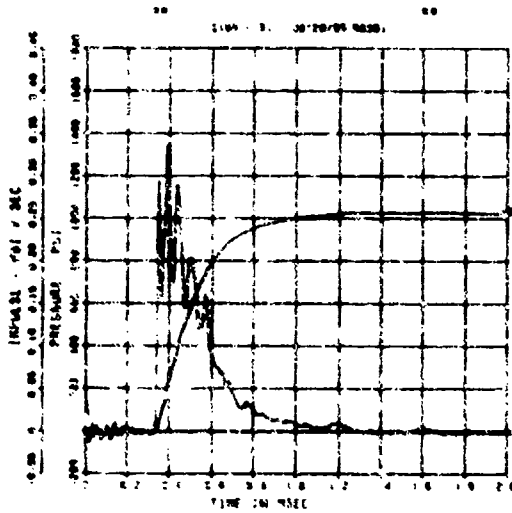
SPALL TEST 7B
PM-0
200000. HZ CAL= 4008.



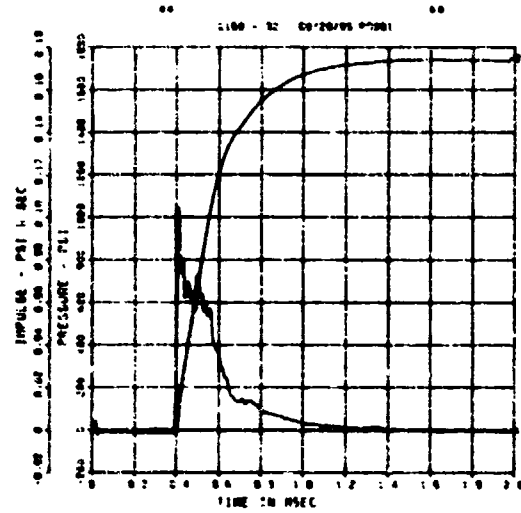
SPALL TEST 7B
PM-1
200000. HZ CAL= 3447.



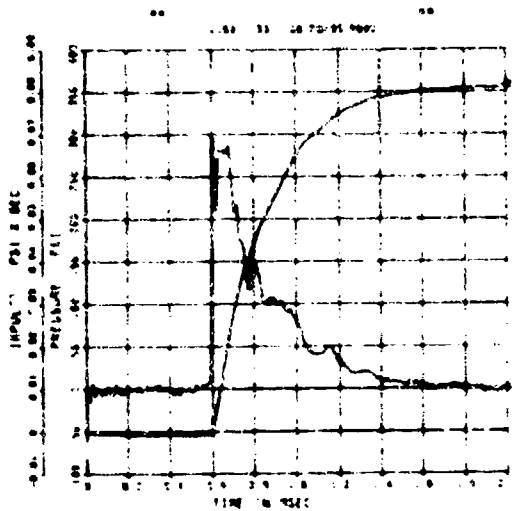
SPALL TEST 7B
PM-2
200000. HZ CAL= 2938.



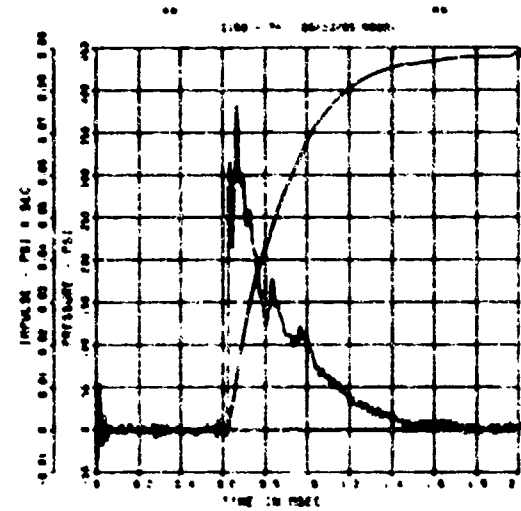
SPALL TEST 7B
PM-3
200000. HZ CAL= 1448.



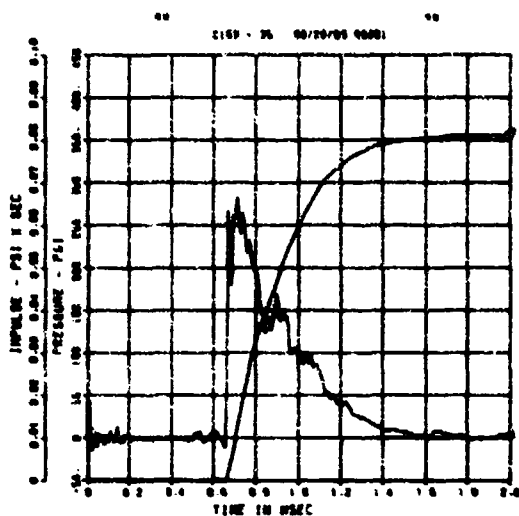
SPALL TEST 7B
PI-0
200000. HZ CAL= 294.5



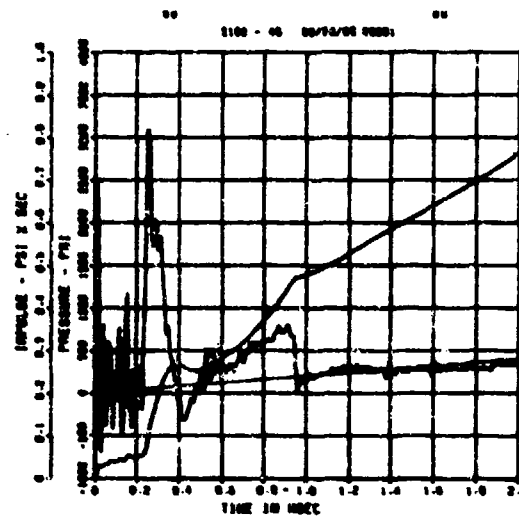
SPALL TEST 7B
PI-2
200000. HZ CAL= 213.7



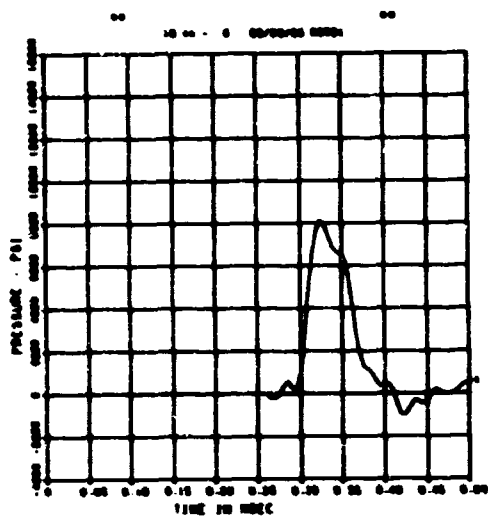
SPALL TEST 7B
PT-3
200000. HZ CAL= 533.4



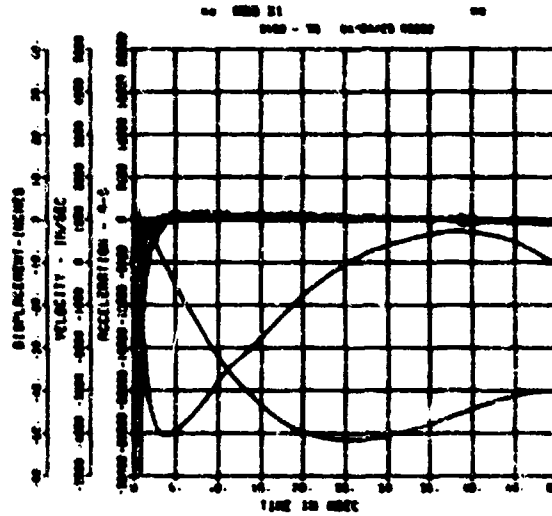
SPALL TEST 7B
BP-6
200000. HZ CAL= 7303.



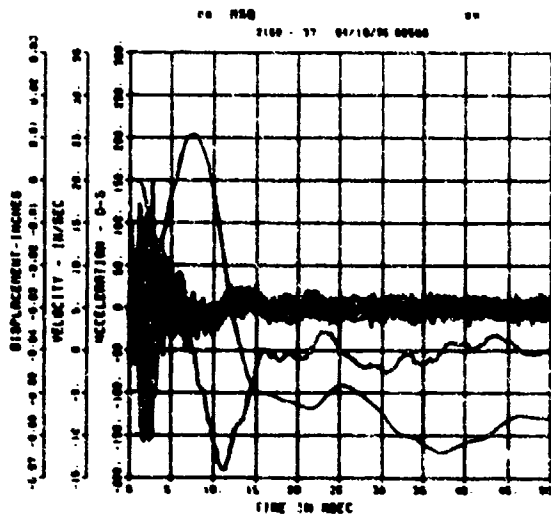
SPALL TEST 7B
FP-8
200000. HZ CAL= -0.055



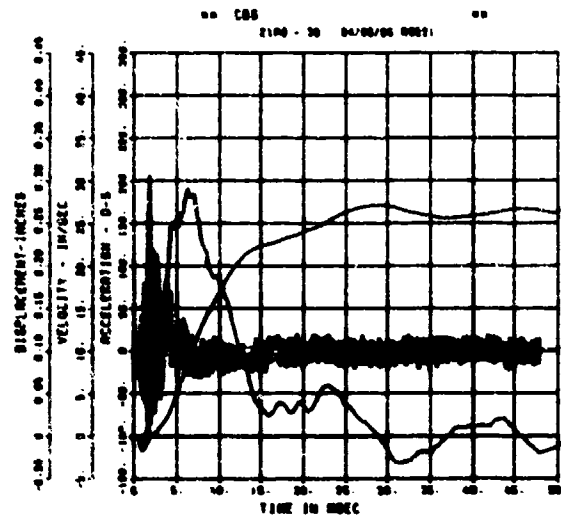
SPALL TEST 7B
AMMR
200000. HZ CAL= 26659.



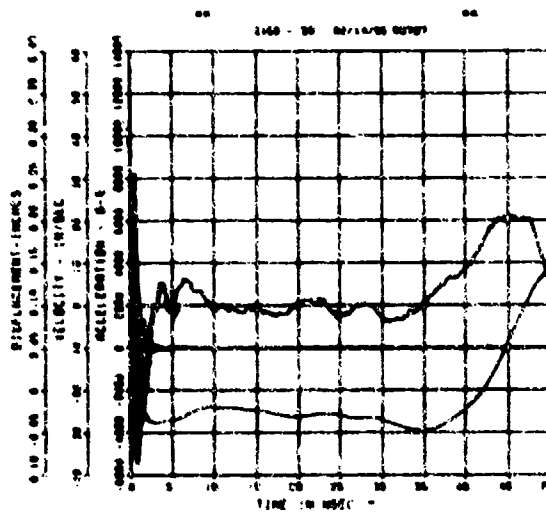
SPALL TEST 7B
ARV
200000. HZ CAL= 1807.



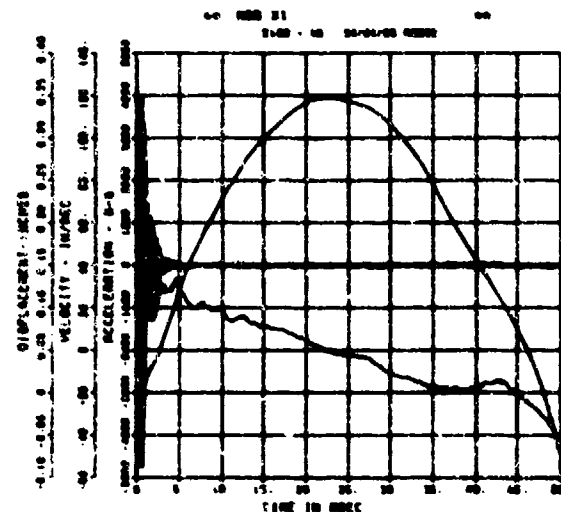
SPALL TEST 7B
ARM
200000. HZ CAL= 1832.



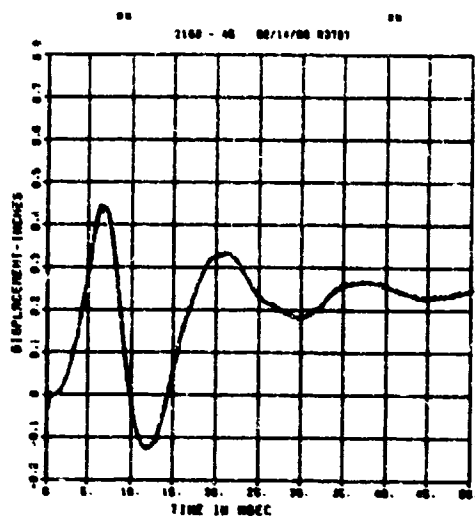
SPALL TEST 7B
AFV
200000. HZ CAL= 6396.



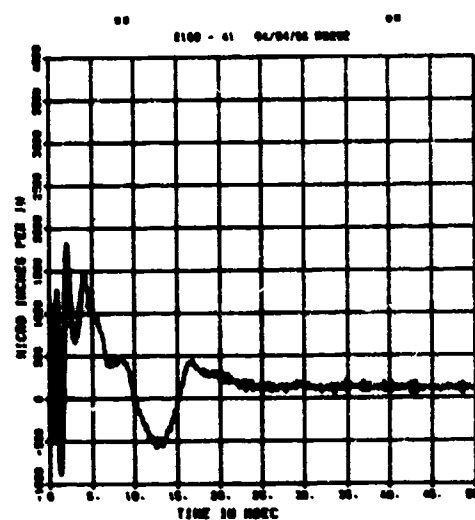
SPALL TEST 7B
AFH
200000. HZ CAL= 7036.



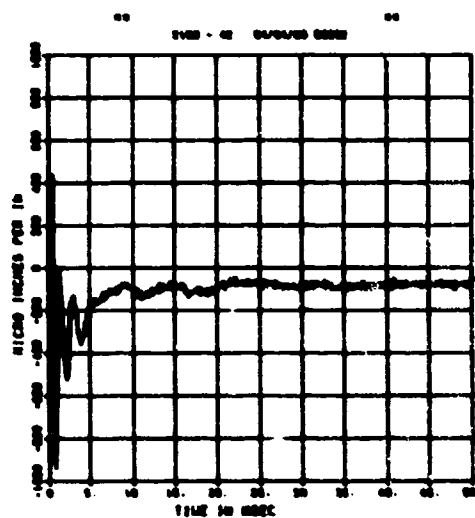
SPALL TEST 7B
DM
200000. HZ CAL= 0.435



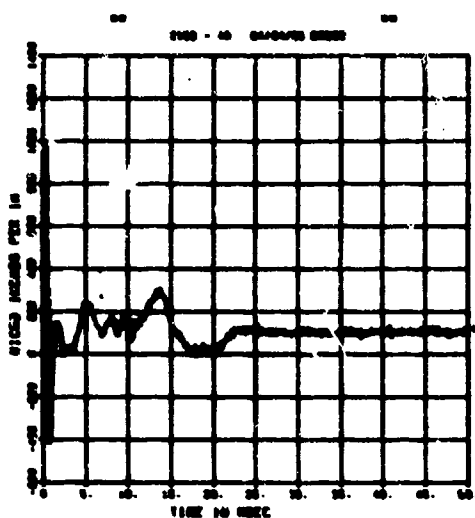
SPALL TEST 7B
EDT
200000. HZ CAL= 11175.
LP4/8 TOL CUTOFF= 5000. HZ



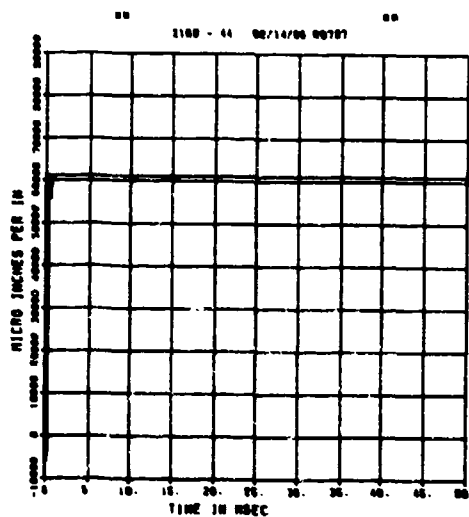
SPALL TEST 7B
EIT
200000. HZ CAL= 5004.
LP4/8 TOL CUTOFF= 5000. HZ



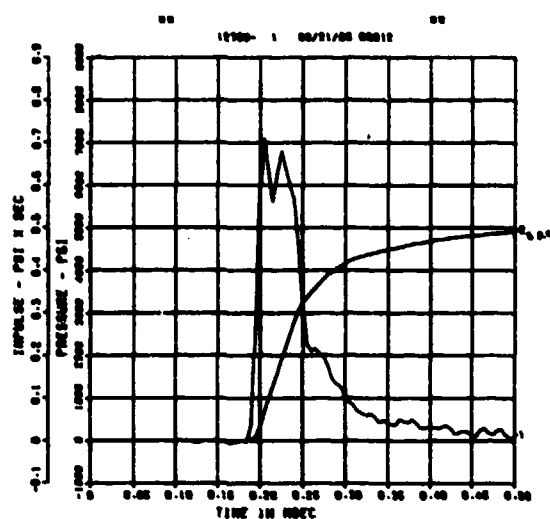
SPALL TEST 7B
EOM
200000. HZ CAL= 5004.
LP4/8 TOL CUTOFF= 5000. HZ



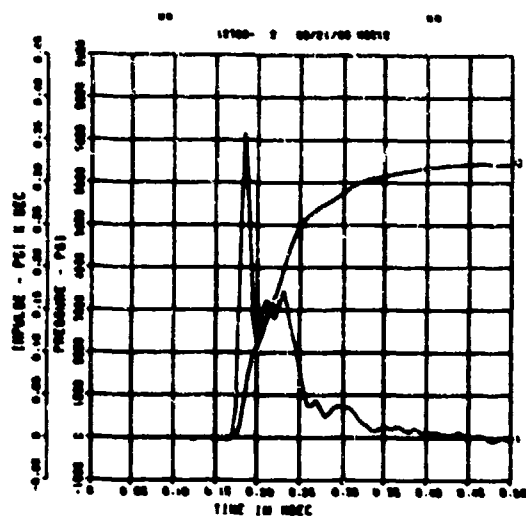
SPALL TEST 7B
 EOB
 200000. HZ CAL= 30324.



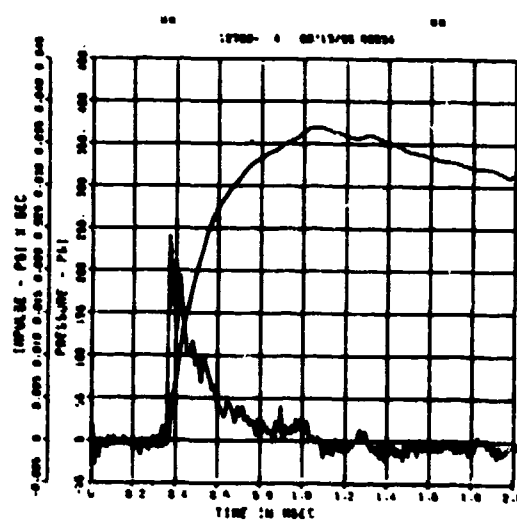
SPALL TEST 8A
 PQ-0
 200000. HZ CAL= 14725.



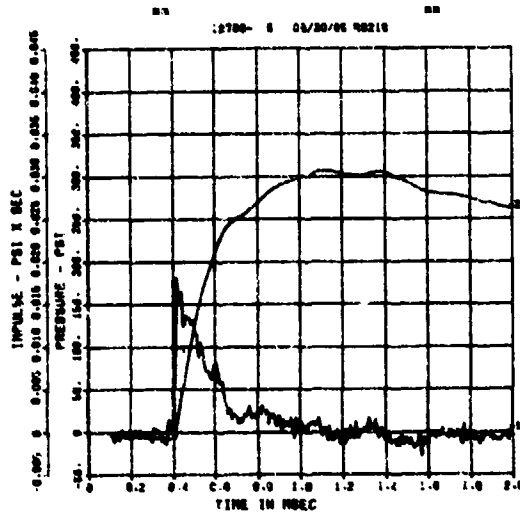
SPALL TEST 8A
 PQ-1
 200000. HZ CAL= 10544.



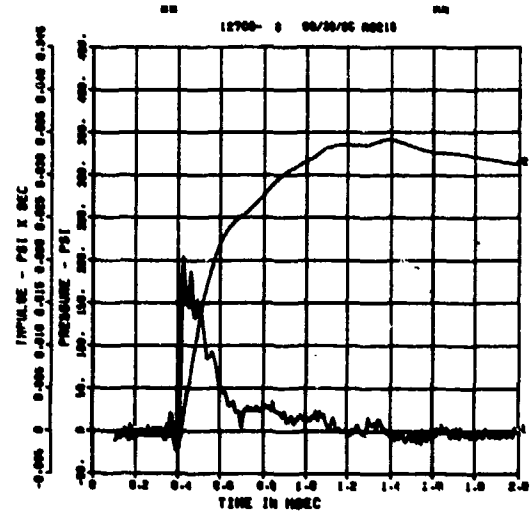
SPALL TEST 8A
 PM-0
 200000. HZ CAL= 3001.



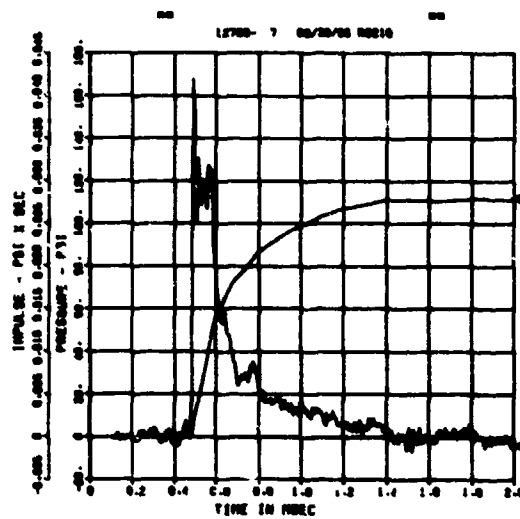
SPALL TEST 8A
PM-1
200000. HZ CAL= 2663.



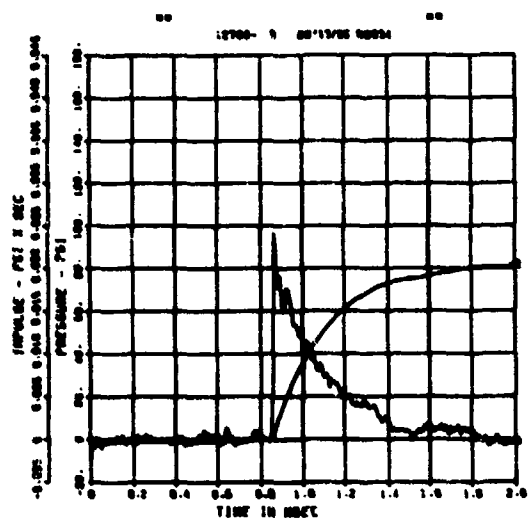
SPALL TEST 8A
PM-2
200000. HZ CAL= 1981.



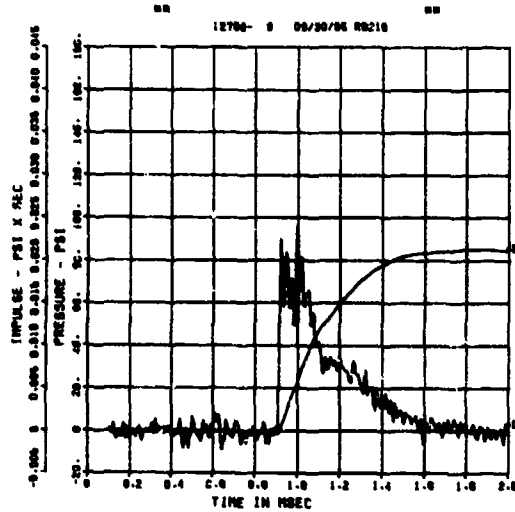
SPALL TEST 8A
PM-3
200000. HZ CAL= 1025.



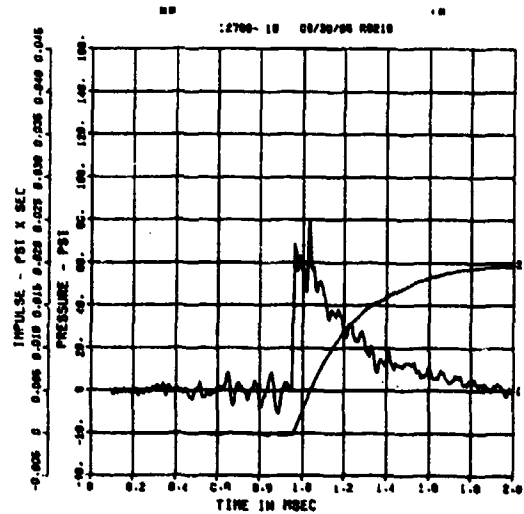
SPALL TEST 8A
PT-0
200000. HZ CAL= 593.0



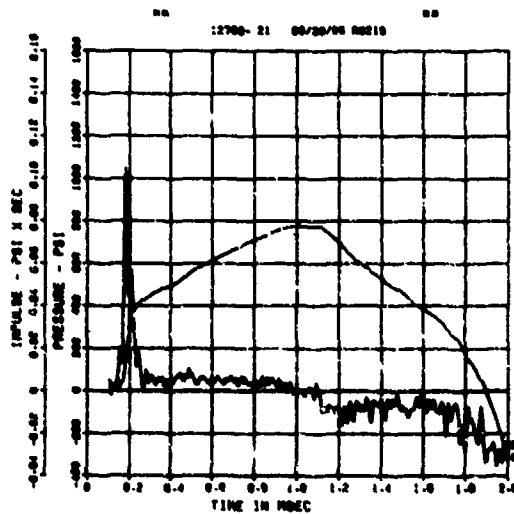
SPALL TEST 8A
PT-2
200000. HZ CAL= 512.0



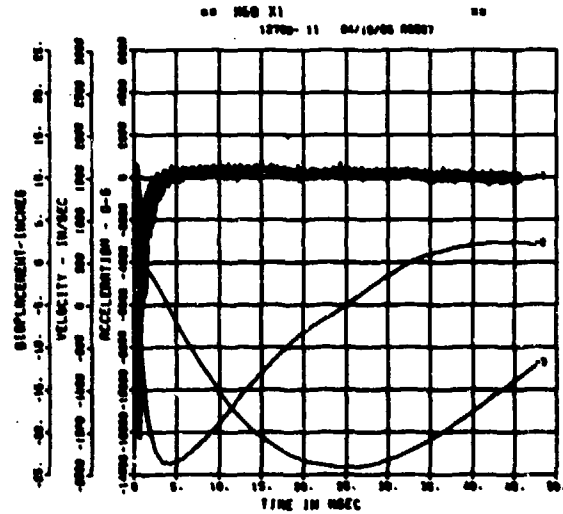
SPALL TEST 8A
PT-3
200000. HZ CAL= 405.0



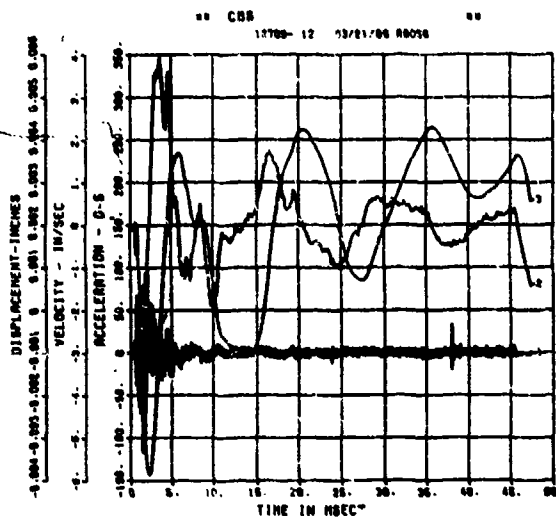
SPALL TEST 8A
BP-A
200000. HZ CAL= 6356.



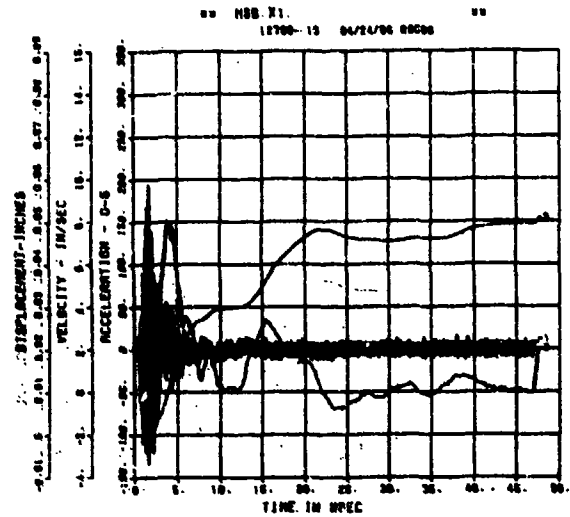
SPALL TEST 8A
AWHM
200000. HZ CAL= 34987.



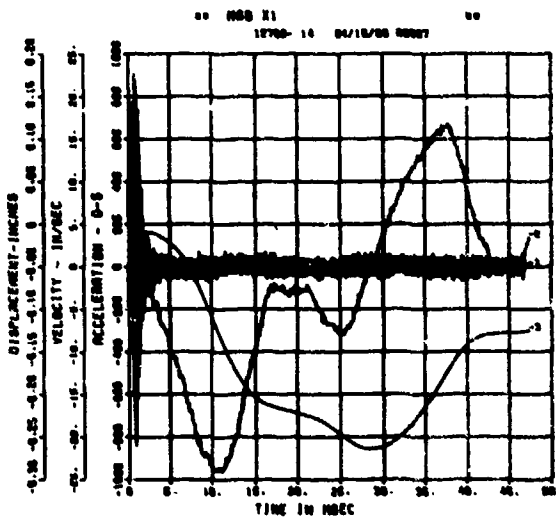
SPALL TEST 8A
ARV
200000. HZ CAL= 811.0



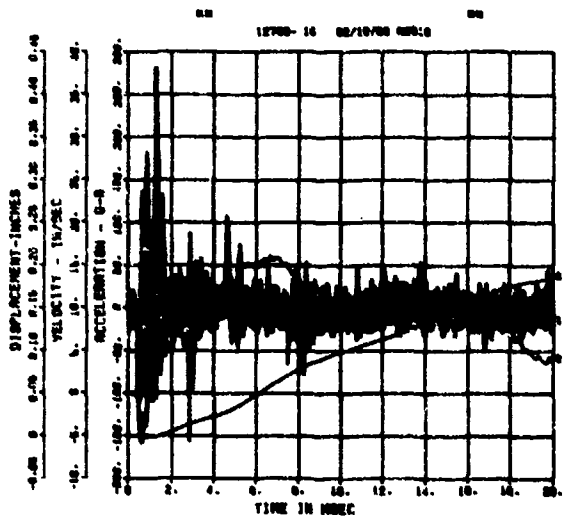
SPALL TEST 8A
ARRH
200000. HZ CAL= 1019.



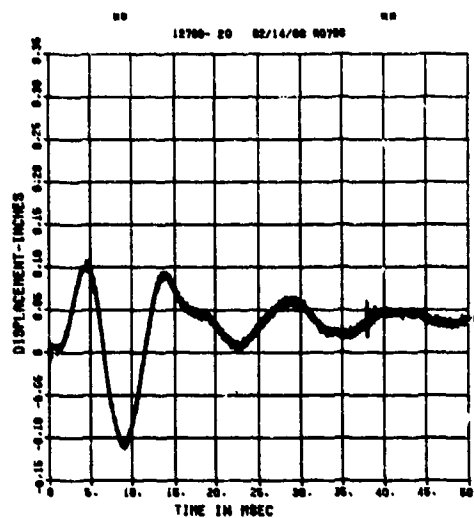
SPALL TEST 8A
AFV
200000. HZ CAL= 4966.



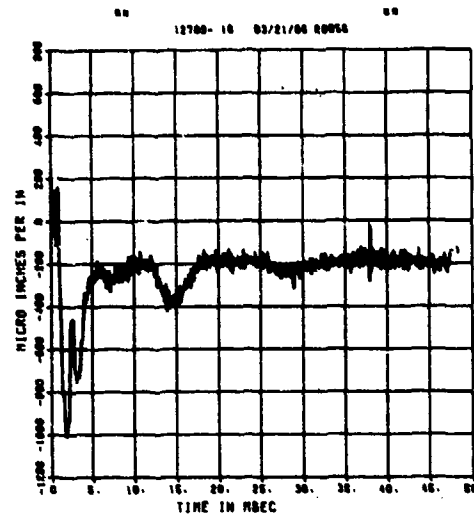
SPALL TEST 8A
AFH
200000. HZ CAL= 4944.



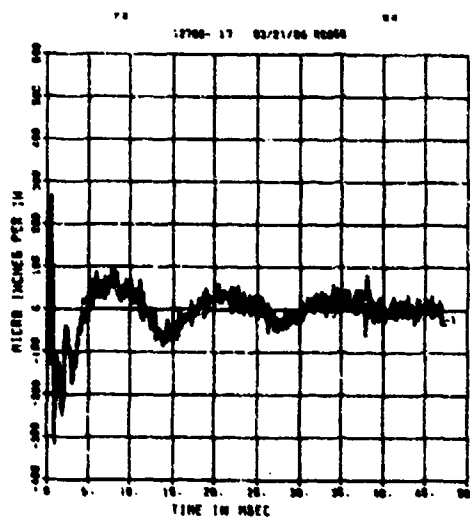
SPALL TEST 8A
DM
200000. HZ CAL= 0.715



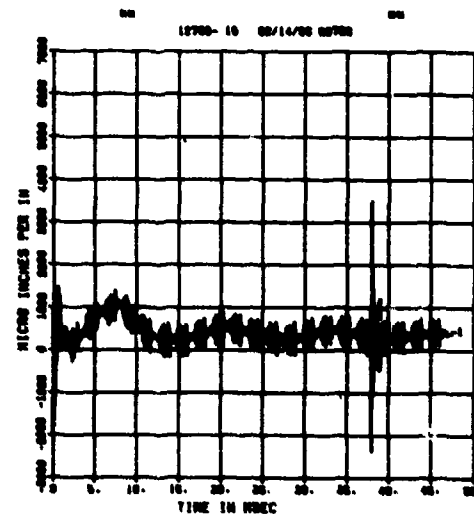
SPALL TEST 8A
EOT
200000. HZ CAL= 11176.
LP4/0 70K CUTOFF= 8000. HZ



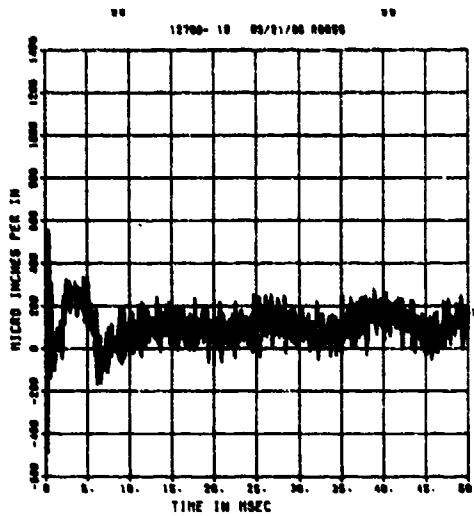
SPALL TEST 8A
EIT
200000. HZ CAL= 7469.
LP4/0 70K CUTOFF= 8000. HZ



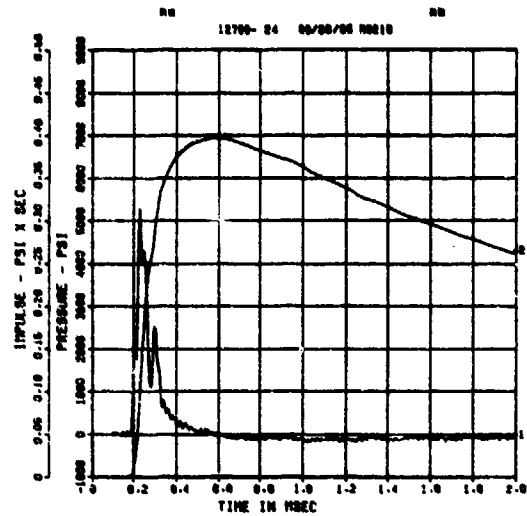
SPALL TEST 8A
EOM
200000. HZ CAL= 7469.



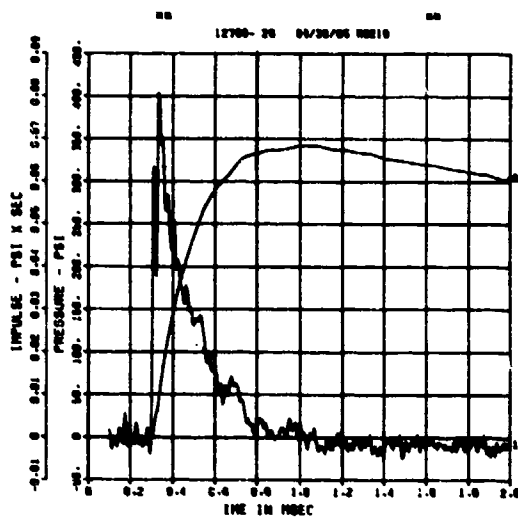
SPALL TEST 8A
E08
200000. HZ CAL= 31027.
LP4/0 70X CUTOFF= 9000. HZ



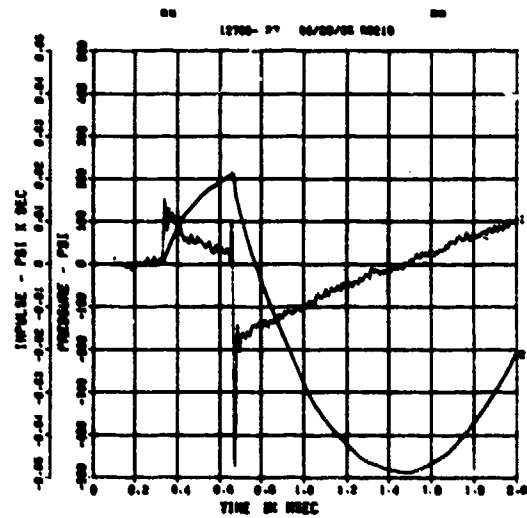
SPALL TEST 8B
PQ-2
200000. HZ CAL= 9965.



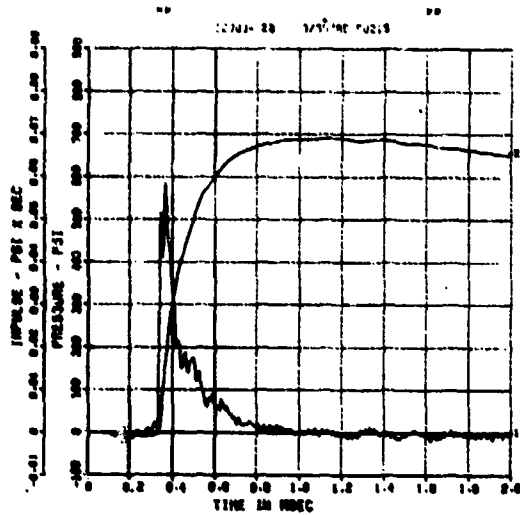
SPALL TEST 8B
PM-0
200000. HZ CAL= 2758.



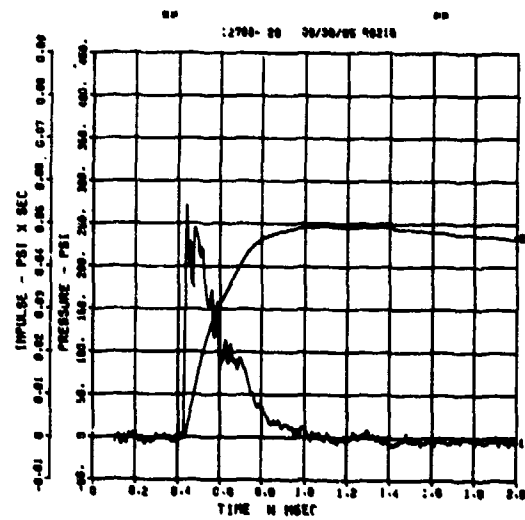
SPALL TEST 8B
PM-1
200000. HZ CAL= 2169.



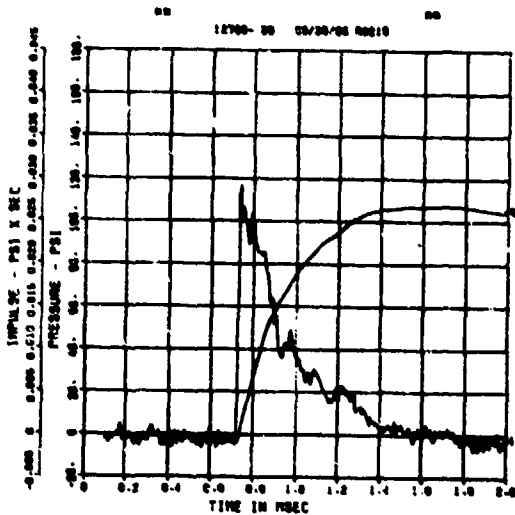
SPALL TEST 8B
PM-2
200000. HZ CAL= 128



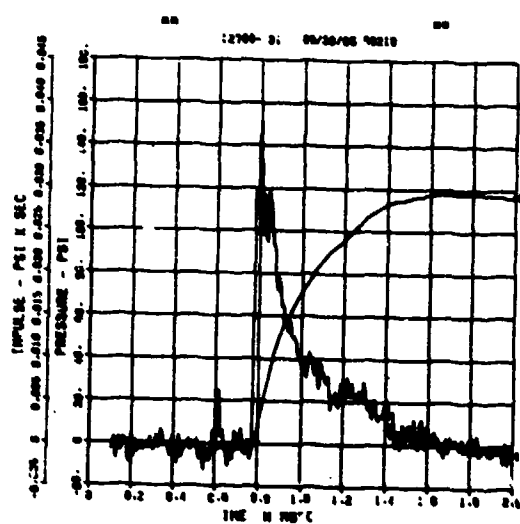
SPALL TEST 8B
PM-3
200000. HZ CAL= 1248.



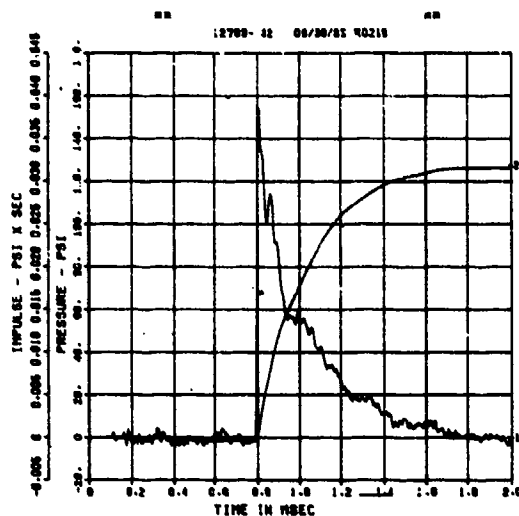
SPALL TEST 8B
PT-0
200000. HZ CAL= 88.7



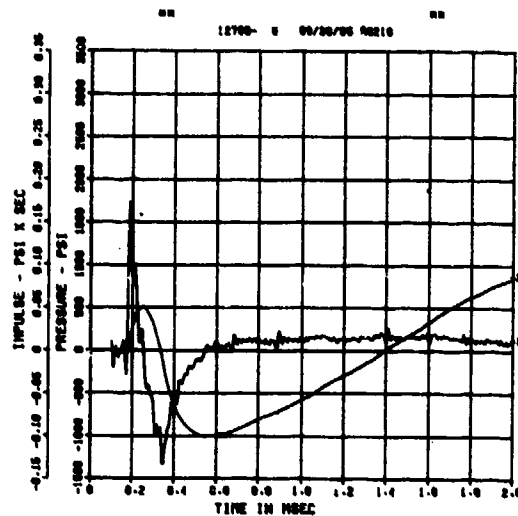
SPALL TEST 8B
PT-2
200000. HZ CAL= 38.5



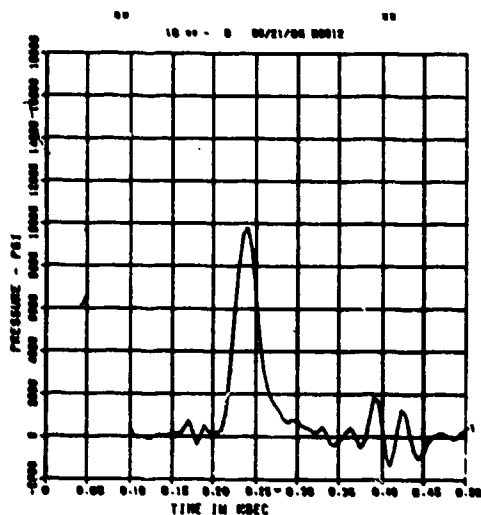
SPALL TEST 8B
PT-3
200000. HZ CR = 505.0



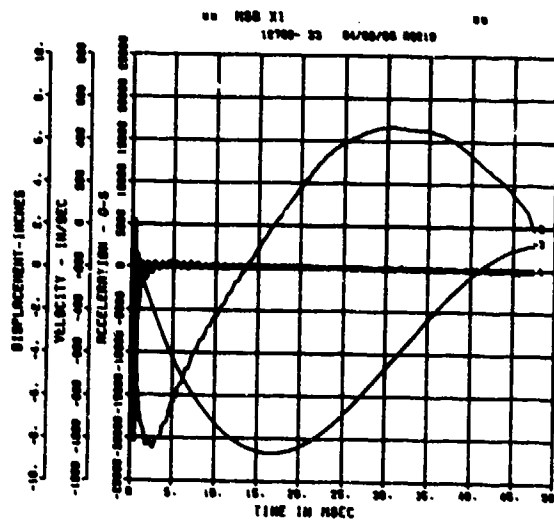
SPALL TEST 8B
BP-B
200000. HZ CAL = 3°58.



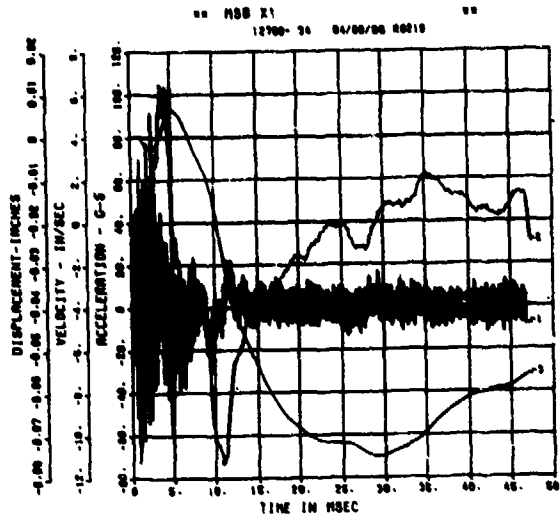
SPALL TEST 8B
FP-B
200000. HZ CAL = -0.055



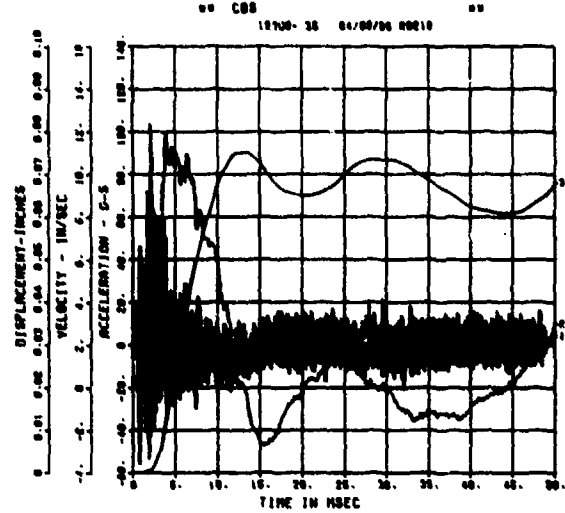
SPALL TEST 8B
AWHM
200000. HZ CAL = 34987.



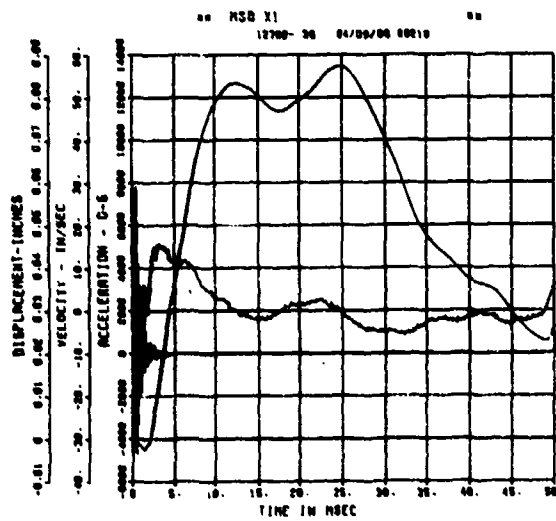
SPALL TEST 8B
ARV
200000. HZ CAL= 1211.



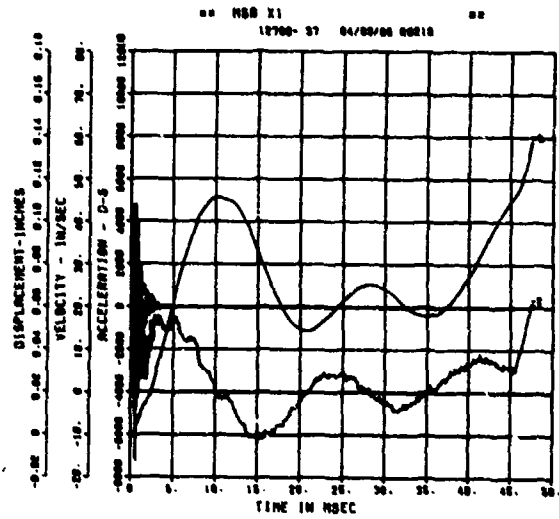
SPALL TEST 8B
ARM
200000. HZ CAL= 1228.



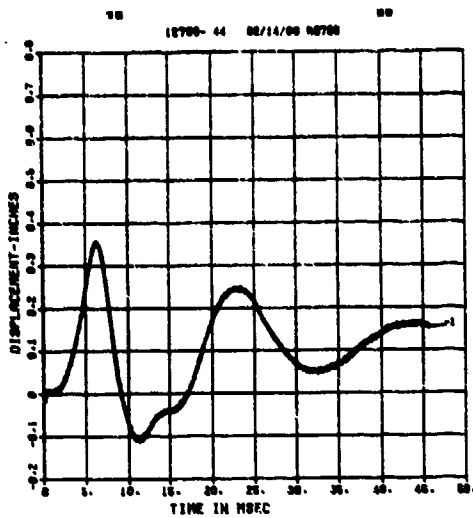
SPALL TEST 8B
AFV
200000. HZ CAL= 6015.



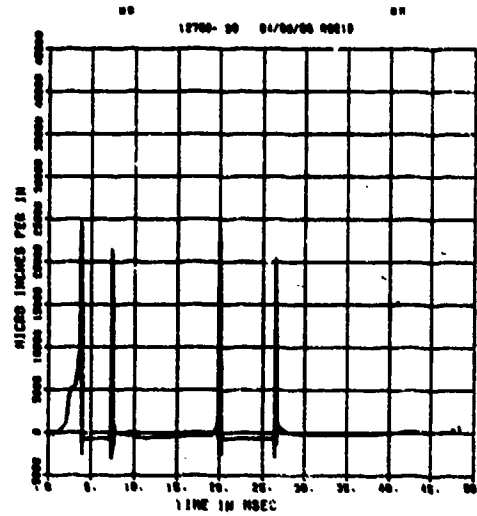
SPALL TEST 8B
AFH
200000. HZ CAL= 7934.



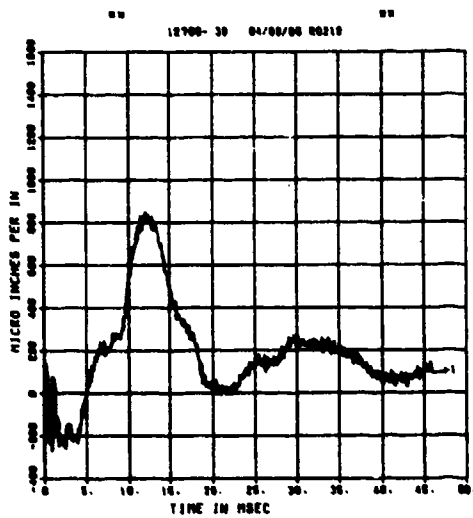
SPALL TEST 8B
DM
200000. HZ CAL= 0.720



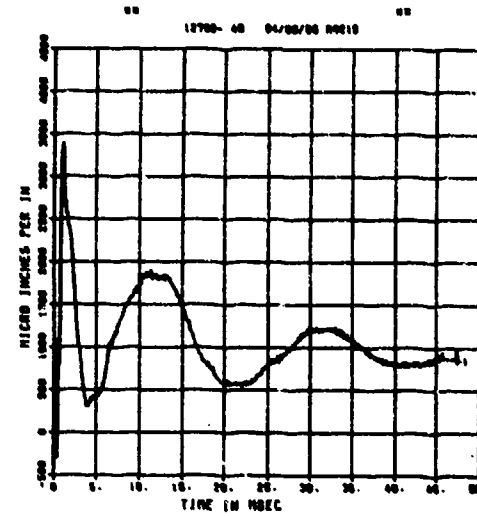
SPALL TEST 8B
EOT
200000. HZ CAL= 11176.
LP4/0 70% CUTOFF= 9000. HZ



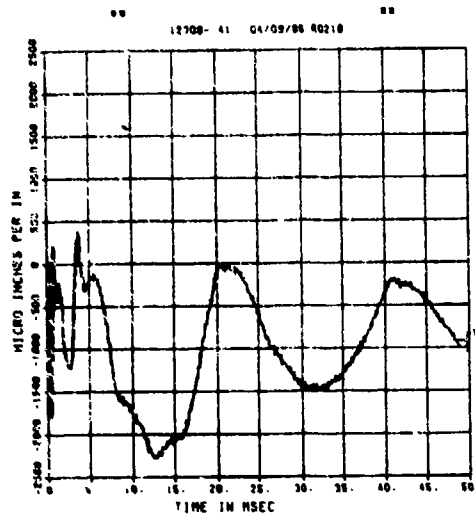
SPALL TEST 8B
EIT
200000. HZ CAL= 7469.
LP4/0 70% CUTOFF= 9000. HZ



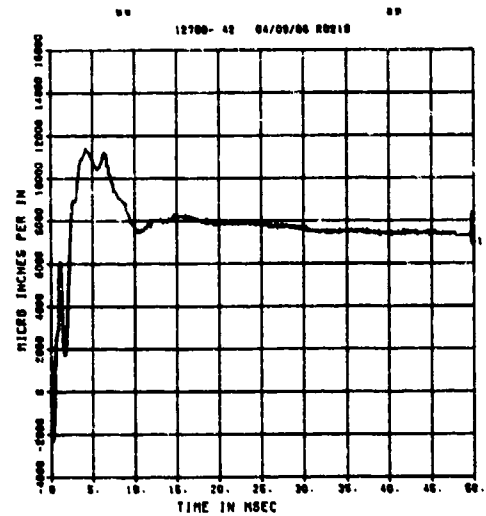
SPALL TEST 8B
EOM
200000. HZ CAL= 7469.
LP4/0 70% CUTOFF= 9000. HZ



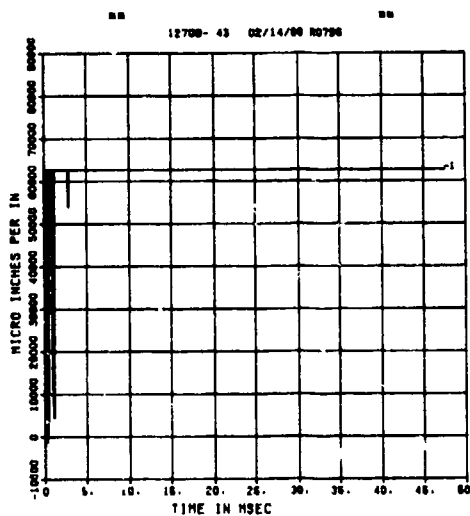
SPALL TEST 8B
EIM
200000. HZ CAL= 11176.
LP4/O 70% CUTOFF= 9000. HZ



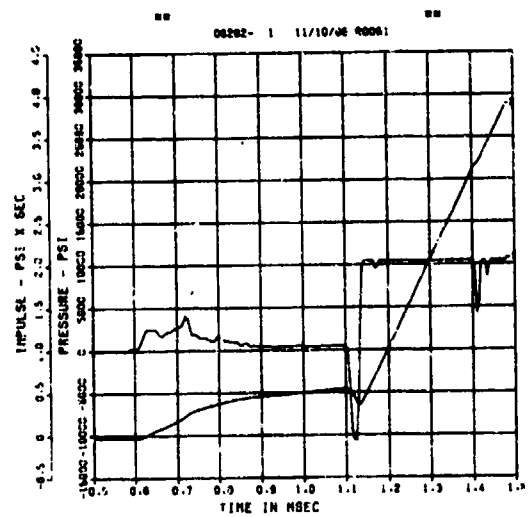
SPALL TEST 8B
EIM
200000. HZ CAL= 30324.
LP4/O 70% CUTOFF= 9000. HZ



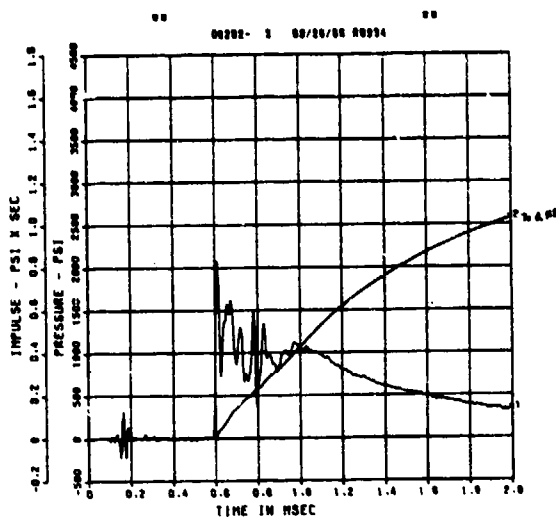
SPALL TEST 8B
EIM
200000. HZ CAL= 30324.



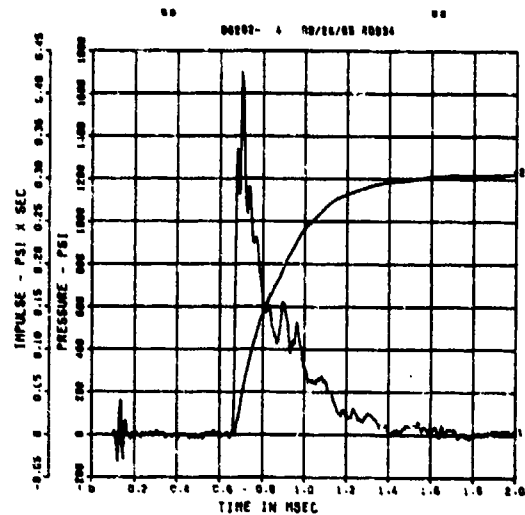
SPALL TEST 9A
PQ-0
200000. HZ CAL= 4987.



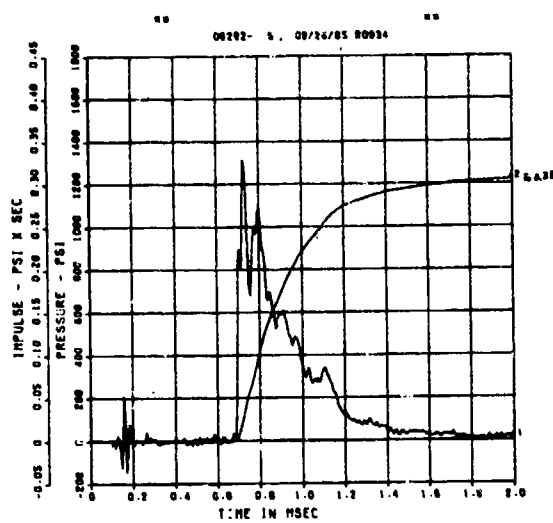
SPALL TEST 9A
PQ-2
200000. HZ CAL= 3008.



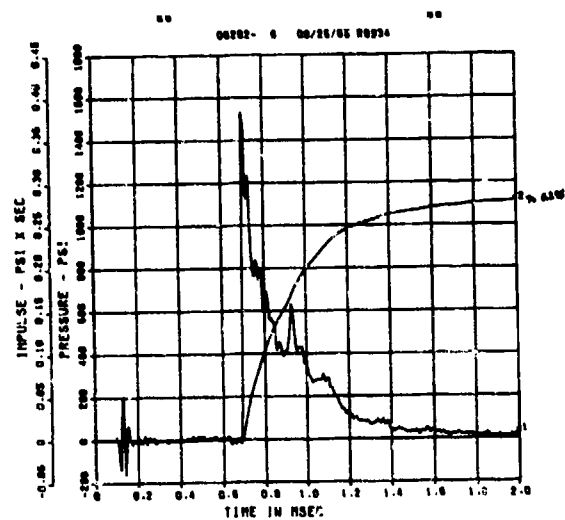
SPALL TEST 9A
PM-0
200000. HZ CAL= 4008.



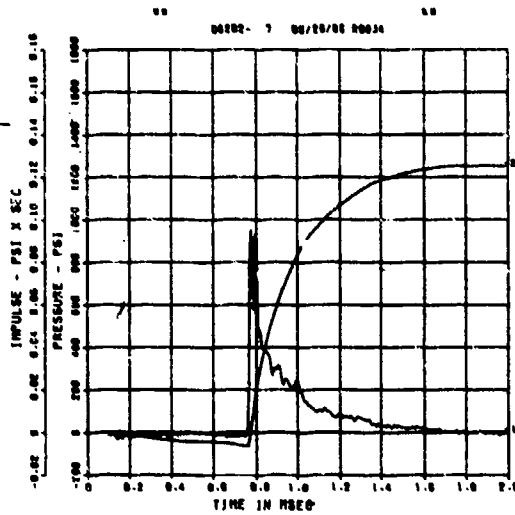
SPALL TEST 9A
PM-1
200000. HZ CAL= 3026.



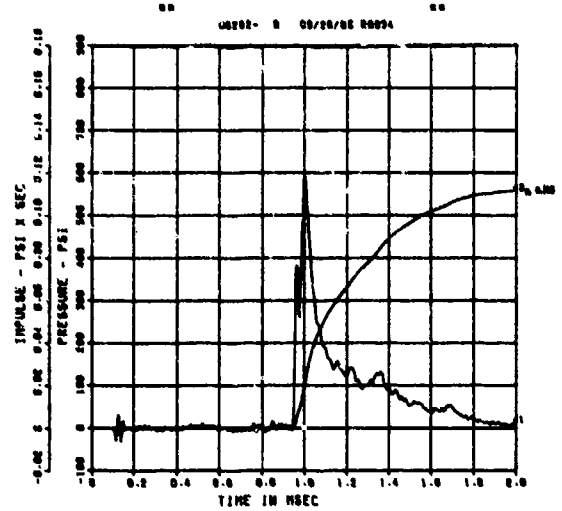
SPALL TEST 9A
PM-2
200000. HZ CAL= 2462.



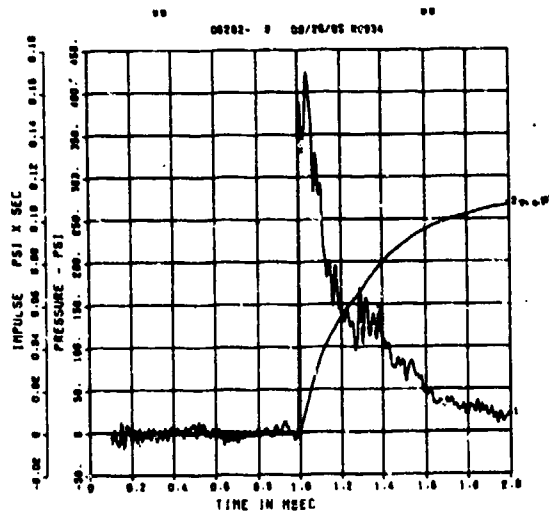
SPALL TEST 9A
PM-3
200000. HZ CAL= 1987.



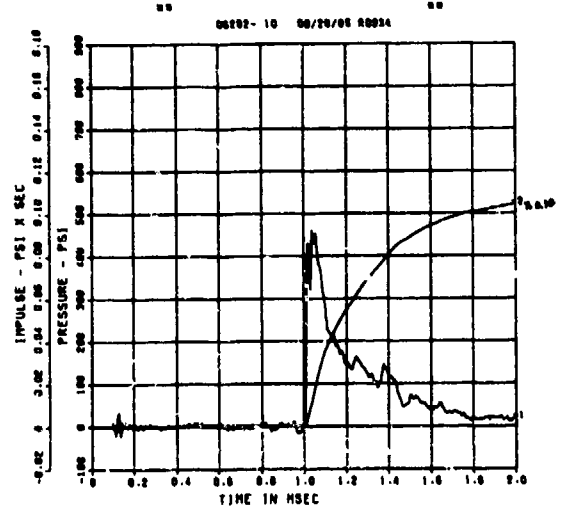
SPALL TEST 9A
PT-0
200000. HZ CAL= 1292.



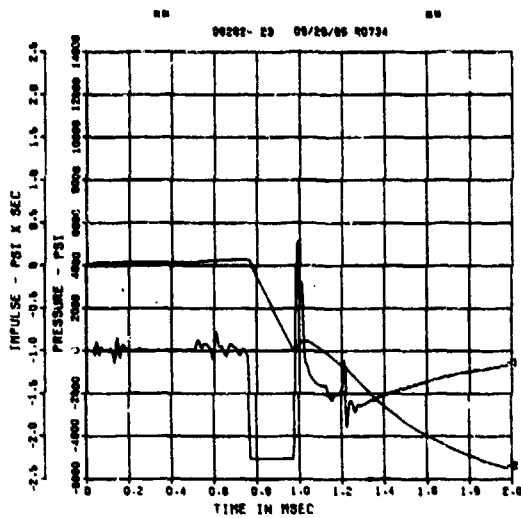
SPALL TEST 9A
PT-2
200000. HZ CAL= 1136.



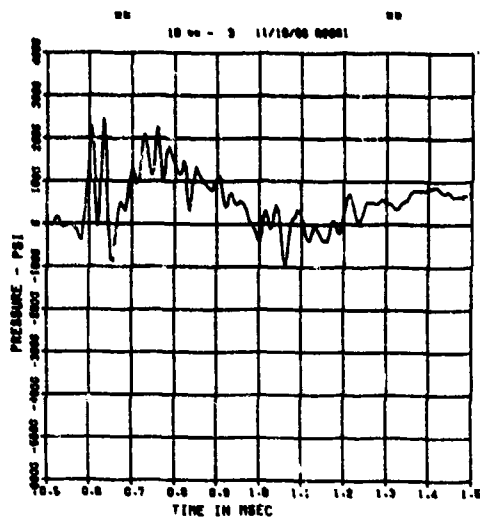
SPALL TEST 9A
PT-3
200000. HZ CAL= 1247.



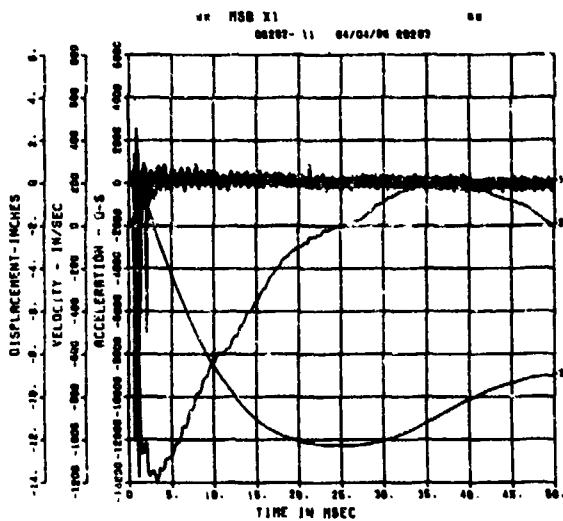
SPALL TEST 9A
BP-A
200000. HZ CAL= 2538.



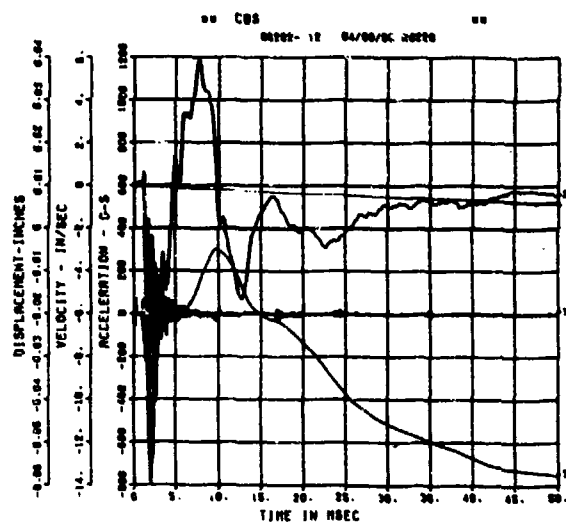
SPALL TEST 9A
FP-A
200000. HZ CAL= -0.025



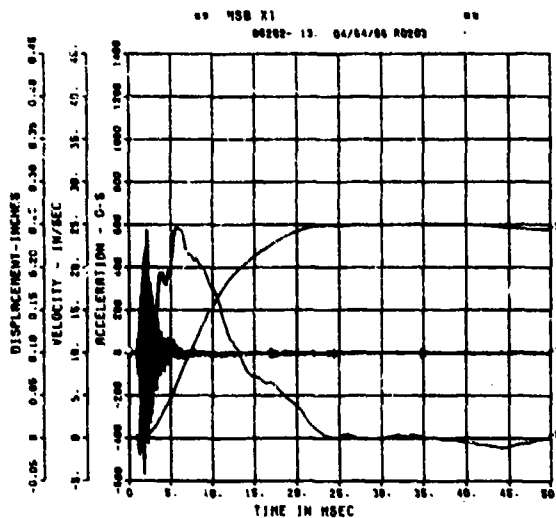
SPALL TEST 9A
AWHM
200000. HZ CAL= 41314.



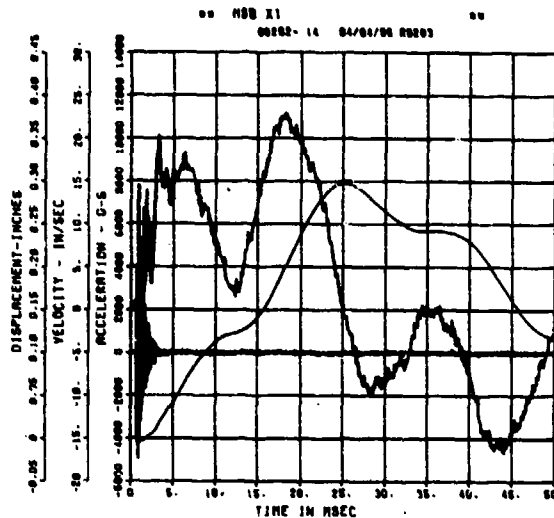
SPALL TEST 9A
ARV
200000. HZ CAL= 612.0



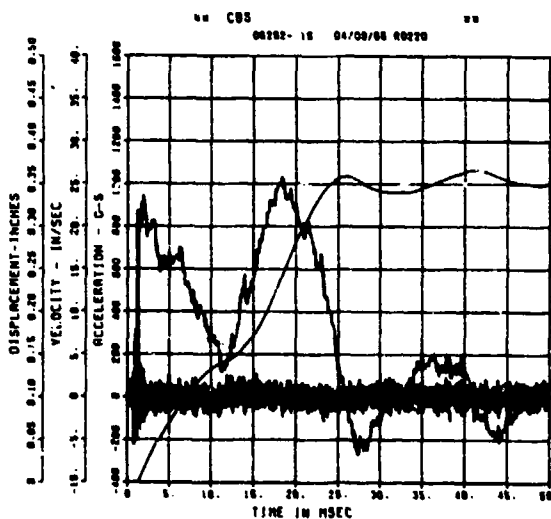
SPALL TEST 9A
ARH
200000. HZ CAL= 591.0



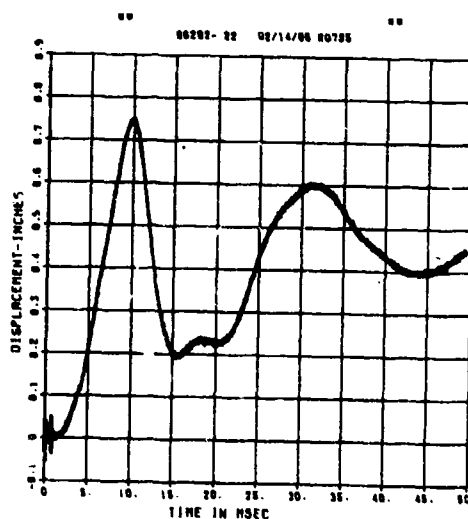
SPALL TEST 9A
AFV
200000. HZ CAL= 8462.



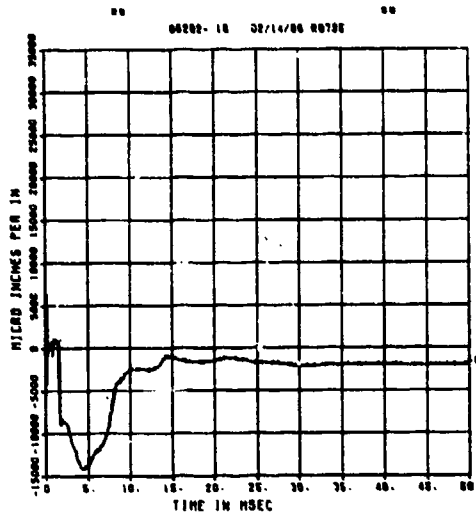
SPALL TEST 9A
AFH
200000. HZ CAL= 10167.



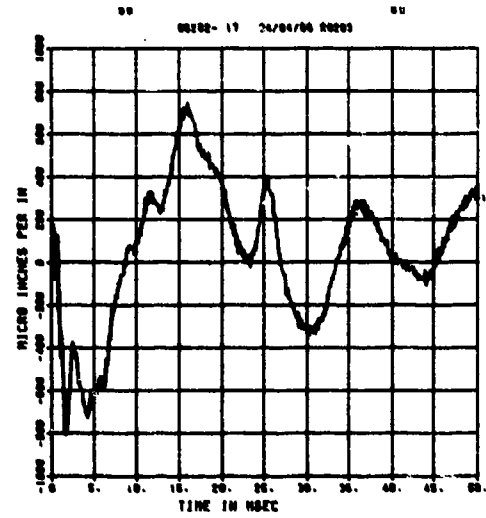
SPALL TEST 9A
DM
200000. HZ CAL= 1.076



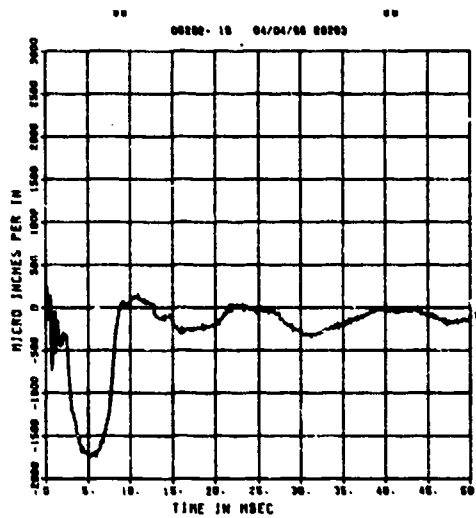
SPALL TEST 9A
EOT
200000. HZ CAL= 14816.



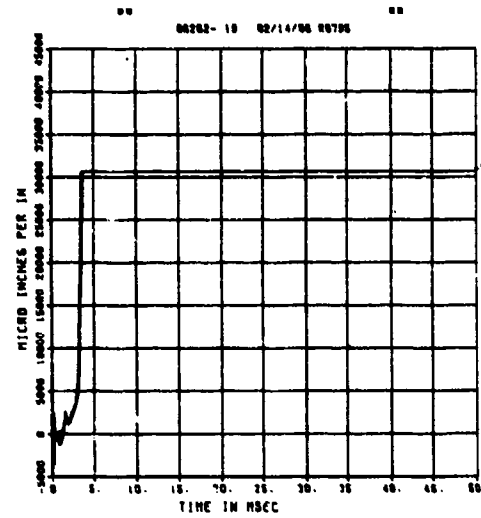
SPALL TEST 9A
EIT
200000. HZ CAL= 7469.
LP4/0 70% CUTOFF= 9000. HZ



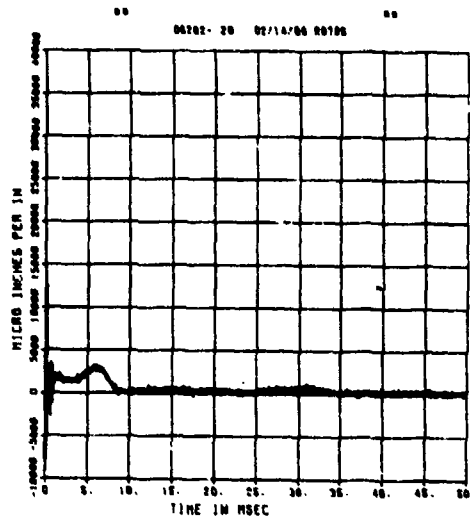
SPALL TEST 9A
EOM
200000. HZ CAL= 7469.
LP4/0 70% CUTOFF= 9000. HZ



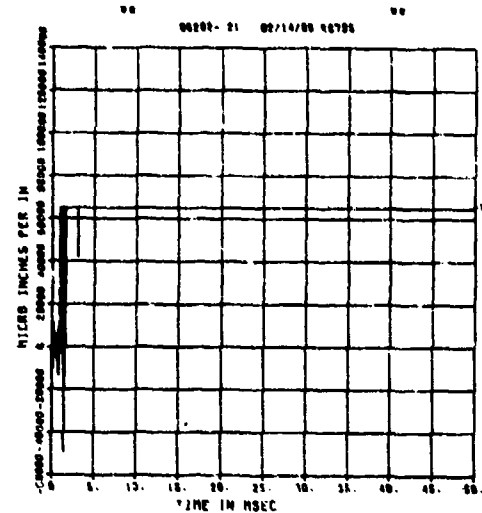
SPALL TEST 9A
EIM
200000. HZ CAL= 14816.



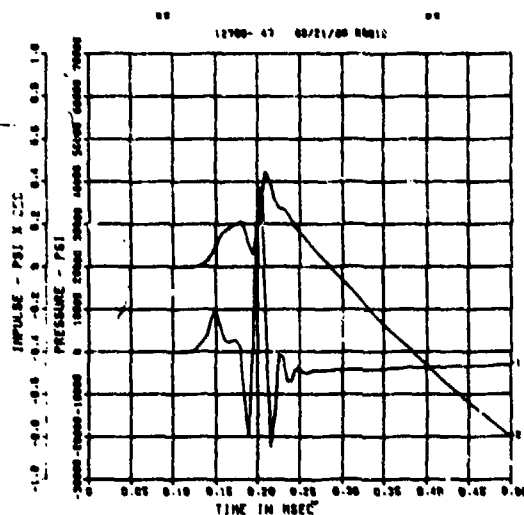
SPALL TEST 9A
E08
200000. HZ CAL= 30324.



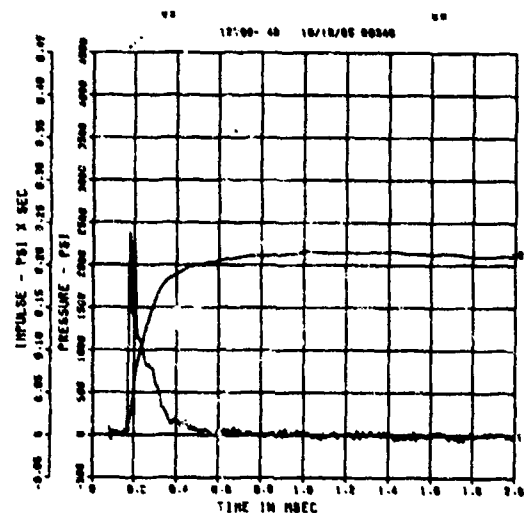
SPALL TEST 9A
E18
200000. HZ CAL= 30324.



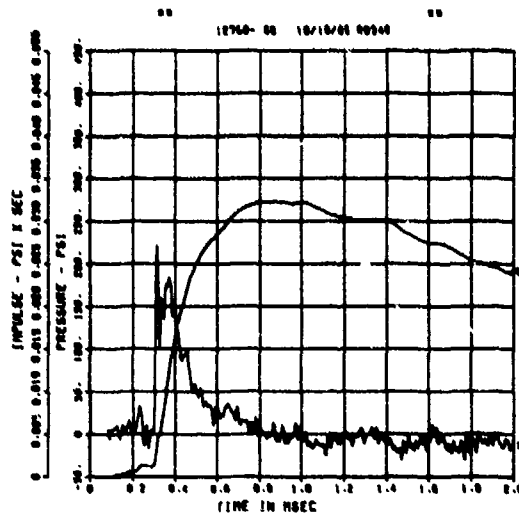
SPALL TEST 9B
PQ-0
200000. HZ CAL= 18808.



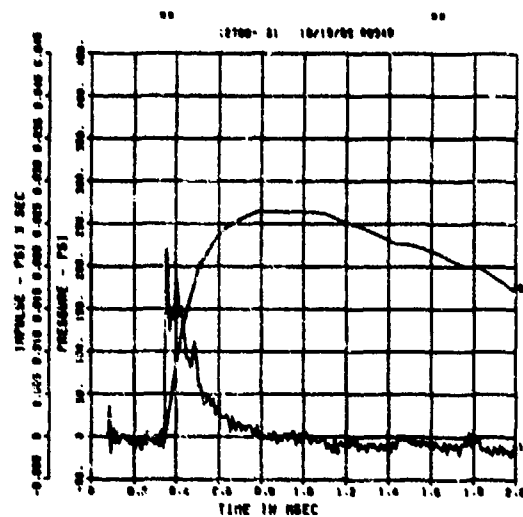
SPALL TEST 9B
PQ-2
200000. HZ CAL= 9965.



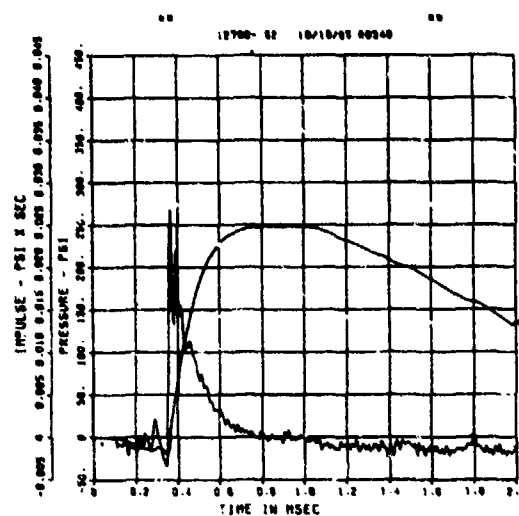
SPALL TEST 9B
PM-0
200000. HZ CAL= 2758.



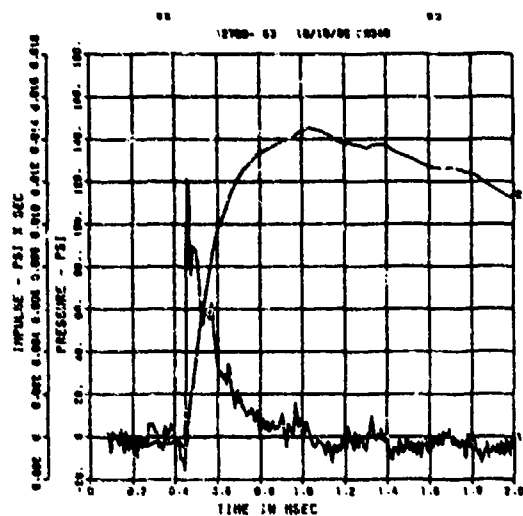
SPALL TEST 9B
PM-1
200000. HZ CAL= 1952.



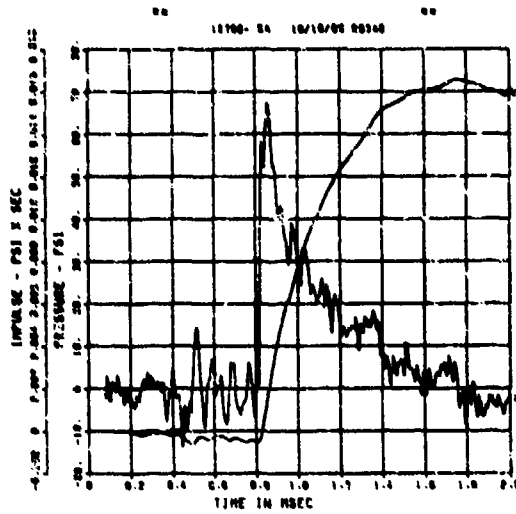
SPALL TEST 9B
PM-2
200000. HZ CAL= 1703.



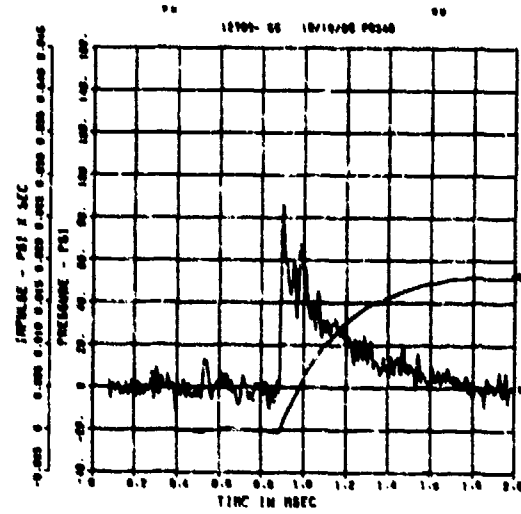
SPALL TEST 9B
PM-3
200000. HZ CAL= 1248.



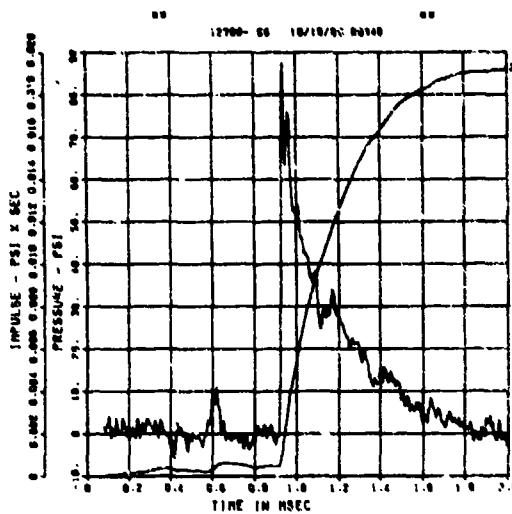
SPALL TEST 9B
PT-0
200000. HZ CAL= 818.0



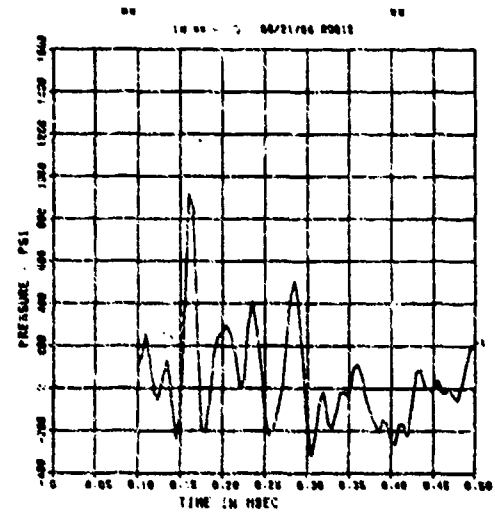
SPALL TEST 9B
PT-2
200000. HZ CAL= 639.0



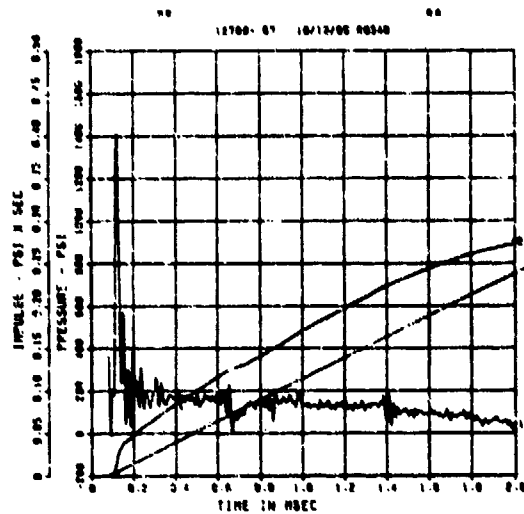
SPALL TEST 9B
PT-3
200000. HZ CAL= 505.0



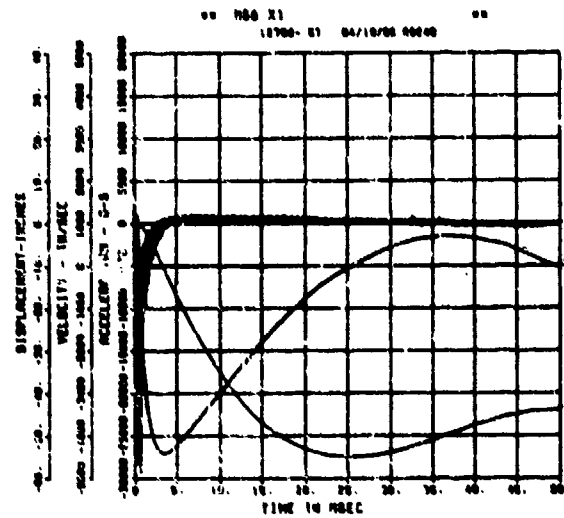
SPALL TEST 9B
FP-B
200000. HZ CAL= -0.065



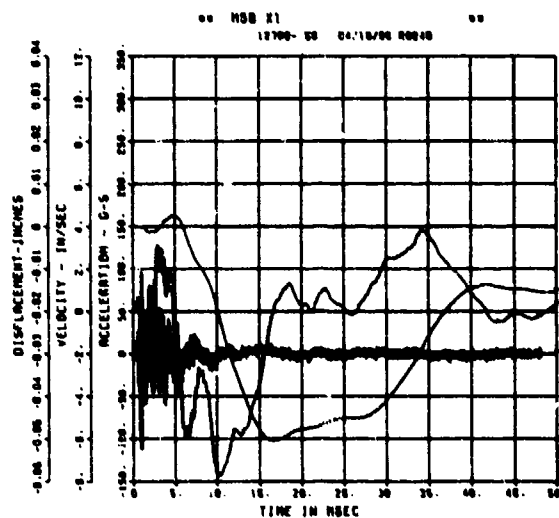
SPALL TEST 9B
BP-B
200000. HZ CAL= 3924.



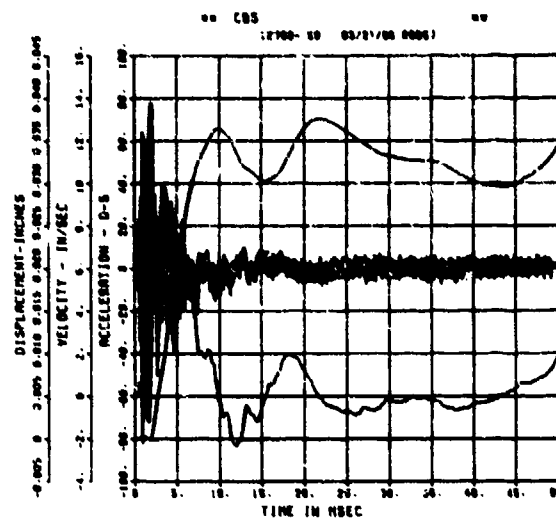
SPALL TEST 9B
AWHM
200000. HZ CAL= 35478.



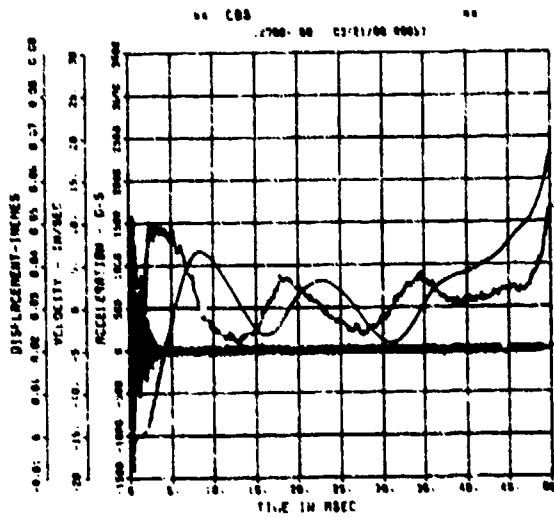
SPALL TEST 9B
ARV
200000. HZ CAL= 611.0



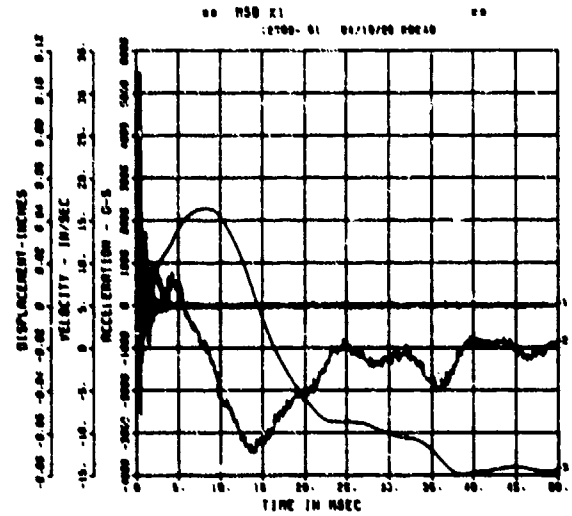
SPALL TEST 9B
ARR
200000. HZ CAL= 499.6



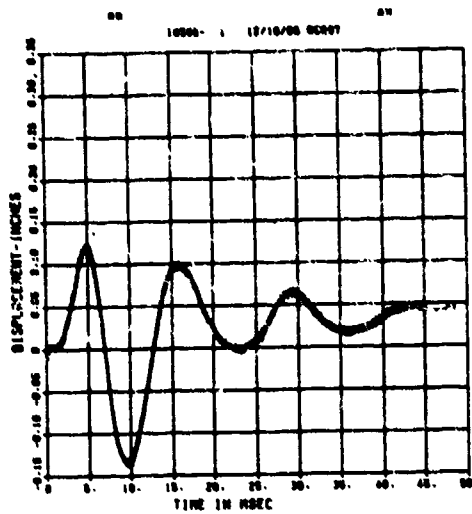
SPALL TEST 98
 AFV
 200000. HZ CAL= 4963.



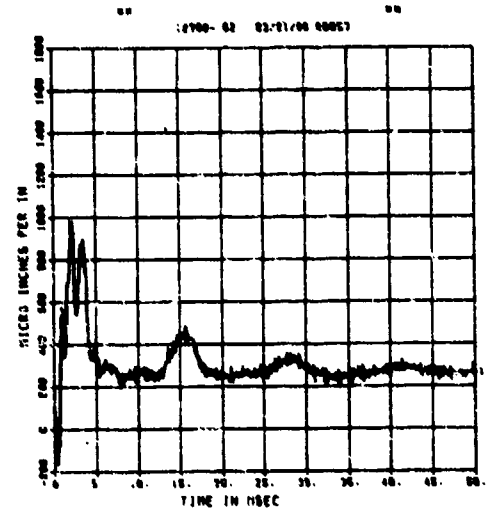
SPALL TEST 98
 AFH
 200000. HZ CAL= 7020.



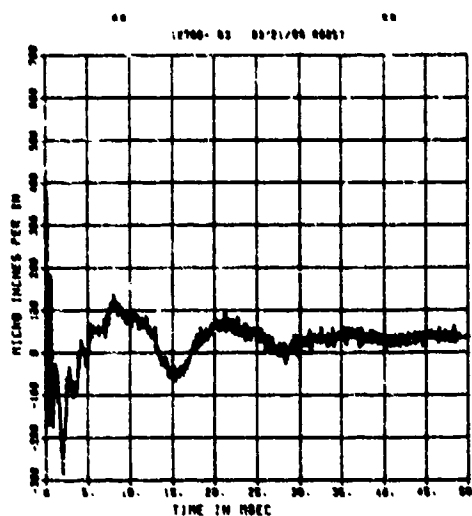
SPALL TEST 98
 DM
 200000. HZ CAL= 5.715



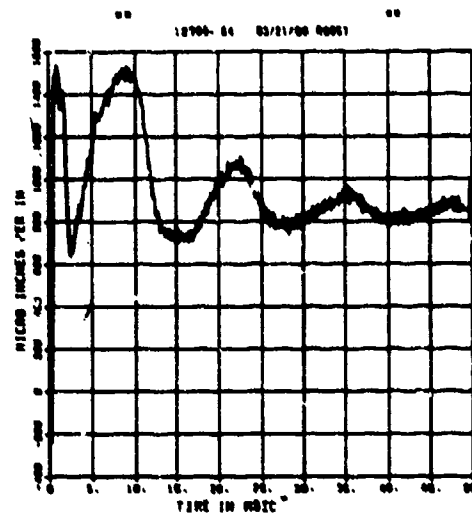
SPALL TEST 98
 EOT
 200000. HZ CAL= 7469.
 LP4:G 70% CUTOFF 4 9000. HZ



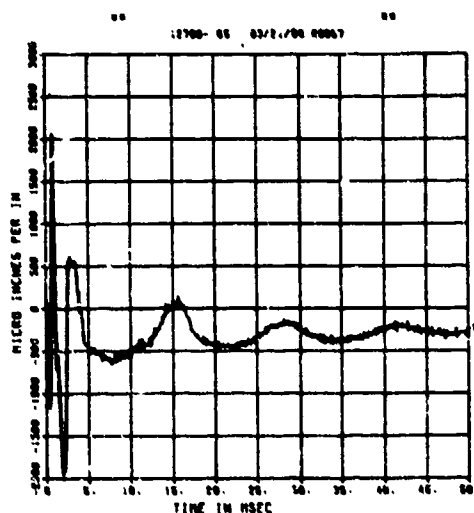
SPALL TEST 9B
EIT
200000. HZ CAL= 5005.
LP4/0 70X CUTOFF= 8000. HZ



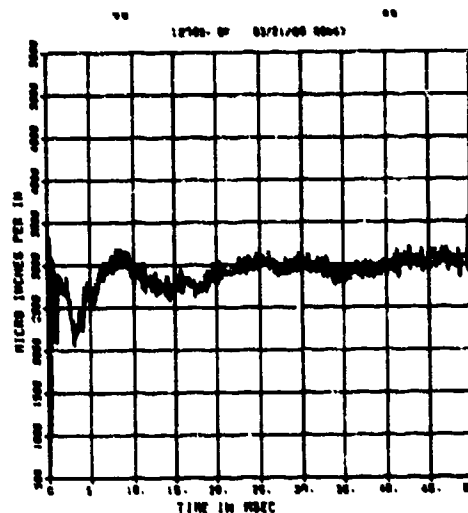
SPALL TEST 9B
EOM
200000. HZ CAL= 7489.
LP4/0 70X CUTOFF= 8000. HZ



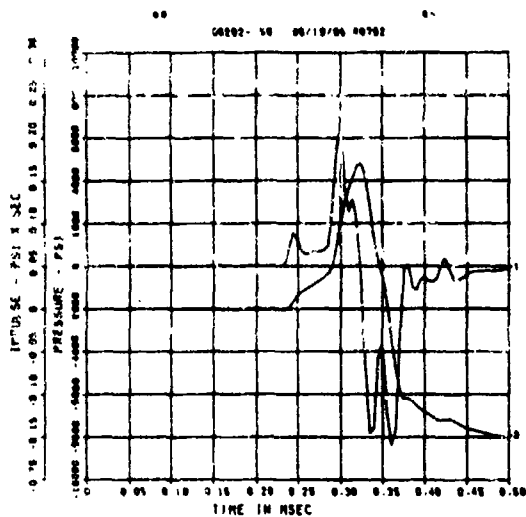
SPALL TEST 9B
EIM
200000. HZ CAL= 11176.
LP4/0 70X CUTOFF= 8000. HZ



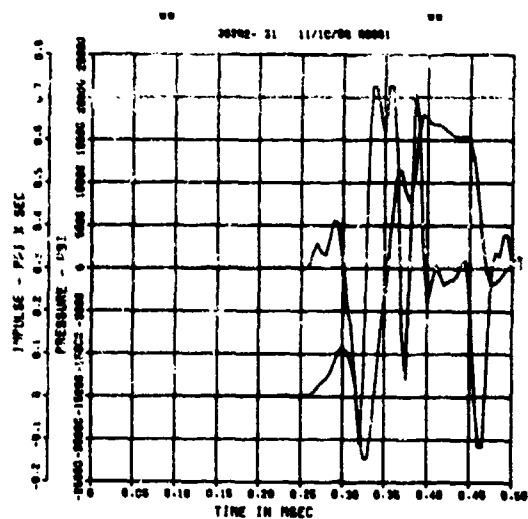
SPALL TEST 9B
E0B
200000. HZ CAL= 30324.
LP4/0 70X CUTOFF= 8000. HZ



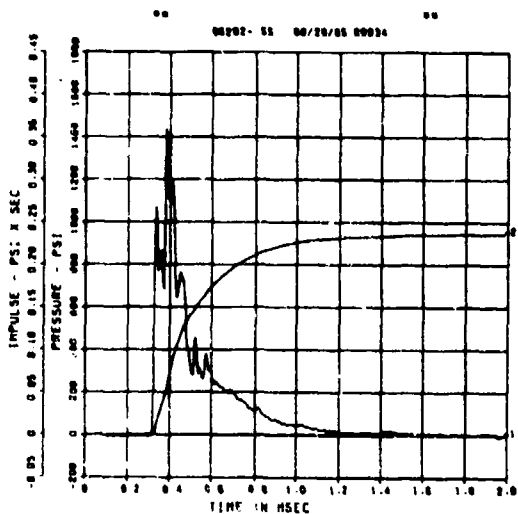
SPALL TEST 10A
PQ-0
200000. HZ CAL= 3556.



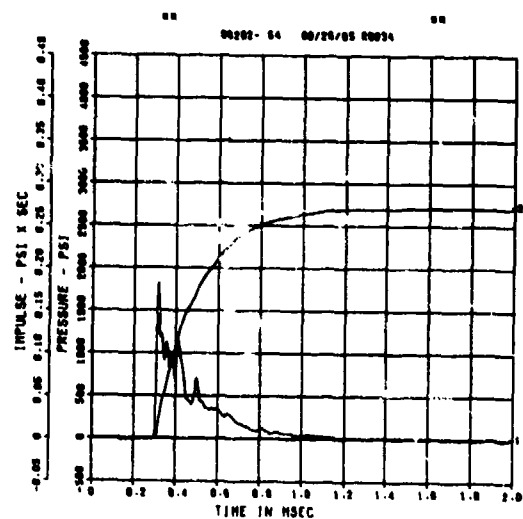
SPALL TEST 10A
PQ-1
200000. HZ CAL= 9152.



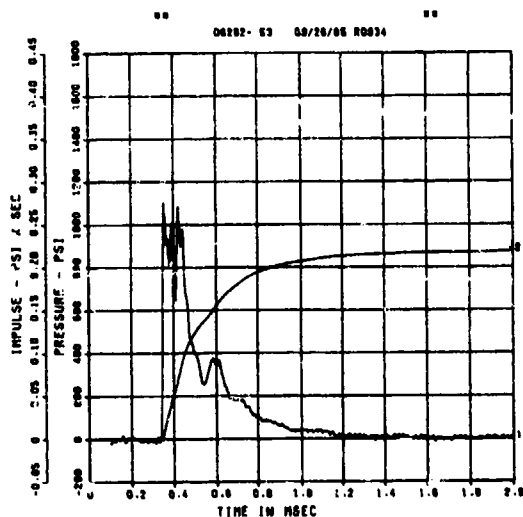
SPALL TEST 10A
PM-0
200000. HZ CAL= 1448.



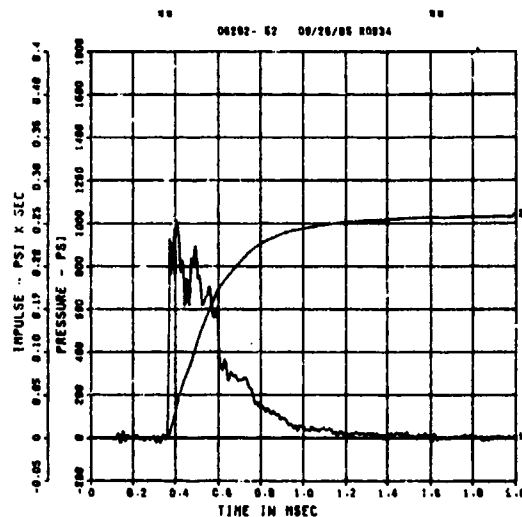
SPALL TEST 10A
PM-1
200000. HZ CAL= 2270.



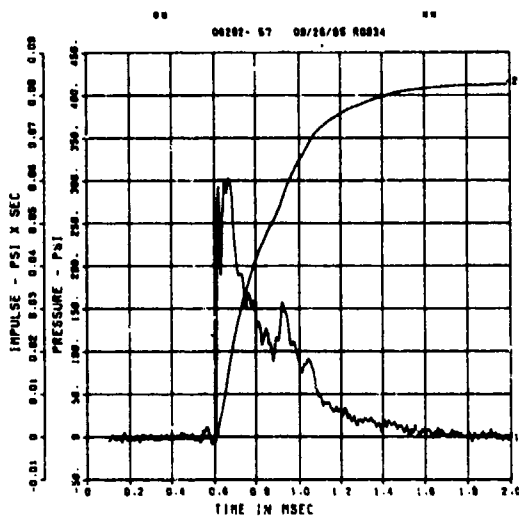
SPALL TEST 10A
PM-2
200000. HZ CAL= 2431.



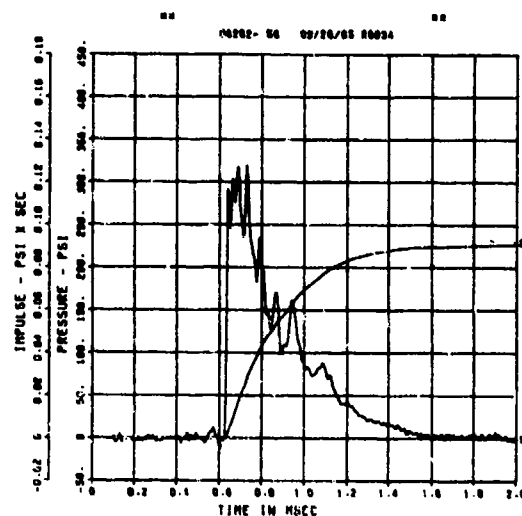
SPALL TEST 10A
PM-3
200000. HZ CAL= 3001.



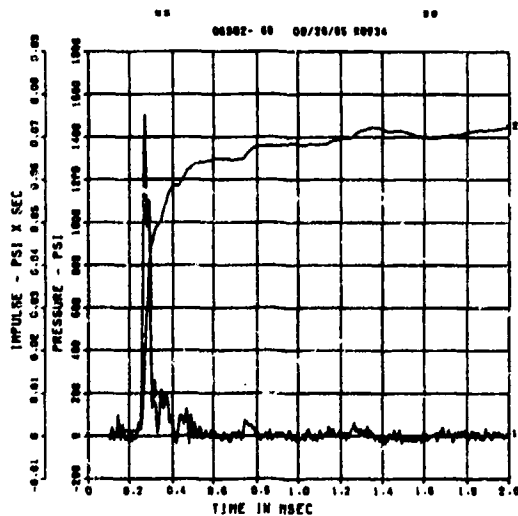
SPALL TEST 10A
PT-2
200000. HZ CAL= 726.0



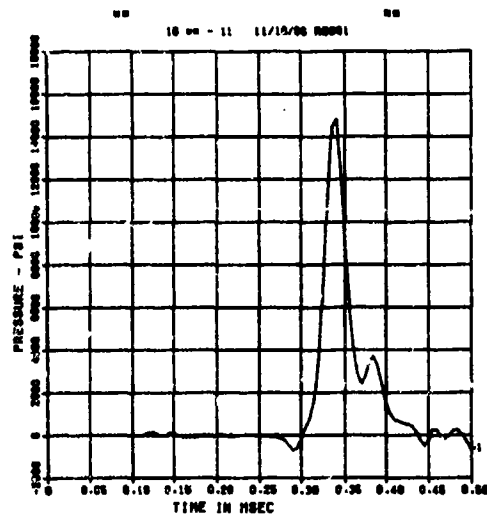
SPALL TEST 10A
PT-3
200000. HZ CAL= 631.3



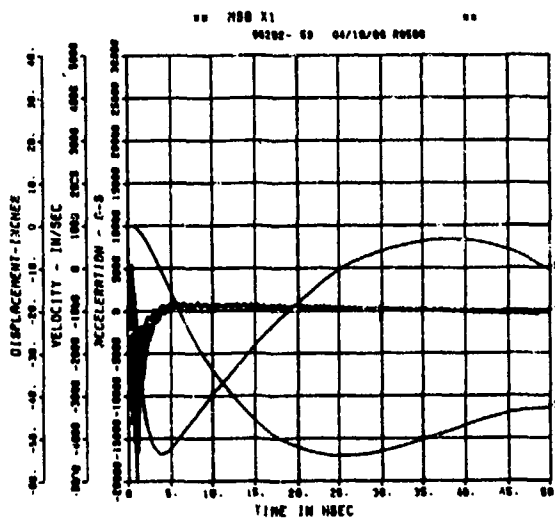
SPALL TEST 10A
BP-A
200000. HZ CAL= 5934.



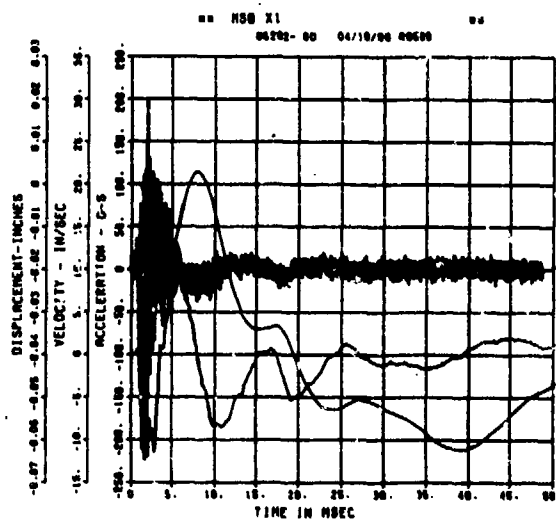
SPALL TEST 10A
FP-A
200000. HZ CAL= -0.045



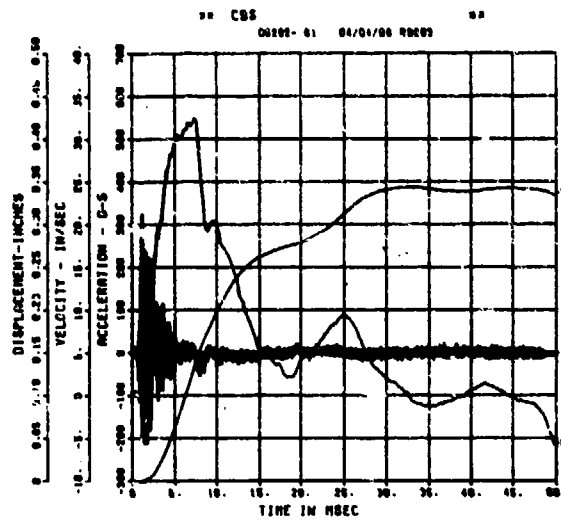
SPALL TEST 10A
AWHM
200000. HZ CAL= 27133.



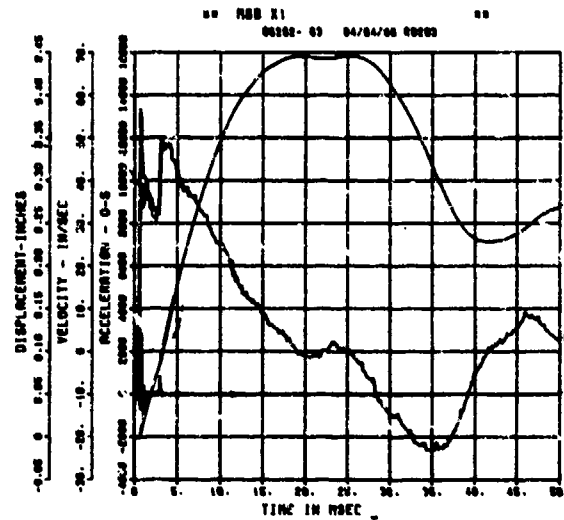
SPALL TEST 10A
ARV
200000. HZ CAL= 1630.



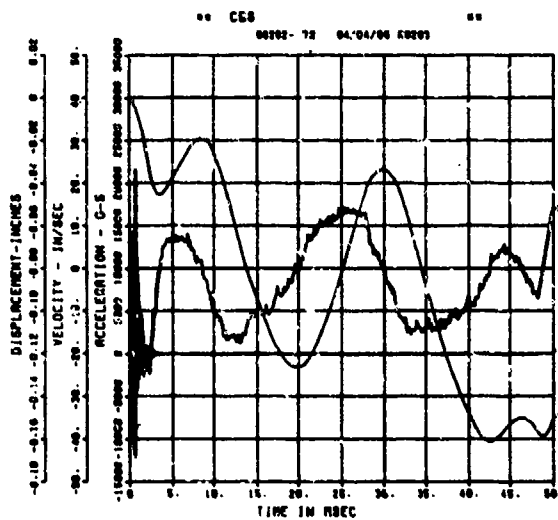
SPALL TEST 10A
ARM
200000. HZ CAL= 1503.



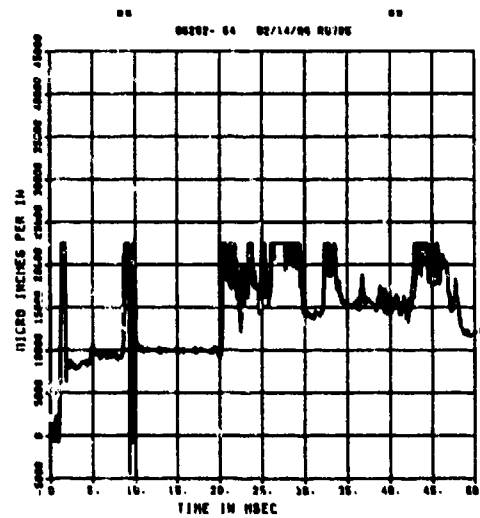
SPALL TEST 10A
AFM
200000. HZ CAL= 7519.



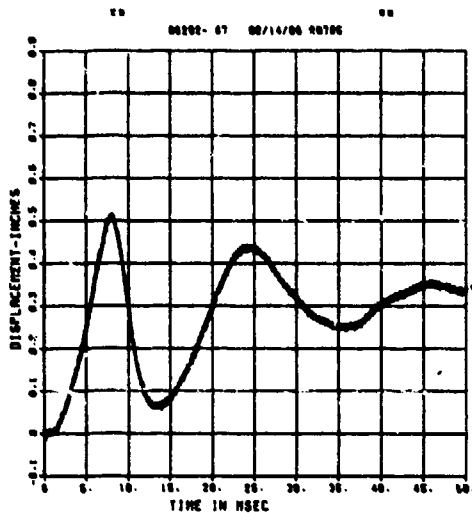
SPALL TEST 10A
AFV
200000. HZ CAL= 6259.



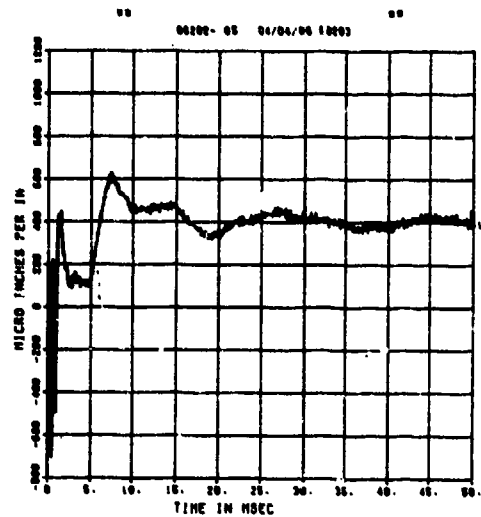
SPALL TEST 10A
EOT
200000. HZ CAL= 11176.



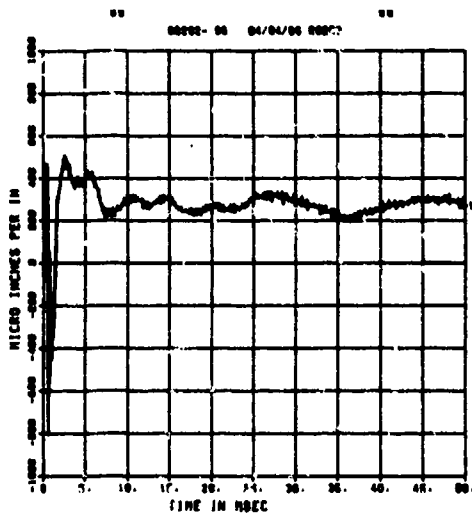
SPALL TEST 10A
DM
200000. HZ CAL= 1.076



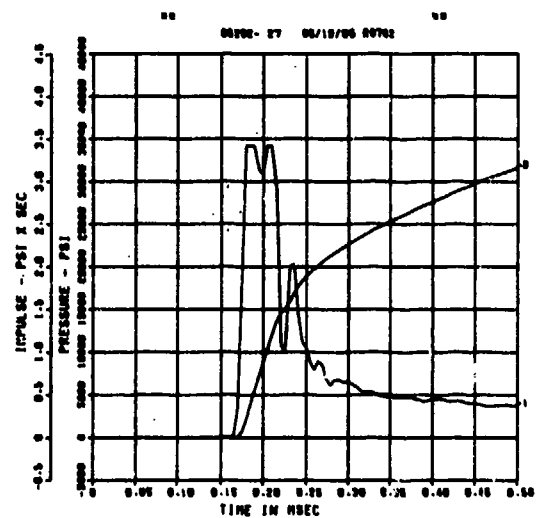
SPALL TEST 10A
EIT
200000. HZ CAL= 5004.
LP4/0 70X CUTOFF= 9000. HZ



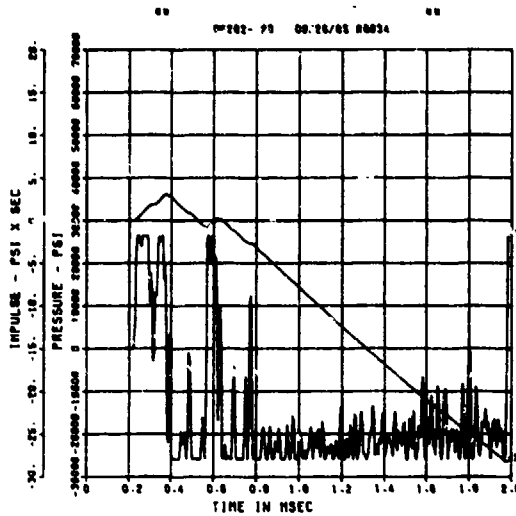
SPALL TEST 10A
EOM
200000. HZ CAL= 5004.
LP4/0 70X CUTOFF= 9000. HZ



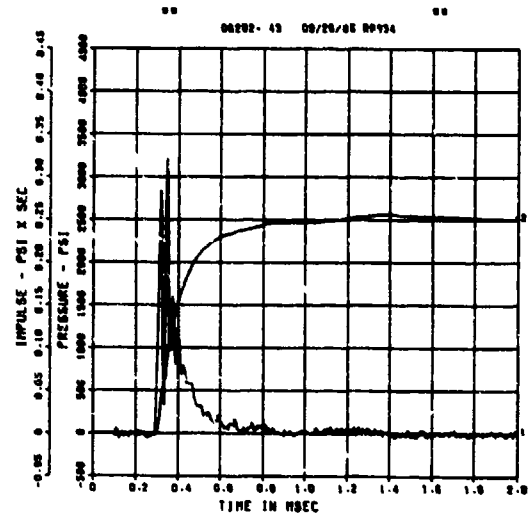
SPALL TEST 10B
PQ-1
200000. HZ CAL= 16440.



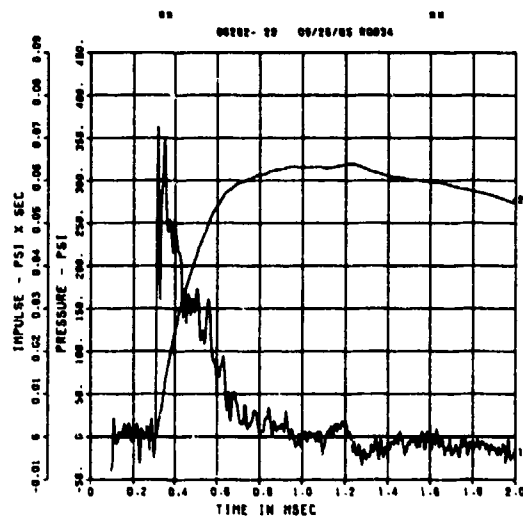
SPALL TEST 10B
PQ-2
200000. HZ CAL= 12568.



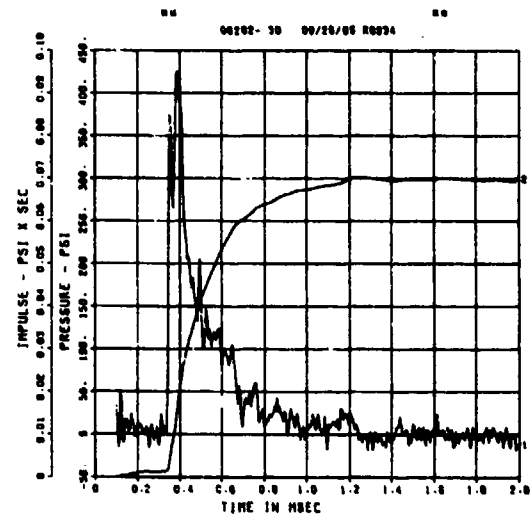
SPALL TEST 10B
PQ-3
200000. HZ CAL= 6664.



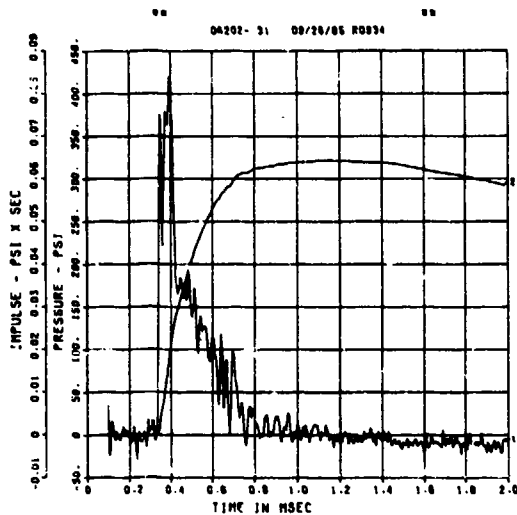
SPALL TEST 10B
PM-0
200000. HZ CAL= 3001.



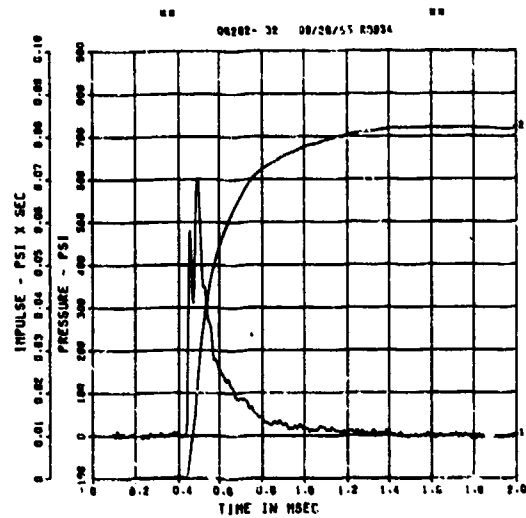
SPALL TEST 10B
PM-1
200000. HZ CAL= 3026.



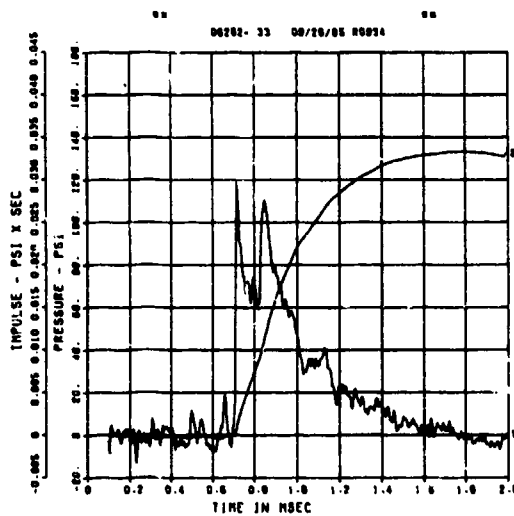
SPALL TEST 10B
PM-2
200000. HZ CAL= 1981.



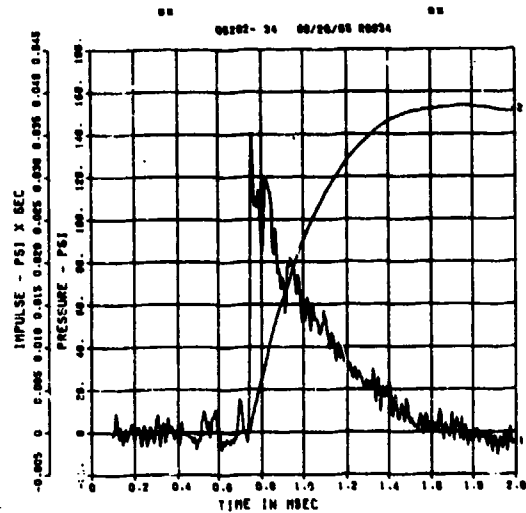
SPALL TEST 10B
PM-3
200000. HZ CAL= 127.



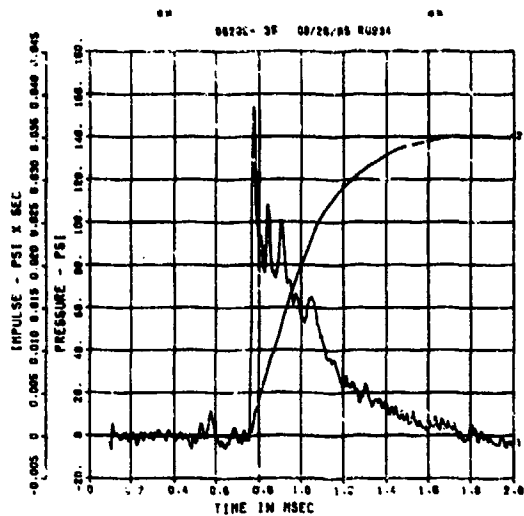
SPALL TEST 10B
PT-0
200000. HZ CAL= 936.0



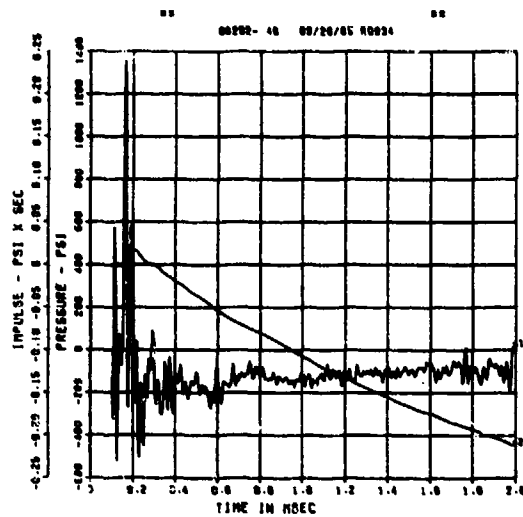
SPALL TEST 10B
PT-2
200000. HZ CAL= 809.0



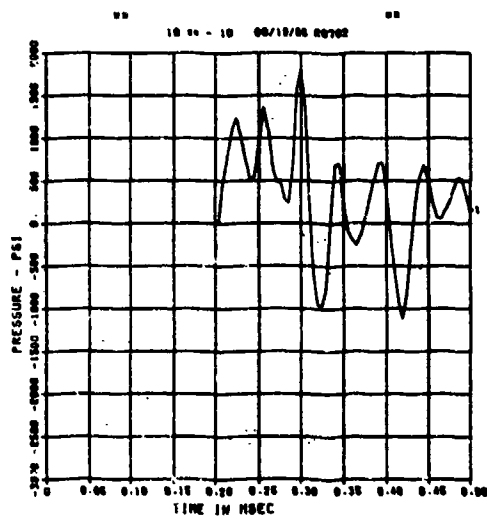
SPALL TEST 108
PT-3
200000. HZ CAL= 533.0



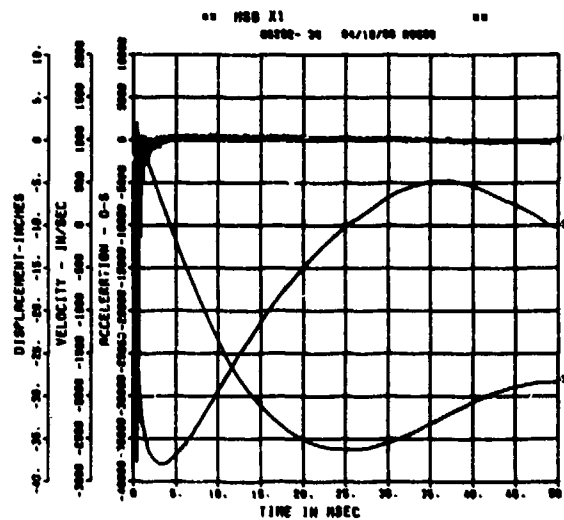
SPALL TEST 108
BP-B
200000. HZ CAL= 4365.



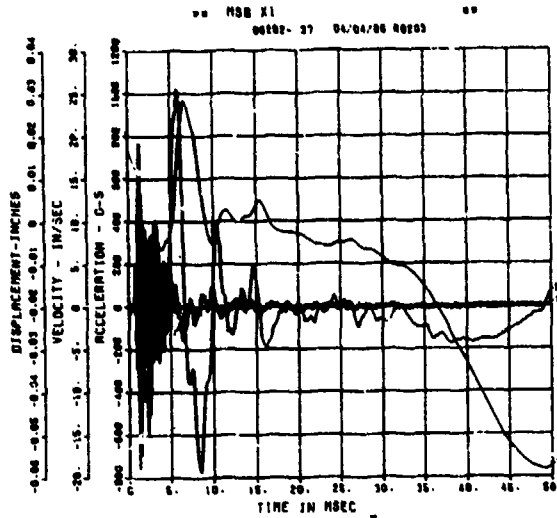
SPALL TEST 108
FP-B
200000. HZ CAL= -0.045



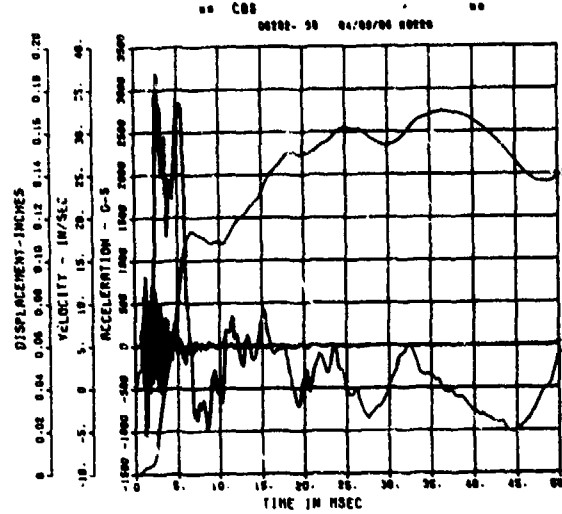
SPALL TEST 108
AWHM
200000. HZ CAL= 26659.



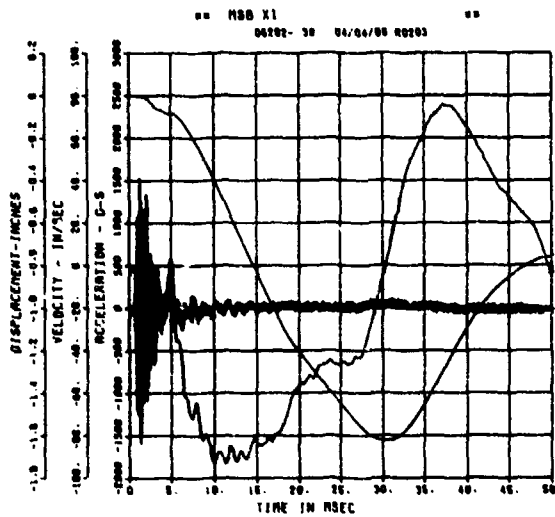
SPALL TEST 10B
ARV
200000. HZ CAL= 1211.



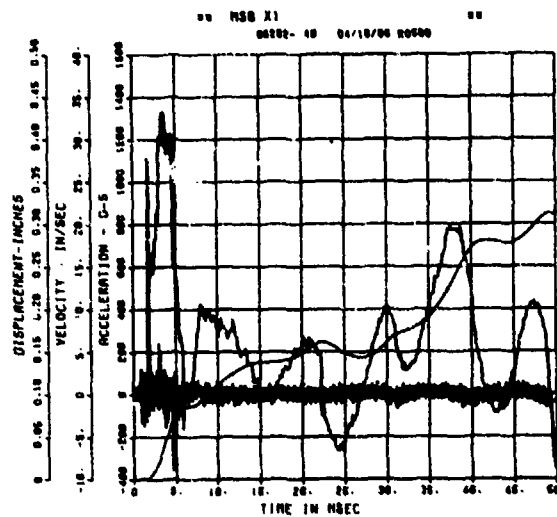
SPALL TEST 10B
ARH
200000. HZ CAL= 1228.



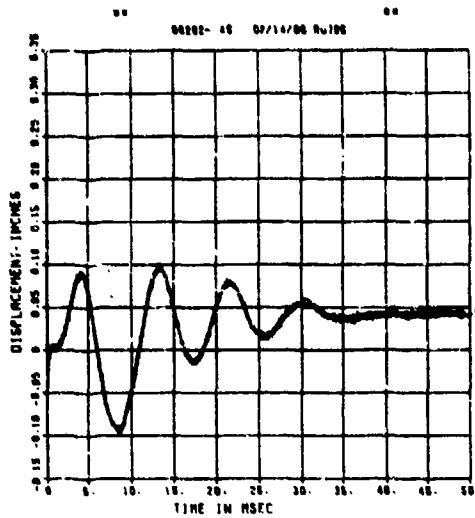
SPALL TEST 10B
AFV
200000. HZ CAL= 4963.



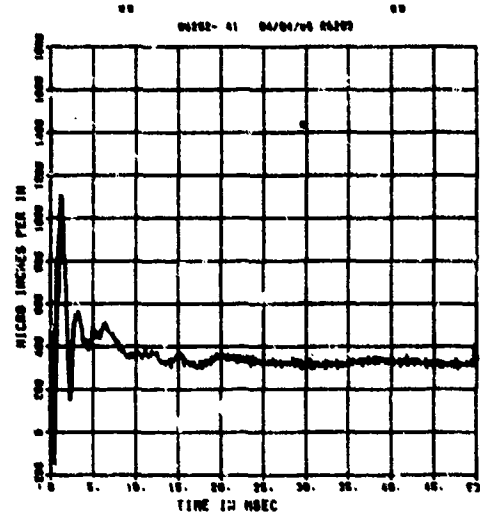
SPALL TEST 10B
AFH
200000. HZ CAL= 5624.



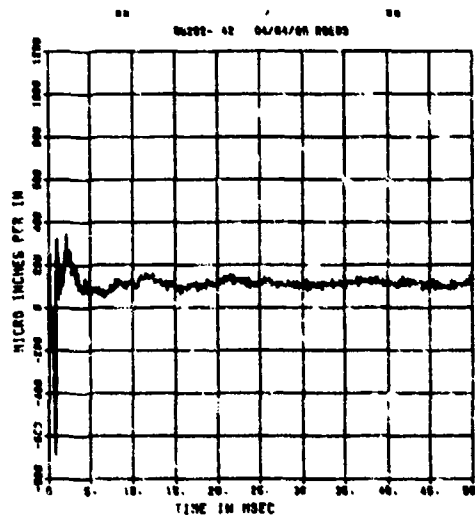
SPALL TEST 10B
DM
200000. HZ CAL= 0.431



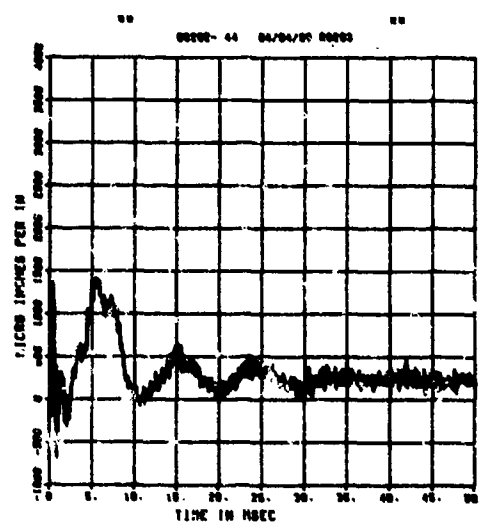
SPALL TEST 10B
EOT
200000. HZ CAL= 5004.
LP4/0 70% CUTOFF= 9000. HZ



SPALL TEST 10B
EIT
200000. HZ CAL= 5004.
LP4/0 70% CUTOFF= 9000. HZ

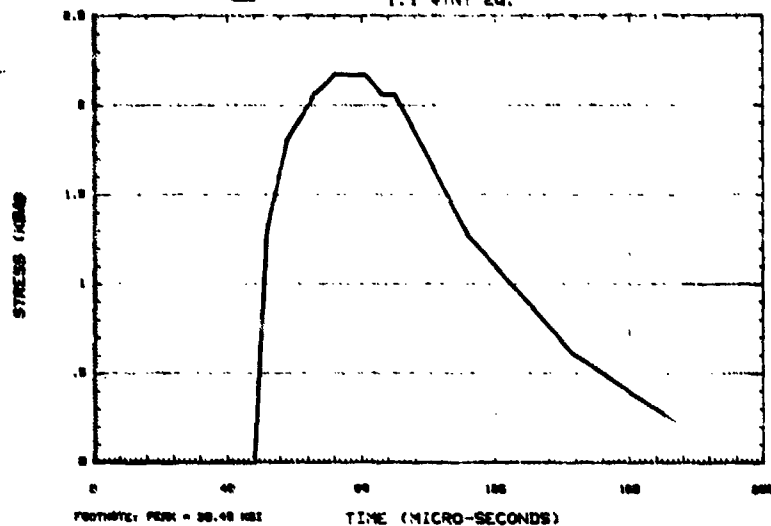


SPALL TEST 10B
E0B
200000. HZ CAL= 30324.
LP4/0 70% CUTOFF= 9000. HZ



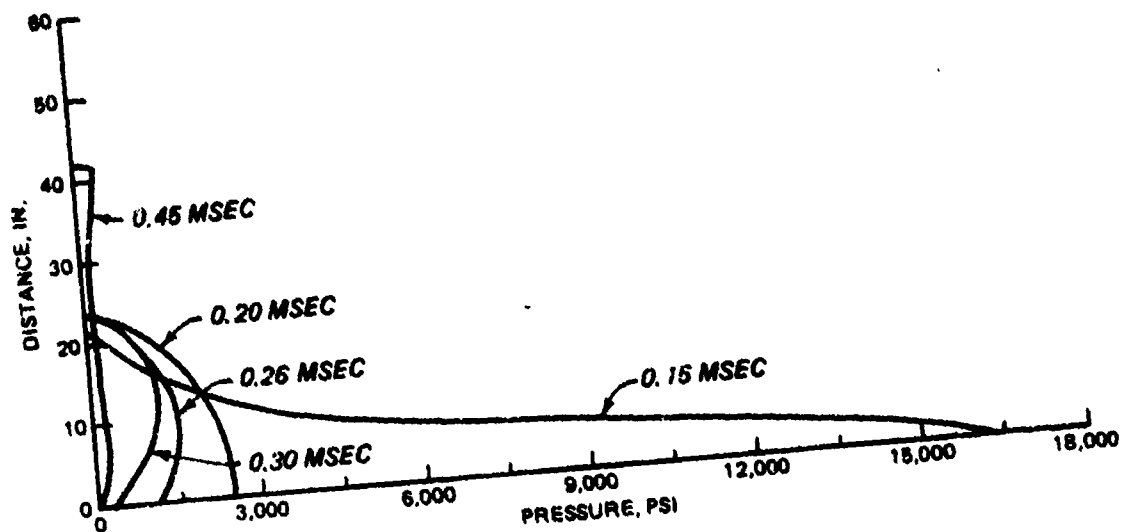
PP-1

STRESS VS TIME TEST 100- CONTRACT SHOT ON BASE CONCRETE WALL I. I. VINEY, JR.

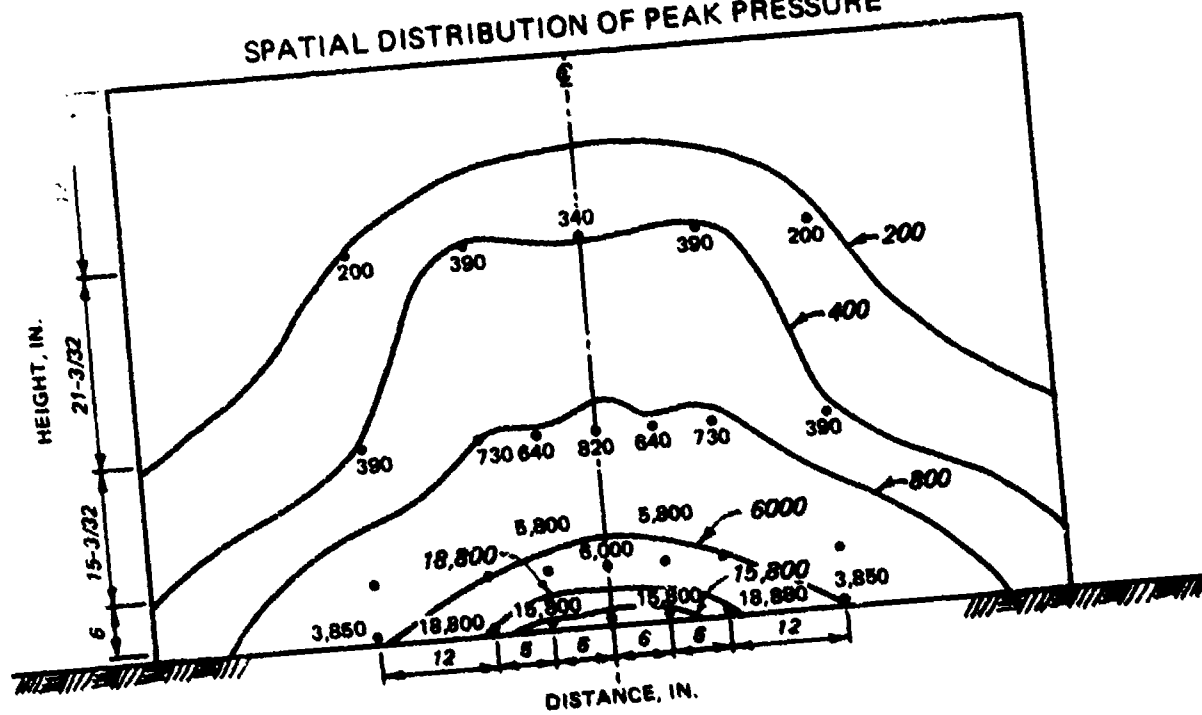


APPENDIX B
PRESSURE DISTRIBUTIONS ON THE WALL PANELS

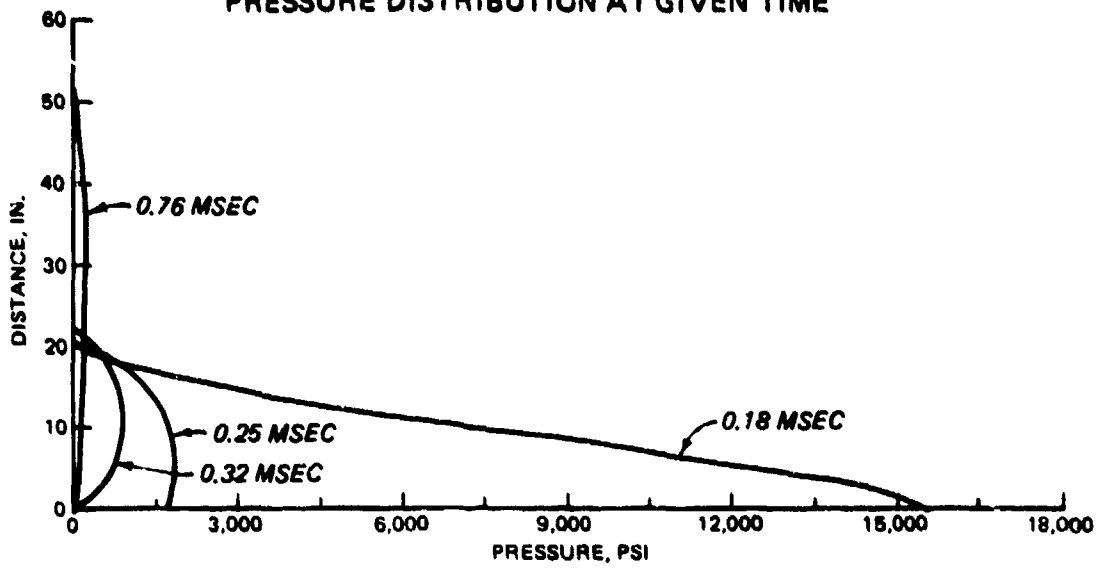
TEST 1A PRESSURE DISTRIBUTION AT GIVEN TIME



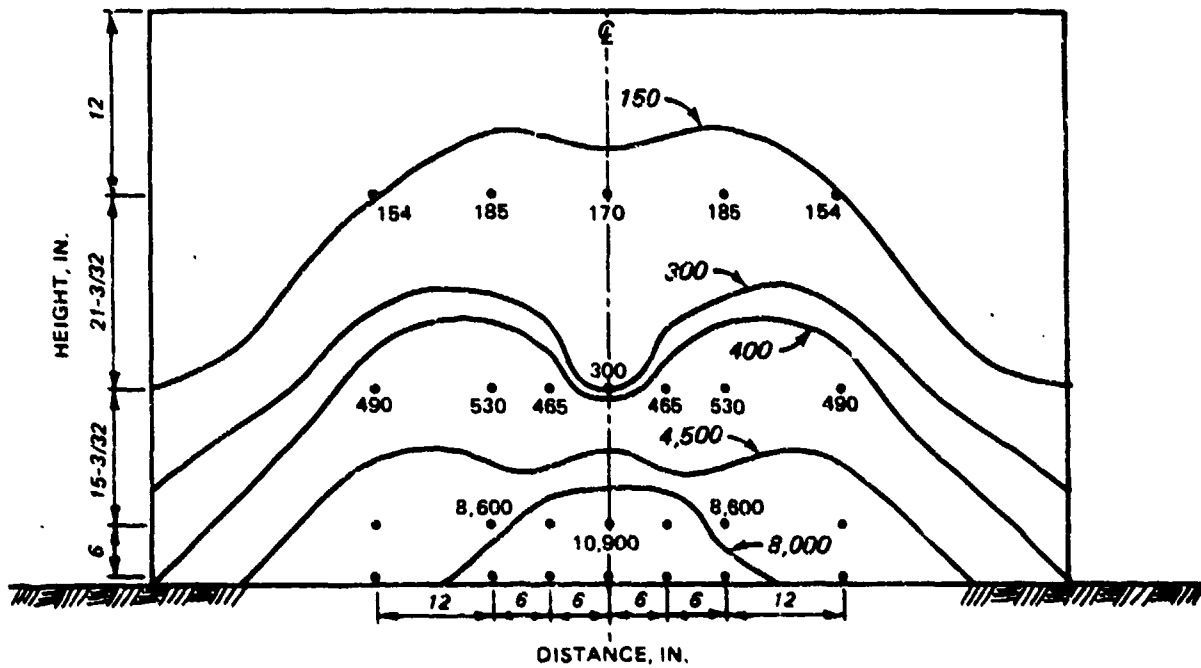
SPATIAL DISTRIBUTION OF PEAK PRESSURE



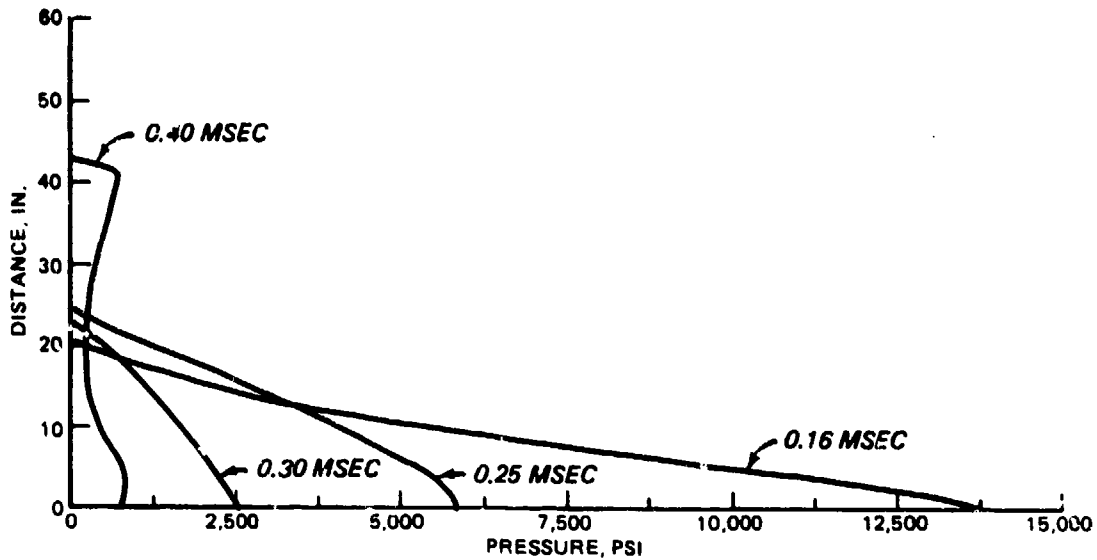
TEST 1B PRESSURE DISTRIBUTION AT GIVEN TIME



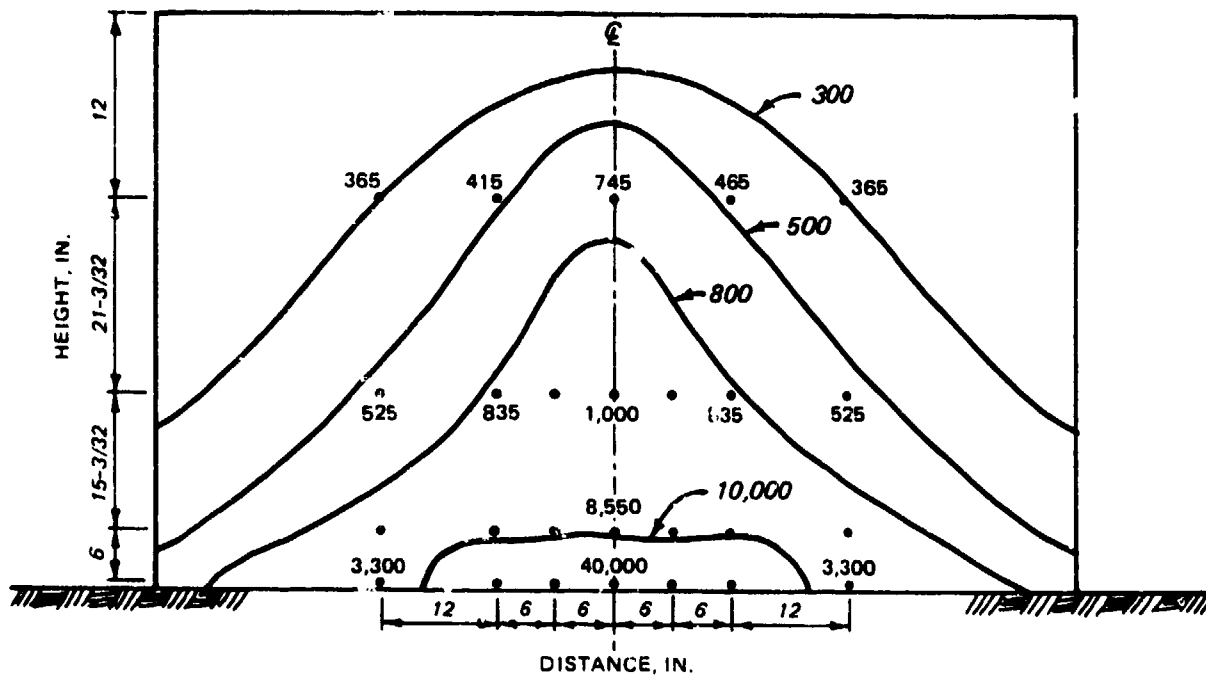
SPATIAL DISTRIBUTION OF PEAK PRESSURE



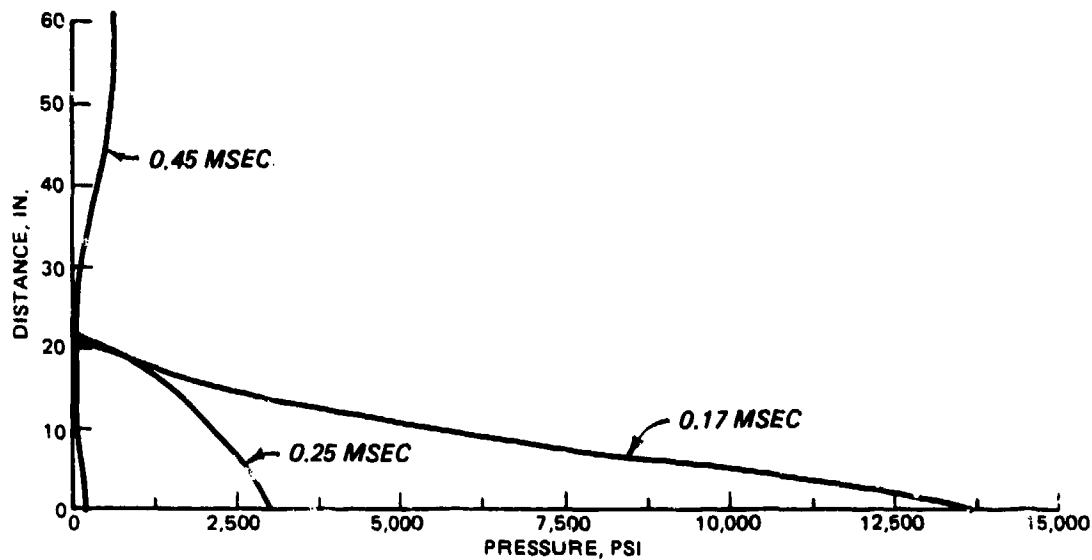
TEST 1D PRESSURE DISTRIBUTION AT GIVEN TIME



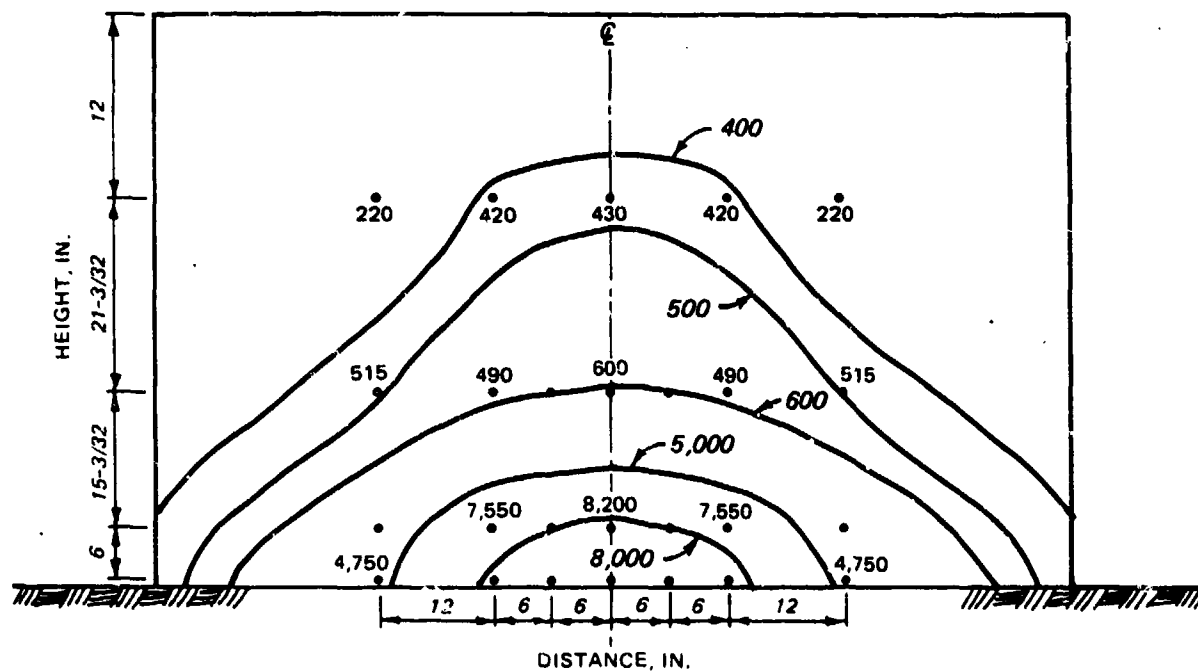
SPATIAL DISTRIBUTION OF PEAK PRESSURE



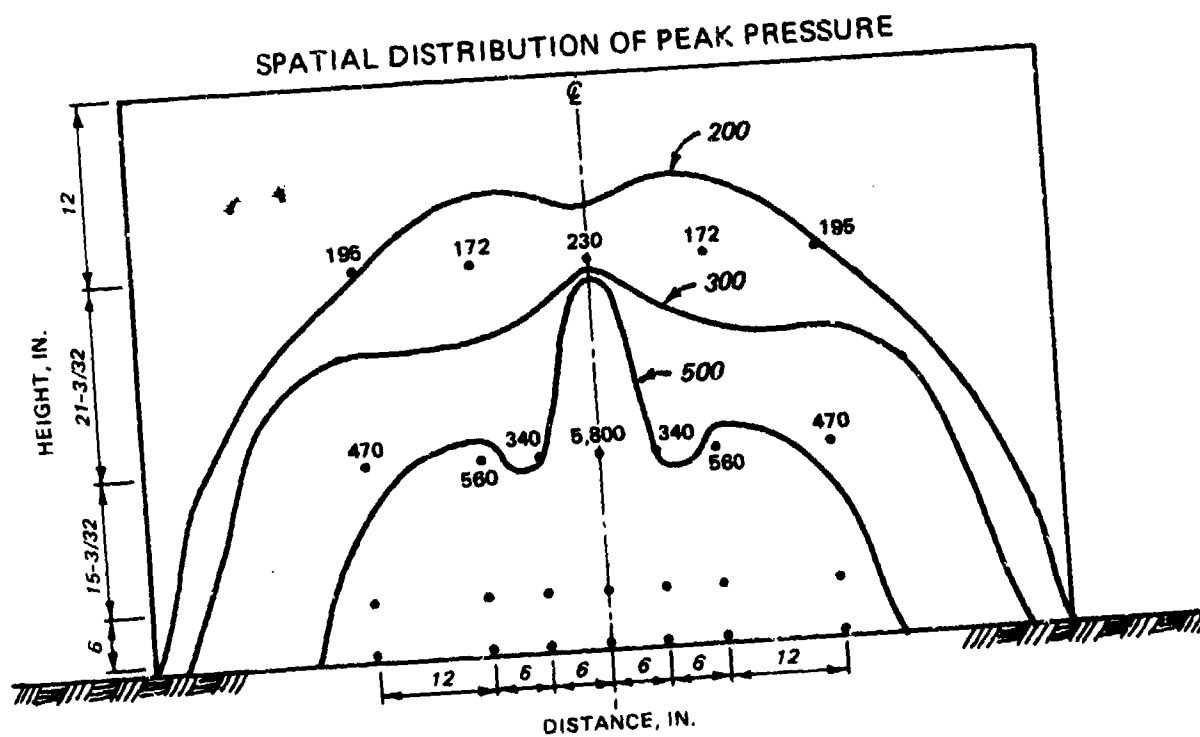
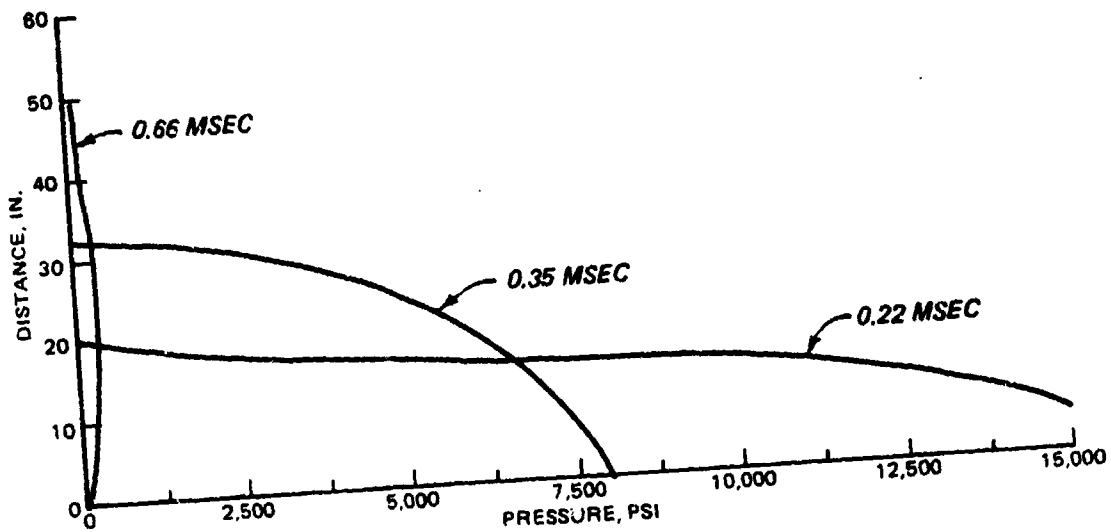
TEST 2A PRESSURE DISTRIBUTION AT GIVEN TIME



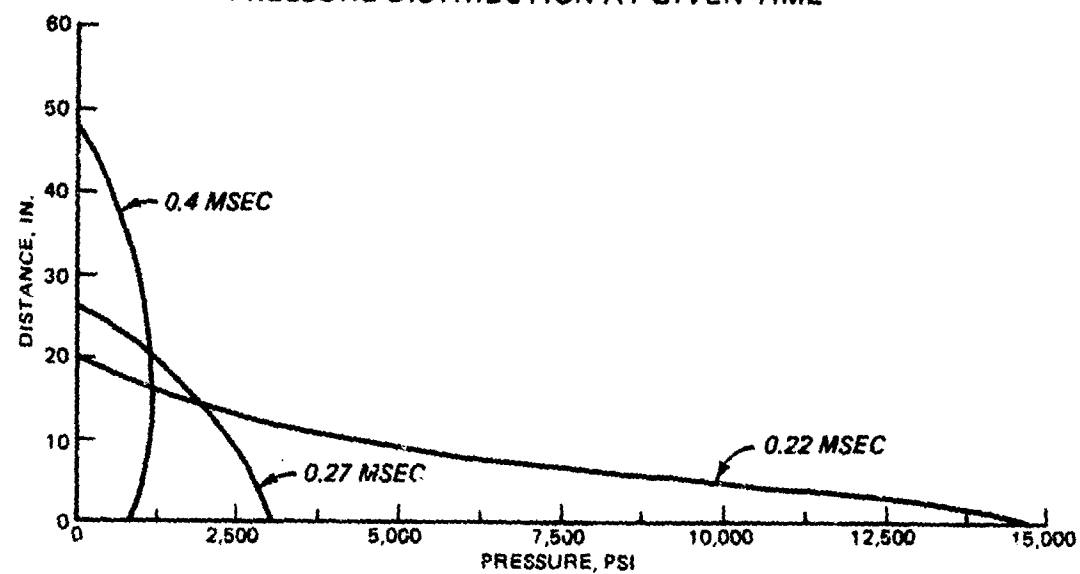
SPATIAL DISTRIBUTION OF PEAK PRESSURE



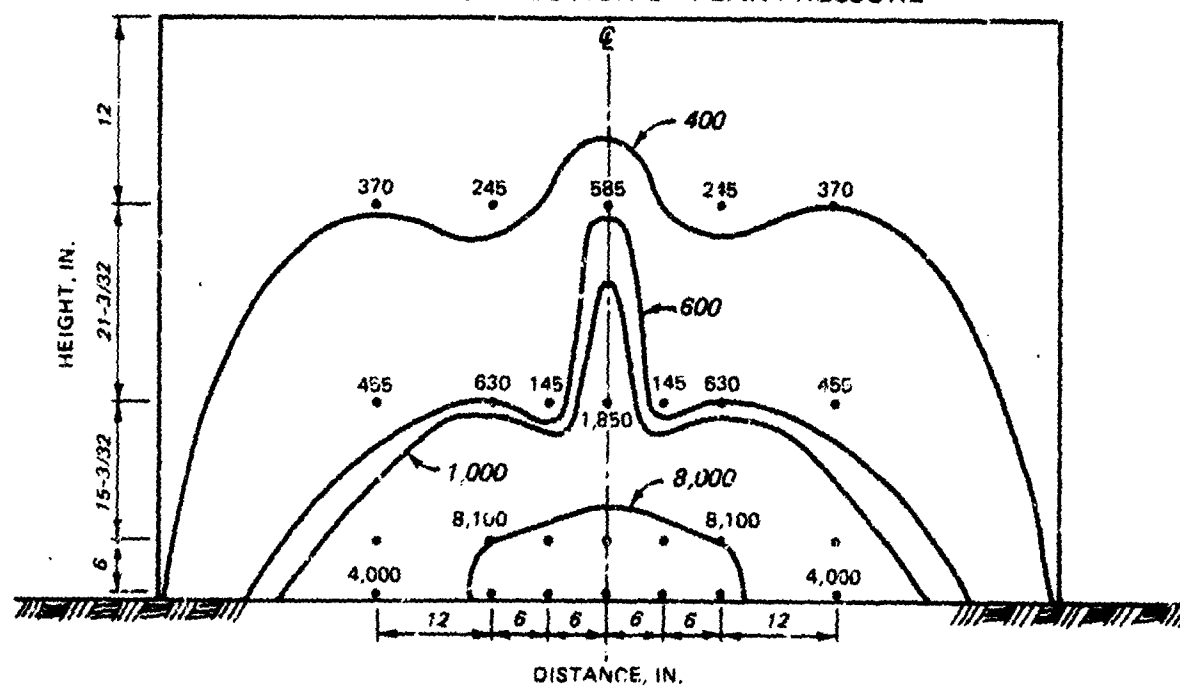
TEST 2B PRESSURE DISTRIBUTION AT GIVEN TIME



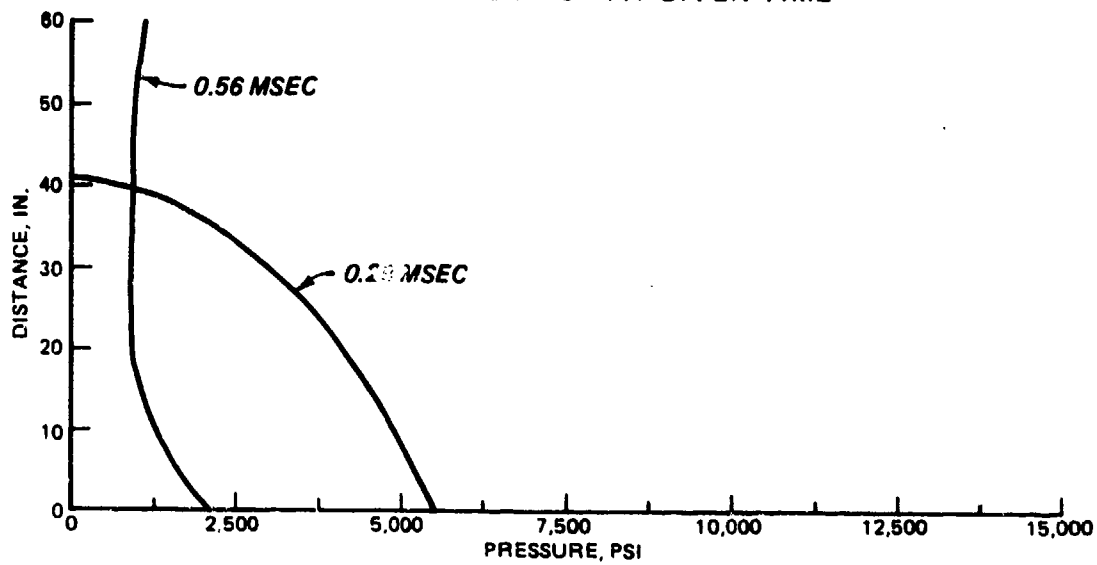
TEST 20
PRESSURE DISTRIBUTION AT GIVEN TIME



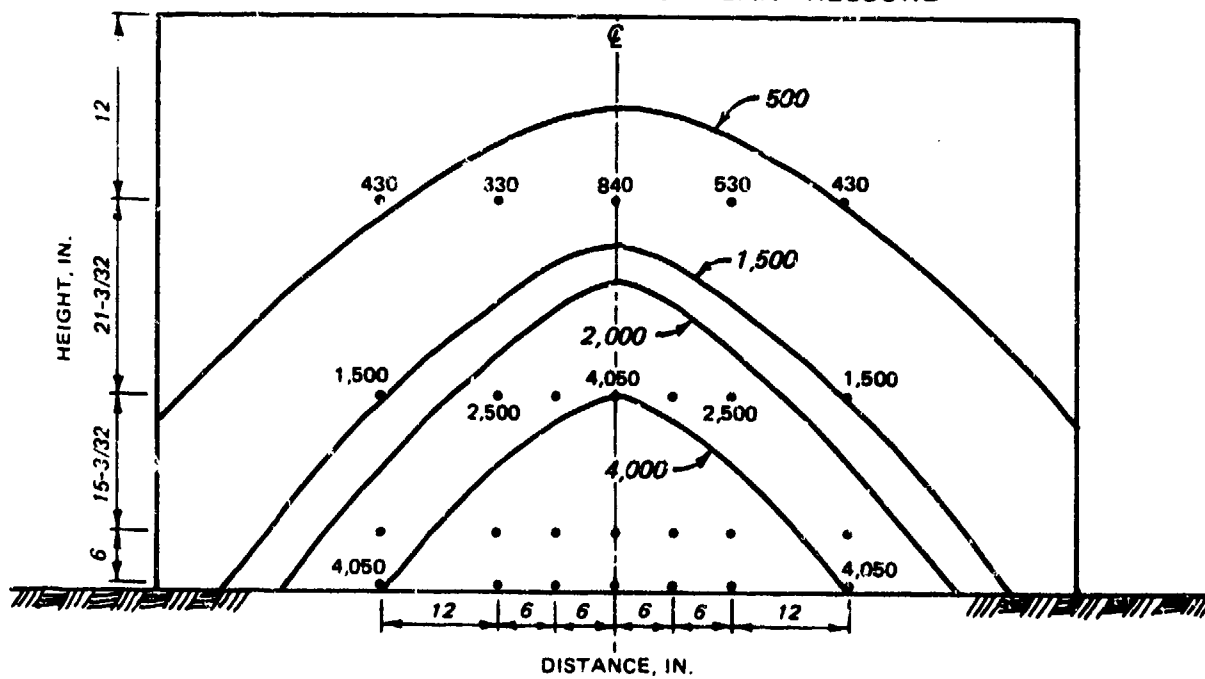
SPATIAL DISTRIBUTION OF PEAK PRESSURE



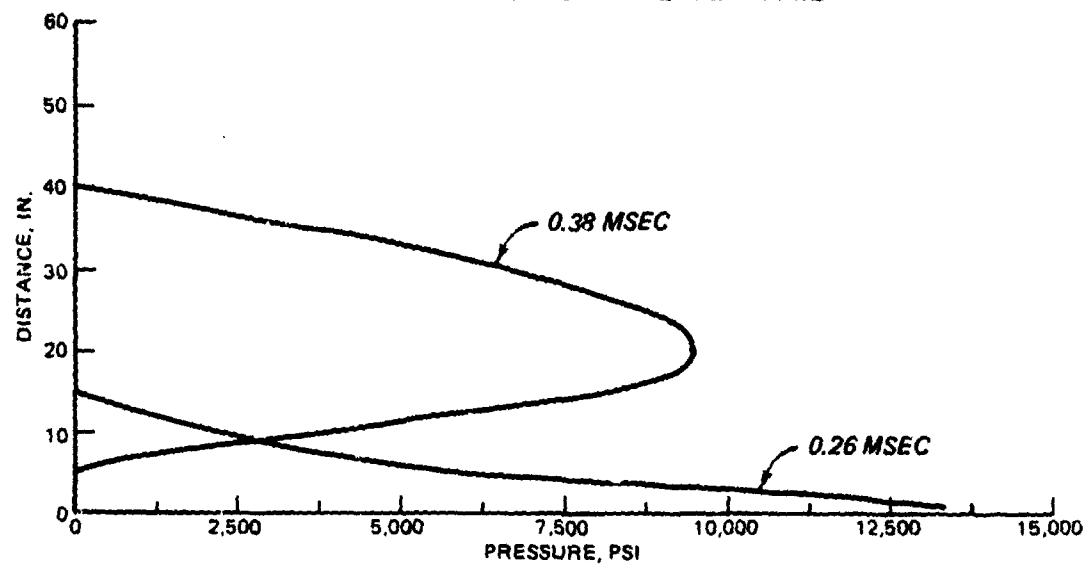
TEST 3A PRESSURE DISTRIBUTION AT GIVEN TIME



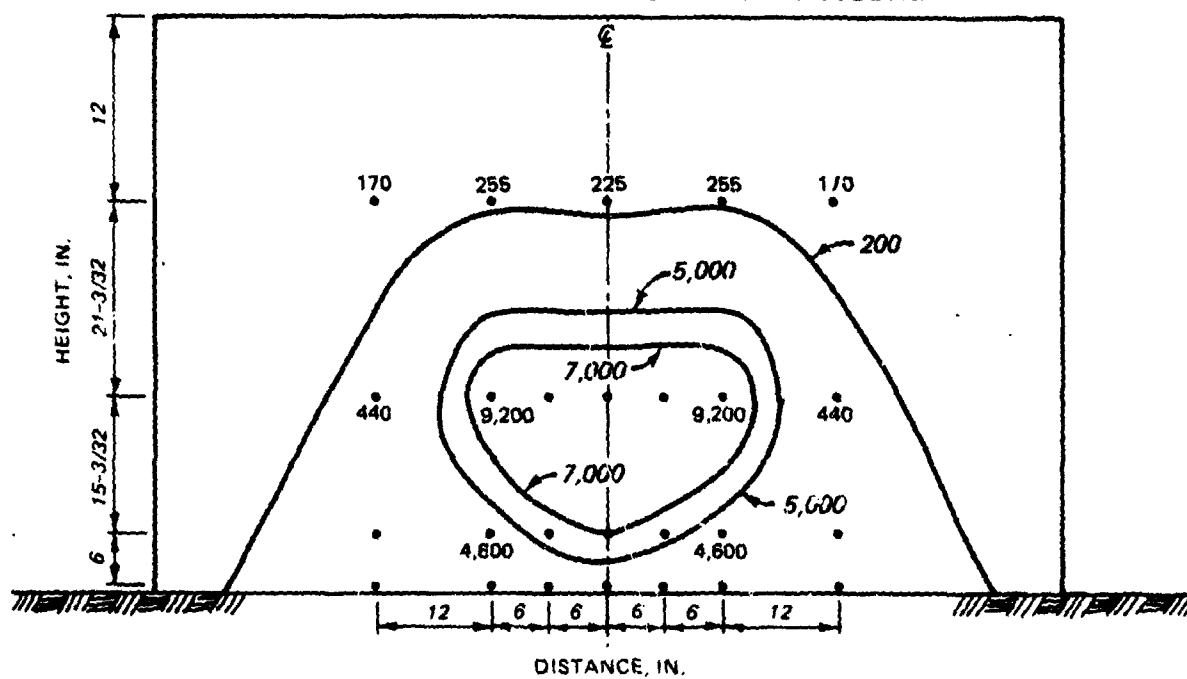
SPATIAL DISTRIBUTION OF PEAK PRESSURE



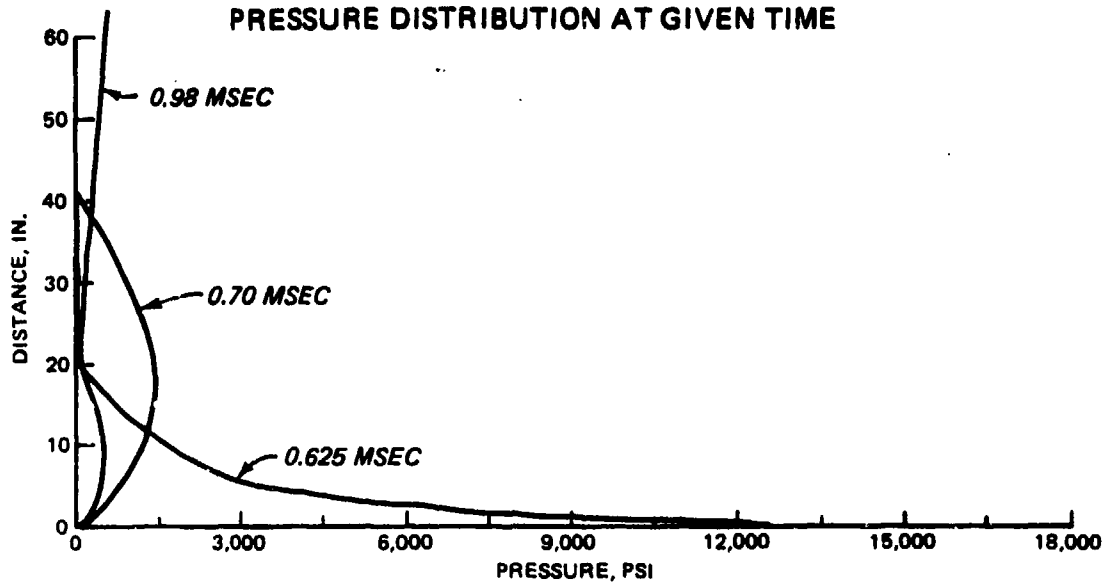
TEST 3B PRESSURE DISTRIBUTION AT GIVEN TIME



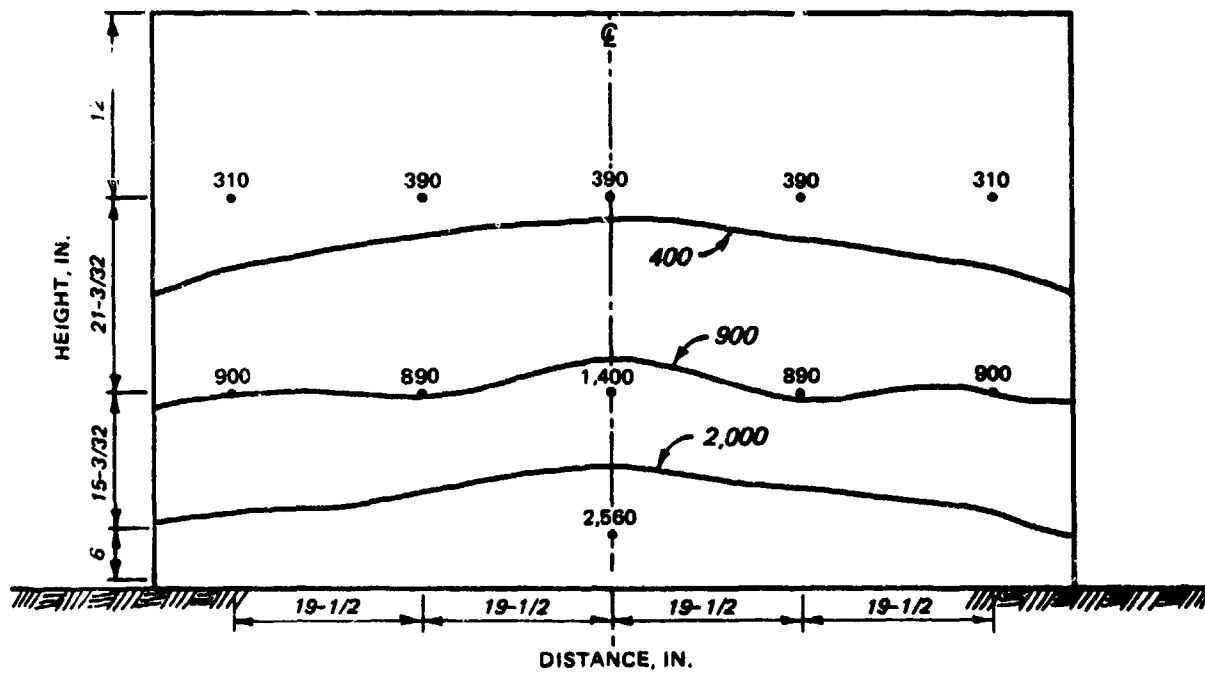
SPATIAL DISTRIBUTION OF PEAK PRESSURE



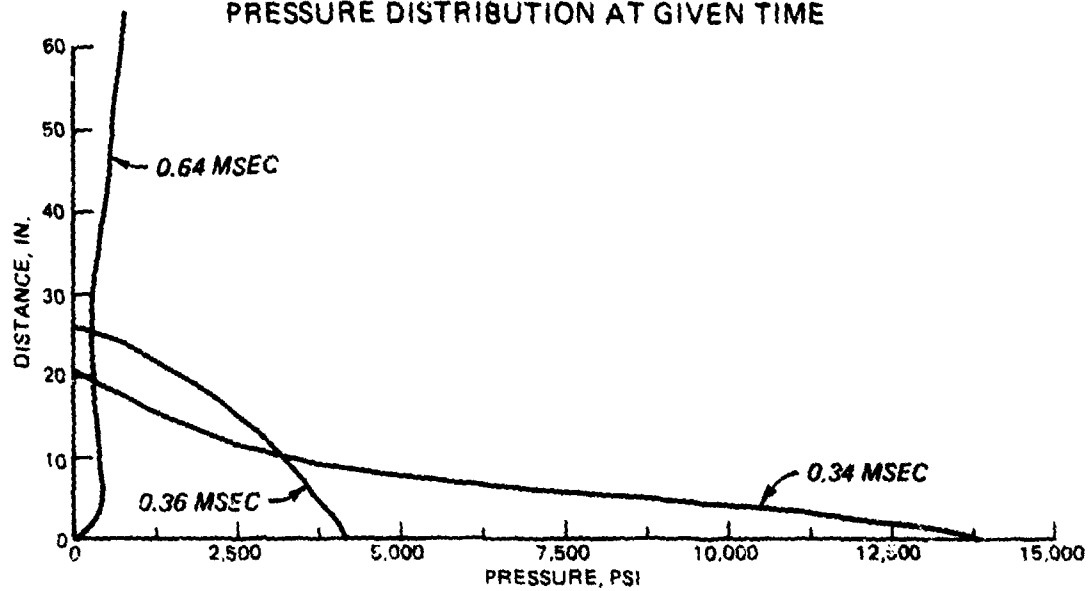
TEST 4A PRESSURE DISTRIBUTION AT GIVEN TIME



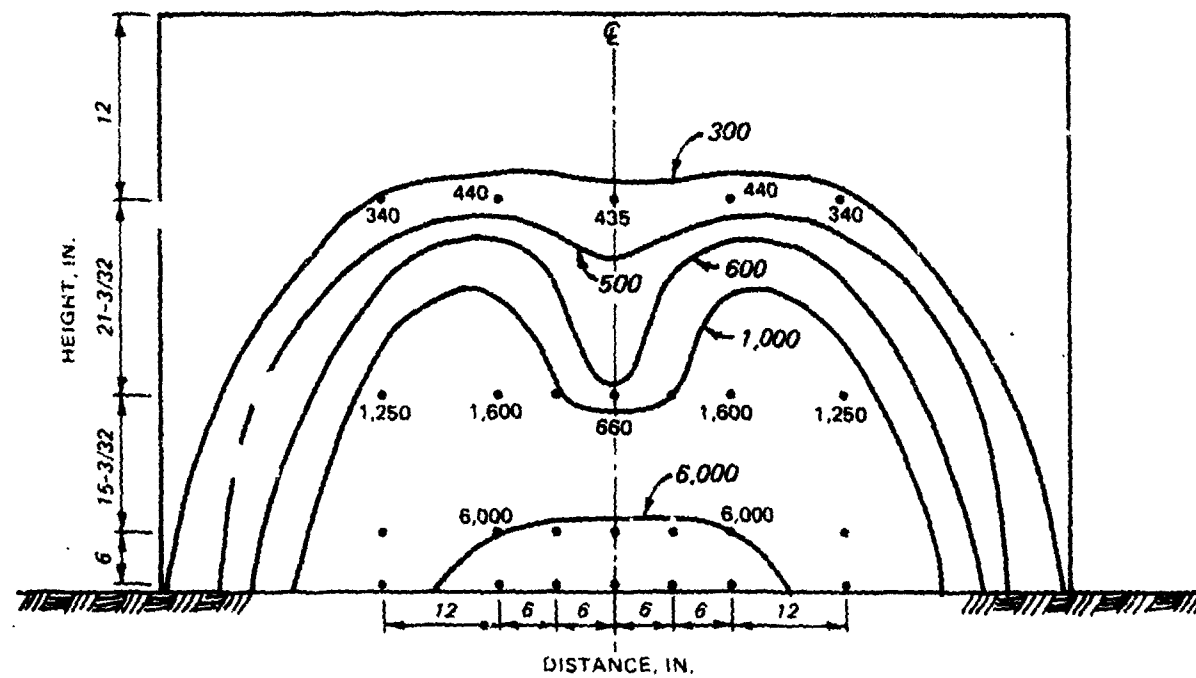
SPATIAL DISTRIBUTION OF PEAK PRESSURE



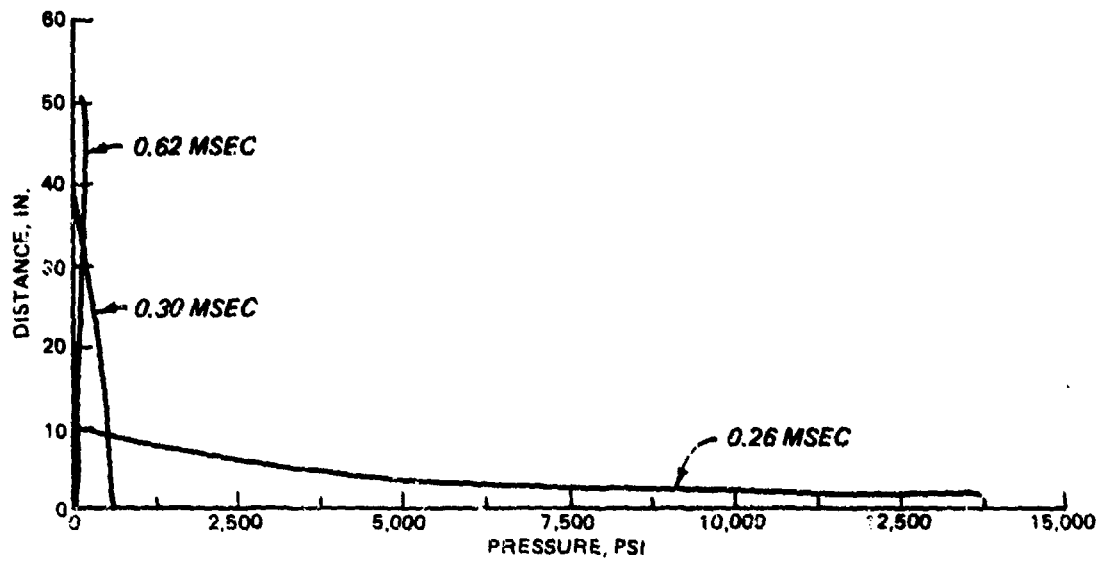
TEST 48
PRESSURE DISTRIBUTION AT GIVEN TIME



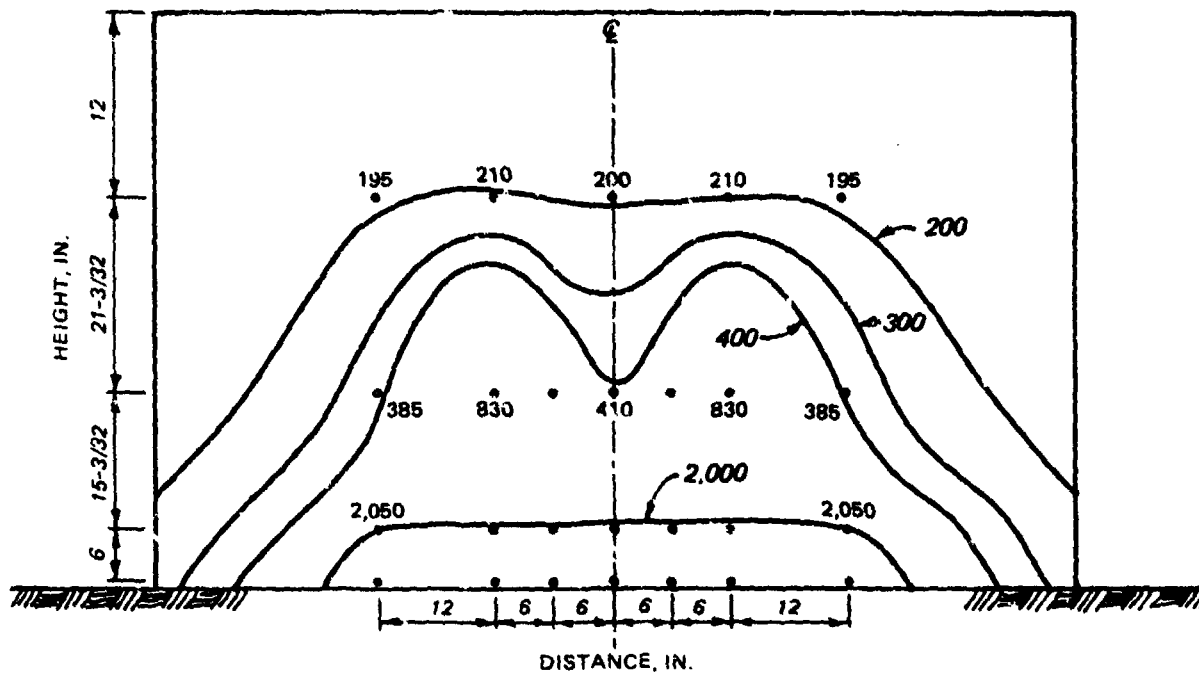
SPATIAL DISTRIBUTION OF PEAK PRESSURE

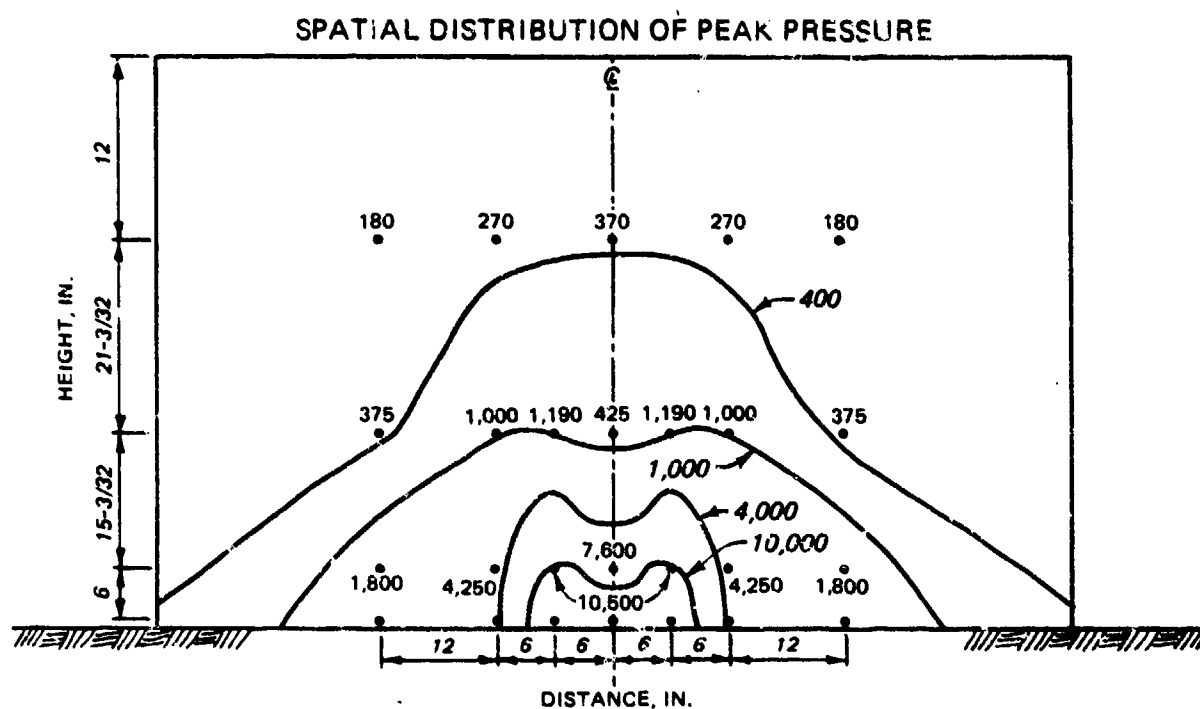
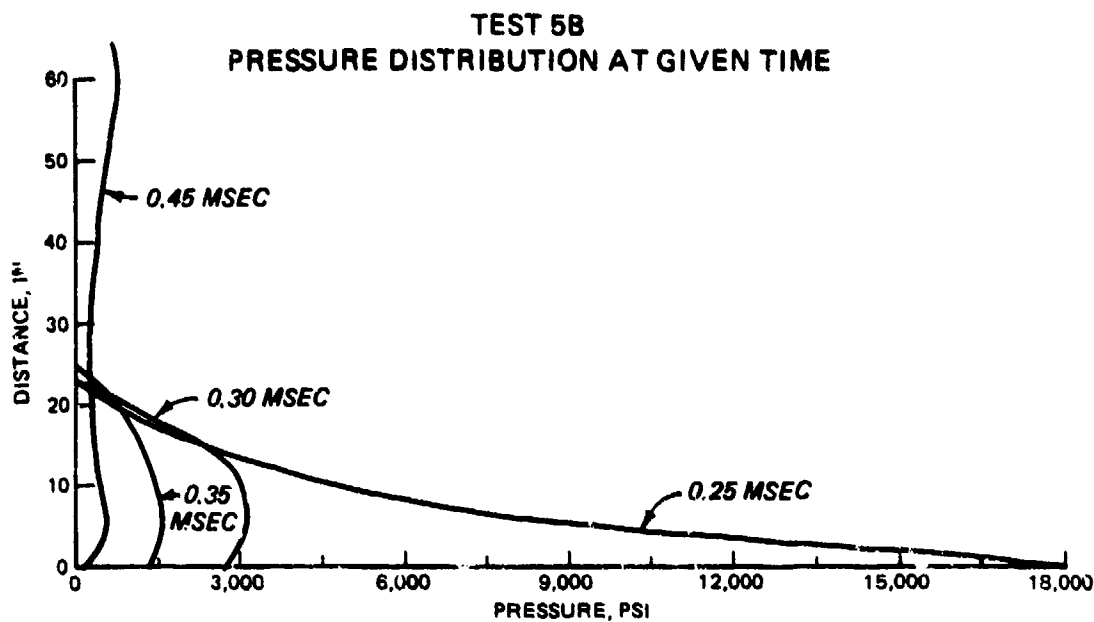


TEST 5A PRESSURE DISTRIBUTION AT GIVEN TIME

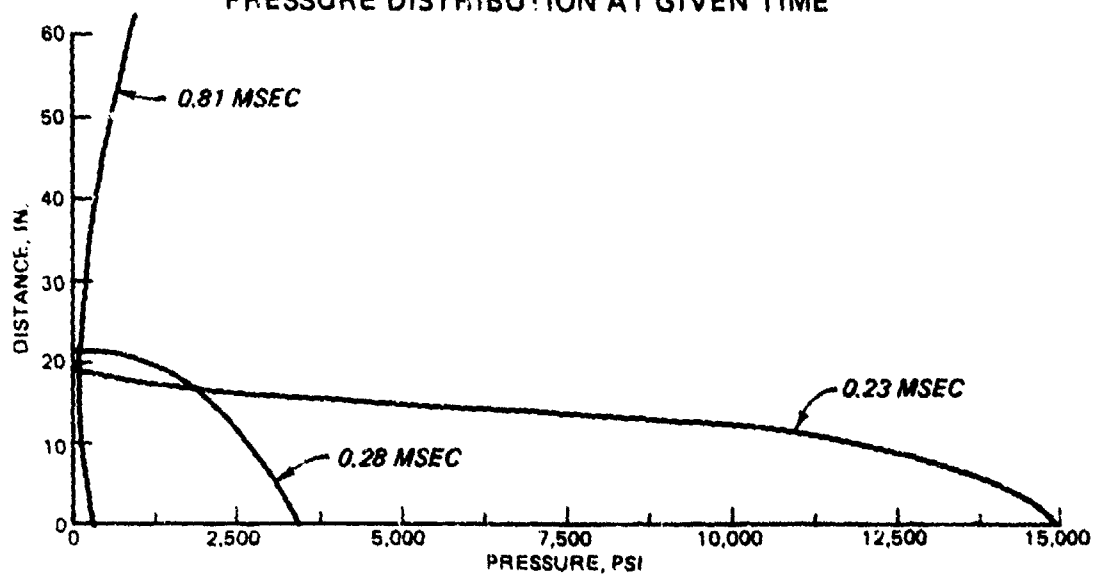


SPATIAL DISTRIBUTION OF PEAK PRESSURE

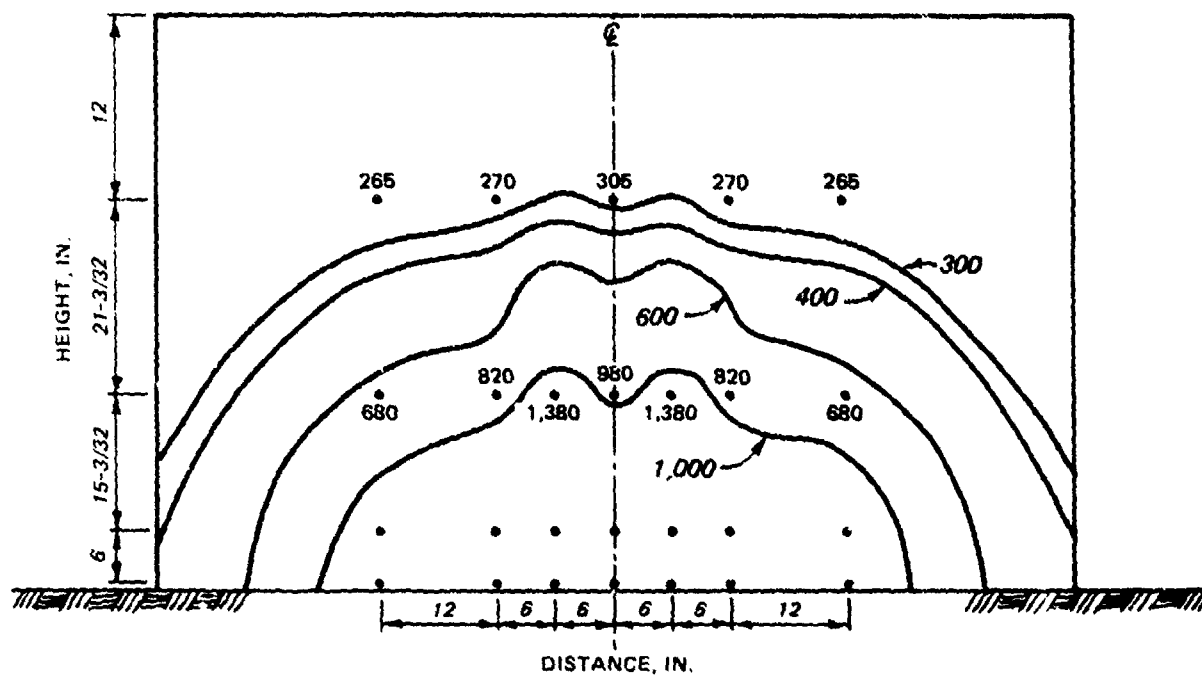




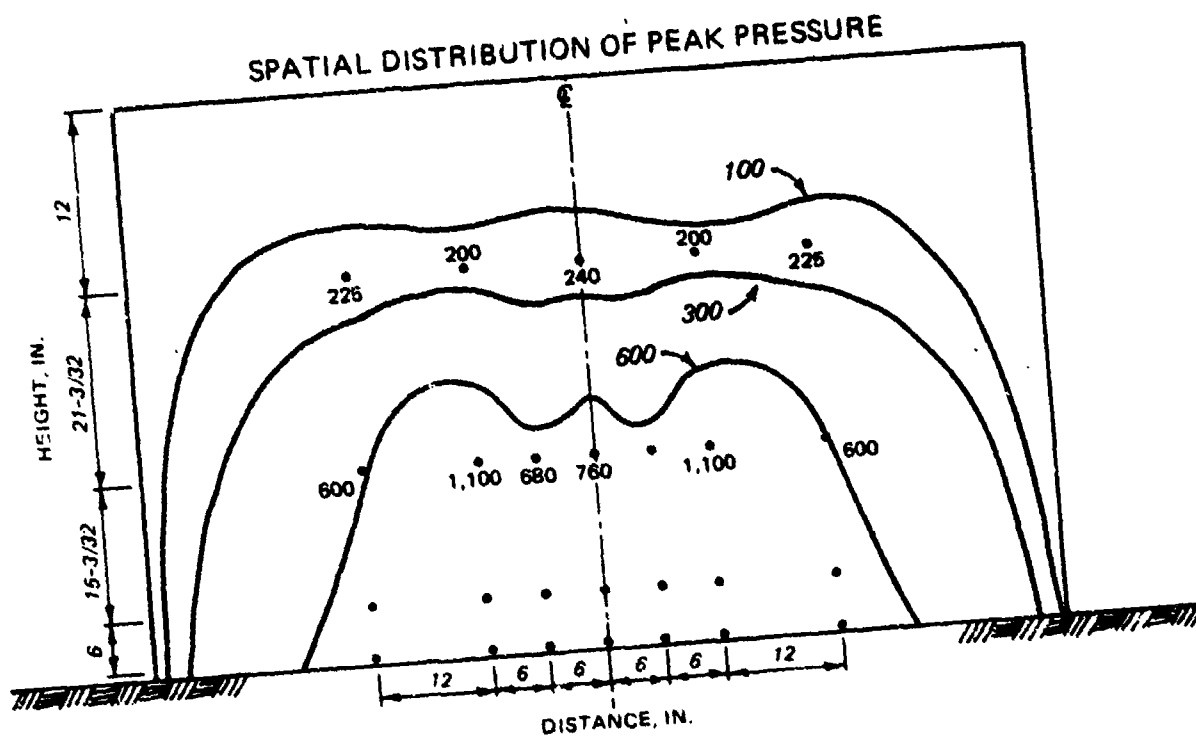
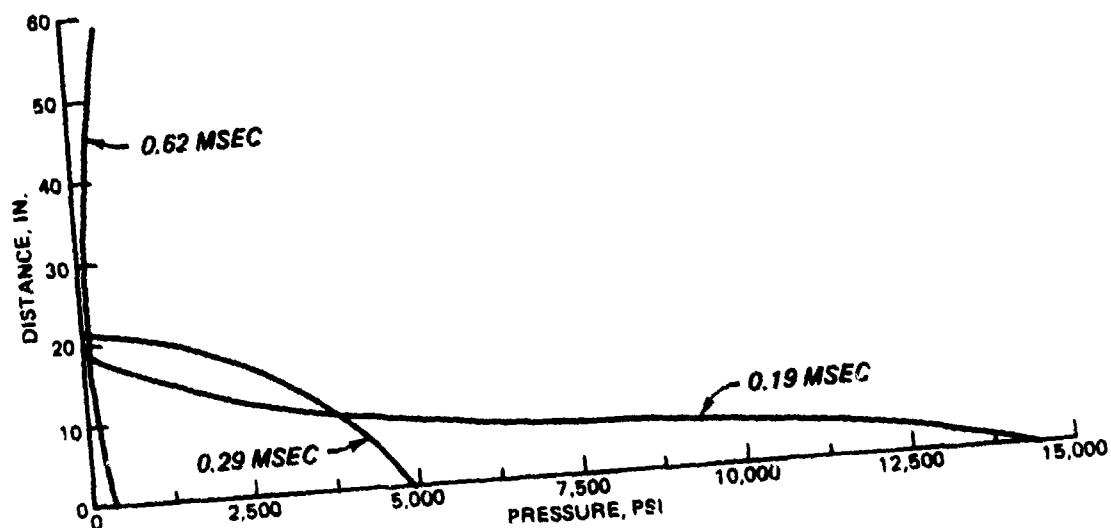
TEST 6A PRESSURE DISTRIBUTION AT GIVEN TIME



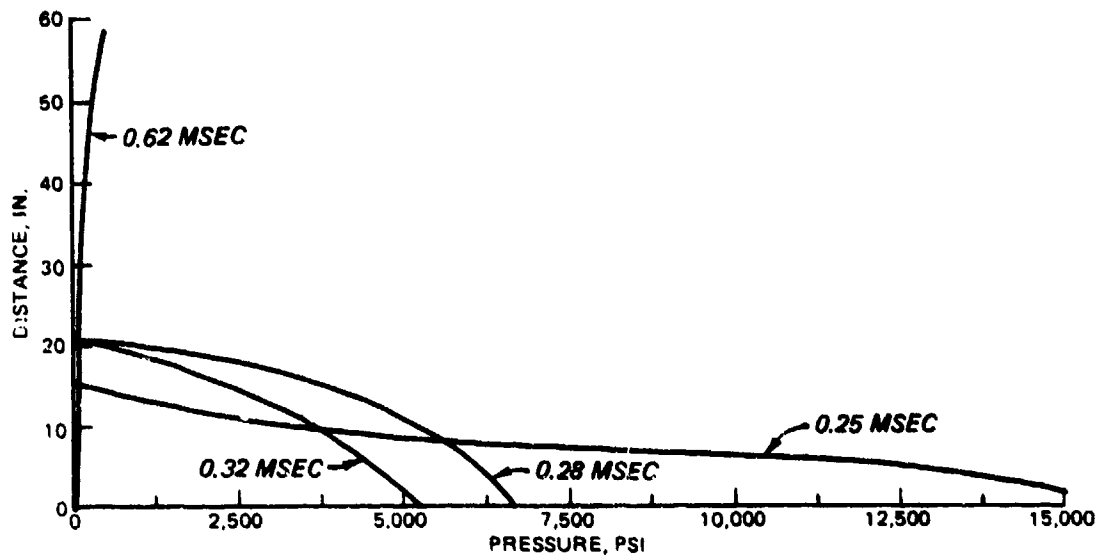
SPATIAL DISTRIBUTION OF PEAK PRESSURE



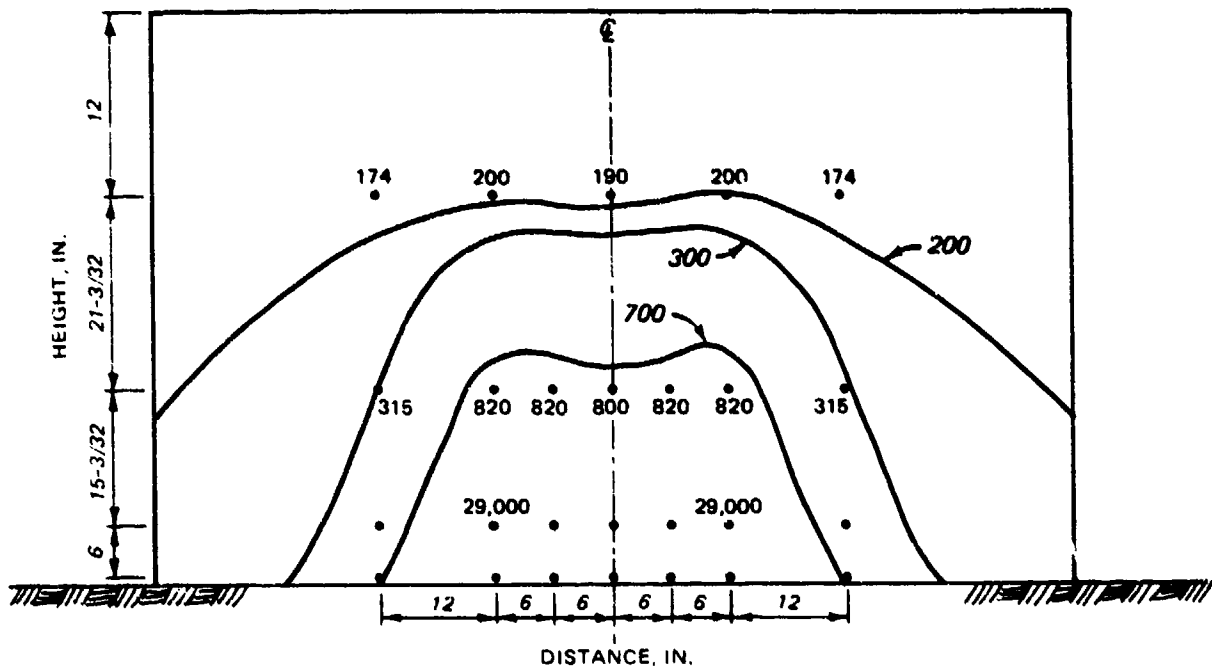
TEST 6B PRESSURE DISTRIBUTION AT GIVEN TIME



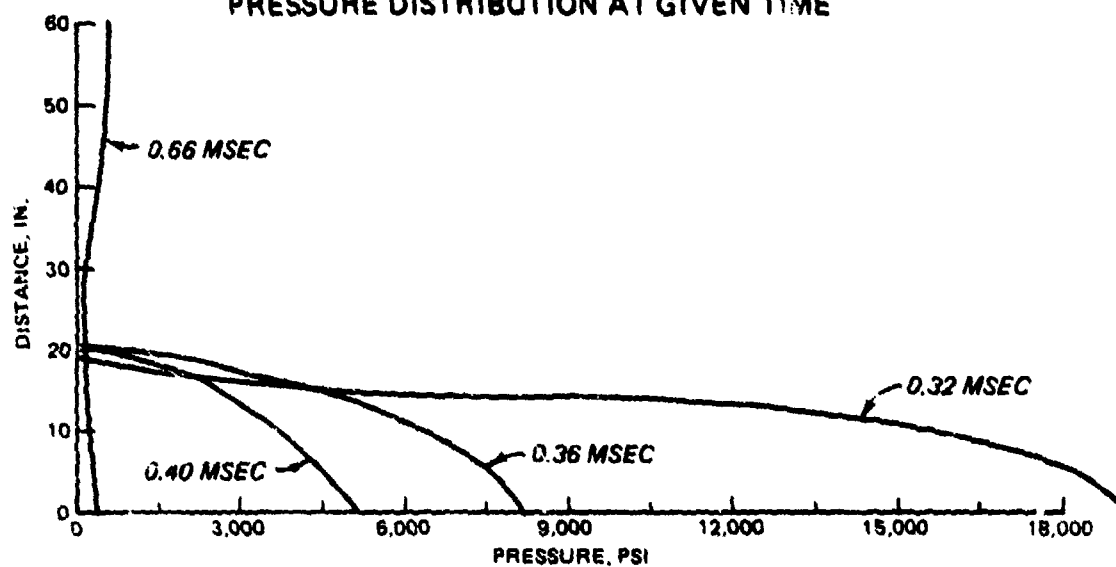
TEST 7A PRESSURE DISTRIBUTION AT GIVEN TIME



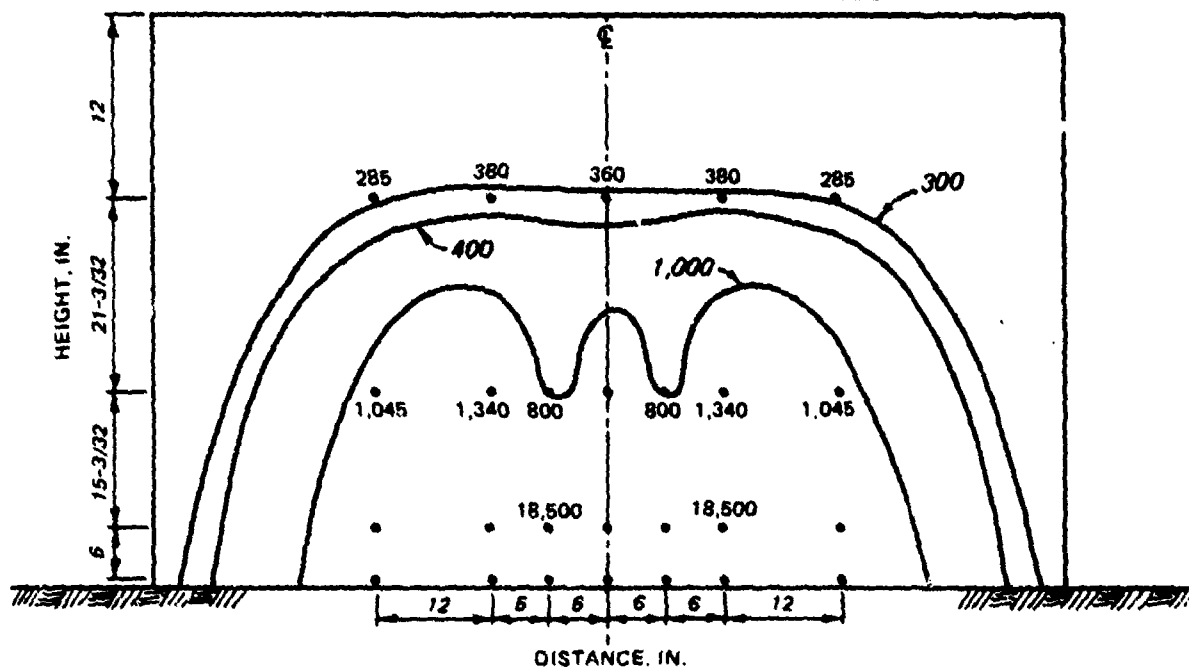
SPATIAL DISTRIBUTION OF PEAK PRESSURE



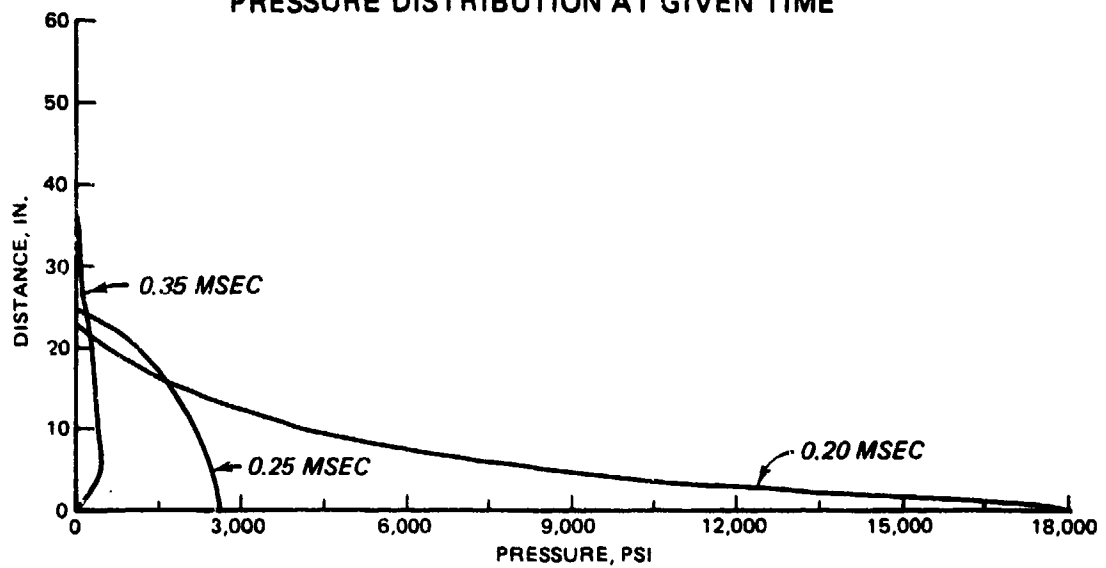
TEST 7B PRESSURE DISTRIBUTION AT GIVEN TIME



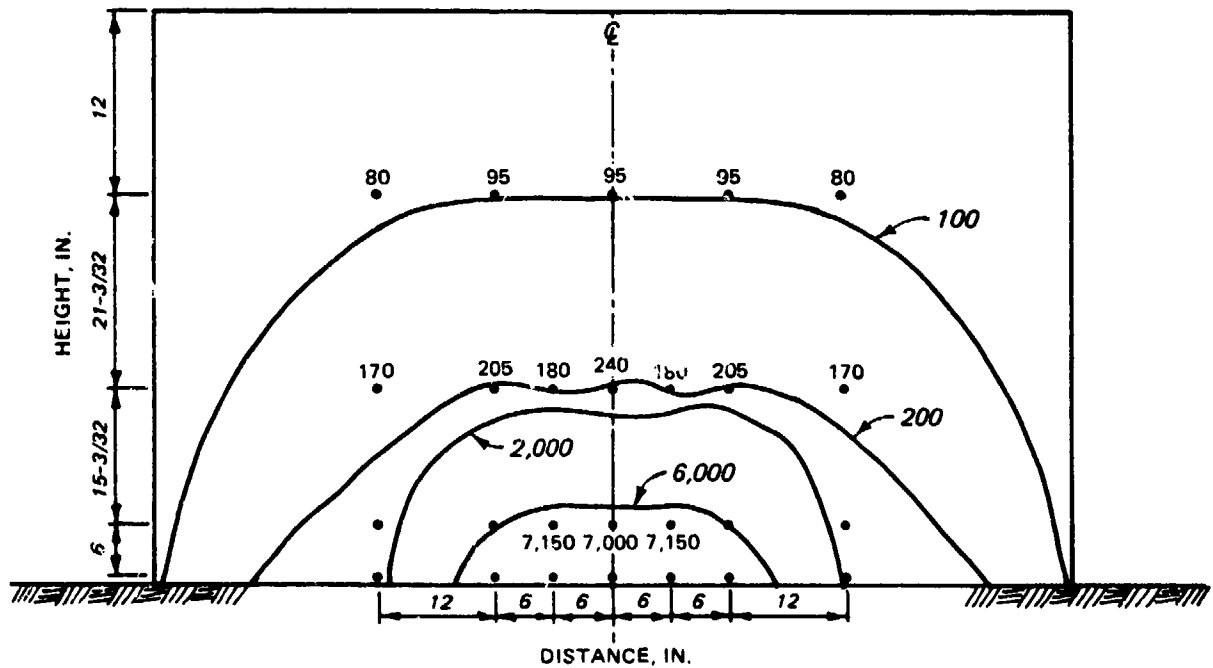
SPATIAL DISTRIBUTION OF PEAK PRESSURE



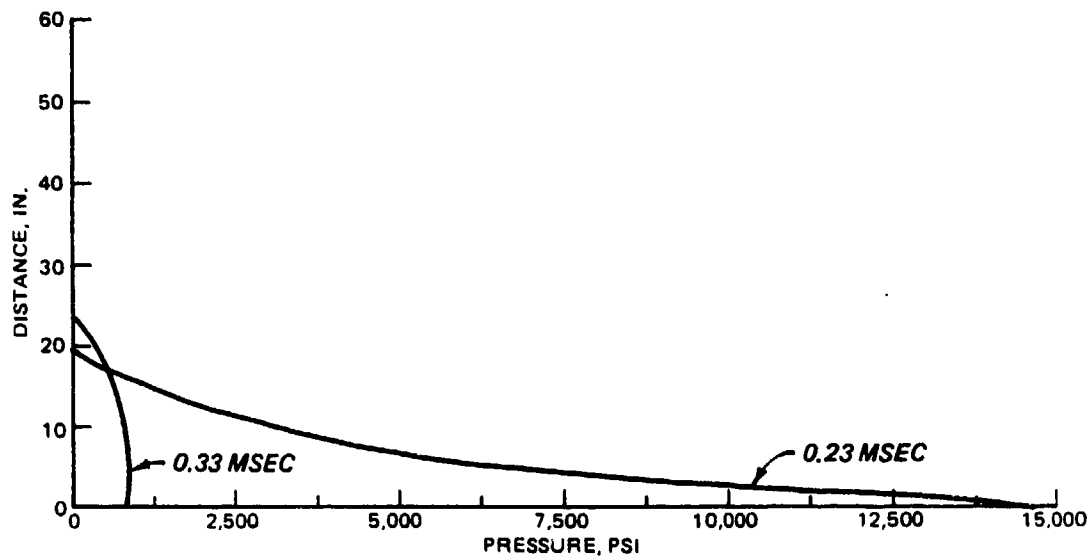
TEST 8A PRESSURE DISTRIBUTION AT GIVEN TIME



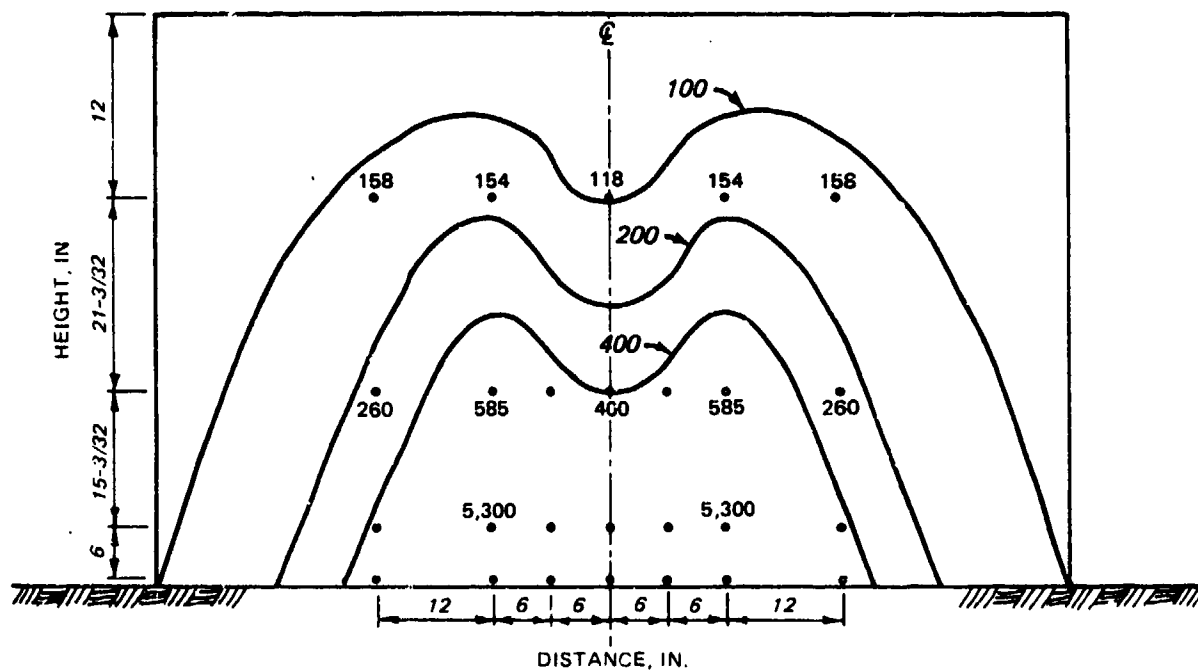
SPATIAL DISTRIBUTION OF PEAK PRESSURE



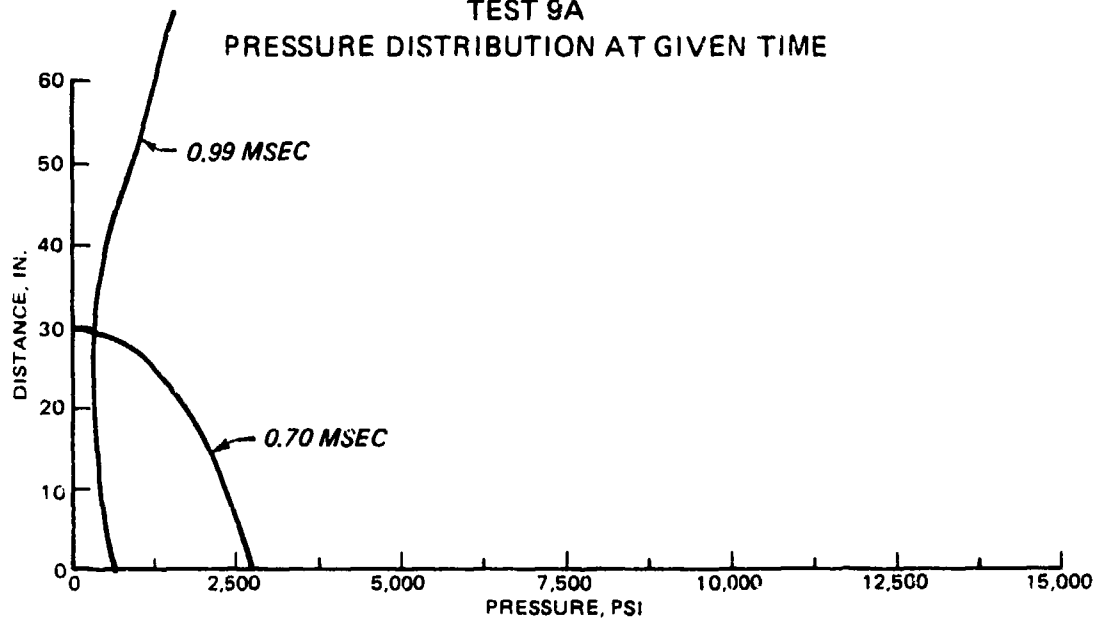
TEST 8B PRESSURE DISTRIBUTION AT GIVEN TIME



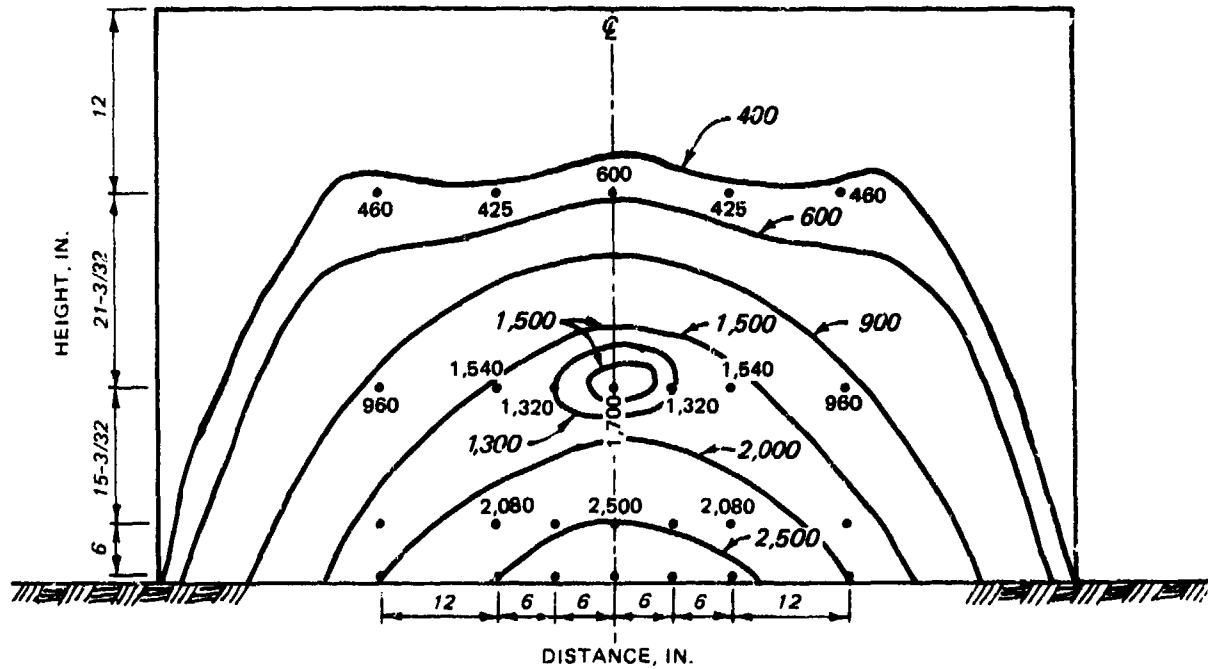
SPATIAL DISTRIBUTION OF PEAK PRESSURE



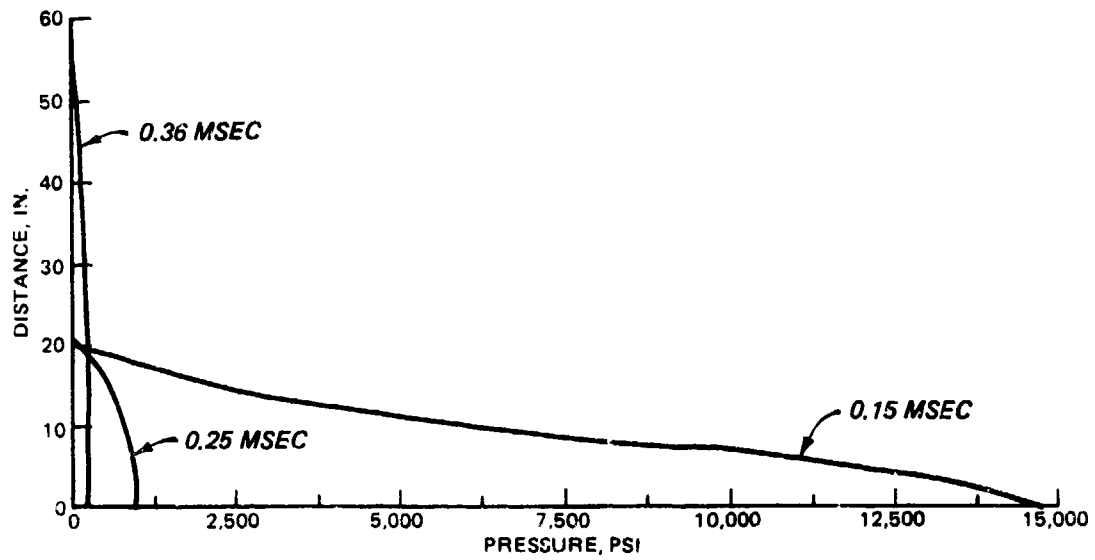
TEST 9A PRESSURE DISTRIBUTION AT GIVEN TIME



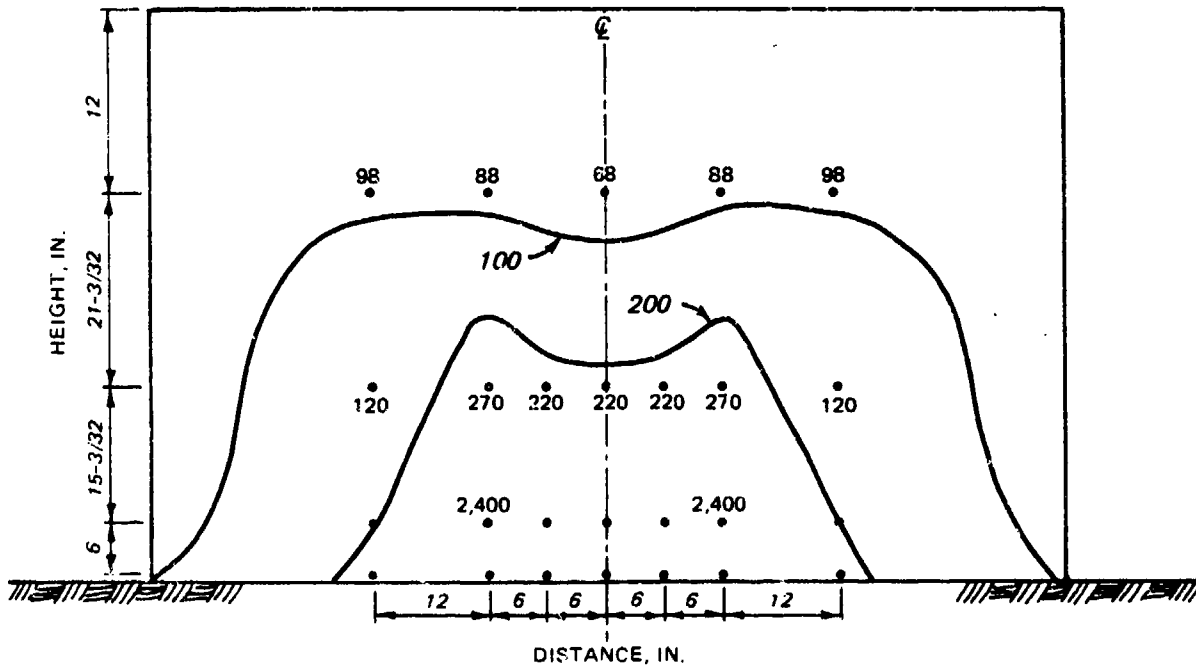
SPATIAL DISTRIBUTION OF PEAK PRESSURE



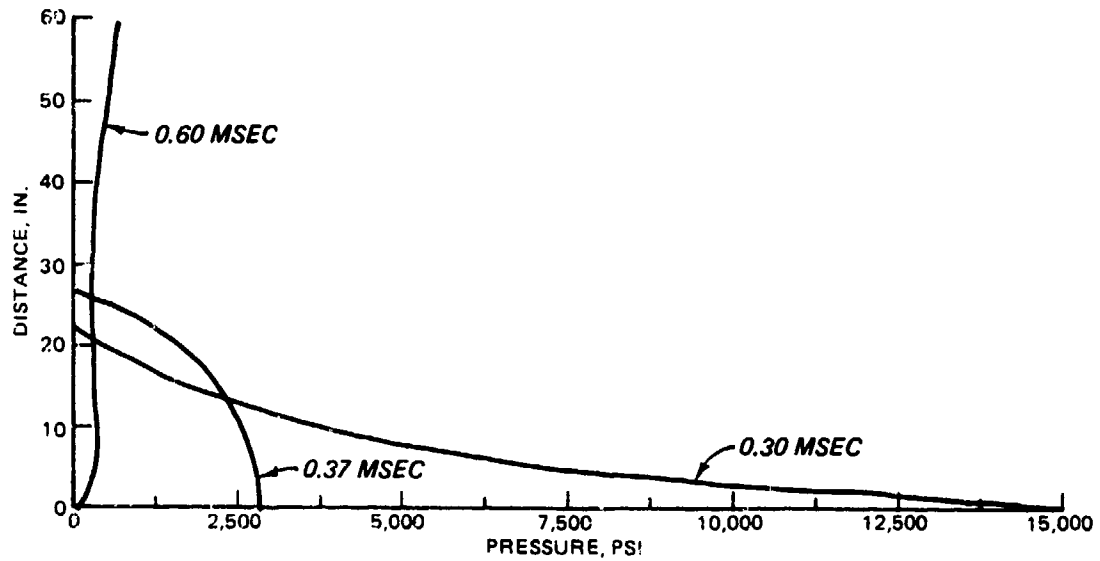
TEST 9B PRESSURE DISTRIBUTION AT GIVEN TIME



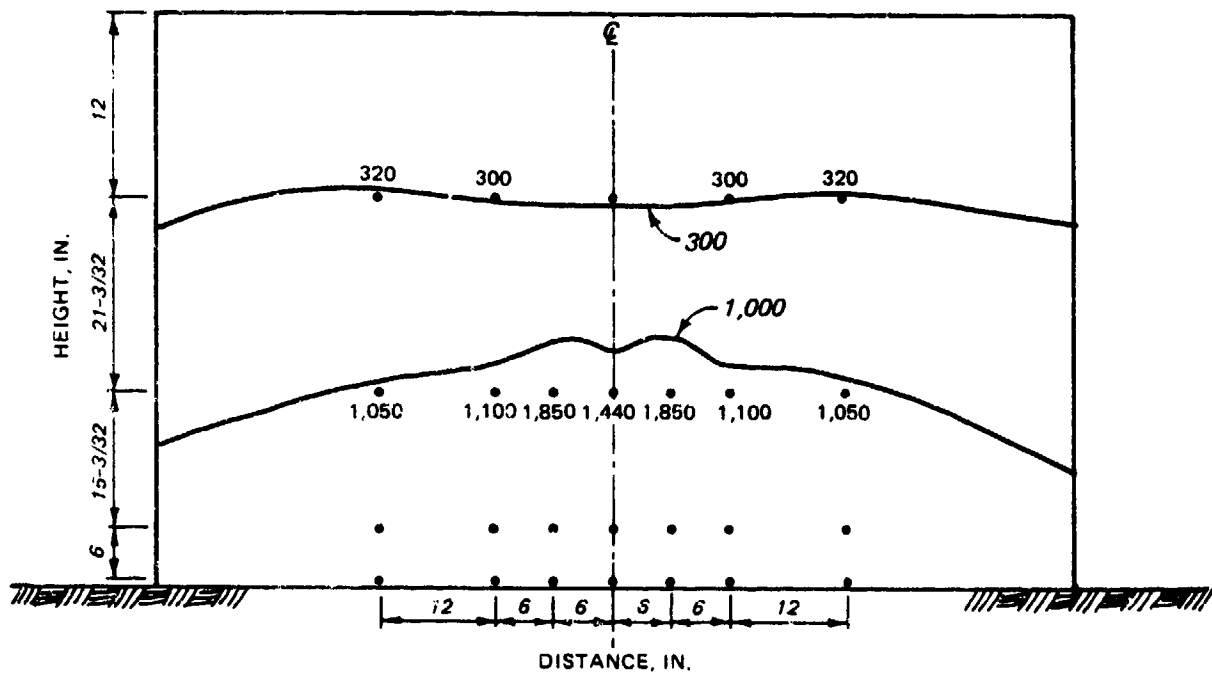
SPATIAL DISTRIBUTION OF PEAK PRESSURE



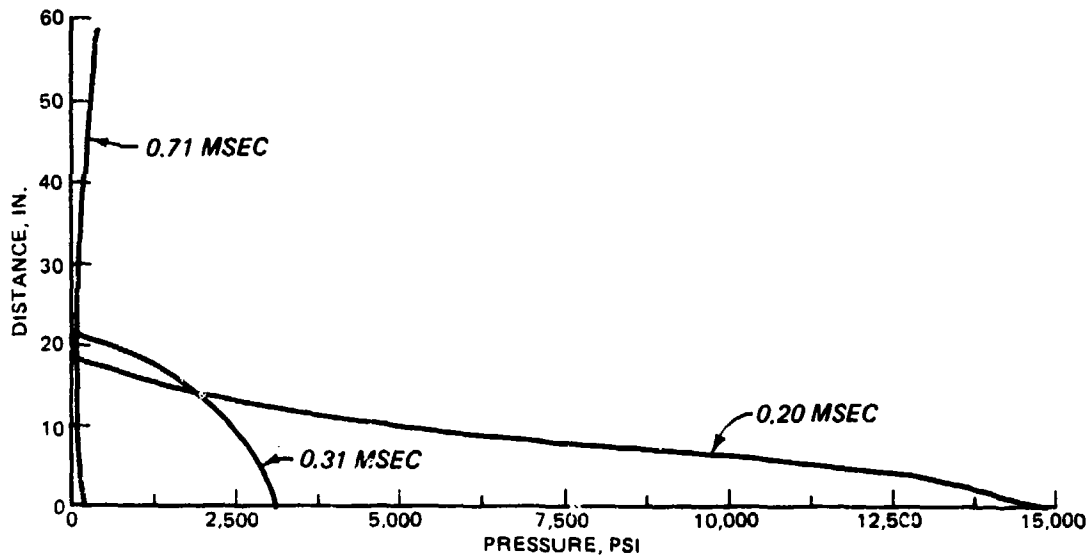
TEST 10A PRESSURE DISTRIBUTION AT GIVEN TIME



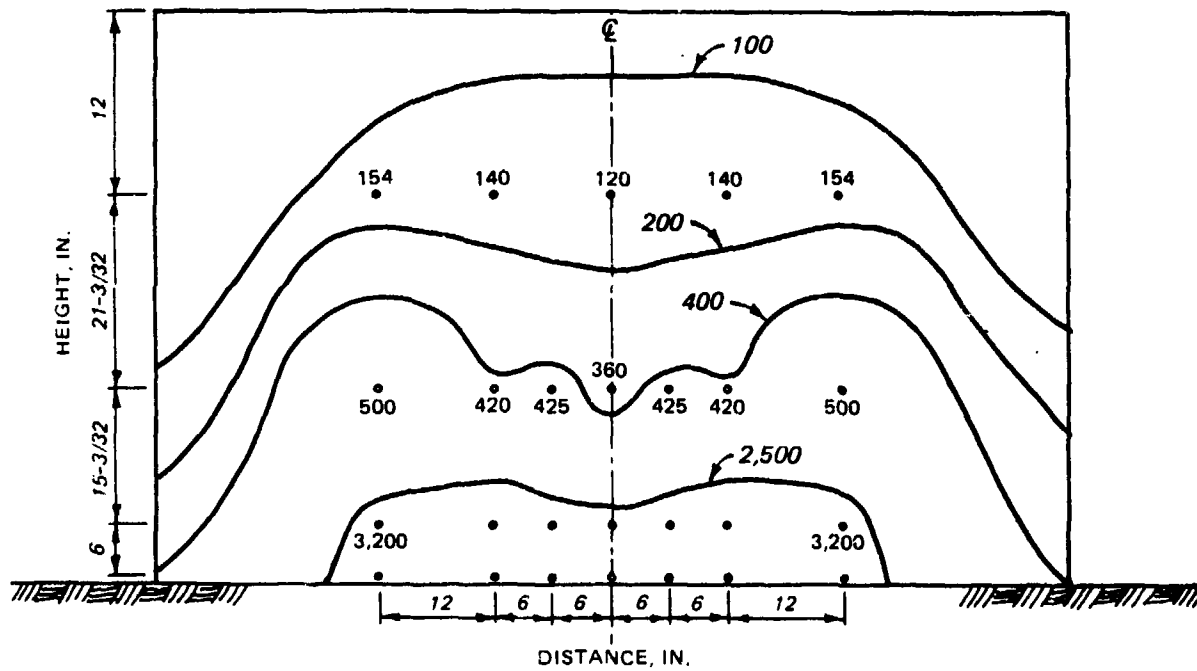
SPATIAL DISTRIBUTION OF PEAK PRESSURE



TEST 10B PRESSURE DISTRIBUTION AT GIVEN TIME



SPATIAL DISTRIBUTION OF PEAK PRESSURE



APPENDIX C
PRETEST AND POSTTEST PICTURES OF EACH TEST



Figure C.1. Test 1A with 3.626 pounds of C-4 in a cardboard tube 1.54 feet from an 8.5-inch-thick wall.

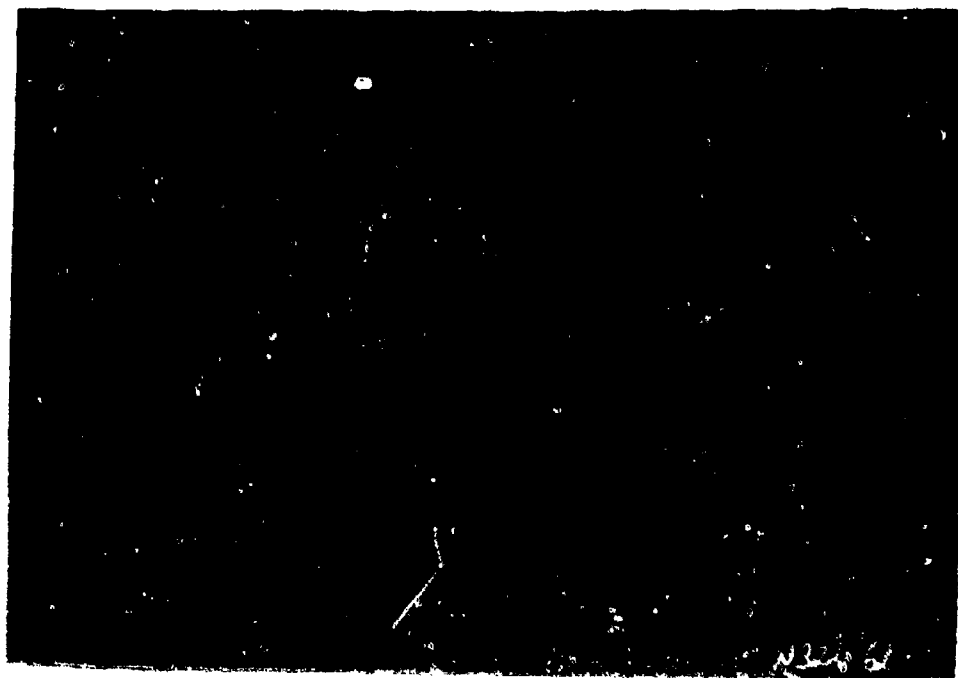


Figure C.2. Test 1A did not damage the front of the wall.

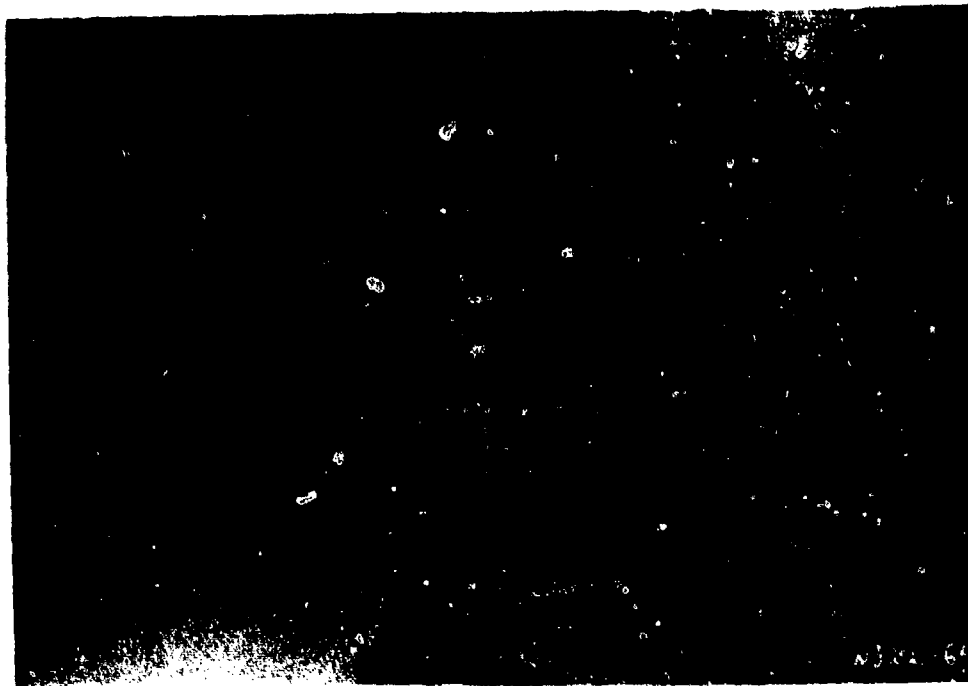


Figure C.3. Test 1A did not damage the back of the wall.

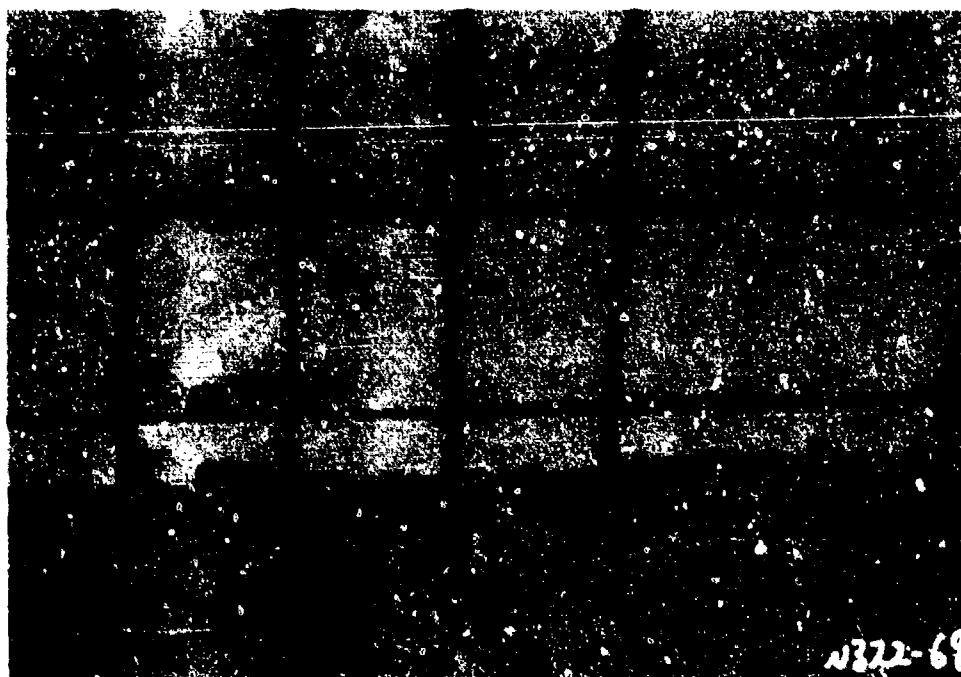


Figure C.4. Test 1B setup with 3.626 pounds of C-4 in a 0.70-inch-thick casing at a stand-off distance of 1.54 feet from an 8.5-inch-thick wall.

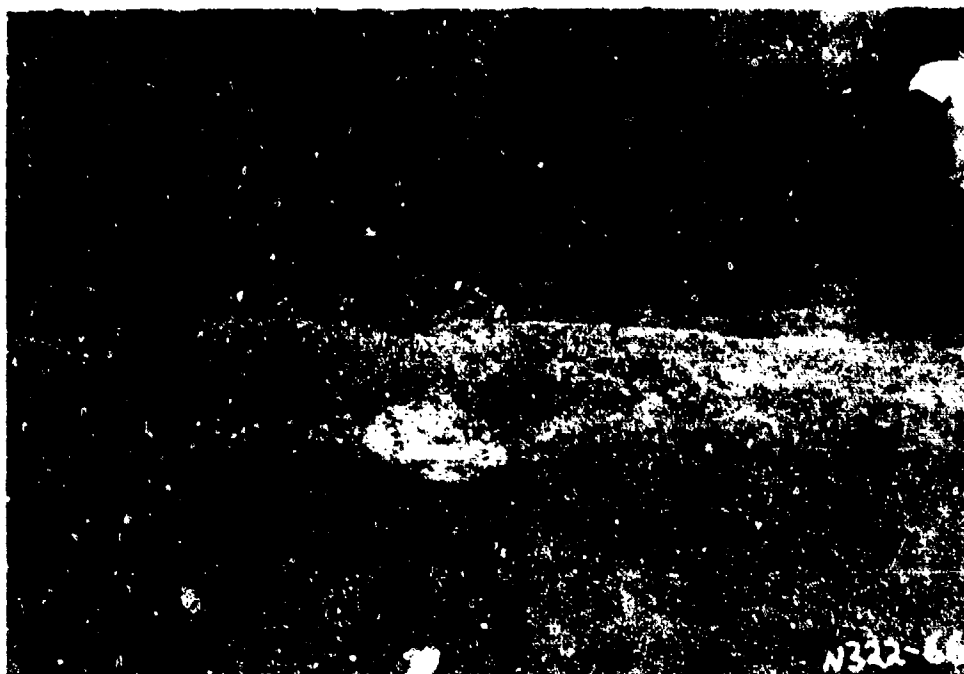


Figure C.5. The fragment damage to the front of the wall caused by test 1B. The deepest penetration was 0.75 to 1.0 inch.

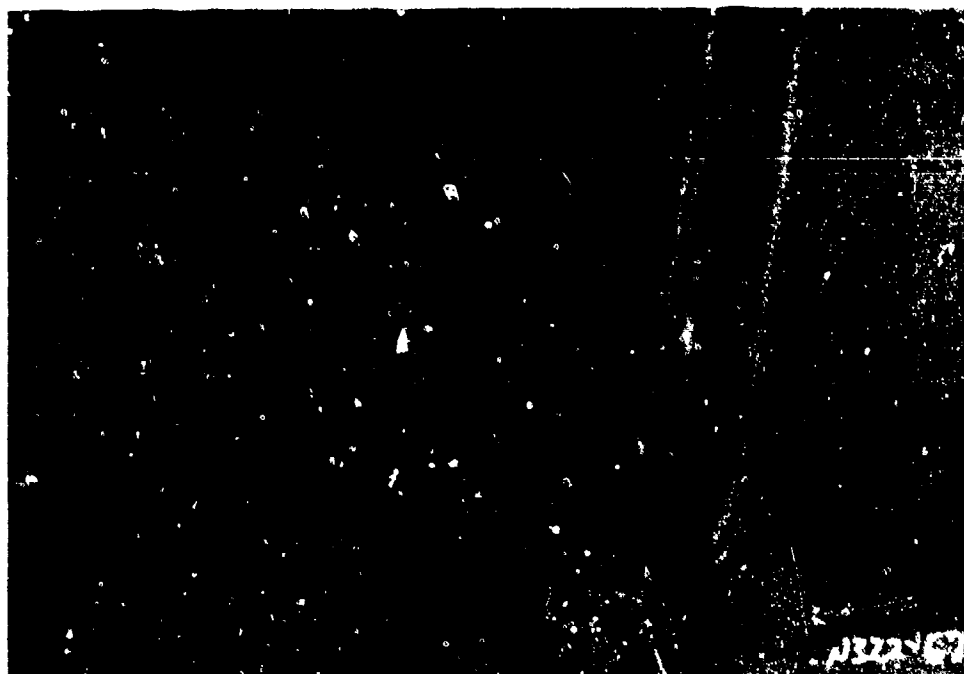


Figure C.6. The threshold spall caused by test 1B.



Figure C.7. Cross-sectional view of the wall in test 1B. The crack depth was 2.62 inches.





Figure C.8. Test 1C setup with a 1.074-pound C-4 bare charge in contact with an 8.5-inch wall.



Figure C.9. The crater blown in the wall by test 1C. The crater was 2.44 inches deep.

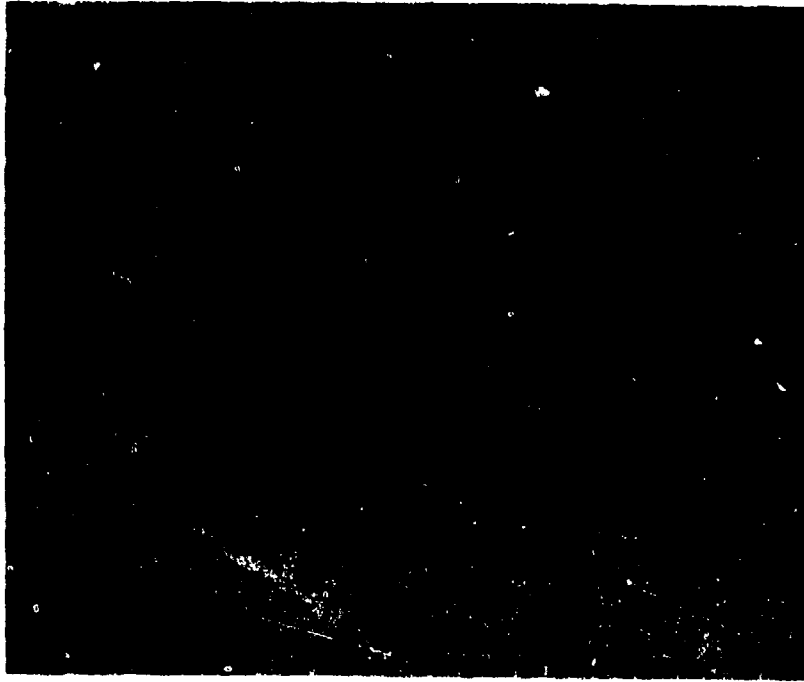


Figure C.10. Spall caused by test 1C. Spall depth was 2.5 inches and spall velocity was 53 ft/sec.



Figure C.11. Cross-sectional view of the wall in test 1C.

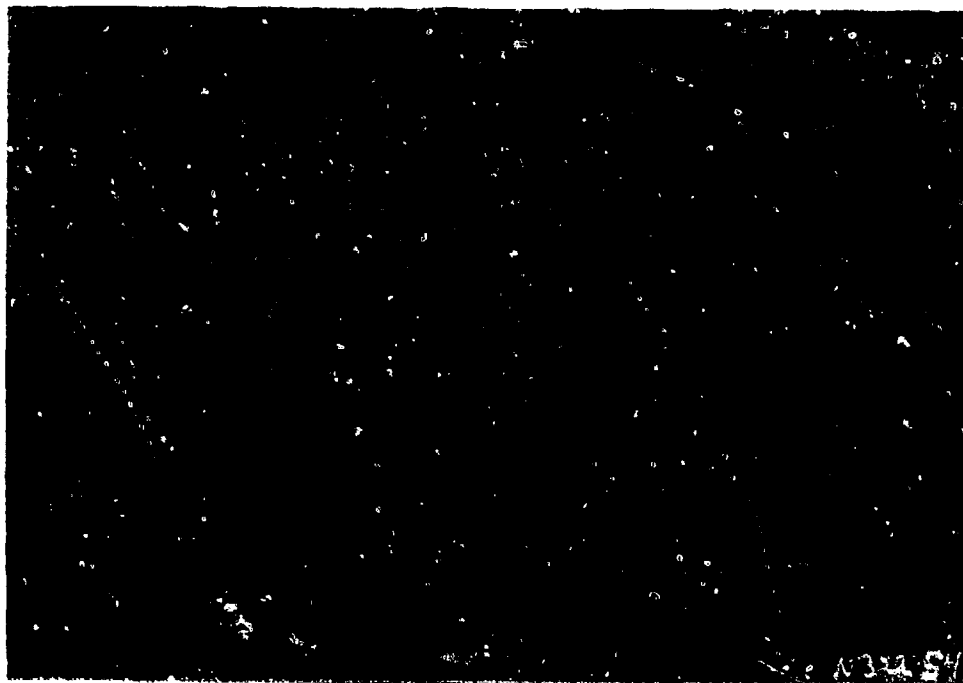


Figure C.12. Test 1D setup with a 7.44-pound bare C-4 charge 1.54 feet from an 8.5-inch-thick wall.



Figure C.13. Very light scabbing of the wall caused by test 1D.



Figure C.14. Spall caused by test 1D. Spall depth was 2.25 inches and spall velocity was 28 ft/s.

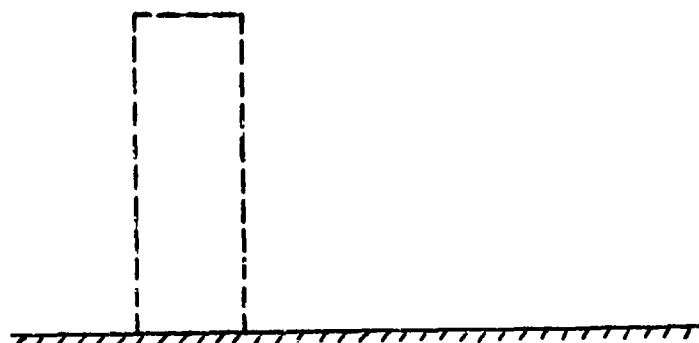
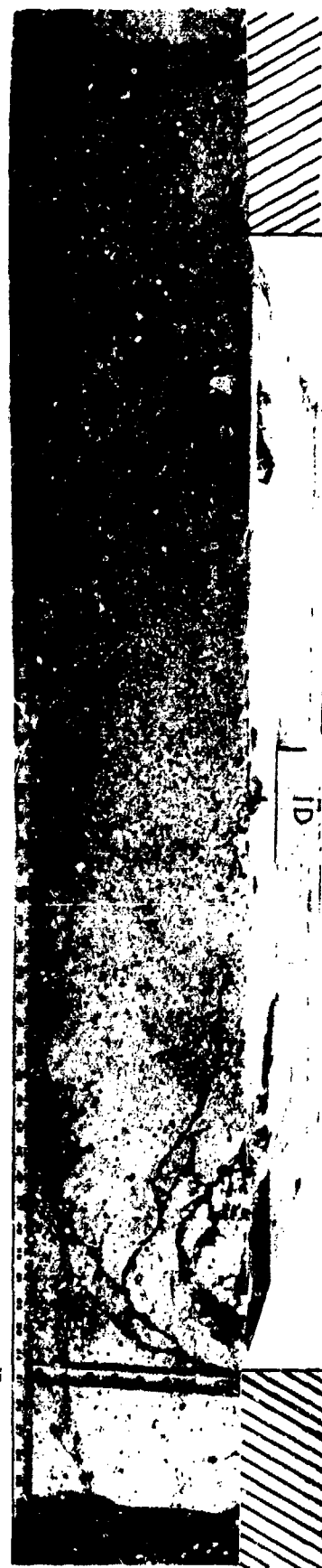


Figure C.15. Cross-sectional view of wall in test 1C. The main cracks were 2.44 inches and 4.5 inches deep.



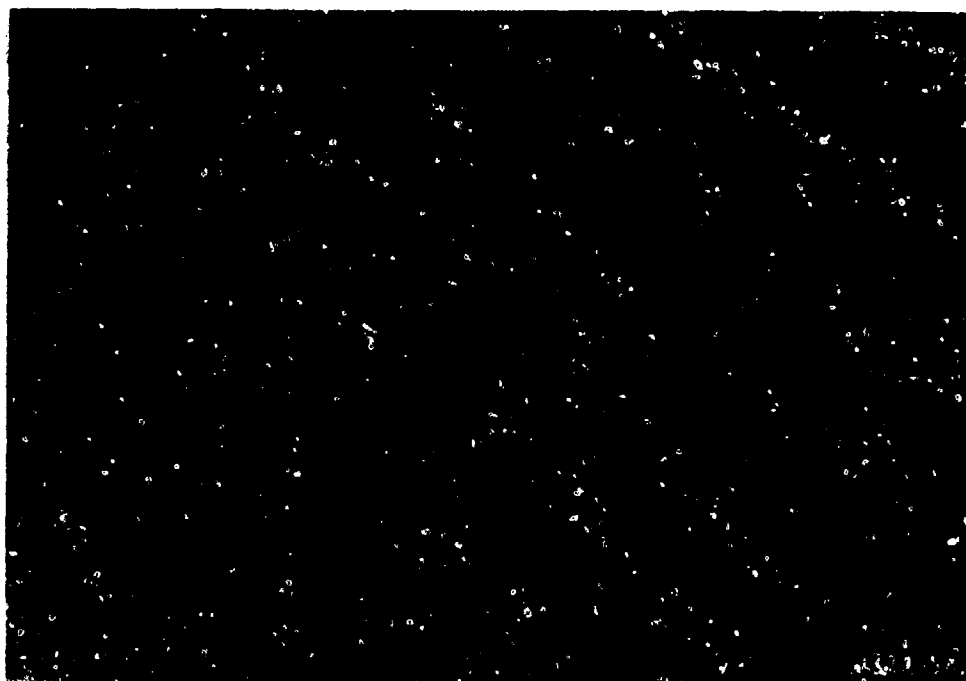


Figure C.16. Test 2A with a 4.70-pound bare C-4 charge at 1.54 feet from an 8.5-inch-thick wall.

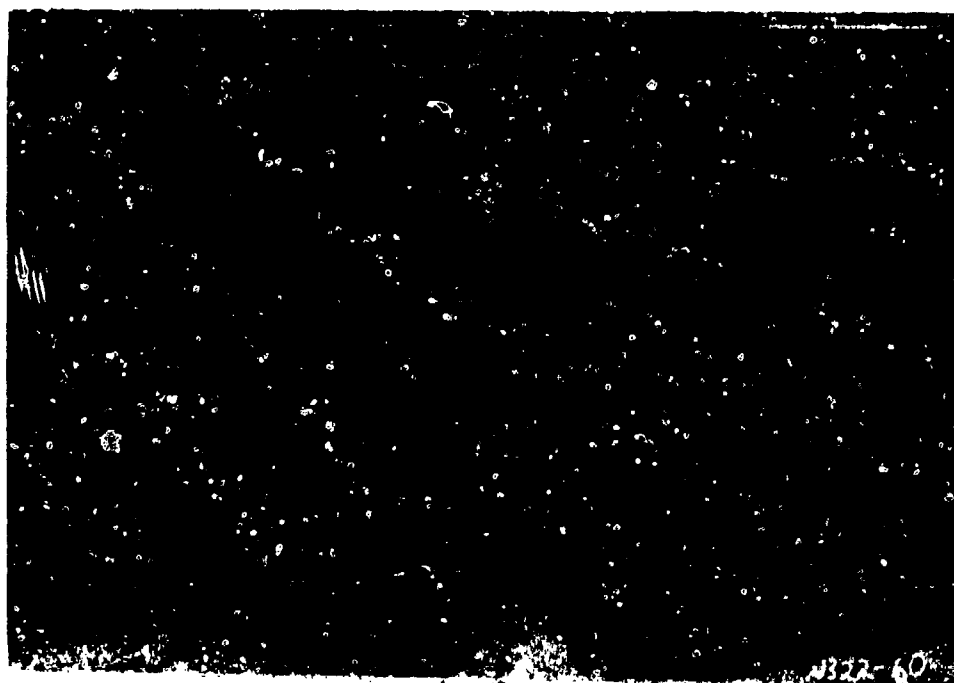


Figure C.17. Test 2A did not damage the front of the wall.

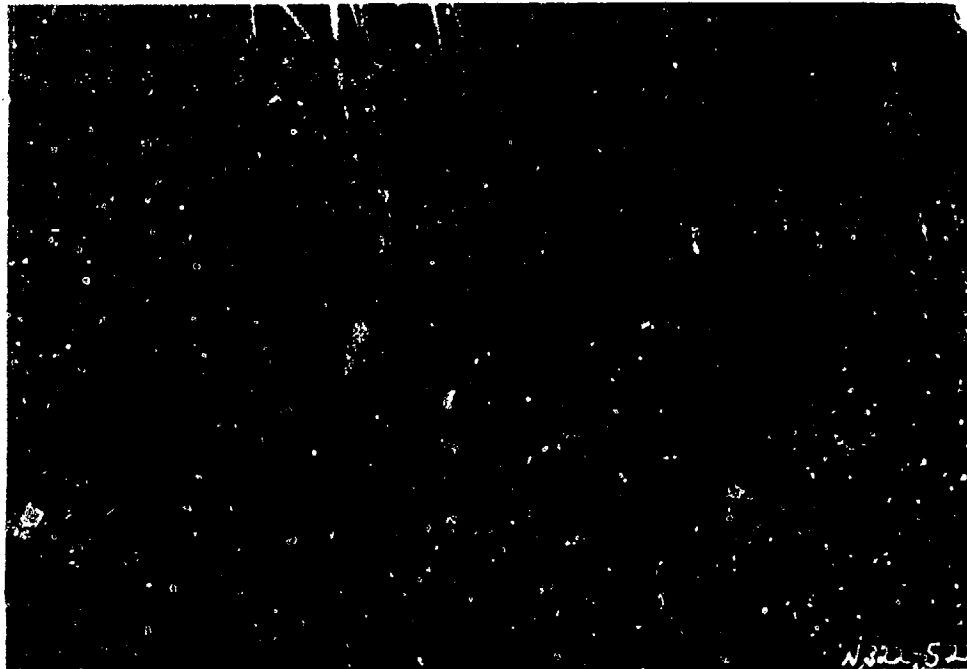


Figure C.18. Test 2A did not damage the back of the wall.

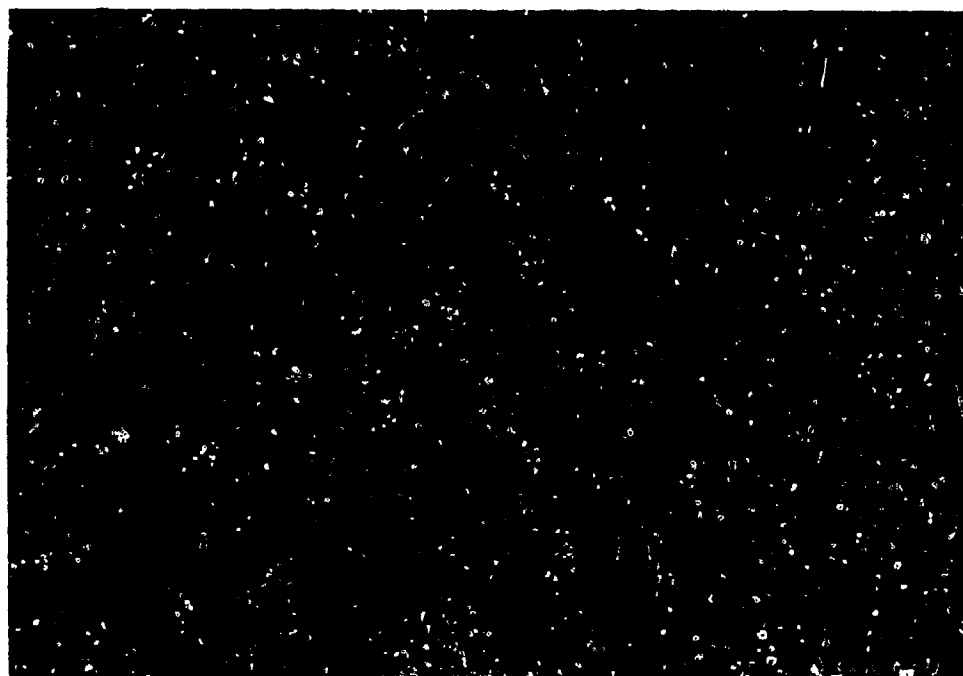


Figure C.19. Test 2B with a 5.45-pound C-4 charge in a 0.088-inch-thick casing at 1.54 feet from an 8.5-inch-thick wall.



Figure C.20. Fragment damage caused by test 2E. Scab depth was 1.25 inches.



Figure C.21. Cracks and a hollow area in the back of wall caused by test 2B.

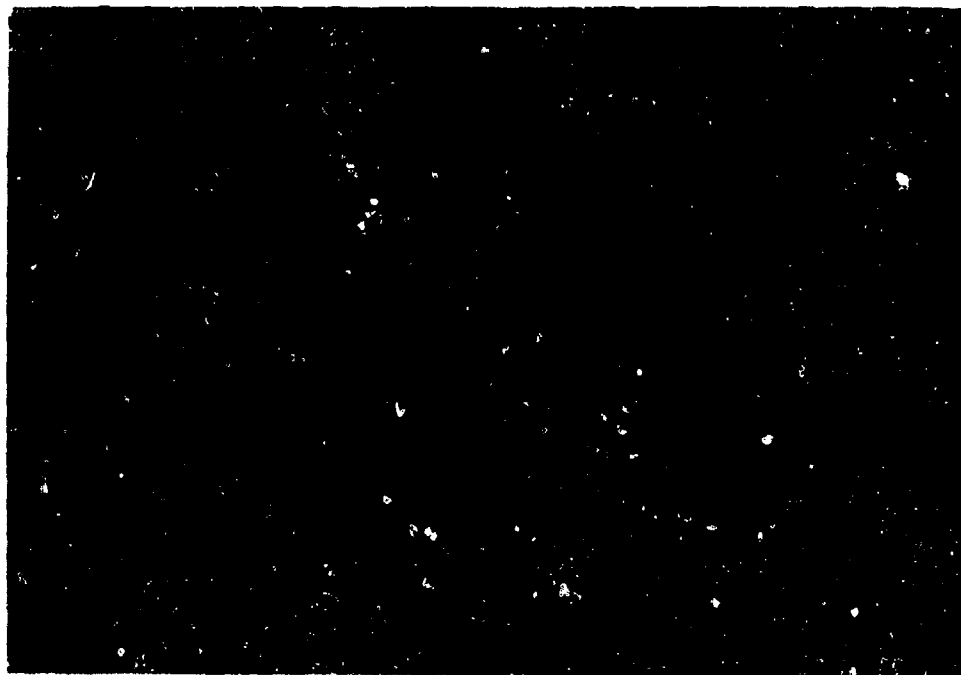


Figure C.22. Test 2C with a 1.07-pound C-4 charge in 0.04-inch-thick casing 1.54 feet from an 8.5-inch-thick wall.



Figure C.23. Crater 2.50 inches deep, blown in the front of the wall by the contact charge in test 2C.

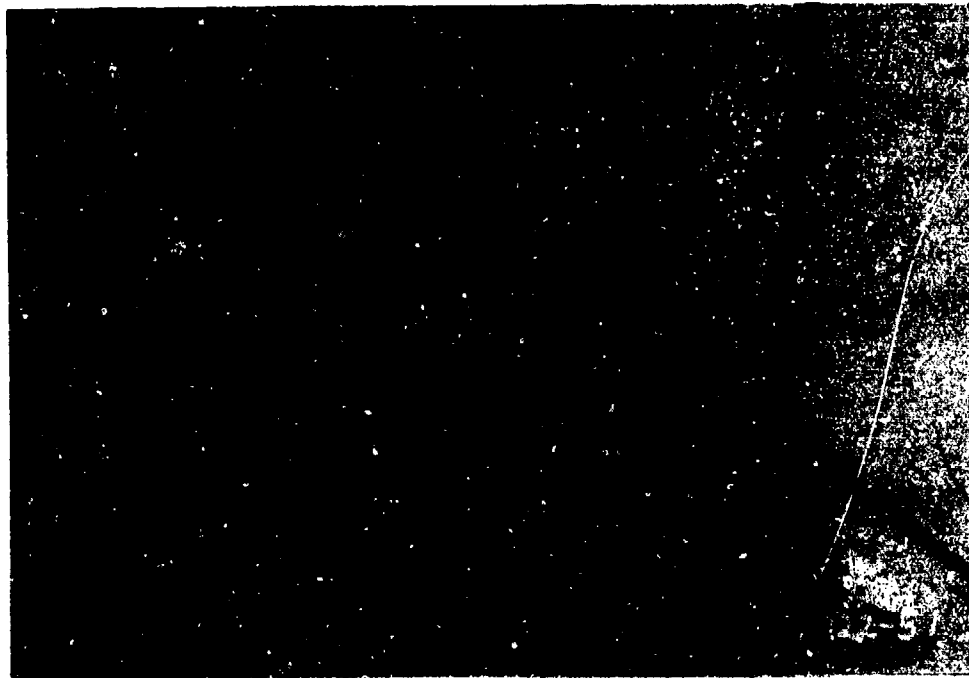


Figure C.24. Spall caused by test 2C. Spall depth was 2.0 inches and spall velocity was 53.5 ft/s.

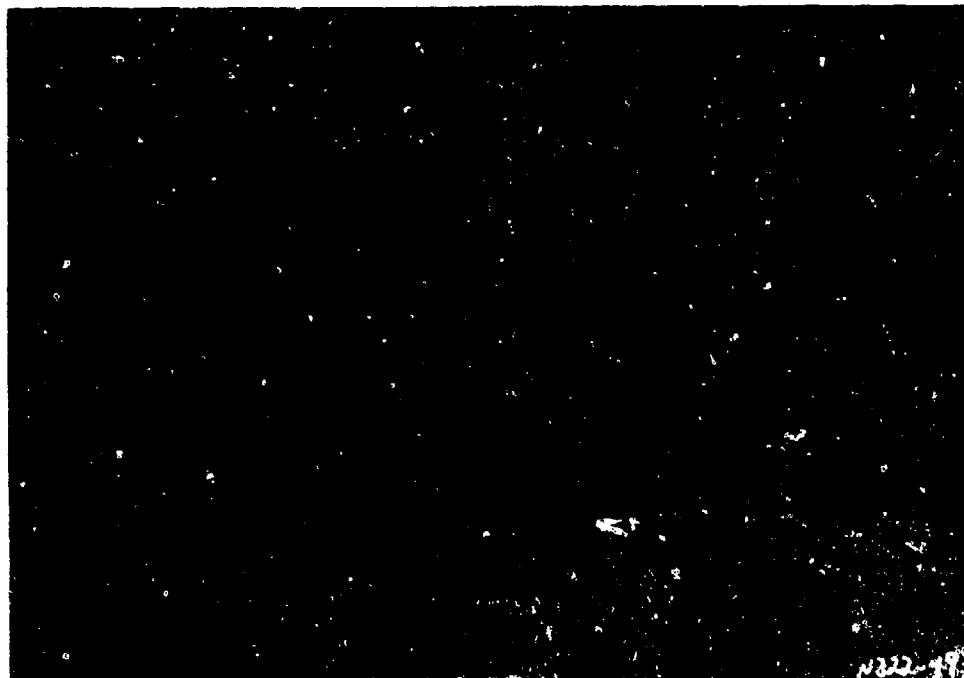


Figure C.25. Test 2D with a 5.45-pound C-4 bare charge 1.54 feet from an 8.5-inch-thick wall.

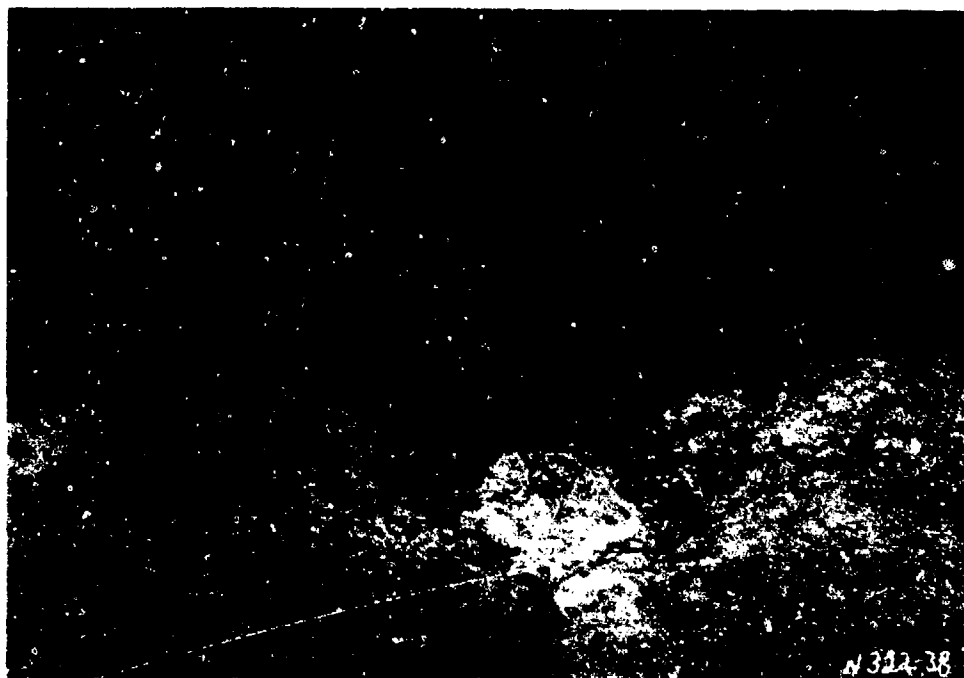


Figure C.26. Test 2D did not damage the front of the wall.

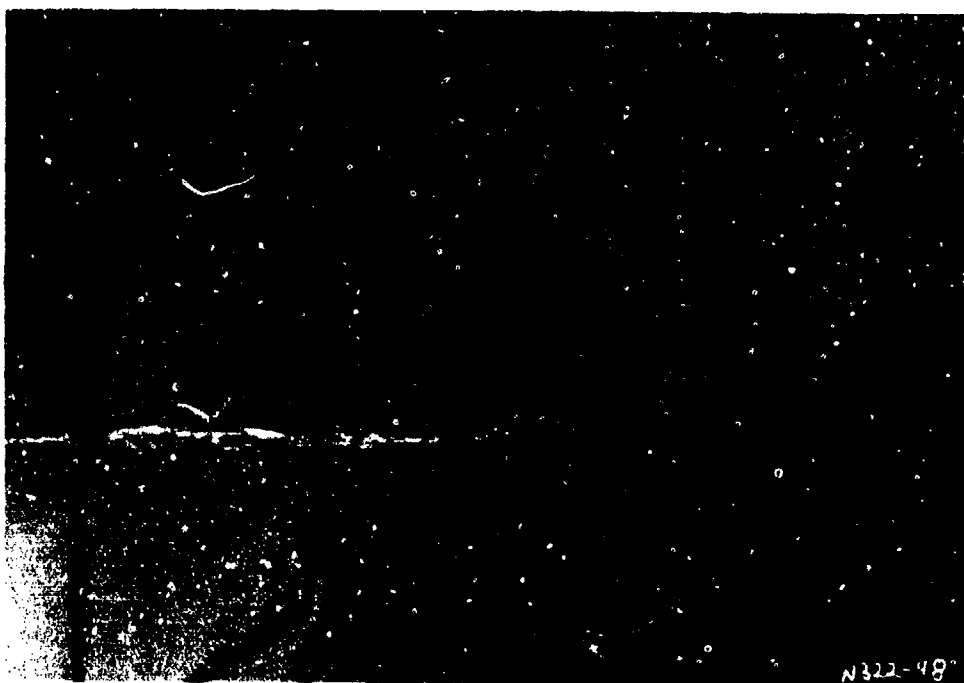


Figure C.27. Test 2D caused cracks and a hollow area in the back of the wall.



Figure C.28. Test 3A with a 29.41-pound bare C-4 charge at 2.44 feet from an 8.5-inch-thick wall.

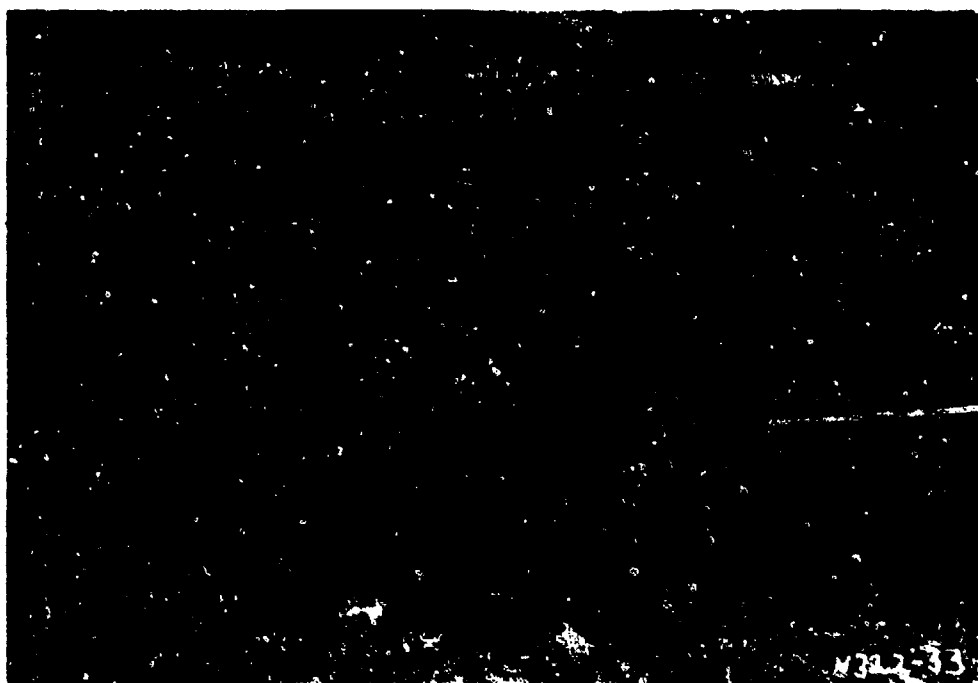


Figure C.29. Outside view of the severe damage to the wall caused by test 3A.

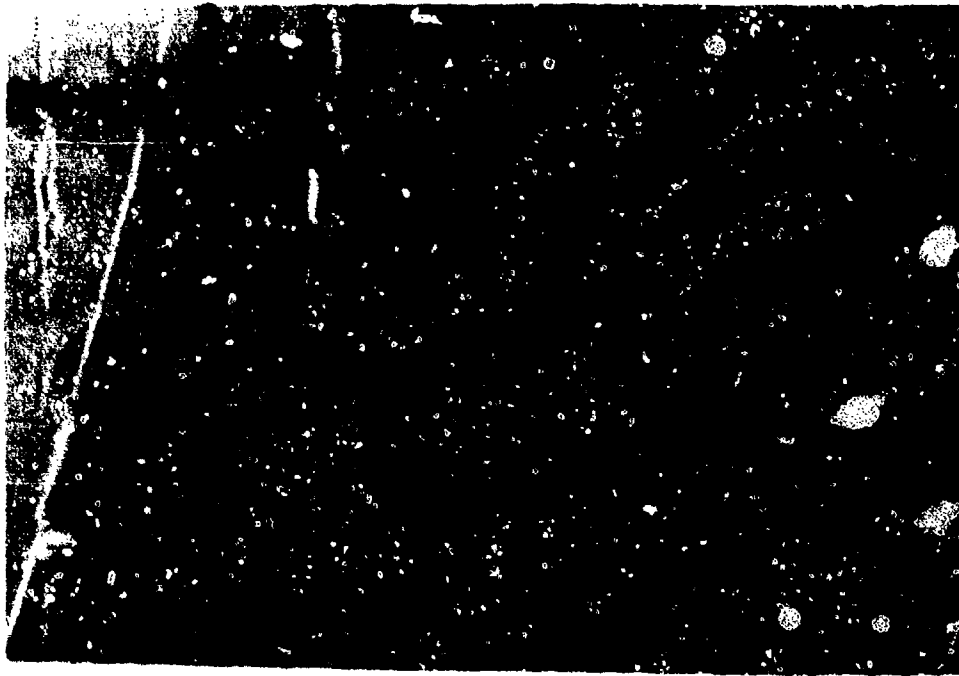


Figure C.30. The scattered spall damage and large flexural cracks in the back of the wall caused by test 3A. Spall depth was 4.87 inches and spall velocity was 69 ft/s.

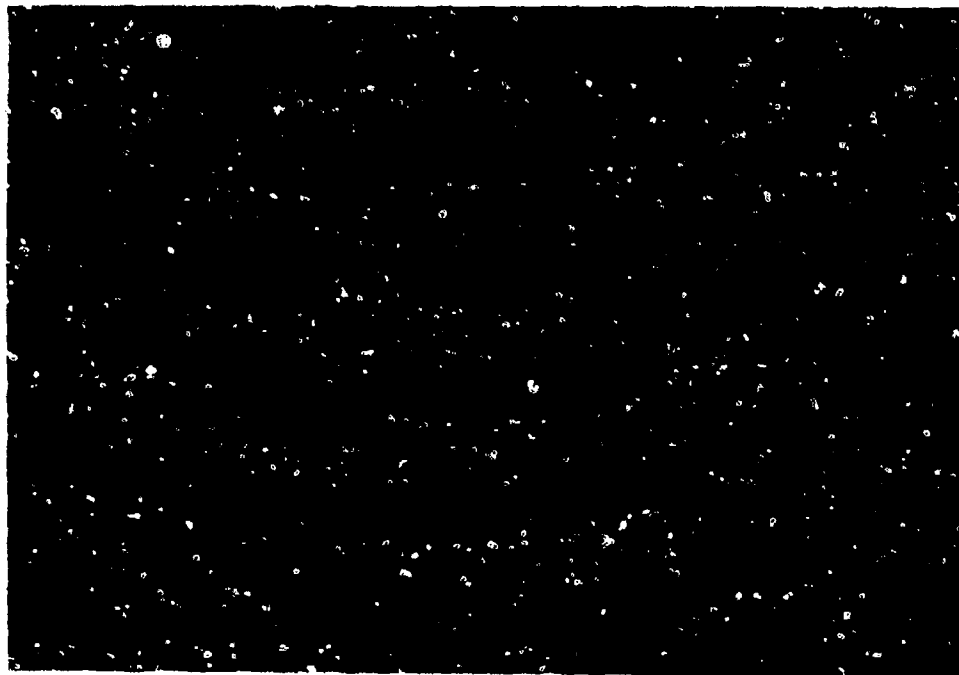


Figure C.31. The uncovered breach and 1.59-inch displacement of the bottom of the wall caused by test 3A.

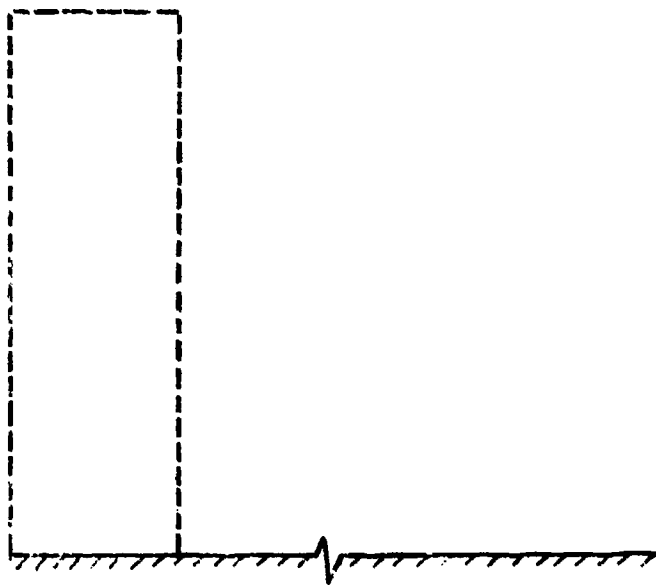


Figure C.32. Cross sectional view of
the wall in test 3A.

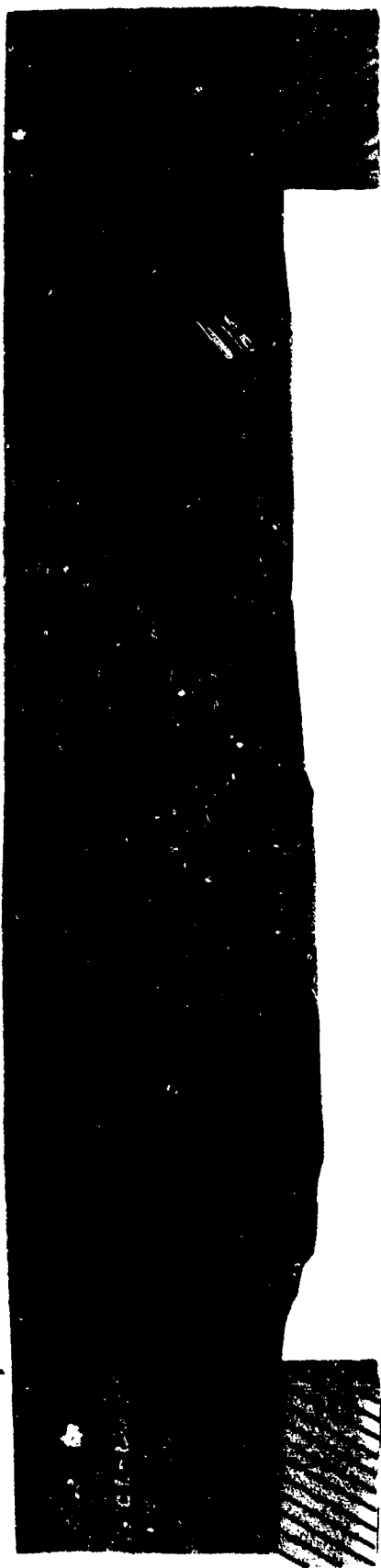




Figure C.33. Test 3B with 7.08 pounds of C-4 in 0.088-inch-thick casing at 1.54 feet from on 8.5-inch wall.

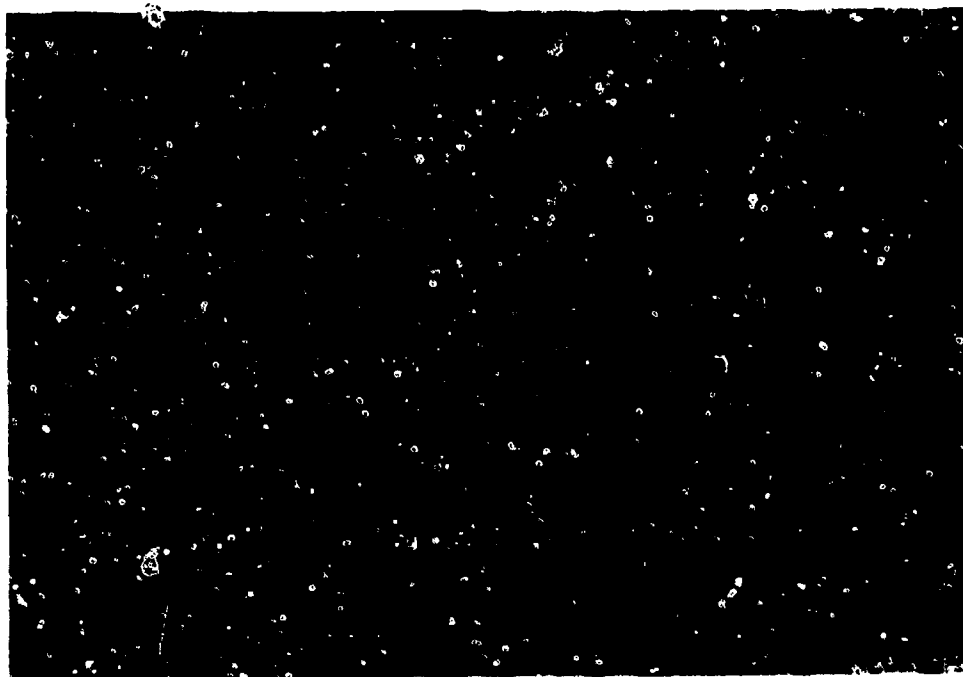


Figure C.34. Bomb fragment damage to the front of the wall caused by test 3B. Scab depth was 2 inches.

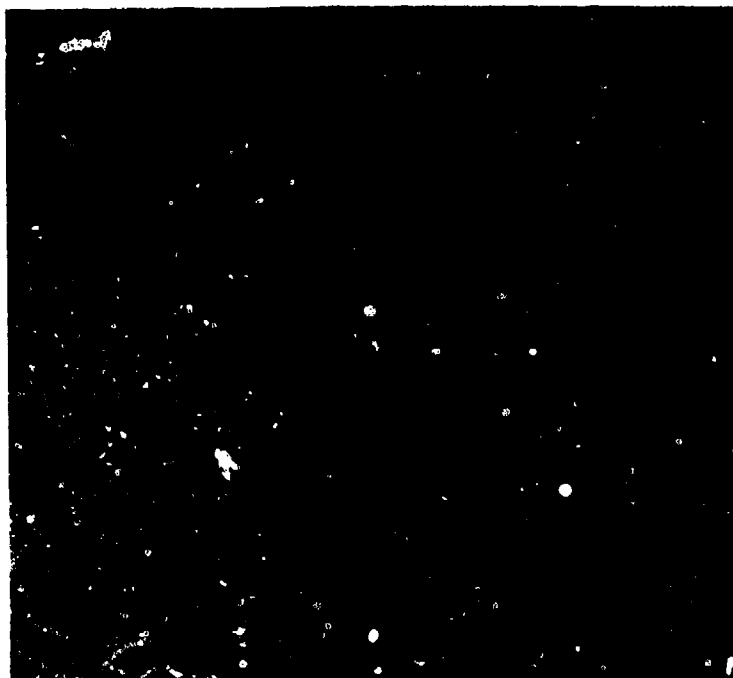


Figure C.35. 1.38-inch-deep spall caused by test 3E. Spall velocity was 39 ft/sec.

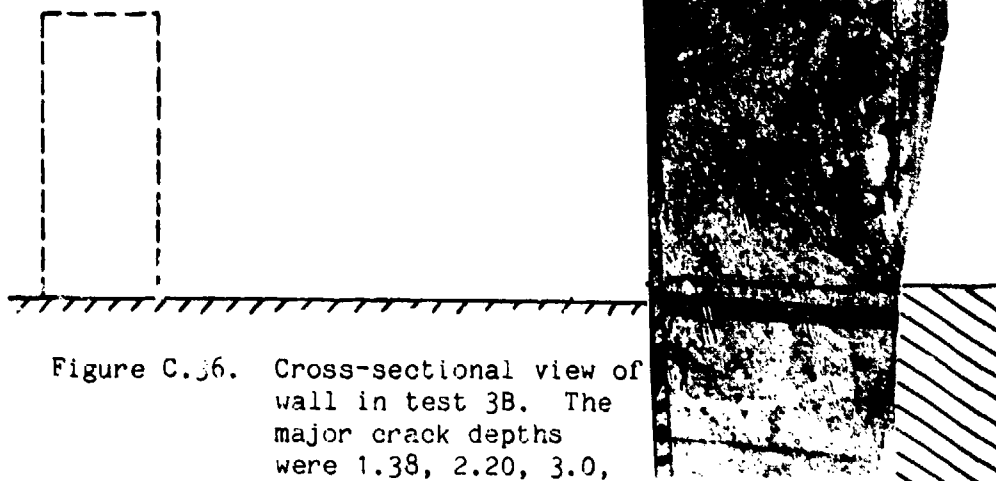


Figure C.36. Cross-sectional view of wall in test 3B. The major crack depths were 1.38, 2.20, 3.0, and 4.50 inches.

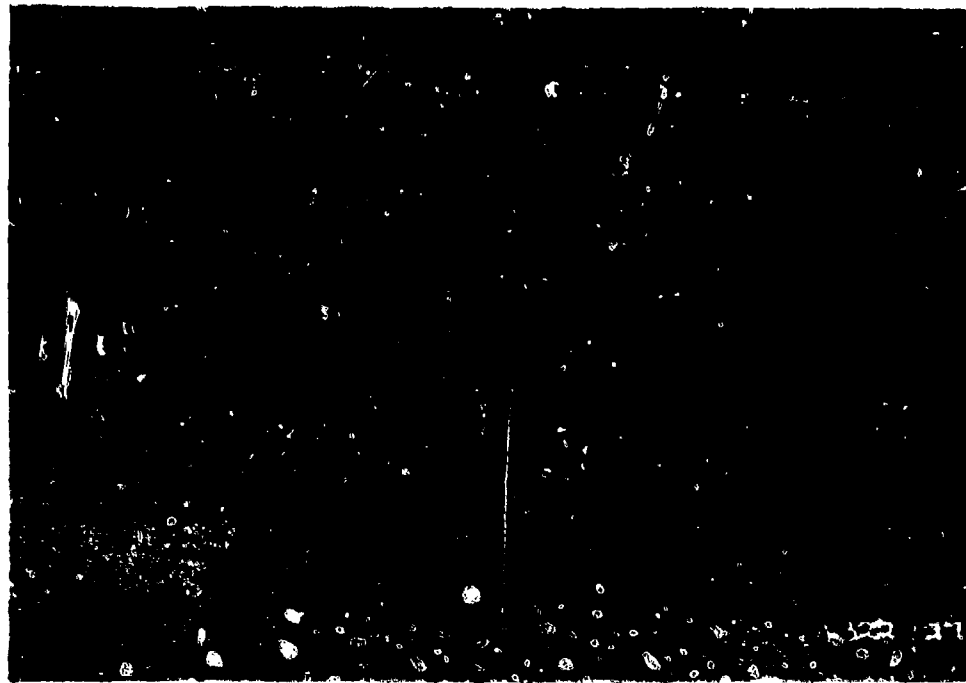


Figure C.37. Test 4A with a 14.39-pound C-4 charge in a 0.111-inch-thick casing at 5.0 feet from an 8.5-inch-thick wall.



Figure C.38. Scab damage (2.25 inches deep) caused by the bomb fragments in test 4A.

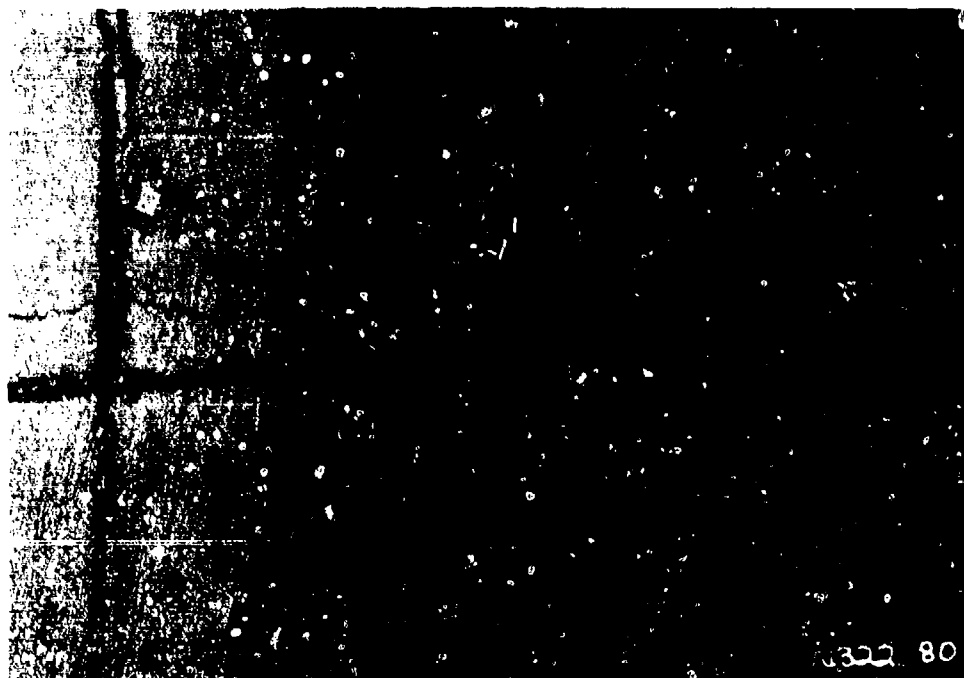


Figure C.39. Hairline cracks in the back of the wall in test 4A.

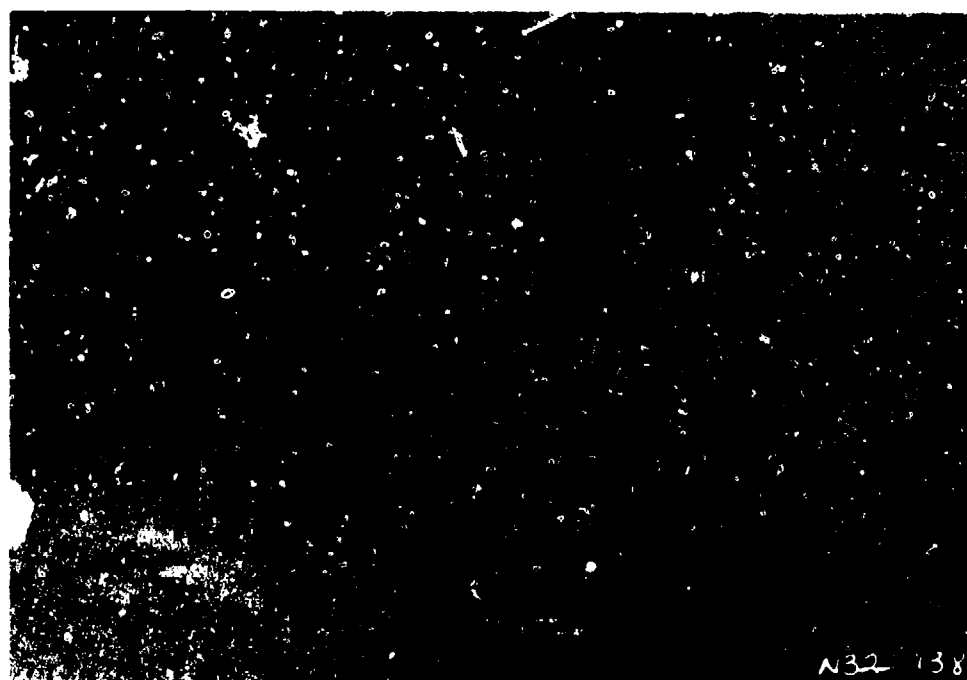


Figure C.40. Hollow zone in the back of wall in test 4A.

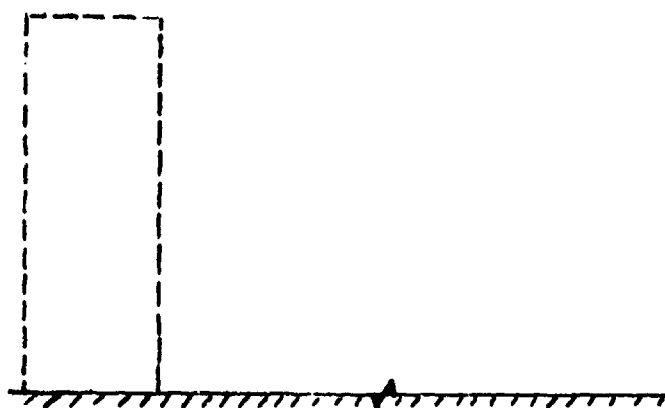


Figure C.41. Cross-sectional view of wall in test 4A.

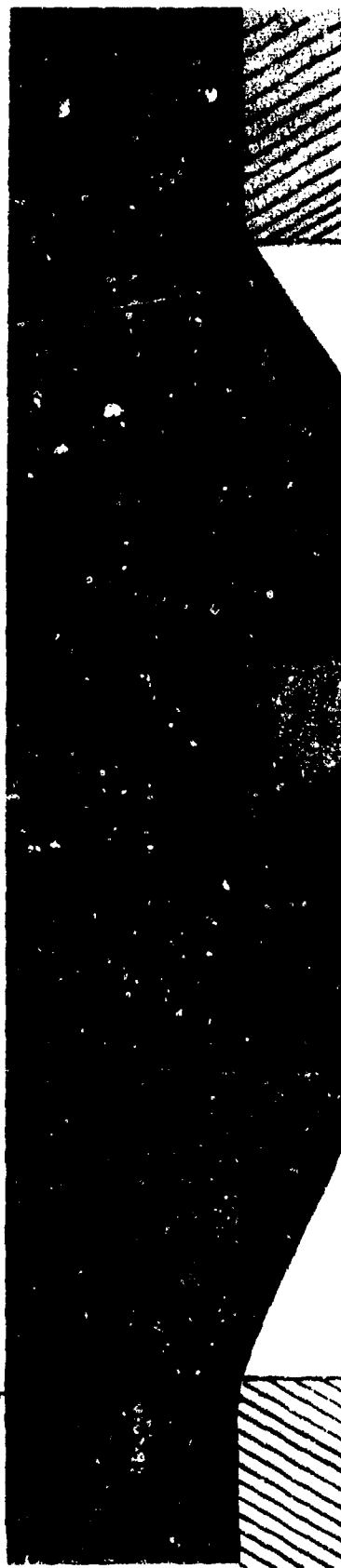




Figure C.42. Test 4B with a 14.39-pound C-4 charge in a 0.111-thick casing at 2.44 inches from an 8.5-inch-thick wall.



Figure C.43. 2.25-inch deep scab in the front of the wall caused by bomb fragments in test 4B.

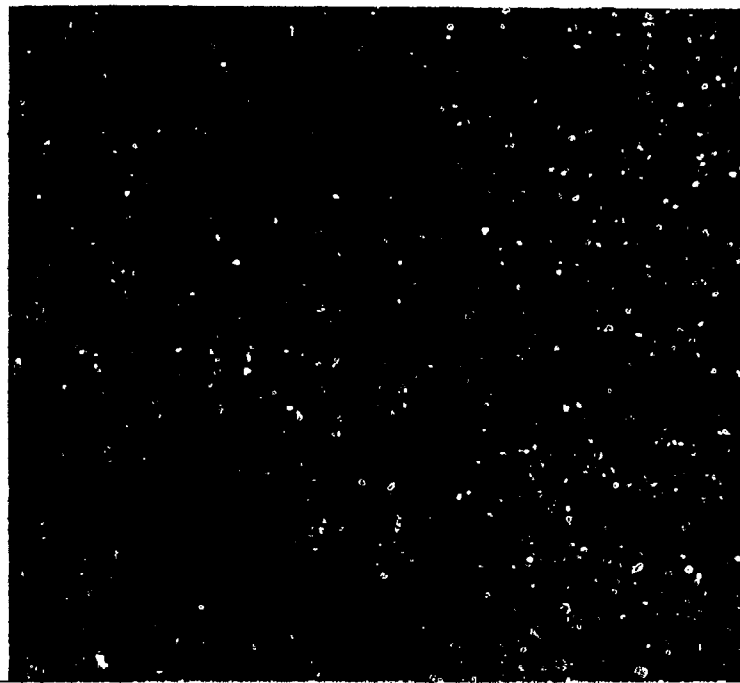


Figure C.44. 1.81-inch-deep spall caused by test 4B. Spall velocity was 44 ft/s.

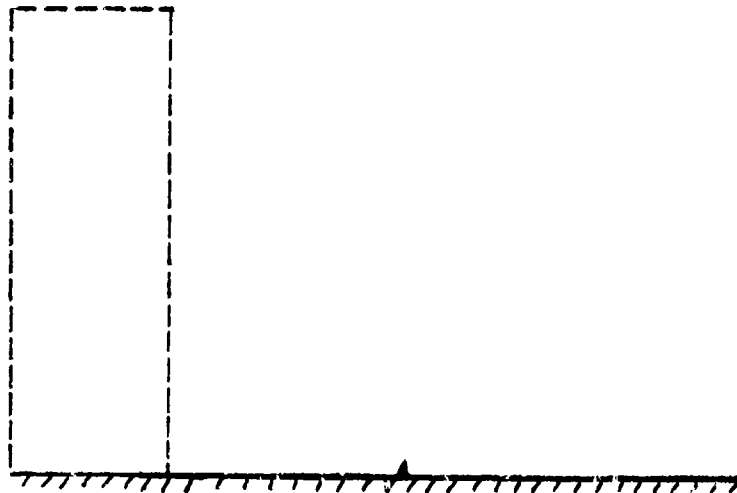


Figure C.45. Cross-sectional view of the wall in test 4B. Main crack depths were 1.81, 3.75, and 4.75 inches deep.





Figure C.46. Test 5A with a 7.08-pound C-4 charge in a 0.088-inch-thick casing at 1.54 feet from an 8.5-inch thick wall made of high-strength concrete.



Figure C.47. Scab damage (1.25 inches deep) in the front of the wall caused by bomb fragments from test 5A.

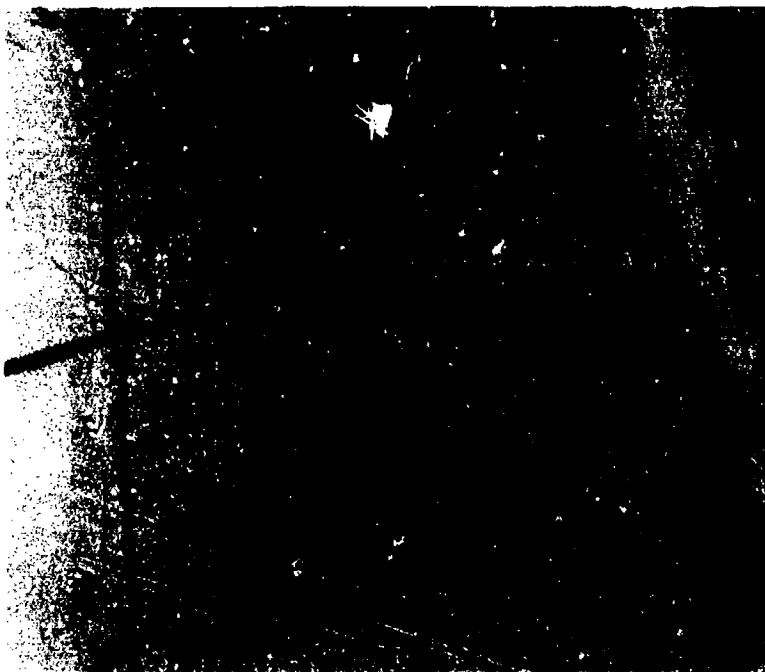


Figure C.48. Spall damage (3.75 inches deep)
in the back of the wall in
test 5A.

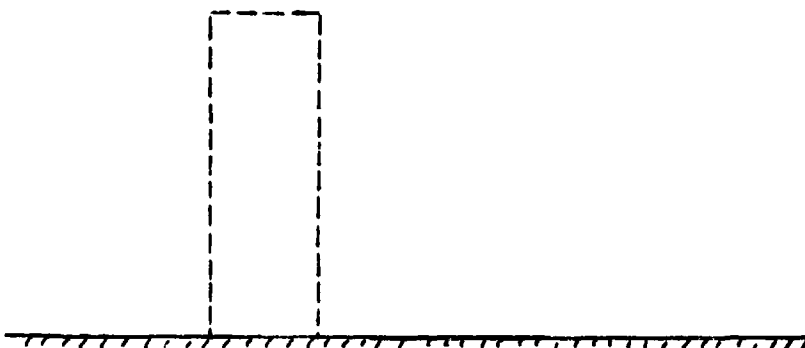


Figure C.49. Cross-sectional view of the wall
in test 5A.

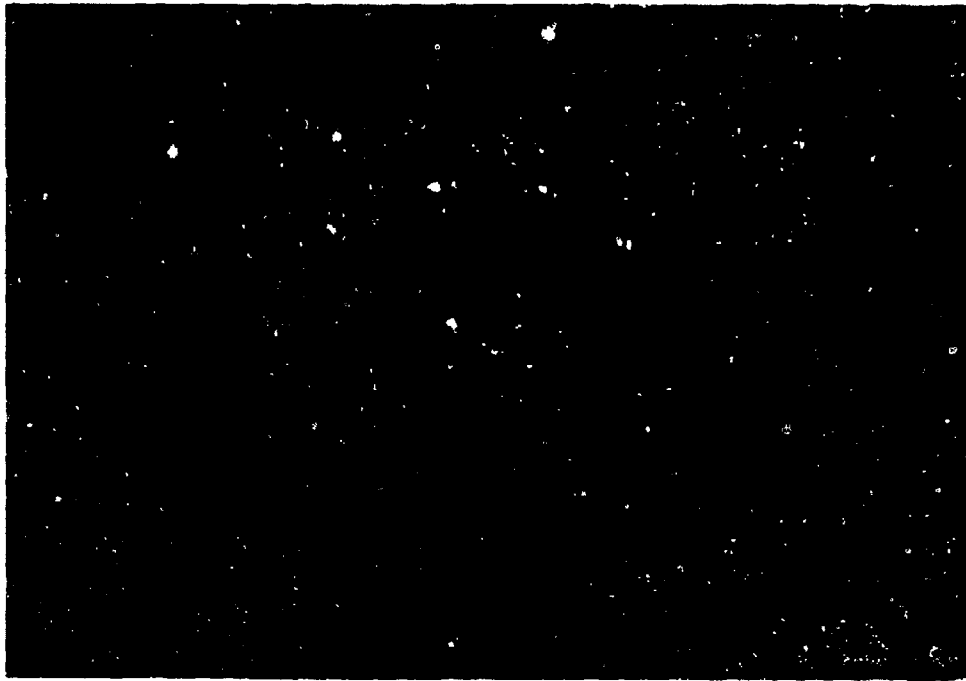


Figure C.50. Test 5B with a 3.63-pound C-4 charge in a 0.07-inch-thick casing 1.54 feet from an 8.5-inch-thick wall of high-strength concrete.



Figure C.51. Scab damage (0.94 inch deep) to the front of the wall caused by bomb fragments from test 5B.

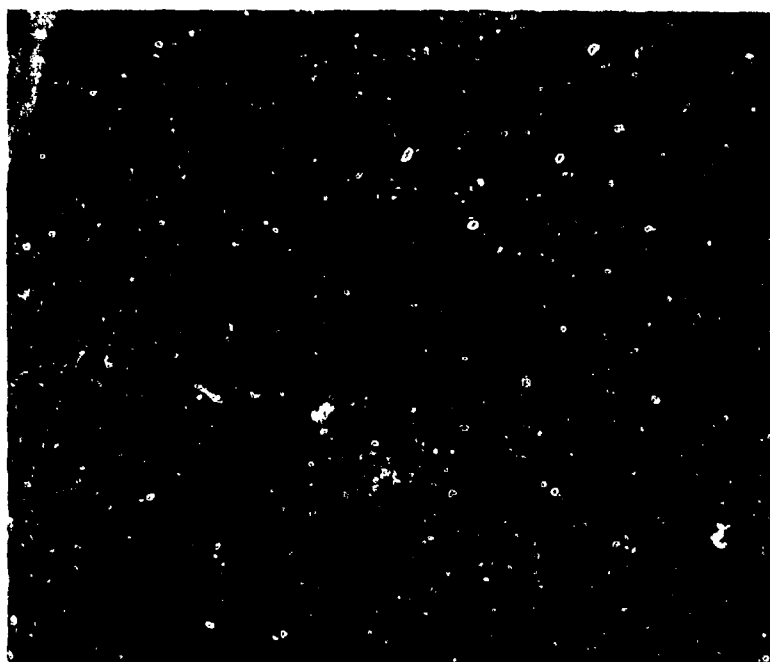


Figure C.52. Spall damage (1.06 inches deep) to the back of the wall in test 5B. Spall velocity was 14.41 ft/s.

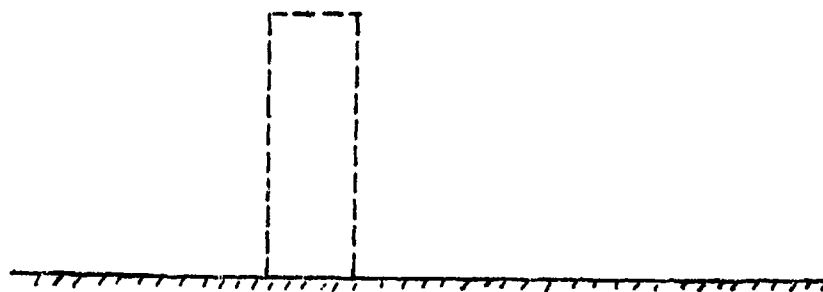


Figure C.53. Cross-sectional view of the wall in test 5B. Main crack depths were 1.06, 1.5, 2.12, and 3.38 inches.

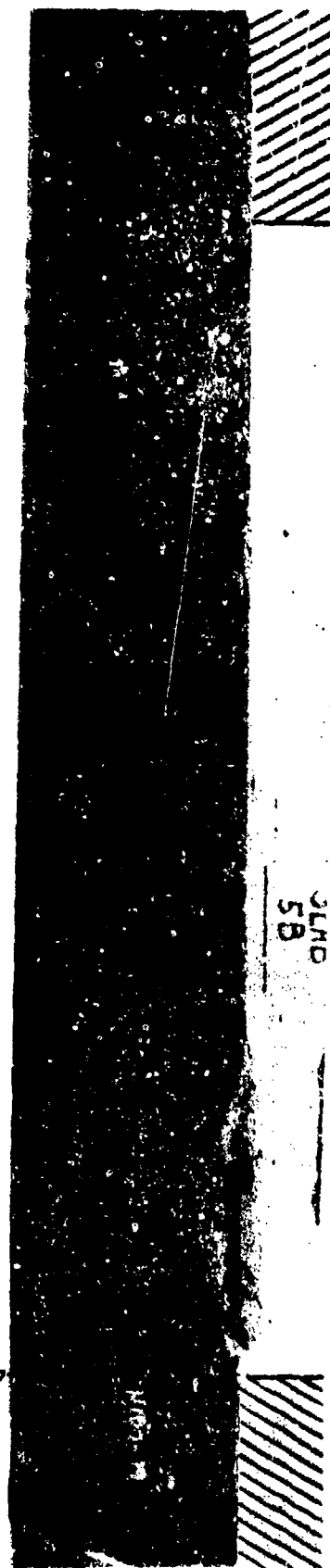




Figure C.54. Test 5C with a 1.07-pound C-4 charge in a 0.047-inch-thick casing in contact with the 8.5-inch-thick wall of high-strength concrete.



Figure C.55. Scab damage (1.85 inches deep) to the front of the wall caused by test 5C.

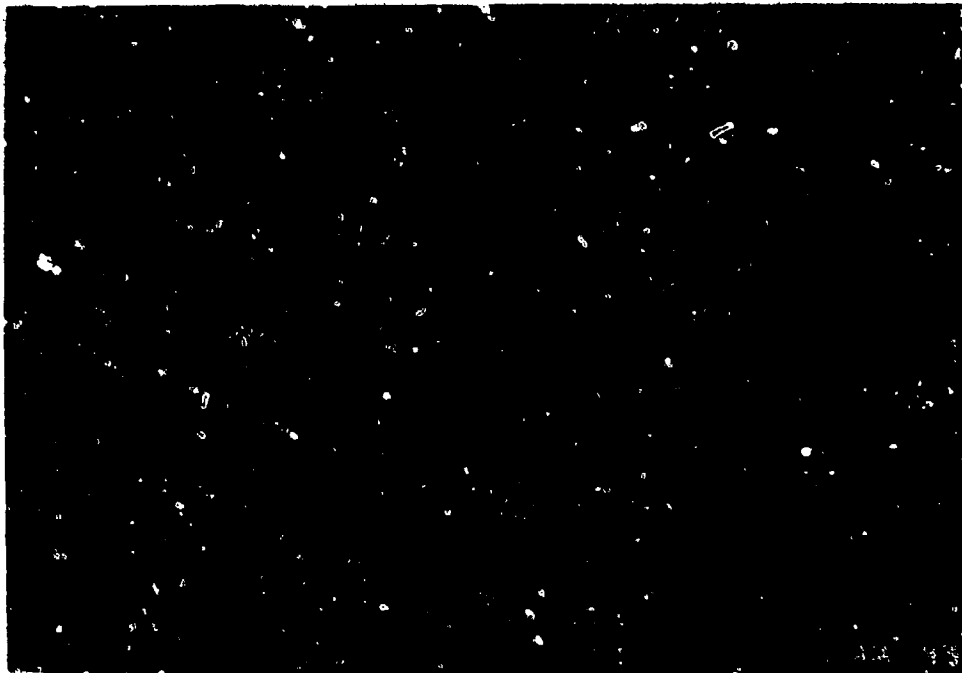


Figure C.56. Close-up of the scab damage,
1.85 inches deep.

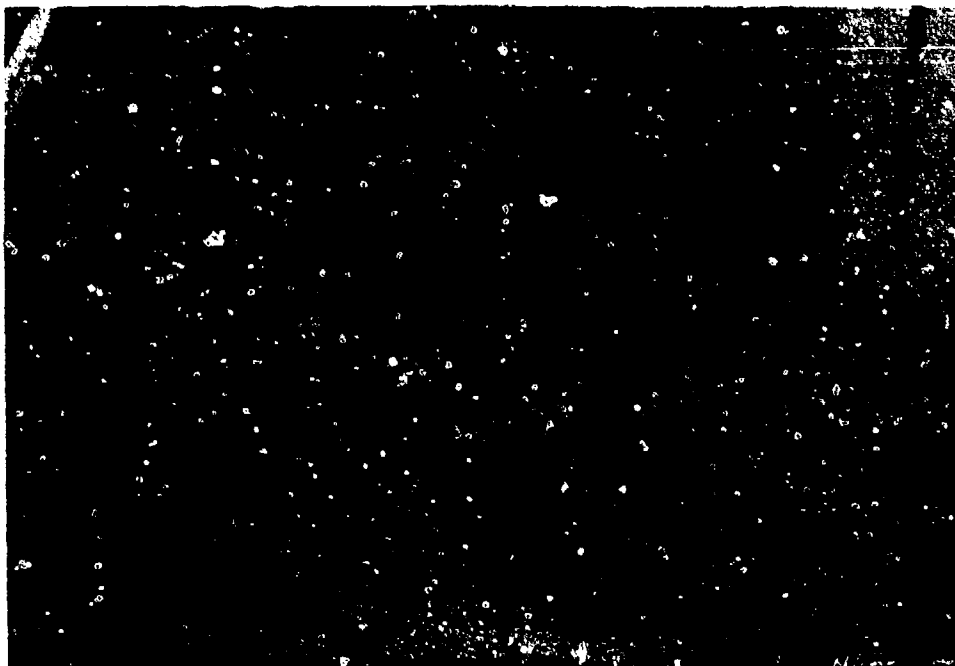


Figure C.57. Spall damage (3.38 inches deep) to the
back of the wall in test 5C.

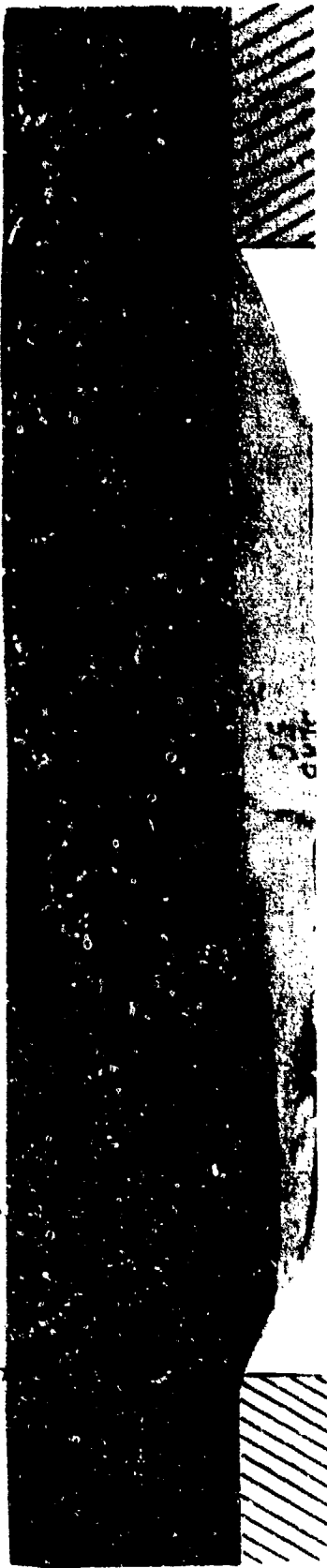


Figure C.58. Cross-sectional view of wall in test 5C. Main cracks were 3.38, 4.5, and 5.38 inches deep.

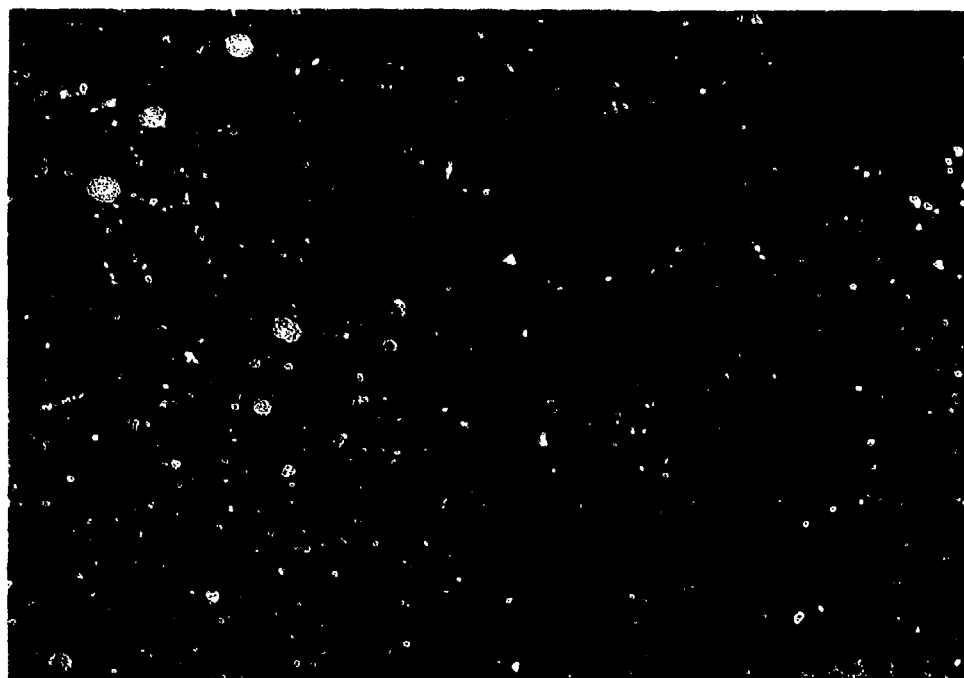


Figure C.59. Test 6A with a 7.08-pound C-4 charge in a 0.088-inch-thick casing at 1.54 feet from an 8.5-inch wall of concrete with acrylic latex additive.

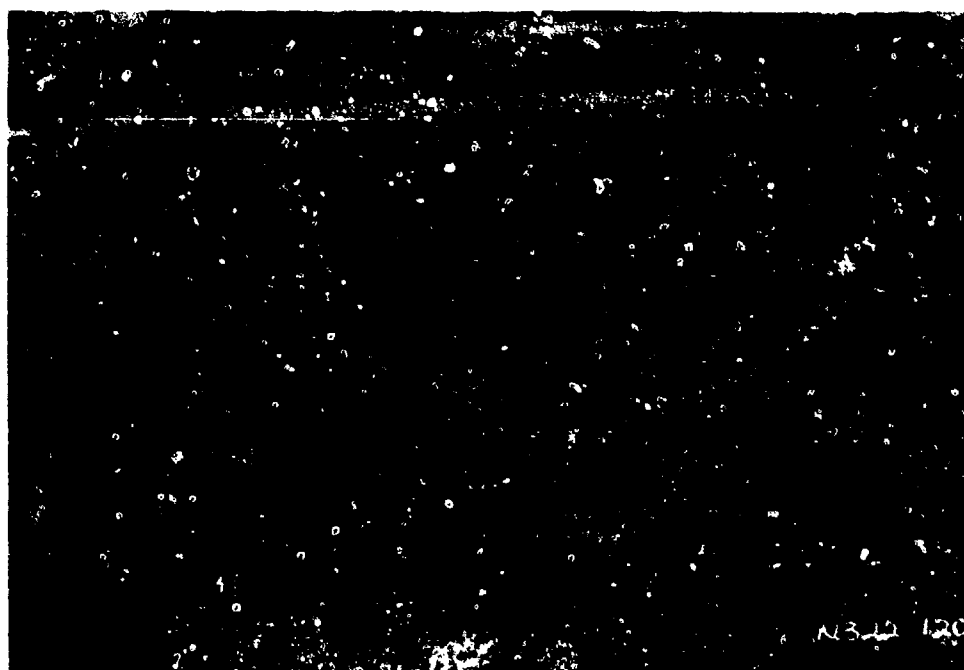


Figure C.60. Scab damage (1.08 inches deep) to the front of the wall in test 6C.

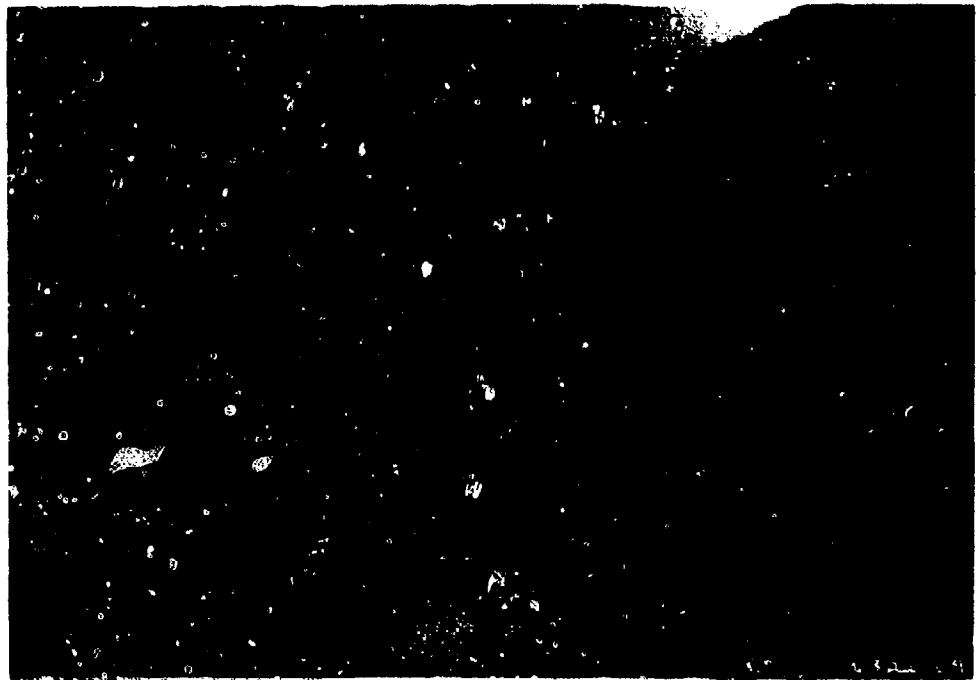


Figure C.61. Close-up of scab damage which was up to 1.08 inches deep

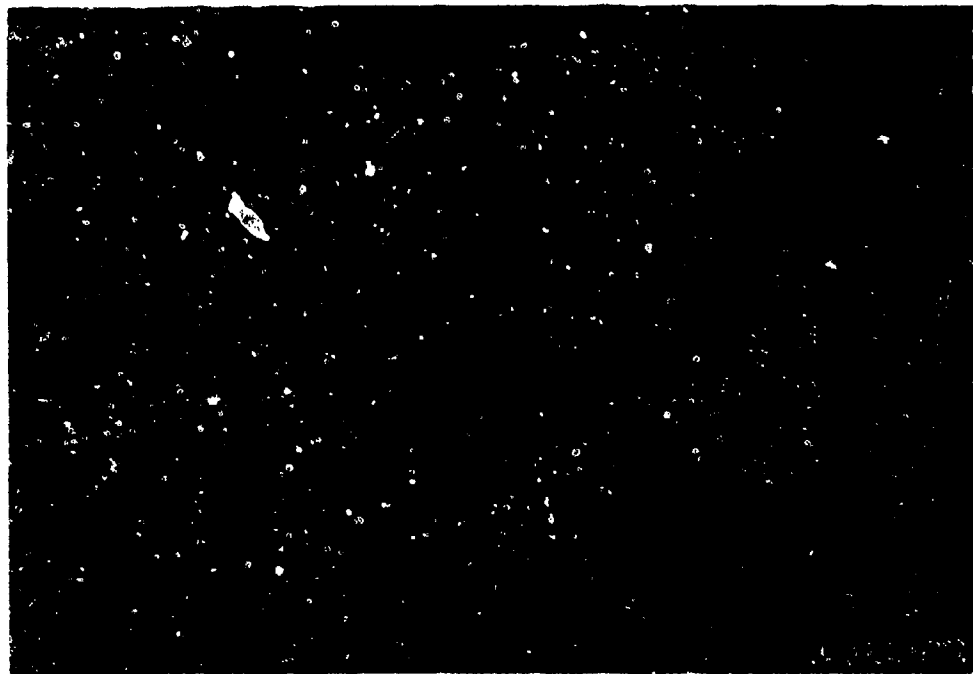


Figure C.62. Threshold spall in the back of the wall in test 6A.

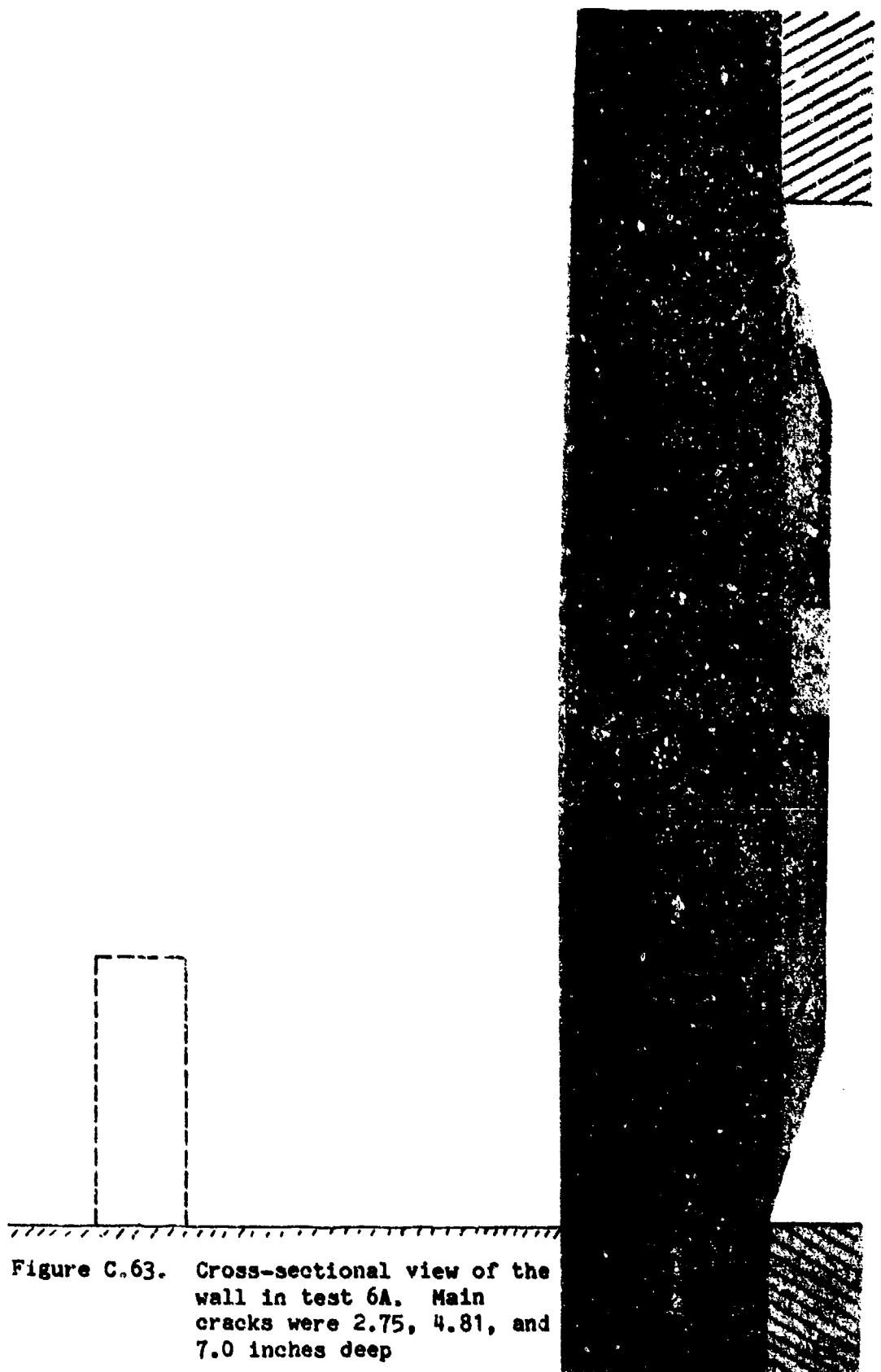


Figure C.63. Cross-sectional view of the wall in test 6A. Main cracks were 2.75, 4.81, and 7.0 inches deep

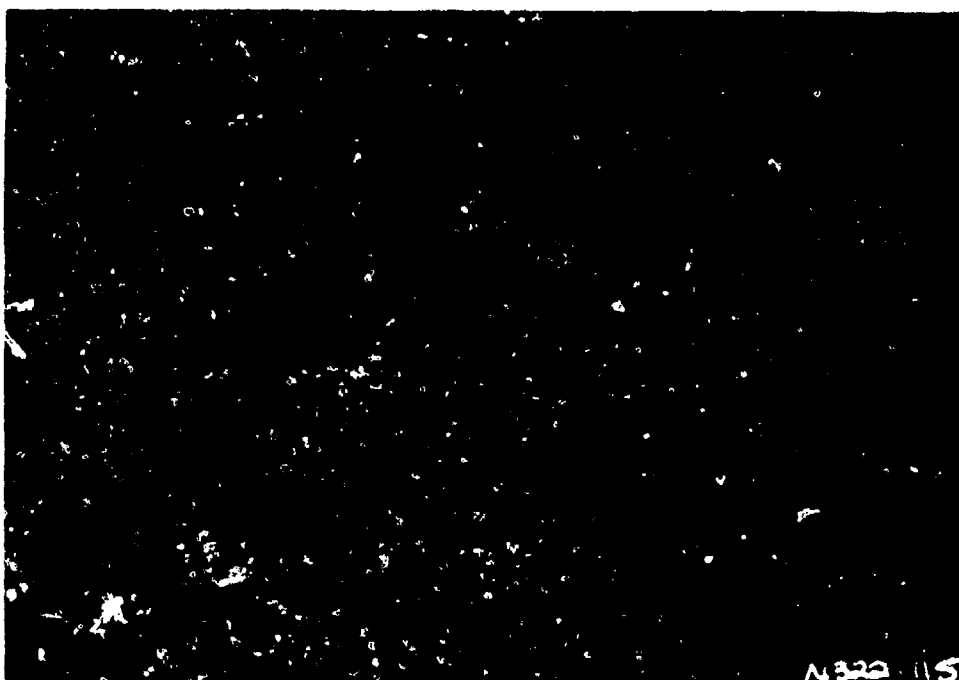


Figure C.64. Test 6B with a 3.63-pound C-4 charge in a 0.070-inch-thick casing at 1.54 feet from an 8.5-inch-thick wall of concrete with acrylic latex additive.

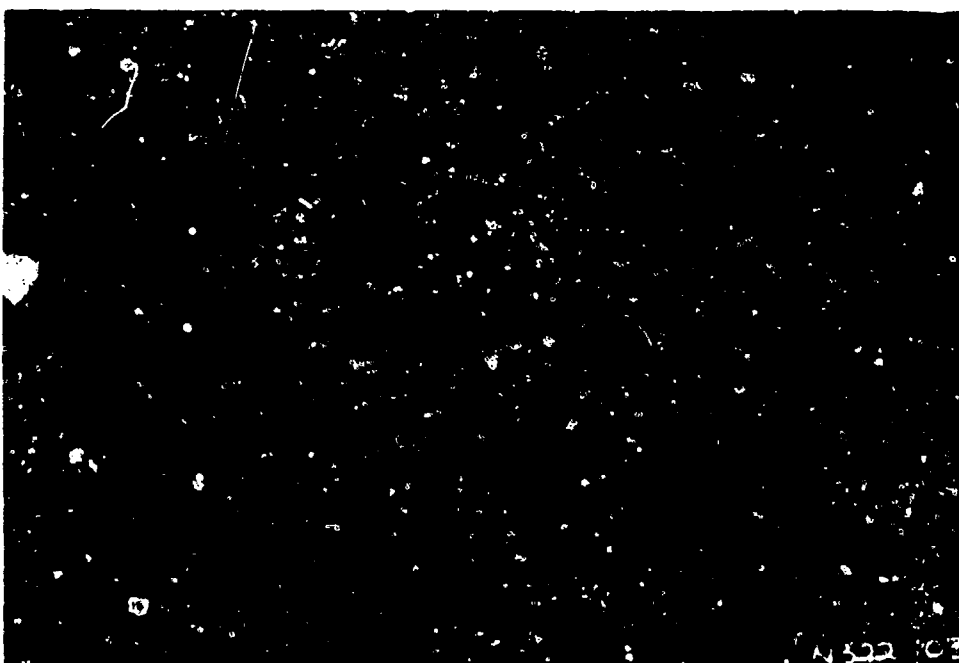


Figure C.65. Scab damage (1.5 inches deep) to the front of the wall in test 6B.

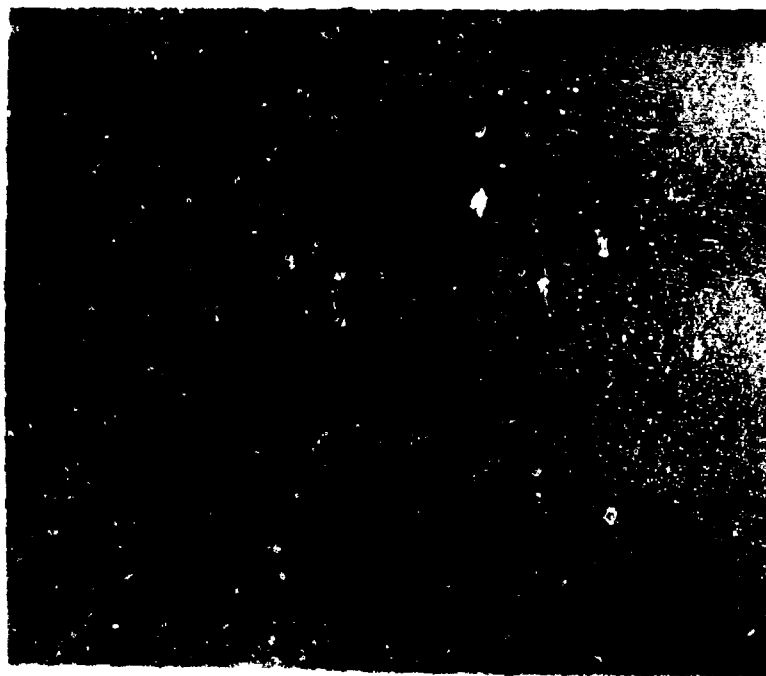


Figure C.66. Threshold spall damage to the backside of the wall in test 6B.



Figure C.67. Cross-sectional view of the wall in test 6B. The main cracks were 2.43, 3.83, 4.38, and 5.25 inches deep.





Figure C.68. Test 6C with a 1.07-pound C-4 charge in a 0.047-inch-thick casing in contact with an 8.5-inch-thick wall of concrete with acrylic latex additive.

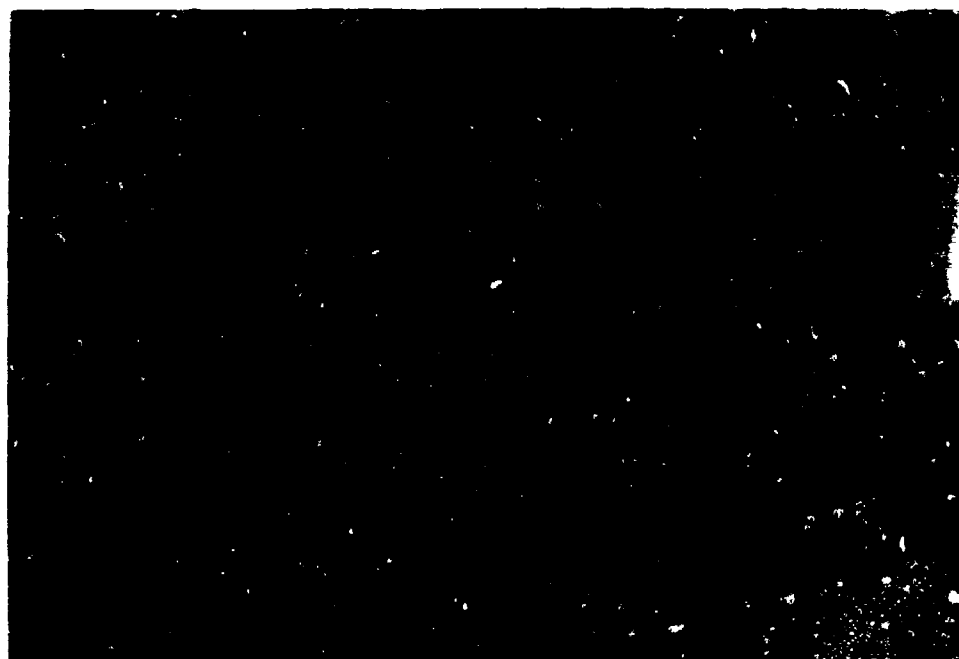


Figure C-69. Scab damage (2.00 in. deep) to the front of the wall in test 6C.



Figure C.70. Spall damage (3.75 inches deep) to back of the wall in test 6C.

Figure C.71. Cross-sectional view of the wall in test 6C. Main cracks were 3.75 and 4.75 inches deep.



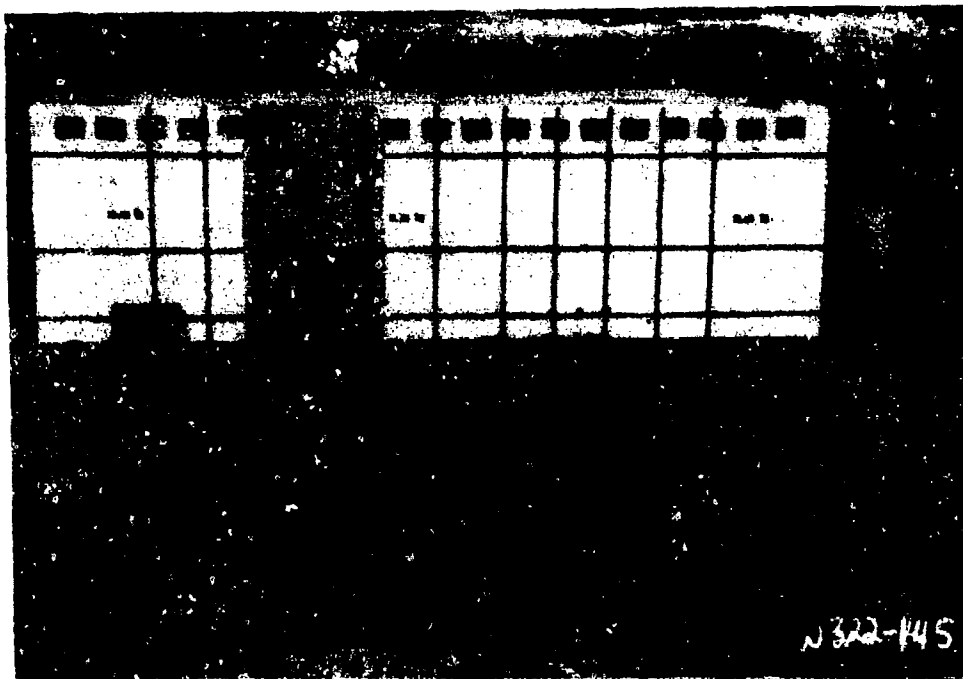


Figure C.72. Test 7A with a 7.08 pound C-4 charge in a 0.088-inch-thick casing at 1.54 feet from an 8.5-inch-thick wall of steel fiber concrete.



Figure C.73. Scab damage (2.00 inches deep) caused by bomb fragments from test 7A.



Figure C.74. Threshold spall damage to the back of the wall in test 7A.

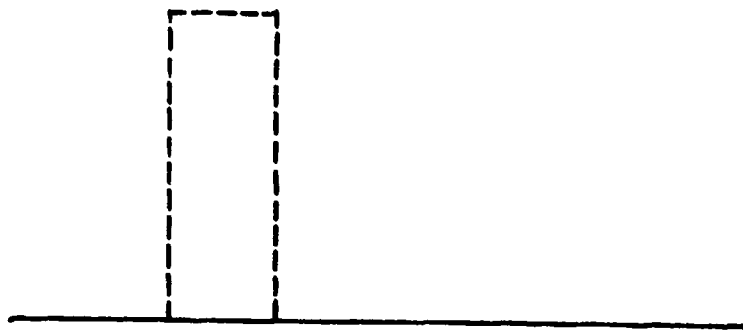


Figure C.75. Cross-sectional view of the wall in test 7A. Main cracks were 2.0, 3.25, 5.0, and 6.5 inches deep.

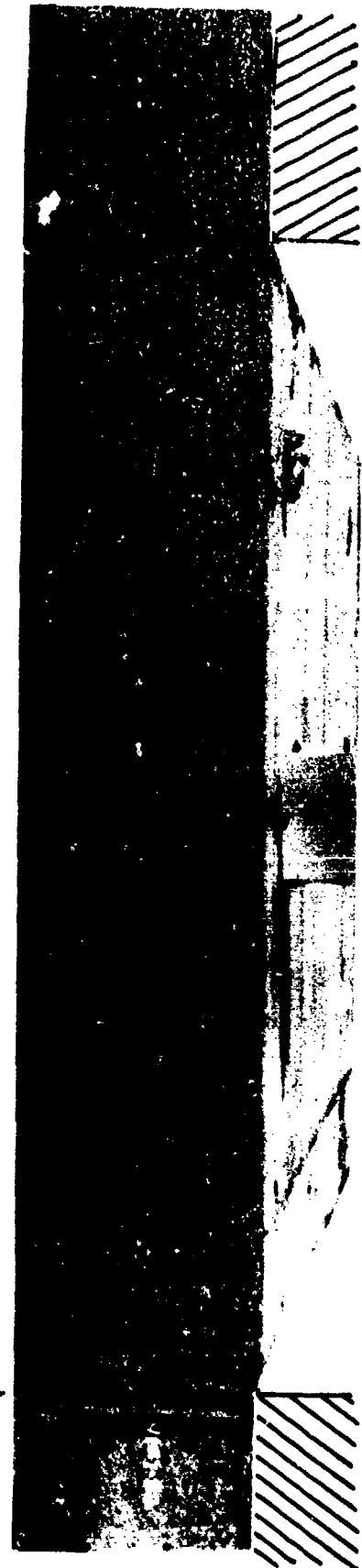




Figure C.76. Test 7B with a 14.39-pound charge in a 0.111-inch-thick casing at 2.44 feet from an 8.5-inch-thick wall of steel fiber concrete.

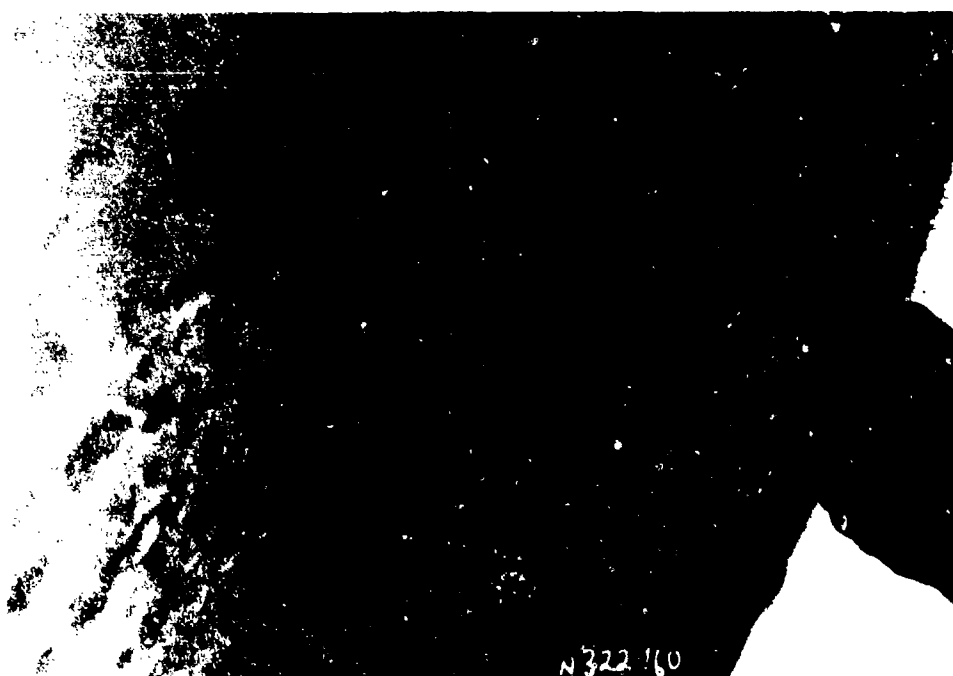


Figure C.77. Scab damage (1.38 inches deep) caused by the bomb fragments in test 7B.

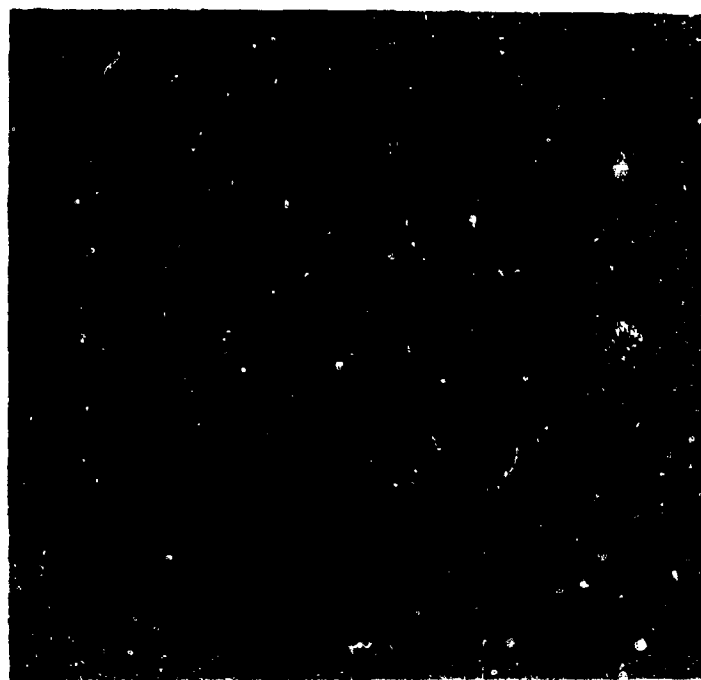


Figure C.78. Threshold spall damage to the back of the wall in test 7B.

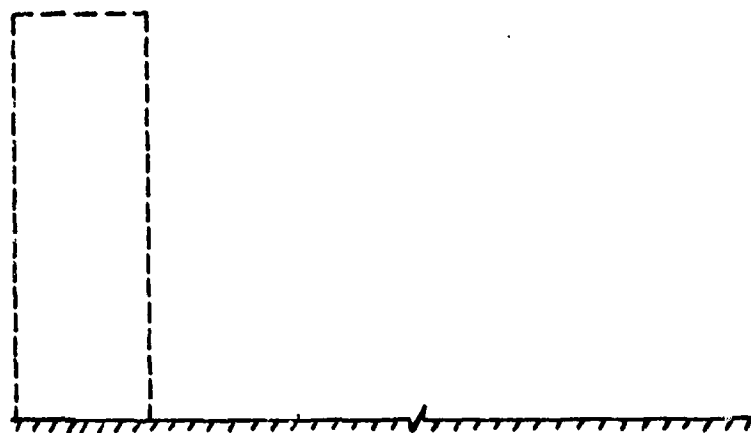


Figure C.79. Cross-sectional view of the wall in test 7B. Main cracks were 2.25, 3.5, and 5 inches deep.





Figure C.80. Test 7C with a 1.07-pound C-4 charge in a 0.047-inch-thick casing in contact with an 8.5-inch-thick wall of steel fiber concrete.

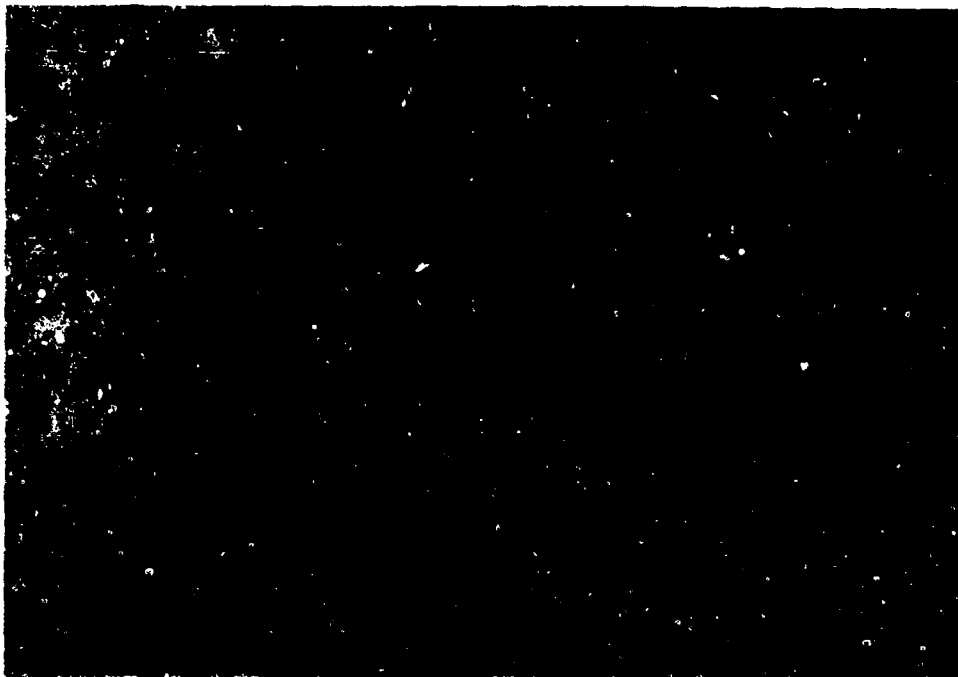


Figure C.81. Scab crater (2.25 inches deep) blown out of the front of the wall in test 7C.



Figure C.82. Spall damage (1.75 inches deep) to back of the wall in test 7C.

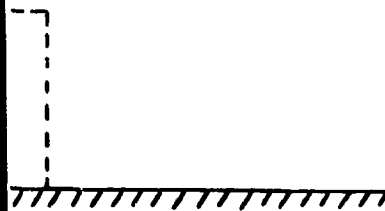


Figure C.83. Cross-sectional view of the wall in test 7C. Main crack depths were 1.75, 3.0, 3.75, and 6.25 inches.

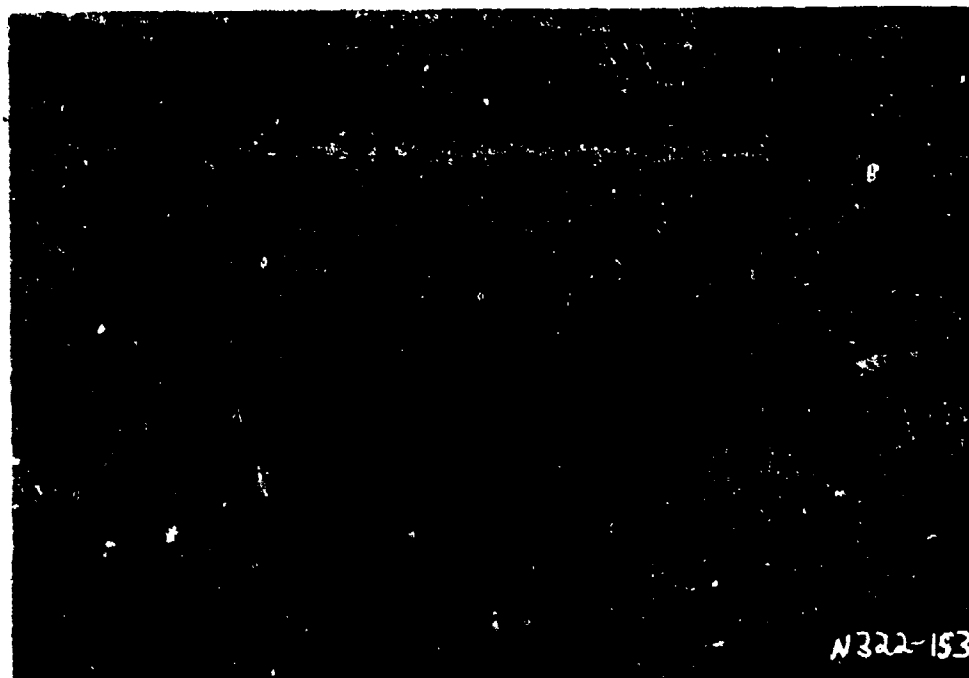


Figure C.84. Test 8A with a 1.66-pound C-4 charge in a 0.054-inch-thick casing at 1.54 feet from a 5.38-inch-thick wall.

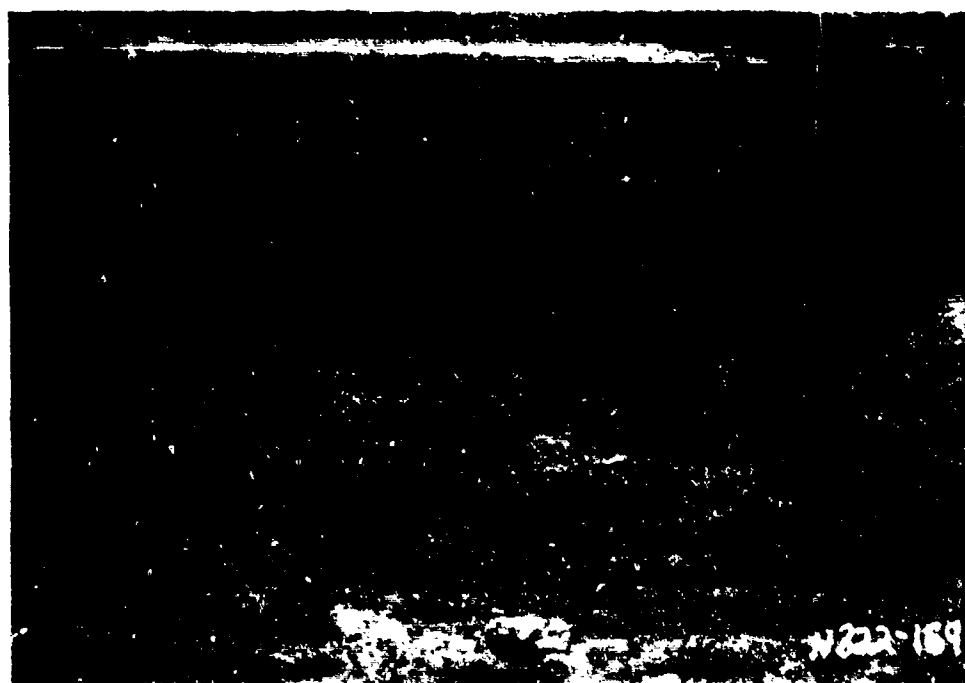


Figure C.85. Bomb fragment damage up to 0.88 inches deep in the front side of the wall in test 8A.



Figure C.86. Faint hairline cracks on the back of the wall in test 8A.

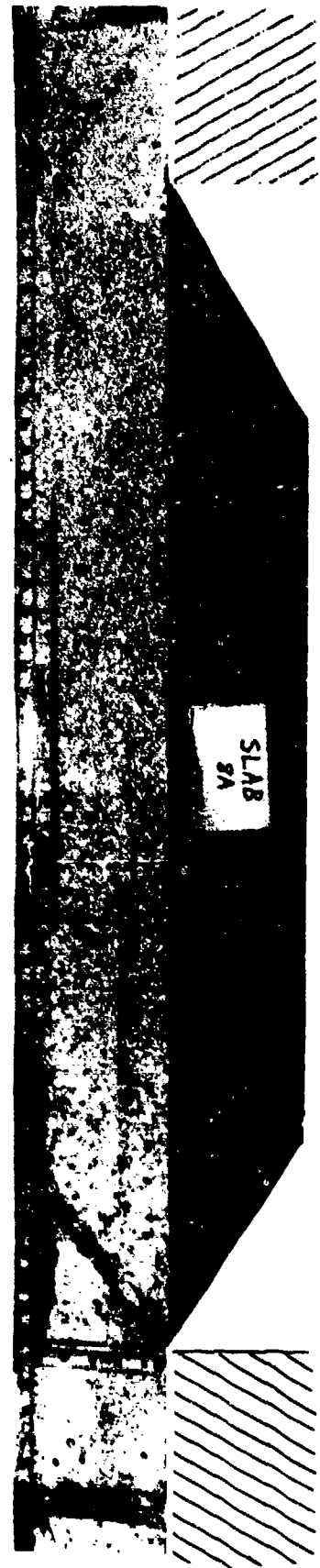


Figure C.87. Cross-sectional view of the wall in test 8A. The main crack goes all the way through at approximately a 45-degree angle.



Figure C.88. Test 8B with a 3.63-pound C-4 charge in a 0.07-inch-thick casing at 1.54 feet from a 5.38-inch-thick wall.

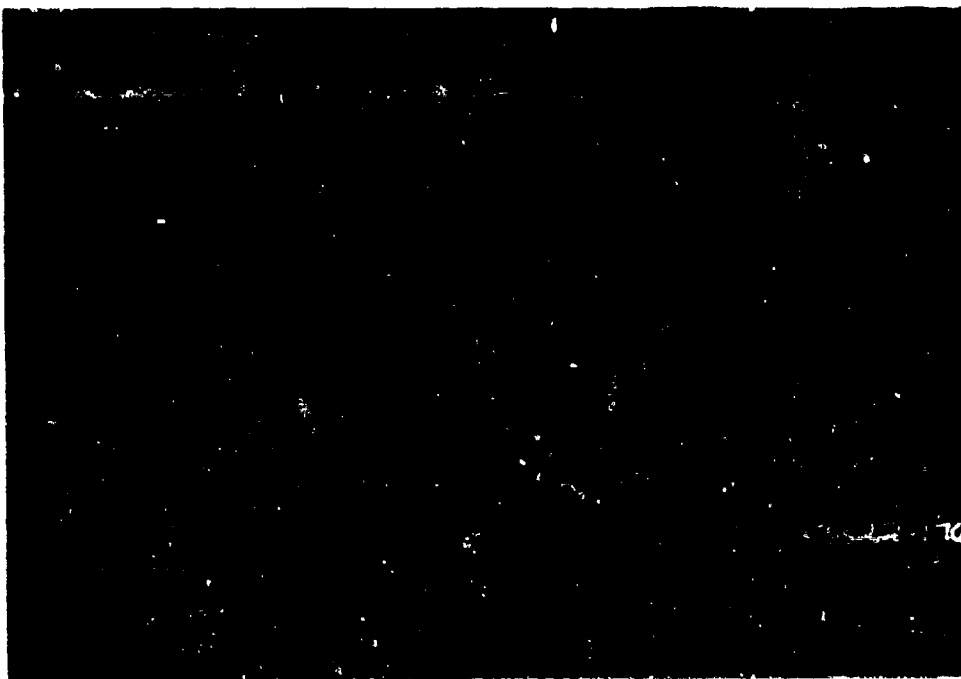


Figure C.89. Bomb fragment damage up to 1.40 inches deep in the front side of the wall in test 8B.

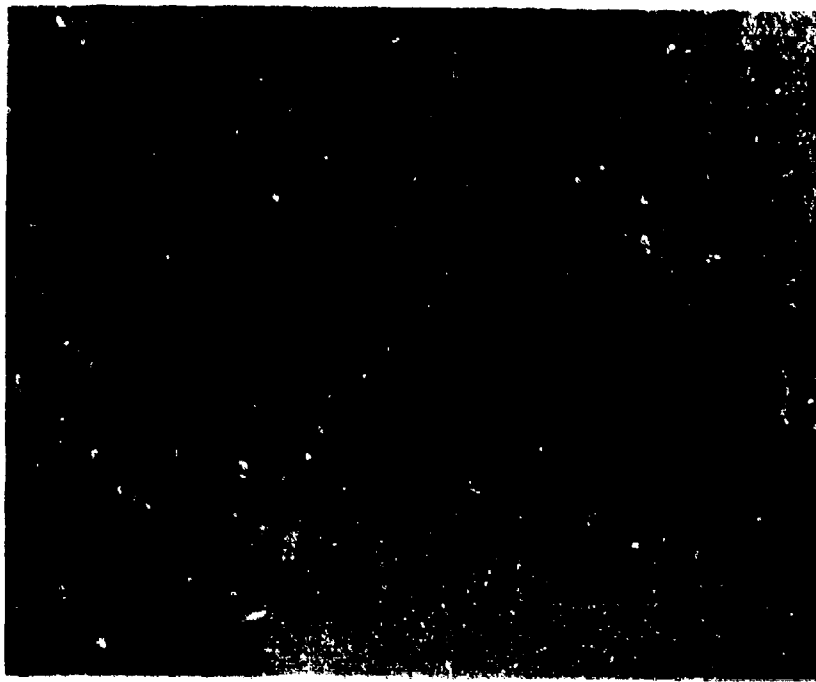


Figure C.90. Threshold spall in the back of the wall in test 8B. A few small fragments left the wall at 57 ft/s.

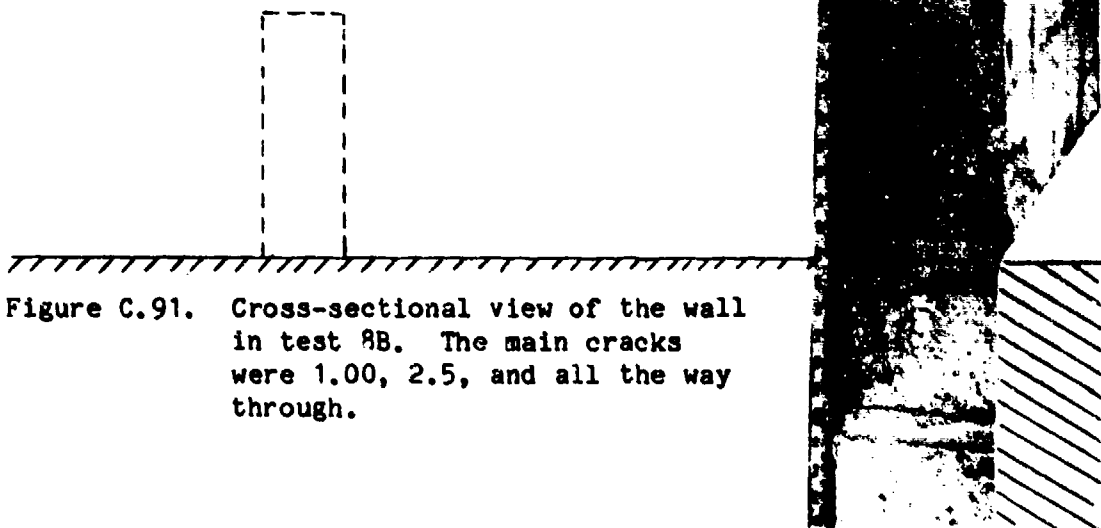


Figure C.91. Cross-sectional view of the wall in test 8B. The main cracks were 1.00, 2.5, and all the way through.

THIS
PAGE
IS
MISSING
IN
ORIGINAL
DOCUMENT

C51

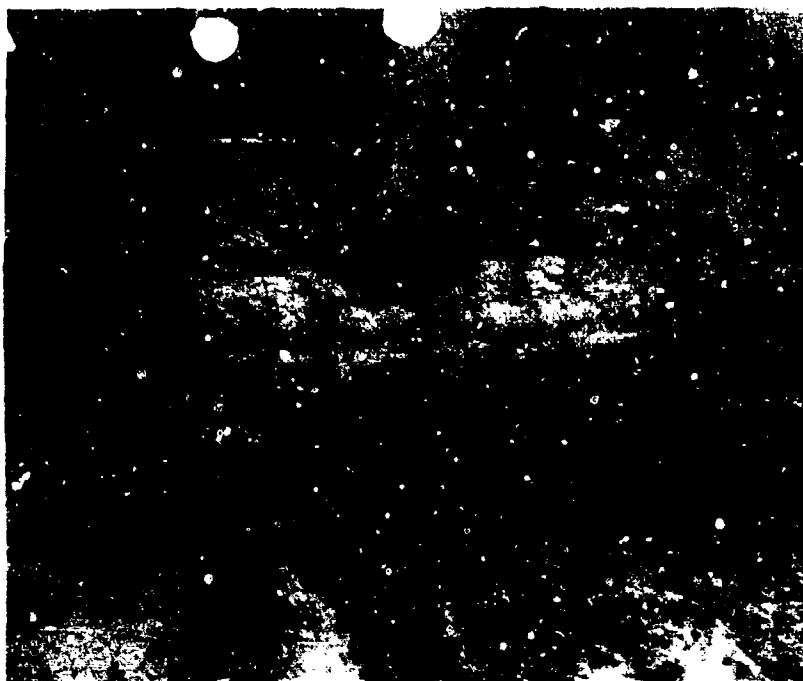


Figure C.94. Close-up of the wall with the debris cleaned away. The lead spall velocity was 65 ft/s.

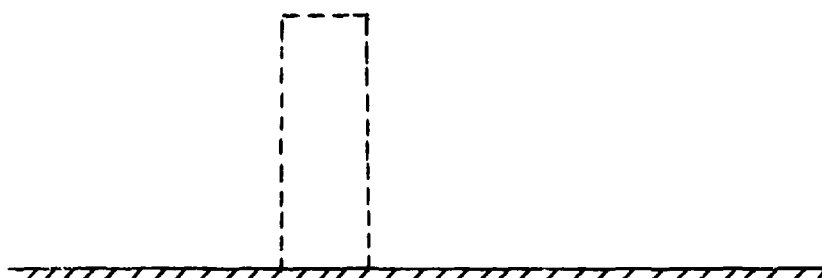


Figure C.95. Cross-sectional view of the wall breached by test 8C.

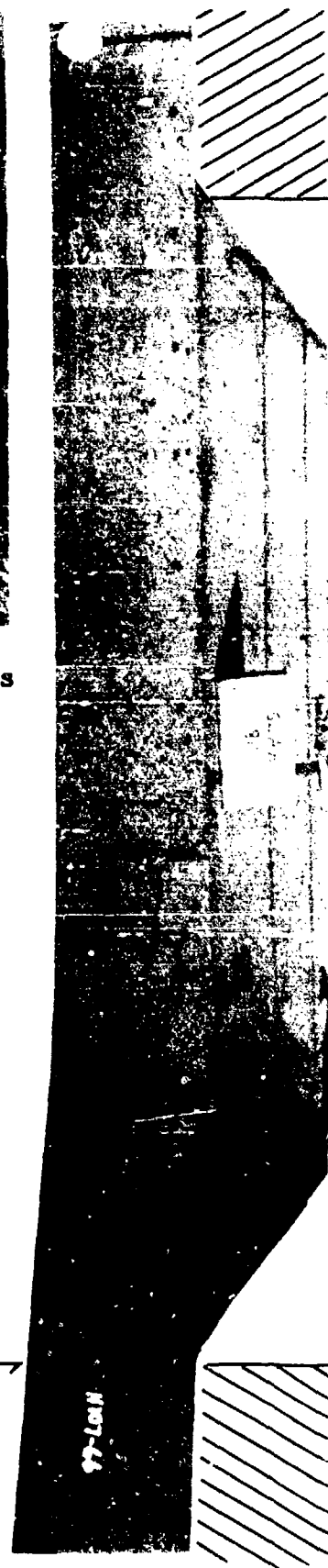




Figure C.96. Test 9A with a 14.39-pound C-4 charge in a 0.111-inch-thick casing at 5.0 feet from a 5.38-inch-thick wall.



Figure C.97. Scab damage up to 2.5-inch-deep caused by bomb fragments from test 9A.



Figure C.98. Threshold spall in the back of the wall in test 9A.



Figure C.99. Cross-sectional view of the wall in test 9A. Main cracks were 0.87, 1.62, and 3.25-inches deep. The crack all the way through was at a 28-degree angle.



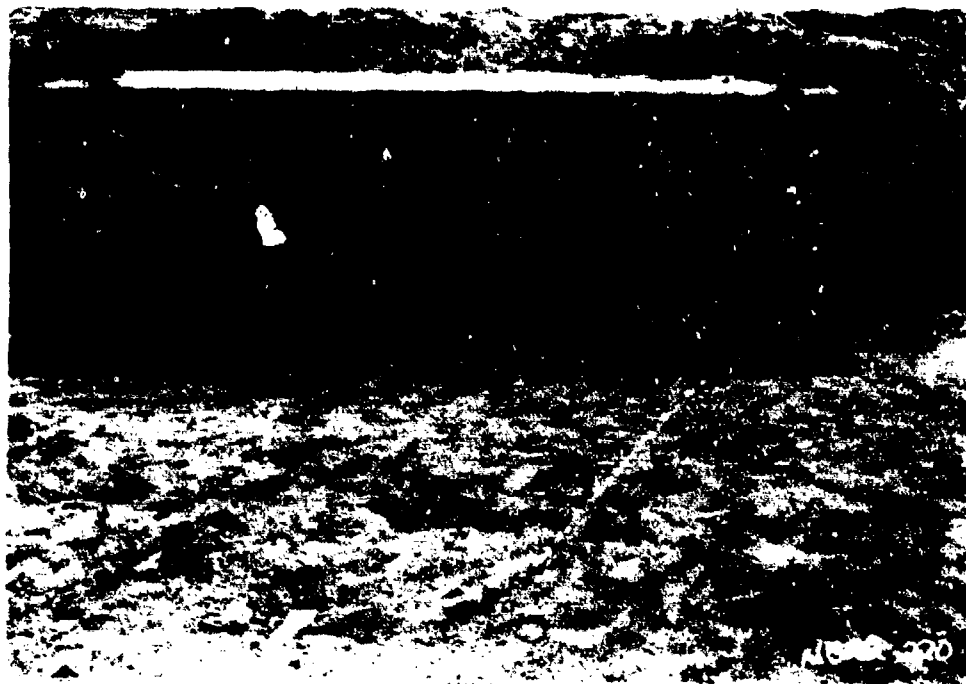


Figure C.100. Test 9B with a 1.66-pound C-4 charge in a 0.54-inch-thick casing at 1.54 feet from a 5.38-inch-thick wall.



Figure C.101. Scab damage up to 0.62-inch-deep in the front of the wall in test 9B.



Figure C.102. Threshold spall in the back of the wall in test 9B.

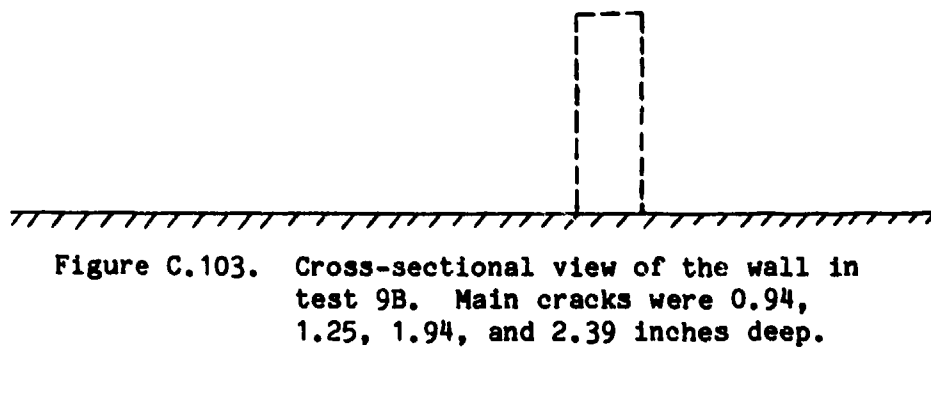


Figure C.103. Cross-sectional view of the wall in test 9B. Main cracks were 0.94, 1.25, 1.94, and 2.39 inches deep.

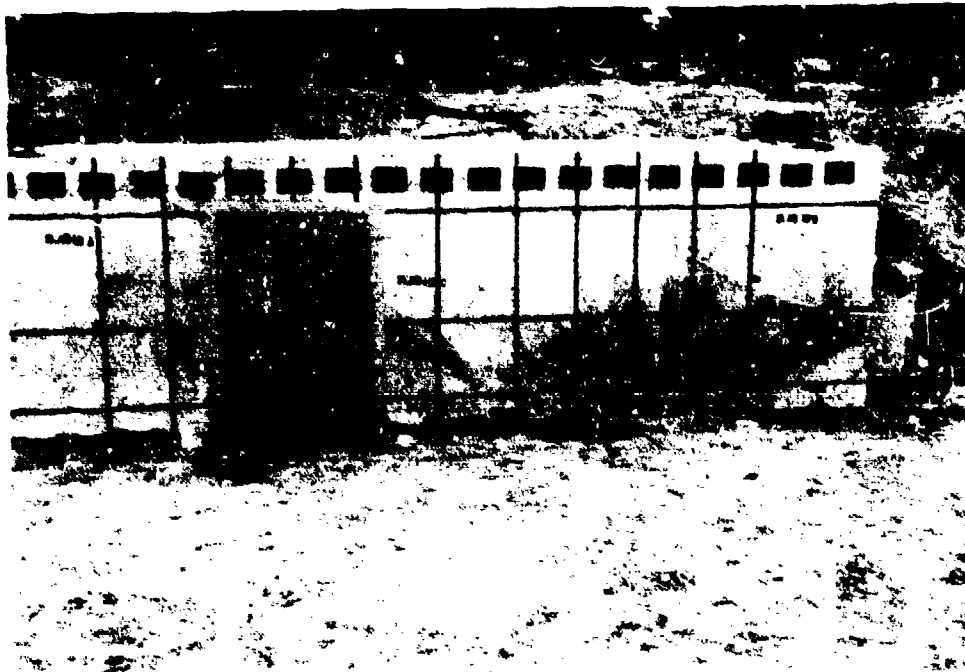


Figure C.104. Test 10A with a 14.39-pound C-4 charge in a 0.111-inch-thick casing at 2.44 feet from an 8.5-inch-thick wall with closely spaced reinforcing (1.5 inch).



Figure C.105. Scab damage up to 1.75-inch-deep caused by the bomb fragments from test 10A.

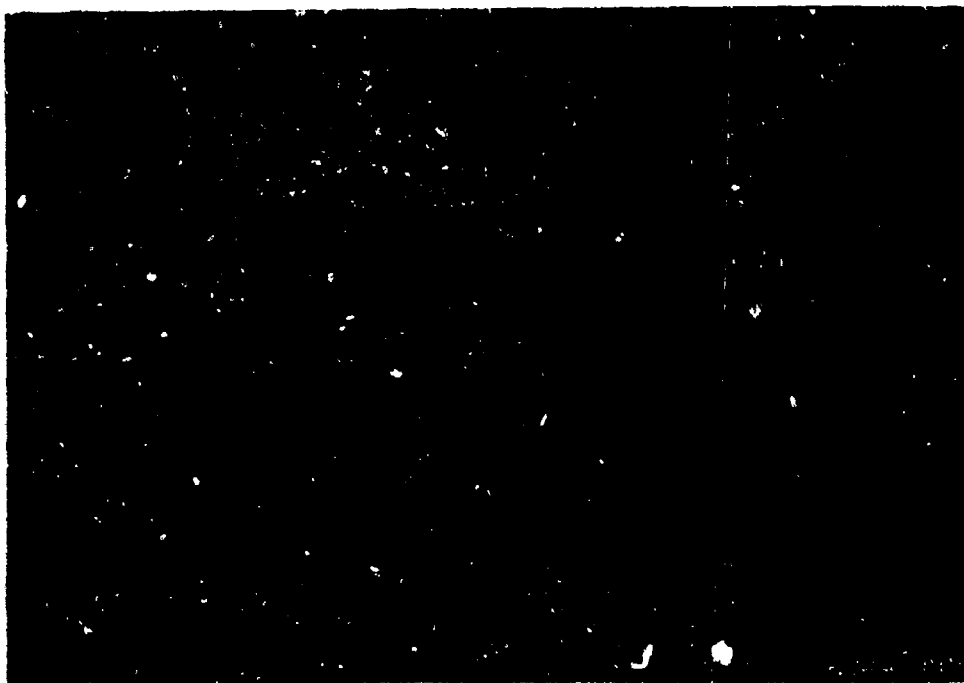


Figure C.106. Close-up of scab damage up to 1.75 inches deep.



Figure C.107. Spall of up to 1.25 inches from the back of the wall in test 10A. The spall velocity was 37.1 ft/s.

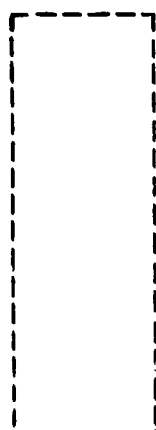


Figure C.108. Cross-sectional view of the wall in test 10A. Main cracks were 1.25, 2.0, 2.5, 3.89, 4.75, and 6.0 inches deep.

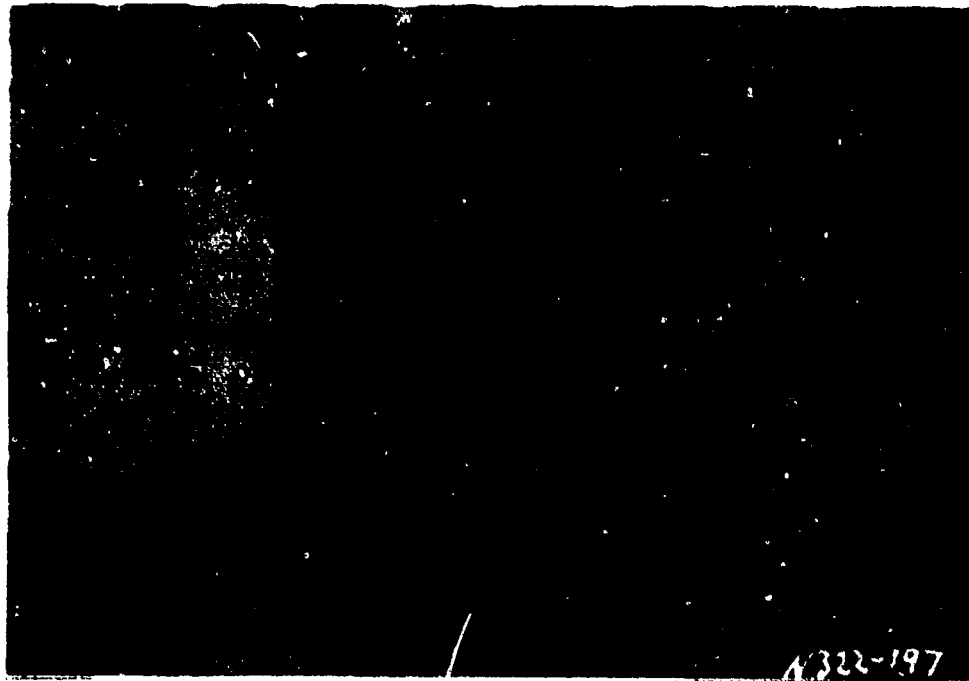


Figure C.109. Test 10B with a 3.63-pound C-4 charge in a 0.07-inch-thick casing at 1.54 feet from an 8.5-inch-thick wall with closely spaced reinforcing (1.5 inches).

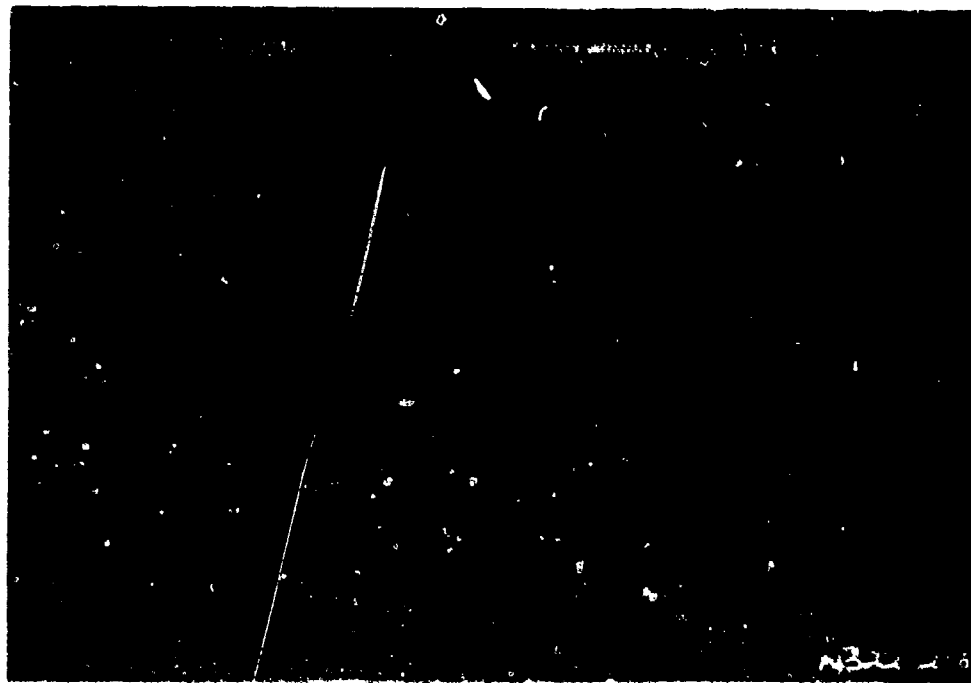


Figure C.110. Scab damage up to 1.00 inch deep in test 10B.

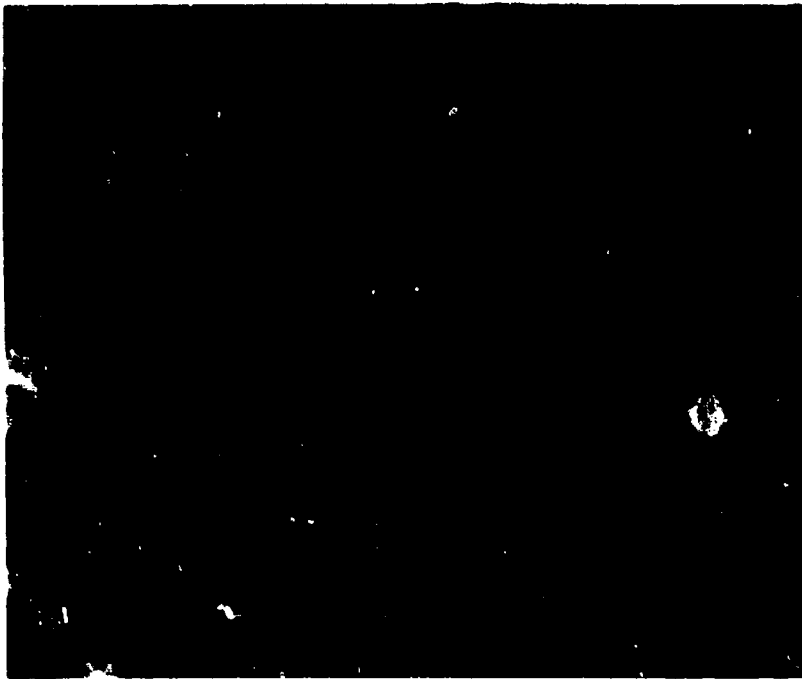


Figure C.111. Hairline cracks in the back of the wall in test 10B.

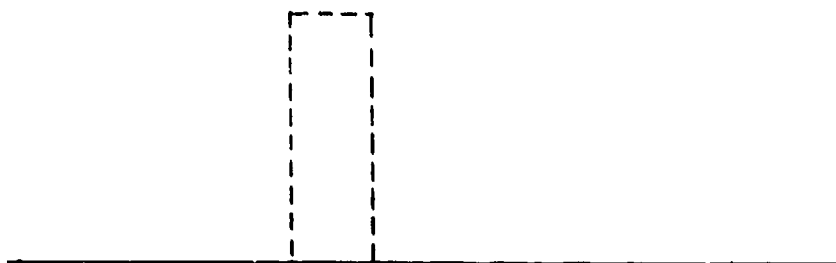


Figure C.112. Cross-sectional view of the wall in test 10B. No major cracks were found.



Figure C.113. Test 10C with a 1.07-pound C-4 charge in a 0.047-inch-thick casing in contact with an 8.5-inch-thick wall with closely spaced reinforcing (1.5 inches).



Figure C.114. Scab damage up to 1.88 inches deep in the front of the wall in test 10C.

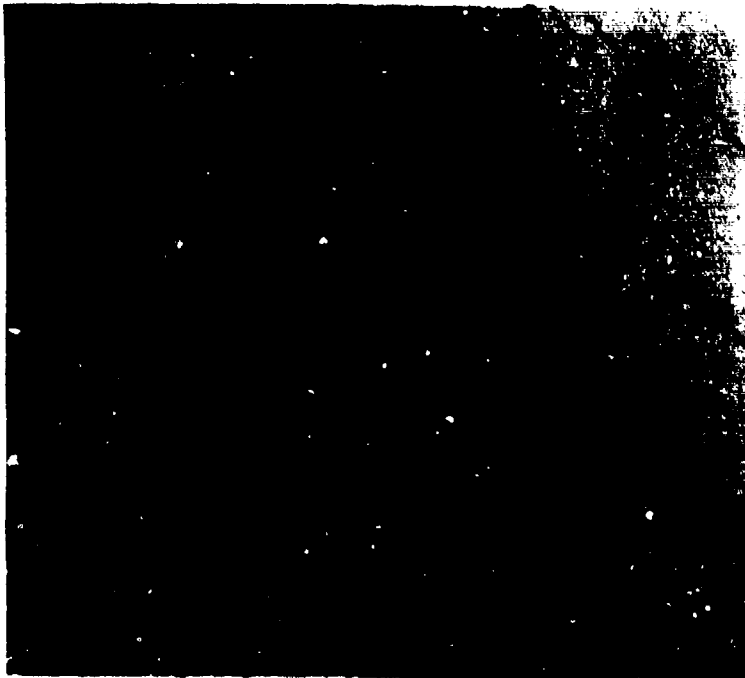


Figure C.115. 0.5-inch-deep spall damage to the back of the wall in test 10C.



Figure C.116. Cross-sectional view of the wall in test 10C. Main cracks were 1.38, 2.00, 2.75, 3.12, and 4 inches deep.

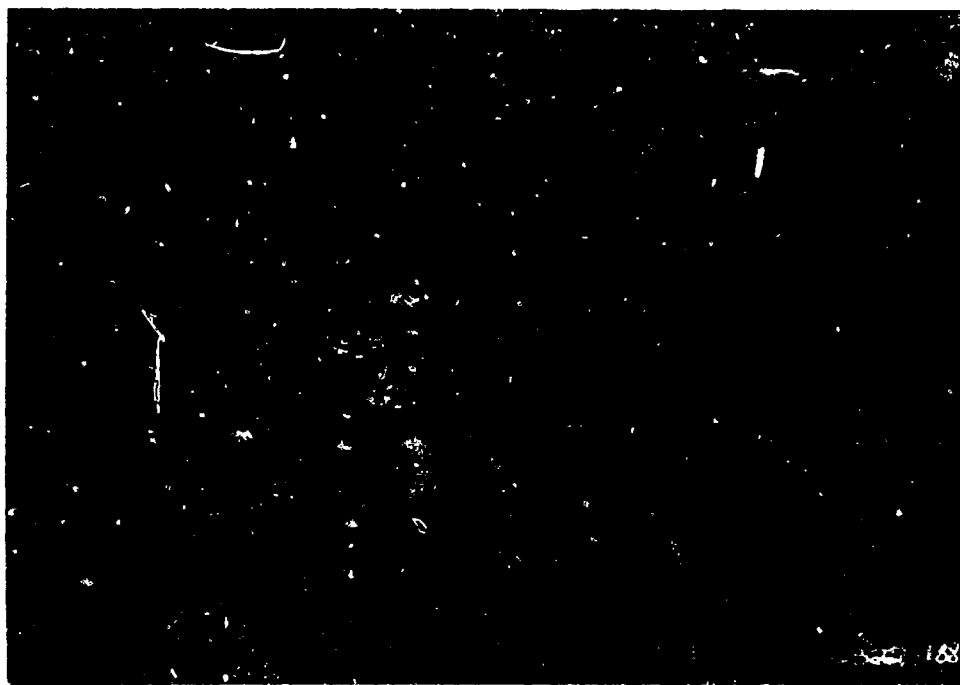


Figure C.117. Test Box-1 with bare 3.63-pound C-4 charge at 1.54 feet from an 11.25-inch-thick wall.



Figure C.118. Front of wall after charge was detonated in test Box-1.

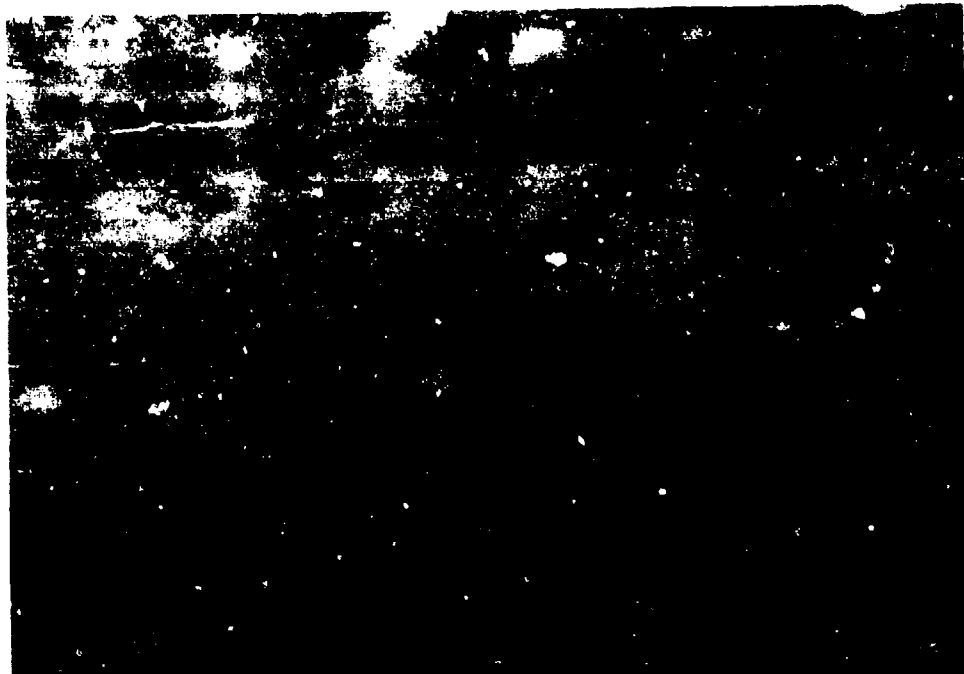


Figure C.119. Hairline cracks in the back of the wall in test Box-1.

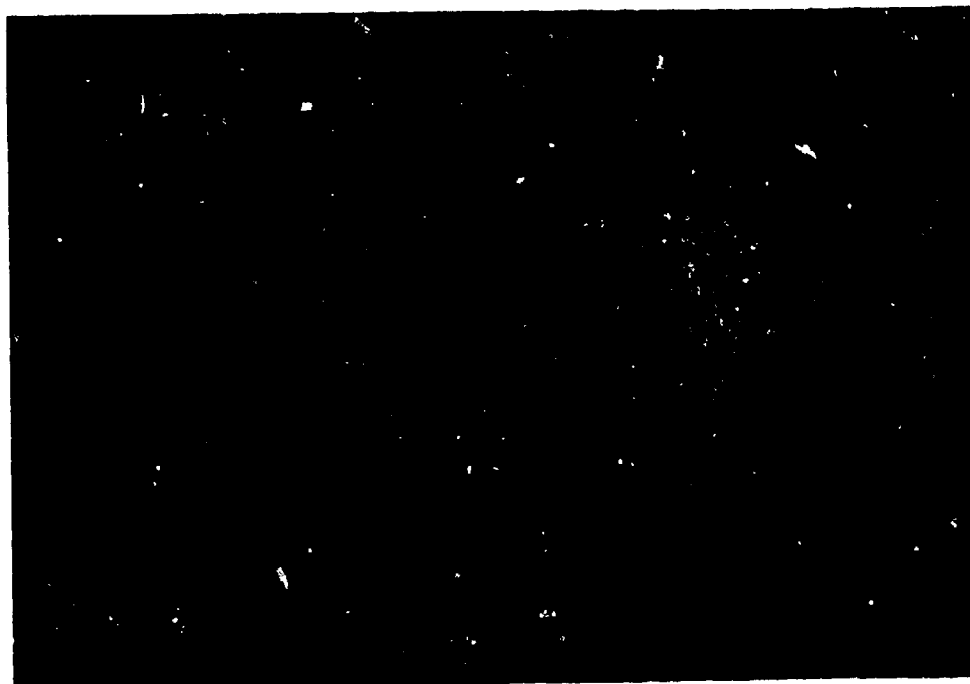


Figure C.120. Test Box-2 with a 3.63-pound C-4 charge in a 0.070-inch-thick casing at 1.54 feet from an 11.25-inch-thick wall.



Figure C.121. Damage to the front of the wall in test Box-2.



Figure C.122. Close-up of the scab damage up to 1.0-inch deep in the front of the wall in test Box-2.

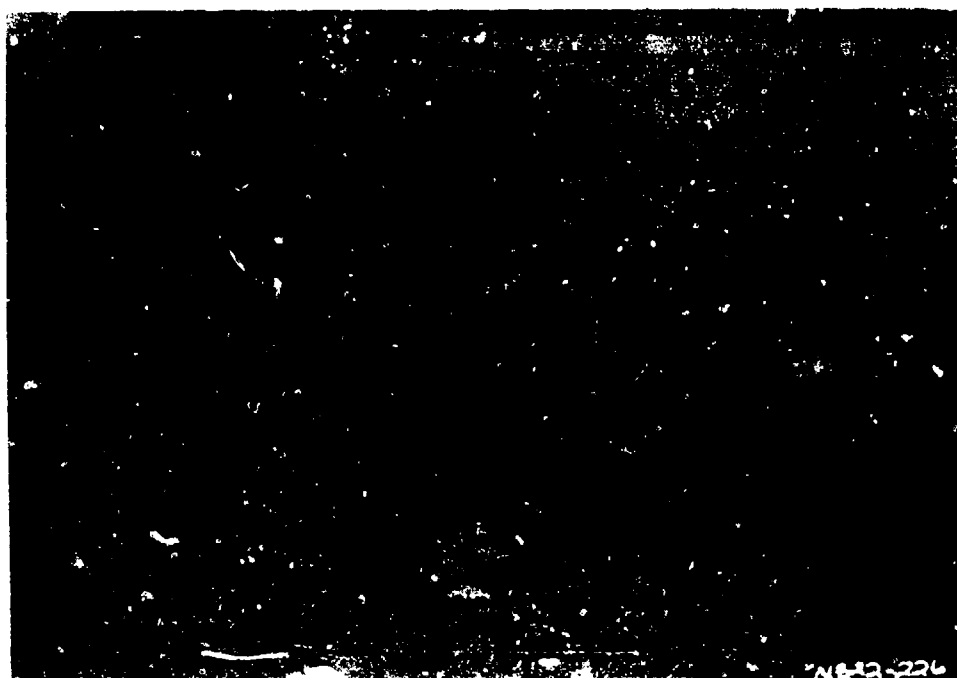


Figure C.123. Spall damage (2.50 inches deep) to the back of the wall in test Box-2.



Figure C.124. Test Box-3 with a 3.63-pound C-4 charge in a 0.22-inch-thick casing at 1.54 feet from a 11.25-inch-thick wall.

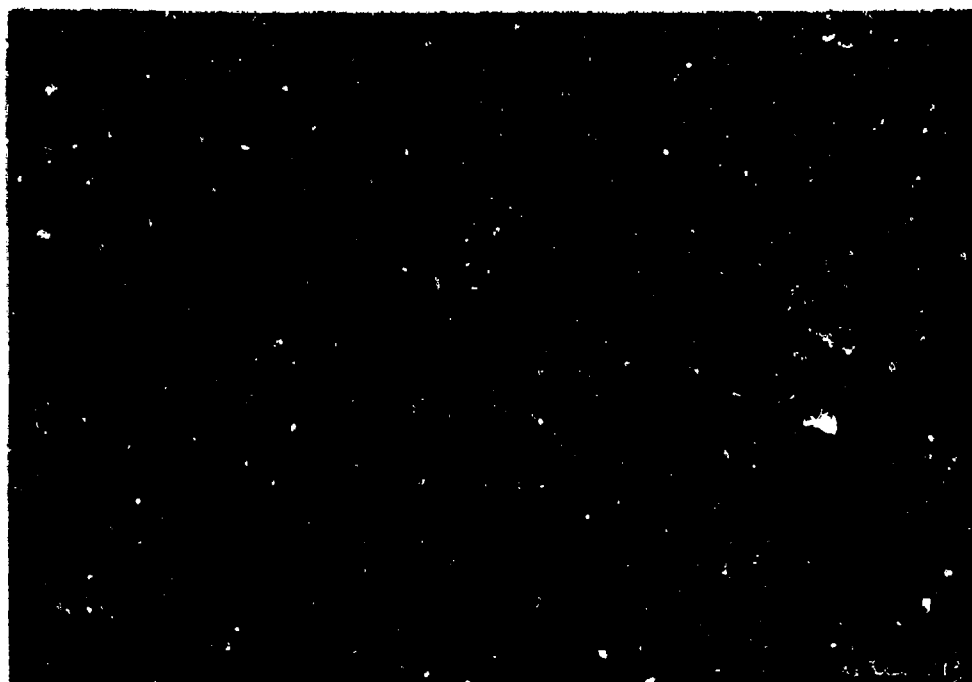


Figure C.125. Damage to the front of the wall in test Box-3.



Figure C.126. Scab damage up to 2.50 inches deep in the front of the wall in test Box-3.

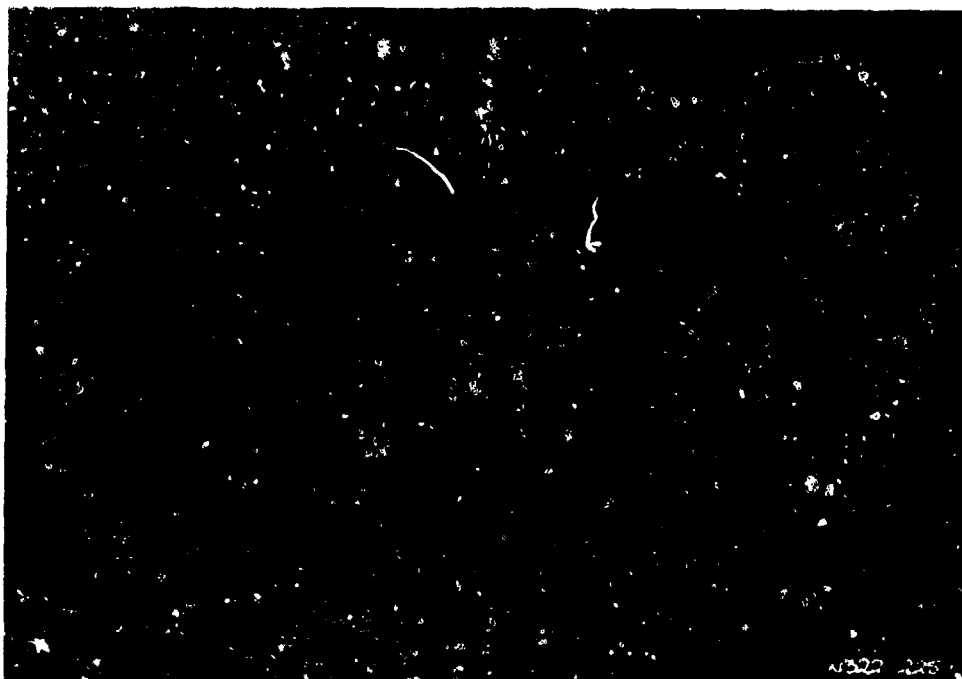


Figure C.127. Spall damage up to 3.00 inches deep in the back of the wall in test Box-3.



Figure C.128. Test Box-4 with a bare 7.44-pound C-4 charge at 1.54 feet from a 11.25-inch-thick wall.

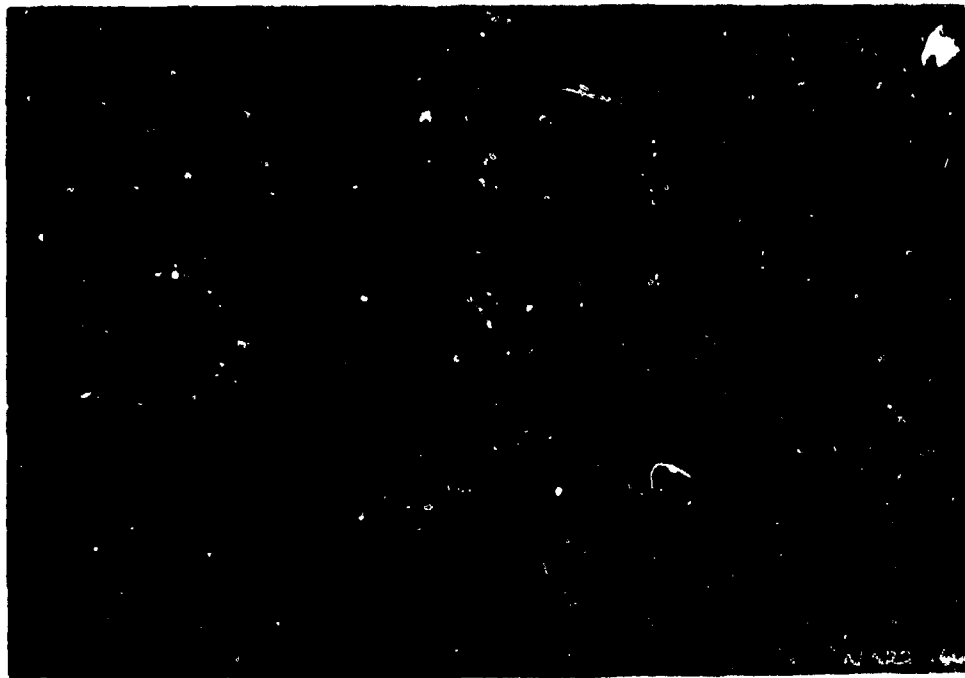


Figure C.129. The front of the wall in test Box-4 incurred no damage.

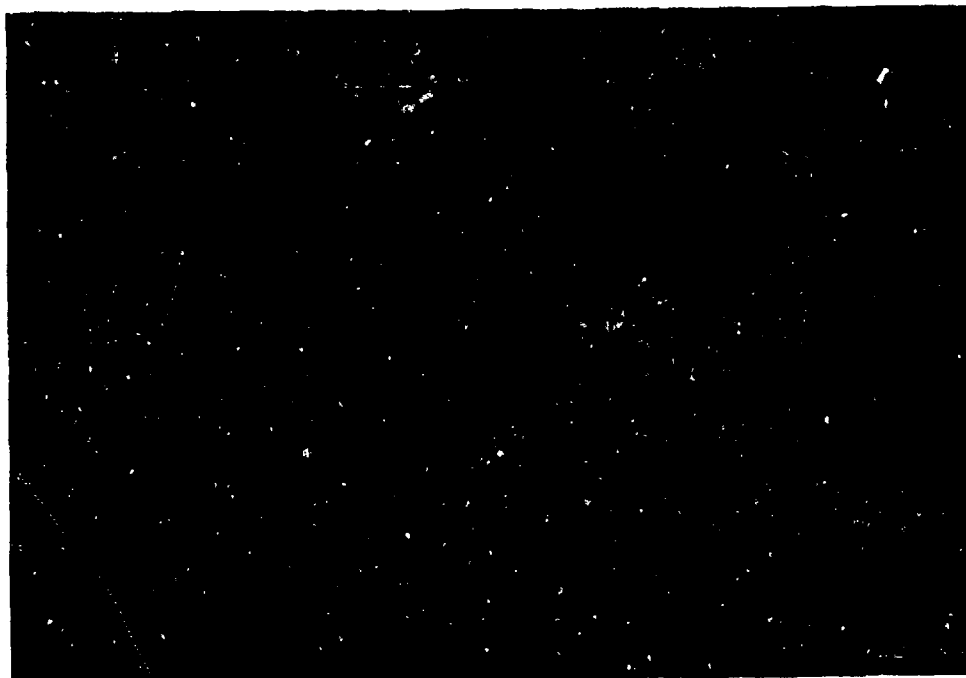


Figure C.130. Back of the wall in test Box-4 suffered only a few small patches of spall.

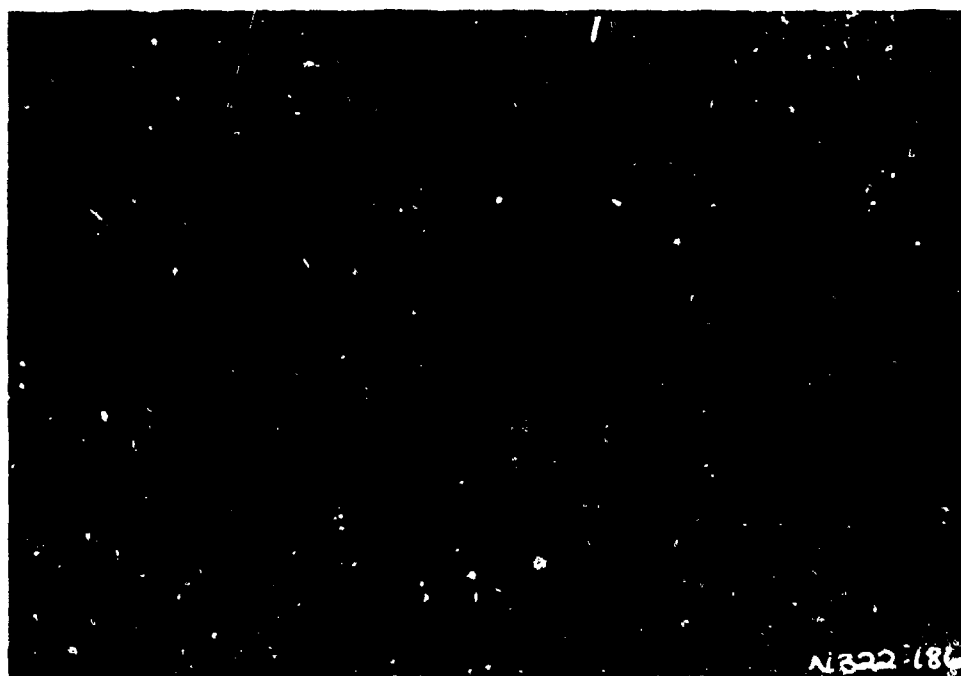


Figure C.131. Test Box-5 with a 7.44-pound C-4 charge in a 0.088-inch-thick casing at 1.54 feet from a 11.25-inch-thick wall.



Figure C.132. Damage to the front of the wall caused by bomb fragments in test Box-5.



Figure C.133. Close-up of the crater and scab damage caused by test Box-5. Scab depth was up to 1.00 inch deep.

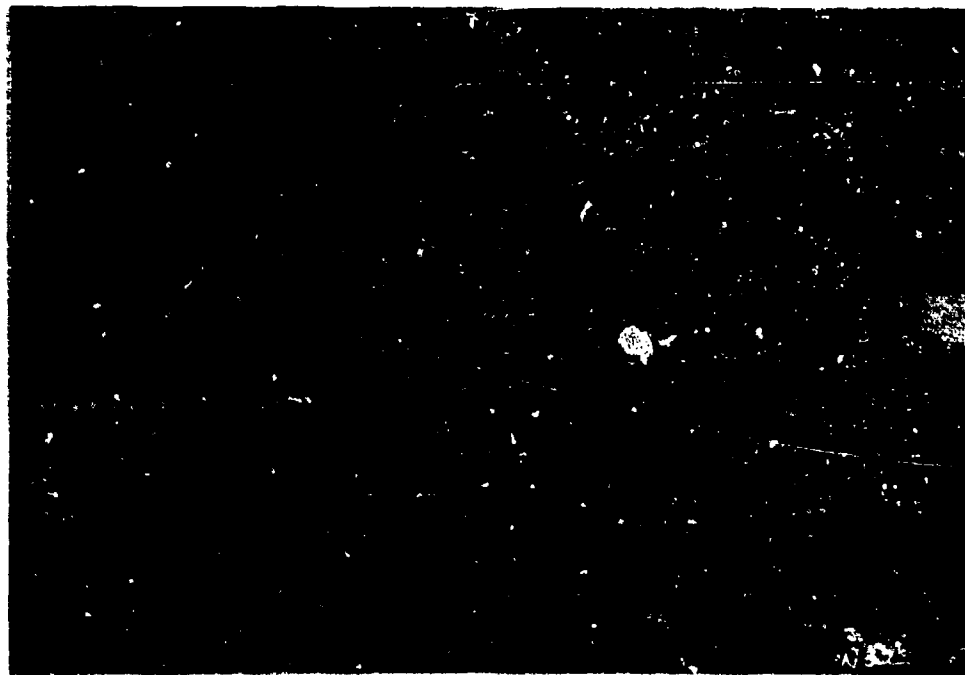


Figure C.134. Spall damage up to 3.75 inches deep in the back of the wall in test Box-5.

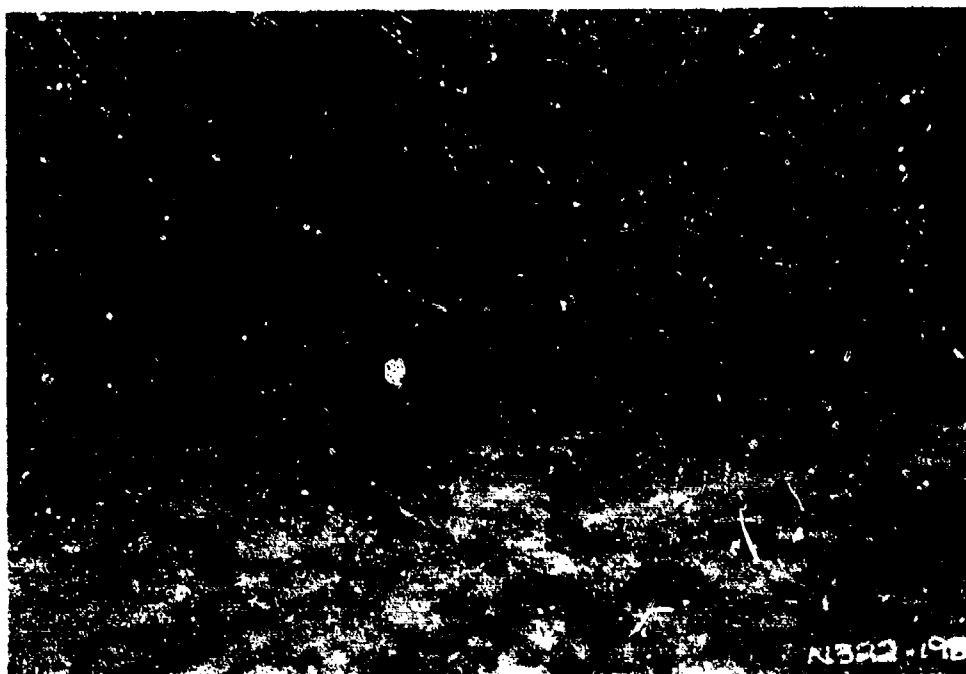


Figure C.135. Test Box-6 with a 7.44-pound C-4 charge in a 0.344-inch-thick casing at 1.54 feet from a 11.25-inch-thick wall.

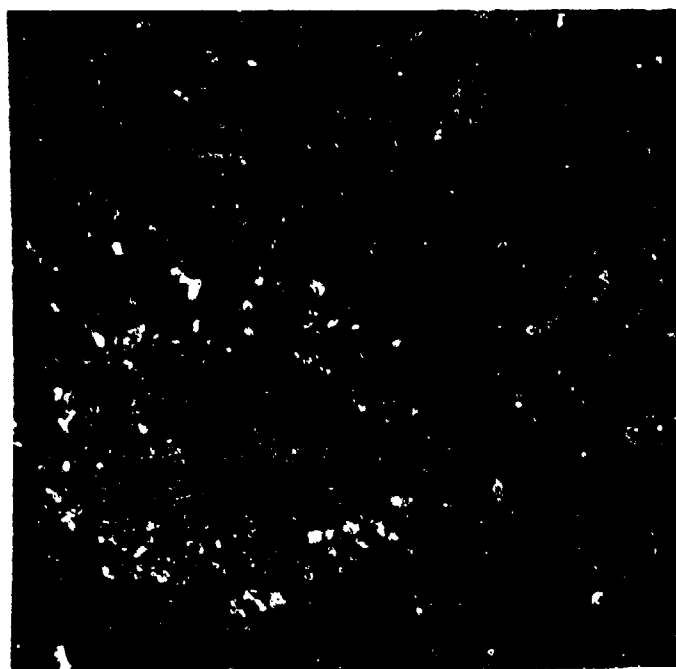


Figure C.136. Scab damage up to 2.50 inches deep in the front of the wall in test Box-6.

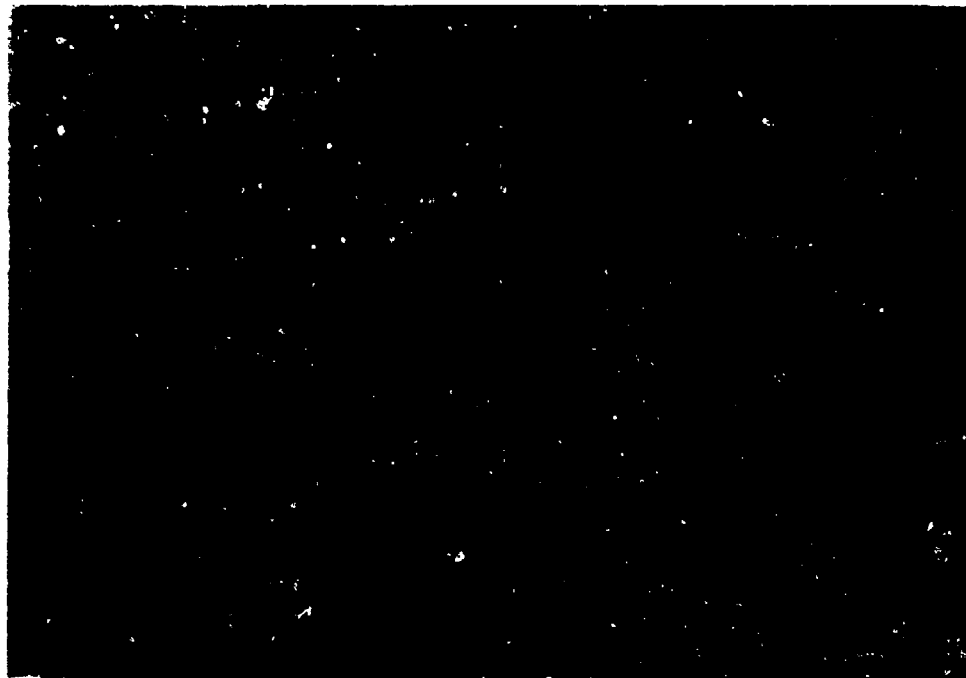


Figure C.137. Spall damage up to 3.75 inches deep in the back of the wall in test Box-6.

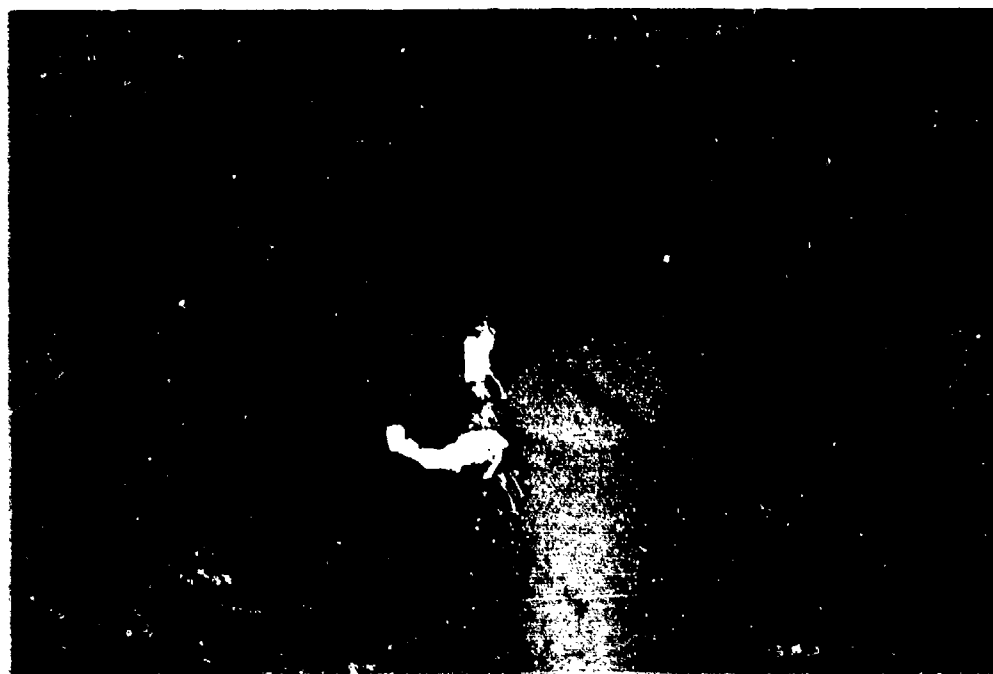


Figure C.138. Test Box-7 with a 12.0-pound C-4 charge in a plastic pipe at 2.0 feet from a 11.25-inch-thick wall.



Figure C.139. The front of the wall in test Box-7
slightly pitted.



Figure C.140. Spall damage up to 3.00 inches deep in the
back of the wall in test Box-7.

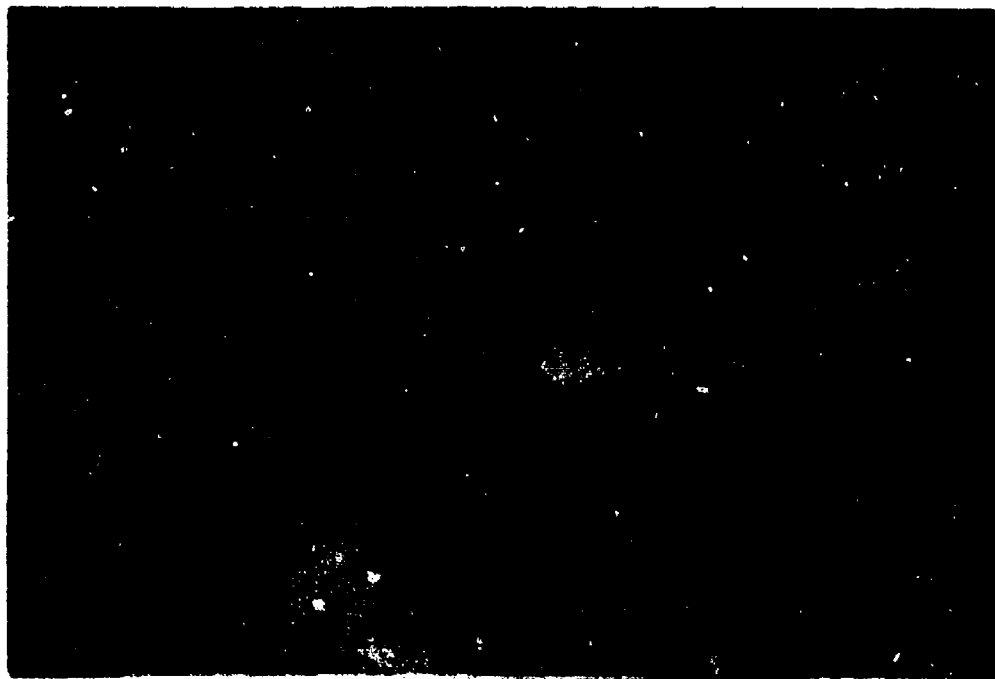


Figure C.141. Test Box-8 with a 6.25-pound C-4 charge in a cardboard tube at 2.00 feet from a 11.25-inch-thick wall.



Figure C.142. The front of the wall in test Box-8 showing no damage.

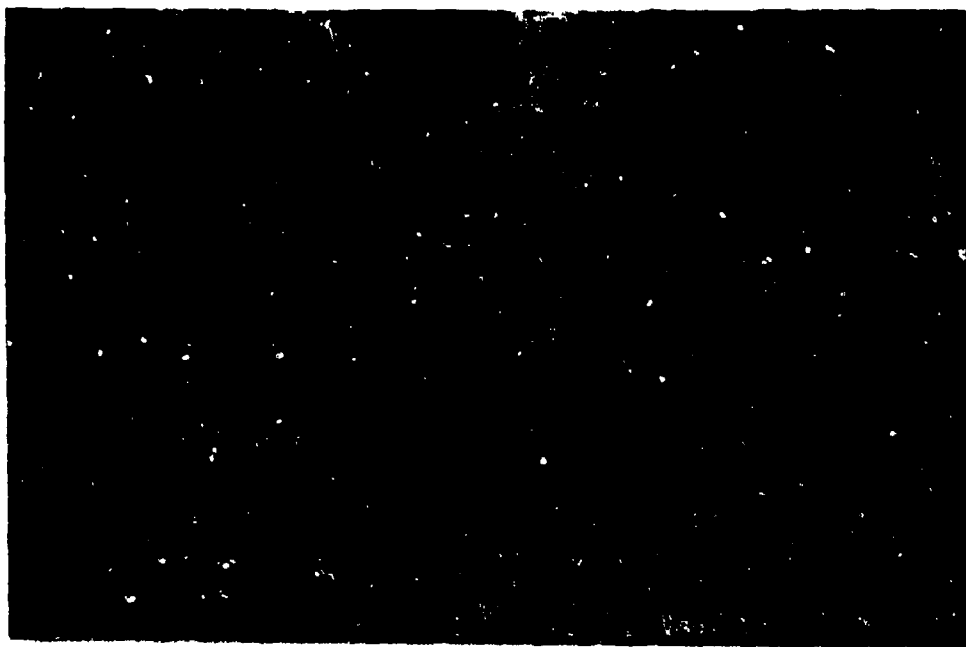


Figure C.143. The back of the wall in test Box-8 showing no damage.



Figure C.144. Test Box-9 with a 6.25-pound C-4 charge in a 0.156-inch-thick casing at 2.00 feet from a 11.25-inch-thick wall.

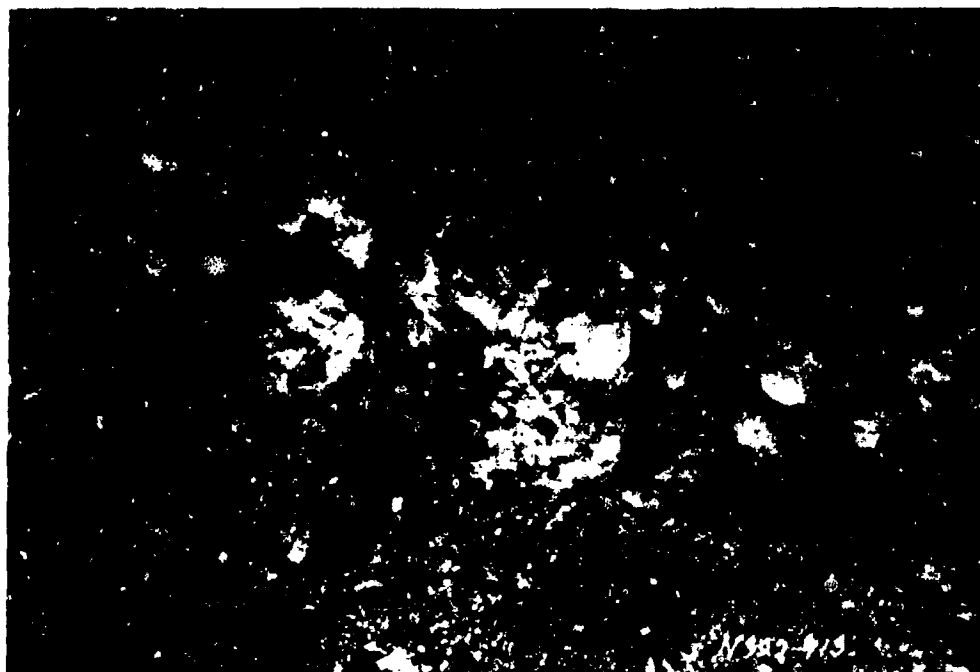


Figure C.145. Damage up to 1.5 inches deep to the front of the wall in test Box-9.



Figure C.146. Spall damage up to 3.00 inches deep in the back of the wall in test Box-9.



Figure C.147. Test Box-10 with a 9.00-pound C-4 charge in a plastic pipe at 2.00 feet from a 11.25-inch-thick wall.

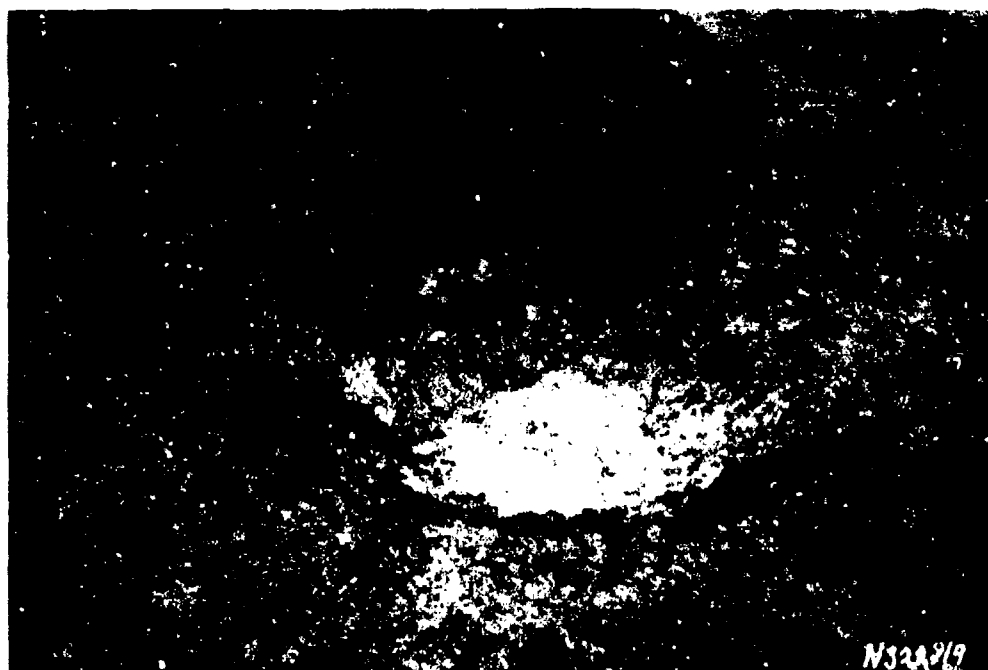


Figure C.148. Light damage to the front of the wall in test Box-10.



Figure C.149. Threshold spall in the back of the wall in test Box-10.

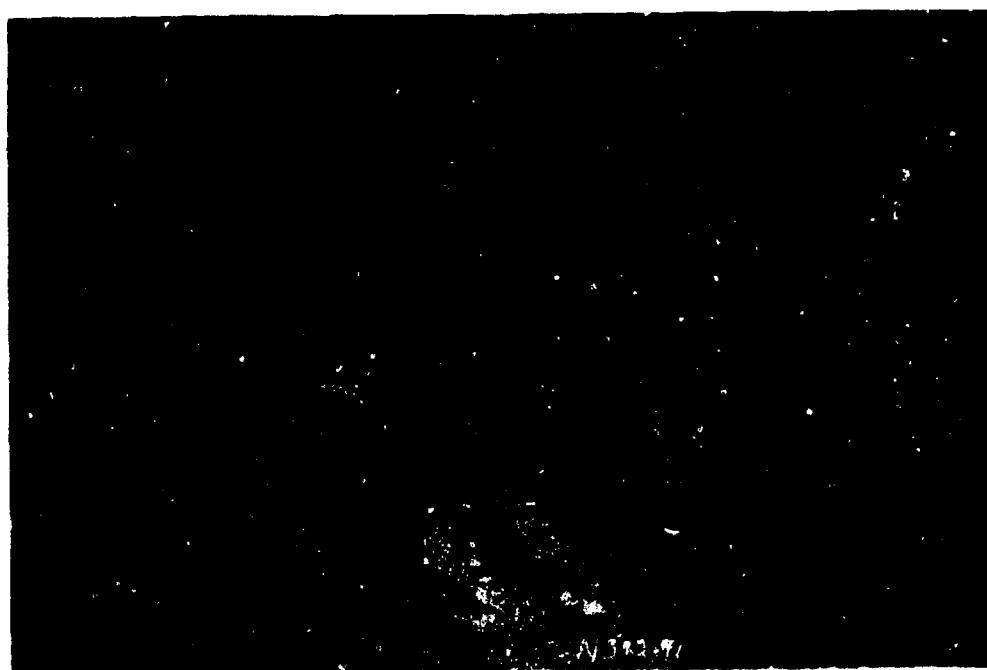


Figure C.150. Test Box-11 with a 3.86-pound C-4 charge in a 0.25-inch-thick casing at 2.00 feet from a 11.25-inch-thick wall.

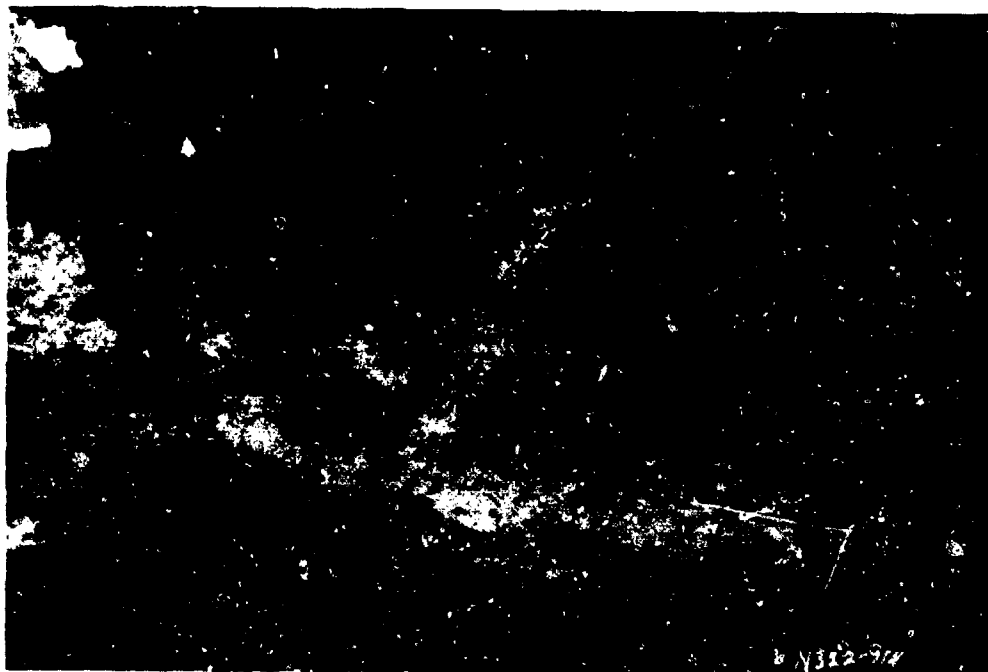


Figure C.151. Scab damage up to 1.25 inches deep in the front of the wall in test Box-11.



Figure C.152. Threshold to light spall damage (1.5 inches deep) in the back of the wall in test Box-11.

APPENDIX D

**DATA ON DAMAGE OF REINFORCED CONCRETE STRUCTURES
CAUSED BY NEARBY BOMB DETONATIONS**

POINT	REFERENCE	TEST	R (in)	W (in) (lb)	BOMB SIZE ID (in) X Ht. (in)	CASING (in)	R/W=1/3 11/lb=1/3	T (in)
1	---	1 A	18.5	4.968	3.0 X 9.0	---	0.9035	8.5
2	---	B	18.5	4.968	"	.070	0.9035	8.5
3	---	C	1	1.472	2.0 X 6.0	---	0.0733	8.5
4	---	D	18.5	10.195	3.81 X 11.44	---	0.7110	8.5
5	---	2 A	18.5	6.439	3.25 X 9.75	---	0.8287	8.5
6	---	B	18.5	7.473	3.75 X 8.69	.088	0.7885	8.5
7	---	C	1	1.472	2.0 X 6.0	.047	0.0767	8.5
8	---	D	18.5	7.473	3.44 X 10.31	---	0.7885	8.5
9	---	3 A	29.25	40.295	6.0 X 18.25	---	0.7110	8.5
10	---	B	18.5	10.195	3.75 X 11.25	.088	0.7228	8.5
11	---	4 A	60.0	19.719	4.75 X 14.25	.111	1.8507	8.5
12	---	B	29.25	19.719	"	.111	0.9022	8.5
13	---	5 A	18.5	9.702	3.75 X 11.25	.088	0.7228	8.5
14	---	B	18.5	4.968	3.0 X 9.0	.070	0.9035	8.5
15	---	C	1	1.472	2.0 X 6.0	.047	0.0767	8.5
16	---	6 A	18.5	9.702	3.75 X 11.25	.088	0.7228	8.5
17	---	B	18.5	4.968	3.0 X 9.0	.070	0.9035	8.5
18	---	C	1	1.472	2.0 X 6.0	.047	0.0767	8.5
19	---	7 A	18.5	9.702	3.75 X 11.25	.088	0.7228	8.5
20	---	B	29.25	19.719	4.75 X 14.25	.111	0.9022	8.5
21	---	C	1	1.472	2.0 X 6.0	.047	0.0767	8.5
22	---	8 A	18.5	2.275	2.31 X 6.94	.054	1.1720	5.38
23	---	B	18.5	4.968	3.0 X 9.0	.070	0.9035	5.38
24	---	C	18.5	4.968	3.03 X 9.0	.21875	0.9035	5.38
25	---	9 A	60.0	19.719	4.75 X 14.25	.111	1.8507	5.38
26	---	B	11.375	2.275	2.31 X 6.94	.054	0.7207	5.38
27	---	10 A	29.25	19.719	4.75 X 14.25	.111	0.9022	8.5
28	---	B	18.5	4.968	3.0 X 9.0	.070	0.9035	8.5
29	---	C	1	1.472	2.0 X 6.0	.047	0.0767	8.5
30	---	DNA 3-1	18.5	4.968	3.0 X 9.0	.070	0.9035	11.25
31	---	3-2	18.5	4.968	"	---	0.9035	11.25
32	---	3-3	18.5	4.968	"	.21875	0.9035	11.25
33	---	DNA 7-1	18.5	10.189	3.81 X 11.69	---	0.7111	11.25
34	---	7-2	18.5	10.189	"	.088	0.7111	11.25
35	---	7-3	18.5	10.189	"	.34375	0.7111	11.25
36	---	DNA 1	24.0	16.440	3.94 X 17.5	---	0.7885	11.25
37	---	2	24.0	8.562	3.19 X 13.5	---	0.9776	11.25
38	---	3	24.0	8.062	3.06 X 14.31	.15625	0.9974	11.25
39	---	4	24.0	12.330	3.94 X 13.12	---	0.8657	11.25
40	---	5	24.0	4.979	3.06 X 9.38	.250	1.1712	11.25
41	48	1 FRONT	88.5	218.500	12.75 X 30.0	---	1.2240	18
42	48	2 FRONT	88.5	299.340	12.75 X 30.0	---	1.1020	18
43	48	3 FRONT	88.5	218.500	12.75 X 30.0	.250	1.2240	18
44	48	4 SIDE1	66.0	218.500	12.75 X 30.0	---	0.9130	18
45	48	5 SIDE2	66.0	218.500	12.75 X 30.0	.250	0.9130	18
46	---	1	22.5	4.411	2.88 X 4.5	0.125	1.1430	9
47	---	2	27.12	7.836	4.0 X 8.5	0.25	1.1380	9
48	---	3	33	14.138	4.0 X 15.38	0.25	1.1370	9
49	---	4	41.25	27.605	6.89 X 11.3	0.3	1.1370	9

T/W ² =1/3 (1/1b ² =1/3)	CONCRETE (psi)	W/(W+C) ² R/W ² =1/3	REBAR VERT. (in)	REBAR HORIZ. (in)	DAMAGE
0.4150	5090		#3 @ 5.5	#2 @ 5.5	NO DAMAGE
0.4151	5090	0.67114055	#3 @ 5.5	#2 @ 5.5	THRESHOLD
0.6227	5090		#3 @ 5.5	#2 @ 5.5	MEDIUM (2 3/8" DEEP)
0.3267	5090		#3 @ 5.5	#2 @ 5.5	MEDIUM (2 1/4" DEEP)
0.3807	4850		#3 @ 5.5	#2 @ 5.5	NO DAMAGE
0.3823	4850	0.58439556	#3 @ 5.5	#2 @ 5.5	THRESHOLD
0.6227	4850	0.05687778	#3 @ 5.5	#2 @ 5.5	MEDIUM (2" DEEP)
0.3623	4850		#3 @ 5.5	#2 @ 5.5	BARELY THRESHOLD
0.2086	5080		#3 @ 5.5	#2 @ 5.5	PATCHED SPALL & FLEXURE BREACH
0.3267	5080	0.57547411	#3 @ 5.5	#2 @ 5.5	MEDIUM (1 9/16" DEEP)
0.2622	5290	1.37407106	#3 @ 5.5	#2 @ 5.5	NO VISIBLE SPALL BUT HOLLOW
0.2622	5290	0.66984757	#3 @ 5.5	#2 @ 5.5	MEDIUM-HOLLOW OVER 86" SPACE
0.3321	13815	0.56957485	#3 @ 5.5	#2 @ 5.5	MEDIUM OVER A LARGE AREA
0.4151	13815	0.67114055	#3 @ 5.5	#2 @ 5.5	MEDIUM
0.6227	13815	0.05687778	#3 @ 5.5	#2 @ 5.5	SEVERE
0.3321	4605	0.56957485	#3 @ 5.5	#2 @ 5.5	THRESHOLD TO BARELY SPALL
0.4151	4605	0.67114055	#3 @ 5.5	#2 @ 5.5	THRESHOLD TO BARELY SPALL
0.6227	4605	0.05687778	#3 @ 5.5	#2 @ 5.5	MEDIUM TO SEVERE
0.3321	5050	0.56957485	#3 @ 5.5	#2 @ 5.5	THRESHOLD "CRACKING"
0.2622	5050	0.66984757	#3 @ 5.5	#2 @ 5.5	THRESHOLD/SHEAR/FLEXURE
0.6227	5050	0.05687778	#3 @ 5.5	#2 @ 5.5	MEDIUM
0.3406	4000	0.87048645	#2 @ 4.125	D2.5 @ 4.5	BARELY CRACKED-HALLOW AREA
0.2625	4000	0.67114055	#2 @ 4.125	D2.5 @ 4.5	OUTSIDE-SEVERE FRAG. DAMAGE
0.2625	4000	0.42114730	#2 @ 4.125	D2.5 @ 4.5	BREACHED
0.1658	4605	1.37407106	#2 @ 4.125	D2.5 @ 4.5	FLEXURE & SHEAR @ BOTTOM
0.3406	4605	0.53528974	#2 @ 4.125	D2.5 @ 4.5	THRESHOLD
0.2622	4300	0.66984757	D3 @ 1.5	D1 @ 1.25	SPALL
0.4151	4300	0.67114055	D3 @ 1.5	D1 @ 1.25	LIGHT CRACKS
0.6227	4300	0.05687778	D3 @ 1.5	D1 @ 1.25	MEDIUM SPALL
0.5495	5010	0.67114531	#6 @ 8.0	#6 @ 8.0	LIGHT (2 - 2 1/2" DEEP)
0.5495	5010		#6 @ 8.0	#6 @ 8.0	HAIRLINE CRACKS - NO DAMAGE
0.5495	5010	0.42110337	#6 @ 8.0	#6 @ 8.0	LIGHT TO MEDIUM (3" DEEP)
0.4324	5010		#6 @ 8.0	#6 @ 8.0	LIGHT SPALL (1 5/8" DEEP)
0.4324	5010	0.52659334	#6 @ 8.0	#6 @ 8.0	MEDIUM SPALL (2 1/2" DEEP)
0.4324	5010	0.28936450	#6 @ 8.0	#6 @ 8.0	MEDIUM TO SEVERE (3 1/4" DEEP)
0.3687	5010		#6 @ 8.0	#6 @ 8.0	MEDIUM SPALL (3" x 40")
0.4583	5010		#6 @ 8.0	#6 @ 8.0	NO DAMAGE
0.4675	5010	0.55639826	#6 @ 8.0	#6 @ 8.0	MEDIUM SPALL
0.4058	5010		#6 @ 8.0	#6 @ 8.0	THRESHOLD OF LIGHT SPALL
0.5490	5010	0.49090869	#6 @ 8.0	#6 @ 8.0	THRESHOLD SPALL
0.2490	4321		#8 @ 8.0	#4 @ 9.0	HAIRLINE CRACKS
0.2242	4321		#8 @ 8.0	#4 @ 9.0	HEAVY SPALL-WALL MOVED 2" @ BOTTOM
0.2490	4321	0.87629095	#8 @ 8.0	#4 @ 9.0	BREACHED SAMEPLACE AS SHOT 2
0.2490	4321		#9 @ 7.0	#5 @ 11.0	CRACKS-WALL MOVED 4.5" @ BOTTOM
0.2490	4321	0.65363859	#9 @ 7.0	#5 @ 11.0	BREACH-WALL MOVED 4"
0.4573	6500	0.85294755	#6 @ 4.0	#3 @ 4.0	NO DAMAGE
0.3776	6500	0.56204280	#6 @ 4.0	#3 @ 4.0	THRESHOLD
0.3100	6500	0.56072645	#6 @ 4.0	#3 @ 4.0	SPALL
0.2480	6500	0.64442839	#6 @ 4.0	#3 @ 4.0	SPALL

POINT	REFERENCE	TEST	R (in)	W (in) (lb)	BOMB SIZE ID (in) X Ht (in)	CASING (in)	R/WRA1/3 (t/lbRA1/3)	T (in)
50	---	---	59.0	80.460	8.09 X 23.31	.197	1.1400	12.5
51	---	---	59.0	80.460	8.09 X 23.31	.197	1.1400	12.5
52	---	---	59.0	80.460	8.09 X 23.31	.197	1.1400	12.5
53	---	---	59.0	80.460	8.09 X 23.31	.197	1.1400	12.5
54	---	---	59.0	80.460	8.09 X 23.31	.197	1.1400	12.5
55	---	---	59.0	80.460	8.09 X 23.31	.197	1.1400	12.5
56	---	---	59.0	80.460	8.09 X 23.31	.197	1.1400	12.5
57	---	---	59.0	80.460	8.09 X 23.31	.197	1.1400	12.5
58	---	---	59.0	80.460	8.09 X 23.31	.197	1.1400	12.5
59	---	---	59.0	80.460	8.09 X 23.31	.197	1.1400	12.5
60	---	---	59.0	80.460	8.09 X 23.31	.197	1.1400	15.75
61	---	---	59.0	80.460	8.09 X 23.31	.197	1.1400	21.625
62	---	---	59.0	80.460	8.09 X 23.31	.197	1.1400	18.75
63	---	---	59.0	80.460	8.09 X 23.31	.197	1.1400	12.5
64	49	---	1.02	1	(SPHERES) 3.24	---	0.1350	6
65	49	---	2.04	2	4.08	---	0.1349	6
66	49	---	2.58	4	5.16	---	0.1354	6
67	49	---	3.54	10	7.08	---	0.1369	6
68	49	---	1.02	1	3.24	---	0.1350	10
69	49	---	2.04	2	4.08	---	0.1349	10
70	49	---	2.58	4	5.16	---	0.1354	10
71	49	---	3.54	10	7.08	---	0.1369	10
72	49	---	4.08	16	8.16	---	0.1349	10
73	49	---	4.5	21	9.00	---	0.1359	10
74	49	---	6	50	12.00	---	0.1357	20
75	50	S3A 1-5	2.87	5.5	(SPHERE) 5.74	---	0.1354	10.25
76	2	1-S111B	59.05	80.46	8.6 X 23.6	---	1.1396	19.7
77	2	2-S1B	59.05	80.46	8.6 X 23.6	---	1.1396	12.8
78	2	4-S11B	59.05	80.46	8.6 X 23.6	---	1.1396	12.8
79	2	7-S1A	66.14	65.98	8.6 X 23.6	---	1.3640	19.7
80	2	9-S111A	59.05	65.98	8.6 X 23.6	---	1.2180	12.8
81	2	11-S1A	59.05	78.99	8.6 X 23.6	---	1.1470	19.7
82	2	12	59.05	66.14	9.0 X 25.6	---	1.2170	12.8
83	2	13	59.05	66.140	9.0 X 25.6	.236	1.2170	12.8
84	2	14	59.05	66.14	9.0 X 25.6	---	1.2170	22.6
85	2	15	59.05	92.600	8.66 X 23.92	.236	1.0880	12.8
86	51		60	15.400	4.99 X 23.74	FW=.00181	2.0100	6.0
87	51		60	15.400	4.99 X 23.74	FW=.00181	2.0100	6.0
88	51		60	15.400	4.99 X 23.74	FW=.00181	2.0100	6.0
89	51		240	16.000		---	7.9340	6.0
90	51		120	16.000		---	3.9685	6.0
91	51		60	2.331		FW=.00172	3.7710	6.0
92	51		60	3.300		?	3.3580	6.0
93	51		60			?	?	6.0
94	51		120	7.700		TOT=47.8	5.0000	6.0
95	51		60	7.700		TOT=47.8	2.5320	6.0
96	51		60	2.331		FW=.00172	3.7710	6.0
97	51		60	3.300		?	3.3580	6.0
98	51		60			?	?	6.0
99	51		60	7.100		FW=.00335	2.5015	6.0
100	51		60	7.700		TOT=47.8	2.5320	6.0
101	51		360	15.400	4.99 X 23.74	FW=.00181	12.0580	6.0
102	51		60	15.400	4.99 X 23.74	FW=.00181	2.0100	6.0

T/W=1/3 1/1b=1/3	CONCRETE (psi)	W/(W+C)* R/W=1/3	REBAR VERT (in)	HEBAR HORIZ. (in)	DAMAGE
0.2413	5684	ERR	2 x #6 @ 4.0	#3 @ 4.0	MEDIUM SPALL
0.2413	5684	ERR	#4 @ 7.0	#3 @ 4.0	MEDIUM (2-2 3/4" DEEP)
0.2413	4952	ERR	#6 @ 4.0	#3 @ 4.0	"
0.2413	4952	ERR	#4 @ 3.5	#3 @ 4.0	"
0.2413	5004	ERR	#4 @ 3.5	#3 @ 4.0	"
0.2413	5004	ERR	#4 @ 7.0	#3 @ 8.0	"
0.2413	5233	ERR	#3 @ 9.0	#3 @ 9.0	NO DAMAGE EXCEPT FRAGMENTS
0.2413	5233	ERR	#3 @ 9.0	#3 @ 9.0	NO DAMAGE EXCEPT FRAGMENTS
0.2413	5352	ERR	#4 @ 3.5	#3 @ 9.0	SPALL PLATE DEFLECTED 7"
0.2413	5352	ERR	#3 @ 3.75	#3 @ 9.0	SPALL PLATE DEFLECTED 8"
0.3040	6184	ERR	#3 @ 5.0	#3 @ 7.0	MED (1-1 1/2" DEEP)-SHEAR @ FL
0.4174	6184	ERR	#3 @ 7.0	#3 @ 5.0	LIGHT TO MED.-SHEAR @ FLOOR
0.3619	5488	ERR	#3 @ 6.0	#3 @ 8.0	LIGHT TO MED.-SHEAR @ FLOOR
0.2413	5488	ERR	#3 @ 3.75	#3 @ 9.0	SPALL PLATE DEFLECTED 8"
0.5000	3500		#3 @ 11.75	#3 @ 12.0	SPALL (2.4" DEEP X 17.4" DIA.)
0.3976	3500		#3 @ 11.75	#3 @ 12.0	BREACH (18.36" DIA.)
0.3150	3500		#3 @ 11.75	#3 @ 12.0	BREACH (26.4" DIA.)
0.2320	3500		#3 @ 11.75	#3 @ 12.0	BREACH (28.8" DIA.)
0.8330	3500		#4 @ 11.75	#4 @ 12.0	NO SPALL
0.6610	3500		#4 @ 11.75	#4 @ 12.0	NO SPALL
0.5250	3500		#4 @ 11.75	#4 @ 12.0	SEVERE (5.76" DEEP X 10.2" DIA)
0.3870	3500		#4 @ 11.75	#4 @ 12.0	BREACH (38.28" DIA)
0.3310	3500		#4 @ 11.75	#4 @ 12.0	BREACH (42.72" DIA)
0.3020	3500		#4 @ 11.75	#4 @ 12.0	BREACH (47.52" DIA)
0.4520	3500		#4 @ 10.75	#4 @ 12.0	BREACH (66.28" DIA)
0.4840	4870		RAT. = .0025	?	MEDIUM SPALL (2-2 1/2" DEEP)
0.3803	3655		RAT. = .00085	RAT. = .000956	MED. TO HEAVY SPALL 3/4"
0.2471	3655		RAT. = .00085	RAT. = .000956	BREACH-HOLE
0.2471	3655		RAT. = .00085	RAT. = .000956	BREACH & SPALL PLATE TORN AWAY
0.4062	3655		RAT. = .00085	RAT. = .000956	CRACK & .31" PERMANENT DEFL.
0.2640	3655		RAT. = .00085	RAT. = .000956	LARGE CRACKS, 5.9" PERM. DEFL.
0.3828	3655		RAT. = .00085	RAT. = .000956	WALLS SEPERATED, HEAVY DAMAGE
0.2638	5917		RAT. = .0017	RAT. = .0017	MED. SPALL, 1 1/2" PERM. DEFL.
0.2638	5917	0.69545881	RAT. = .0017	RAT. = .0017	CRACKS, 1 1/4" PERM. DEFL.
0.2638	5917		RAT. = .00087	RAT. = .00087	LIGHT CRACKS, LIGHT SPALL
0.2658	5917	0.73700658	7mm @ 5.9"	5mm @ 5.9"	NO DAMAGE, HAIRLINE CRACKS
0.2010	4000	0.35111161	#4 @ 11.0	#4 @ 11.0	BREACHED
0.2010	4000	0.35111161	#4 @ 11.0	#4 @ 11.0	HAIRLINE CRACKS
0.2010	2500	0.35111161	#4 @ 11.0	#4 @ 11.0	NO SPALL
0.1984	2500		#5 @ 7.8	#5 @ 11.0	NO DAMAGE
0.1984	2500		#5 @ 7.8	#5 @ 11.0	NO DAMAGE
0.3771	2500	1.23267437	#5 @ 7.8	#5 @ 11.0	NO SPALL
0.3358	2500		#5 @ 7.8	#5 @ 11.0	CRACKS
	2500		#5 @ 6.0	#5 @ 10.0	CRACKS
0.2532	2500		#5 @ 7.8	#5 @ 11.0	SEVERE SPALL
0.2532	2500		#5 @ 7.8	#5 @ 11.0	BREACHED
0.3771	2500	1.23267437	#6 @ 10.0	#5 @ 12.0	NO SPALL, OUTSIDE SCABBED
0.3358	2500		#6 @ 10.0	#5 @ 12.0	NO SPALL, OUTSIDE SCABBED
	2500		#5 @ 10.0	#5 @ 12.0	NO SPALL, OUTSIDE SCABBED
0.2602	2500		#6 @ 10.0	#5 @ 12.0	MEDIUM SPALL & CRACKING
0.2532	2500		#6 @ 10.0	#5 @ 12.0	SEVERE SPALL
0.2010	2500	2.10632032	#6 @ 10.0	#5 @ 12.0	SMALL BREACH
0.2010	2500	0.35111161	#6 @ 10.0	#5 @ 12.0	BREACHED

POINT	REFERENCE	TEST	R (in)	W (Int) (lb)	BOMB SIZE ID (in) X Ht. (in)	CASING (in)	R/WAF1/3 12/16RA1/3	T (in)
103	52	1	?	47.950		---	0.1350	20.0
104	52	2	?	47.950		---	0.1350	8.0
105	53	1	59.05	76.240	7.87" X 25.59"	.236	1.1605	12.8
106	53	2	33.46	15.763	4.13" X 19.85"	.197	1.1120	12.8
107	53	3	59.05	76.240	7.87" X 25.5"	.236	1.1605	7.87
108	53	4	33.46	15.763	4.13" X 19.85"	.197	1.1120	12.8
109	53	13	118.11	445.320	?	?	1.2890	25.50
(O.D. X HEIGHT)								
110	54	H1	39.37	15.102	6.22 X 23.74	.615	1.3270	11.81
111	54	H2	19.68	15.102	6.22 X 23.74	.615	0.8635	11.81
112	54	H3	39.37	15.102	6.22 X 23.74	.615	1.3270	15.75
113	54	H4	9.84	15.102	6.22 X 23.74	.615	0.3317	15.75
114	54	H5	39.37	22.040	? IN BAG	---	1.1702	11.81
115	54	H6	19.68	22.040	? IN BAG	---	0.5849	11.81
116	54	H7	9.84	22.040	? IN BAG	---	0.2925	11.81
117	54	H8	39.37	22.040	? IN BAG	---	1.1702	7.87
118	54	H9	19.68	22.040	? IN BAG	---	0.5849	7.87
119	54	H10	9.84	22.040	? IN BAG	---	0.2925	7.87
120	54	H11	19.68	22.040	? IN BAG	---	0.5849	15.75
121	54	H12	9.84	22.040	? IN BAG	---	0.2925	15.75
122	54	H13	9.84	22.040	? IN BAG	---	0.2925	15.75
123	54	H14	9.84	44.050	? IN BAG	---	0.2321	11.81
124	54	H15	2	14.000	9.00 X 9.00 X 3.6	?	0.0691	15.75
125	55	1	0.4	0.028	.7978 CUBED	---	0.1100	3.94
126	55	2	0.5	0.055	1.0048 CUBED	---	0.1100	3.94
127	55	3	0.63	0.110	1.2657 CUBED	---	0.1100	3.94
128	55	4	0.8	0.221	1.5949 CUBED	---	0.1100	3.94
129	55	5	0.8	0.221	1.5949 CUBED	---	0.1100	3.94
130	55	6	1.77	0.221	1.5949 CUBED	---	0.2440	3.94
131	55	7	2.76	0.221	1.5949 CUBED	---	0.3610	3.94
132	55	8	0.91	0.331	1.8256 CUBED	---	0.1700	3.94
133	55	9	2.17	0.331	1.8256 CUBED	---	0.2610	3.94
134	55	10	3.15	0.331	1.8256 CUBED	---	0.3600	3.94
135	55	11	1	0.441	2.0086 CUBED	---	0.1100	3.94
136	55	12	2.36	0.441	2.0086 CUBED	---	0.2580	3.94
137	55	13	3.54	0.441	2.0086 CUBED	---	0.3600	3.94
138	55	14	4.72	0.441	2.0086 CUBED	---	0.5170	3.94
139	55	15	1.97	0.661	2.3001 CUBED	---	0.1860	3.94
140	55	16	1.97	1.102	2.7269 CUBED	---	0.1590	3.94
141	55	17	3.15	1.102	2.7269 CUBED	---	0.2540	3.94
142	55	18	5.90	2.204	3.4366 CUBED	---	0.3750	3.94
143	55	19	4.92	4.409	4.3290 CUBED	---	0.2500	3.94
144	55	20	5.66	6.614	4.9555 CUBED	---	0.3840	3.94
145	55	21	0	0.825	1.323 LB	.62	0.1400	3.94
146	55	22	4.92	0.825	1.323 LB	.62	0.4372	3.94
147	55	23	9.842	0.825	1.323 LB	.62	0.8746	3.94
148	55	24	19.685	0.825	1.323 LB	.62	1.7494	3.94
149	55	25	27.560	0.825	1.323 LB	.62	2.4492	3.94
150	55	26	0	4.365	33.07 LB	.13	0.1200	3.94
151	55	27	19.685	4.365	33.07 LB	.13	1.0040	3.94
152	55	28	39.370	4.365	33.07 LB	.13	2.0070	3.94
153	55	29	76.74	4.365	33.07 LB	.13	4.0150	3.94
154	55	30	118.110	4.365	33.07 LB	.13	6.0220	3.94
155	55	31	196.850	4.365	33.07 LB	.13	10.0370	3.94

T/WAR1/3 1/1bAR1/3	CONCRETE (psi)	W/(W+C) ² R/WAR1/3	REBAR VER1 (in)	REBAR HORIZ (in)	DAMAGE
0.4687	3600		#4 @ 12.0	#4 @ 12.0	BREACHED 28"HOLE x 84"SPALL
0.1835	3600		#4 @ 12.0	#4 @ 12.0	BREACHED 26"HOLE x 60"SPALL
0.2516	6817	0.73890529	RAT=.000829	RAT=.000829	BREACHED 15.8" x 68.9"
0.4254	6817	0.56905028	RAT=.000829	RAT=.000829	SPALL 6.7"DEEP 23.6" x 27.6"
0.1547	4000	0.73970638	RAT=.000829	RAT=.000829	SHEILD WALL DESTROYED MAIN WALL
0.2516	4000	0.56905028	RAT=.000829	RAT=.000829	SHEILD WALL DESTROYED MAIN WALL
0.2793	7252		RAT=.000829	RAT=.000829	MEDIUM SPALL (2"DEEP) + 2" SCAB
0.3981	4267	0.22808898	mm @ in	mm @ in	MEDIUM SPALL (3.6"DEEP)
0.3981	4267	0.11404449	16 @ 5.9	16 @ 5.9	TOTALLY DESTROYED
0.5310	4267	0.22808898	20 @ 9.84	20 @ 9.84	FLEXURE + SEVERE SCABBING
0.5310	4267	0.05701365	20 @ 9.84	14 @ 5.9	SEVERE SPALL + SEVERE SCABBING
0.3510	4267		16 @ 5.9	16 @ 5.9	NO DAMAGE
0.3510	4267		16 @ 5.9	16 @ 5.9	HAIRLIKE FLEXURE CRACKS
0.3510	4267		16 @ 5.9	16 @ 5.9	MED SPALL (2.7"DEEP) + SCABBED
0.2339	4267		10 @ 3.94	10 @ 3.94	NO DAMAGE
0.2339	4267		10 @ 3.94	10 @ 3.94	MED SPALL 2"DEEPEST
0.2339	4267		10 @ 3.94	10 @ 3.94	COMPLETELY DESTROYED
0.4681	4267		20 @ 9.84	20 @ 9.84	HAIRLIKE FLEXURE CRACKS
0.4681	4267		20 @ 9.84	20 @ 9.84	CRACKS, SMALL THRESHOLD SPALL
0.4681	4267		20 @ 9.84	14 @ 5.9	FLEXURAL CRACKS
0.2788	4267		16 @ 5.9	16 @ 5.9	HEAVY SPALL & WALL LEANED OVER
0.5448	4267		16 @ 5.9	16 @ 5.9	TOTALLY DESTROYED
1.0660	6670		RAT=.00406	RAT=.00406	NO DAMAGE
0.8630	6670		RAT=.00406	RAT=.00406	NO DAMAGE
0.6850	6670		RAT=.00406	RAT=.00406	MEDIUM SPALL
0.5430	6670		RAT=.00406	RAT=.00406	MEDIUM SPALL
0.5430	6670		RAT=.00406	RAT=.00406	MEDIUM SPALL
0.5430	6670		RAT=.00406	RAT=.00406	MEDIUM SPALL
0.5430	6670		RAT=.00406	RAT=.00406	THRESHOLD SPALL
0.4750	6670		RAT=.00406	RAT=.00406	SEVERE SPALL
0.4750	6670		RAT=.00406	RAT=.00406	SEVERE SPALL
0.4750	6670		RAT=.00406	RAT=.00406	MEDIUM SPALL
0.4310	6670		RAT=.00406	RAT=.00406	BREACHED
0.4310	6670		RAT=.00406	RAT=.00406	SEVERE SPALL
0.4310	6670		RAT=.00406	RAT=.00406	SEVERE SPALL
0.4310	6670		RAT=.00406	RAT=.00406	THRESHOLD
0.3770	7250		RAT=.00406	RAT=.00406	SEVERE SPALL
0.3180	7250		RAT=.00406	RAT=.00406	BREACHED
0.3180	7250		RAT=.00406	RAT=.00406	SEVERE SPALL
0.3180	7250		RAT=.00406	RAT=.00406	SEVERE SPALL
0.2520	7250		RAT=.00406	RAT=.00406	BREACHED
0.2000	7250		RAT=.00406	RAT=.00406	BREACHED
0.1750	7250		RAT=.00406	RAT=.00406	BREACHED
0.3502	7110	0.08724867	RAT=.00411	RAT=.00411	BREACHED
0.3502	7110	0.27246515	RAT=.00411	RAT=.00411	BREACHED
0.3502	7110	0.54505495	RAT=.00411	RAT=.00411	BREACHED
0.3502	7110	1.09023454	RAT=.00411	RAT=.00411	BREACHED
0.3502	7110	1.52636328	RAT=.00411	RAT=.00411	BREACHED
0.2009	7110	0.02816888	RAT=.00411	RAT=.00411	BREACHED
0.2009	7110	0.23567948	RAT=.00411	RAT=.00411	BREACHED
0.2009	7110	0.47112422	RAT=.00411	RAT=.00411	BREACHED
0.2009	7110	0.94248319	RAT=.00411	RAT=.00411	BREACHED
0.2009	7110	1.41360742	RAT=.00411	RAT=.00411	BREACHED
0.2009	7110	2.35609061	RAT=.00411	RAT=.00411	BREACHED

POINT	REFERENCE	TEST	R (in)	W (in) (lb)	BOMB SIZE ID (in) X Ht. (in)	CASING (in)	R/WRA1/3 11/1bRA1/3	1 (in)
156	56		157.48	48.501	SWISS 50kg BOMB	.44	3.5980	5.9~11.8
157	57	WAND B	0	48.501	SWISS 50kg BOMB	.44	0.1000	47.24
158	57	PECKE	0	48.501	SWISS 50kg BOMB	.44	0.1000	43.307
159	25	400	36	26.000	?	---	1.0130	18
160	25	401	18	26.000	?	---	0.5063	18
161	25	402	10	26.000	?	---	0.2810	18
162	25	403	10	26.000	?	---	0.2810	18
163	58	1	2.05	2.205	1 BLK=4X5X7 cm 5 BLOCKS	---	0.1312	8.66
164	58	2	.7874	0.441	1 BLOCK	---	0.0862	8.66
165	58	3	1.18	0.661	1.5 BLOCKS	---	0.1129	8.66
166	56	4	.787	0.441	1BLOCK	---	0.0862	15.35
167	56	5	1.18	0.661	1.5 BLOCKS	---	0.1129	15.35
168	58	6	2.05	2.205	5 BLOCKS	---	0.1312	15.35
169	58	7	2.52	4.409	10 BLOCKS	---	0.1281	15.35
170	58	8	2.56	6.614	15 BLOCKS	---	0.1136	15.35
171	58	9	3.35	11.023	25 BLOCKS	---	0.1254	43.31
172	60	1A	1.1	2.205	STACKED BLOCKS	---	0.0700	13.78
173	60	2A	1.1	2.205	STACKED BLOCKS	---	0.0700	13.78
174	60	3A	1.1	2.205	STACKED RLOCKS	---	0.0700	13.78
175	60	4A	1.1	2.205	STACKED BLOCKS	---	0.0700	13.78
176	60	5A	1.1	2.205	STACKED BLOCKS	---	0.0700	13.78
177	60	1B	1.26	4.409	STACKED BLOCKS	---	0.0640	13.78
178	60	2B	1.26	4.409	STACKED BLOCKS	---	0.0640	13.78
179	60	3B	1.26	4.409	STACKED BLOCKS	---	0.0640	13.78
180	60	4B	1.26	4.409	STACKED BLOCKS	---	0.0640	13.78
181	60	5B	1.26	4.409	STACKED BLOCKS	---	0.0640	13.78
182	60	1C	2.48	6.614	STACKED BLOCKS	---	0.1100	13.78
183	60	2C	2.48	6.614	STACKED BLOCKS	---	0.1100	13.78
184	60	3C	2.48	6.614	STACKED BLOCKS	---	0.1100	13.78
185	60	4C	2.48	6.614	STACKED BLOCKS	---	0.1100	13.78
186	60	5C	2.48	6.614	STACKED BLOCKS	---	0.1100	13.78
187	61	11	.5905	0.110	CYL ON SIDE	---	0.1026	3.937
188	61	12	.5905	0.165	CYL ON SIDE	---	0.0898	3.937
189	61	19	1.7716	0.220	CYL ON END	---	0.2444	3.937
190	61	9	.7874	0.309	STACKED BLOCKS	---	0.0971	3.937
191	61	7	.7874	0.441	STACKED BLOCKS	---	0.0862	3.937
192	61	24	.5905	0.066	CYL ON SIDE	---	0.1217	9.4488
193	61	16	.5905	0.220	CYL ON SIDE	---	0.0815	9.4488
194	61	21	.5905	0.220	CYL ON SIDE	---	0.0815	9.4488
195	61	20	.7874	0.441	STACKED BLOCKS	---	0.0862	9.4488
196	61	17	.9842	0.882	STACKED BLOCKS	---	0.0855	9.4488
197	61	23	1.3780	1.543	SPHERE	---	0.0994	9.4488
198	61	22	1.8110	3.086	SPHERE	---	0.1036	9.4488
199	61	18	2.1653	4.409	SPHERE	---	0.1100	9.4488

T/W=1/3 F1/1bP=1/3	CONCRETE (psi)	W/(W+C)* R/W=1/3	REBAR VERT. (in)	REBAR HORIZ. (in)	DAMAGE
0.2020	1	1.58642361	RAT=.092407		LIGHT FLEXURAL + SEVERE SCABBING
1.0795 0.9896	4977 7110	0.04409181 0.04409181	RAT=.00071 RAT=.0008		SEVERE FLEXURE + SPALL FLEXURAL BENDING, DEEP SPALL
0.5063 0.5063 0.5063 0.5063	5800 5800 5800 5800		RAT=.00875 RAT=.00875 RAT=.00875 RAT=.00875		NO DAMAGE NO DAMAGE NO DAMAGE NO DAMAGE
0.5545 0.8498 0.8283 1.8800 1.4881 0.9828 0.7801 0.8815 1.6217	5365 5365 5365 5365 5365 5365 5365 5365 5365		3mm @ 1.575 3mm @ 1.575 3mm @ 1.575 5mm @ 2.755 5mm @ 2.755 5mm @ 2.755 5mm @ 2.755 5mm @ 2.755 5mm @ 2.755	3mm @ 1.575 3mm @ 1.575 3mm @ 1.575 5mm @ 2.755 5mm @ 2.755 5mm @ 2.755 5mm @ 2.755 5mm @ 2.755 5mm @ 2.755	SEV.SPALL TO CONT. BREACH, SEV.SPALL TO CONT. BREACH, SEV.SPALL TO CONT. BREACH, NO SPALL, FRONT CRATER NO SPALL, FRONT CRATER THRESHOLD, FRONT CRATER MED SPALL TO BREACH, BACK BULGE BREACHED NO SPALL, FRONT CRATER
0.8823 0.8823 0.8823 0.8823 0.8823 0.7003 0.7003 0.7003 0.7003 0.7003 0.6117 0.6117 0.6117 0.6117 0.6117	7975 7975 7975 7975 7975 7975 7975 7975 7975 7975 7975 7975 7975 7975 7975		STIRRUPS STIRRUPS STIRRUPS STIRRUPS STIRRUPS STIRRUPS STIRRUPS STIRRUPS STIRRUPS STIRRUPS STIRRUPS STIRRUPS STIRRUPS STIRRUPS STIRRUPS	TOT RAT=.0117 TOT RAT=.0126 TOT RAT=.0110 TOT RAT=.0124 TOT RAT=.0120 TOT RAT=.0117 TOT RAT=.0126 TOT RAT=.0110 TOT RAT=.0124 TOT RAT=.0120 TOT RAT=.0117 TOT RAT=.0126 TOT RAT=.0110 TOT RAT=.0124 TOT RAT=.0120	LIGHT SPALL LIGHT SPALL LIGHT SPALL LIGHT SPALL LIGHT SPALL LIGHT TO MED SPALL LIGHT TO MED SPALL LIGHT TO MED SPALL LIGHT TO MED SPALL LIGHT TO MED SPALL MEDIUM SPALL MEDIUM SPALL MEDIUM SPALL MEDIUM SPALL MEDIUM SPALL
0.6842 0.5977 0.5431 0.4854 0.4311 1.9470 1.3034 1.3034 1.3045 0.8211 0.8814 0.5408 0.4802	4060 4060 4060 4060 4060 5670 5670 5670 4675 5670 4625 4625 5670		TOT RAT=.00534 TOT RAT=.00534 TOT RAT=.00534 TOT RAT=.00534 TOT RAT=.00534 TOT RAT=.0038 TOT RAT=.0038 TOT RAT=.0038 TOT RAT=.0038 TOT RAT=.0038 TOT RAT=.0038 TOT RAT=.0038 TOT RAT=.0038		MEDIUM SPALL MEDIUM SPALL OR SEVERE BREACH BREACH BREACH NO DAMAGE NO DAMAGE NO DAMAGE NO DAMAGE NO DAMAGE MEDIUM SPALL BREACH BREACH

POINT	REFERENCE	TEST	R (in)	W (in) (lb)	BOMB SIZE ID (in) X HL. (in)	CASING (in)	H/WAR1/3 (1/1000) 1/3	T (in)
200	61	6	1.4667	1.323	TNT SPHERE	---	0.1106	13.7706
201	61	13	2.2441	4.860	TNT SPHERE	---	0.1106	13.7706
202	61	3	2.4409	6.173	TNT SPHERE	---	0.1109	13.7706
203	61	10	3.1496	13.226	TNT SPHERE	---	0.1110	13.7706
204	61	6	3.7401	22.040	TNT SPHERE	---	0.1111	13.7706
205	61	14	3.1496	13.226	TNT SPHERE	---	0.1110	27.0627
206	61	1	3.9370	26.456	TNT SPHERE	---	0.1101	27.0627
207	61	2	4.3307	33.069	TNT SPHERE	---	0.1124	27.0627
208	61	8	4.7244	39.683	TNT SPHERE	---	0.1154	27.0627
209	61	15	4.7244	39.683	TNT SPHERE	---	0.1154	27.0627
210	61	4	4.7244	44.092	TNT SPHERE	---	0.1116	27.0627
211	47	FS-2	240	64	8 X 24	---	5	14
212	47	FS-3	240	64	8 X 24	---	5	14
213	47	FS-4	180	27	8 X 18	---	5	14
214	47	FS-7	60	64	8 X 24	---	1.26	8
215	47	FS-8	240	64	8 X 24	---	5	14
216	47	FS-10	60	64	8 X 24	---	1.26	14
217	47	FS-11	240	64	8 X 24	---	5	15
218	47	FS-13	240	64	8 X 24	---	5	16
219	47	FS-14	180	27	8 X 18	---	5	16
220	47	FS-15	240	64	8 X 24	---	5	16
221	47	FS-16	180	27	8 X 18	---	5	16
222	47	FS-17	60	64	8 X 24	---	1.26	16
223	47	FS-20	60	64	8 X 24	20--25	1.26	16
224	47	FS-21	60	64	8 X 24	---	1.26	16
225	47	FS-22	240	263.58	10.8 X 60	WT=311	3.119	14
226	47	FS-23	60	263.58	10.8 X 60	WT=311	1.17	16
227	47	OS-1	60	1	2 X 6	---	5	4
228	47	OS-2	60	1	2 X 6	---	5	3.5
229	47	OS-4	15	1	2 X 6	---	1.26	3.5
230	47	OS-6	60	1	2 X 6	---	5	2.5
231	47	OS-6	15	1	2 X 6	---	1.26	2.5
232	47	OS-7	60	1	2 X 6	---	5	2.5
233	47	OS-8	15	1	2 X 6	---	1.26	2.5
234	47	OS-10	15	1	2 X 6	---	1.26	2
235	63	DB1 A	1.625	0.5	1.75 X 3.25	---	0.1706	6
236	63	B	1.625	0.5	1.75 X 3.25	---	0.1706	6
237	63	C	1.6875	0.5	1.75 X 3.25	---	0.1772	6
238	63	D	1.75	0.5	1.75 X 3.25	---	0.1837	6
239	63	DB2 A	1.625	0.5	1.75 X 3.25	---	0.1706	6
240	63	B	1.625	0.5	1.75 X 3.25	---	0.1706	6
241	63	C	1.6875	0.5	1.75 X 3.25	---	0.1772	6
242	63	D	1.75	0.5	1.75 X 3.25	---	0.1837	6
243	63	DB3 A	1.625	0.5	1.75 X 3.25	---	0.1706	6
244	63	B	1.625	0.5	1.75 X 3.25	---	0.1706	6
245	63	C	1.6875	0.5	1.75 X 3.25	---	0.1772	6
246	63	D	1.75	0.5	1.75 X 3.25	---	0.1837	6
247	63	DB4 A	1.625	0.5	1.75 X 3.25	---	0.1706	6.5
248	63	B	1.625	0.5	1.75 X 3.25	---	0.1706	6.5
249	63	C	1.6875	0.5	1.75 X 3.25	---	0.1772	6.5
250	63	D	1.75	0.5	1.75 X 3.25	---	0.1837	6.5
251	63	DB5 A	1.625	0.5	1.75 X 3.25	---	0.1706	6.5
252	63	B	1.625	0.5	1.75 X 3.25	---	0.1706	6.5
253	63	C	1.6875	0.5	1.75 X 3.25	---	0.1772	6.5
254	63	D	1.75	0.5	1.75 X 3.25	---	0.1837	6.5
255	63	DB6 A	1.625	0.5	1.75 X 3.25	---	0.1706	6.5
256	63	B	1.625	0.5	1.75 X 3.25	---	0.1706	6.5
257	63	C	1.6875	0.5	1.75 X 3.25	---	0.1772	6.5
258	63	D	1.75	0.5	1.75 X 3.25	---	0.1837	6.5
259	63	DB7 A	1.625	0.5	1.75 X 3.25	---	0.1706	6.5
260	63	B	1.625	0.5	1.75 X 3.25	---	0.1706	6.5
261	63	C	1.6875	0.5	1.75 X 3.25	---	0.1772	6.5
262	63	D	1.75	0.5	1.75 X 3.25	---	0.1837	6.5
263	63	DB8 A	1.625	0.5	1.75 X 3.25	---	0.1706	6.5
264	63	B	1.625	0.5	1.75 X 3.25	---	0.1706	6.5
265	63	C	1.6875	0.5	1.75 X 3.25	---	0.1772	6.5
266	63	D	1.75	0.5	1.75 X 3.25	---	0.1837	6.5
267	63	DB9 A	1.625	0.5	1.75 X 3.25	---	0.1706	6.5
268	63	B	1.625	0.5	1.75 X 3.25	---	0.1706	6.5
269	63	C	1.6875	0.5	1.75 X 3.25	---	0.1772	6.5
270	63	D	1.75	0.5	1.75 X 3.25	---	0.1837	6.5
271	63	DB10 A	1.625	0.5	1.75 X 3.25	---	0.1706	6
272	63	B	1.625	0.5	1.75 X 3.25	---	0.1706	6
273	63	C	1.6875	0.5	1.75 X 3.25	---	0.1772	6

1/W#1/3	CONCRETE (psi)	W/(W+C)#	REBAR VERT.(in)	REBAR HORIZ.(in)	DAMAGE
1.0460	8758		STEEL FIBERS	TOT RAT=.0136	NO DAMAGE
0.6784	7728		STEEL FIBERS	TOT RAT=.0136	NO DAMAGE
0.6260	8758		STEEL FIBERS	TOT RAT=.0136	LIGHT SPALL
0.4855	7728		STEEL FIBERS	TOT RAT=.0136	MEDIUM SPALL TO SEVERE
0.4095	8758		STEEL FIBERS	TOT RAT=.0136	BREACH
0.9850	8888		STEEL FIBERS	TOT RAT=.0136	NO DAMAGE
0.7818	7902		STEEL FIBERS	TOT RAT=.0068	NO DAMAGE
0.7257	8816		STEEL FIBERS	TOT RAT=.0068	THRESHOLD OR NO DAMAGE
0.6829	7700		STEEL FIBERS	TOT RAT=.0068	LIGHT SPALL
0.6829	8888		STEEL FIBERS	TOT RAT=.0068	LIGHT SPALL
0.6594	8511		STEEL FIBERS	TOT RAT=.0068	MEDIUM SPALL
0.2917	5800		RAT=.00123	RAT=.00123	HAIRLIKE FLEXURE
0.2917	5800		RAT=.00123	RAT=.00123	HAIRLIKE FLEXURE
0.3889	5800		RAT=.00123	RAT=.00123	HAIRLIKE FLEXURE
0.1667	5800		RAT=.00187	RAT=.00119	BREACHED
0.2917	5800		RAT=.00123	RAT=.00123	HAIRLIKE FLEXURE
0.3889	5800		RAT=.00123	RAT=.00123	THRESHOLD SPALL
?	5800		?	?	HAIRLIKE CRACKS, FLEXURE
0.3333	5800		RAT=.0018	RAT=.00145	HAIRLIKE CRACKS
0.4444	5800		RAT=.0018	RAT=.00145	NO DAMAGE
0.3333	5800		RAT=.0018	RAT=.00145	HAIRLIKE FLEXURE
0.2778	5800		RAT=.0025	RAT=.0025	HAIRLIKE FLEXURE
0.2083	5800		RAT=.0025	RAT=.0025	THRESHOLD SPALL/MEDIUM FLEXURE
0.2083	5800	0.74074074	RAT=.0025	RAT=.0025	BREACHED
?	5800		RAT=.0025	RAT=.0025	LIGHT SPALL/FLEXURE SKIP
0.182	5800	2.64342771	RAT=.00123	RAT=.00123	MEDIUM SPALL
0.208	5800	0.99180321	RAT=.0018	RAT=.00145	BREACHED BIG AREA
0.3333	5000		RAT=.0018	RAT=.00145	NO DAMAGE
0.2917	5000		RAT=.00123	RAT=.00123	NO DAMAGE
0.2917	5000		RAT=.00123	RAT=.00123	NO DAMAGE
0.2083	5000		RAT=.0025	RAT=.0025	NO DAMAGE
0.2083	5000		RAT=.0025	RAT=.0025	NO DAMAGE
0.2083	5000		RAT=.0025	RAT=.0025	NO DAMAGE
0.2083	5000		RAT=.0025	RAT=.0025	NO DAMAGE
0.1667	5000		RAT=.00187	RAT=.0019	HAIRLIKE FLEXURE
0.8399	1535		03 @ 9"	03 @ 15"	THRESHOLD
0.8399	1535		03 @ 9"	03 @ 15"	NO SPALL
0.8399	1535		03 @ 9"	03 @ 15"	NO SPALL
0.8399	1535		03 @ 9"	03 @ 15"	NO SPALL
0.8399	1535		03 @ 9"	03 @ 15"	THRESHOLD
0.8399	1535		03 @ 9"	03 @ 15"	NO SPALL
0.8399	1535		03 @ 9"	03 @ 15"	NO SPALL
0.8399	1535		03 @ 9"	03 @ 15"	THRESHOLD
0.8399	1535		03 @ 9"	03 @ 15"	NO SPALL
0.8399	1535		03 @ 9"	03 @ 15"	NO SPALL
0.8399	1535		03 @ 9"	03 @ 15"	THRESHOLD
0.8399	1535		03 @ 9"	03 @ 15"	NO SPALL
0.8399	1535		03 @ 9"	03 @ 15"	NO SPALL
0.8399	1535		03 @ 9"	03 @ 15"	THRESHOLD
0.8399	1535		03 @ 9"	03 @ 15"	NO SPALL
0.8399	1535		03 @ 9"	03 @ 15"	NO SPALL
0.8399	1535		03 @ 9"	03 @ 15"	THRESHOLD
0.8399	1535		03 @ 9"	03 @ 15"	NO SPALL
0.8399	1535		03 @ 9"	03 @ 15"	NO SPALL
0.8399	1535		03 @ 9"	03 @ 15"	THRESHOLD
0.8399	1535		03 @ 9"	03 @ 15"	NO SPALL
0.8399	1535		03 @ 9"	03 @ 15"	NO SPALL
0.8399	1535		03 @ 9"	03 @ 15"	THRESHOLD
0.8399	1535		03 @ 9"	03 @ 15"	NO SPALL
0.8399	1535		03 @ 9"	03 @ 15"	NO SPALL
0.8399	1535		03 @ 9"	03 @ 15"	THRESHOLD
0.8399	1535		03 @ 9"	03 @ 15"	NO SPALL
0.8399	1535		03 @ 9"	03 @ 15"	NO SPALL
0.8399	1535		03 @ 9"	03 @ 15"	THRESHOLD
0.8399	1535		03 @ 9"	03 @ 15"	NO SPALL
0.8399	1535		03 @ 9"	03 @ 15"	NO SPALL
0.8399	1535		03 @ 9"	03 @ 15"	THRESHOLD
0.8399	1535		03 @ 9"	03 @ 15"	NO SPALL
0.8399	1535		03 @ 9"	03 @ 15"	NO SPALL
0.8399	1535		03 @ 9"	03 @ 15"	THRESHOLD
0.8399	1535		03 @ 9"	03 @ 15"	NO SPALL
0.8399	1535		03 @ 9"	03 @ 15"	NO SPALL
0.8399	1535		03 @ 9"	03 @ 15"	THRESHOLD
0.8399	1535		03 @ 9"	03 @ 15"	NO SPALL
0.8399	1535		03 @ 9"	03 @ 15"	NO SPALL
0.8399	1535		03 @ 9"	03 @ 15"	THRESHOLD
0.8399	1535		03 @ 9"	03 @ 15"	NO SPALL
0.8399	1535		03 @ 9"	03 @ 15"	NO SPALL
0.8399	1535		03 @ 9"	03 @ 15"	THRESHOLD
0.8399	1535		03 @ 9"	03 @ 15"	NO SPALL
0.8399	1535		03 @ 9"	03 @ 15"	NO SPALL
0.8399	1535		03 @ 9"	03 @ 15"	THRESHOLD
0.8399	1535		03 @ 9"	03 @ 15"	NO SPALL
0.8399	1535		03 @ 9"	03 @ 15"	NO SPALL
0.8399	1535		03 @ 9"	03 @ 15"	THRESHOLD
0.8399	1535		03 @ 9"	03 @ 15"	NO SPALL
0.8399	1535		03 @ 9"	03 @ 15"	NO SPALL
0.8399	1535		03 @ 9"	03 @ 15"	THRESHOLD
0.8399	1535		03 @ 9"	03 @ 15"	NO SPALL
0.8399	1535		03 @ 9"	03 @ 15"	NO SPALL
0.8399	1535		03 @ 9"	03 @ 15"	THRESHOLD
0.8399	1535		03 @ 9"	03 @ 15"	NO SPALL
0.8399	1535		03 @ 9"	03 @ 15"	NO SPALL
0.8399	1535		03 @ 9"	03 @ 15"	THRESHOLD
0.8399	1535		03 @ 9"	03 @ 15"	NO SPALL
0.8399	1535		03 @ 9"	03 @ 15"	NO SPALL
0.8399	1535		03 @ 9"	03 @ 15"	THRESHOLD
0.8399	1535		03 @ 9"	03 @ 15"	NO SPALL
0.8399	1535		03 @ 9"	03 @ 15"	NO SPALL
0.8399	1535		03 @ 9"	03 @ 15"	THRESHOLD
0.8399	1535		03 @ 9"	03 @ 15"	NO SPALL
0.8399	1535		03 @ 9"	03 @ 15"	NO SPALL
0.8399	1535		03 @ 9"	03 @ 15"	THRESHOLD
0.8399	1535		03 @ 9"	03 @ 15"	NO SPALL
0.8399	1535		03 @ 9"	03 @ 15"	NO SPALL
0.8399	1535		03 @ 9"	03 @ 15"	THRESHOLD
0.8399	1535		03 @ 9"	03 @ 15"	NO SPALL
0.8399	1535		03 @ 9"	03 @ 15"	NO SPALL
0.8399	1535		03 @ 9"	03 @ 15"	THRESHOLD
0.8399	1535		03 @ 9"	03 @ 15"	NO SPALL
0.8399	1535		03 @ 9"	03 @ 15"	NO SPALL
0.8399	1535		03 @ 9"	03 @ 15"	THRESHOLD
0.8399	1535		03 @ 9"	03 @ 15"	NO SPALL
0.8399	1535		03 @ 9"	03 @ 15"	NO SPALL
0.8399	1535		03 @ 9"	03 @ 15"	THRESHOLD
0.8399	1535		03 @ 9"	03 @ 15"	NO SPALL
0.8399	1535		03 @ 9"	03 @ 15"	NO SPALL
0.8399	1535		03 @ 9"	03 @ 15"	THRESHOLD
0.8399	1535		03 @ 9"	03 @ 15"	NO SPALL
0.8399	1535		03 @ 9"	03 @ 15"	NO SPALL
0.8399	1535		03 @ 9"	03 @ 15"	THRESHOLD
0.8399	1535		03 @ 9"	03 @ 15"	NO SPALL
0.8399	1535		03 @ 9"	03 @ 15"	NO SPALL
0.8399	1535		03 @ 9"	03 @ 15"	THRESHOLD
0.8399	1535		03 @ 9"	03 @ 15"	NO SPALL
0.8399	1535		03 @ 9"	03 @ 15"	NO SPALL
0.8399	1535		03 @ 9"	03 @ 15"	THRESHOLD
0.8399	1535		03 @ 9"	03 @ 15"	NO SPALL
0.8399	1535		03 @ 9"	03 @ 15"	NO SPALL
0.8399	1535		03 @ 9"	03 @ 15"	THRESHOLD
0.8399	1535		03 @ 9"	03 @ 15"	NO SPALL
0.8399	1535		03 @ 9"	03 @ 15"	NO SPALL
0.8399	1535		03 @ 9"	03 @ 15"	THRESHOLD
0.8399	1535		03 @ 9"	03 @ 15"	NO SPALL
0.8399	1535		03 @ 9"	03 @ 15"	NO SPALL
0.8399	1535		03 @ 9"	03 @ 15"	THRESHOLD
0.8399	1535		03 @ 9"	03 @ 15"	NO SPALL
0.8399	1535		03 @ 9"	03 @ 15"	NO SPALL
0.8399	1535		03 @ 9"	03 @ 15"	THRESHOLD
0.8399	1535		03 @ 9"	03 @ 15"	NO SPALL
0.8399	1535		03 @ 9"	03 @ 15"	NO SPALL
0.8399	1535		03 @ 9"	03 @ 15"	THRESHOLD
0.8399	1535		03 @ 9"	03 @ 15"	NO SPALL
0.8399	1535		03 @ 9"	03 @ 15"	NO SPALL
0.8399	1535		03 @ 9"	03 @ 15"	THRESHOLD
0.8399	1535		03 @ 9"	03 @ 15"	NO SPALL
0.8399	1535		03 @ 9"	03 @ 15"	NO SPALL
0.8399	1535		03 @ 9"	03 @ 15"	THRESHOLD
0.8399	1535		03 @ 9"	03 @ 15"	NO SPALL
0.8399	1535		03 @ 9"	03 @ 15"	NO SPALL
0.8399	1535		03 @ 9"	03 @ 15"	THRESHOLD
0.8399	1535		03 @ 9"	03 @ 15"	NO SPALL
0.8399	1535		03 @ 9"	03 @ 15"	NO SPALL
0.8399	1535		03 @ 9"	03 @ 15"	THRESHOLD
0.8399	1535		03 @ 9"	03 @ 15"	NO SPALL
0.8399	1535		03 @ 9"	03 @ 15"	NO SPALL
0.8399	1535		03 @ 9"	03 @ 15"	THRESHOLD
0.8399	1535		03 @ 9"	03 @ 15"	NO SPALL
0.8399	1535		03 @ 9"	03 @ 15"	NO SPALL
0.8399	1535		03 @ 9"	03 @ 15"	THRESHOLD
0.8399	1535		03 @ 9"	03 @ 15"	NO SPALL
0.8399	1535		03 @ 9"	03 @ 15"	NO SPALL
0.8399	1535		03 @ 9"	03 @ 15"	THRESHOLD
0.8399	1535		03 @ 9"	03 @ 15"	NO SPALL
0.8399	1535		03 @ 9"	03 @ 15"	NO SPALL
0.8399	1535		03 @ 9"	03 @ 15"	THRESHOLD
0.8399	1535		03 @ 9"	03 @ 15"	NO SPALL
0.8399	1535		03 @ 9"	03 @ 15"	NO SPALL
0.8399	1535		03 @ 9"	03 @ 15"	THRESHOLD
0.8399	1535		03 @ 9"	03 @ 15"	NO SPALL
0.8399	1535		03 @ 9"	03 @ 15"	NO SPALL
0.8399	1535		03 @ 9"	03 @ 15"	THRESHOLD
0.8399	1535		03 @ 9"	03 @ 15"	NO SPALL
0.8399	1535		03 @ 9"	03 @ 15"	NO SPALL
0.8399	1535		03 @ 9"	03 @ 15"	THRESHOLD
0.8399	1535		03 @ 9"	03 @ 15"	NO SPALL
0.8399	1535		03 @ 9"	03 @ 15"	NO SPALL
0.8399	1535		03 @ 9"	03 @ 15"	THRESHOLD
0.8399	1535		03 @ 9"	03 @ 15"	NO SPALL
0.8399	1535		03 @ 9"	03 @ 15"	NO SPALL
0.8399	1535		03 @ 9"	03 @ 15"	THRESHOLD
0.8399	1535		03 @ 9"	03 @ 15"	NO SPALL
0.8399	1535		03 @ 9"	03 @ 15"	NO SPALL
0.8399	1535		03 @ 9"	03 @ 15"	THRESHOLD
0.8399	1535		03 @ 9"	03 @ 15"	NO SPALL
0.8399	1535		03 @ 9"	03 @ 15"	NO SPALL
0.8399	1535		03 @ 9"	03 @ 15"	THRESHOLD
0.8399	1535		03 @ 9"	03 @ 15"	NO SPALL
0.8399	1535		03 @ 9"	03 @ 15"	NO SPALL
0.8399	1535		03 @ 9"	03 @ 15"	THRESHOLD
0.8399	1535		03 @ 9"	03 @ 15"	NO SPALL
0.8399	1535		03 @ 9"	03 @ 15"	NO SPALL
0.8399	1535		03 @ 9"	03 @ 15"	THRESHOLD
0.8399	1535		03 @ 9"	03 @ 15"	NO SPALL
0.8399	1535		03 @ 9"	03 @ 15"	NO SPALL
0.8399	1535		03 @ 9"	03 @ 15"	THRESHOLD
0.8399	1535		03 @ 9"	03 @ 15"	NO SPALL
0.8399	1535		03 @ 9"	03 @ 15"	NO SPALL
0.8399	1535		03 @ 9"	03 @ 15"	THRESHOLD
0.8399	1535		03 @ 9"	03 @ 15"	NO SPALL
0.8399	1535		03 @ 9"	03 @ 15"	NO SPALL
0.8399	1535		03 @ 9"	03 @ 15"	THRESHOLD
0.8399	1535		03 @ 9"	03 @ 15"	NO SPALL
0.8399	1535		03 @ 9"	03 @ 15"	NO SPALL
0.8399	1535		03 @ 9"	03 @ 15"	THRESHOLD
0.8399	1535		03 @ 9"	03 @ 15"	NO SPALL
0.8399	1535		03 @ 9"	03 @ 15"	NO SPALL
0.8399	1535		03 @ 9"	03 @ 15"	THRESHOLD
0.8399	1535		03 @ 9"	03 @ 15"	NO SPALL
0.8399	1535		03 @ 9"	03 @ 15"	NO SPALL
0.8399	1535		03 @ 9"	03 @ 15"	THRESHOLD
0.8399	1535		03 @ 9"	03 @ 15"	NO SPALL
0.8399	1535		03 @ 9"	03 @ 15"	NO SPALL
0.8399	1535		03 @ 9"	03 @ 15"	THRESHOLD
0.8399	153				

POINT	REFERENCE	TEST	R (in)	W (lnt) (lb)	BOMB SIZE ID (in) X Ht. (in)	CASING (in)	R/W**1/3 ft/lb**1/3	T (in)
274	63	D	1.75	0.5	1.75 X 3.25	---	0.1837	5
275	63	DB11 A	1.625	0.5	1.75 X 3.25	---	0.1706	5
276	63	B	1.625	0.5	1.75 X 3.25	---	0.1706	5
277	63	C	1.6875	0.5	1.75 X 3.25	---	0.1772	5
278	63	D	1.75	0.5	1.75 X 3.25	---	0.1837	5
279	63	DB12 A	1.625	0.5	1.75 X 3.25	---	0.1706	5
280	63	B	1.625	0.5	1.75 X 3.25	---	0.1706	5
281	63	C	1.6875	0.5	1.75 X 3.25	---	0.1772	5
282	63	D	1.75	0.5	1.75 X 3.25	---	0.1837	5
283	63	DB16 A	1.625	0.5	1.75 X 3.25	---	0.1706	3.5
284	63	B	1.625	0.5	1.75 X 3.25	---	0.1706	6.5
285	63	C	1.6875	0.5	1.75 X 3.25	---	0.0919	6.5
286	63	D	1.75	0.5	1.75 X 3.25	---	0.0919	6.5
287	63	DB17 A	1.625	0.5	1.75 X 3.25	---	0.1706	3.5
288	63	B	1.625	0.5	1.75 X 3.25	---	0.1706	6.5
289	63	C	1.6875	0.5	1.75 X 3.25	---	0.0919	6.5
290	63	D	1.75	0.5	1.75 X 3.25	---	0.0919	6.5
291	63	DB18 A	1.625	0.5	1.75 X 3.25	---	0.1706	6.5
292	63	B	1.625	0.5	1.75 X 3.25	---	0.1706	6.5
293	63	C	1.6875	0.5	1.75 X 3.25	---	0.0919	6.5
294	63	D	1.75	0.5	1.75 X 3.25	---	0.0919	6.5
295	63	DB13 A	1.625	0.5	1.75 X 3.25	---	0.1706	6.5
296	63	B	1.625	0.5	1.75 X 3.25	---	0.1706	6.5
297	63	C	1.6875	0.5	1.75 X 3.25	---	0.1772	6.5
298	63	D	1.75	0.5	1.75 X 3.25	---	0.1772	6.5
299	63	E	0.875	0.5	1.75 X 3.25	---	0.0919	6.5
300	63	DB14 A	1.625	0.5	1.75 X 3.25	---	0.1706	6.5
301	63	B	1.625	0.5	1.75 X 3.25	---	0.1706	6.5
302	63	C	1.6875	0.5	1.75 X 3.25	---	0.1772	6.5
303	63	D	1.75	0.5	1.75 X 3.25	---	0.1772	6.5
304	63	E	0.875	0.5	1.75 X 3.25	---	0.0919	6.5
305	63	DB15 A	1.625	0.5	1.75 X 3.25	---	0.1706	6.5
306	63	B	1.625	0.5	1.75 X 3.25	---	0.1706	6.5
307	63	C	1.6875	0.5	1.75 X 3.25	---	0.1772	6.5
308	63	D	1.75	0.5	1.75 X 3.25	---	0.1772	6.5
309	63	E	0.875	0.5	1.75 X 3.25	---	0.0919	6.5
310	63	25 A	1.625	0.5	1.75 X 3.25	---	0.1706	8
311	63	B	1.625	0.5	1.75 X 3.25	---	0.1706	8
312	63	C	1.6875	0.5	1.75 X 3.25	---	0.1772	8
313	63	D	1.75	0.5	1.75 X 3.25	---	0.1837	8
314	63	26 A	1.625	0.5	1.75 X 3.25	---	0.1706	8
315	63	B	1.625	0.5	1.75 X 3.25	---	0.1706	8
316	63	C	1.6875	0.5	1.75 X 3.25	---	0.1772	8
317	63	D	1.75	0.5	1.75 X 3.25	---	0.1837	8
318	63	27 A	1.625	0.5	1.75 X 3.25	---	0.1706	8
319	63	B	1.625	0.5	1.75 X 3.25	---	0.1706	8
320	63	C	1.6875	0.5	1.75 X 3.25	---	0.1772	8
321	63	D	1.75	0.5	1.75 X 3.25	---	0.1837	8
322	63	37 A	1.625	0.5	1.75 X 3.25	---	0.1706	8
323	63	B	1.625	0.5	1.75 X 3.25	---	0.1706	8
324	63	C	0.875	0.5	1.75 X 3.25	---	0.0919	8
325	63	D	0.875	0.5	1.75 X 3.25	---	0.0919	8
326	63	38 A	1.625	0.5	1.75 X 3.25	---	0.1706	8
327	63	B	1.625	0.5	1.75 X 3.25	---	0.1706	8
328	63	C	0.875	0.5	1.75 X 3.25	---	0.0919	8
329	63	D	0.875	0.5	1.75 X 3.25	---	0.0919	8
330	63	39 A	1.625	0.5	1.75 X 3.25	---	0.1706	8
331	63	B	1.625	0.5	1.75 X 3.25	---	0.1706	8
332	63	C	0.875	0.5	1.75 X 3.25	---	0.0919	8
333	63	D	0.875	0.5	1.75 X 3.25	---	0.0919	8
334	63	40 A	1.5	0.783	2" DIA X 3" LONG	---	0.1358	8
335	63	B	1.5	0.551	2" DIA X 3" LONG	---	0.1525	8
336	63	C	1.5	0.5	2" DIA X 3" LONG	---	0.1706	8
337	63	41 A	1.5	0.783	2" DIA X 3" LONG	---	0.1358	8
338	63	B	1.5	0.551	2" DIA X 3" LONG	---	0.1525	8
339	63	C	1.5	0.5	2" DIA X 3" LONG	---	0.1706	8

D13

POINT	REFERENCE	TEST	R (in)	W (lbt) (lb)	BOMB SIZE ID (in) X Ht. (in)	CASING (in)	R/W**1/3 ft/lb**1/3	1 (in)
340	63	43 A	1.5	0.763	2" DIA X 3" LONG	---	0.1356	8
341	63	B	1.5	0.551	2" DIA X 3" LONG	---	0.1525	8
342	63	C	1.5	0.5	2" DIA X 3" LONG	---	0.1706	8
343	63	D	1.625	0.5	1.75 X 1.75 X 3.2	---	0.1706	8
344	63	44 A	1.5	0.763	2" DIA X 3" LONG	---	0.1356	8
345	63	B	1.5	0.551	2" DIA X 3" LONG	---	0.1525	8
346	63	C	1.5	0.5	2" DIA X 3" LONG	---	0.1706	8
347	63	D	1.625	0.5	1.75 X 1.75 X 3.2	---	0.1706	8
348	63	61 A	1.625	0.5	1.75 X 1.75 X 3.2	---	0.1706	5
349	63	B	1.625	0.5	1.75 X 1.75 X 3.2	---	0.1706	5
350	63	C	1.6875	0.5	1.75 X 1.75 X 3.2	---	0.1772	5
351	63	D	2.125	0.5	1.75 X 1.75 X 3.2	---	0.2231	5
352	63	62 A	1.625	0.5	1.75 X 1.75 X 3.2	---	0.1706	5
353	63	B	1.625	0.5	1.75 X 1.75 X 3.2	---	0.1706	5
354	63	C	1.6875	0.5	1.75 X 1.75 X 3.2	---	0.1772	5
355	63	D	2.125	0.5	1.75 X 1.75 X 3.2	---	0.2231	5
356	63	63 A	1.625	0.5	1.75 X 1.75 X 3.2	---	0.1706	5
357	63	B	1.625	0.5	1.75 X 1.75 X 3.2	---	0.1706	5
358	63	C	1.6875	0.5	1.75 X 1.75 X 3.2	---	0.1772	5
359	63	D	2.125	0.5	1.75 X 1.75 X 3.2	---	0.2231	5
360	63	67 A	1.625	0.5	1.75 X 1.75 X 3.2	---	0.1706	5
361	63	B	1.625	0.5	1.75 X 1.75 X 3.2	---	0.1706	5
362	63	C	1.75	0.5	1.75 X 1.75 X 3.2	---	0.1772	5
363	63	D	1.875	0.5	1.75 X 1.75 X 3.2	---	0.2231	5
364	63	68 A	1.625	0.5	1.75 X 1.75 X 3.2	---	0.1706	5
365	63	B	1.625	0.5	1.75 X 1.75 X 3.2	---	0.1706	5
366	63	C	1.75	0.5	1.75 X 1.75 X 3.2	---	0.1772	5
367	63	D	1.875	0.5	1.75 X 1.75 X 3.2	---	0.2231	5
368	63	69 A	1.625	0.5	1.75 X 1.75 X 3.2	---	0.1706	5
369	63	B	1.625	0.5	1.75 X 1.75 X 3.2	---	0.1706	5
370	63	C	1.75	0.5	1.75 X 1.75 X 3.2	---	0.1772	5
371	63	D	1.875	0.5	1.75 X 1.75 X 3.2	---	0.2231	5
372	64	1	7.143	438.4	24"DIA X 12"HIGH	16	0.0783	60
373	64	2	7.576	895.08	30"DIA X 12"HIGH	16	0.0786	60
374	64	3	11.364	2298.86	40"DIA X 18"HIGH	16	0.0787	84

[illegible]